SINTEF

F26123- Restricted

Report

Danish Seine: Computer based Development and Operation

Reporting on the expert workshop activities March 2013 – May 2014

Author
Bent Herrmann

SINTEF Fisheries and Aquaculture
SINTEF Fisheries and Aquaculture
2014-05-20

SINTEF

SINTEF Fiskeri og havbruk AS
SINTEF Fisheries and Aquaculture

P.b. 4762 Sluppen
NO-7465 Trondheim
NORWAY

Telephone:+47 40005350
Telefax:+47

fish@sintef.no
www.sintef.no/fisk
Enterprise /VAT No:
NO 980 478 270 MVA

KEYWORDS:
Danish Seine
Simulation
Gear behaviour
Selectivity
Expert workshop

Report

Danish Seine: Computer based Development and Operation

Reporting on the expert workshop activities March 2013 – May 2014

VERSION
1.0

DATE
2014-05-20

AUTHOR
Bent Herrmann

CLIENT(S)
RCN / FHF

CLIENT'S REF.
225193 / 900861

PROJECT NO.
225193 (MAROFF-2) / 900861 (FHF) / 6020699 (SFH)

NUMBER OF PAGES/APPENDICES:
8 + Appendices

ABSTRACT
The purpose of the project "Danish Seine: Computer based Development and Operation" (MAROFF-2 project no. 225193 / FHF 900861), funded by Research Council of Norway (RCN) and Norwegian Seafood Research Fund (FHF), is to develop software tools to investigate Danish Seine fishing. These tools cover both the physical behaviour of the Danish Seine gear during the fishing process and the selectivity inside the Seine net. International knowledge is transferred to the project through an expert group established in connection with the project to assist development of models and software tools in the project. This report summarizes the expert group activities carried out inside the project in the period March 2013 to May 2014.

PREPARED BY
Bent Herrmann

SIGNATURE


CHECKED BY
Nina Madsen

SIGNATURE


APPROVED BY
Vegar Johansen

SIGNATURE
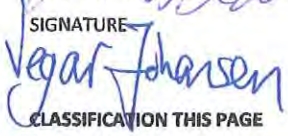

REPORT NO. F26123

ISBN ISBN

CLASSIFICATION Restricted

CLASSIFICATION THIS PAGE Restricted

Document history

VERSION	DATE	VERSION DESCRIPTION
Version No. 1	2014-05-20	

SINTEF

Table of contents

APPENDICES

1 Introduction

The purpose of the project "Danish Seine: Computer based Development and Operation" (MAROFF-2 project no. 225193 / FHF project no. 900861), funded by Research Council of Norway (RCN) and Norwegian Seafood Research Fund (FHF), is to develop software tools to investigate Danish Seine fishing. These tools cover both the physical behaviour of the Danish Seine gear during the fishing process and the selectivity inside the Seine net. The project is led by Sintef Fisheries and Aquaculture (SFH), and is carried out in collaboration with the Norwegian College of Fishery Science at the University in Tromsø (UiT). To provide expert knowledge about physical modelling of fishing gear behaviour, simulation of selectivity, Danish Seine fishing and Seining selectivity to the development team in the project an expert group has been created. Three international specialists, covering different scientific disciplines and fields of experience of importance for the development team participate in the expert group. Transfer of knowledge from these international experts to the members of the development team in the project has during the period March 2013 to May 2014 been provided through: i) Skype and telephone meetings between one expert and one member of the development team; ii) mail correspondence; iii) a workshop between all the members of the development team and the experts (May 2014).
The purpose of this report is to document which knowledge have been transferred from the experts to the project and to outline how it has been achieved. The main parts of the report are therefore in a comprehensive appendix indexed A1 to A17 which contain the information transferred in the form of data, documents, presentations, and presentations discussed. The report then outlines how the transfer of knowledge has been obtained while referring to the appendices.

2 Description of the expert group

Three experts from internal research institutes participate in the expert group. The role of these experts is to transfer knowledge to the project which will ensure that the development inside the project is based on knowledge which is at the international forefront.

IFREMER in France participates with Dr. Daniel Priour. He is regarded an international expert in modelling of netting behaviour in towed fishing gears and has recently initiated national research in France regarding simulation of Danish Seine behaviour.

Fisheries Research Service at the Marine Laboratory, Aberdeen, Scotland (FRS) participates through Dr. Barry O' Neill. He has expertise in hydrodynamics, modelling of netting behaviour in towed fishing gears, physical modelling of the seabed impact by active fishing gears, size selectivity, fish behaviour and simulation of fishing gear selectivity. Further, Dr. O' Neill has experiences and access to experimental data regarding size selectivity in Seine fishing.

The Johann Heinrich von Thünen Institute (TI) is represented by Dr. Daniel Stepputtis. He has his main expertise in conducting full scale sea trials measuring various biological parameters, gear behaviour during fishing and is in charge of a team conducting selectivity experiments.
Experimental data and underwater observations from Dr. Stepputtis' team are used in the development and verification processes for the simulation models in the project. Specifically, test of some aspects of the codend size selectivity simulation model is possible through this collaboration.

3 Description of the projects development team

To implement the simulations tools being developed in the project a software development team with three members from SFH has been setup. They are the one who has the task of implementing the different models into the computer code which form the software tools being developed in the project. The main flow of

information from the group of experts is therefore to be directed towards this development team. The software development team consists of:

- Dr. Bent Herrmann who is responsible for development of the seine selectivity models in the project. He further acts as project manager for the project.
- Dr. Karl Gunnar Aarsæther who works on the physical modelling of gear behaviour with main focus on implementing the core model.
- Dr. Nina A.H. Madsen who works on the physical modelling of gear behaviour with main focus on the user interface implementation.

Besides these three members specific parts of the models will be implemented by other SFH-staff with special and specific know how.

To support the software development team with basic knowledge about Norwegian fishery and in particular Danish seine fishing MSc. Roger B. Larsen from UiT is part of the project team. Further are these activities supplemented by Dr. Manu Sistiaga and Dr. Eduardo Grimaldo, both from SFH.

4 Transfer of knowledge from Dr. Priour prior to the expert workshop

During several telephone meetings and Skype meetings in the period March 2013 to April 2014 between Dr. Herrmann and Dr. Priour have various technical subjects been discussed regarding the application of finite elements methods to simulate the physical behaviour of active fishing gears like trawls and seines. Key subjects covered in these discussions have included:

- Use of 2D triangular elements to model the physical behaviour of diamond mesh, square mesh and hexagonal mesh netting.
- Application of different drag models with specific focus on problems with realistic modelling when small angles of attack occur between netting and the current.
- Application of the Newton-Raphson method versus the Newmark's method in the estimation algorithm.
- Application of different types of convergence criteria's to stop the estimation algorithm.
- Models for the interaction between fishing gear and seabed.
- Temporary use of additional model stiffness by adding a virtual contribution to the diagonal in the stiffness matrix for the model to mitigate matrix singularity problems during estimations.
- Use of stepwise model refinement in estimation as method to reduce overall model estimation time.
- Strategies for acquisition of experimental data to validate the physical behaviour of different parts of the Danish Seine fishing gear.

Many of the different subjects addressed in these discussions with Priour are covered by the descriptions in [A7].

5 Transfer of knowledge from Dr. O'Neill prior to the expert workshop

Telephone and Skype meetings between Dr. O'Neill and Dr. Herrmann have been conducted in the period March 2013 and April 2014. Key subjects discussed have covered:

- Methods for comparing codend size selectivity in Danish/ Scottish Seines and demersal trawls.
- Simulation of codend selectivity
- Modelling of fish herding in active fishing gears like Danish seines and demersal trawls.

Some information is described in [A8]

6 Transfer of knowledge from Dr. Stepputtis prior to the expert workshop

Dr. Herrmann have in the initial part of the project (March 2013 – February 2014) had telephone meetings with Dr. Stepputtis aiming at identifying German collected experimental codend selectivity data which might have relevance for the current project. This was concentrated around codends made of square mesh netting and codends where the selectivity mainly would be attributable to the use of square mesh panels. The species in focus was cod. Some information is documented in [A9].

The discussions with Dr. Stepputtis also aimed at identifying underwater recordings which could learn the project something about fish escape behaviour in relation to square mesh panels and codends. [A11] show a few examples of screen dumps.

Another subject discussed was experimental method and data to assess fish herding efficiency of cables /warps when dragged over the seabed during fishing with active gears like trawls and Danish seines. A German experimental dataset will be applied as a basis to model flatfish herding efficiency.

7 Description of activities during the expert workshop

It was found to be practical to coordinate the expert workshop in the project with the venue of the ICES working group for Fisheries Technology and Fish Behaviour (ICES WGFTFB) 2014 annual meeting because: i) the project had to report to ICES WGFTFB as part of the scientific dissemination activities in the project; ii) it would provide the platform to exchange the ideas with national and international scientists not being part of the expert group; iii) it would be easier to coordinate the participation of the expert group members; iv) further it would provide the chance to introduce some of the younger members of the development team to the international scientific environment on Fishing gear technology around the ICES WGFTFB. The expert workshop was therefore conducted in the period May 4th – 9th, 2014 in parallel with ICES WGFTFB in New Bedford, MA, US. The workshop activities are described in the subsequent subsections.

7.1 Meeting with Dr. Benoit Vincent

May 6th did Dr. Madsen, Dr. Aarsæther and Dr. Herrmann meet with Dr. Vincent from France to discuss simulations modelling of the physical behaviour of Danish seines. Dr. Vincent is the developer of the internationally recognized commercial software *Dynamit* (http://wwz.ifremer.fr/dynamit) which simulates the physical behaviour of trawls. Parts of the discussion with Dr. Vincent was rather technical with one of the subjects being the use of different convergence criteria's in the simulation of dynamic fishing gear behaviour. Furthermore Dr. Vincent informed that he is going to build a simulation model for the physical behaviour of Danish seines. In this context it was agreed to share ideas and information. Dr. Vincent also informed that some of his colleagues are going to work with size selectivity in Danish Seine netting. That work was going to be coordinated by MSc Pascal Laurent who will be contacted to investigate potential collaborations with regarding the size selectivity part of the project.

7.2 Meeting with Dr. Antonello Sala

May 8th did Bent Herrmann meet with Dr. Sala from CNR in Italy to discuss the project. The background for the meeting was that Dr. Sala expressed interest in the project and potentially would consider national research activities on the Danish seine fishing method. In this context he was interested in a future collaboration. It was agreed to further investigate the possibilities for a future collaboration.

7.3 Meeting with Dr. Priour

On the May 8th a two and a half hour Skype meeting was held with Dr. Priour with participation of Dr. Madsen, Dr. Aarsæther and Dr. Herrmann from the project group. This had to be conducted as a Skype meeting since Dr. Priour few weeks before the planned workshop activities was prevented to travel to the workshop. The purpose of the meeting was mainly to let Dr. Priour give lectures in his long standing experience in modelling of physical behaviour of active fishing gears including Danish Seines. It was also a

main objective of this meeting to introduce the younger members of the development team in the project to Dr. Priour with the purpose to enable direct collaboration in the later stages of the project.

One of the key subjects in the lectures by Priour was the application of the finite element method to model the physical behaviour of active fishing gears. Dr. Priour is considered an internationally leading scientist. Dr. Priour has developed an estimation tool FEMNET which can predict the physical behaviour of active fishing gears like trawls and Danish seines. Priour introduced the basic ideas of the finite element method and showed a few very simple examples [A1] on how to estimate the equilibrium state for simple systems model by the finite element method and by applying the Newton Raphson method. He continued by explaining how triangular elements can be applied to model netting when this is considered as a 3D surface. He showed how to derive the stiffness matrix for the triangular element [A1] and [A5]. Priour explained how he mitigates singularity or near-singularity in the stiffness matrix by use of temporal added stiffness to the diagonal elements in the matrix.

Dr. Priour explained about the national French project he is heading regarding Danish seine fishing [A3]. He did explain how he had adopted his FEMNET estimation tool to simulate the Danish seine fishing process and showed an example of the estimated physical behaviour [A2]. It was clear from this part of the lecture that the knowledge of Dr. Priour can be very valuable to this project.

Further Dr. Priour did lecture on the very recent sea trials which were carried out April 2014 in the French project. The purpose of those sea trials was to provide experimental data on the physical behaviour of the Danish seine gear during fishing operations which could be applied to validate/adjust the simulation model [A4]. Besides given a lecture on the data collected Dr. Priour also provided an access to the French data which will enable a potential the use of these data in the model validation work to be carried out in the current project both on qualitative and quantitative level.

7.4 Group Meeting

A four hour workshop meeting did take place May 7th, 2014 in New Bedford. This meeting had participation by: Dr. O'Neill, Dr. Stepputtis, Dr. Grimaldo, MSc. Larsen, Dr. Aarsæther, Dr. Madsen and Dr. Herrmann.

Dr. O'Neill presented Scottish codends selectivity data where results from Seining were compared to from demersal trawling [A8]. The Scottish-based results, for mainly haddock, did not show significant difference from those obtained from trawling. Confidence limits where however wide for the seining results and the validity of the model with the trawls results were based on can be questioned. Potential availability of older Scottish seining codend selectivity was also discussed and it was agreed to investigate this further to see if other data which could be of value for the project should exist.

Dr. Stepputtis presented codend selectivity data collected for cod during German sea trials with trawls [A9]. These codend selectivity data involved different codends which has a square mesh panel integrated and a full square mesh codend (120 mm). Even through this data was from bottom trawling and not seining, they were considered to be relevant for the project to learn something about square mesh selectivity of cod. The results demonstrated significant difference in size selectivity of cod between when the codend only partly is built of square meshes compared to when it is fully built of square meshes. In the discussion it came up how this demonstrate the relevance of the specific square mesh codend designs applied in some of the Norwegian Danish seine fishing. The results have relevance for the codend size selection simulator of the project. Further Dr. Stepputtis gave a presentation on a study on factors which affects the codend square mesh release efficiency in codends [A10]. In addition Dr. Stepputtis showed several video clips demonstrating the behaviour of cod and other roundfish species when inside a fishing gear and in particular the behaviour in vicinity of codend square meshes. A few still pictures are shown in [A11].

MSc. Larsen was showing video clips demonstrating the different operational steps in Norwegian Danish seine fishing. The material and the discussion on it provided information with was relevant to consider when designing the user-interface for the simulation tool regarding which facilities there needed to be available. Further MSc. Larsen did make a presentation covering different technical aspects on how Danish Seine fishing is carried out in Norwegian fishery [A12]. The information presented and discussed are relevant for the design options in the tools being developed and for the selection of case designs during the development stages of the project.
Some historical Danish seine selectivity work which MSc. Larsen has been involved in was presented and discussed in the meeting. This information is of key importance for the development of the selectivity simulator in the project. Some of the results of the work MSc. Larsen has been involved in are described in [A13] and [A14].

Dr. Grimaldo presented several very recent underwater video clips from Norwegian Danish Seine fishing. These video clips provide valuable information about when during the Danish seine fishing process cod and haddock escape from the seine. Further these underwater recordings seem to be able to provide detailed information for the selectivity simulator regarding which of the different mesh distortions model that should be considered. These different models are outlined and applied in [A17]. It was discussed how this could be achieved and what additional information that would be relevant to collect for the benefit of this project.

Based on Dr. O'Neill expertise regarding modelling of interaction between fishing gear elements and the seabed there was a discussion on how best to model the interaction between seine ropes and the seabed in the simulation tools. An important part would here be to obtain realistic values for the model parameters. It was discussed whether parts of the work Dr. O'Neill presented in the WGFTFB-meeting could provide some information [A15].

7.5 Activities within the WGFTFB meeting

Inside the WGFTFB meeting did Dr. Madsen give a presentation about the project with a focus on the physical behaviour of the seine ropes [A16]. One purpose of this presentation was to provide a broader international collaboration around the current project and feed-back from a large group of scientists. The presentation did lead to some discussion about the differences and similarities between the different variants seining fishing including what could be defined as Danish seining and Scottish seining.

Also inside the WGFTFB meeting did Dr. Herrmann give a presentation with the title Understanding and predicting size selection of cod (Gadus morhua) in square-mesh codends for Danish Seining: a simulation-based approach. The purpose was here to get some response on the work being conducted in the project regarding simulation of size selectivity [A17]. Member, MSc. Thomas Moth Poulsen (FAO), of WGFTFB responded by stating that some experimental data might be available which could potentially be of interest for the project. This will be investigated further. Further did Dr. Michael Breen from IMR Norway express interest in potentially applying the model in the work of another ICES working group.

Technology for a better society

www.sintef.no

Appendix A1

Finite Element Method for netting

Finite Element Method for netting

Daniel.Priour@ifremer.fr

IFREMER

November 4, 2010

Fish cages

- Salmon in Norway (1Mtons/y)
- Sea-bass in Greece
- Tuna in Japan (Ktons/y)

Fish cages

- What are the tension in cables?
- What is the volume inside the cage?

Fishing gears

- Bottom trawl common in Europe
- Purse seine
- Dredge
- Fish trap

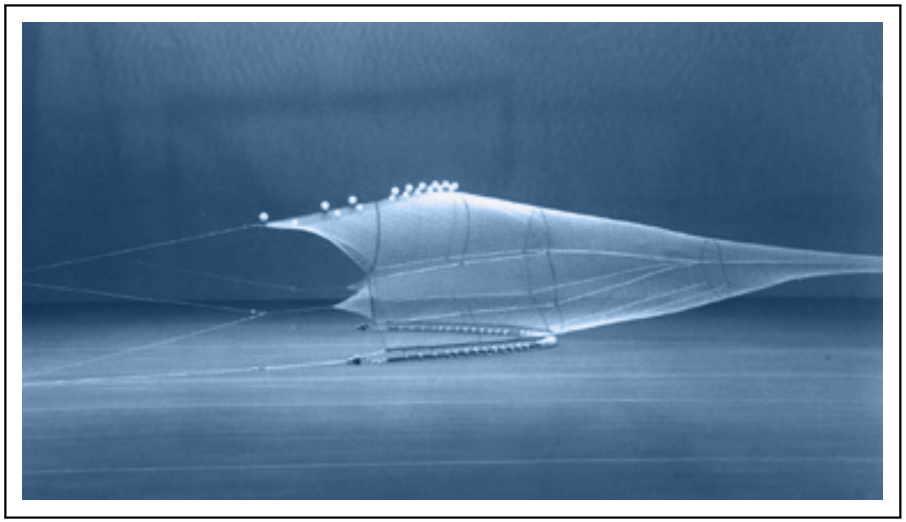

Fishing gears

- What is the drag of the trawl? And the fuel consumption? $(\frac{1/}{Kg})$
- What are the mesh opening in the cod-end? And the fish escapment?

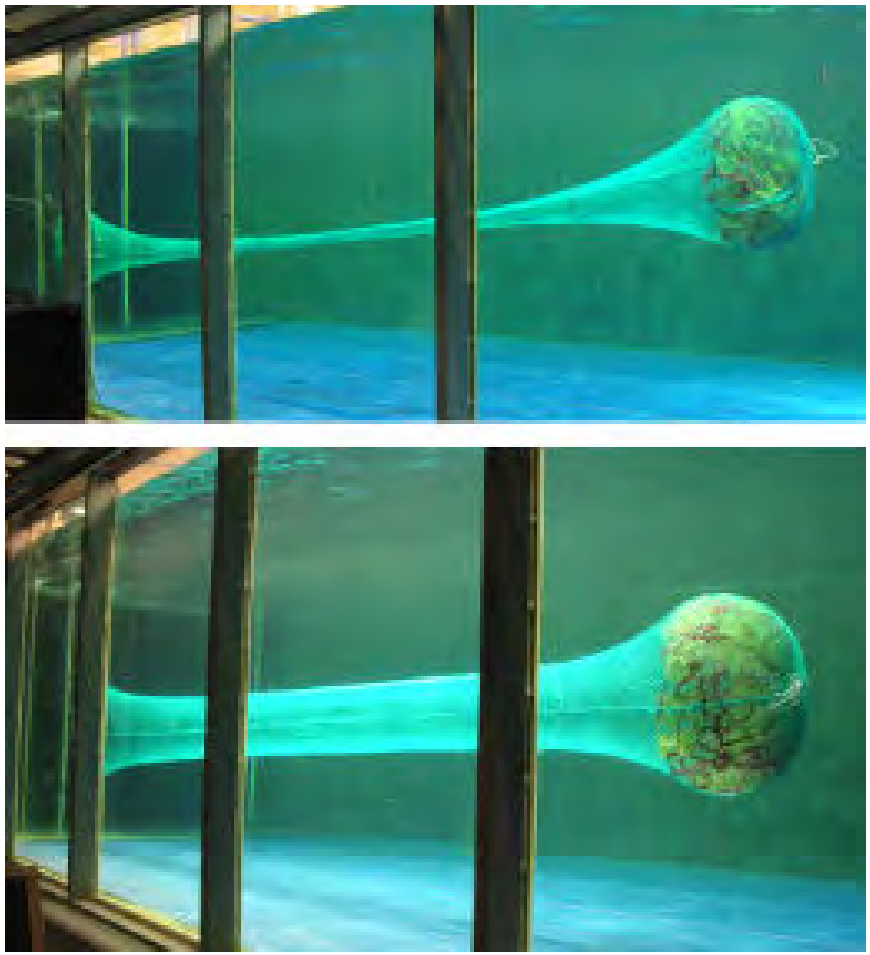

Newton Raphson method: Spring with 1DOF

Question: What is its length?

- $F(x) = Ax\frac{x-l_0}{l_0} - Mg$
- Stiffness not constant
- What is the length (x) at equilibrium?
- Equilibrium: $F(x) = 0$

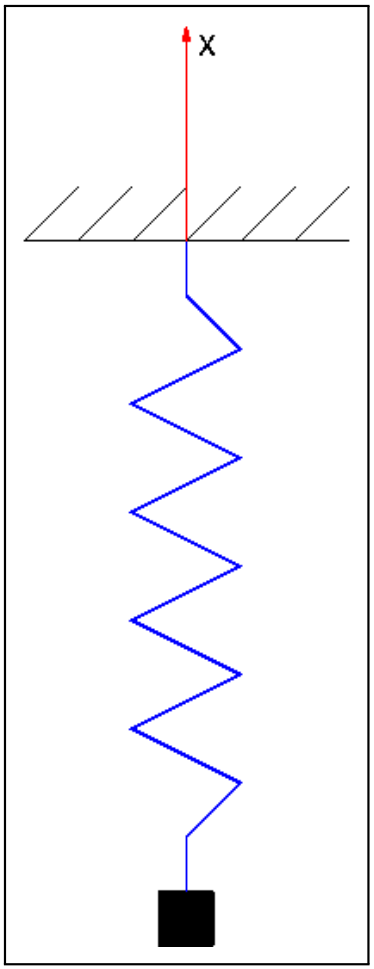

Spring with 1DOF

- Arbitrary length $x = x_0$
- $F(x) = Ax\frac{x-l_0}{l_0} - Mg$
- $F'(x) = \frac{A}{l_0}(2x - l_0)$
- Newton Raphson leads to:
- $x_{k+1} = x_k + \frac{F(x_k)}{-F'(x_k)}$
- $x_0 -> F(x_0) -> F'(x_0) -> x_1$
- $F'(x) = \lim_{h\to 0} \frac{F(x+h)-F(x)}{h}$

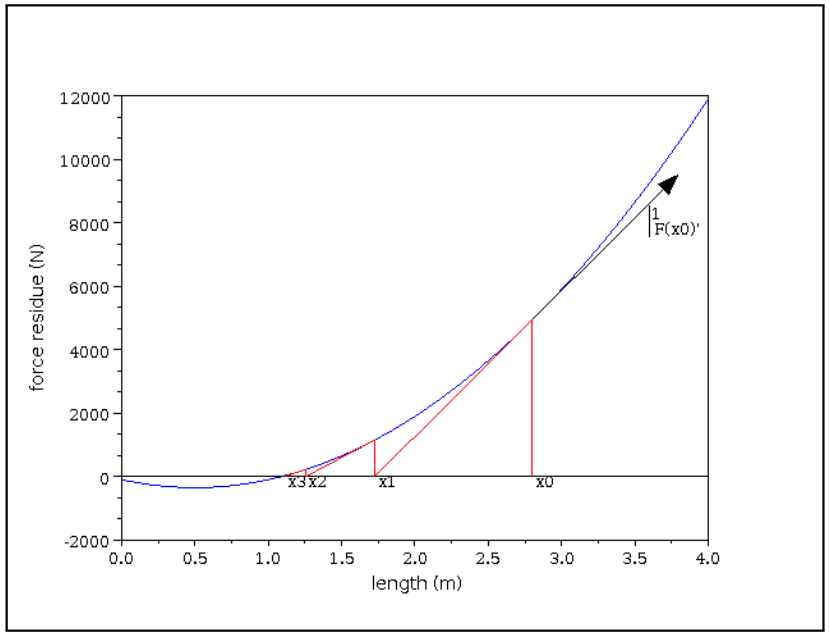

Spring with 1DOF

- Convergence is pretty quick
- But sometimes $F'(x) = 0$
- $x_{k+1} = x_k + \frac{F(x_k)}{-F'(x_k)}$
- Additional stiffness

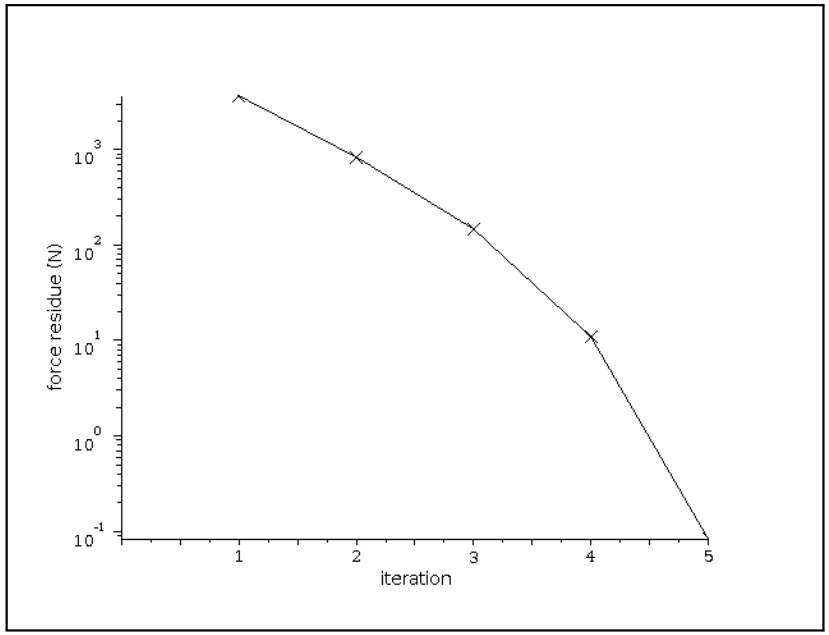

Spring with 2DOF

- $l = \sqrt{x^2 + y^2}$
- $T = Al\frac{l-l_0}{l_0}$ Stiffness not constant
- $F_x(\mathbf{X}) = T\frac{x}{l}$
- $F_y(\mathbf{X}) = T\frac{y}{l} - Mg$

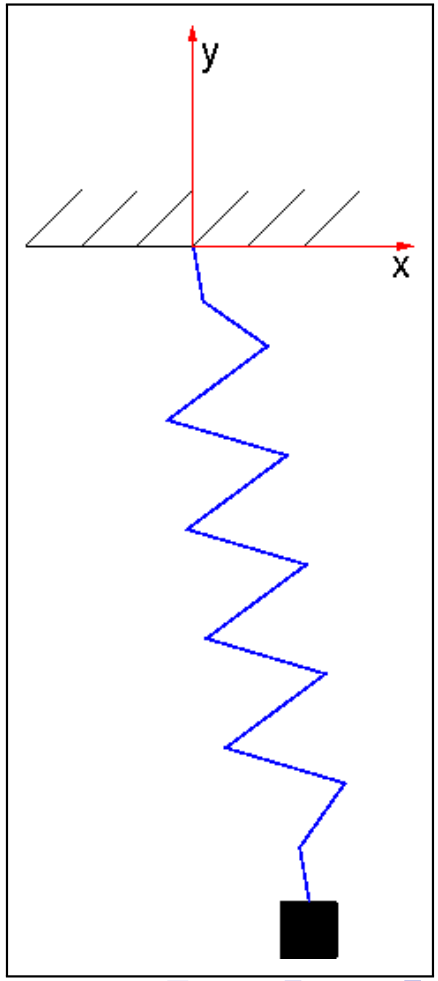

Spring with 2DOF

$$\mathbf{X}_k = \begin{cases} x_k \\ y_k \end{cases}$$

$$\mathbf{F}(\mathbf{X}_k) = \begin{cases} F_x(\mathbf{X}_k) \\ F_y(\mathbf{X}_k) \end{cases}$$

$$F'(\mathbf{X}_k) = \frac{A}{l_0 l_k} \begin{cases} l_k^2 - l_0 l_k + y_k^2 & x_k y_k \\ x_k y_k & l_k^2 - l_0 l_k + y_k^2 \end{cases}$$

$$\mathbf{X}_{k+1} = \mathbf{X}_k + \frac{\mathbf{F}(\mathbf{X}_k)}{-F'(\mathbf{X}_k)}$$

Spring with 2DOF

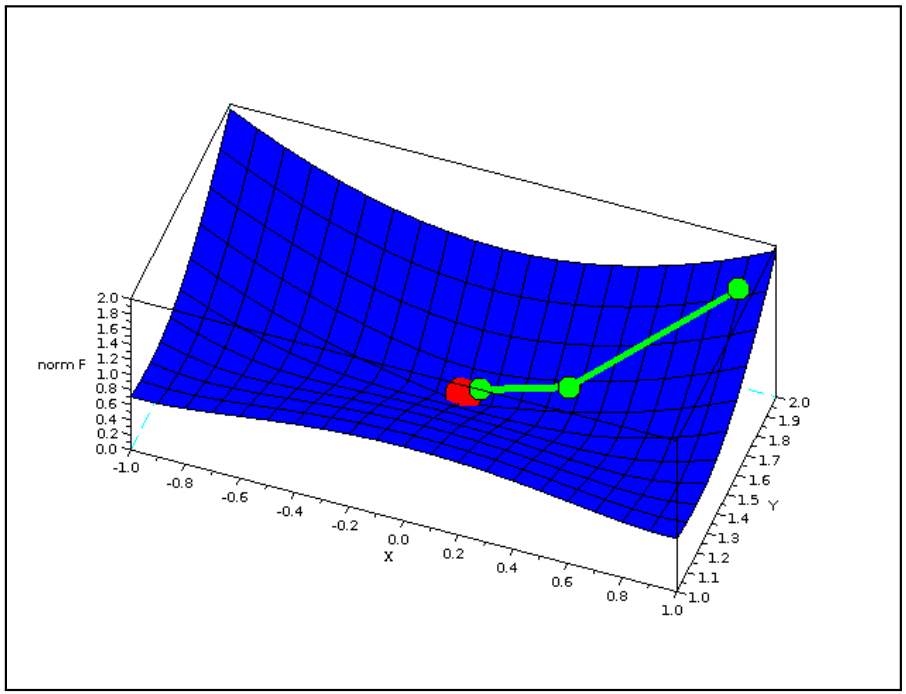

force norme: $\sqrt{F_x^2 + F_y^2}$

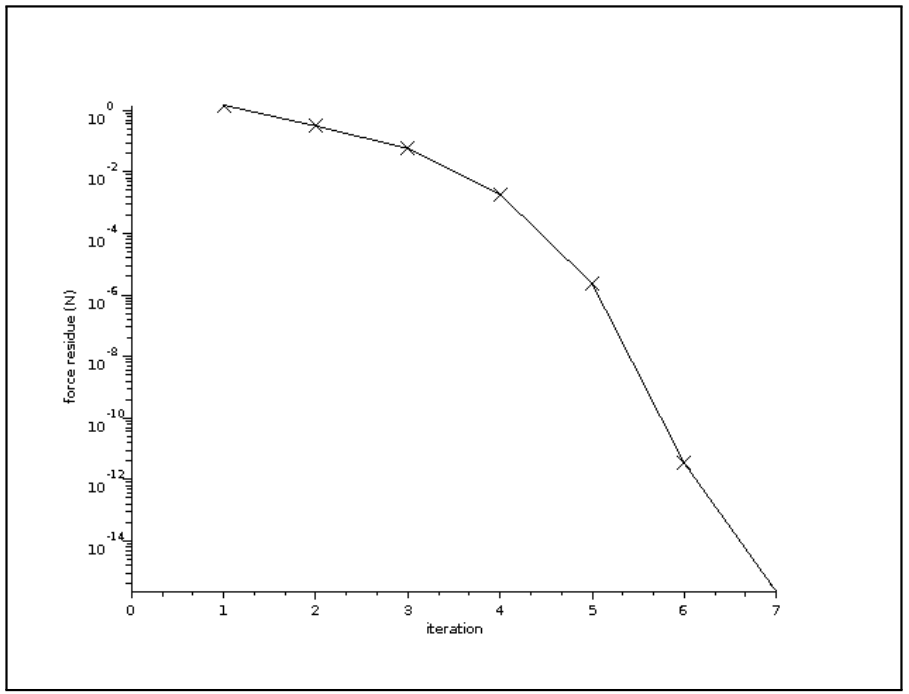

Residue of force norme

Structure with several DOF

$$\mathbf{X}_k = \begin{cases} x_{1k} \\ x_{2k} \\ . \\ x_{nk} \end{cases} \qquad \mathbf{F}(\mathbf{X}_k) = \begin{cases} F_{1k}(\mathbf{X}_k) \\ F_{2k}(\mathbf{X}_k) \\ . \\ F_{nk}(\mathbf{X}_k) \end{cases}$$

$$-F'(\mathbf{X}_k) = \begin{cases} -\frac{dF_1}{dx_1} & -\frac{dF_1}{dx_2} & . & -\frac{dF_1}{dx_n} \\ -\frac{dF_2}{dx_1} & -\frac{dF_2}{dx_2} & . & -\frac{dF_2}{dx_n} \\ . & . & . & . \\ -\frac{dF_n}{dx_1} & -\frac{dF_n}{dx_2} & . & -\frac{dF_n}{dx_n} \end{cases}$$

$$\mathbf{X}_{k+1} = \mathbf{X}_k + \frac{\mathbf{F}(\mathbf{X}_k)}{-F'(\mathbf{X}_k)}$$

Structure with several DOF: Risk of singularity

$$-F'(\mathbf{X}_k) = \begin{Bmatrix} -\frac{dF_1}{dx_1} + K & -\frac{dF_1}{dx_2} & . & -\frac{dF_1}{dx_n} \\ -\frac{dF_2}{dx_1} & -\frac{dF_2}{dx_2} + K & . & -\frac{dF_2}{dx_n} \\ . & . & .+K & . \\ -\frac{dF_n}{dx_1} & -\frac{dF_n}{dx_2} & . & -\frac{dF_n}{dx_n} + K \end{Bmatrix}$$

The additional stiffness K is tuned

Spring with 1DOF: Newmark vs Newton

- $F(x) = Ax\frac{x-l_0}{l_0} - Mg$
- $M\gamma = F(x)$
- Δt is choosen
- $v_{k+1} = v_k + \gamma_k \Delta t$
- $x_{k+1} = x_k + v_k \Delta t + \gamma_k \frac{\Delta t^2}{2}$

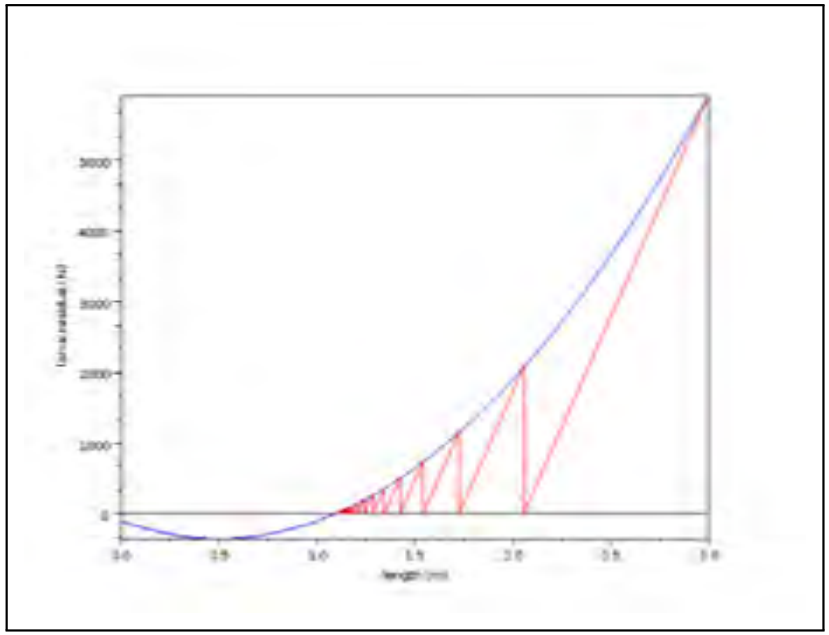

Circle perimeter

- The perimeter is $2\pi R$
- The perimeter approximated by n times cord length
- Cord length $2Rsin(\frac{\alpha}{2})$
- or $2Rtan(\frac{\alpha}{2})$ (outside)

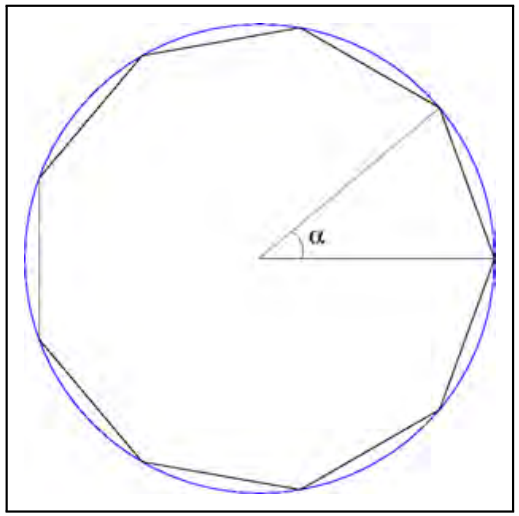

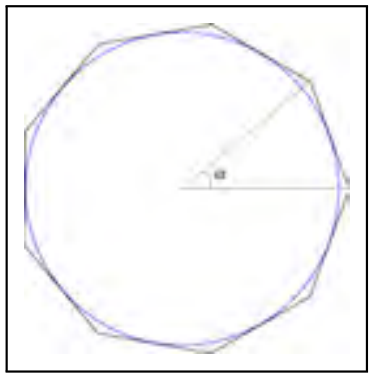

Circle perimeter

Finite Element basic idea:

- Divided in finite elements
- Approximation by element
- Rebuilding all the elements

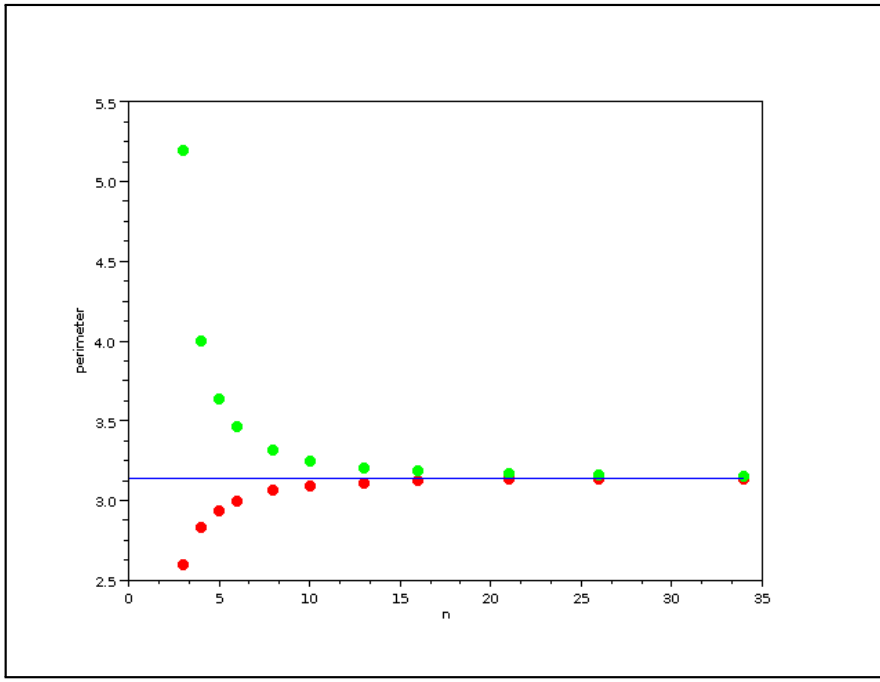

Perimeter vs elements number

Finite element for netting: How?

Netting behaviour:

- Surface
- Elastic

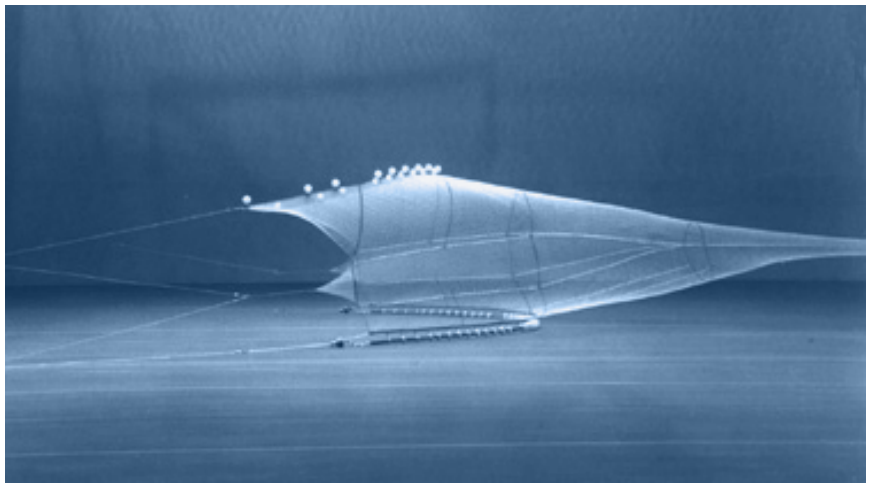

Model test in flume tank

Finite element for netting: Triangle

Triangular element for netting:

- twines parallel
- linear elasticity

Triangular elements model all the netting

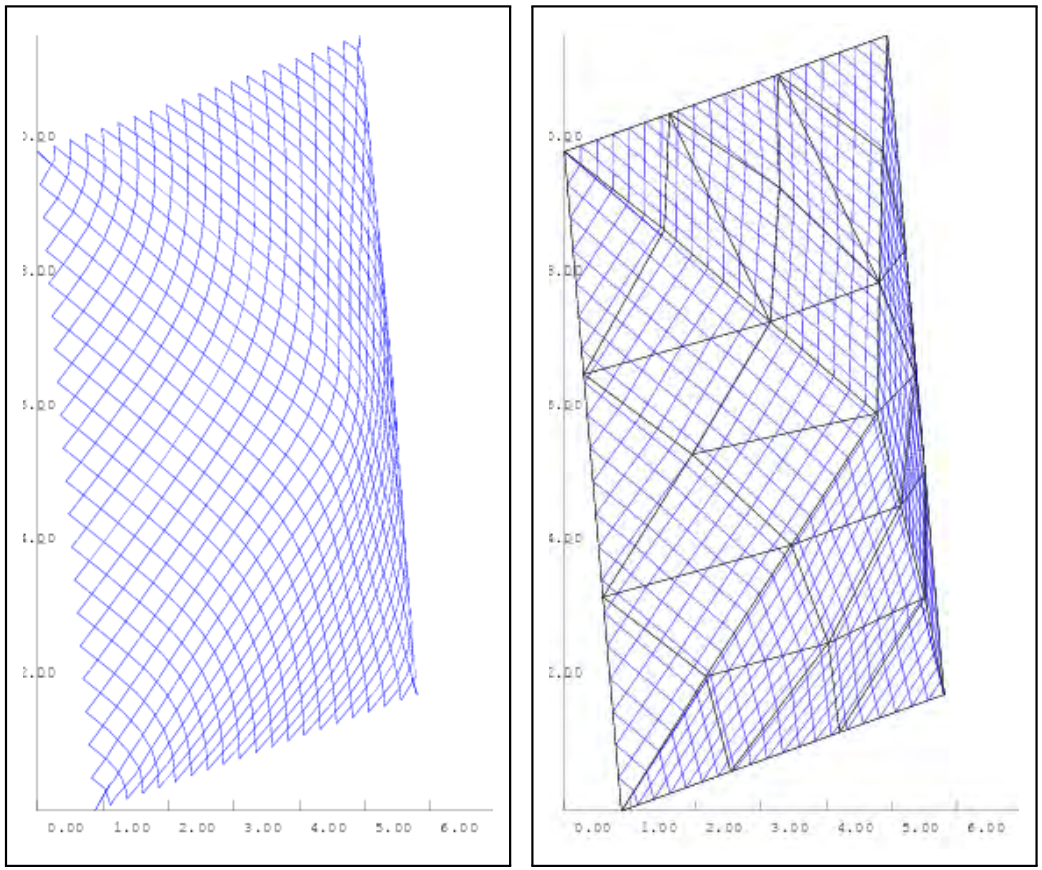

Netting decomposed in triangular elements

Finite element for netting: calculation of mesh sides $(\mathbf{U}, \mathbf{V})$

- Nodes are fixed to the netting
- Cartesian coordinates: $x_1 \ldots z_3$
- Twine coordinates: $U_1 \ldots V_3$
- Triangle side **12** is linear combinaison of mesh sides $\mathbf{U}, \mathbf{V}$

$$\mathbf{12} = (U_2 - U_1)\mathbf{U} + (V_2 - V_1)\mathbf{V}$$
$$\mathbf{13} = (U_3 - U_1)\mathbf{U} + (V_3 - V_1)\mathbf{V}$$

- 2 equations, 2 unknowns $(\mathbf{U}, \mathbf{V})$

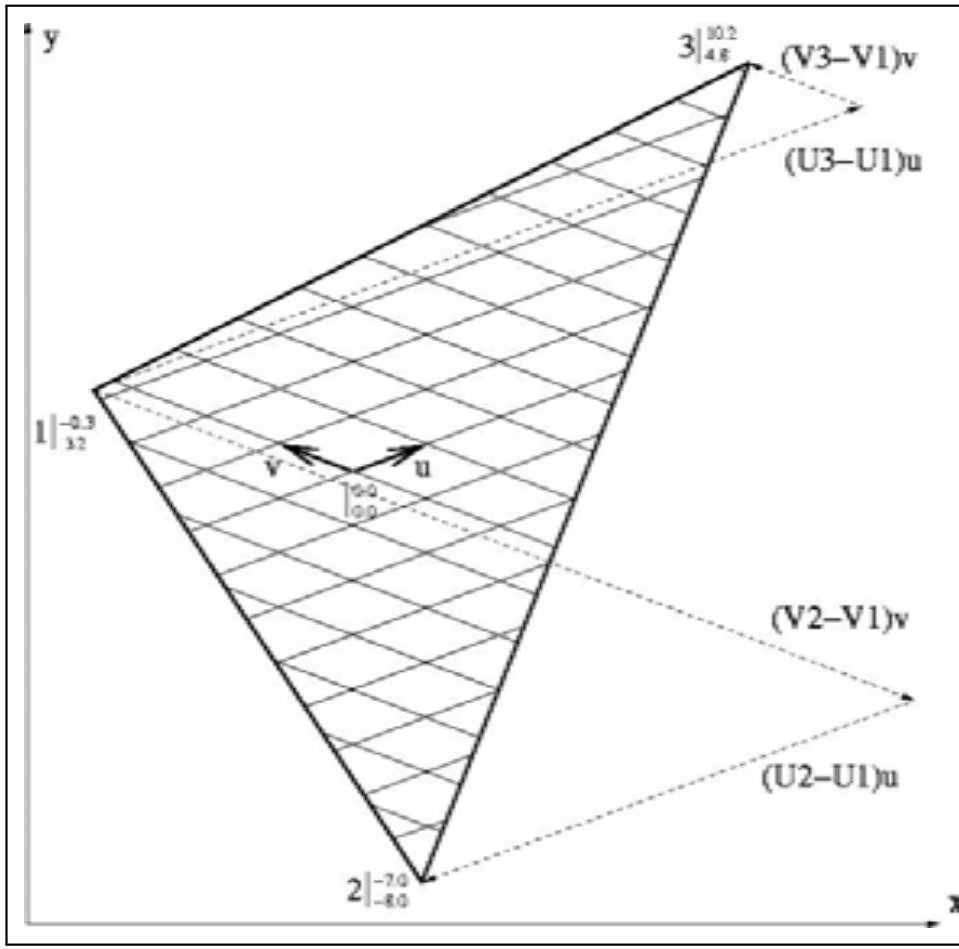

Finite element for netting: calculation of mesh sides ($\mathbf{U}, \mathbf{V}$)

2 previous equations with 2 unknowns ($\mathbf{U}$ and $\mathbf{V}$):

$$\mathbf{U} = \frac{V_3 - V_1}{d}\mathbf{12} - \frac{V_2 - V_1}{d}\mathbf{13}$$
$$\mathbf{V} = \frac{U_3 - U_1}{d}\mathbf{12} - \frac{U_2 - U_1}{d}\mathbf{13}$$

Sides vectors:

$$\mathbf{12} = \begin{vmatrix} X_2 - X_1 \\ Y_2 - Y_1 \\ Z_2 - Z_1 \end{vmatrix}$$
$$\mathbf{13} = \begin{vmatrix} X_3 - X_1 \\ Y_3 - Y_1 \\ Z_3 - Z_1 \end{vmatrix}$$

and

$$d = (U_2 - U_1)(V_1 - V_3) - (U_3 - U_1)(V_1 - V_2)$$

Finite element for netting: number of mesh sides (**U**, **V**)

meaning of d:

- Nb of meshes $= d/4$
- Nb of mesh sides $\mathbf{U} = d/2$
- Nb of mesh sides $\mathbf{V} = d/2$
- Nb of knots $= d/4$

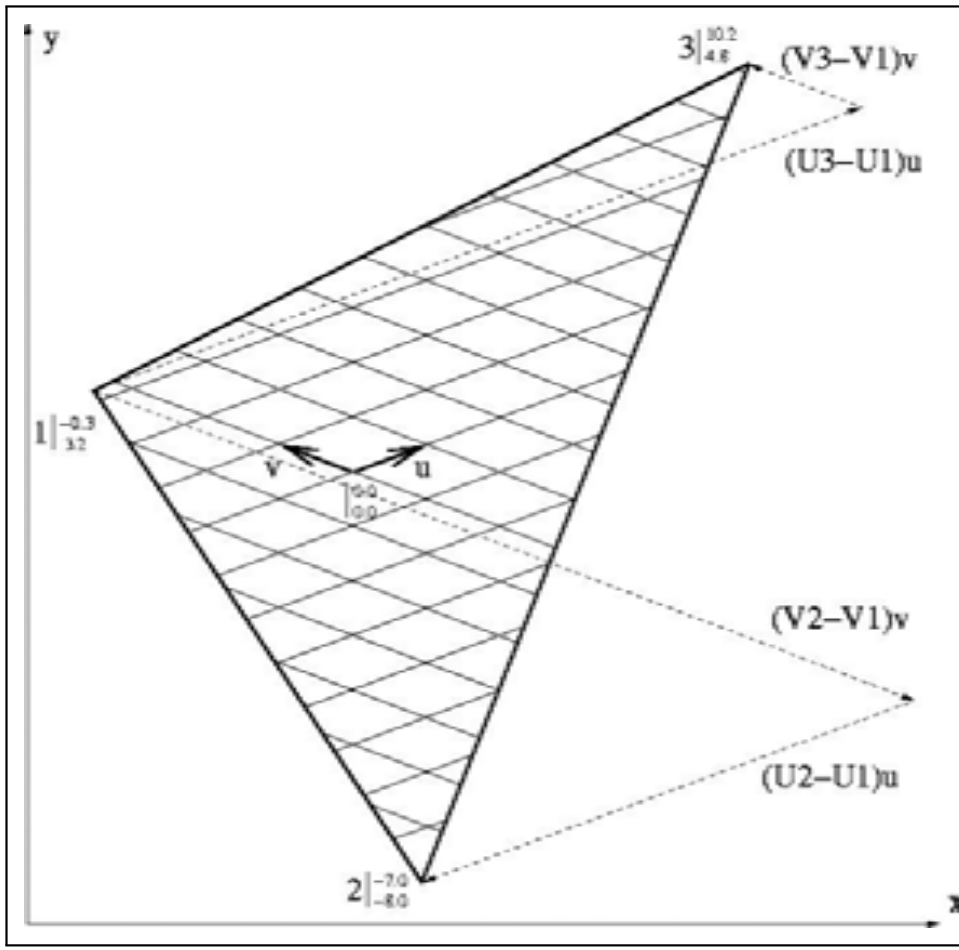

$$d = (U_2 - U_1)(V_1 - V_3) - (U_3 - U_1)(V_1 - V_2):$$

Finite element for netting: tension in mesh sides (T_u, T_v)

Twines are elastic:

$$T_u = EA_u \frac{|\mathbf{U}| - l_0}{l_0}$$
$$T_v = EA_v \frac{|\mathbf{V}| - l_0}{l_0}$$

E: Young's modulus of the material (N/m^2),
A_u, A_v: section of the twines(m^2),
l_o: un-stretched length of mesh sides (m).

Finite element for netting: Principle of virtual work

Force on vertices due to twine tension

Virtual displacement ($\partial x1$):

$W_e = F_{x1}\partial x1$

$W_i = (\partial|\mathbf{U}|\,T_u + \partial|\mathbf{V}|\,T_v)\frac{d}{2}$

$F_{x1} = (T_u\frac{\partial|\mathbf{U}|}{\partial x1} + T_v\frac{\partial|\mathbf{V}|}{\partial x1})\frac{d}{2}$

$\mathbf{F}_1 = (V_3 - V_2)\,T_u\frac{\mathbf{U}}{2|\mathbf{U}|} + (U_2 - U_3)\,T_v\frac{\mathbf{V}}{2|\mathbf{V}|}$

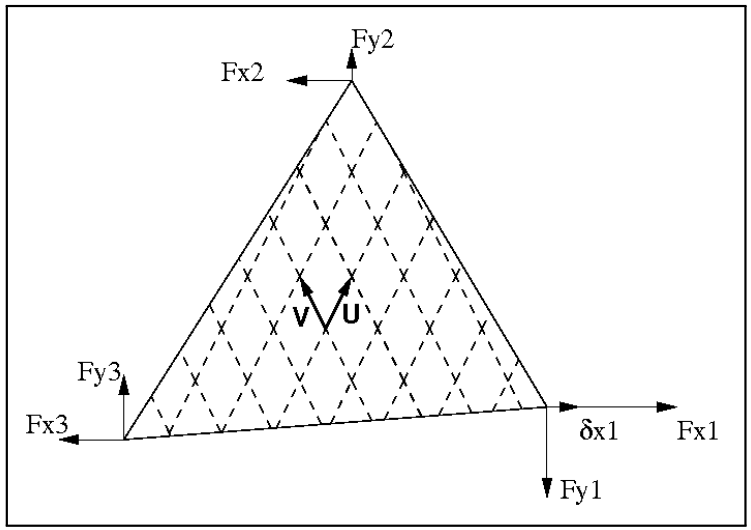

$$\frac{\partial F_{x1}}{\partial x1} = \frac{EA_u(V_3-V_2)}{2}\left[\frac{\partial U_x}{\partial x1}\left(\frac{1}{n_0} - \frac{1}{|\mathbf{U}|}\right) + \frac{\partial|\mathbf{U}|}{\partial x1}\frac{U_x}{|\mathbf{U}|^2}\right] + \frac{EA_v(U_2-U_3)}{2}\left[\frac{\partial V_x}{\partial x1}\left(\frac{1}{n_0} - \frac{1}{|\mathbf{V}|}\right) + \frac{\partial|\mathbf{V}|}{\partial x1}\frac{V_x}{|\mathbf{V}|^2}\right]$$

Drag ($\mathbf{F}, \mathbf{T}$) per triangular element

Amplitude of drag on **U** twine:

$$|\mathbf{F}| = \frac{1}{2}\rho C_d D|\mathbf{U}|(|\mathbf{v}|sin\theta)^2$$

$$|\mathbf{T}| = f\frac{1}{2}\rho C_d D|\mathbf{U}|(|\mathbf{v}|cos\theta)^2$$

Direction of drag on **U** twine:

$$\frac{\mathbf{F}}{|\mathbf{F}|} = \frac{\mathbf{U}}{|\mathbf{U}|} \wedge \frac{\mathbf{v}\wedge\mathbf{U}}{|\mathbf{v}||\mathbf{U}|}$$

$$\frac{\mathbf{T}}{|\mathbf{T}|} = \frac{\mathbf{F}}{|\mathbf{F}|} \wedge \frac{\mathbf{v}\wedge\mathbf{U}}{|\mathbf{v}||\mathbf{U}|}$$

Force on vertex 1 due to drag on **U** twine:

$$\mathbf{D1} = \frac{1}{3}\frac{d}{2}(\mathbf{F} + \mathbf{T})$$

Angle between **v** and **U** twine:

$$cos\theta = \frac{\mathbf{v}.\mathbf{U}}{|\mathbf{v}||\mathbf{U}|}$$

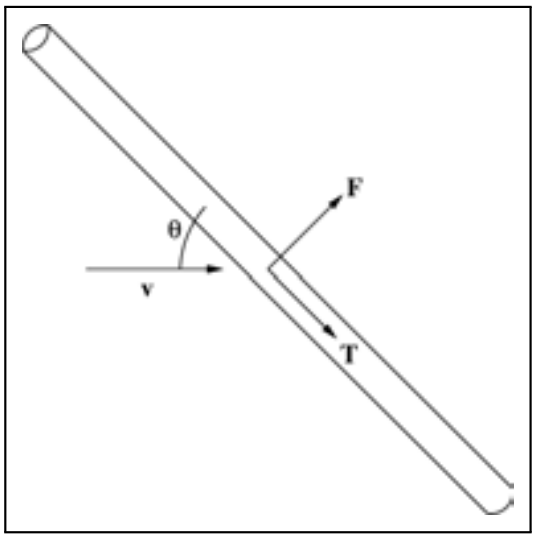

Twines flexion per triangular element

Angle between twines **U** and **V**:
$\alpha = \frac{1}{2} acos(\frac{\mathbf{UV}}{|\mathbf{U}||\mathbf{V}|})$

Couple on knot due to flexion of **U** twine:
$C_u = -C_v = H(\alpha - \alpha_0)$

α_0 angle between unstressed twines

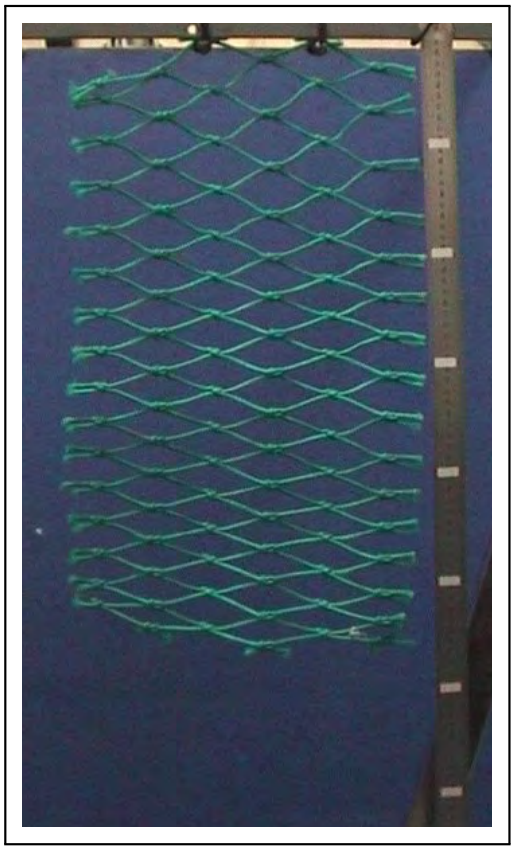

Twines flexion per triangular element

Virtual works:

$$W_e = Fx_1 \partial x_1$$
$$W_i = \frac{d}{2}(C_u \partial\alpha - C_v \partial\alpha)$$

Forces on vertex 1 along X axis:

$$Fx_1 = C_u d \frac{\partial\alpha}{\partial x_1}$$
$$Fx_1 = H(\alpha - \alpha_0) d \frac{\partial\alpha}{\partial x_1}$$

Derivative of α:

$$\frac{\partial\alpha}{\partial x_1} = \frac{V_x V_1 - U_x U_1 - \frac{U_x(\mathbf{U}.\mathbf{V})V_1}{|\mathbf{U}|^2} - \frac{V_x(\mathbf{U}.\mathbf{V})U_1}{|\mathbf{V}|^2}}{2dsin\alpha|\mathbf{U}||\mathbf{V}|}$$

Angle between twines:

$$\alpha = \frac{1}{2} acos(\frac{\mathbf{U}.\mathbf{V}}{|\mathbf{U}||\mathbf{V}|})$$

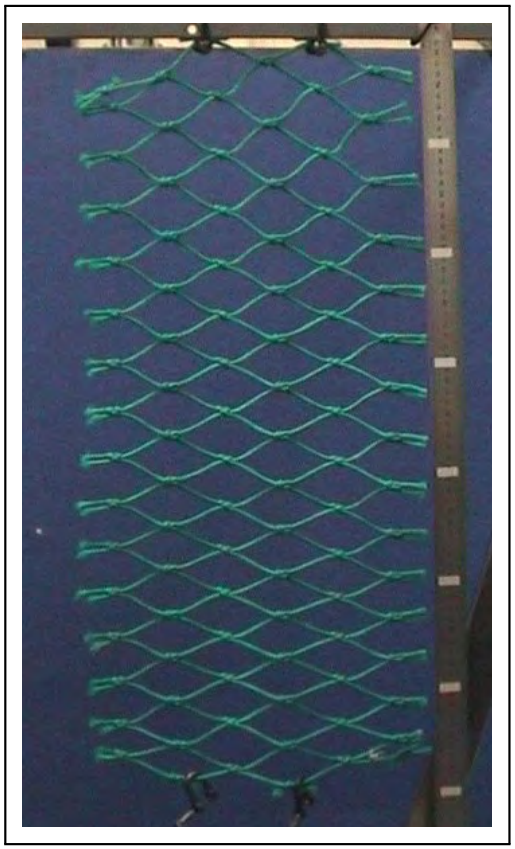

Catch pressure per triangular element

$$p = \frac{1}{2}\rho C_d v^2$$

p: Pressure on the net (Pa),
ρ: density of water (kg/m^3),
C_d: drag coefficient,
v: current amplitude (m/s).

Force on vertex 1:
$\mathbf{F}_1 = \frac{\mathbf{12} \wedge \mathbf{13}}{2} \frac{p}{3}$

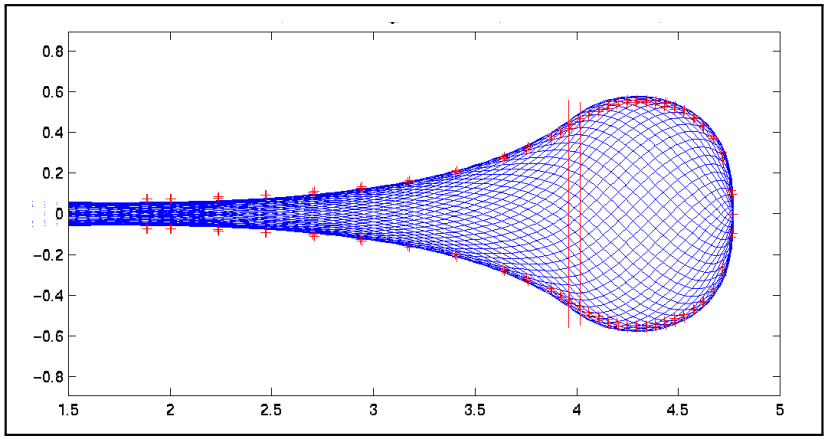

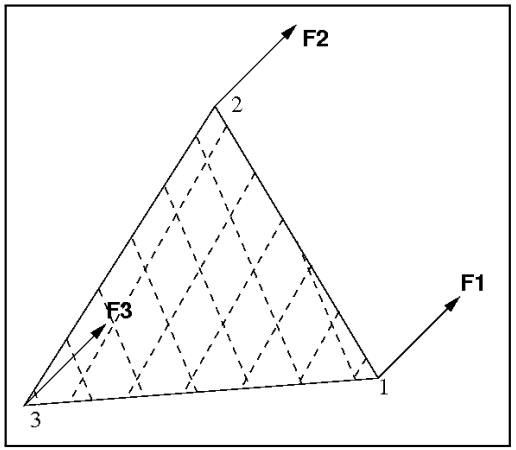

Appendix A2

Danish Seine National project ENERSENNE

Danish Seine
National project ENERSENNE

May 3, 2014

Authors: D.PRIOUR (IFREMER)

MODEL

Top view

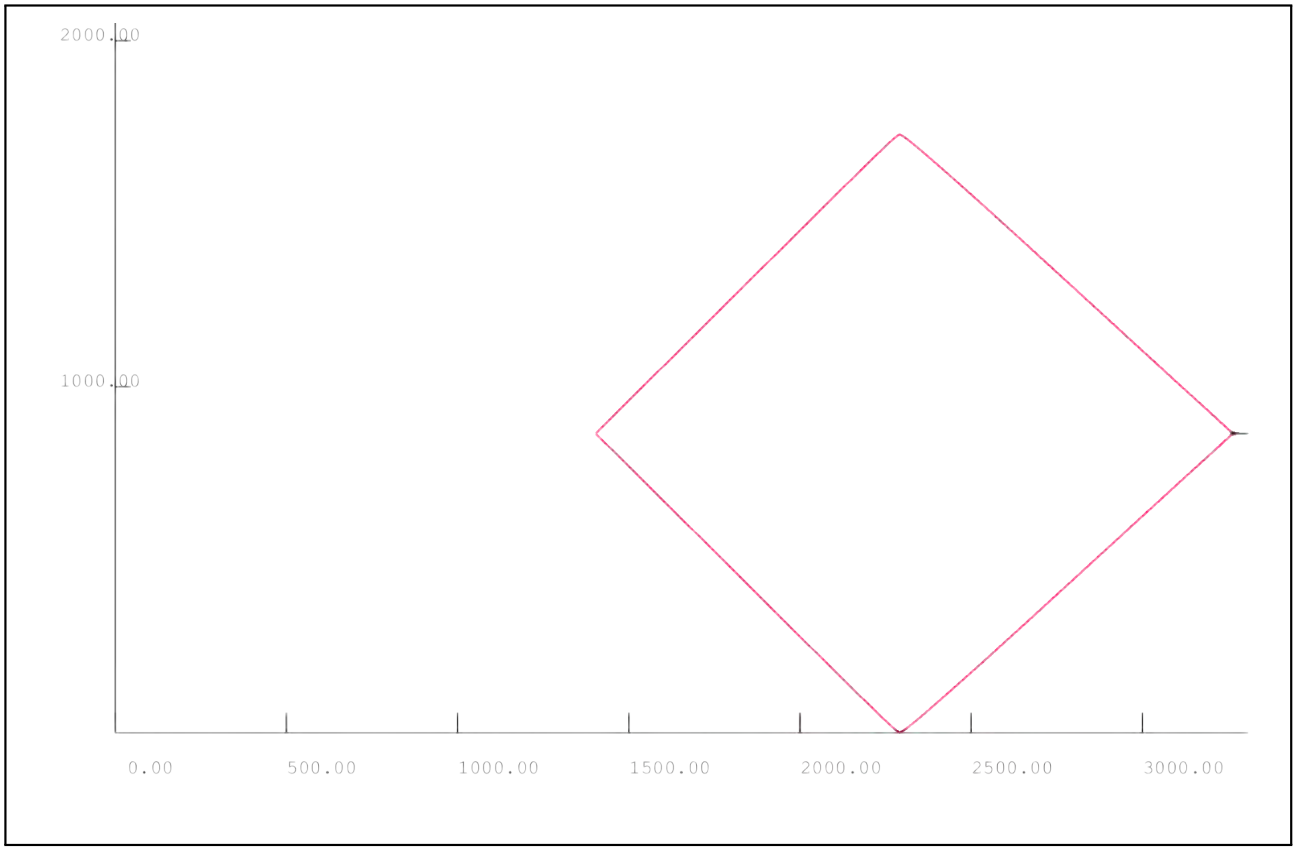
2000.00
1000.00
0.00
500.00
1000.00
1500.00
2000.00
2500.00
3000.00

Top view

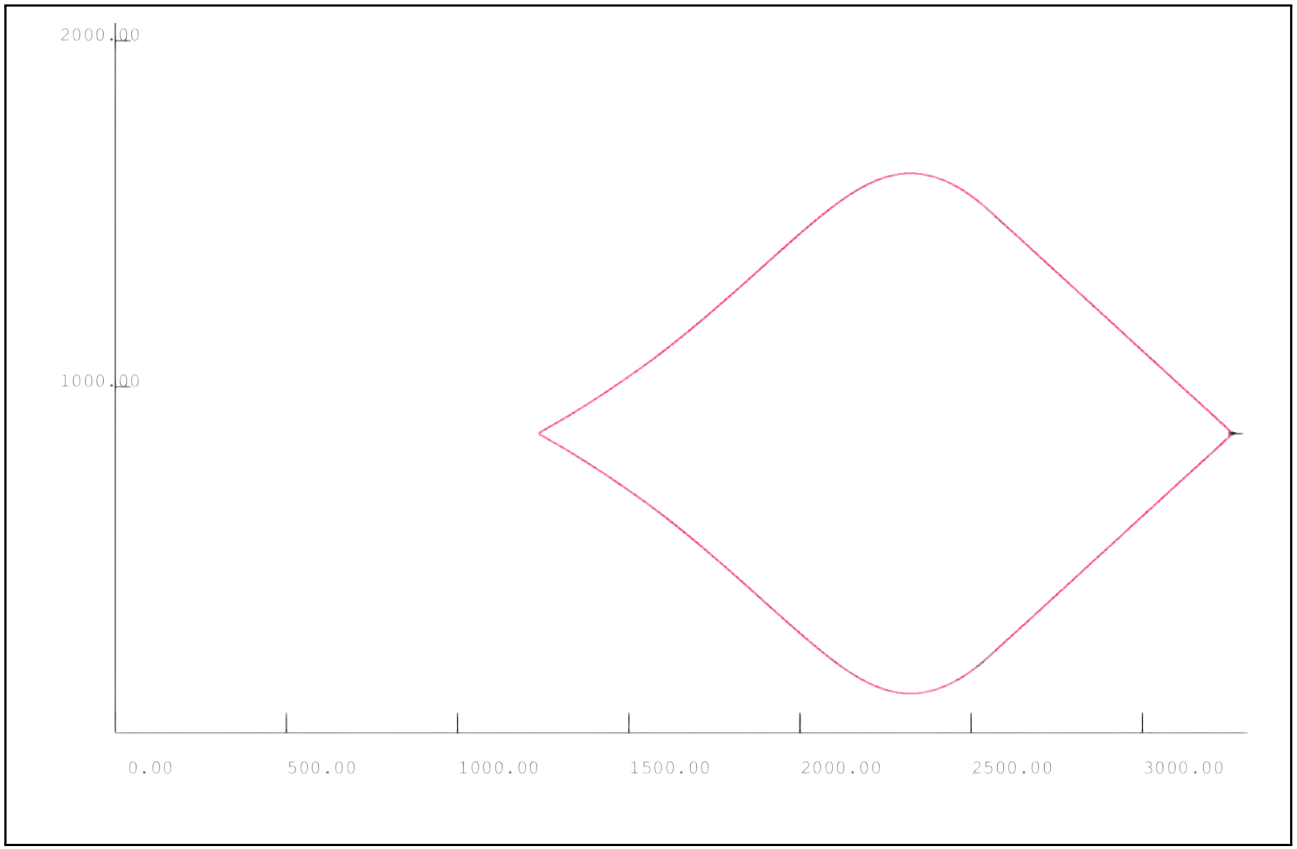
2000.00
1000.00
0.00
500.00
1000.00
1500.00
2000.00
2500.00
3000.00

Top view

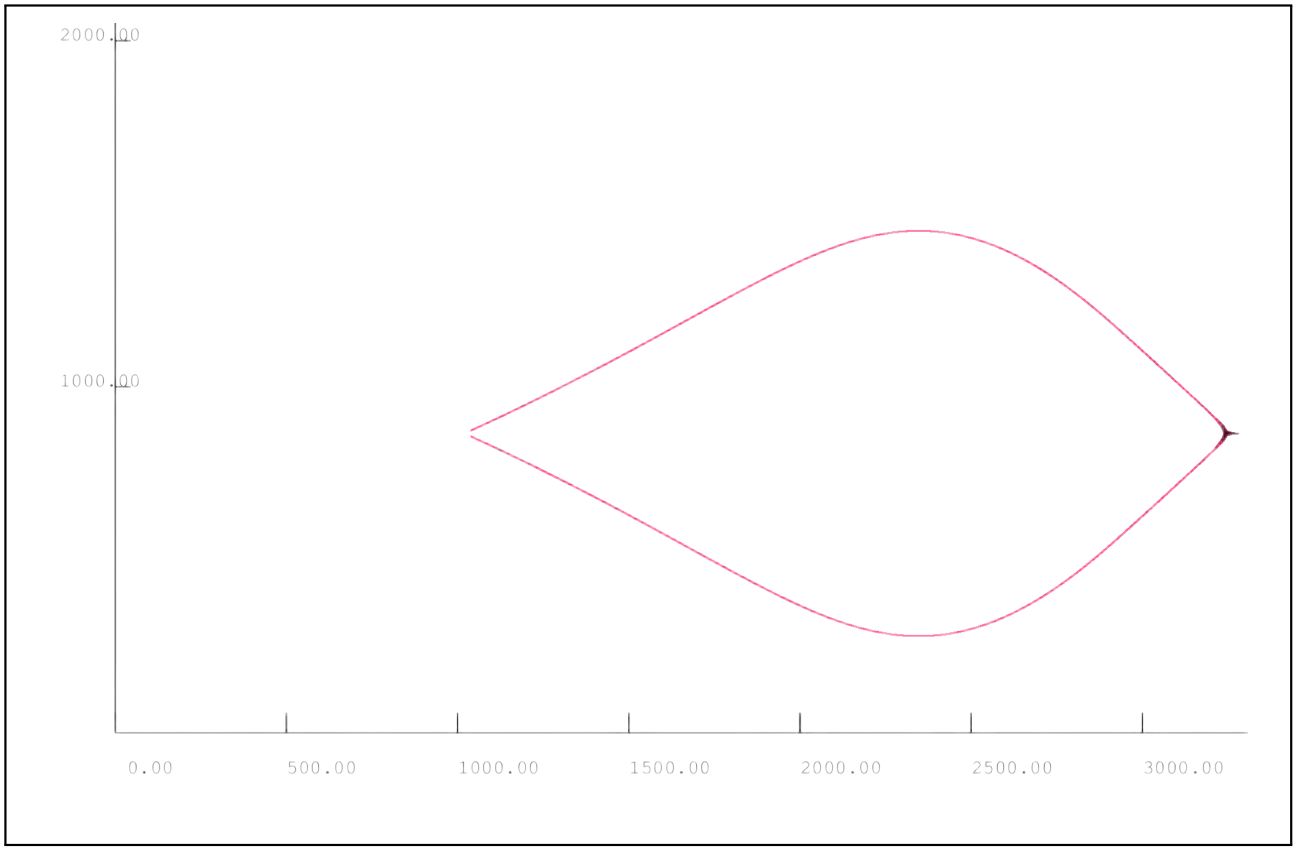
2000.00
1000.00
0.00
500.00
1000.00
1500.00
2000.00
2500.00
3000.00

Top view

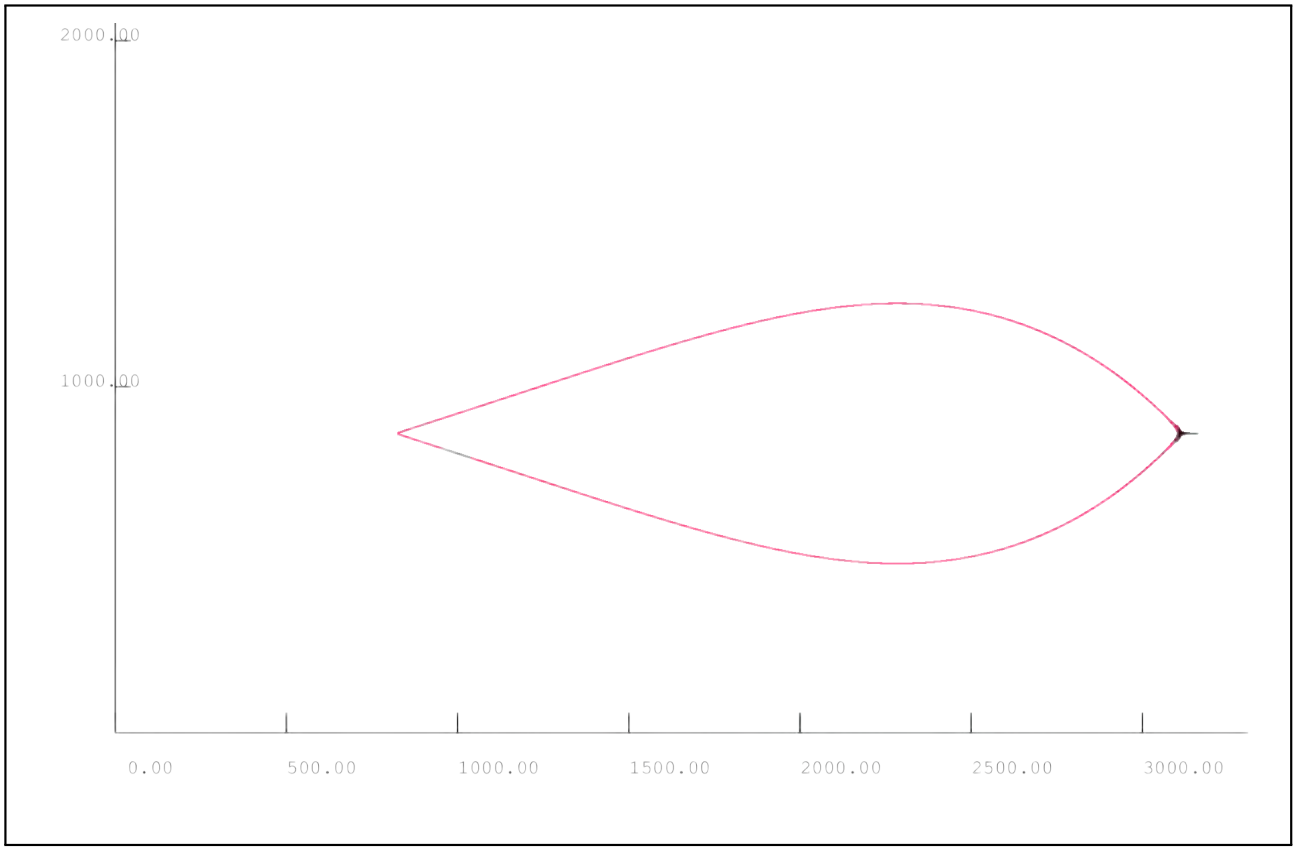
2000.00
1000.00
0.00
500.00
1000.00
1500.00
2000.00
2500.00
3000.00

Top view

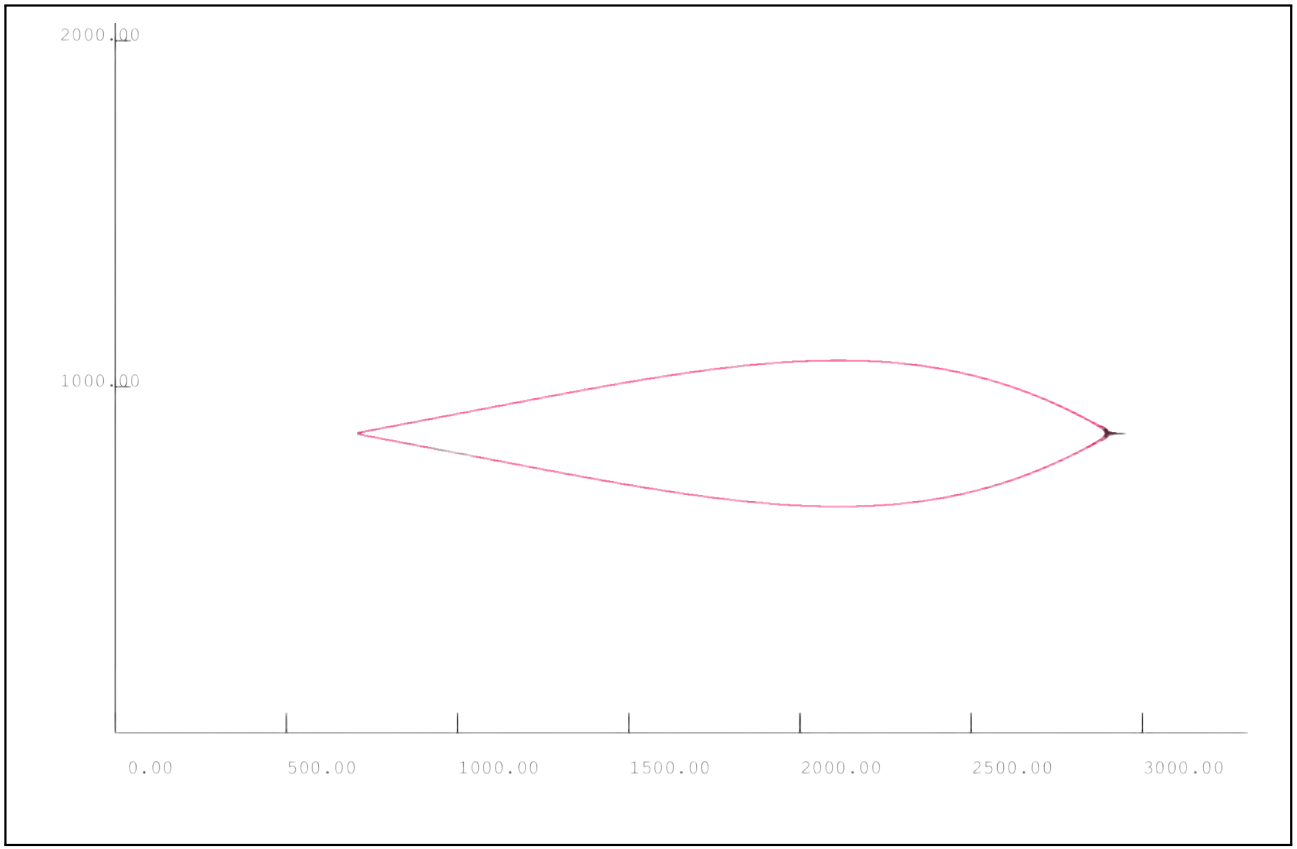
2000.00
1000.00
0.00
500.00
1000.00
1500.00
2000.00
2500.00
3000.00

Top view

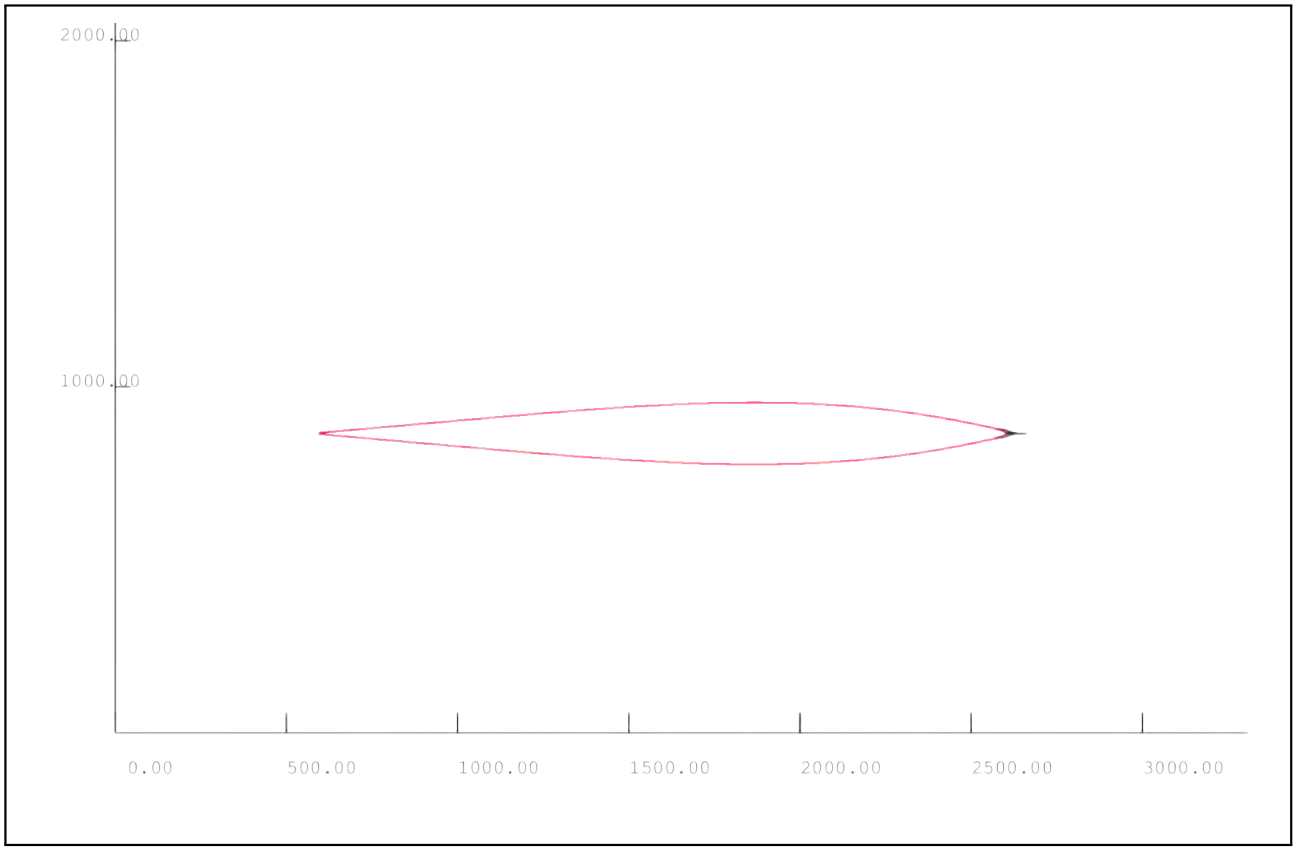
2000.00
1000.00
0.00
500.00
1000.00
1500.00
2000.00
2500.00
3000.00

Top view

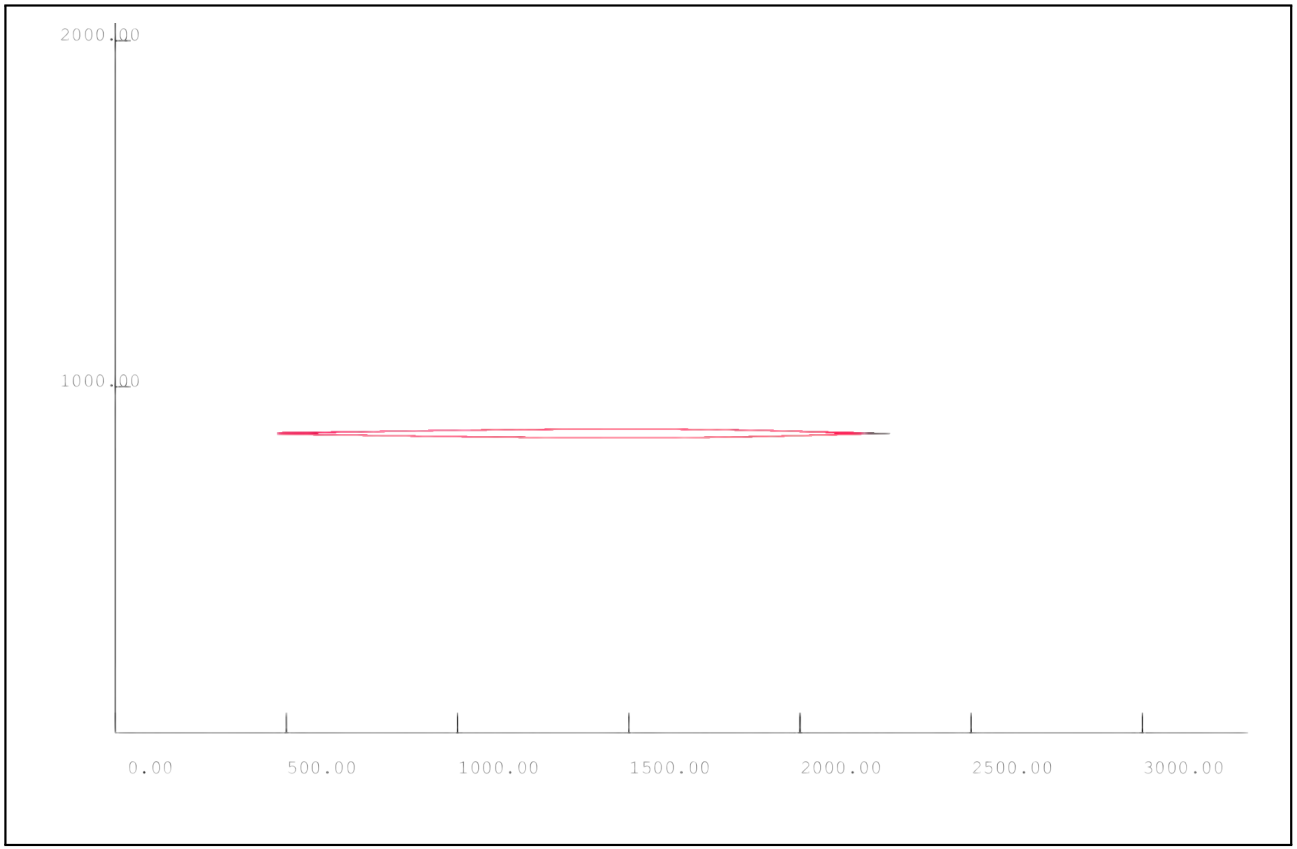
2000.00
1000.00
0.00
500.00
1000.00
1500.00
2000.00
2500.00
3000.00

Top view

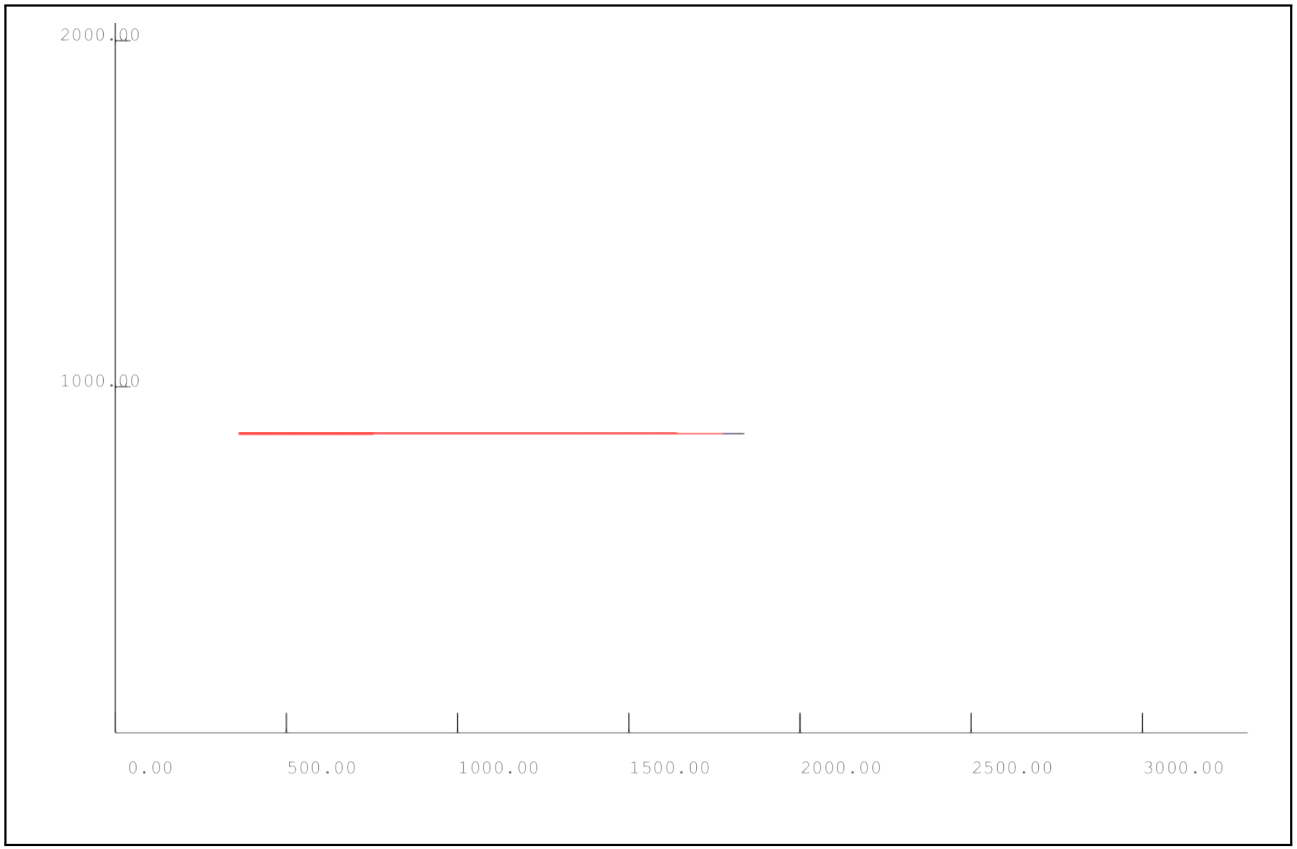
2000.00
1000.00
0.00
500.00
1000.00
1500.00
2000.00
2500.00
3000.00

Top view

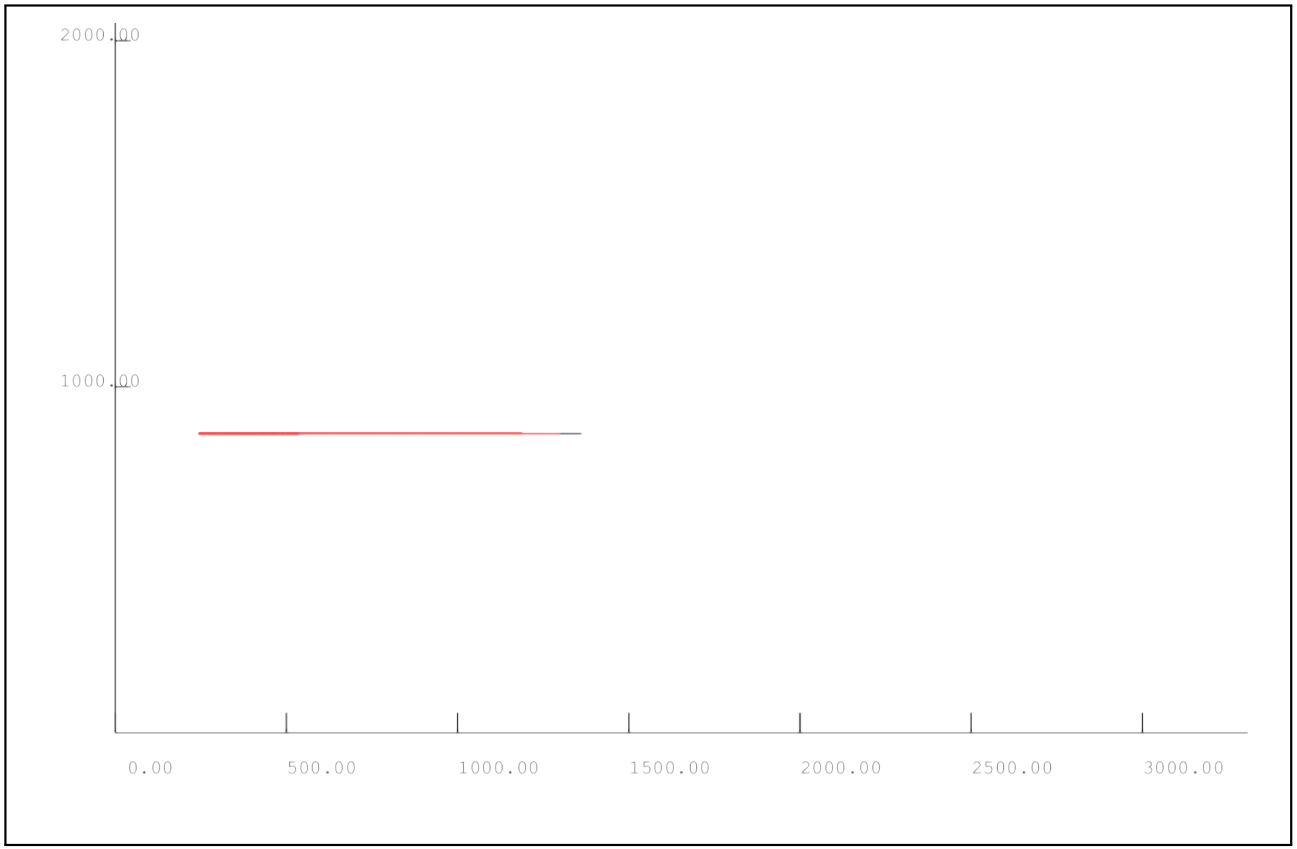
2000.00
1000.00
0.00
500.00
1000.00
1500.00
2000.00
2500.00
3000.00

Top view

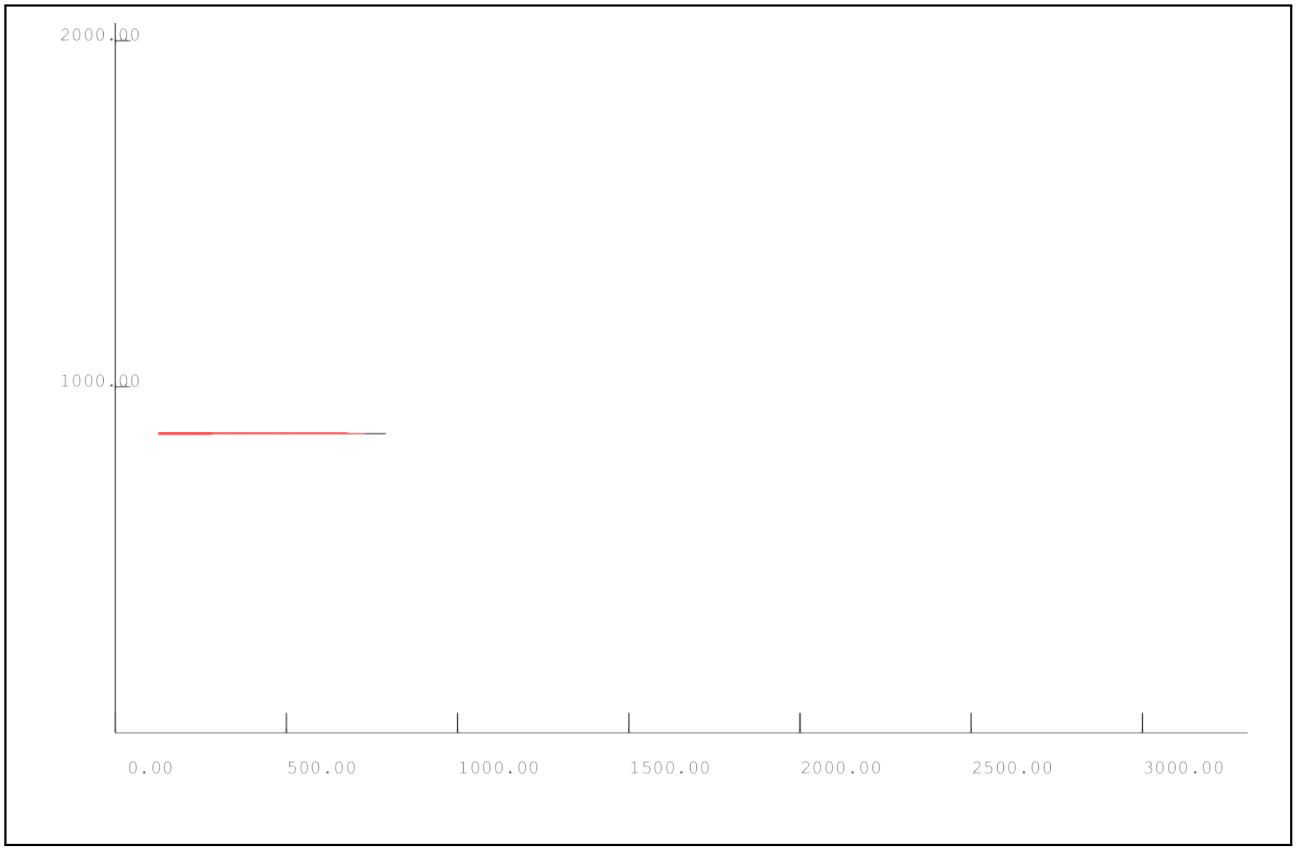
2000.00
1000.00
0.00
500.00
1000.00
1500.00
2000.00
2500.00
3000.00

Top view

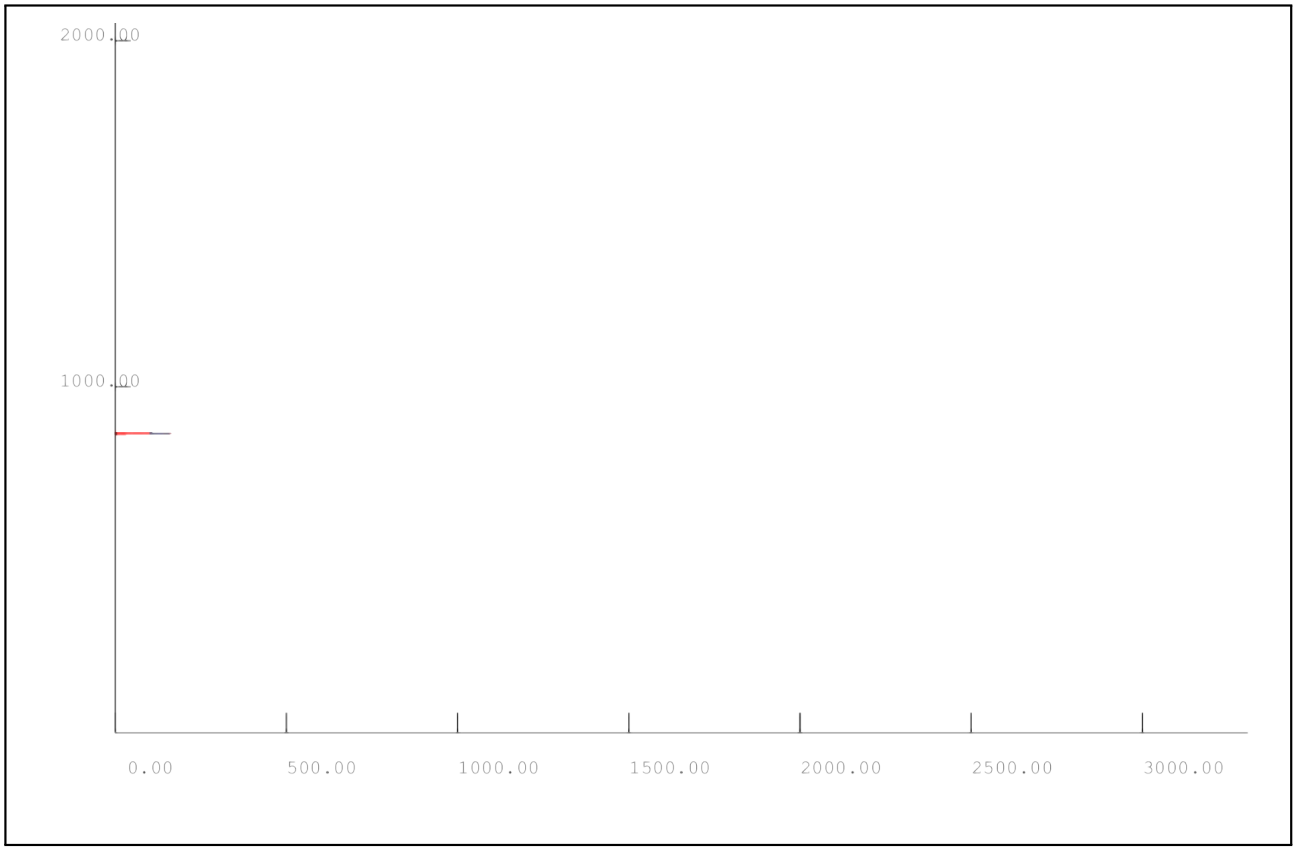
2000.00
1000.00
0.00
500.00
1000.00
1500.00
2000.00
2500.00
3000.00

Side view of trawl

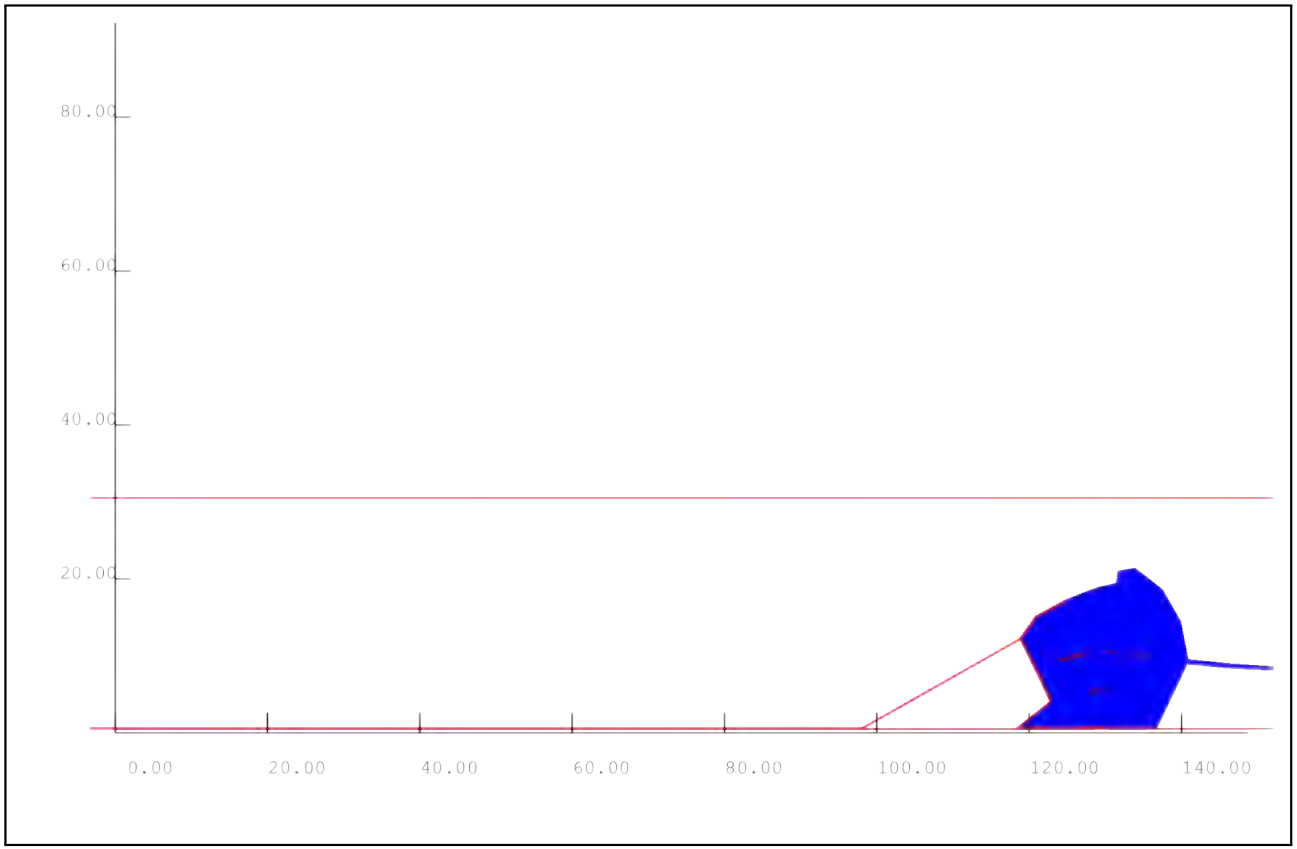

Side view of trawl

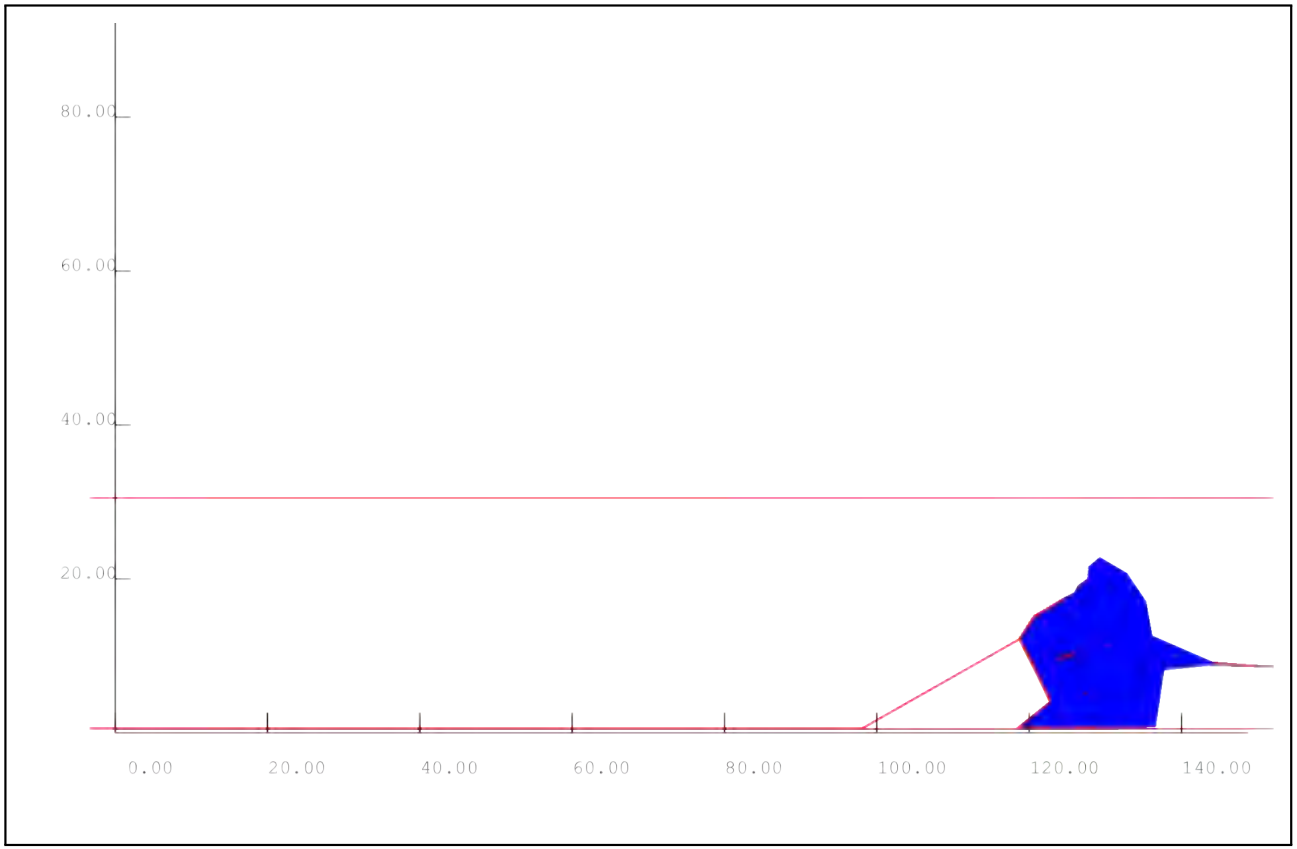

Side view of trawl

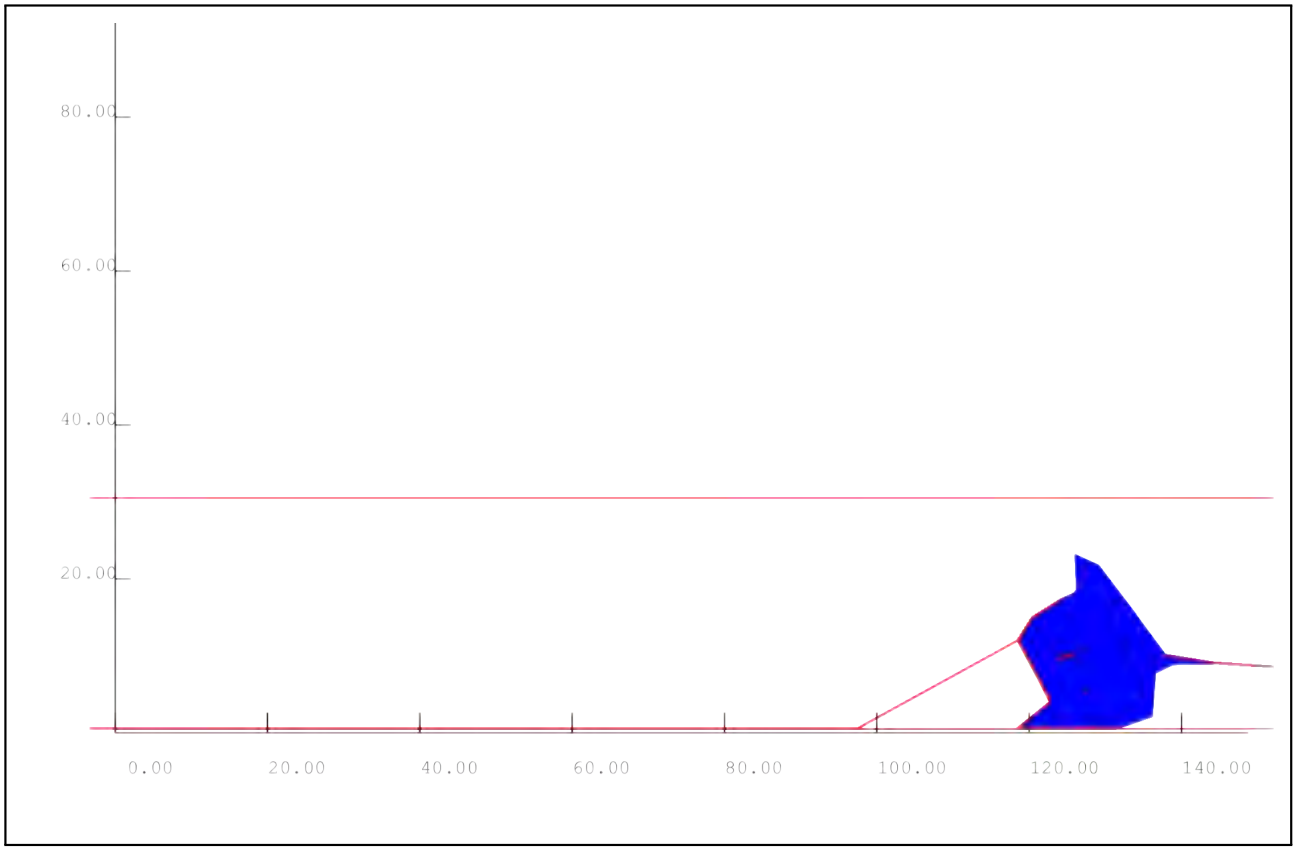

Side view of trawl

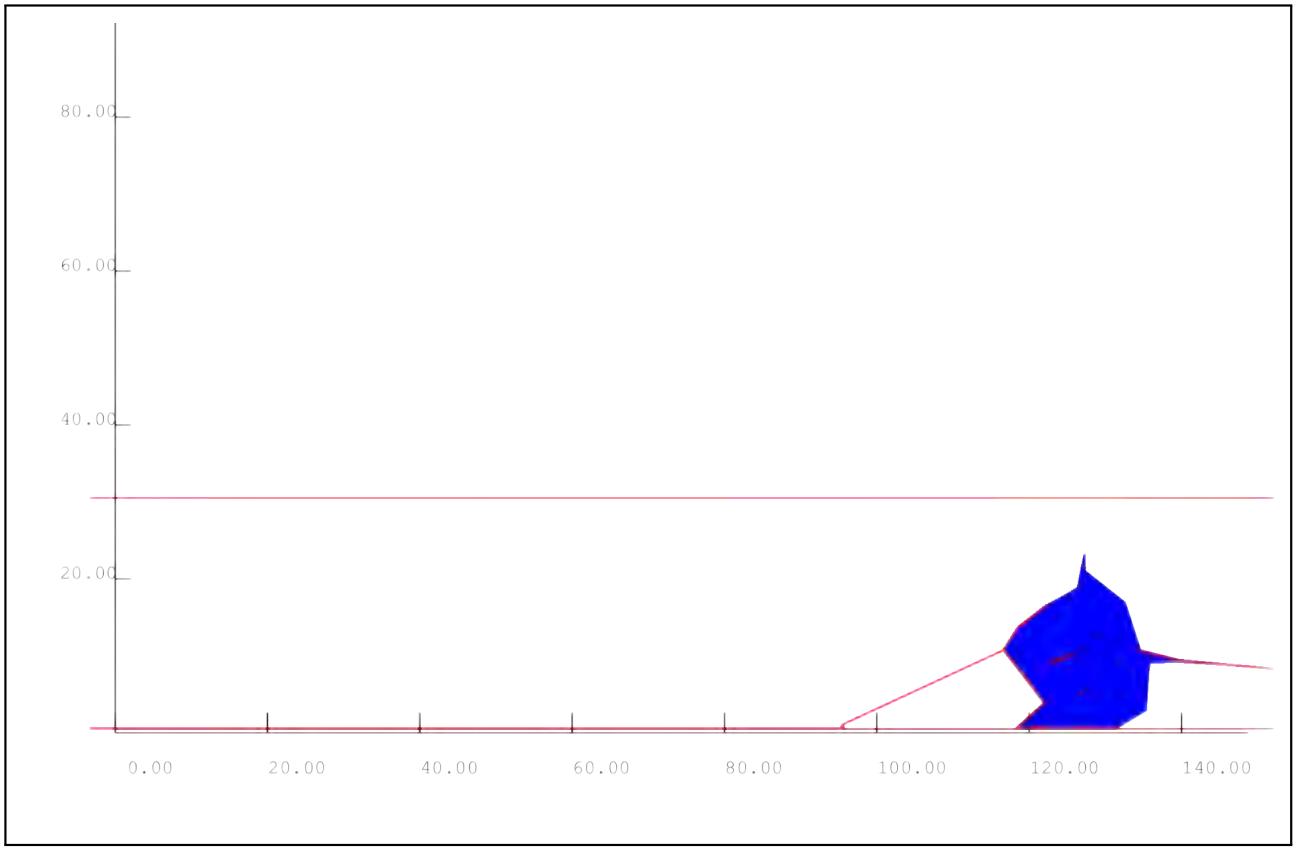

Side view of trawl

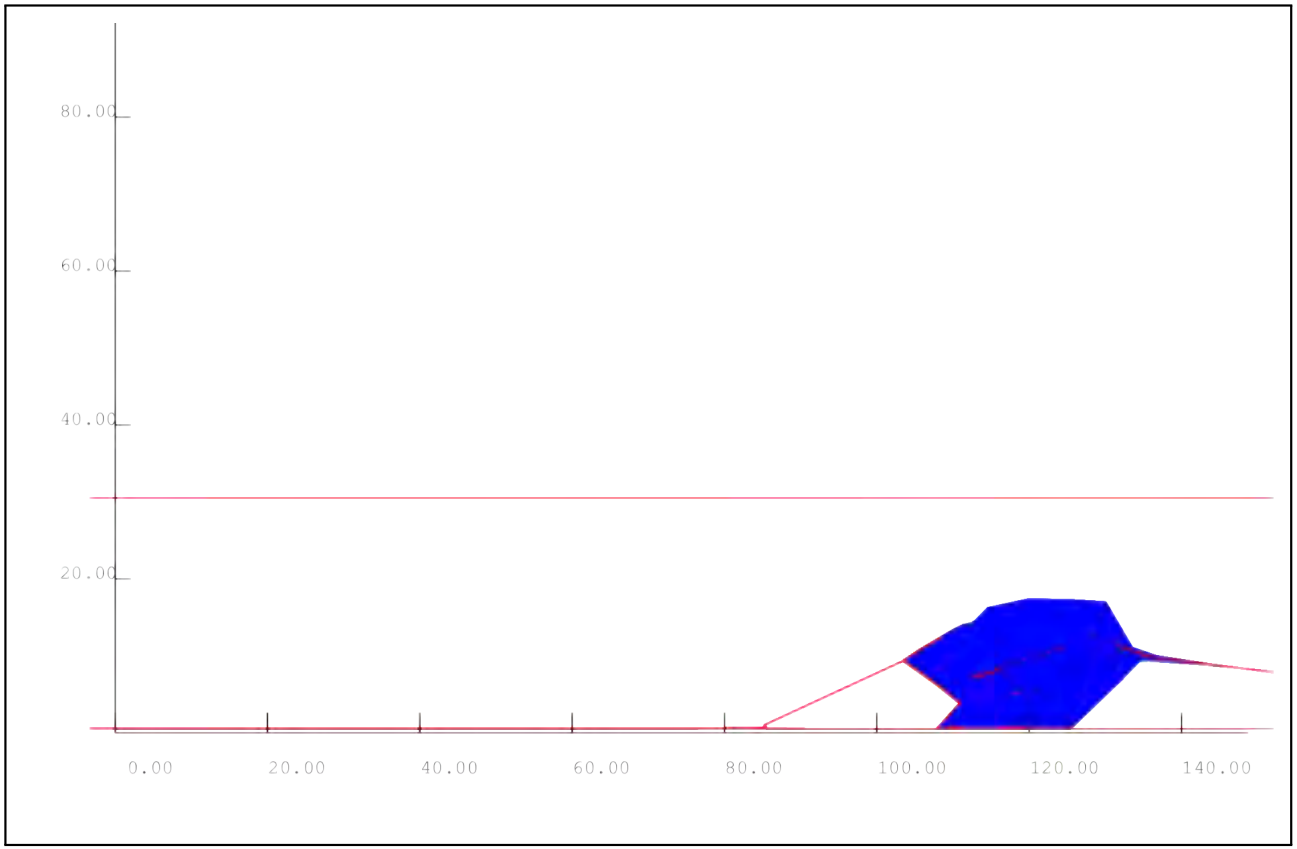

Side view of trawl

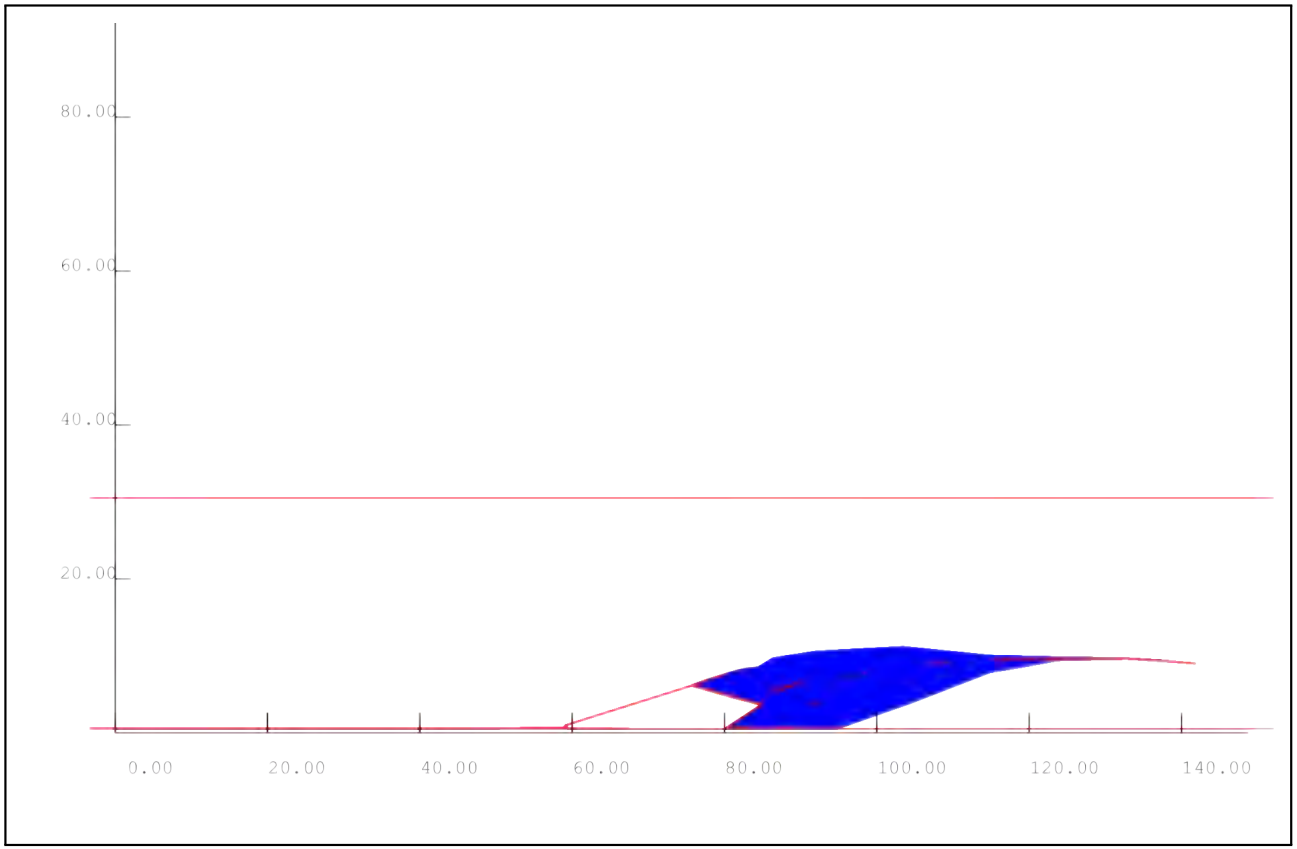

Side view of trawl

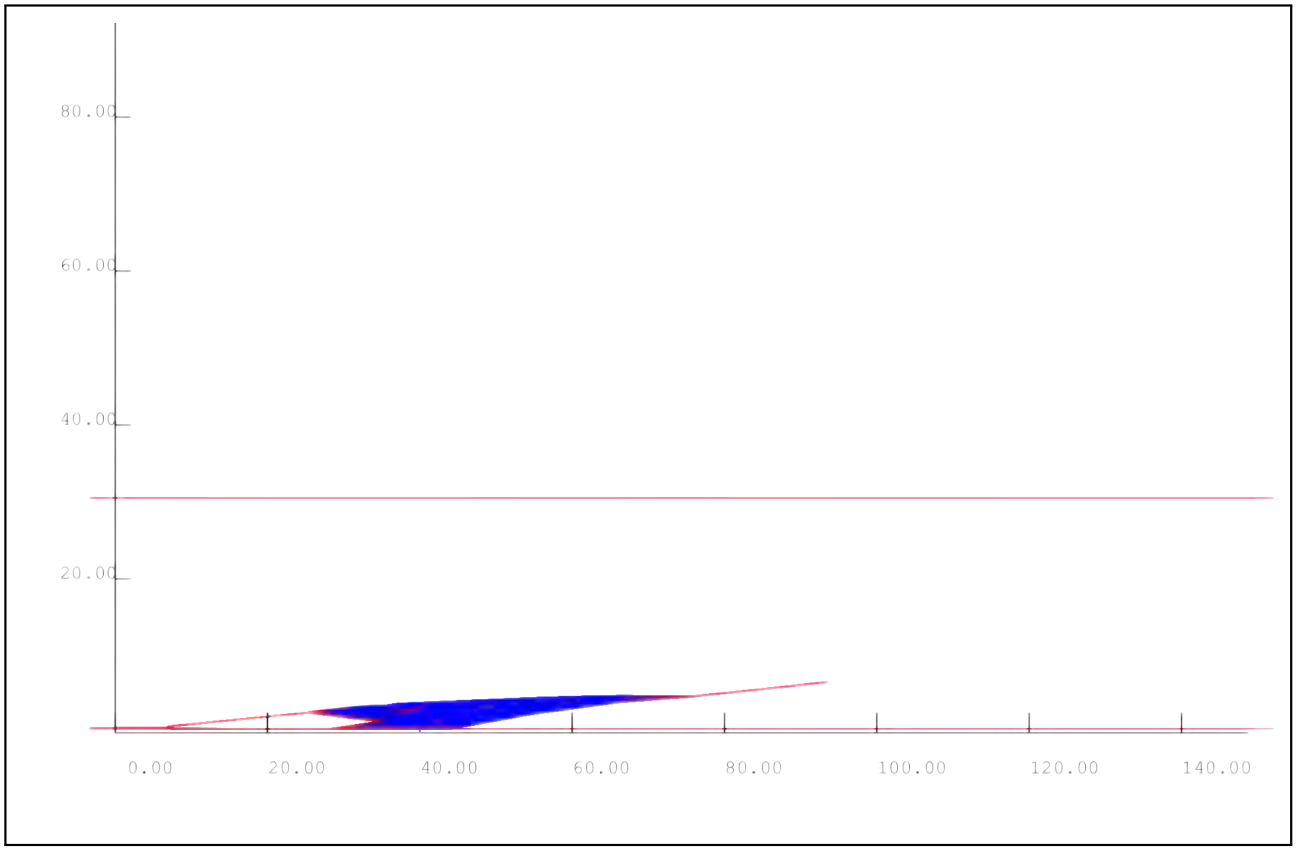

Side view of trawl

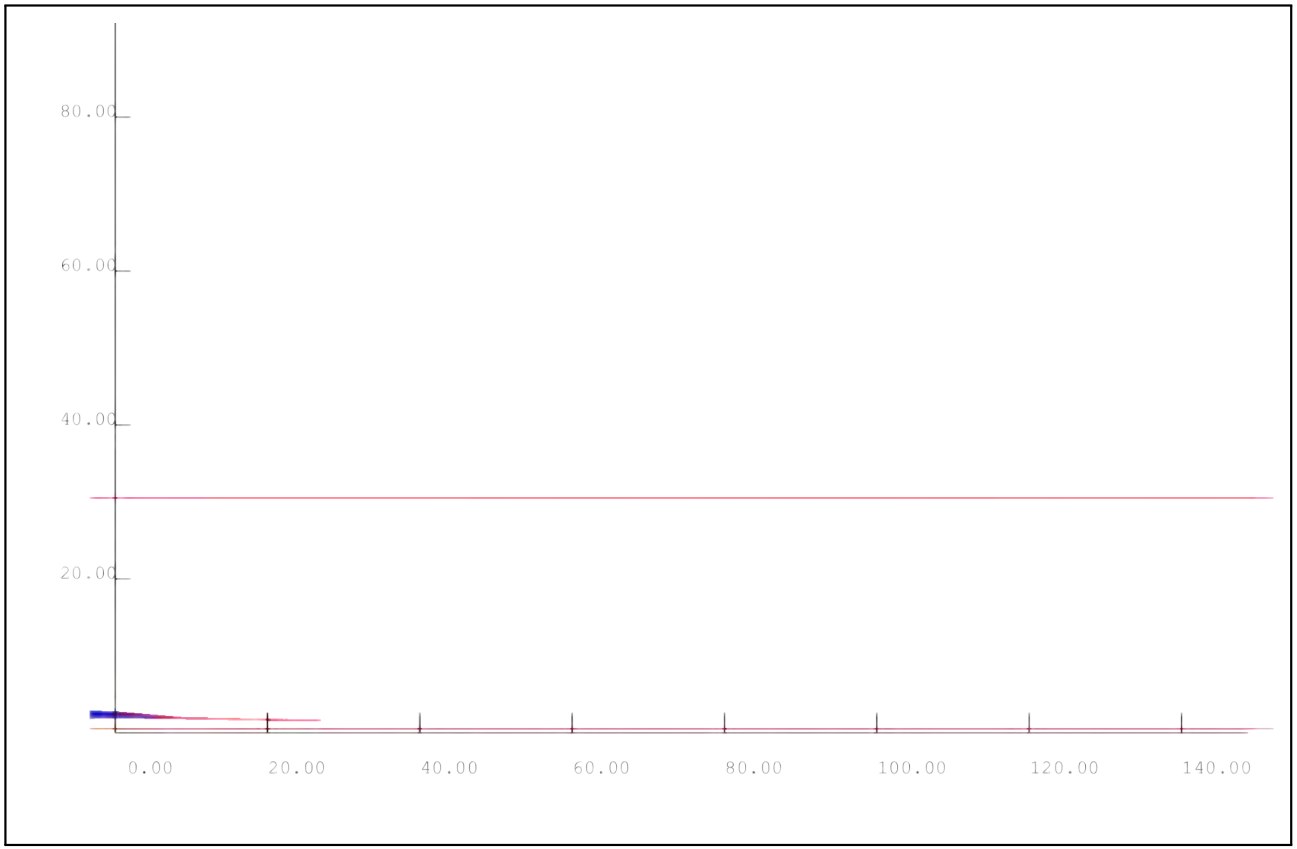

Rear view

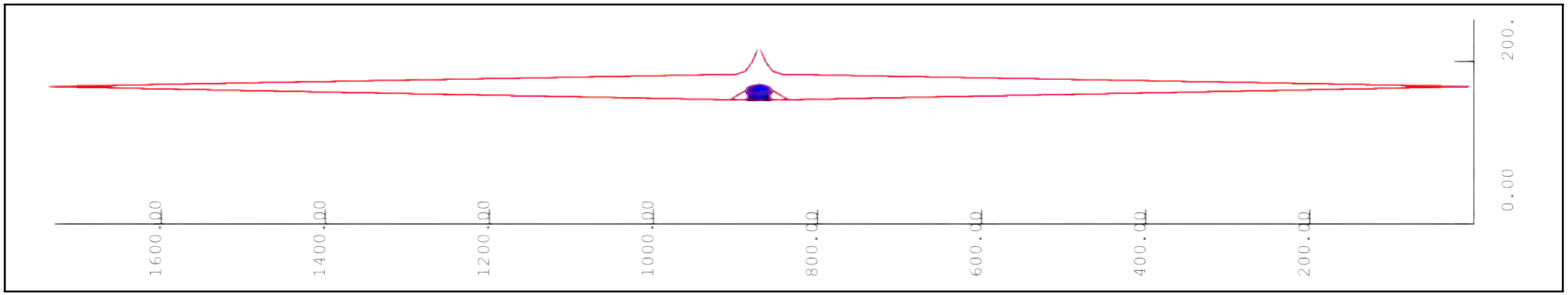
200.
0.00
1600.00
1400.00
1200.00
1000.00
800.00
600.00
400.00
200.00

Rear view

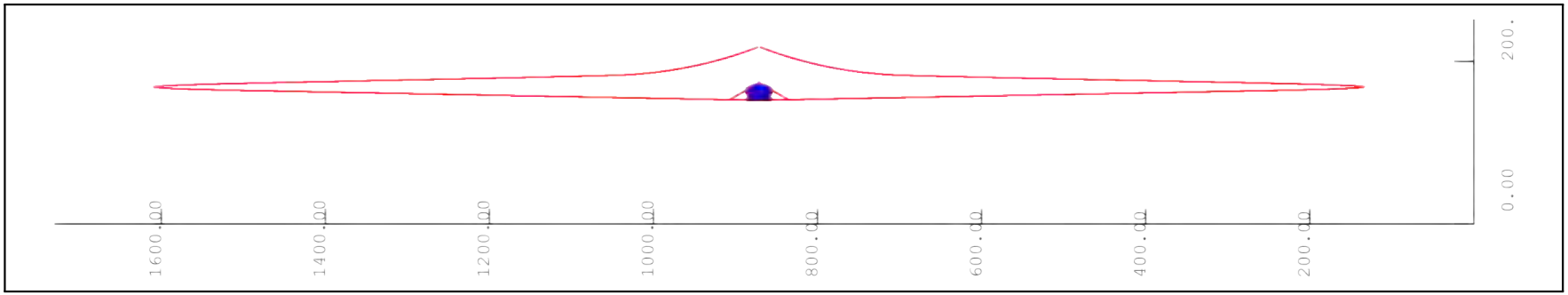
200.
0.00
1600.00
1400.00
1200.00
1000.00
800.00
600.00
400.00
200.00

Rear view

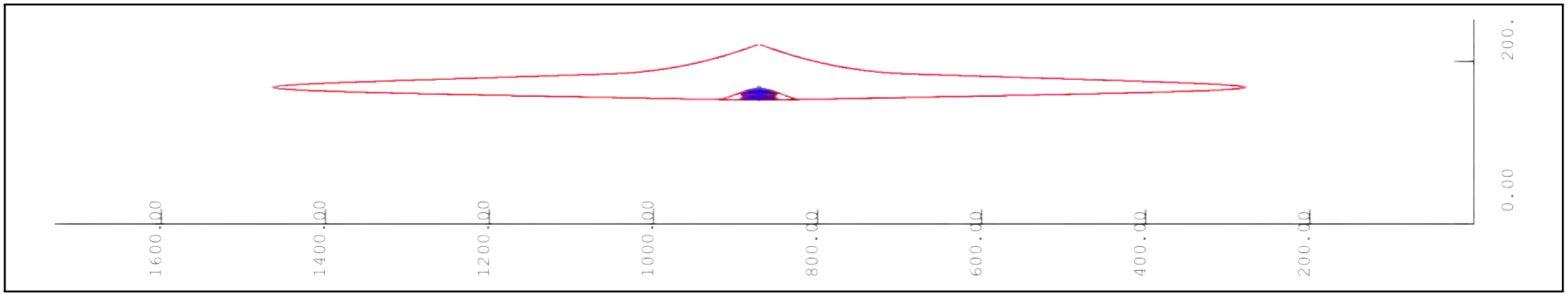
1600.00
1400.00
1200.00
1000.00
800.00
600.00
400.00
200.00
0.00
200.

Rear view

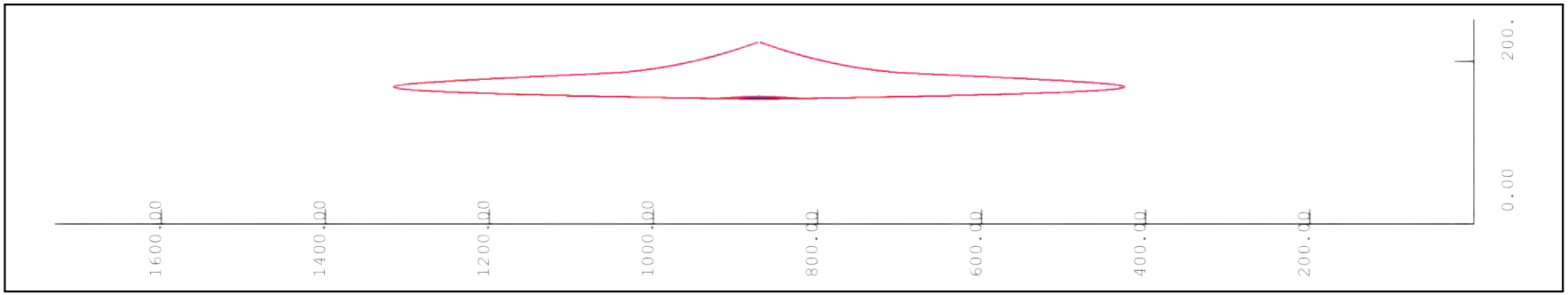
1600.00
1400.00
1200.00
1000.00
800.00
600.00
400.00
200.00
0.00
200.

Rear view

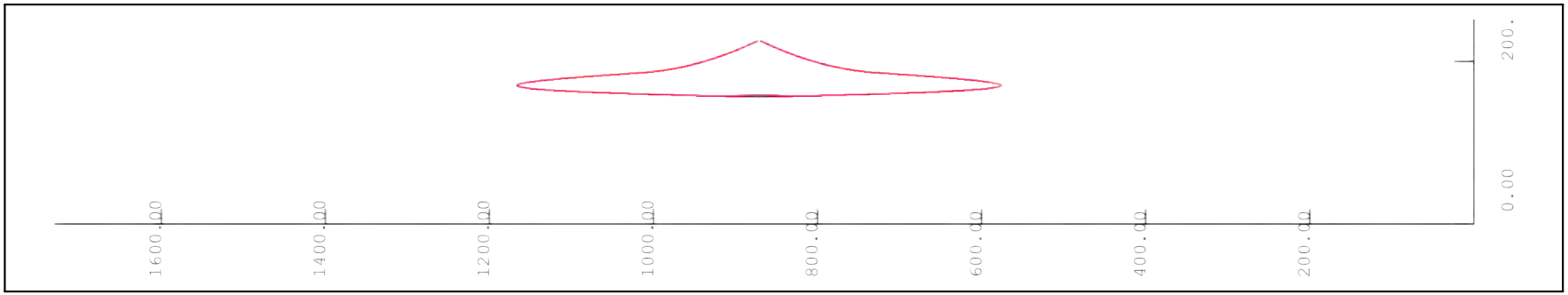
1600.00
1400.00
1200.00
1000.00
800.00
600.00
400.00
200.00
0.00
200.

Rear view

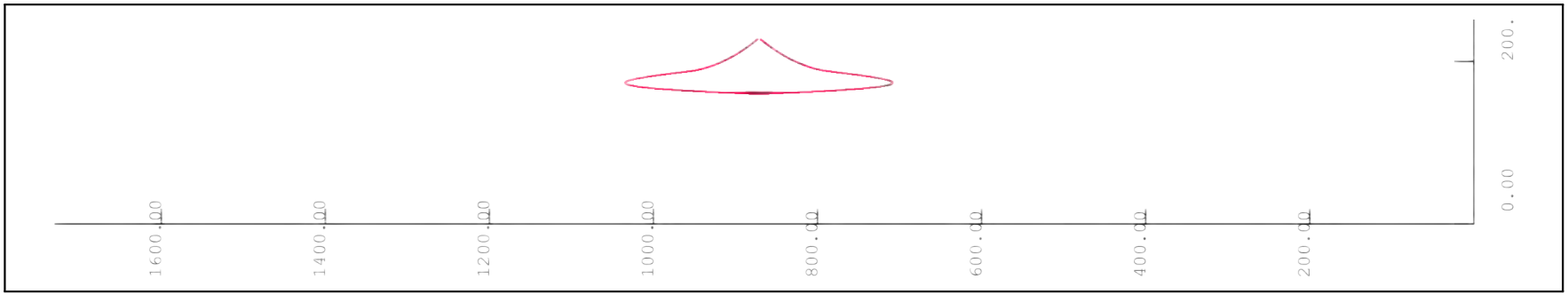
1600.00
1400.00
1200.00
1000.00
800.00
600.00
400.00
200.00
0.00
200.

Rear view

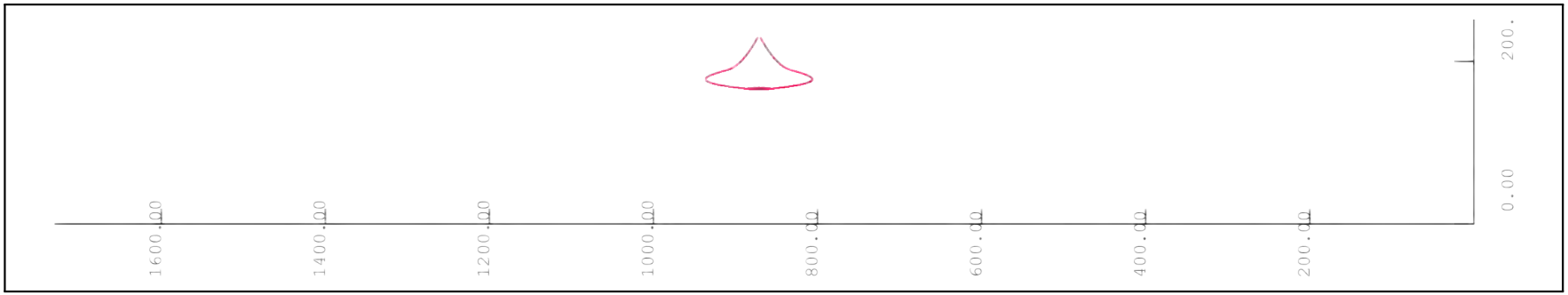
1600.00
1400.00
1200.00
1000.00
800.00
600.00
400.00
200.00
0.00
200.

Trajectory of cables: model and at sea

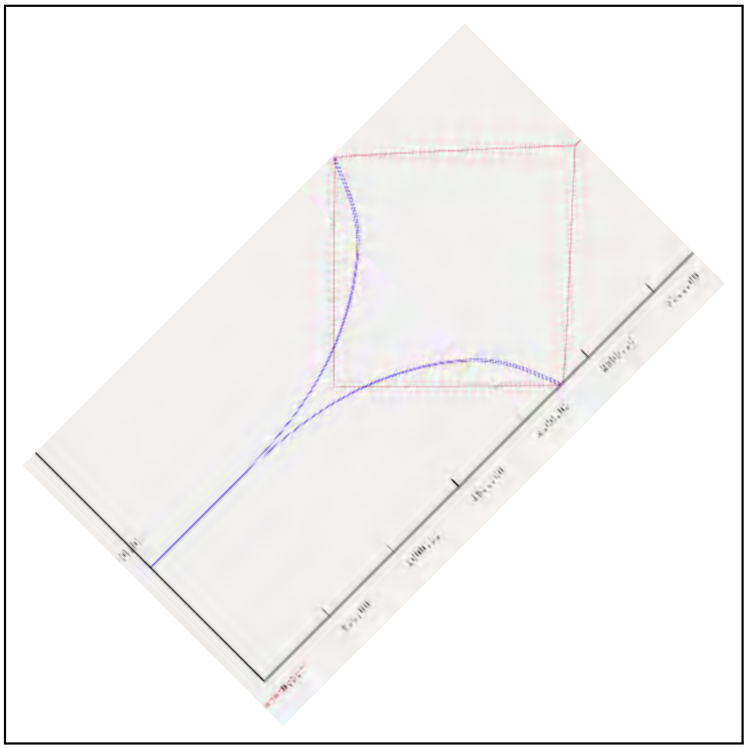

Model

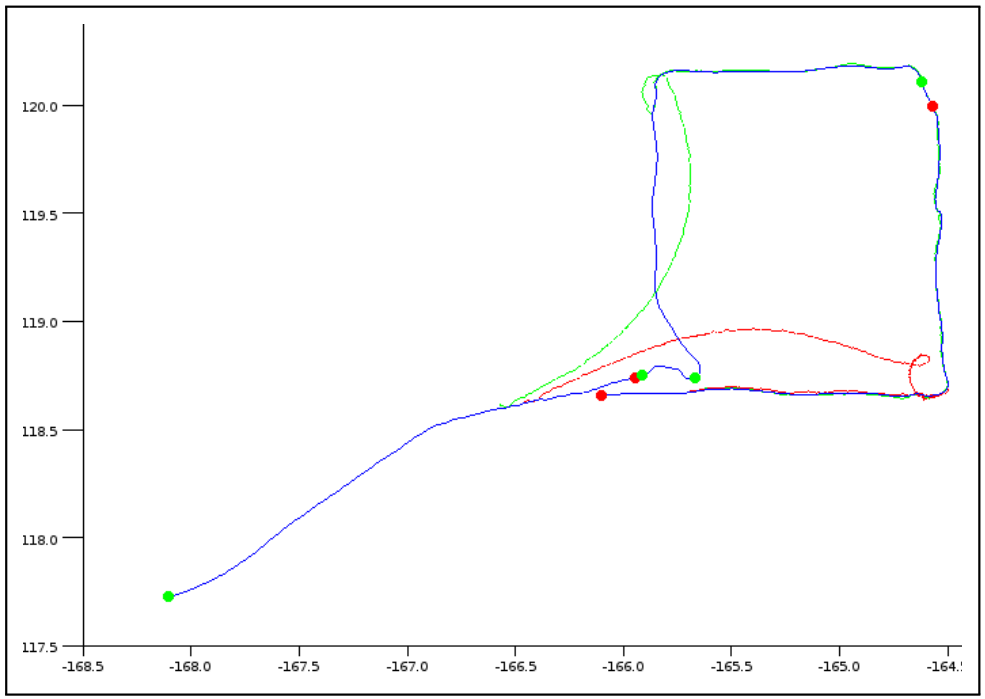

Measurements at sea

Powers during operation

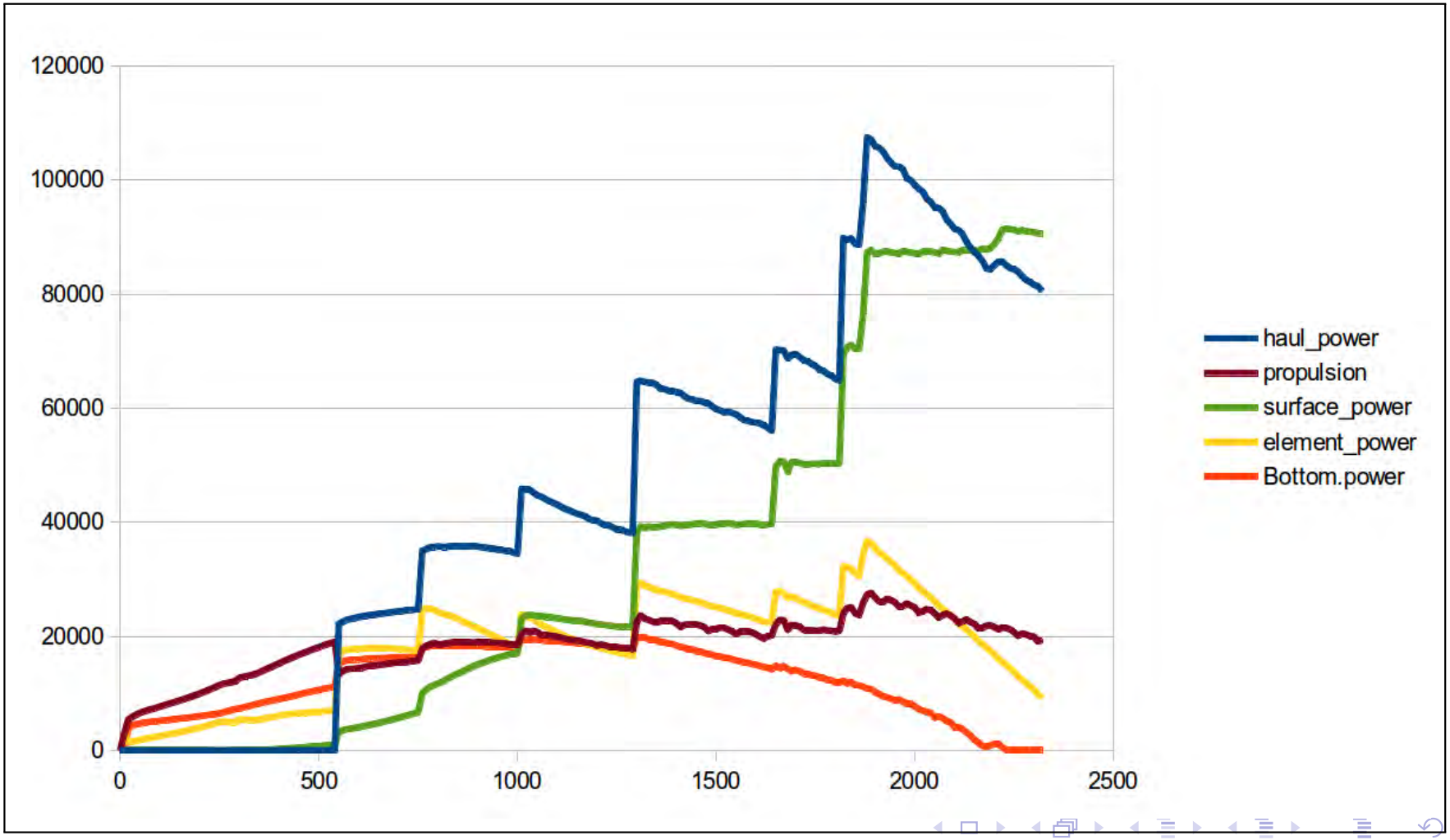

Vertical opening

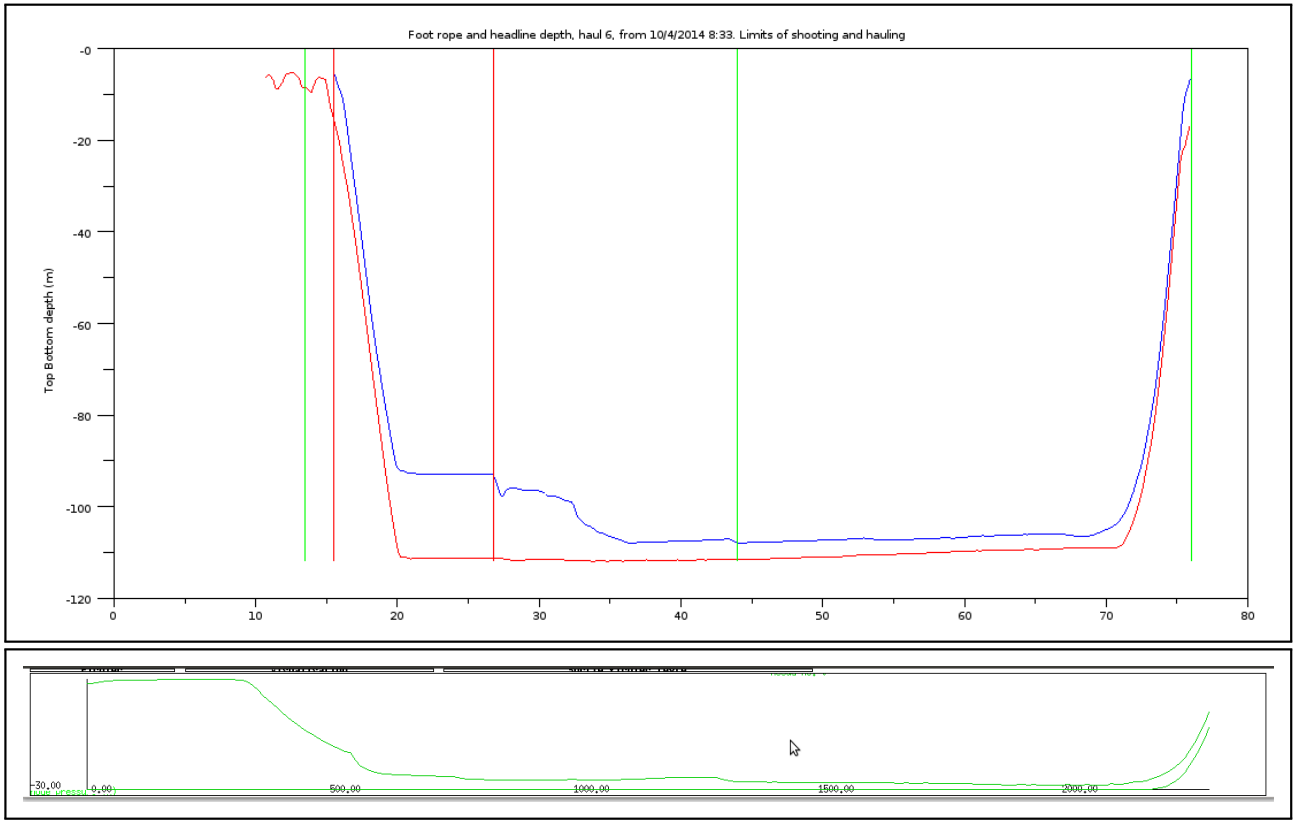

Appendix A3

Danish Seine National project ENERSENNE Introduction

ENERSENNE national project

Daniel PRIOUR

6 march 2014

introduction

The main objective of the project is to estimate the energy requested for the fishing technique of the Danish seine.

Sensors

Sensors have been largely completed during the week of October 21 to 25, 2013 . This arrangement will be finalized over the coming weeks. The following figures were taken on October 25 .

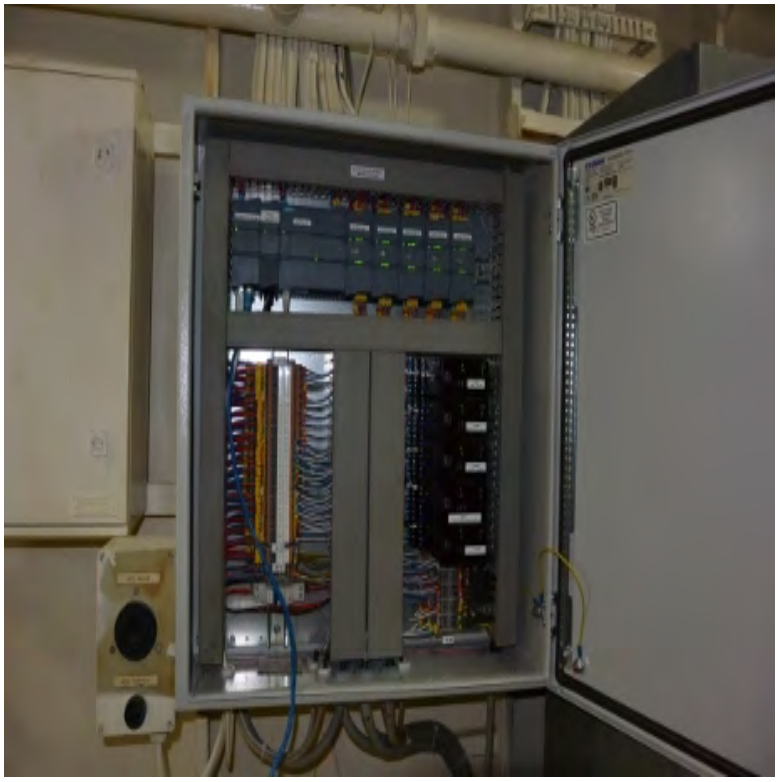

Figure 1: Electrical cabinet for sensors .

Figure 2 : Torsiometer (blue) attached to the propeller shaft .

Figure 3: Control panel including consumption.

Trawl

The trawl was carried out by fishermen.

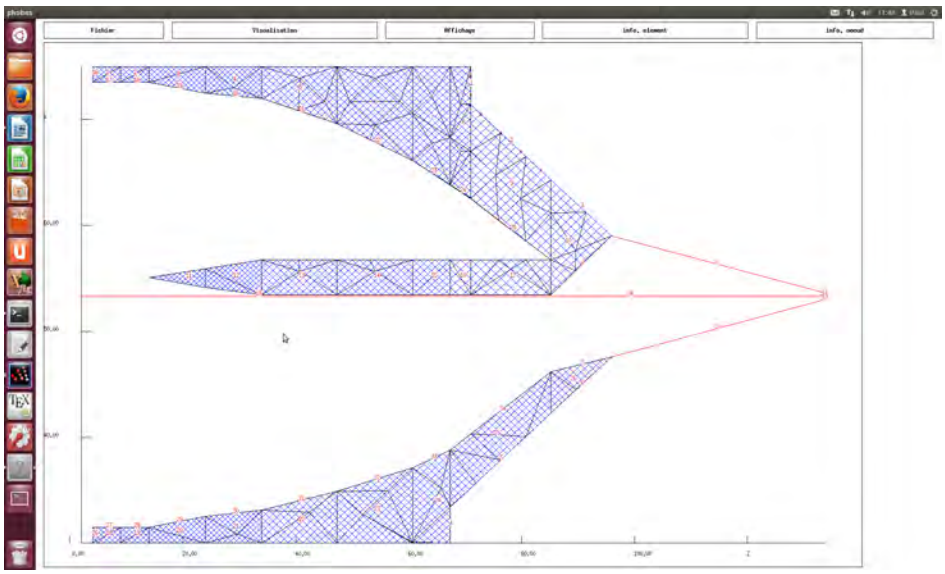

Figure 4: Design of the trawl net (blue) and cables (red) .

Modeling

The modeling the hauling is completed . In the following figure which represents the hauling, 2 phases were modeled : a first from 0s to 2000s when the boat is fixed and the hauling speed of the main cable is 1m / s and a second phase when the hauling speed is still 1m / s and the towing speed is also 1m / s.

Between 0 and 2000s , it should be noted that the power required to haul the main cable (blue curve) is the sum of the drag on the bottom (red curve) of the hydrodynamic drag of the main cable and other cables (yellow curve) and the drag of the trawl net (green curve) . The power consumed by the hauling rises to 15KW during this period.

Between 2000s and 3000s , the boat goes ahead and it can be noted the large increase in drag net (green curve) . Here the power needed to tow the boat is represented by garnet curve. This rises to power 25KW .

We recall that the propulsion efficiency of fishing boats is around 10% , ie the power consumption of fuel should be in the range of 400KW (15 +25 KW divided by 10 %) or fuel consumption 40l / h. Sea trials will adjust the model and get results consumption closer to reality.

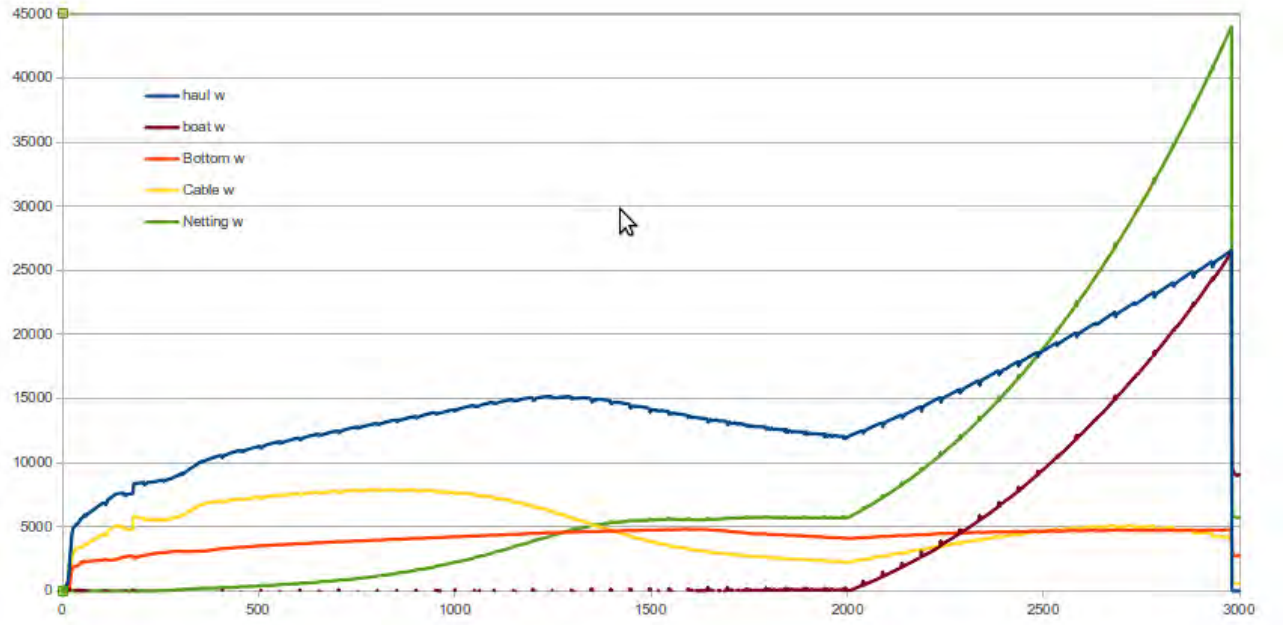

Figure 5: Powers from the model, for winches (blue), towing the boat (garnet) , drag on the bottom (red), hydrodynamic drag cables (yellow) and the hydrodynamic drag of the net (green) . The boat is fixed until 2000s after it moves at 1m / s. Hauling speed is 1m / s.

Appendix A4

Danish Seine National project ENERSENNE Test at sea

Danish Seine
National project ENERSENNE

April 30, 2014

Authors: D.PRIOUR (IFREMER)

BOAT

TESTS AT SEA

Les Barges

Les Barges, 24 m long
Sables d'Olonne

Danish seine
pelagic trawl

Foot rope

Diameter: 55mm

Weight: 350Kg

cables

Diameter: 40mm

Length: 2500m each
Total length: 5000m

NKE

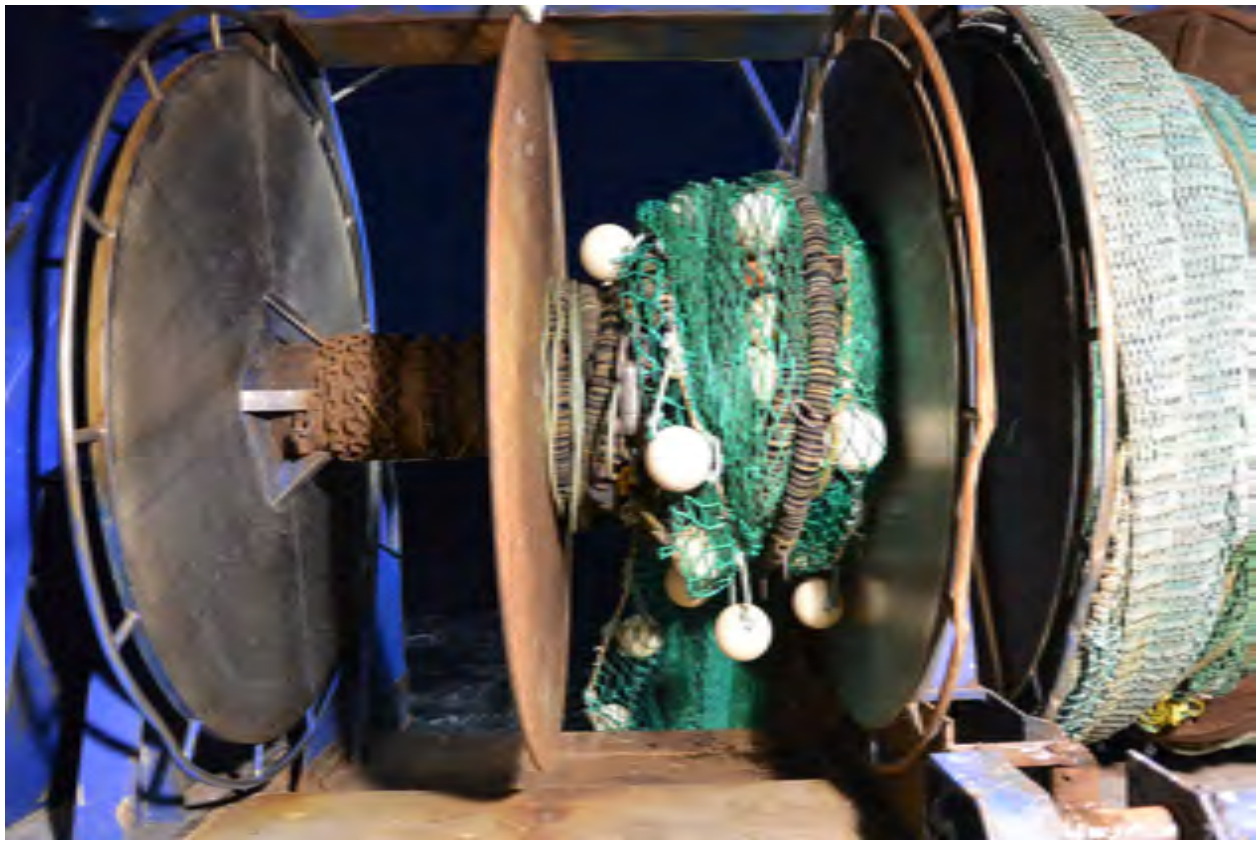

4 tension sensors on bridles

2 pressure sensors on headline and foot rope

MARINELEC

Fuel consumption l/h
Shaft: couple speed
Alternator power

Winches: force speed
GPS
Propeller pitch

For only the haul 13

2 on middle cables
1 on trawl (lost)
1 on boat
1 on float
65 000 way points
each second
around 10l floats

GPS

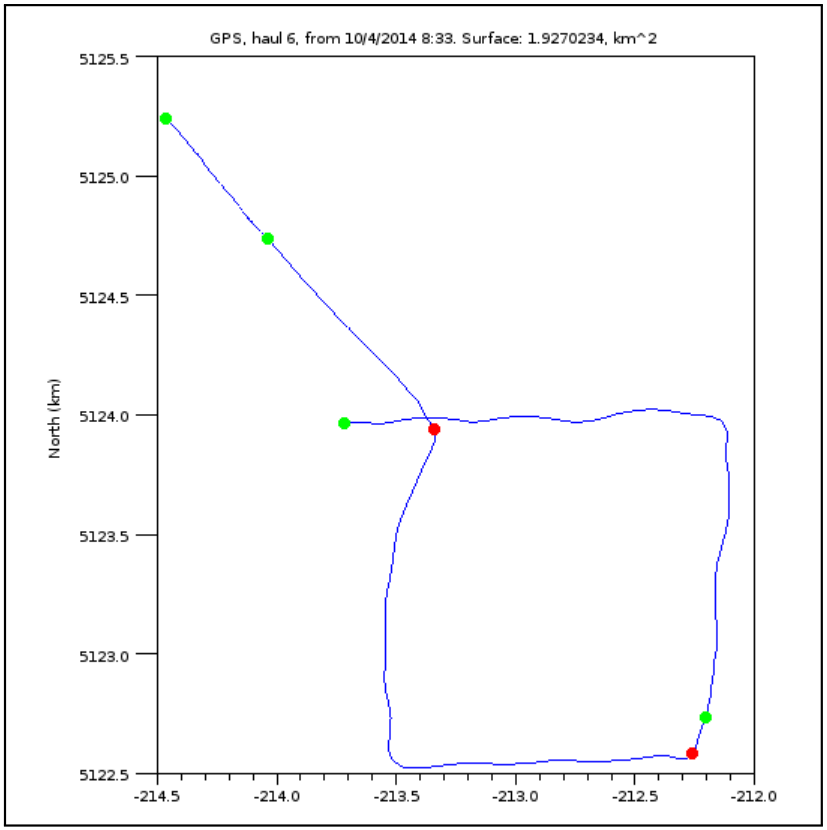

1: shooting right cable
2: shooting trawl
3: shooting left cable
4: hauling float and towing
5: hauling cables and towing

Powers

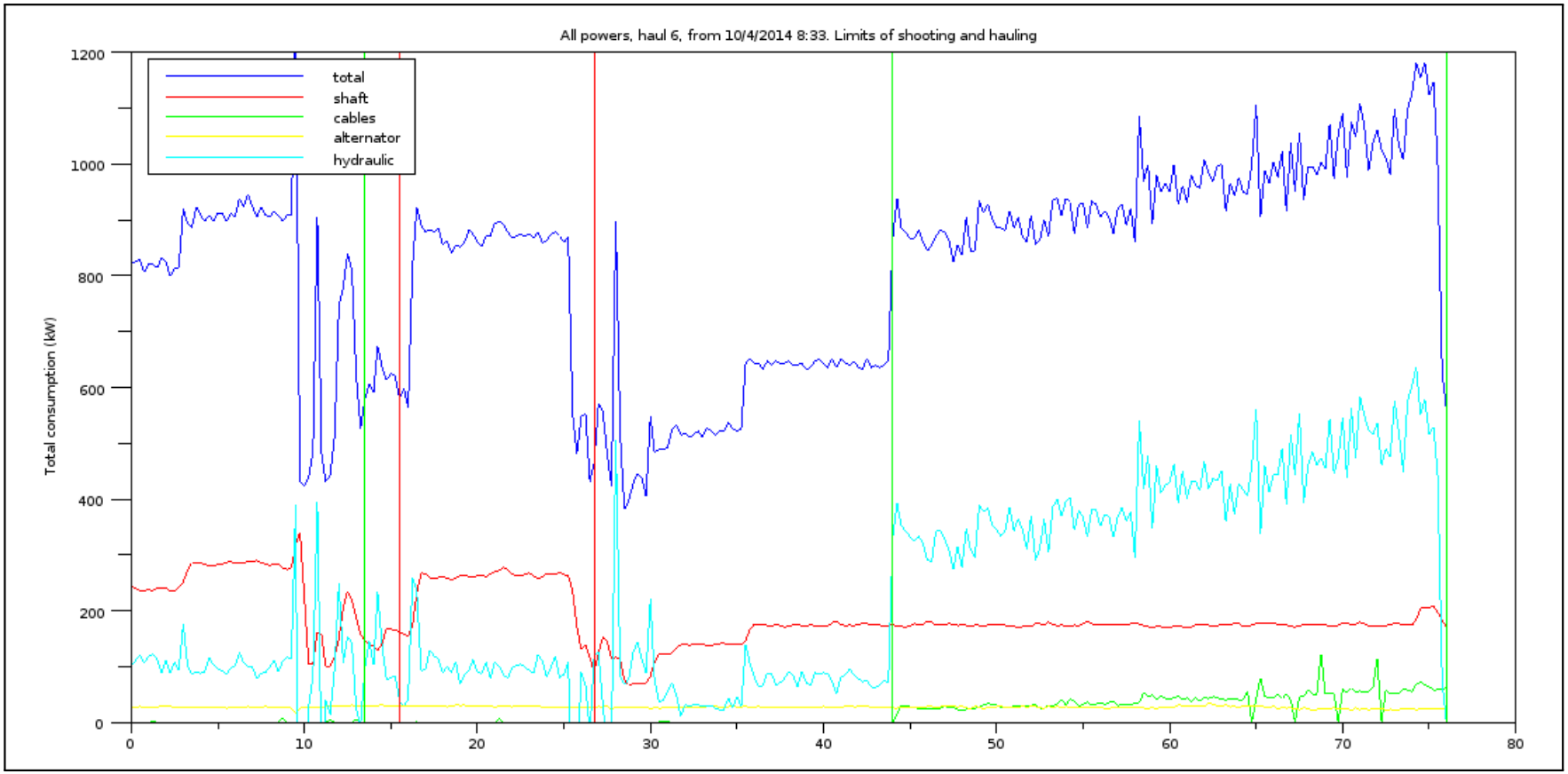
All powers, haul 6, from 10/4/2014 8:33. Limits of shooting and hauling
total
shaft
cables
alternator
hydraulic
Total consumption (kW)
0
200
400
600
800
1000
1200
0
10
20
30
40
50
60
70
80

Tensions

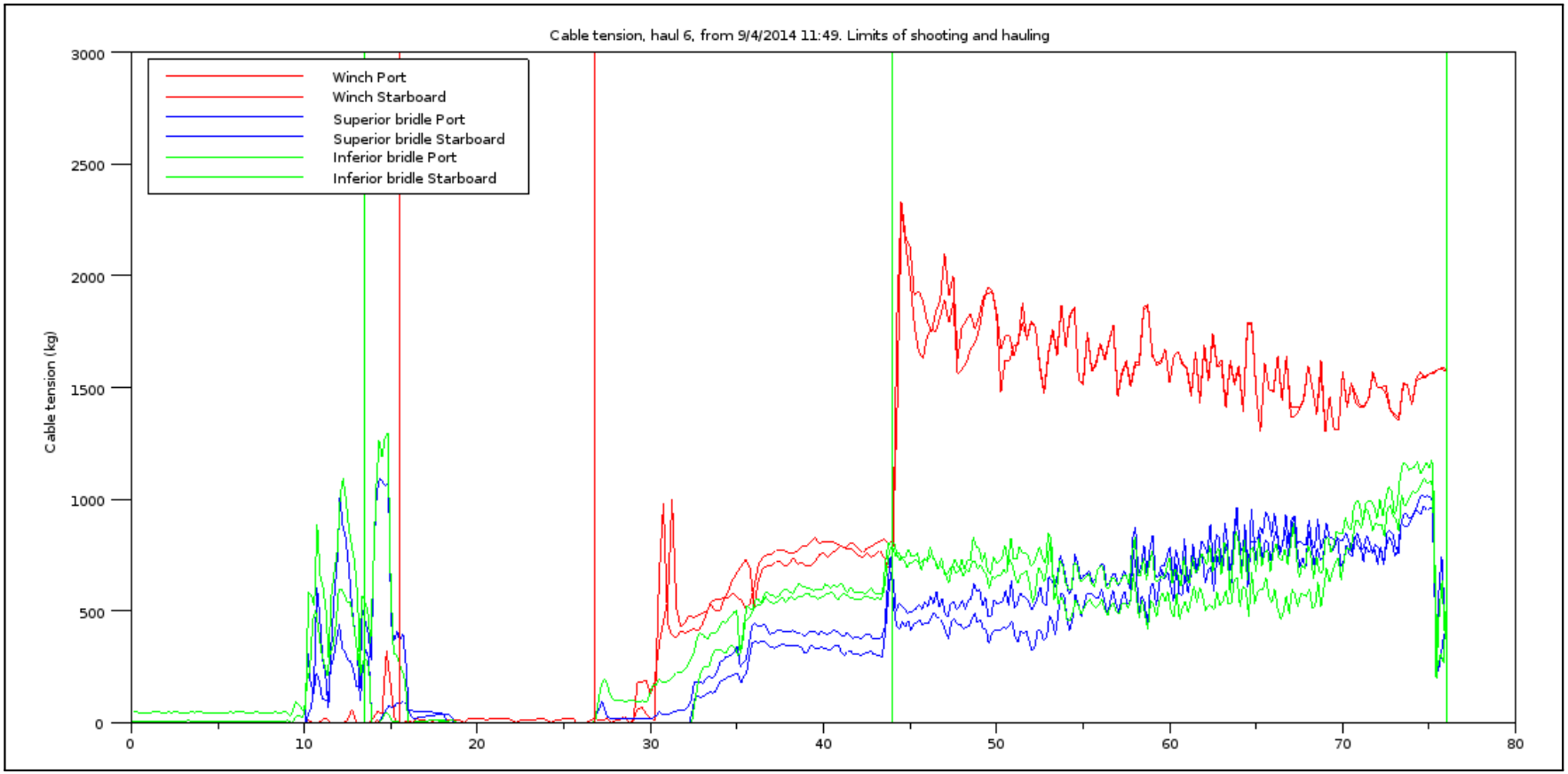
Cable tension, haul 6, from 9/4/2014 11:49. Limits of shooting and hauling
Winch Port
Winch Starboard
Superior bridle Port
Superior bridle Starboard
Inferior bridle Port
Inferior bridle Starboard
Cable tension (kg)
3000
2500
2000
1500
1000
500
0
0
10
20
30
40
50
60
70
80

Cables length

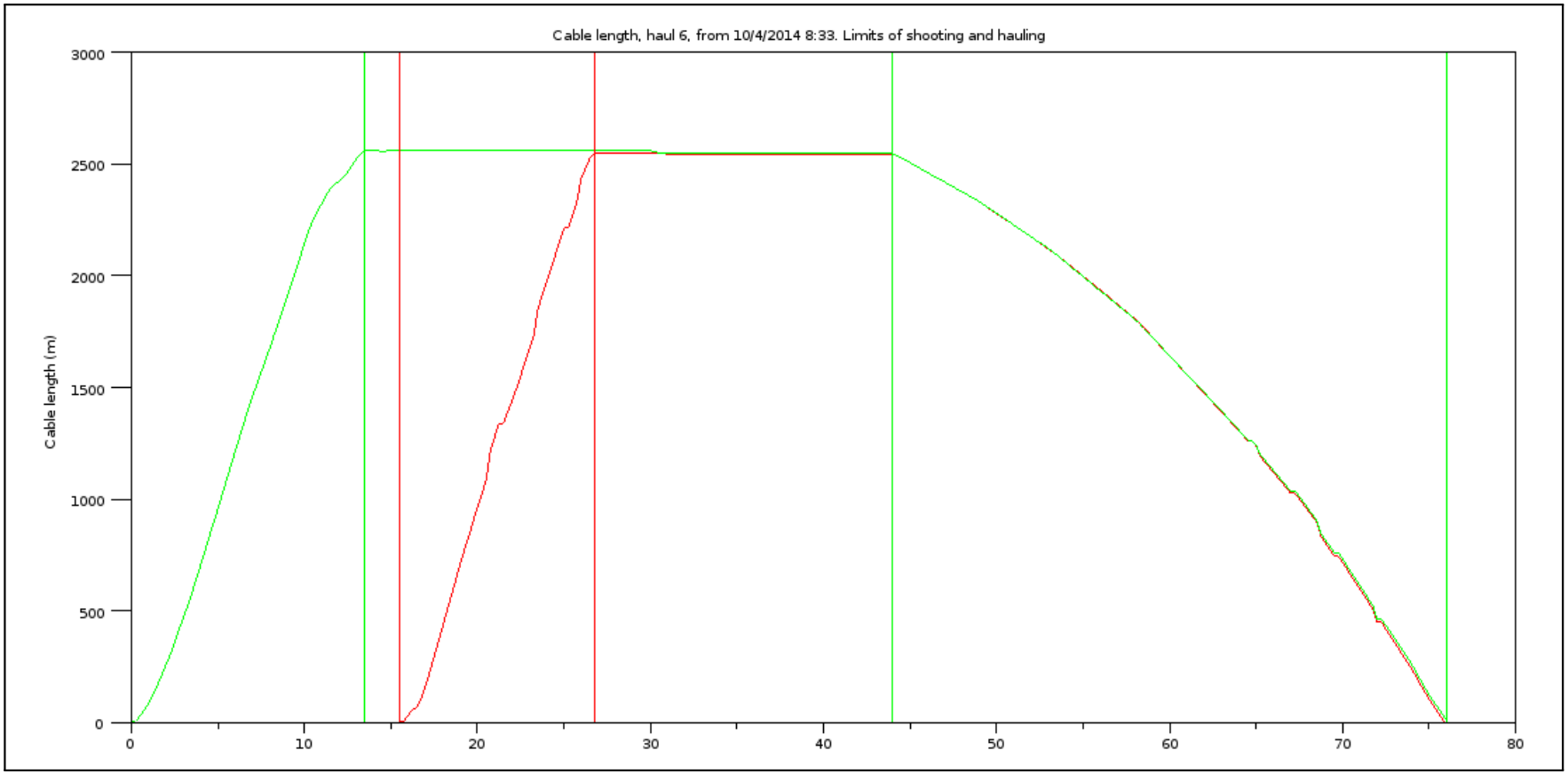

Propeller pitch

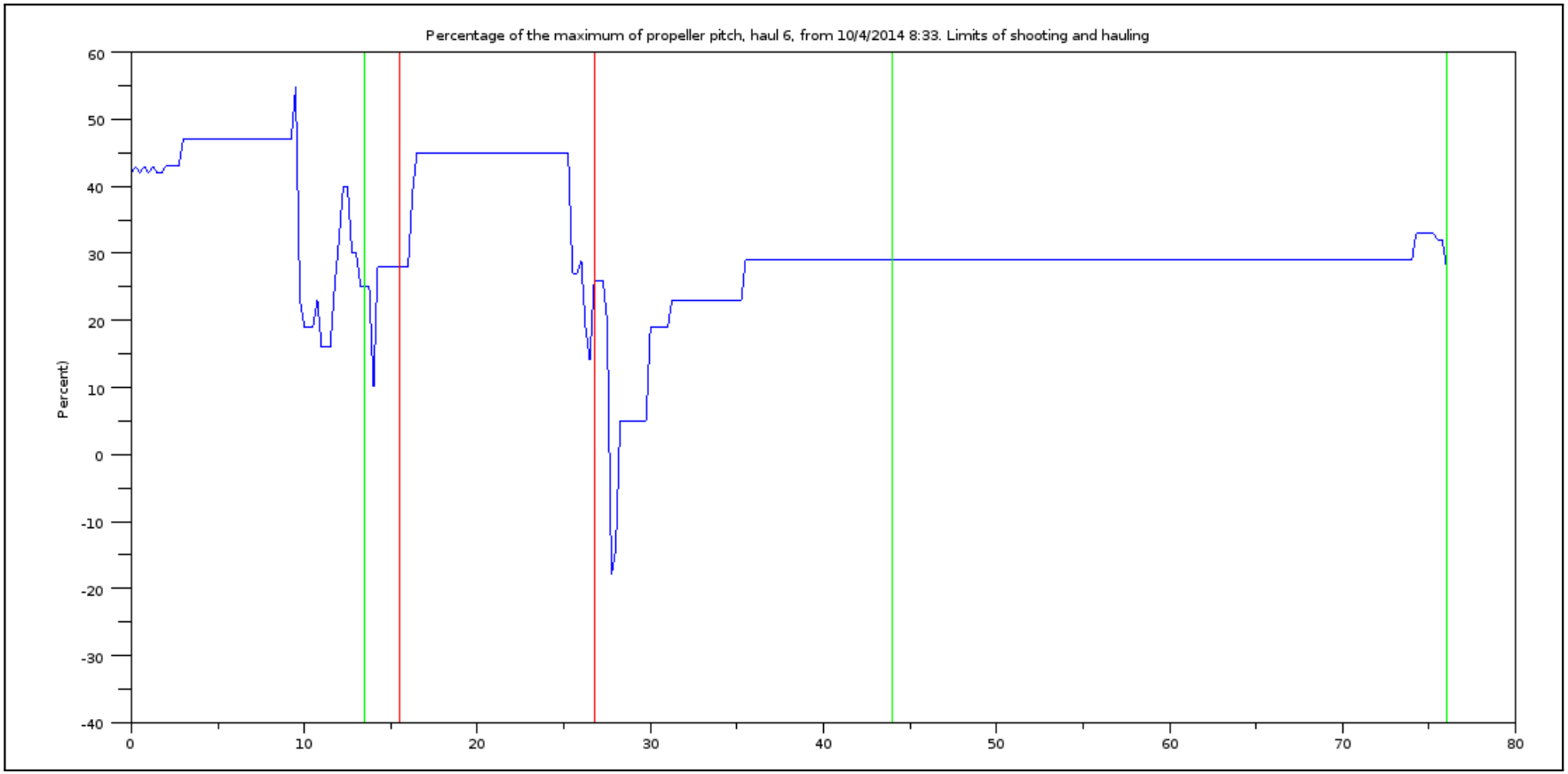

Vertical opening

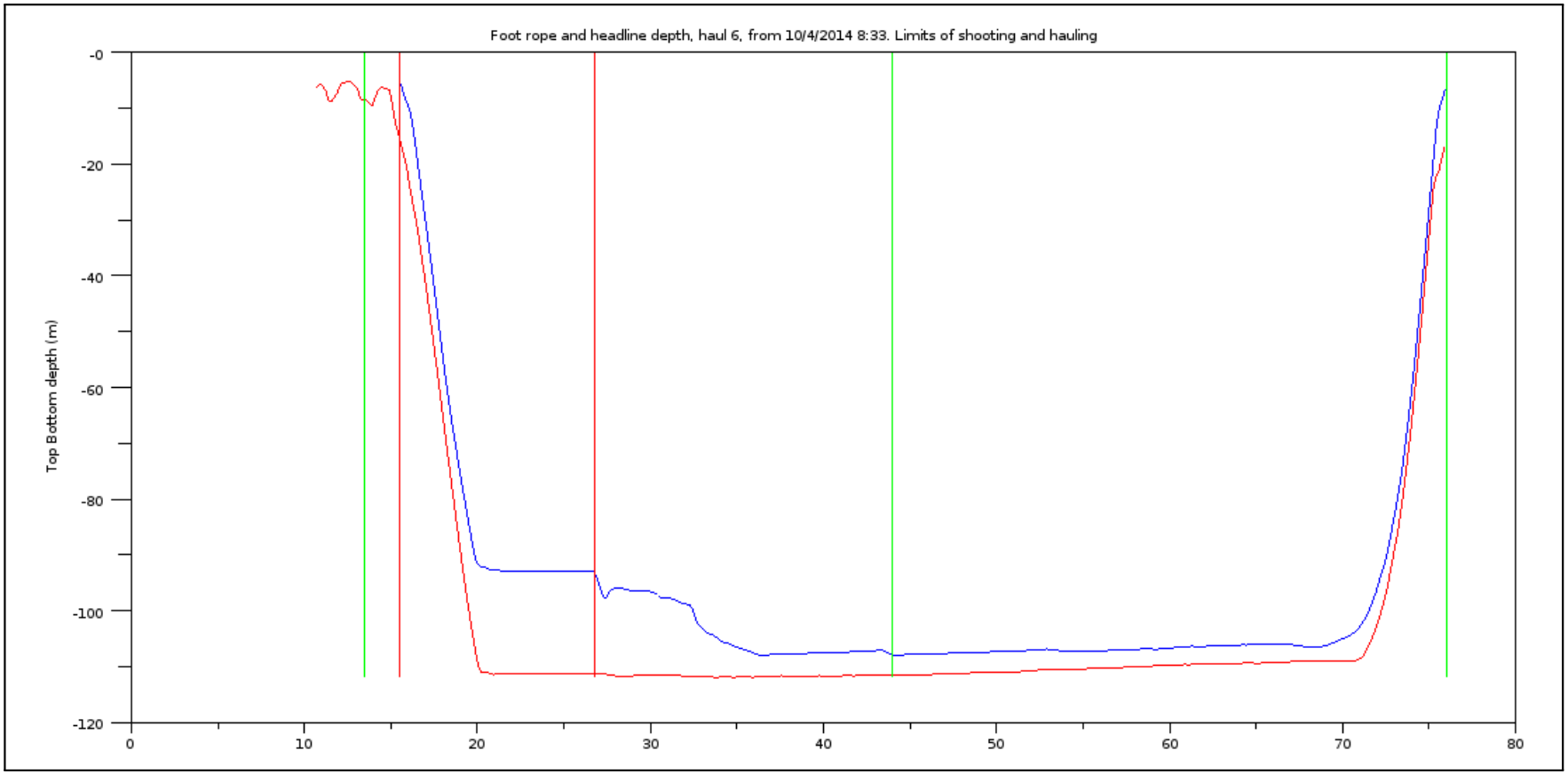

GPS on the middle of the cables

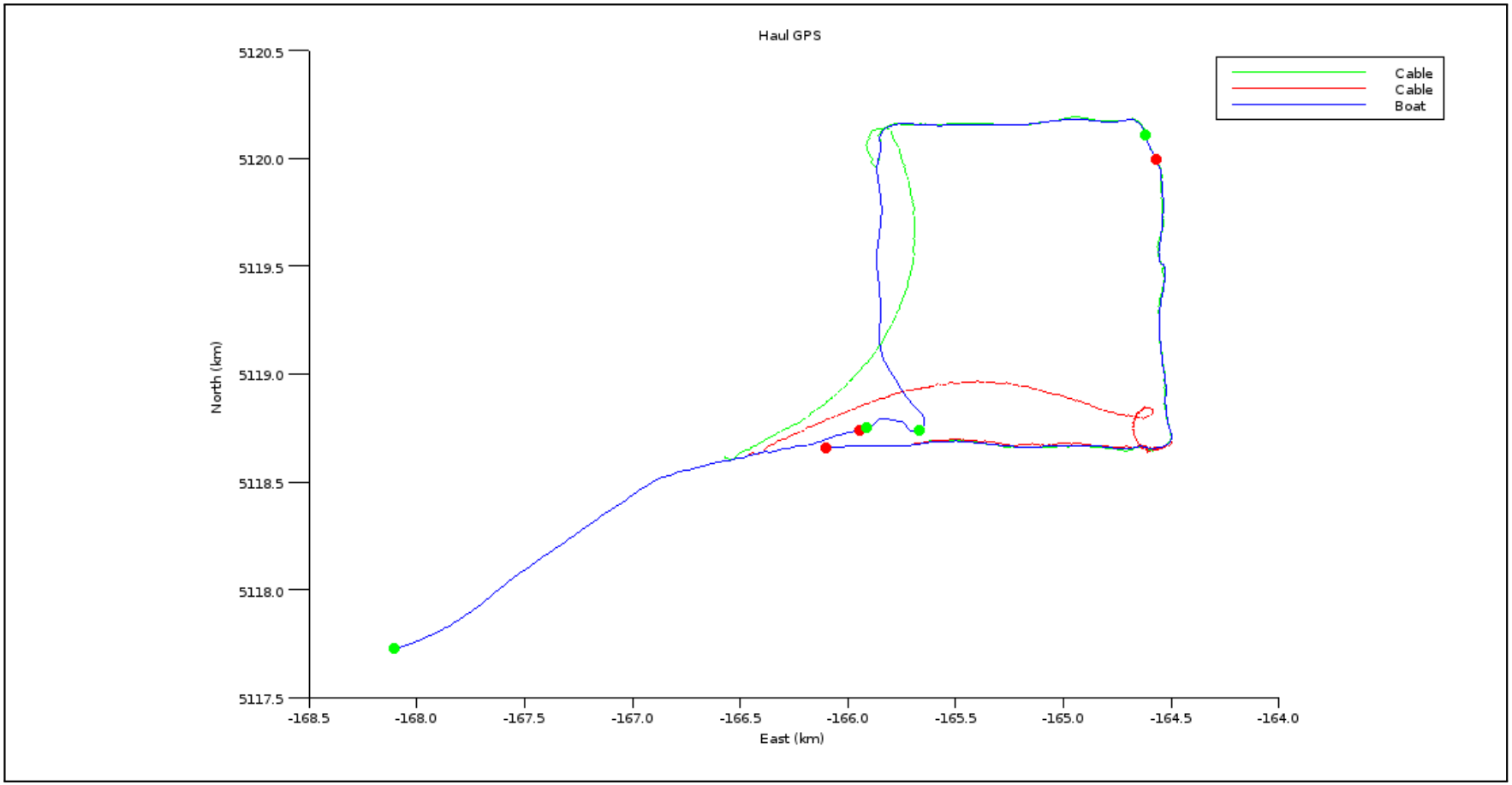

Swept surfaces: around $2km^2$ each haul

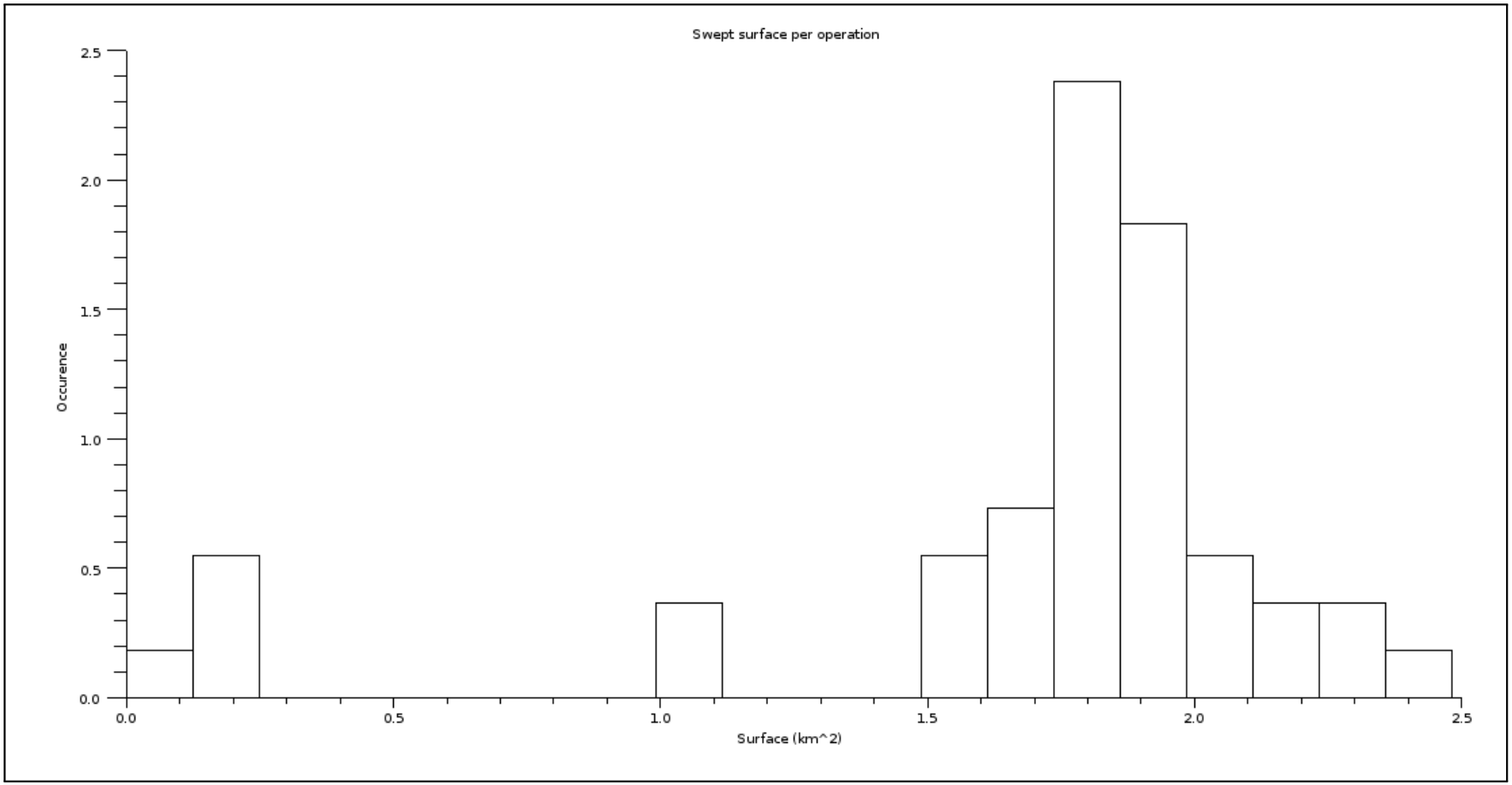

Consumption per operation

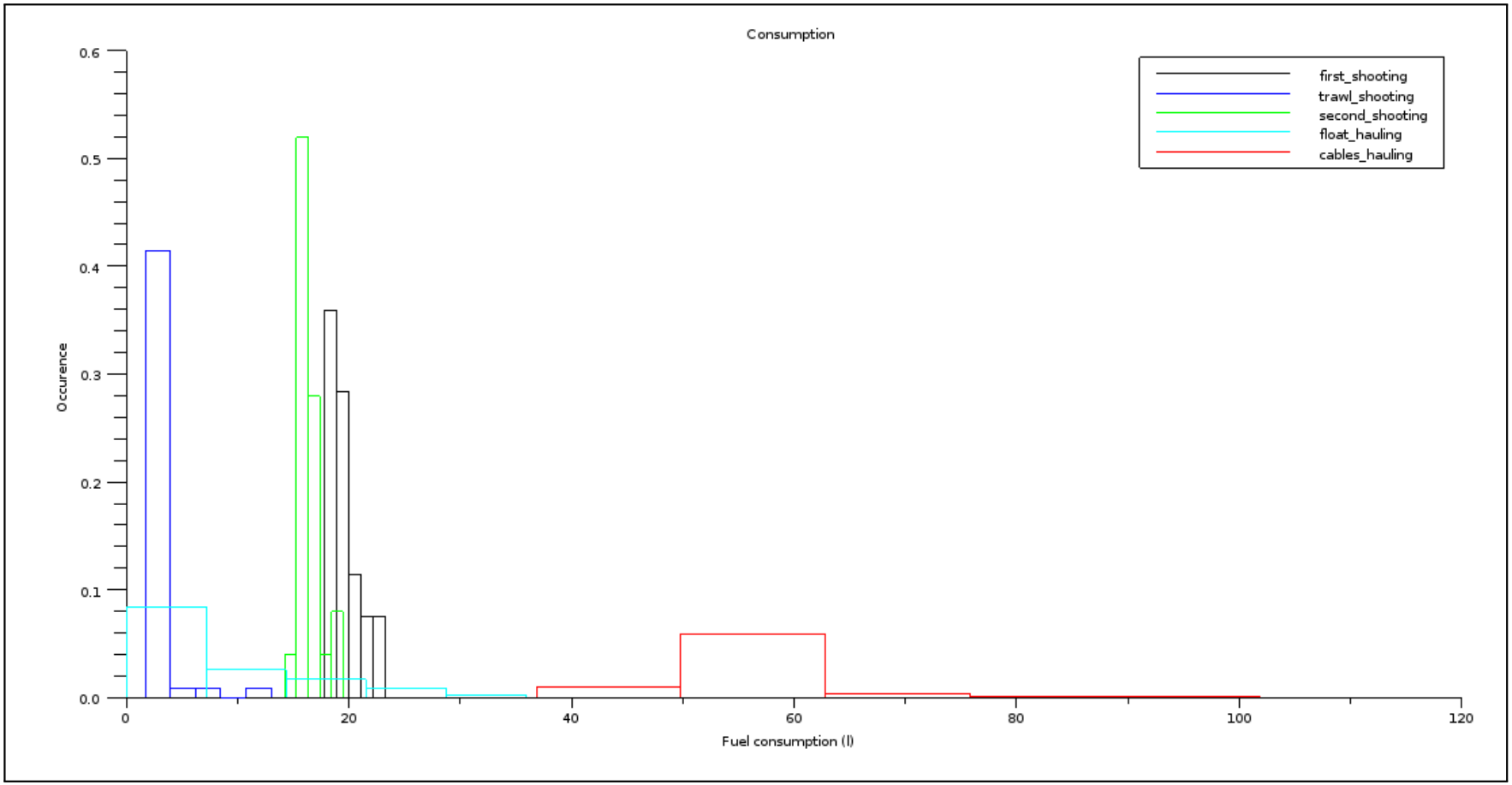

Consumption per surface: around $60l/km^2$

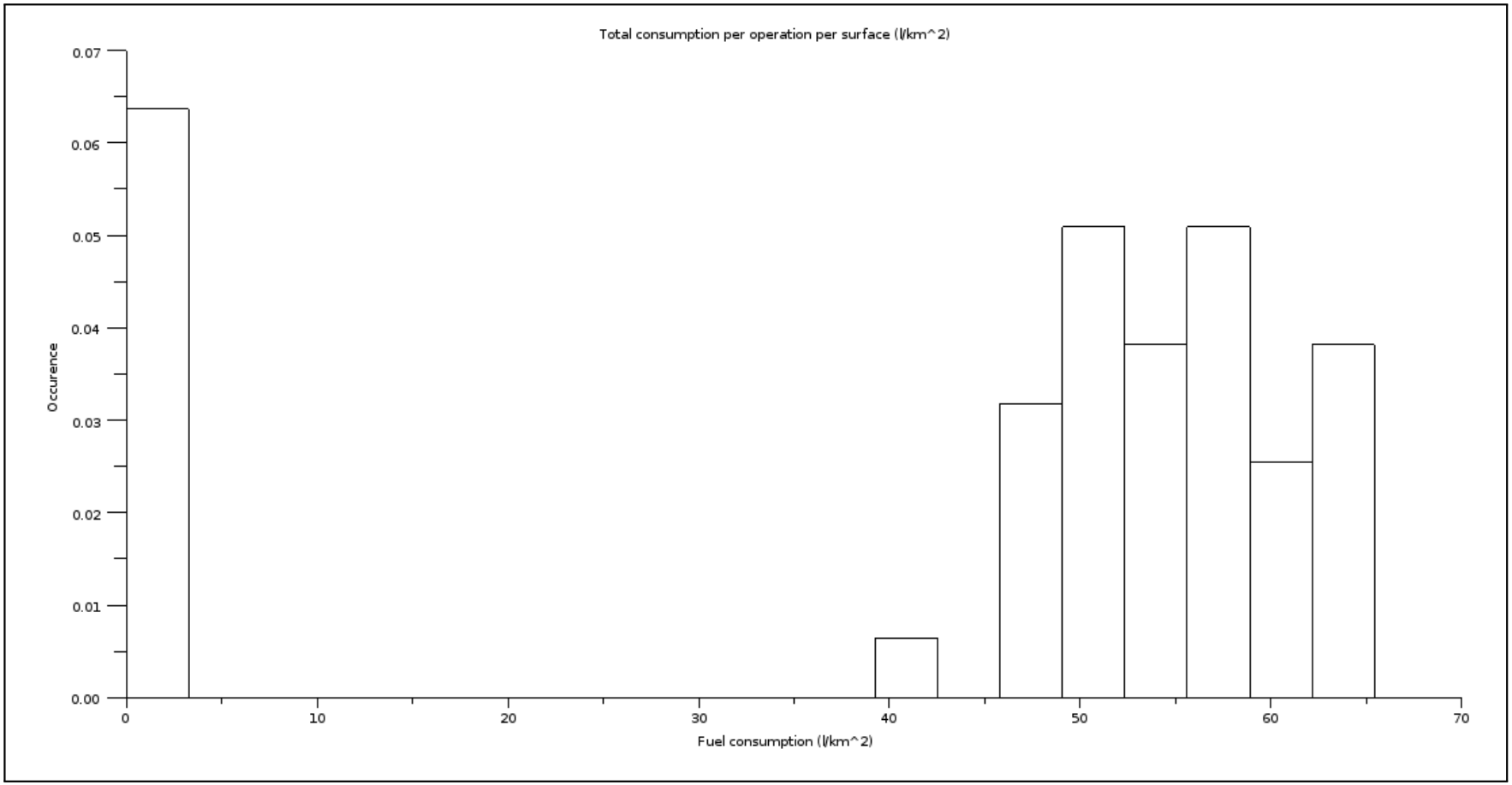

Route: fuel vs speed

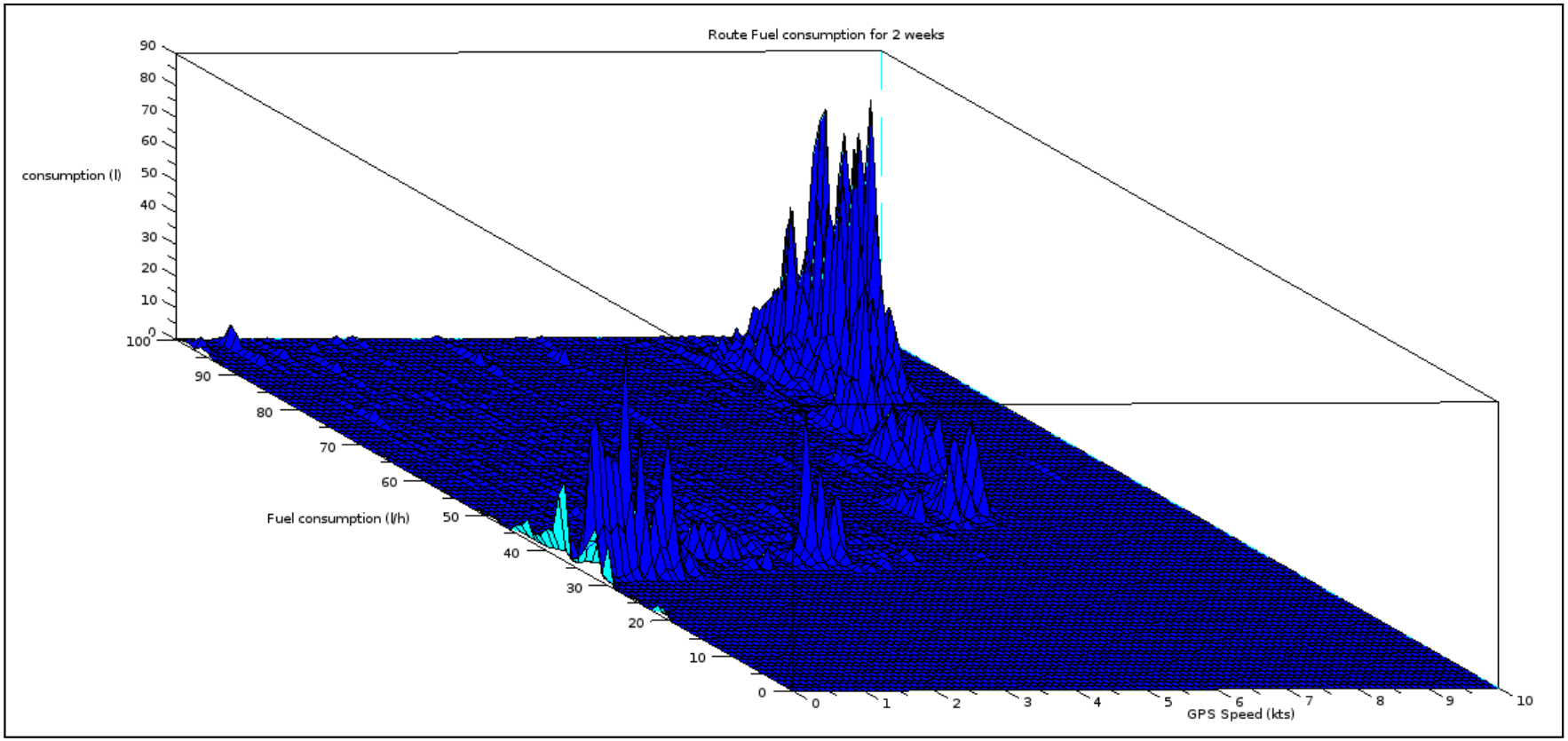

Appendix A5

Netting modeling by Triangular elements

Netting modeling by Triangular elements

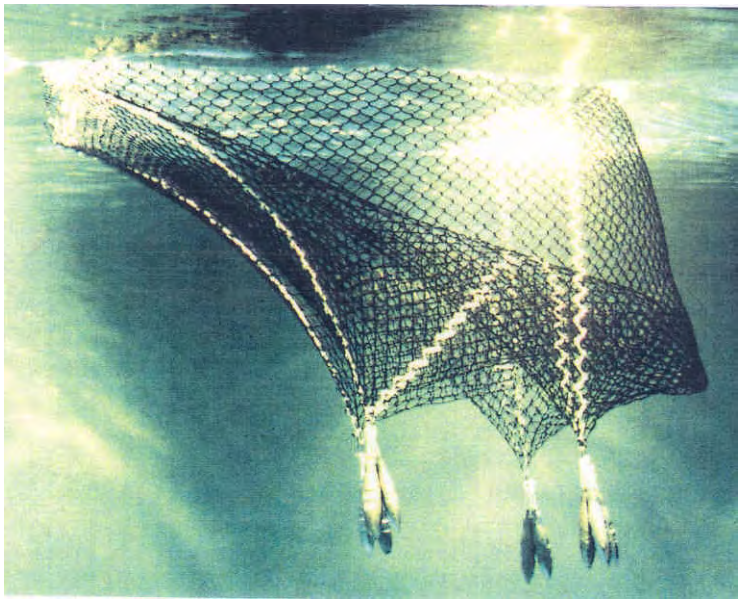

Fish cage

Trawl

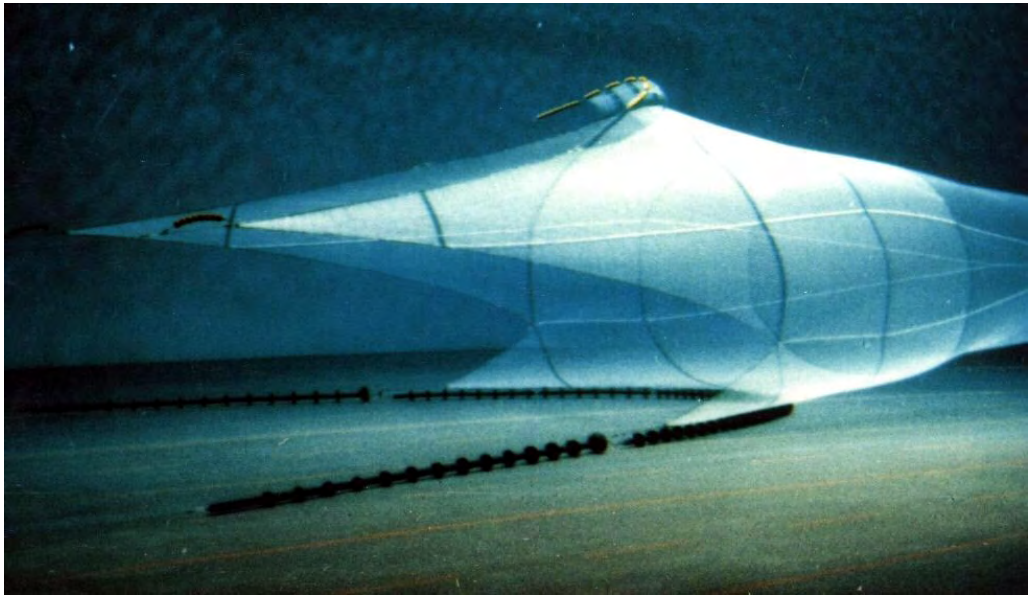

- Netting split in triangles
- Nodes are fixed to the netting
- Constant deformation in each triangle

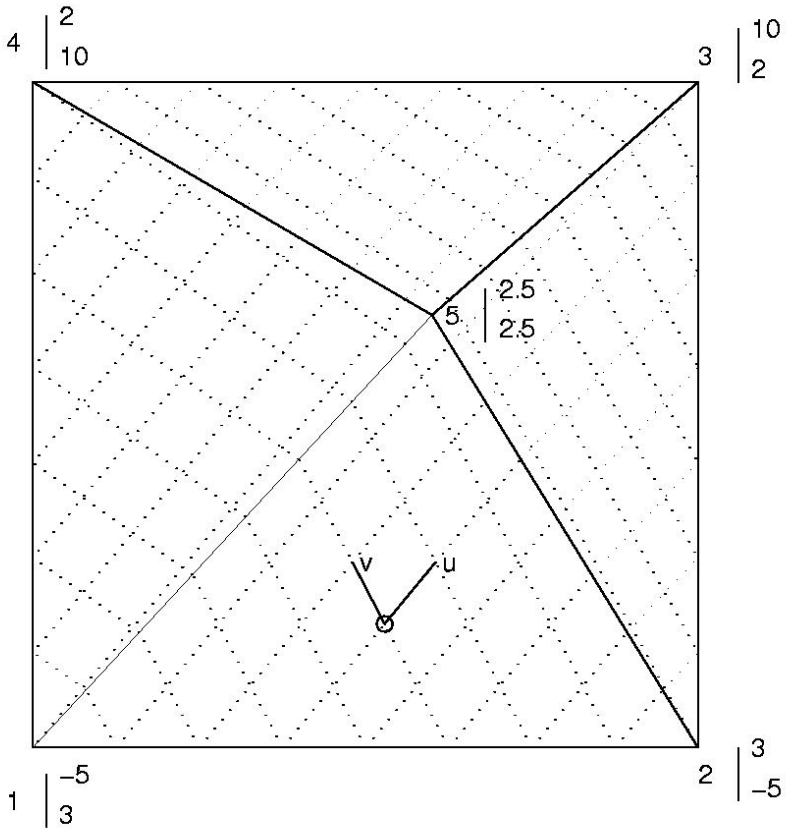

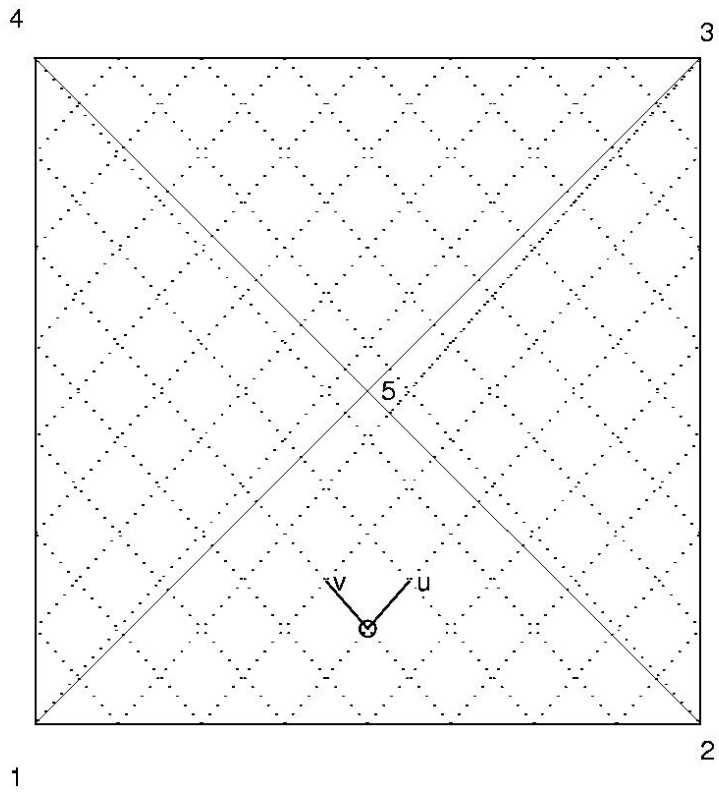

2 geometric relations => **u** & **v**

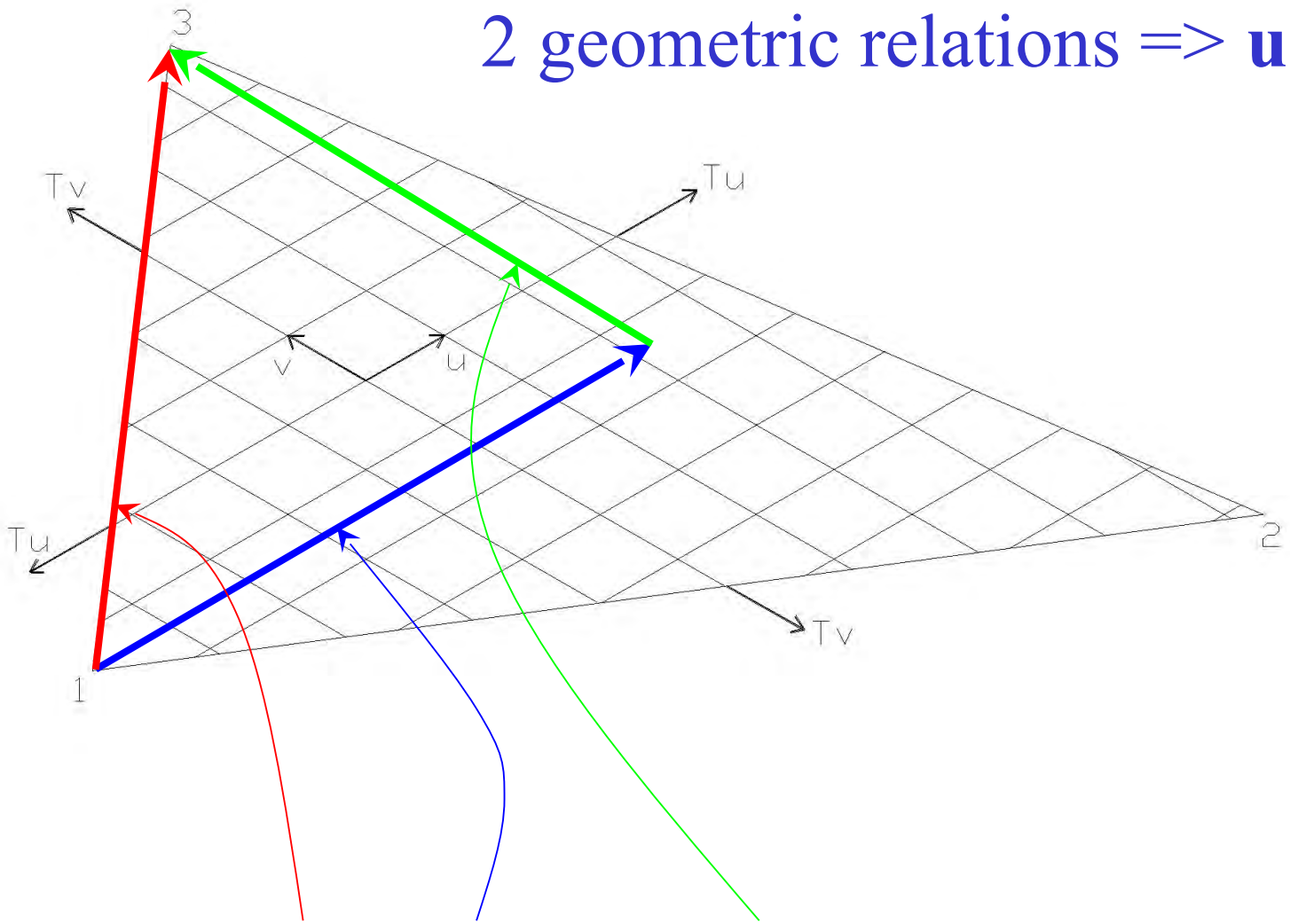

13 = (v3-v1) **u** + (u3-u1) **v**

Idem for the side 12

>> **2 equations & 2 unknowns : u & v**

Twines are elastic

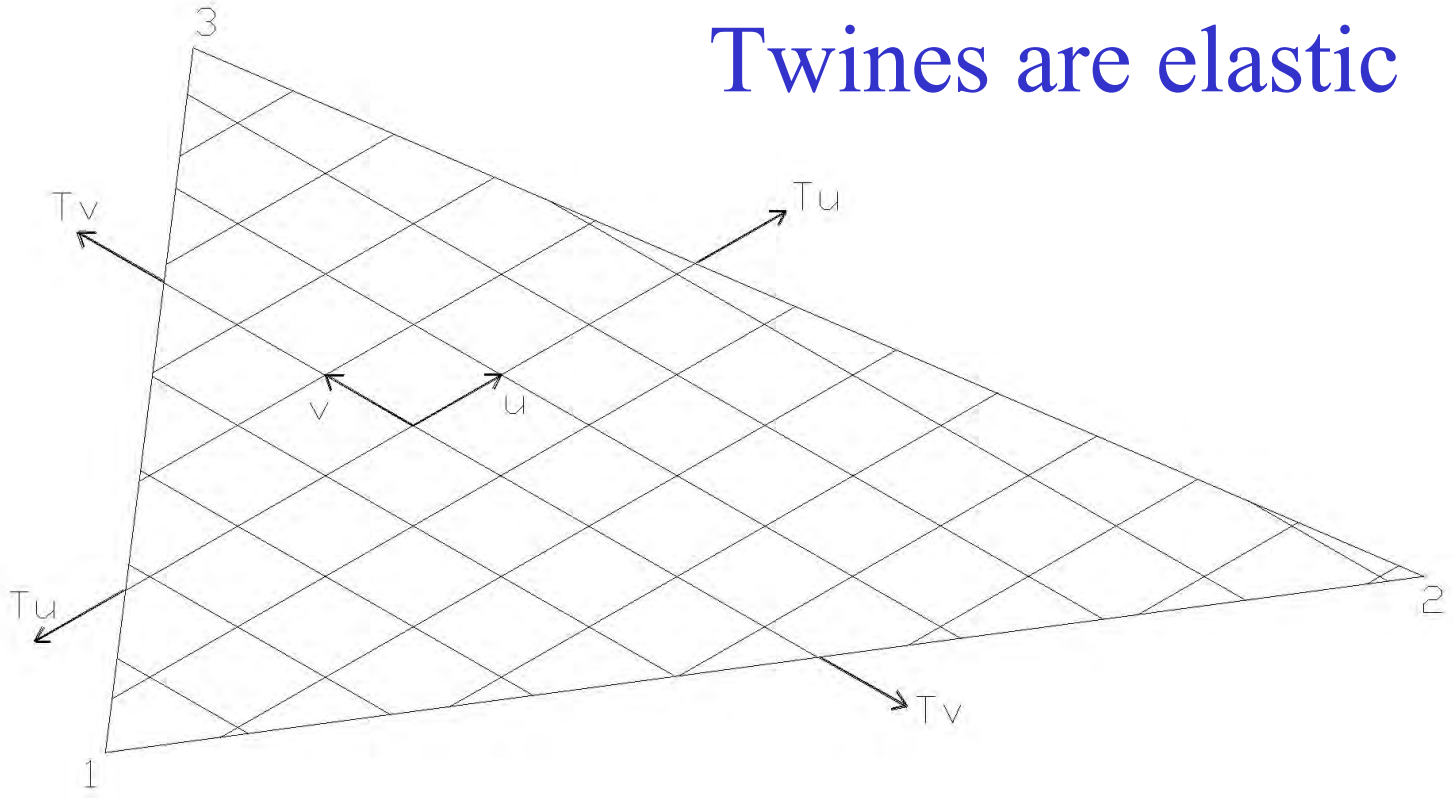

$$Tu = EA\,\frac{|u| - n0}{n0}$$

E traction ≠ E compression

$$Tv = EA\,\frac{|v| - n0}{n0}$$

Principle of virtual work => f

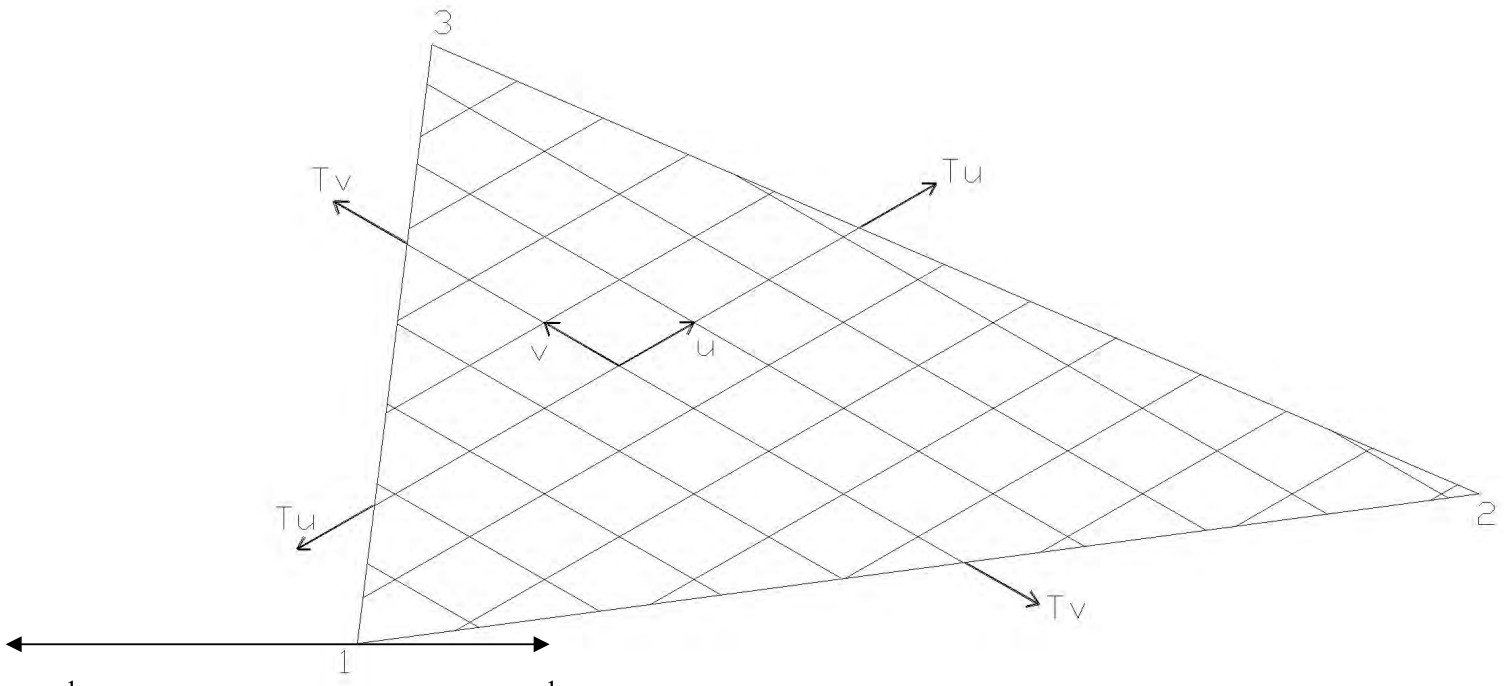

f_x^1 d_x^1

$$We = f_x^1 \; d_x^1$$

$$Wi = nbu \; Tu \; du + nbv \; Tv \; dv$$

$$f_x^1 = (v3 - v2) \; Tu \; \frac{ux}{2|u|} - (u3 - u2) \; Tv \; \frac{vx}{2|v|}$$

Equilibrium by Newton Raphson

$$\mathbf{X}_{k+1} = \mathbf{X}_k - \frac{\mathbf{F}(\mathbf{X}_k)}{\mathbf{F}'(\mathbf{X}_k)}$$

$$\mathbf{F}'(\mathbf{X}) = \frac{\mathbf{F}(\mathbf{X}+\mathbf{h}) - \mathbf{F}(\mathbf{X})}{\mathbf{h}} \quad \begin{cases} \mathbf{F}(\mathbf{X}+\mathbf{h}) = 0 \\ \mathbf{X}_{k+1} - \mathbf{X}_k = \mathbf{h} \end{cases}$$

Netting of 1600 meshes

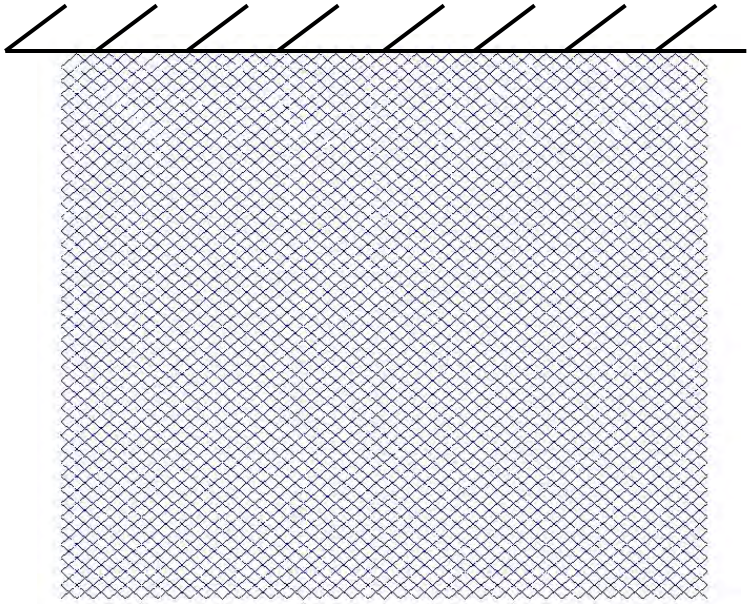

1050 triangular elements

639 nodes

1 symmetry plane

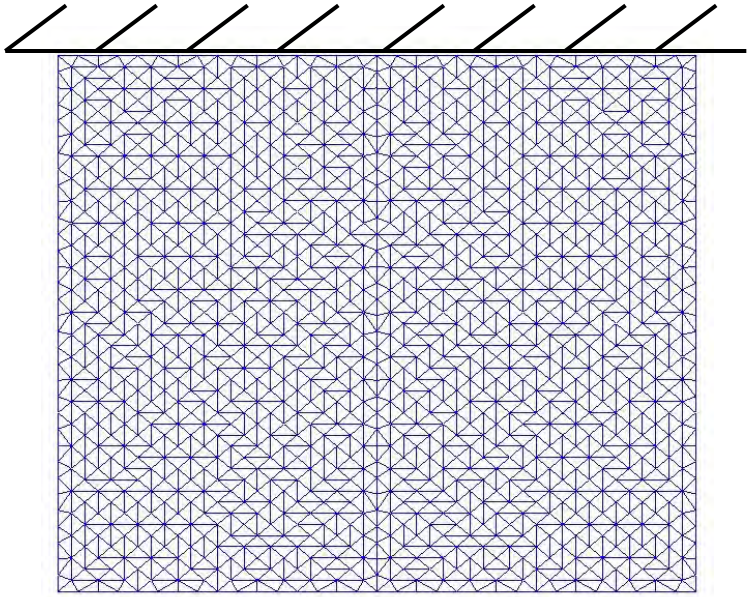

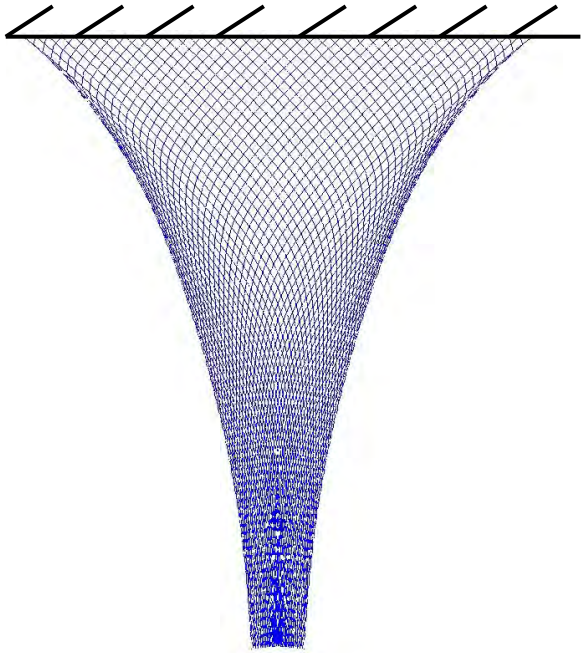

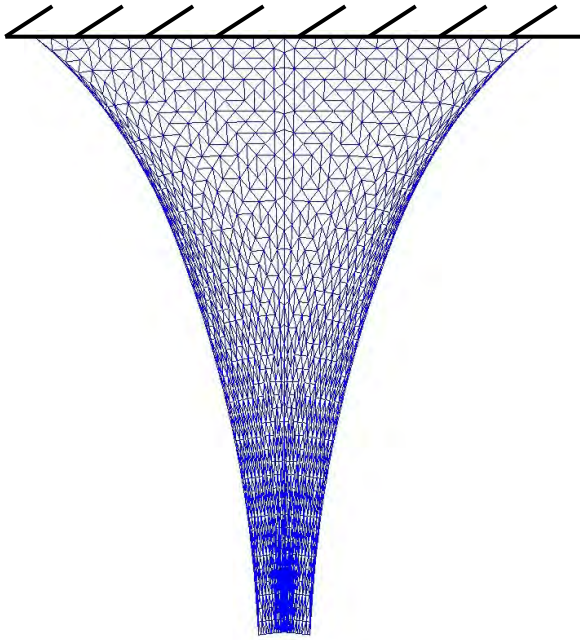

EA=10 000 N

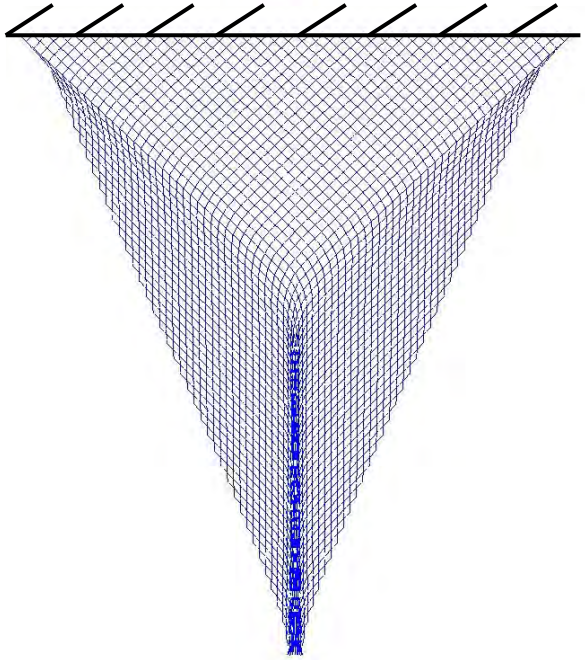

EA=20 000 N

Comparison on cod-end with 25 Kg of water

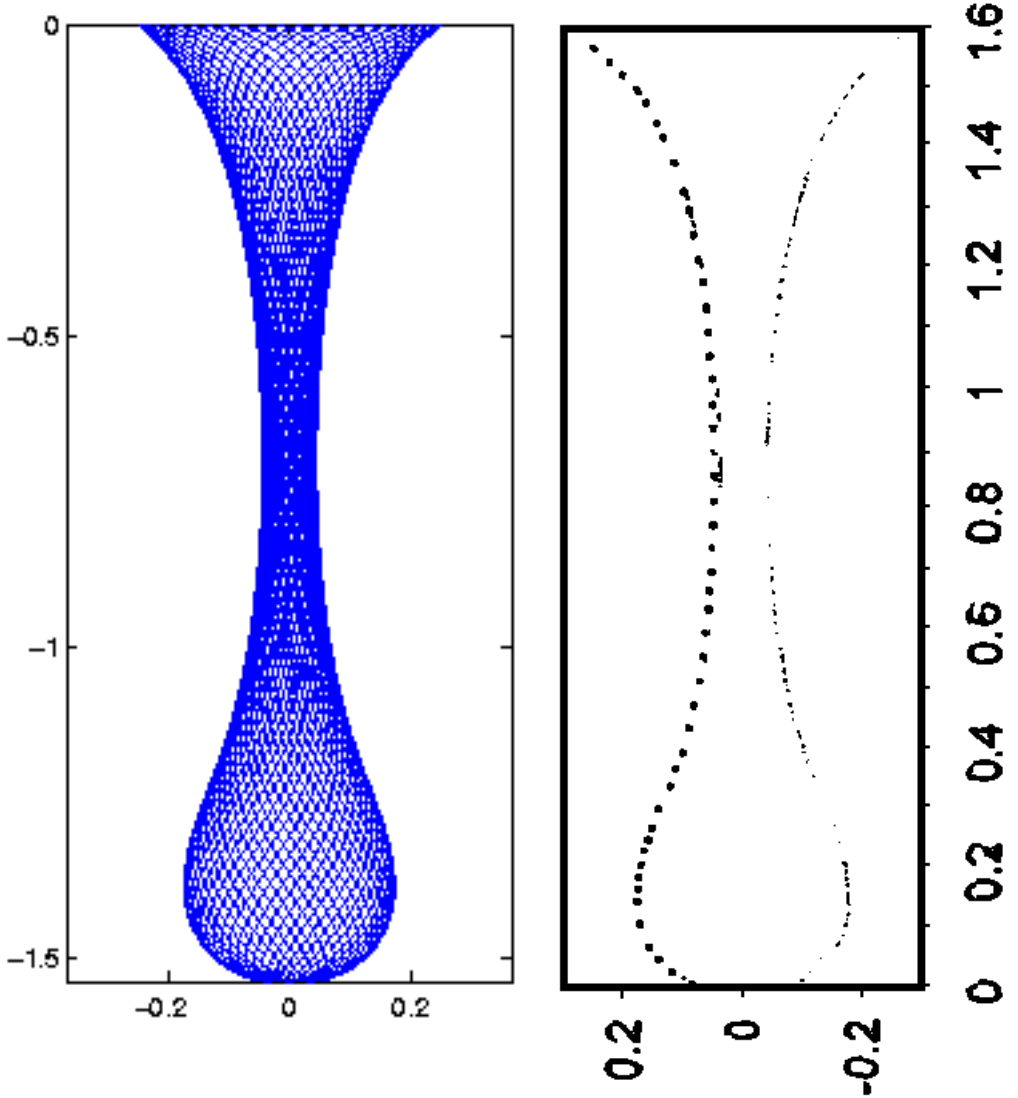

O'Neill and al. (1997)

10 000 twines

1360 triangular elements

742 nodes

2 symmetry planes

$P = \rho g h$

Comparison with flume tank tests (+)

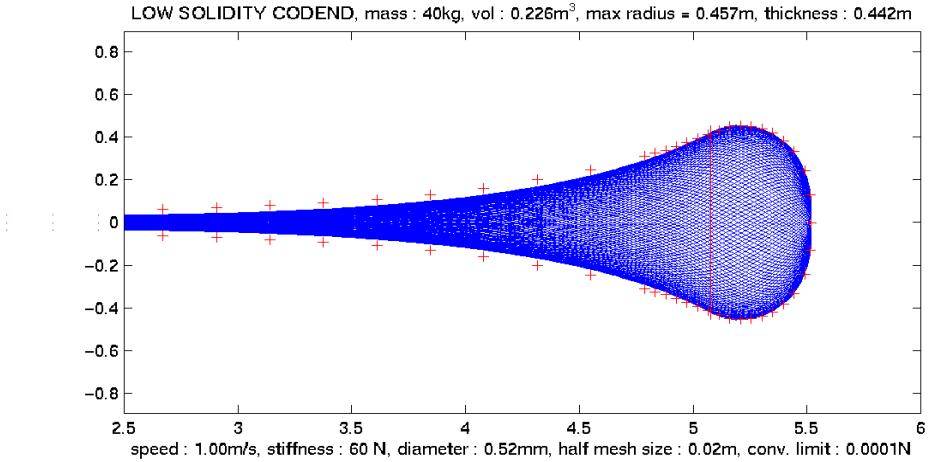

$$P = \frac{1}{2}\rho C d V^2$$

Catch: 40 & 300 Kg

Hirtshals

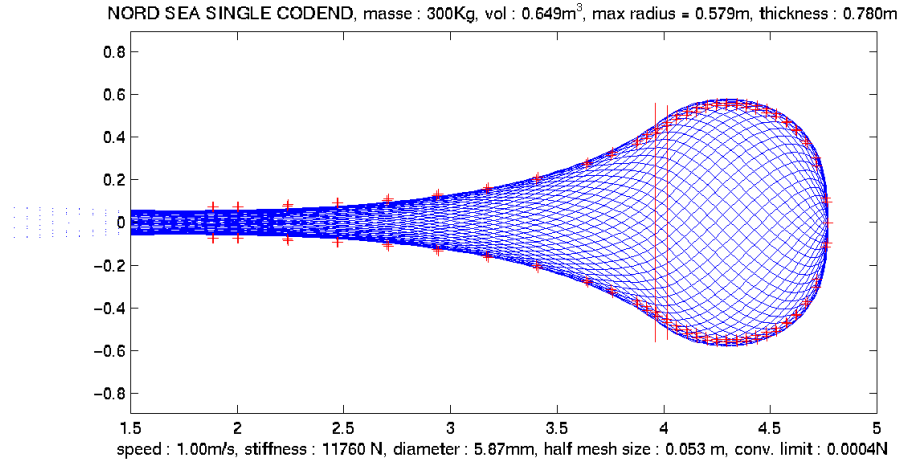

Cubic fish cage

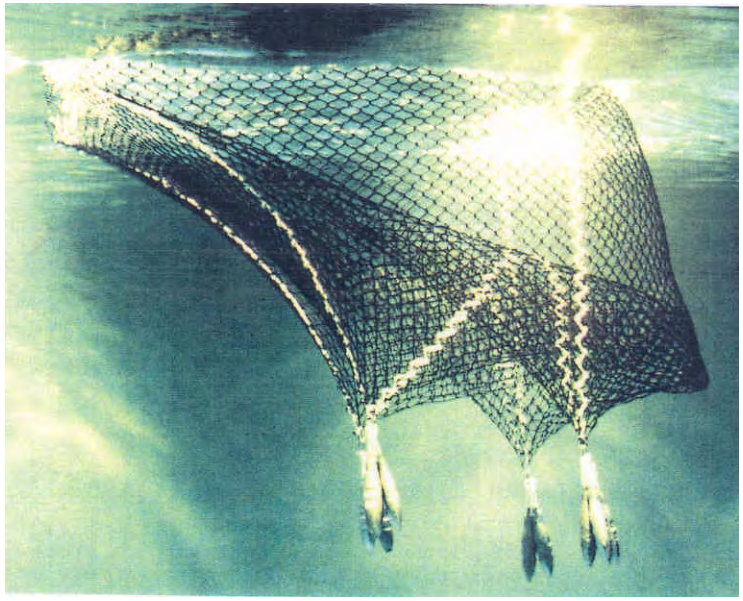

Cube of 1 m^3

4 dead weights: 3 Kg

Current: 1m/s

Boulogne/mer

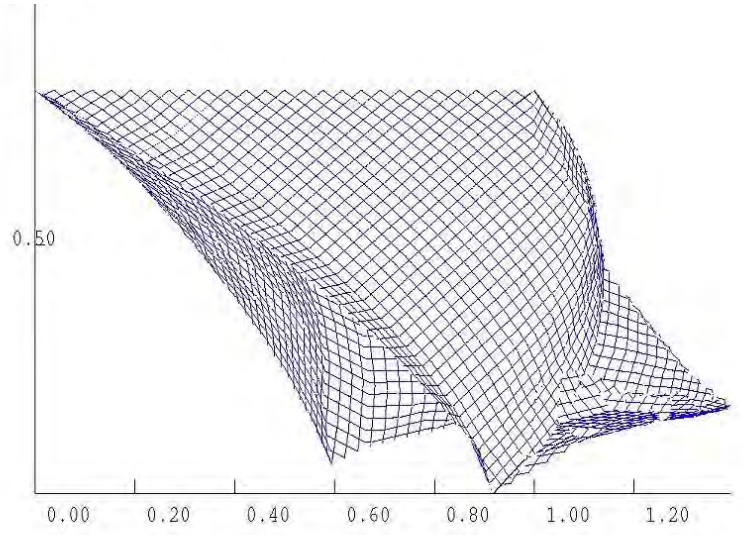

225 nodes

416 triangular elements

1 symmetry plane

Circular fish cage

Diameter: 20m

Dead weights: 1200Kg

3 chains: 150m, 10 Kg/m

3 buoys: 2.3 m^3

Current: 0.5 m/s

800 nodes

165 bars elements

1400 triangular elements

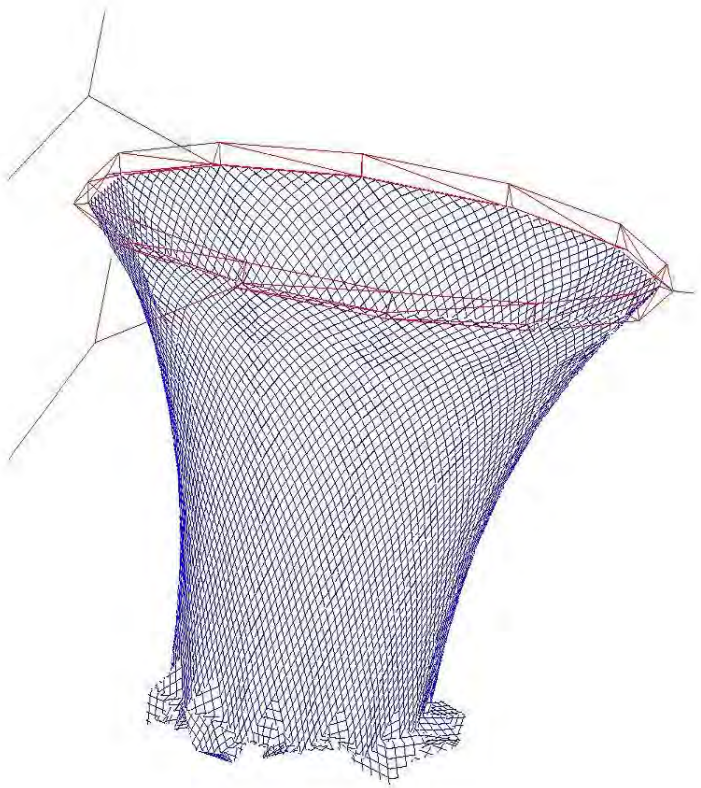

Pelagic trawls

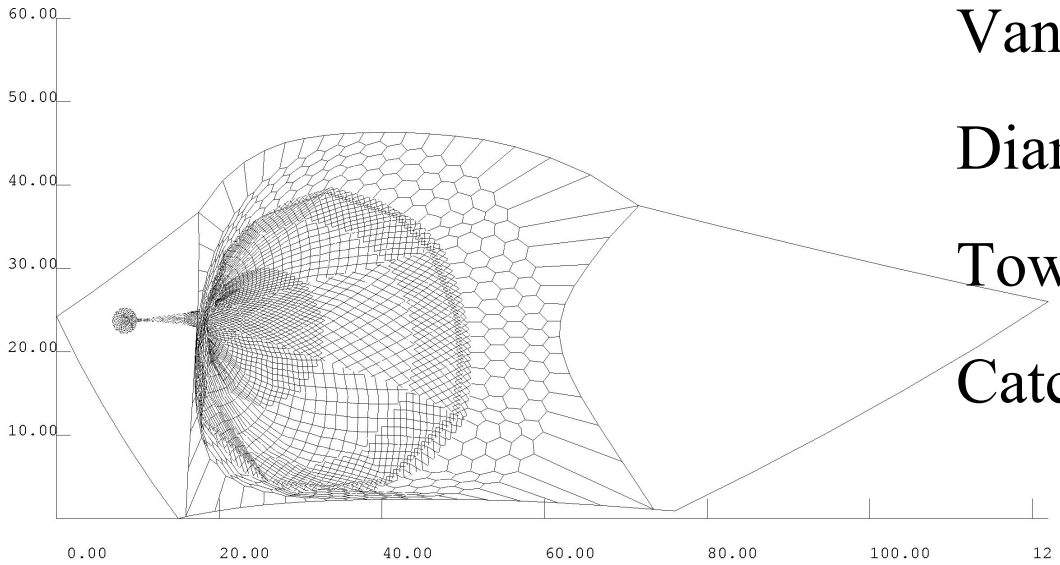

Van Marlen 1980

Diamond & hexagonal meshes

Towing speed 2.08m/s

Catch: 10 m^3

2035 triangular elements

1111 nodes

90 bars elements

1 symmetry plane

Appendix A6

Drag of cables on the sea bottom

Drag of cables on the sea bottom

February 19, 2014

Authors: D.PRIOUR (IFREMER)

Cable modelling

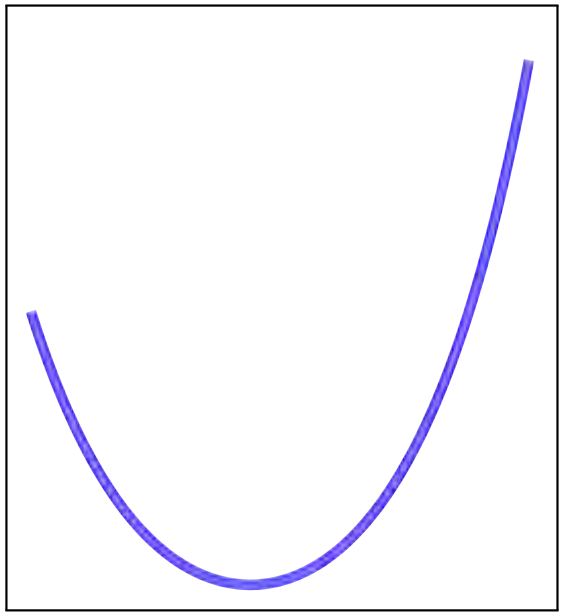

Cable

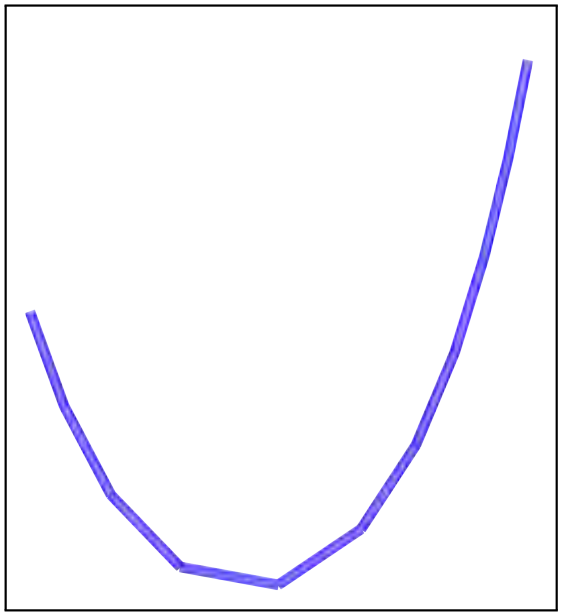

Modelling of the cable by linear elastic elements

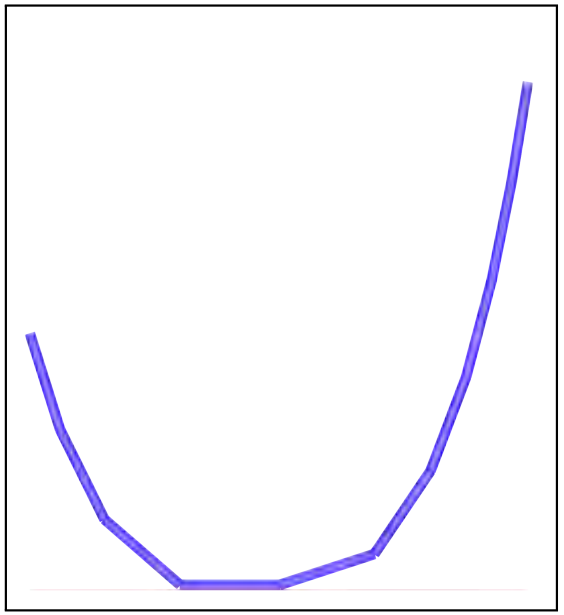

Contact with the bottom

Elastic sea bottom

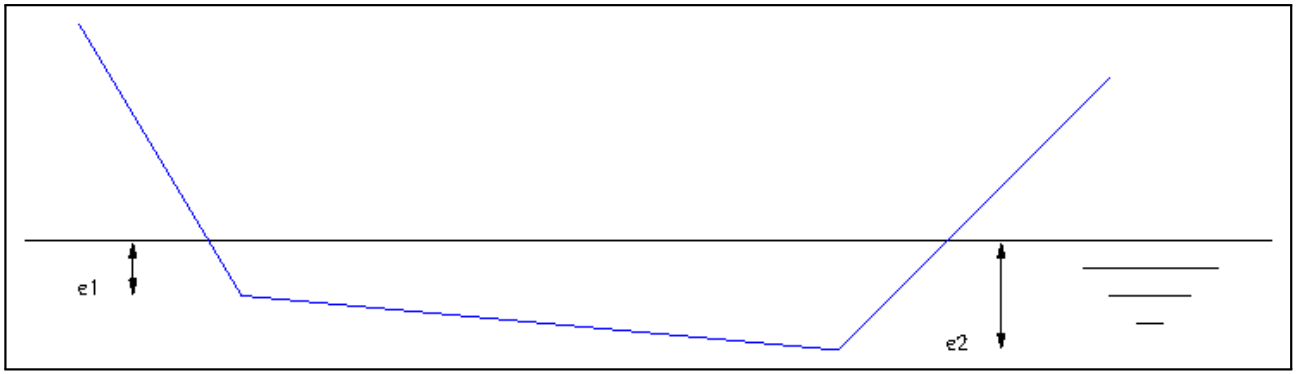

2 nodes of the cable are in the sea bottom

Bottom is elastic (5MN/m)

Sea bottom reaction

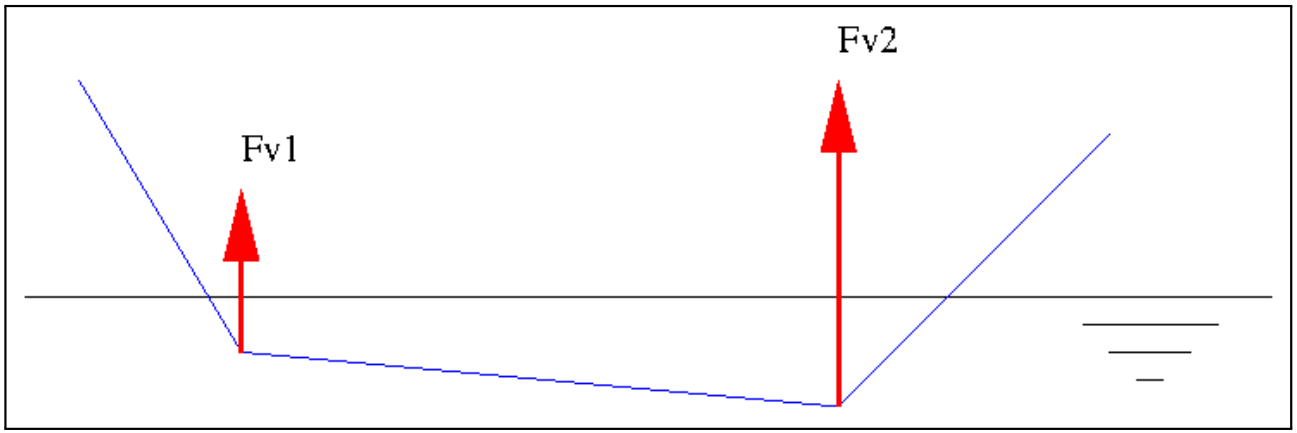

Digging creates vertical reaction

$Fv = K\ e$

e : digging (m)

K : bottom elasticity (N/m)

Fv : vertical reaction (N)

Drag on the sea bottom

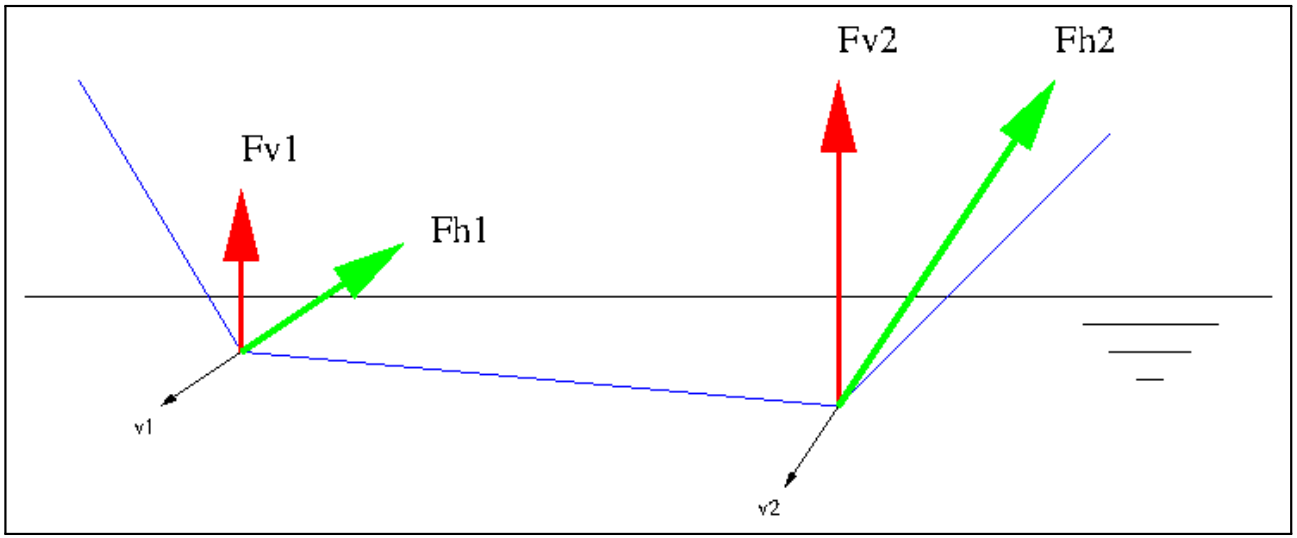

Drag due to the vertical reaction and speed

$Fh = k\ Fv$

$k = 0.5$

Fv : vertical reaction (N)

Fh : horizontal wearing (N)

Sea bottom reaction

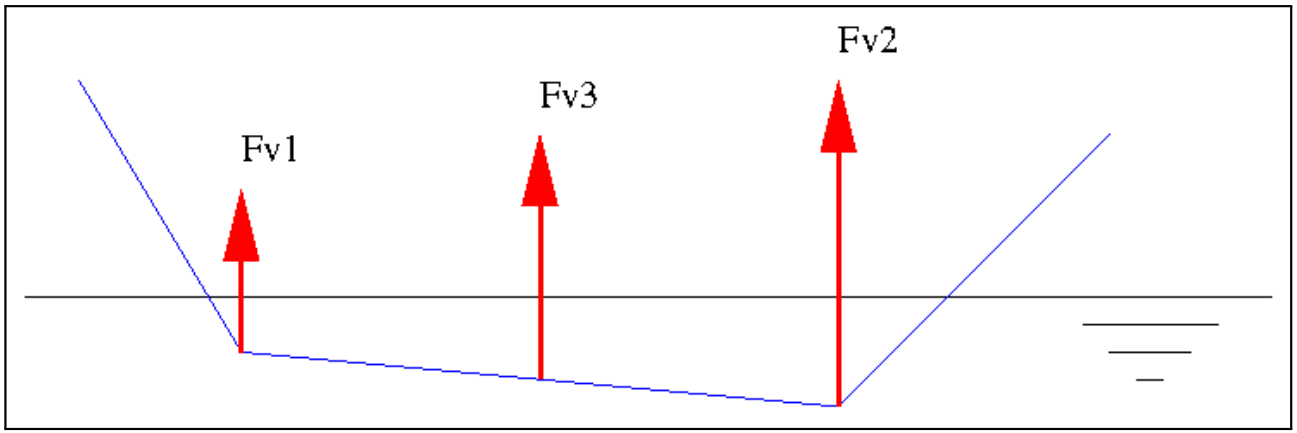

If the discretisation is finer

more nodes are in bottom contact

The same digging will lead to too large vertical reaction

Sea bottom reaction

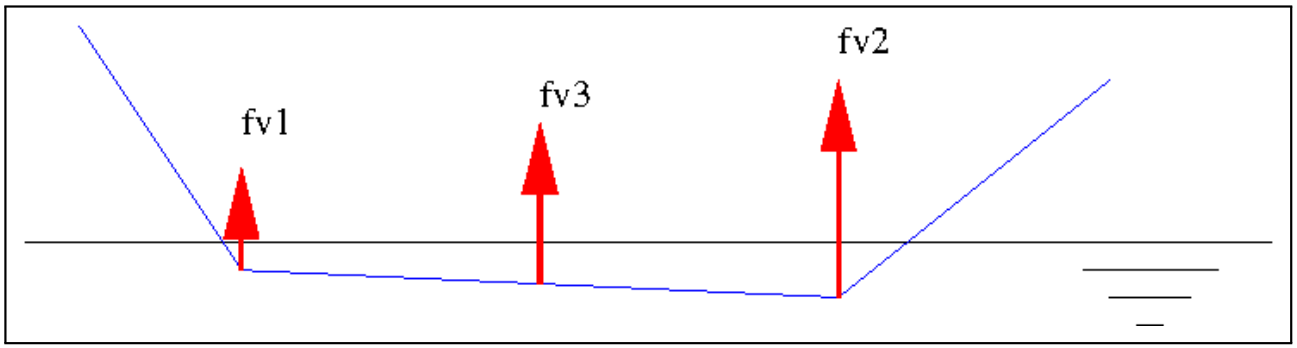

To keep the same global vertical reaction the digging per nodes must be smaller

$fv1 + fv2 + fv3 = Fv1 + Fv2$

Generally it is not a problem because the digging is very small (few mm)

Wearing on the bottom reaction

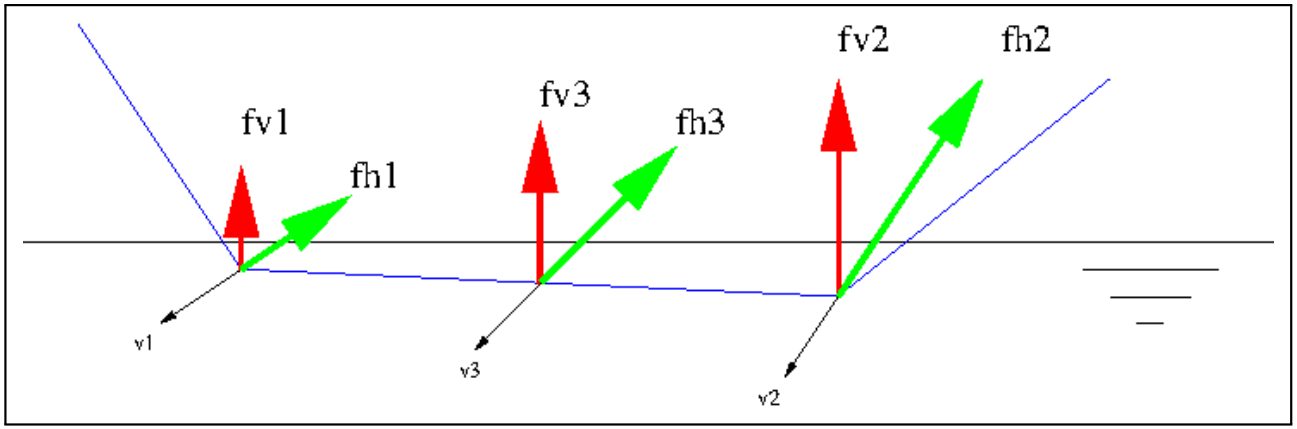

But the drag on the bottom will be the same

$fh1 + fh2 + fh3 = Fh1 + Fh2$

Drag

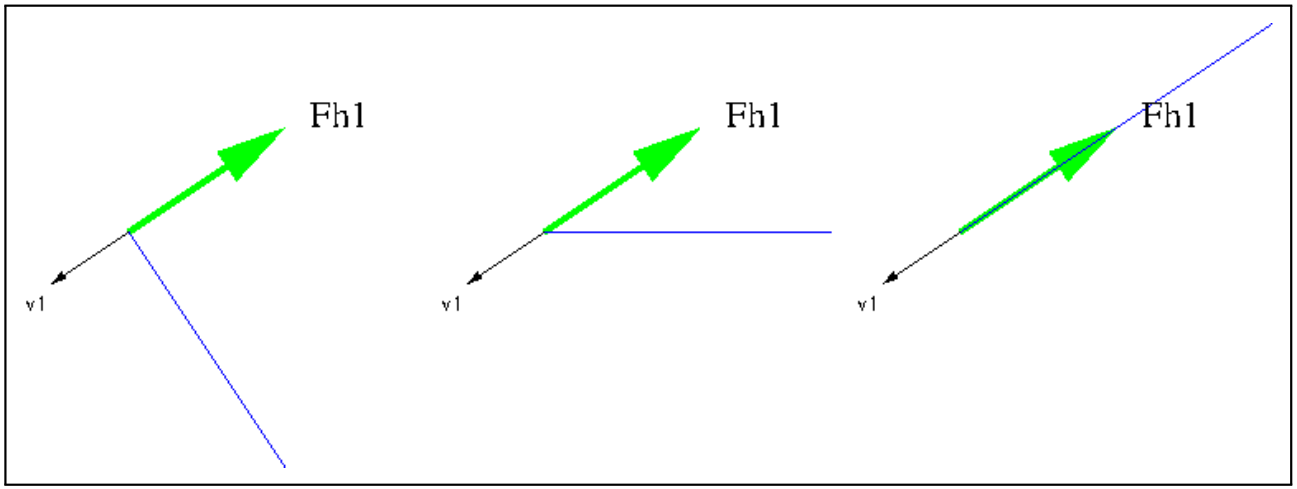

The drag is independent of cable direction

The drag depends on the speed direction only

We suspect a larger normal drag than the tangential one

Sea bottom reaction coarse

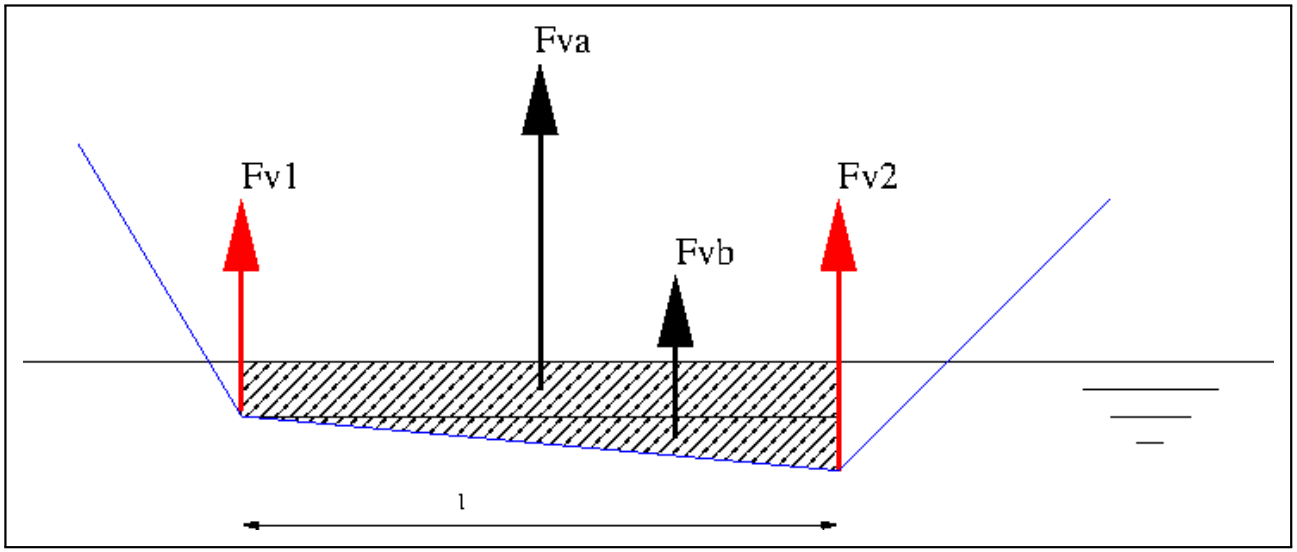

Fv1 = Fva/2 + 1/3 Fvb

Fv1 = Fva/2 + 2/3 Fvb

Fva = e1 diameter l K

Fvb = (e2-e1) diameter l K / 2

K : floattability in the sea bottom (N/m3)

Sea bottom reaction fine

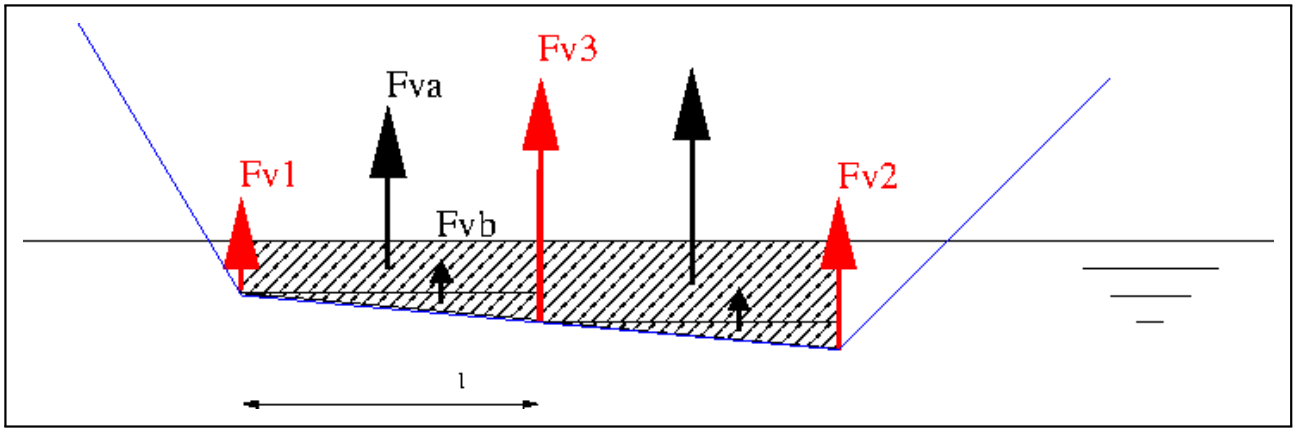

Generally the digging in fine discretisation would be equivalent to the coarse one

Drag

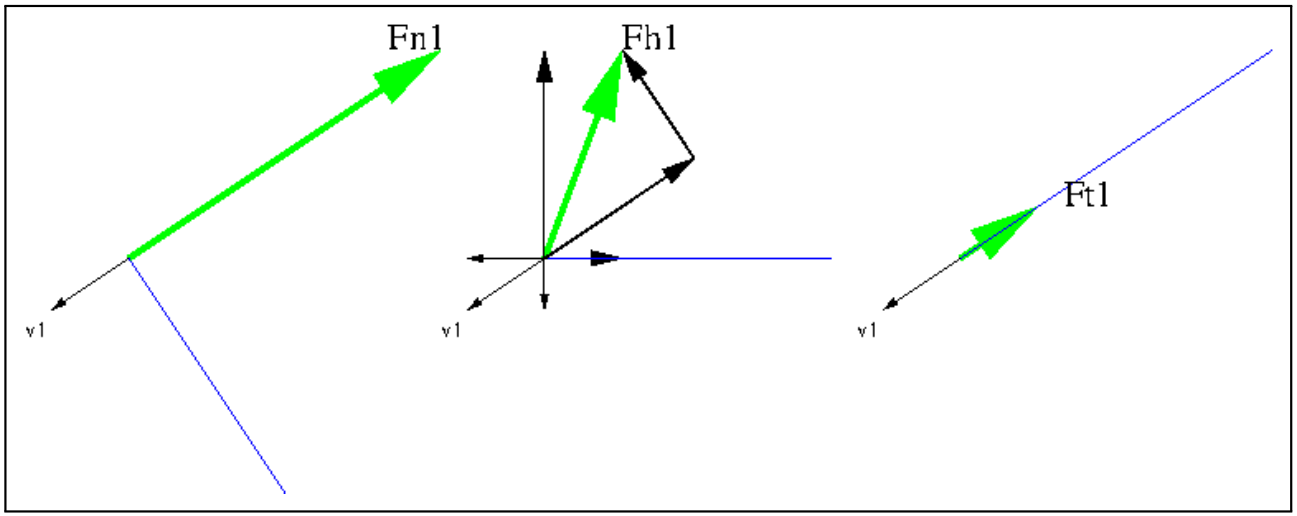

Speed: $v = vn + vt$

Normal force: $Fhn = knFv$

Transverse force: $Fht = ktFv$

with probably $kn > kt$

if $v < vlimit$ weigh by $v/vlimit$

Birger Enerhaug

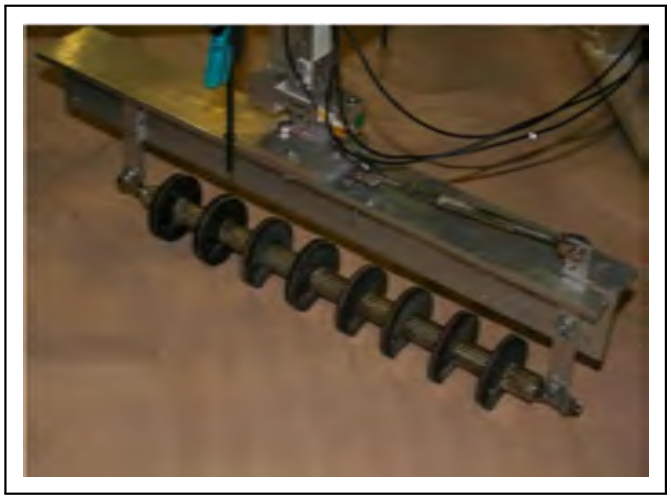

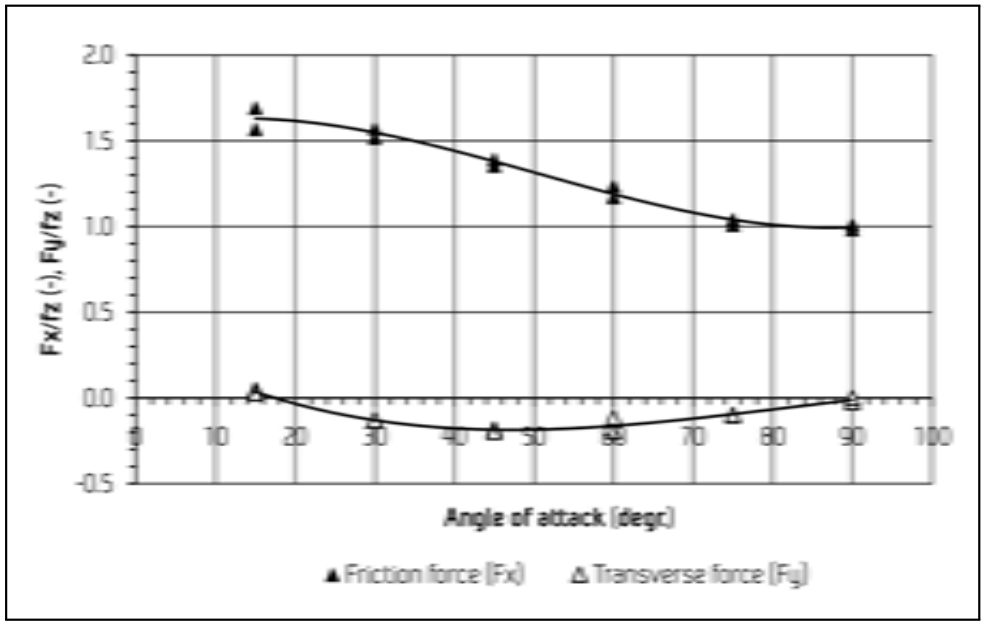

Birger Enerhaug, SINTEF Fisheries and Aquaculture, Trondheim, Norway, DEMat 11, Split, Croatia, 26-28 October, 2011
Drag and transverse forces depends on angle of attack

Appendix A7

A finite element method for netting: application to

Fish cages and fishing gears

A finite element method for netting: application to fish cages and fishing gears

Daniel Priour

December 6, 2012

Contents

Introduction

Chapter 1

Finite element method

1.1 Principle

The finite element method is a method that, at first, approximates the characteristics of a global structure by dividing it into smaller substructures called finite elements. These approximations, in the present case, are performed to estimate efforts on the vertices of these elements. These efforts depend on the position of the vertices of finite elements.

In a second step, these elements are assembled to reconstruct the overall structure and thus obtain the efforts on this structure. These efforts depend on the overall position of the vertices of the elements.

In a third step, the position of the vertices that give a zero overall effort is calculated. This position corresponds to the equilibrium position and therefore to the expected shape of the overall structure.

Field of numerical points

A field of nodes on the structure to be studied is first created. This field of numerical nodes is created so that there are many points in areas of high strain gradient. These nodes serve as the basis for creating finite elements.

The user is often in a position where he does not know *a priori* which areas are with high deformation gradients. The equilibrium positions are calculated successively, refining by adding nodes in areas with steep gradients and removing nodes in areas with low gradients.

Finite elements

Finite elements are created on this field of nodes. These finite elements, in the case of our model, are of several types, depending on whether they are dedicated to cables, bars or nets.

Triangular elements are used for nets (Figure 1.1), since the net is a surface. It seems easier to use the simplest surface, namely, the triangle. The curvature of the net can be represented using several triangular elements. Bar elements are used for cables (Figure 1.2).

1.2 A simple example

The following simple example shows the principle of splitting a global structure into several finite elements. A circle with a diameter of 1m has a perimeter of π ($2\pi R$). To assess this perimeter by the finite element approach, the circle is divided into n identical parts (Figure 1.3). The perimeter is the sum of the length of each circle arc. The length of the arc can be approximated by the circle cord. Each cord has a length of $2Rsin(\frac{\alpha}{2})$.

The perimeter of the circle can be assessed by n times each cord length. Figure 1.4 shows the evaluation accuracy of the perimeter in function of the number of sectors for the approximation. The larger the number of elements, the greater the accuracy.

In other words, a parameter (here the perimeter) can be assessed by dividing the problem into finite elements (sectors) to be able to make acceptable approximations (the arc length approximated by the cord length). The parameter is finally assessed by rebuilding all the finite elements (sum of cord lengths). The principle of the finite element method is to discretize a structure in small (finite) elements to make acceptable approximations in each element and rebuild all the finite elements for assessing parameters on the structure.

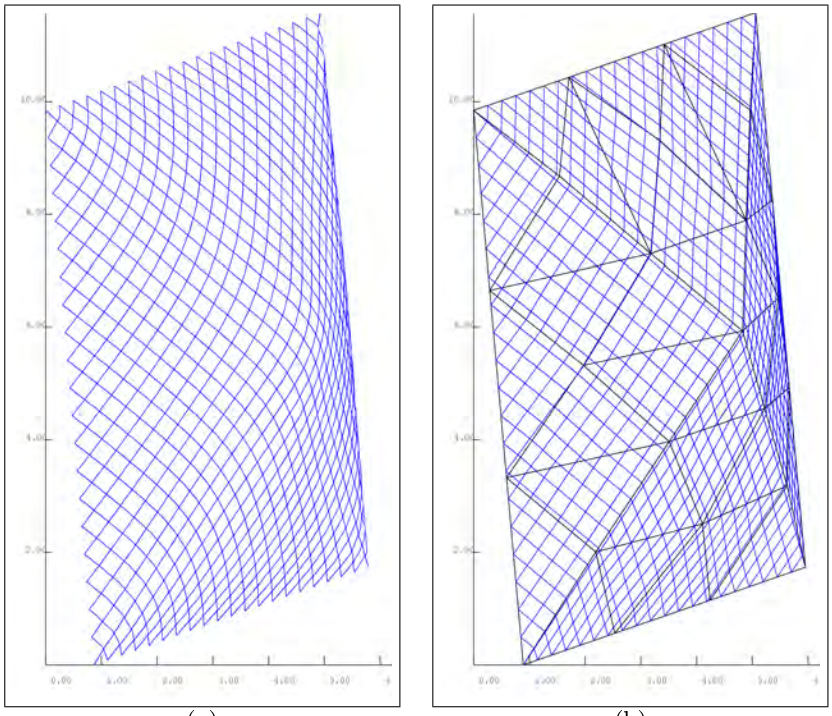

(a) (b)

Figure 1.1: The diamond mesh netting (a) is decomposed into triangular elements (b). The approximation in each triangle is that twines are parallel and therefore have the same deformation, and that the twines are elastic (chapter 3 page 27).

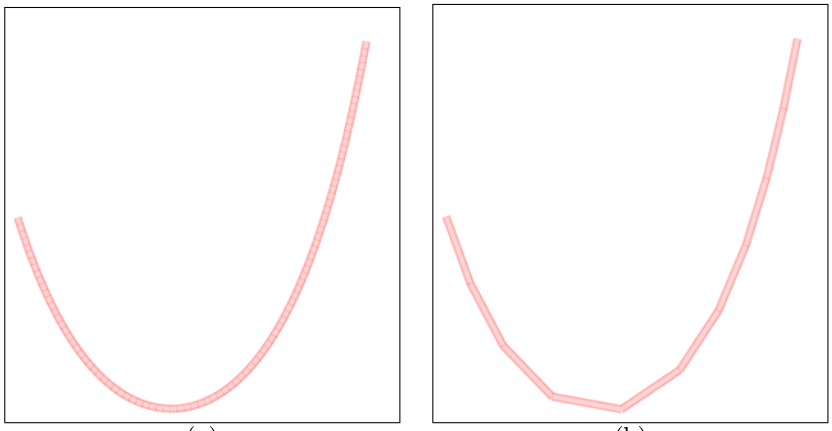

(a) (b)

Figure 1.2: The cable (a) is decomposed into bars elements (b). The approximation in each bar is that bars are straight and elastic (chapter 4 page 71).

1.3 Nodes position, forces on nodes, and stiffness matrix

In case the relationship between efforts on nodes (vertices of the elements) and their position is established, $\mathbf{F}(\mathbf{X})$ is known:

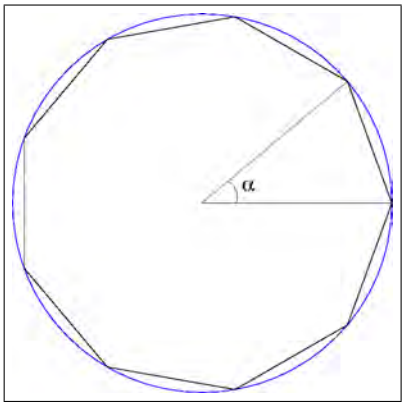

Figure 1.3: Polygon of n cords inside the circle. The length of each cord is 2 R $\sin(\alpha/2)$. The circle perimeter is assessed by n times each cord length.

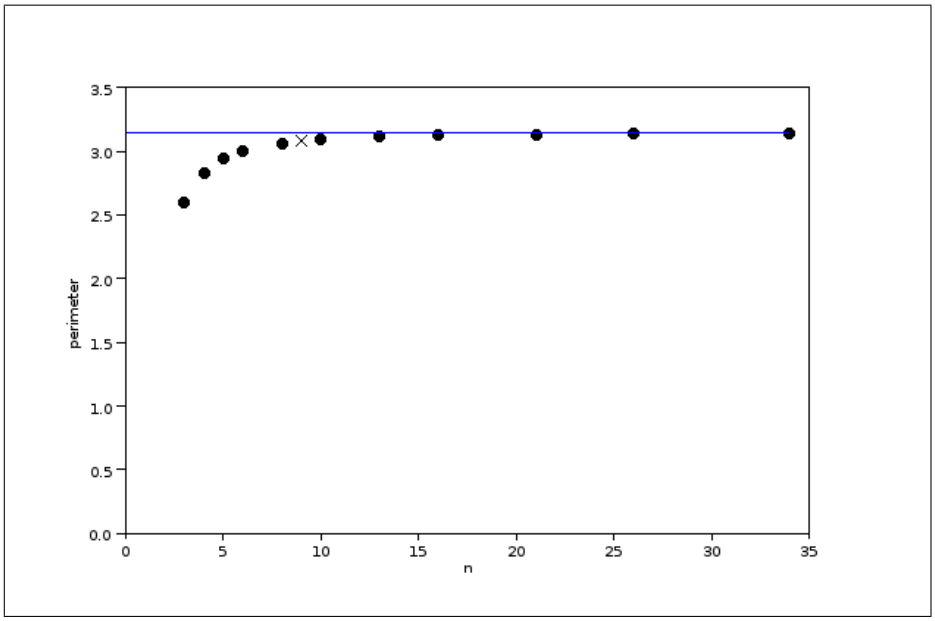

Figure 1.4: Perimeter of the polygon (dots) in function of the number of cords (n) compared with the perimeter of the circle (line). The cross corresponds to the cords in Figure 1.3.

F: force on the nodes (N),

X: node position (m).

The objective of the method is to estimate the equilibrium position ($\mathbf{X}_{final}$), that is to say, such that

$\mathbf{F}(\mathbf{X}_{final}) = 0$

The Newton-Raphson method is generally used to obtain this position ($\mathbf{X}_{final}$) from an initial unbalanced position ($\mathbf{X}_{initial}$). This method iteratively calculates the position at equilibrium. This method relies on the definition of the following derivative:

$$F'(\mathbf{X}) = \frac{\mathbf{F}(\mathbf{X}+\mathbf{h}) - \mathbf{F}(\mathbf{X})}{\mathbf{h}}$$

F': derived efforts with respect to position (N/m),
$\mathbf{h}$: nodes displacement (m).

The displacement $\mathbf{h}$ is sought if $\mathbf{X}$ is not the equilibrium position and such that $\mathbf{X}+\mathbf{h}$ is in equilibrium. Under these conditions:
$\mathbf{F}(\mathbf{X}+\mathbf{h}) = 0$
The previous equation of the derivative gives

$$\mathbf{h} = \frac{\mathbf{F}(\mathbf{X})}{-F'(\mathbf{X})}$$

The term $-F'(\mathbf{X})$ is called the stiffness matrix of the structure. Obviously $\mathbf{h}$ can be large, which means that the definition of the derivative is not completely respected. An iterative calculation is required:

$$\mathbf{X}_{k+1} = \mathbf{X}_k + \frac{\mathbf{F}(\mathbf{X}_k)}{-F'(\mathbf{X}_k)}$$

k: iteration.
Starting from a position $\mathbf{X}_k$, $\mathbf{F}(\mathbf{X}_k)$ and $-F'(\mathbf{X}_k)$ are calculated, then the displacement $\mathbf{h}_k$ is deducted and then the next position $\mathbf{X}_{k+1}$. The iterative calculation is stopped when convergence is achieved, for example when the force $\mathbf{F}(\mathbf{X}_k)$ converges to $\mathbf{0}$.

1.4 Local and global forces and stiffness

In the chapters 3, 4 and 5 the forces and the stiffness are described in local terms.

As mentionned earlier, the structure is split into finite elements in which forces and stiffness are calculated locally. That gives local forces $\mathbf{f}$ and local stiffness k. For example in case of element involving four coordinates, they are as in following:

$$\mathbf{f} = \begin{pmatrix} a \\ b \\ c \\ d \end{pmatrix}$$

$$k = \begin{pmatrix} e & f & g & h \\ i & j & k & l \\ m & n & o & p \\ q & r & s & t \end{pmatrix}$$

To reassemble the finite elements in the global structure, the local forces and the local stiffness have to be added to the global ones ($\mathbf{F}$, K).

For example, if $\mathbf{f}$ and k define the force and the stiffness on an element that involves node components 3, 4, 7, and 8, taking this element into account in the global structure would mean that the local force $\mathbf{f}$ and stiffness k have to be added to the global force $\mathbf{F}$ and stiffness K, as in the following:

$$\mathbf{F}(3) = \mathbf{F}(3) + a$$

$$\mathbf{F}(4) = \mathbf{F}(4) + b$$

$$\mathbf{F}(7) = \mathbf{F}(7) + c$$

$$\mathbf{F}(8) = \mathbf{F}(8) + d$$

$$\begin{array}{cccc} K(3,3) = K(3,3) + e & K(3,4) = K(3,4) + f & K(3,7) = K(3,7) + g & K(3,8) = K(3,8) + h \\ K(4,3) = K(4,3) + i & K(4,4) = K(4,4) + j & K(4,7) = K(4,7) + k & K(4,8) = K(4,8) + l \\ K(7,3) = K(7,3) + m & K(7,4) = K(7,4) + n & K(7,7) = K(3,7) + o & K(7,8) = K(7,8) + p \\ K(8,3) = K(8,3) + q & K(8,4) = K(8,4) + r & K(8,7) = K(8,7) + s & K(8,8) = K(8,8) + t \end{array}$$

In other words:

$$\mathbf{F} = \begin{pmatrix} \cdot \\ \cdot \\ \cdot + a \\ \cdot + b \\ \cdot \\ \cdot \\ \cdot + c \\ \cdot + d \\ \cdot \\ \cdot \end{pmatrix}$$

$$K = \begin{pmatrix} \cdot & \cdot & \cdot & \cdot & \cdot & \cdot & \cdot & \cdot & \cdot & \cdot \\ \cdot & \cdot & \cdot & \cdot & \cdot & \cdot & \cdot & \cdot & \cdot & \cdot \\ \cdot & \cdot & \cdot + e & \cdot + f & \cdot & \cdot & \cdot + g & \cdot + h & \cdot & \cdot \\ \cdot & \cdot & \cdot + i & \cdot + j & \cdot & \cdot & \cdot + k & \cdot + l & \cdot & \cdot \\ \cdot & \cdot & \cdot & \cdot & \cdot & \cdot & \cdot & \cdot & \cdot & \cdot \\ \cdot & \cdot & \cdot & \cdot & \cdot & \cdot & \cdot & \cdot & \cdot & \cdot \\ \cdot & \cdot & \cdot + m & \cdot + n & \cdot & \cdot & \cdot + o & \cdot + p & \cdot & \cdot \\ \cdot & \cdot & \cdot + q & \cdot + r & \cdot & \cdot & \cdot + s & \cdot + t & \cdot & \cdot \\ \cdot & \cdot & \cdot & \cdot & \cdot & \cdot & \cdot & \cdot & \cdot & \cdot \\ \cdot & \cdot & \cdot & \cdot & \cdot & \cdot & \cdot & \cdot & \cdot & \cdot \end{pmatrix}$$

1.5 Symmetry

In the case of symmetrical structures in a symmetrical environment it could be advantageous to use this symmetry to reduce the node number and therefore the computation times.

Figure 1.5 shows a simple bar with a symmetry plane. The plane of symmetry is OYZ and only the node of components a, b, and c, is on the plane of symmetry.

The calculation of force vector on the bar P regardless of the symmetry will give a force such as (cf. Figure 1.5):

$$\mathbf{F} = \begin{vmatrix} F_a \\ F_b \\ F_c \\ F_d \\ F_e \\ F_f \end{vmatrix}$$

The stiffness matrix would be:

$$K = \begin{vmatrix} K_{aa} & K_{ab} & K_{ac} & K_{ad} & K_{ae} & K_{af} \\ K_{ba} & K_{bb} & K_{bc} & K_{bd} & K_{be} & K_{bf} \\ K_{ca} & K_{cb} & K_{cc} & K_{cd} & K_{ce} & K_{cf} \\ K_{da} & K_{db} & K_{dc} & K_{dd} & K_{de} & K_{df} \\ K_{ea} & K_{eb} & K_{ec} & K_{ed} & K_{ee} & K_{ef} \\ K_{fa} & K_{fb} & K_{fc} & K_{fd} & K_{fe} & K_{ff} \end{vmatrix}$$

In this case the ranking of the node coordinates is a, b, c, d, e, f.

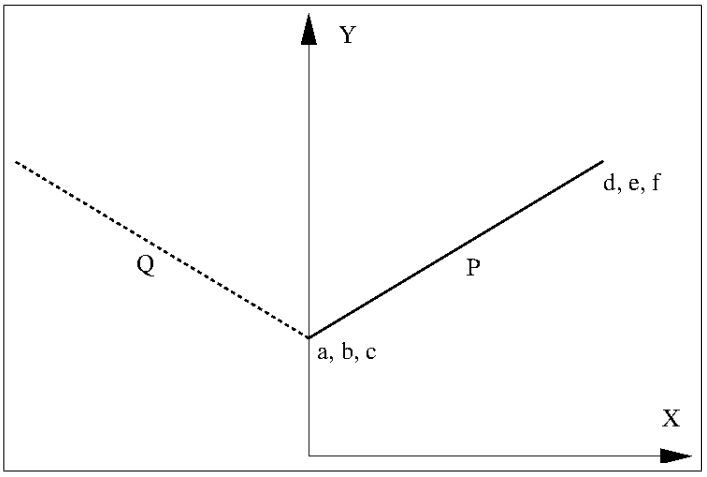

Figure 1.5: The bar P has a node (a, b, c) on the symmetry plane. The other node (d, e, f) is outside the symmetry plane. The symmetric bar is Q.

The calculation of the total force vector on the bar taking into account the symmetry will give a force such as:

$$\mathbf{F} = \left| \begin{array}{ccc} F_a & - & F_a \\ F_b & + & F_b \\ F_c & + & F_c \\ F_d & + & 0 \\ F_e & + & 0 \\ F_f & + & 0 \end{array} \right|$$

The stiffness matrix would be:

$$K = \left| \begin{array}{cccccc} K_{aa} + K_{aa} & K_{ab} - K_{ab} & K_{ac} - K_{ac} & K_{ad} & K_{ae} & K_{af} \\ K_{ba} - K_{ba} & K_{bb} + K_{bb} & K_{bc} + K_{bc} & K_{bd} & K_{be} & K_{bf} \\ K_{ca} - K_{ca} & K_{cb} + K_{cb} & K_{cc} + K_{cc} & K_{cd} & K_{ce} & K_{cf} \\ K_{da} & K_{db} & K_{dc} & K_{dd} & K_{de} & K_{df} \\ K_{ea} & K_{eb} & K_{ec} & K_{ed} & K_{ee} & K_{ef} \\ K_{fa} & K_{fb} & K_{fc} & K_{fd} & K_{fe} & K_{ff} \end{array} \right|$$

That gives for a symmetry plane OXY passing by the node of coordinates a, b, c:

$$\mathbf{F} = \left| \begin{array}{c} 0 \\ 2.F_b \\ 2.F_c \\ F_d \\ F_e \\ F_f \end{array} \right|$$

$$K = \left| \begin{array}{cccccc} 2.K_{aa} & 0 & 0 & K_{ad} & K_{ae} & K_{af} \\ 0 & 2.K_{bb} & 2.K_{bc} & K_{bd} & K_{be} & K_{bf} \\ 0 & 2.K_{cb} & 2.K_{cc} & K_{cd} & K_{ce} & K_{cf} \\ K_{da} & K_{db} & K_{dc} & K_{dd} & K_{de} & K_{df} \\ K_{ea} & K_{eb} & K_{ec} & K_{ed} & K_{ee} & K_{ef} \\ K_{fa} & K_{fb} & K_{fc} & K_{fd} & K_{fe} & K_{ff} \end{array} \right|$$

That gives for a symmetry plane OYZ passing by the node of coordinates a, b, c:

$$\mathbf{F} = \left| \begin{array}{c} 2.F_a \\ 0 \\ 2.F_c \\ F_d \\ F_e \\ F_f \end{array} \right|$$

$$K = \left| \begin{array}{cccccc} 2.K_{aa} & 0 & 2.K_{ac} & K_{ad} & K_{ae} & K_{af} \\ 0 & 2.K_{bb} & 0 & K_{bd} & K_{be} & K_{bf} \\ 2.K_{bc} & 0 & 2.K_{cc} & K_{cd} & K_{ce} & K_{cf} \\ K_{da} & K_{db} & K_{dc} & K_{dd} & K_{de} & K_{df} \\ K_{ea} & K_{eb} & K_{ec} & K_{ed} & K_{ee} & K_{ef} \\ K_{fa} & K_{fb} & K_{fc} & K_{fd} & K_{fe} & K_{ff} \end{array} \right|$$

That gives for a symmetry plane OZX passing by the node of coordinates a, b, c:

$$\mathbf{F} = \begin{vmatrix} 2.F_a \\ 2.F_b \\ 0 \\ F_d \\ F_e \\ F_f \end{vmatrix}$$

$$K = \begin{vmatrix} 2.K_{aa} & 2.K_{ab} & 0 & K_{ad} & K_{ae} & K_{af} \\ 2.K_{ba} & 2.K_{bb} & 0 & K_{bd} & K_{be} & K_{bf} \\ 0 & 0 & 2.K_{cc} & K_{cd} & K_{ce} & K_{cf} \\ K_{da} & K_{db} & K_{dc} & K_{dd} & K_{de} & K_{df} \\ K_{ea} & K_{eb} & K_{ec} & K_{ed} & K_{ee} & K_{ef} \\ K_{fa} & K_{fb} & K_{fc} & K_{fd} & K_{fe} & K_{ff} \end{vmatrix}$$

1.6 Boundary conditions

There are two kinds of boundary conditions: the mechanical and the geometric.

The mechanical boundary conditions are defined through forces on the structure. Such boundary conditions could be the effect of the sea bed; for example, a mooring chain lands on the bottom. This specific case is described in section 5.2 (page 89).

The geometric boundary conditions consist here in displacement boundary conditions; for example, an anchor in the sea bed could be taken into account by a null displacement, or a boat towing a gear could be defined with a null displacement in moving water. These geometric conditions are actually the conditions discussed in this section.

A null displacement for node coordinate c could be taken into account by modifying the force and the stiffness matrix. Generally speaking, the force and the matrix stiffness are such as:

$$\mathbf{F} = \begin{vmatrix} F_a \\ F_b \\ F_c \\ F_d \\ F_e \\ F_f \end{vmatrix}$$

$$K = \begin{vmatrix} K_{aa} & K_{ab} & K_{ac} & K_{ad} & K_{ae} & K_{af} \\ K_{ba} & K_{bb} & K_{bc} & K_{bd} & K_{be} & K_{bf} \\ K_{ca} & K_{cb} & K_{cc} & K_{cd} & K_{ce} & K_{cf} \\ K_{da} & K_{db} & K_{dc} & K_{dd} & K_{de} & K_{df} \\ K_{ea} & K_{eb} & K_{ec} & K_{ed} & K_{ee} & K_{ef} \\ K_{fa} & K_{fb} & K_{fc} & K_{fd} & K_{fe} & K_{ff} \end{vmatrix}$$

When the null displacement for node coordinate c is taken into account, the force and the stiffness matrix become:

$$\mathbf{F} = \begin{vmatrix} F_a \\ F_b \\ 0 \\ F_d \\ F_e \\ F_f \end{vmatrix}$$

$$K = \begin{vmatrix} K_{aa} & K_{ab} & 0 & K_{ad} & K_{ae} & K_{af} \\ K_{ba} & K_{bb} & 0 & K_{bd} & K_{be} & K_{bf} \\ 0 & 0 & 1 & 0 & 0 & 0 \\ K_{da} & K_{db} & 0 & K_{dd} & K_{de} & K_{df} \\ K_{ea} & K_{eb} & 0 & K_{ed} & K_{ee} & K_{ef} \\ K_{fa} & K_{fb} & 0 & K_{fd} & K_{fe} & K_{ff} \end{vmatrix}$$

These modifications of force and stiffness matrix ensure that the displacement of coordinate c is null.

Chapter 2

Equilibrium calculation

2.1 Newton-Raphson method

Finite element methods generally use the Newton-Raphson method (Deuflhard 2004) for the calculation of the equilibrium position of a mechanical structure. The equilibrium position corresponds to that position of the structure in which the sum of forces equals 0. In what follows a few simple examples are given to explain the method under three cases: one dimension, two dimensions and several dimensions.

2.1.1 One dimension

A spring (Figure 2.1) equilibrium is reached when the weight is equilibrated by the spring force. At this position the sum of forces equals 0. This position can be calculated using the Newton-Raphson method. In this example there is just one dimension: the vertical position (x) of the mass relatively to the spring fixation which also equals the length of the spring.

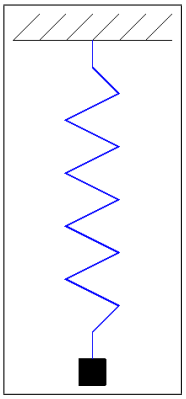

Figure 2.1: The equilibrium of the spring is due to the mass weight and the spring force.

The spring equilibrium is calculated by writing the force on the mass: the weight is $-Mg$ (N), and the force of the spring is $+K\frac{x-l_0}{l_0}$ (N).

With

M: mass (kg),

g: acceleration of gravity (m/s^2),

K: spring stiffness (N),

x: position of the mass along the spring axis relative to the fixed point of the spring (m),

x: length of the stretched spring (m).

In this example the stiffness is not constant in order to give a clearer explanation of the Newton-Raphson method. K is equals to Ax. That means that longer the spring is, the stiffer it is.

The sum of forces on the mass (curve on figure 2.2) is

$$F(x) = K\frac{x - l_0}{l_0} - Mg$$

or, following the previous relations,

$$F(x) = Ax\frac{x - l_0}{l_0} - Mg$$

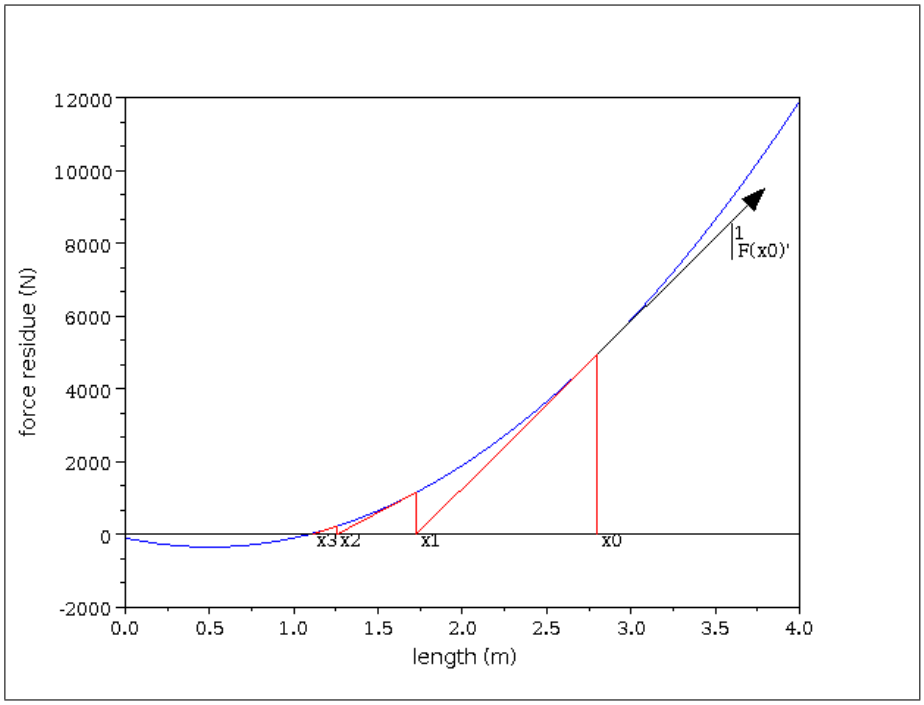

Figure 2.2: Sum of forces on the mass function of spring length. Three Newton-Raphson iterations starting at $x = 2.8m$ are displayed. The vector tangent at x_0 is shown.

Obviously at the equilibrium $F(x) = 0$. It is clear that this simple equation has an analytical solution, which is

$$x = \frac{\sqrt{l_0\,A\,(4\,g\,M + l_0\,A)} + l_0\,A}{2\,A}$$

The Newton-Raphson method could be used to find the length of the spring (x) at the equilibrium. This method requires knowing the force and the derivative of the force relatively to the position.

The method is iterative and approximates the force curve by its tangent (shown in Figure 2.2). From a position (x_k), the force ($F(x_k)$) and the derivative of force ($F'(x_k)$) are calculated, and a new position (x_{k+1}) can be found. This new position is generally closer to the equilibrium and is calculated as follows:

$$x_{k+1} = x_k + \frac{F(x_k)}{-F'(x_k)}$$

Figure 2.2 shows three iterations with an initial value x_0 of the spring length of 2.8m.
With:
The stiffness $A = 1000N/m$,
The mass $M = 10kg$,
The acceleration of gravity $g = 9.81m/s^2$,
The unstretched length of the spring $l_0 = 1m$.
The stretched length at the equilibrium is 1.09m. That means that the spring stretches 9%.

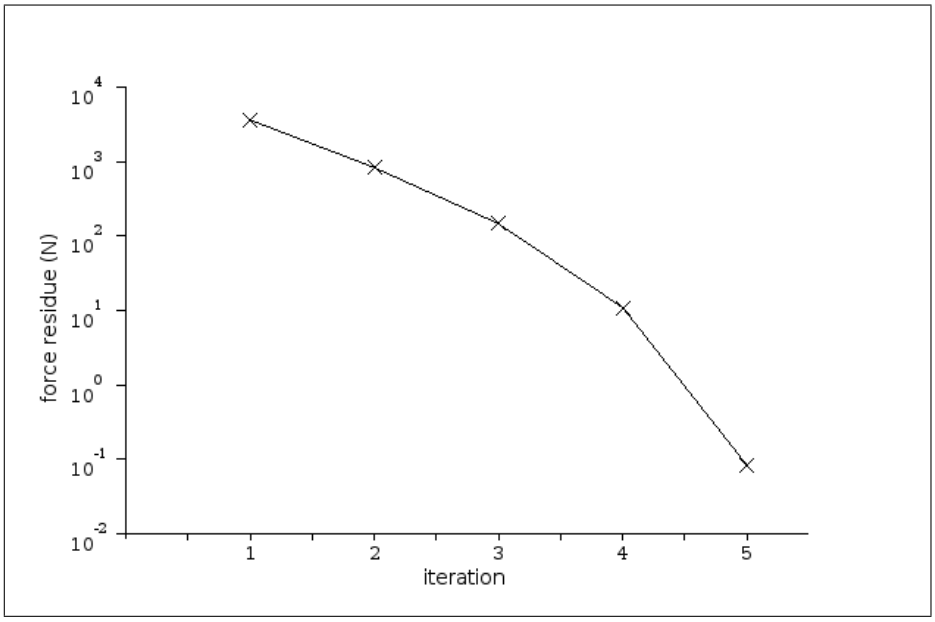

Figure 2.3: Residue of force for each Newton-Raphson method iteration.

After five iterations the equilibrium is reached or more exactly $|F(x)| < 0.1N$. The figure 2.2 shows 3 iterations along the curve of force. Figure 2.3 represents the reduction of the force residue ($|F(x)|$) with the five iterations.

2.1.2 Two dimensions

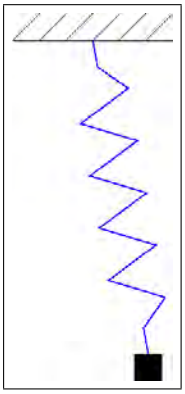

Figure 2.4: Spring with two degrees of freedom: the vertical and horizontal positions of the mass. The equilibrium is due to the mass weight and the spring force.

In this section a simple example in two dimensions is given (Figure 2.4): a spring with two degrees of freedom, i.e., the horizontal (x) and the vertical (y) positions of the mass relative to the spring fixation. The equilibrium of the system is due to the position of the mass along the vertical and the horizontal. Figure 2.5 shows the variation of the norm of the residue of force ($\sqrt{F_x^2 + F_y^2}$) on the mass due to the positions along x and y of the mass. The equilibrium point is noted by the largest dot.

The stiffness (K) of the spring is not constant: K is equal to Al. That means that the longer the spring is, the stiffer it is. In this condition the horizontal and vertical forces on the mass are due to the spring length and the weight of the mass:

$$F_x = T\frac{x}{l}$$

$$F_y = T\frac{y}{l} - Mg$$

With:

$$T = Al\frac{l - l_0}{l_0}$$

$$l = \sqrt{x^2 + y^2}$$

In this case the derivative of the forces is calculated relatively to x and y:

$$\frac{\partial F_x}{\partial x} = A\frac{l - l_0}{l_0} + A\frac{x^2}{ll_0}$$

$$\frac{\partial F_x}{\partial y} = A\frac{xy}{ll_0}$$

$$\frac{\partial F_y}{\partial x} = A\frac{yx}{ll_0}$$

$$\frac{\partial F_y}{\partial y} = A\frac{l - l_0}{l_0} + A\frac{y^2}{ll_0}$$

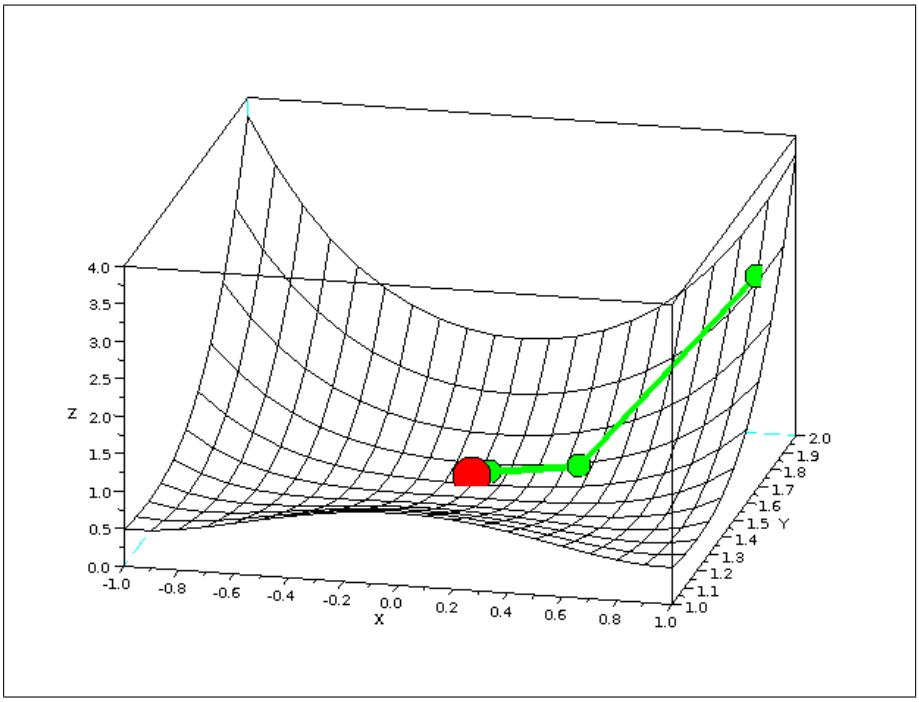

Figure 2.5: Norm of the force ($Z = \sqrt{F_x^2 + F_y^2}$) function of mass coordinates (X, Y). The largest dot is the equilibrium position. The smallest dots are the Newton-Raphson iterations starting at $x = 0.9m$ and $y = 1.9m$.

The Newton-Raphson method accesses the equilibrium solution through iterations. At each iteration the new position is calculated by the following relation:

$$\mathbf{X}_{k+1} = \mathbf{X}_k + \frac{\mathbf{F}(\mathbf{X}_k)}{-F'(\mathbf{X}_k)}$$

With:

$$\mathbf{X}_k = \begin{vmatrix} x_k \\ y_k \end{vmatrix}$$

$$\mathbf{F}(\mathbf{X}_k) = \begin{vmatrix} F_x(X_k) \\ F_y(X_k) \end{vmatrix}$$

The ratio $\frac{\mathbf{F}(\mathbf{X}_k)}{-F'(\mathbf{X}_k)}$ is the displacement $\mathbf{h}$, such as $\mathbf{F}(\mathbf{X}_k) = -F'(\mathbf{X}_k)\mathbf{h}$.

With these equations the equilibrium position is assessed (Figure 2.5). Figure 2.6 represents the reduction of the force residue with the iterations.

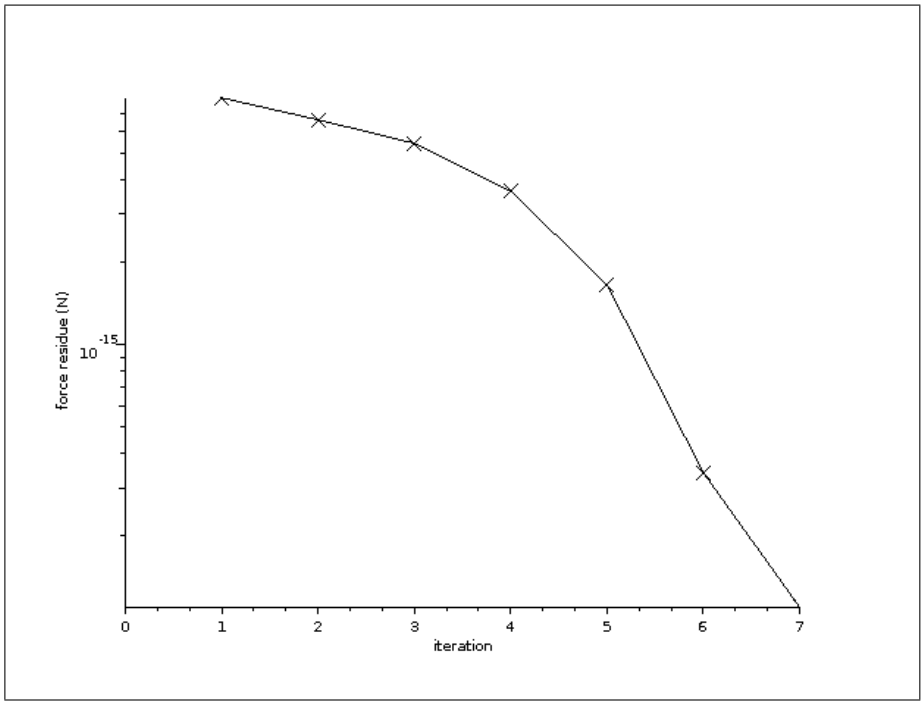

Figure 2.6: Residue of force ($\sqrt{F_x^2 + F_y^2}$) for each Newton-Raphson method iteration.

2.1.3 Several dimensions

Main variables

The positions of the nodes are in vector $\mathbf{X}$, the forces on the nodes are in vector $\mathbf{F}$, and the stiffness matrix is K; x_i and F_i refer to the same node along the same axis.

These variables are as follows:

$$\mathbf{X} = \begin{vmatrix} x_1 \\ x_2 \\ . \\ . \\ x_n \end{vmatrix}$$

$$\mathbf{F} = \begin{vmatrix} F_1 \\ F_2 \\ . \\ . \\ F_n \end{vmatrix}$$

$$K = \begin{vmatrix} -\frac{\partial F_1}{\partial x_1} & -\frac{\partial F_1}{\partial x_2} & . & . & -\frac{\partial F_1}{\partial x_n} \\ -\frac{\partial F_2}{\partial x_1} & -\frac{\partial F_2}{\partial x_2} & . & . & -\frac{\partial F_2}{\partial x_n} \\ . & . & . & . & . \\ . & . & . & . & . \\ -\frac{\partial F_n}{\partial x_1} & -\frac{\partial F_n}{\partial x_2} & . & . & -\frac{\partial F_n}{\partial x_n} \end{vmatrix}$$

From these three variables the displacement vector ($\mathbf{h}$) can be calculated by solving the following system of linear equations:

$$\mathbf{h}K = \mathbf{F}$$

Iterations

As mentioned earlier, the Newton-Raphson-method is an iterative one. The steps are as follows:

From the position ($\mathbf{X}_k$) of the nodes resulting from iteration k:

$$\mathbf{X}_k = \begin{vmatrix} x_{k1} \\ x_{k2} \\ . \\ . \\ x_{kn} \end{vmatrix}$$

The force ($\mathbf{F}_k$) on the nodes and the stiffness (K_k) matrix are calculated:

$$\mathbf{F}_k = \begin{vmatrix} F_{k1} \\ F_{k2} \\ . \\ . \\ F_{kn} \end{vmatrix}$$

$$K_k = \begin{vmatrix} K_{k11} & K_{k12} & . & . & K_{k1n} \\ K_{k21} & K_{k22} & . & . & K_{k2n} \\ . & . & . & . & . \\ . & . & . & . & . \\ K_{kn1} & K_{kn2} & . & . & K_{knn} \end{vmatrix}$$

The node displacements ($\mathbf{h}_k$) are calculated:

$$\mathbf{h}_k K_k = \mathbf{F}_k$$

The new position of nodes are deduced:

$$\mathbf{X}_{k+1} = \mathbf{X}_k + \mathbf{h}_k$$

2.1.4 Singularity of the stiffness matrix

In some cases the stiffness matrix (K) could be singular. In this case solving $\mathbf{h}K = \mathbf{F}$ (section 2.1.3 page 20) could lead to a very large displacement ($h_i >> 1$) and to divergence of the method.

An example can be shown with the unstretched horizontal bar of Figure 2.7. This bar has two extremities. If the first extremity (on the left on Figure 2.7) has the horizontal and vertical coordinates $(0, 0)$, the position vector is:

$$\mathbf{X} = \begin{vmatrix} 0 \\ 0 \\ x_3 \\ 0 \end{vmatrix}$$

With $x_3 \neq 0$

If the force on the second extremity is vertical, the force vector is:

$$\mathbf{F} = \begin{vmatrix} 0 \\ 0 \\ 0 \\ F_4 \end{vmatrix}$$

With $F_4 \neq 0$

As we will see in section 4.2 (page 73) the stiffness matrix is:

$$K = \begin{vmatrix} K_{11} & 0 & -K_{11} & 0 \\ 0 & 0 & 0 & 0 \\ -K_{11} & 0 & K_{11} & 0 \\ 0 & 0 & 0 & 0 \end{vmatrix}$$

The matrix is singular. This is due to the derivative $\frac{\partial F_4}{\partial x_4}$, which is equal to 0 in this case of an unstretched horizontal bar. i) If the bar is not horizontal this derivative will not be equal to 0, because the derivative of the bar length will not equal 0. ii) If the bar is in tension (or compression), even horizontal, the derivative $\frac{\partial F_4}{\partial x_4}$ will not equal 0 because the derivative of the tension direction is not equal to 0.

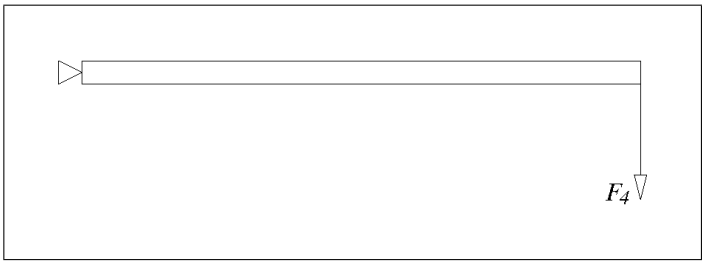

Figure 2.7: This bar is articulated around its left extremity. A vertical force (F_4) is applied on the right extremity. This unstretched bar displays a zero stiffness along the vertical.

To avoid problems due to singularity, precautions are available, as described below.

Additional stiffness

A simple way is to add an arbitrary value (α) along the diagonal of the stiffness matrix, such that the previous matrix becomes:

$$K = \begin{vmatrix} K_{11}+\alpha & 0 & -K_{11} & 0 \\ 0 & \alpha & 0 & 0 \\ -K_{11} & 0 & K_{11}+\alpha & 0 \\ 0 & 0 & 0 & \alpha \end{vmatrix}$$

The added value (α) could decrease along the Newton-Raphson iterations. This added value (α) does not modify the equilibrium position, but only the way to reach this equilibrium.

Additional mechanical behaviour

Another way to remove singularity is to add further mechanical behaviour. For example, if this bar is in a fluid, air, or water, a vertical displacement will generate a drag in the opposite direction, meaning that the components of the stiffness matrix K_{22} and K_{44} will be not equal to 0.

Displacement limit

A displacement limit could be imposed to avoid too large a value:

$$\mathbf{h}K = \mathbf{F}$$

$$\begin{aligned} if \mathbf{h}_i > limit \quad \mathbf{h}_i &= limit \\ if \mathbf{h}_i \leq limit \quad \mathbf{h}_i &= \mathbf{h}_i \end{aligned}$$

2.2 Other resolution methods

2.2.1 Newmark method

The Newmark method is used to find the equilibrium position of a mechanical structure. The following example in one dimension explains the method in a simplified way.

The method consists first in calculating forces on the structure, then calculating the acceleration on the structure using the dynamic equation ($F = M\gamma$). From this acceleration and using a time step, the speed and the new position of the structure can be calculated (Chang 2004).

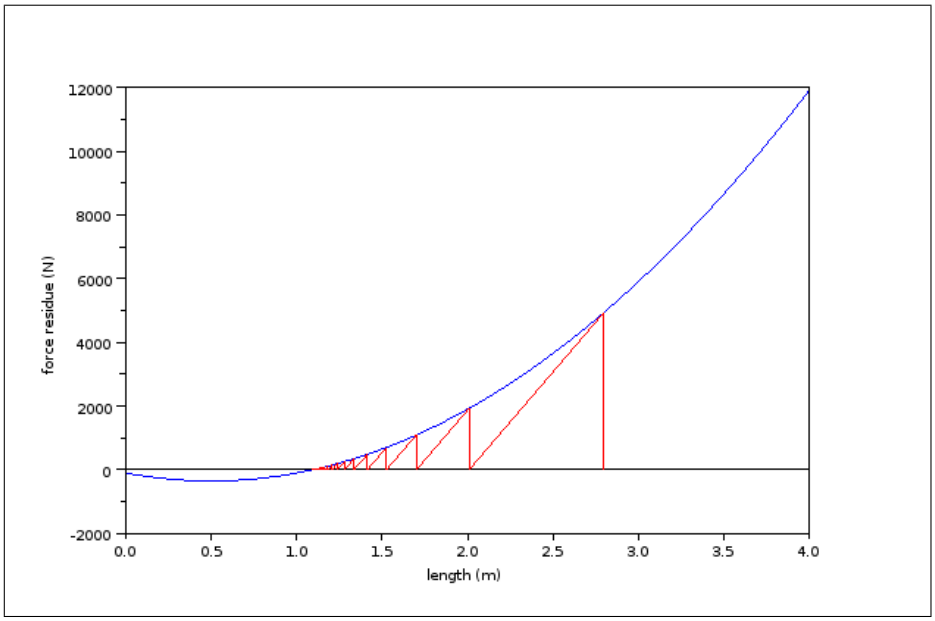

Figure 2.8: Force on the mass function of spring length and Newmark explicit method iterations.

For the example displayed in Figure 2.1, the equilibrium calculation follows the path shown in Figure 2.8 with a time step of $0.04s$. Figure 2.9 shows the residue of force. This calculation follows the Newmark explicit method (Chang 2004).

2.2.2 Energy minimization

This method consists of finding the position of the structure that leads to the minimum of the energy. The energy involved here is the energy due to the conservative forces only. A conservative force is a force that leads to a variation of energy between two positions independent of the path between these two positions. The main conservative forces involved in marine structures are weight and tension in elastic cables and netting twines.

In these cases the energy between two positions are quite simple to calculate:

$$E_W = W\Delta h$$

$$E_T = \frac{1}{2}K\Delta x^2$$

E_W: energy due to the weight (J),

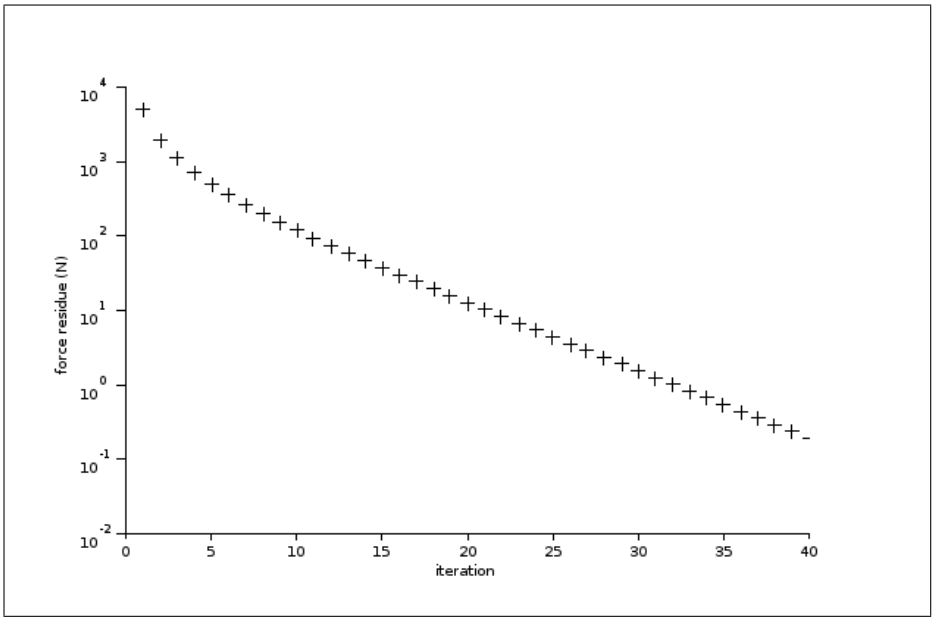

Figure 2.9: Residue of force for each Newmark explicit method iterations.

W: weight (N),
Δh: altitude variation between the two positions (m),
E_T: energy due to the tension (J),
K: constant cable stiffness (N/m),
Δx: cable length variation between the two positions (m).

Some forces are not conservative, as in the case of drag force. In such case the energy consumed by the drag depends on the path followed by the structure between the two positions.

Due to non conservative forces, the method of minimization of energy is not quite adapted to solve the equilibrium of marine structures. In case this method is used, the drag forces could be transformed into constant force.

Chapter 3

The triangular finite element for netting

3.1 State-of-the-art of numerical modelling for nets

3.1.1 Constitutive law for nets

There is little or no published work on the constitutive law for nets. Only Rivlin (1955), to our knowledge, begins to express the stresses in a net surface, but only under conditions of symmetrical deformation twine. If such constitutive law could be defined, usual finite element softwares could be adapted for nettings.

3.1.2 Twine numerical method

The twine numerical method includes almost all the work on numerical modelling of the net (Ferro 1988; Bessonneau and Marichal 1998; Niedzwiedz and Hopp 1998; Tsukrov et al. 2003; Le Dret et al. 2004; Lee et al. 2005). The initial idea is simple: the twines of the net are modelled by bars (called here numerical twines). Then a few adjustments are required.

The twines could be modelled by two bars to account for the shortening, which appears as an angle between the bars. The twines could be modelled with a single bar, but Young's modulus in compression is almost zero to account for the shortening. Given the large number of twines in some structures (up to one million), a numerical bar refers to several true twines (Figure 3.1). This is called globalization.

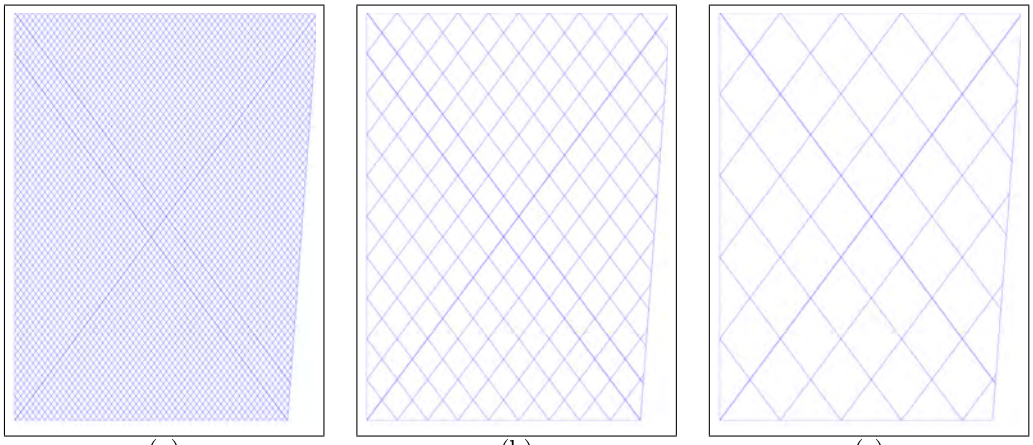

(a) (b) (c)

Figure 3.1: Control net 50 meshes high by 50 and 45 wide (a), with a ratio of globalization of 5 (b) and 10 (c).

The major difficulty with this method of globalization lies in the description of the net by numerical twines. Indeed, a structure is very often the assembly of several panels of nets. Therefore, the creation of numerical twines in a panel will generate nodes on its contour. These nodes are the basis for the creation of numerical twines of the adjacent panel (Figures 3.2 and Figure 3.3).

Figure 3.2 (a) shows four panels (50 by 50 meshes) whose numerical twines connect perfectly (Figure 3.2 (b)): the nodes on the edges are perfectly aligned with the nodes of the adjacent panels.

Figure 3.3 (a) shows the same example, except that panel 1 is only 45 meshes horizontally. In this case the nodes on the borders do not connect perfectly between panels 4 and 1 (Figure

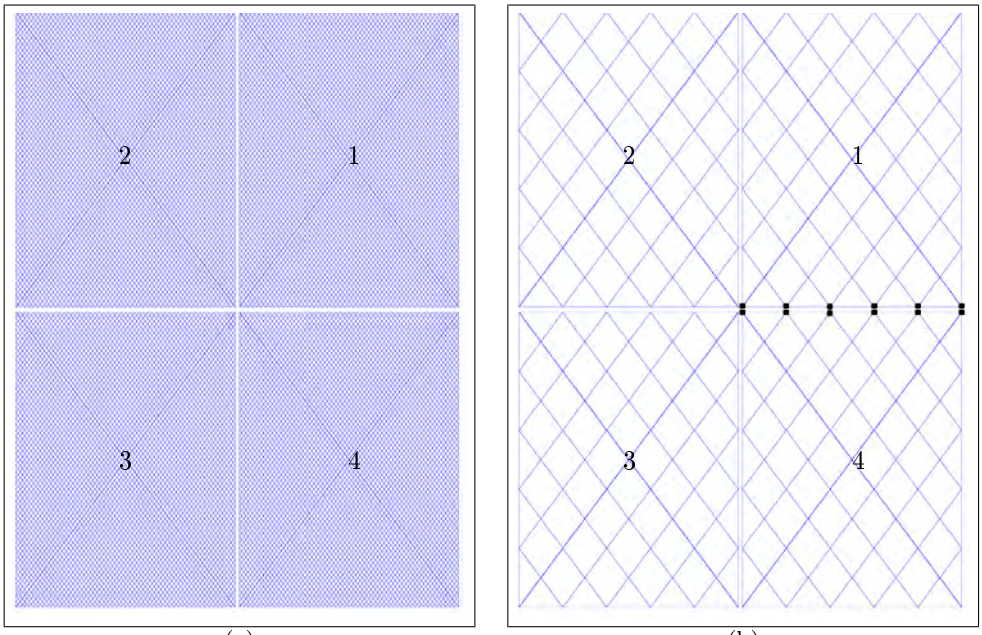

Figure 3.2: Structure of four panels of 50 by 50 meshes (a) discretized in numerical twines (b; globalization ratio of 10): the connection between numerical nodes on the borders of panels is perfect (black dots for the border between panels).

3.3 (b)), whereas the connections are perfect on the other three seams. This approach requires facilities such modification of the design of the netting panels. These facilities are not well described in the literature dedicated to this method.

3.2 The finite element for netting

Triangular elements have been developed to model the net (Figure 3.4). A number of approximations are made in these triangular elements, with the aim of calculating the forces at the vertices of these elements. These are calculated based on the positions of the vertices. The basic assumption in modelling nets by triangular elements is that the twines remain parallel. Under these conditions the twines of the same direction have the same deformation. The second assumption is that the twines are modelled as elastic rods.

One difficulty with the method of numerical globalized twines (or numerical twines) was described earlier: nodes on the edges of the panels do not always coincide perfectly (Figure 3.3 (b)). This difficulty disappears with triangular elements, since the discretization of a netting panel is independent of the discretization of adjacent panels, except on the border. The same panels of Figure 3.3 are discretized in Figure 3.5 with triangular elements. Panel 2 in (Figure 3.5 (a)) is discretized with large triangular elements and in (Figure 3.5 (b)) with smaller elements. It is clear that triangular element discretization is done very easily, unlike the numerical twines technique. This flexibility in the creation of triangular elements overcomes the cumbersome tool for creating globalized twines. This burden results from many different cases to be processed and consequently adjustments that sometimes make it impossible to fully describe the structure

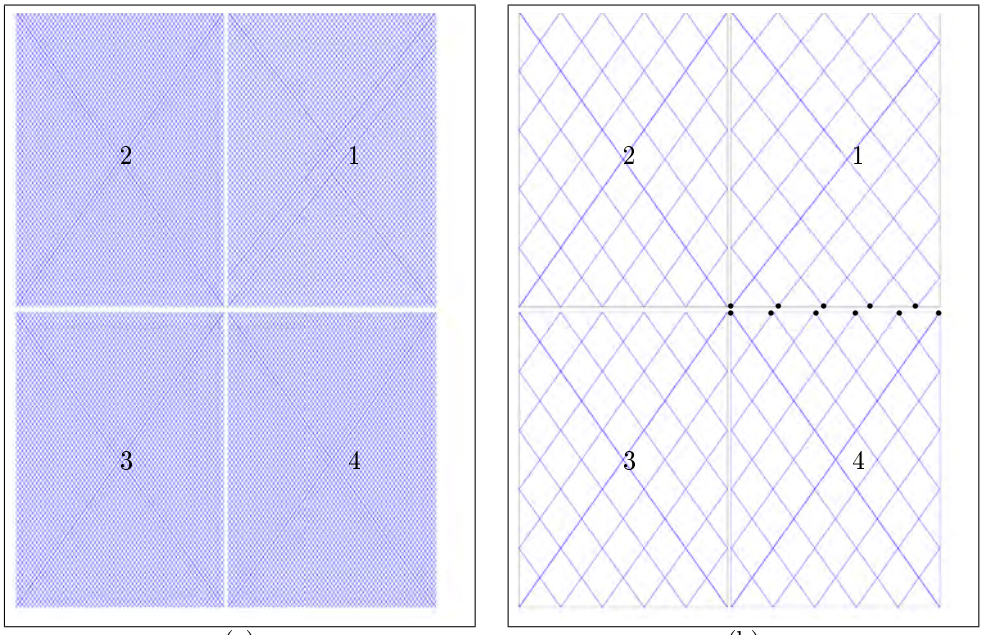

(a) (b)

Figure 3.3: (a) Four netting panels 50 by 50 meshes except for panel 1, which has only 45 meshes horizontally. (b) The globalization of 10 leads the nodes on the common border of panels 1 and 4 to not connect perfectly: panel 1 has five nodes on its bottom border, while the top border of panel 4 has six nodes (black dots).

to be studied with the method of numerical twines.

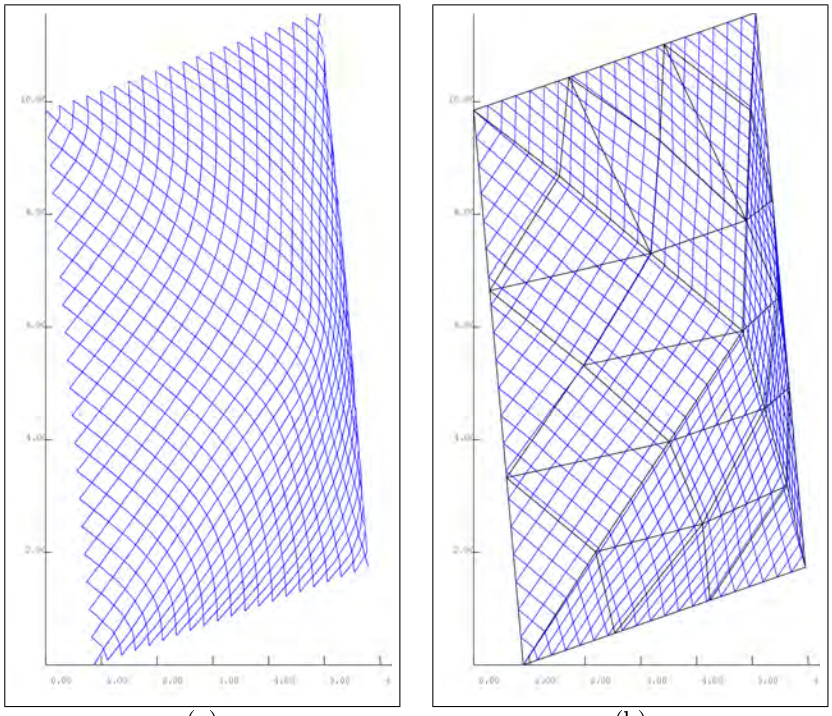

(a) (b)

Figure 3.4: The diamond mesh (a) is decomposed into triangular elements (b). The approximation in each triangle is that twines are parallel and therefore have the same deformation, and that the twines are elastic.

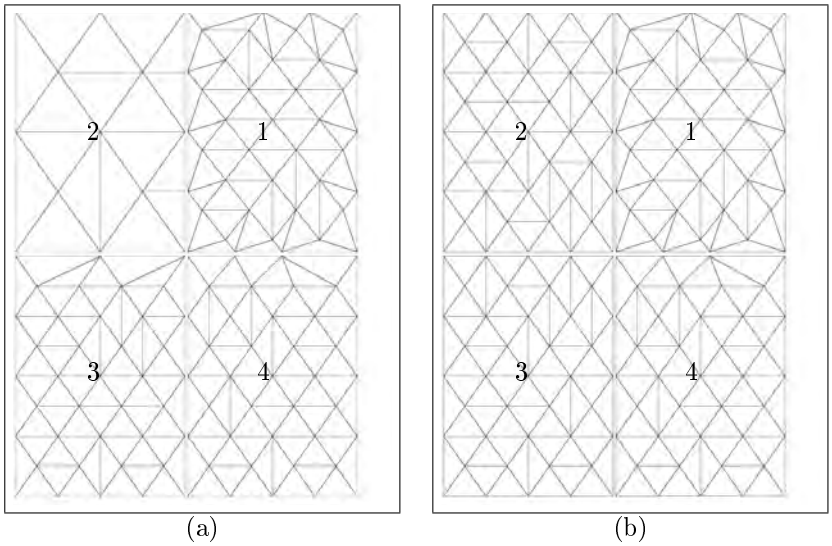

(a) (b)

Figure 3.5: Case identical to Figure 3.3. Although the netting in panel 1 has only 45 meshes horizontally, the triangular element discretization is easy. The step size of panel 2 is larger in (a) than in (b).

3.2.1 The basic method: direct formulation

The triangular finite element dedicated to diamond mesh nets is described here.

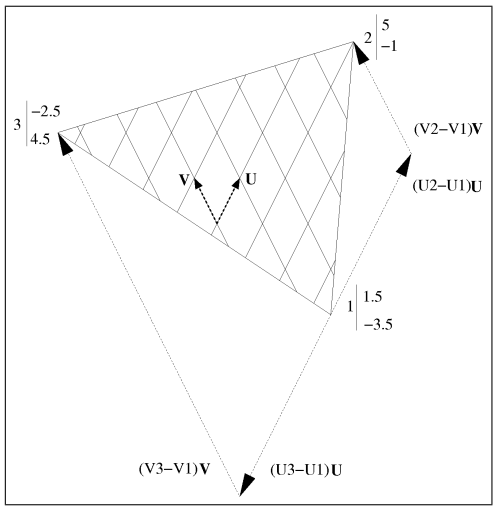

Figure 3.6: A triangular element: the sides of the triangle are linear combinations of twine vectors (**U** and **V**). The coordinates in twine number are noted. The origin of theses coordinates is the intersection of **U** and **V**.

The triangular element is defined by its three vertices, which are connected to the net. The coordinates of the vertices in number of twine vectors are then constant, whatever the deformation of the triangle. Figure 3.6 shows an example. In this example the coordinates in twine number of node 1 are 1.5 along the **U** twine and -3.5 along the **V** twine. It is clear that if the origin of coordinates in twine number changes, the twine coordinates of nodes will change but will not affect the equilibrium position of the net.

These twines are parallel inside the triangular element, which means that the sides of the triangle (**12**, **23**, **31**) are linear combinations of twine vectors (**U** and **V**, cf. Figure 3.6). This point is the main foundation of the model. These combinations are as follows:

$$\mathbf{12} = (U_2 - U_1)\mathbf{U} + (V_2 - V_1)\mathbf{V}$$

$$\mathbf{13} = (U_3 - U_1)\mathbf{U} + (V_3 - V_1)\mathbf{V}$$

12 (**13**): vector from vertex 1 (1) to vertex 2 (3).

The two previous equations with two unknowns (**U** and **V**) then give the following:

$$\mathbf{U} = \frac{V_3 - V_1}{d}\mathbf{12} - \frac{V_2 - V_1}{d}\mathbf{13}$$

$$\mathbf{V} = \frac{U_2 - U_1}{d}\mathbf{13} - \frac{U_3 - U_1}{d}\mathbf{12}$$

With side vectors:

$$\mathbf{12} = \begin{vmatrix} x_2 - x_1 \\ y_2 - y_1 \\ z_2 - z_1 \end{vmatrix}$$

$$\mathbf{13} = \begin{vmatrix} x_3 - x_1 \\ y_3 - y_1 \\ z_3 - z_1 \end{vmatrix}$$

and

$$d = (U_2 - U_1)(V_3 - V_1) - (U_3 - U_1)(V_2 - V_1)$$

x_i, y_i, z_i: Cartesian coordinates of vertex i,
U_i, V_i: coordinates of vertex i in number of twines (twine coordinates).

The twine vectors ($\mathbf{U}$, $\mathbf{V}$) are calculated from the Cartesian coordinates (x_i, y_i, z_i) of the vertices of the triangular element.

It appears that nothing implies that the number of twine coordinates of the vertices of the triangle consists of integers. Therefore, these coordinates can be real. This implies that the vertices of the triangle are not necessarily located on knots of the net (Figure 3.4). Similarly, nothing prevents the triangle from being smaller than a mesh. It appears that while the triangle does not contain any piece of twine of the net, d is not null, and therefore the triangle contains twines and consequently a deformation energy. In other words, the triangular finite element is a homogenization of the mechanical properties of the net.

It also appears that every point of the twines belongs to only one triangular element and still the same, regardless of the deformation of the net. Points on the contour of a triangular element also belong to the neighbours.

3.2.2 Metric of the triangular element

The objective of the finite element method is to calculate the Cartesian coordinates of the numerical nodes. These nodes are, for the netting, the vertices of the triangular elements (Figures 3.7 and 3.8 a).

The nodes are fixed relative to the netting, which means that the coordinates of the nodes in twines or meshes remain constant regardless of the netting deformation.

Figures 3.8 b and c show an example of coordinates of a triangular element. Generally speaking, the mesh coordinates are used by the netting maker.

There are relations between the mesh coordinates and the twine coordinates, the bases of which are noted in Figures 3.8 b and c.

The relations between the bases are the following:

$$\mathbf{u} = \mathbf{U} - \mathbf{V}$$
$$\mathbf{v} = \mathbf{U} + \mathbf{V}$$

This leads to:

$$\mathbf{U} = \frac{\mathbf{u} + \mathbf{v}}{2}$$
$$\mathbf{V} = \frac{\mathbf{v} - \mathbf{u}}{2}$$

This means that the relations between the twine coordinates and the mesh coordinates of the node P are the following:

$$U_P = u_P + v_P$$
$$V_P = v_P - u_P$$

and

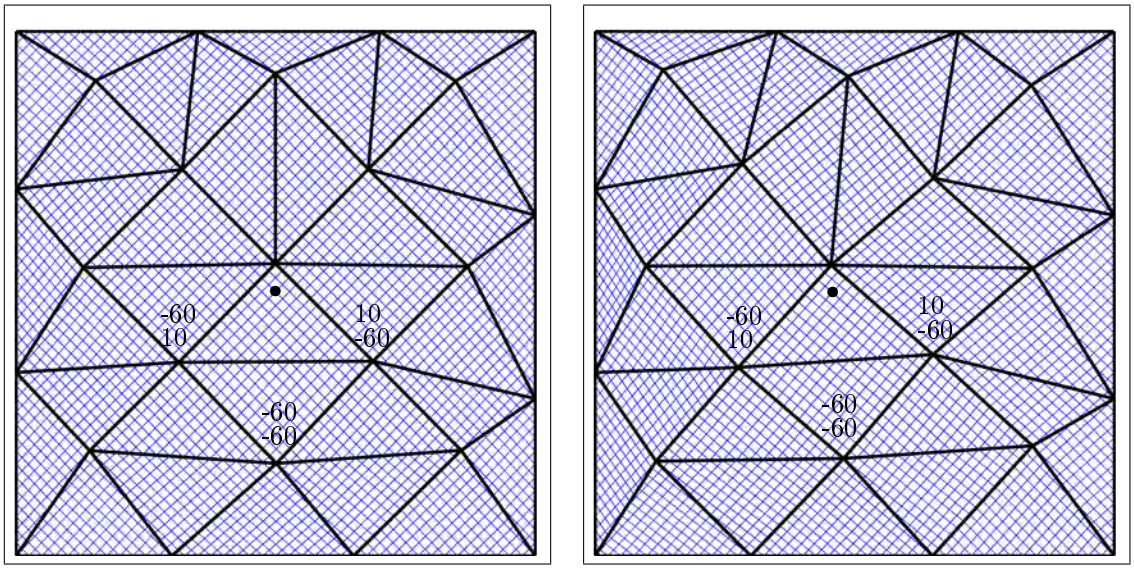

Figure 3.7: Two deformations of the same structure. The twines coordinates of vertices remain constant. The twines coordinates of three vertices are noted. The dot is the origin of twines numbering. Only 1 twine on 5 is drawn.

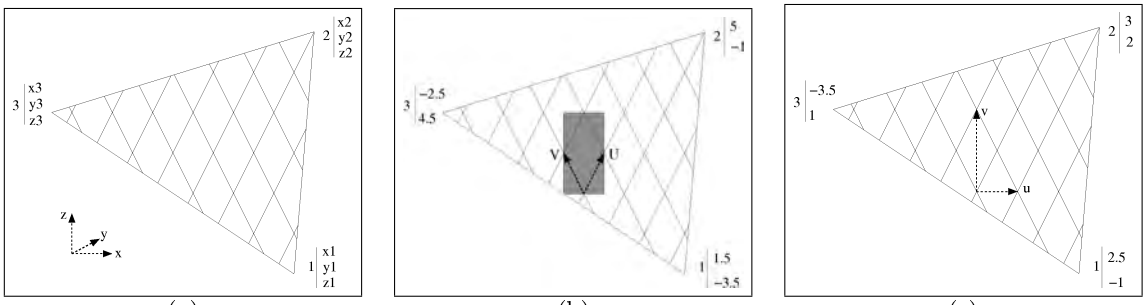

(a) (b) (c)

Figure 3.8: Triangular element: Cartesian coordinates (a), twines coordinates (b), and mesh coordinates (c). The grey surface is a mesh surface (b).

$$u_P = \frac{U_P - V_P}{2}$$

$$v_P = \frac{U_P + V_P}{2}$$

Here, U_P and V_P are the twine coordinates, and u_P and v_P are the mesh coordinates of the same node P. In these conditions the vector from origin to node P could be written as follows:

$$\mathbf{OP} = U_P\mathbf{U} + V_P\mathbf{V}$$

$$\mathbf{OP} = u_P\mathbf{u} + v_P\mathbf{v}$$

Because the amplitude of a cross product of vectors is twice the surface of the triangle made of these two vectors, the Cartesian surface of the triangular element (in m^2) is half the amplitude of the cross product of the side vectors of the triangular element:

$$S = \frac{1}{2}|\mathbf{12} \wedge \mathbf{13}|$$

The side vectors in Cartesian coordinates are as follows:

$$\mathbf{12} = \begin{vmatrix} x_2 - x_1 \\ y_2 - y_1 \\ z_2 - z_1 \end{vmatrix}$$

$$\mathbf{13} = \begin{vmatrix} x_3 - x_1 \\ y_3 - y_1 \\ z_3 - z_1 \end{vmatrix}$$

By the same way, the number of meshes, as defined in Figure 3.8b, is

$$nb_m = \frac{1}{4}|\vec{12} \wedge \vec{13}|$$

with side vectors in twine coordinates:

$$\vec{12} = \begin{vmatrix} U_2 - U_1 \\ V_2 - V_1 \\ 0 \end{vmatrix}$$

$$\vec{13} = \begin{vmatrix} U_3 - U_1 \\ V_3 - V_1 \\ 0 \end{vmatrix}$$

The number of meshes in a triangular element is

$$nb_m = \frac{1}{4}\left[(U_2 - U_1)(V_3 - V_1) - (U_3 - U_1)(V_2 - V_1)\right] = \frac{d}{4}$$

Because there are two twines U and two twines V per mesh, the number of twines U and V is calculated as follows:

$$nb_U = \frac{d}{2}$$

$$nb_V = \frac{d}{2}$$

Because there are also two knots per mesh, the number of knots in a triangular element is

$$nb_k = \frac{d}{2}$$

The surface of one mesh is calculated through the cross product of twines vectors (**U** and **V**):

$$Ms = 2|\mathbf{U} \wedge \mathbf{V}|$$

which is also the surface of the triangular element divided by the number of meshes in the element:

$$Ms = \frac{S}{nb_m}$$

In the case of Figures 3.6 and 3.8, $d = 38$, the number of meshes is 9.5, the number of **U** twines is 18, the number of **V** twines is 18, and the number of knots is 18.

3.3 The forces on the netting

3.3.1 Twine tension in diamond mesh

The tensions in the twines are required to estimate the forces on the vertices due to these tensions. In the hypothesis of linear elasticity, these tensions are deduced from **U** and **V**, which have been previously calculated. In these conditions the twine tensions are as follows:

$$T_u = EA\frac{|\mathbf{U}| - l_0}{l_0}$$

$$T_v = EA\frac{|\mathbf{V}| - l_0}{l_0}$$

E : Young's modulus of the material (N/m^2),
A : mechanical section of the twines U and V (m^2),
l_o : unstretched length of twine vectors (m).

The principle of virtual work is used here to calculate the forces on the vertices due to the tension in the twines.

The force component along X on vertex 1 of a triangular element is estimated by considering a virtual displacement $(\partial x1)$ along the axis x of vertex 1. This displacement leads to an external work:

$$W_e = F_{x1}\partial x1$$

This displacement also induces a change in the length of mesh bars ($\partial|\mathbf{U}|$ and $\partial|\mathbf{V}|$), an internal work per twine $\partial|\mathbf{U}|T_u$ and $\partial|\mathbf{V}|T_v$ and therefore an internal work for the triangular element:

$$W_i = (\partial|\mathbf{U}|T_u + \partial|\mathbf{V}|T_v)\frac{d}{2}$$

The principle of virtual work implies that the external work equals the internal work, since the forces represent the tension in the twines. That gives for each component of force on the three vertices:

$$F_{x1} = (T_u\frac{\partial|\mathbf{U}|}{\partial x1} + T_v\frac{\partial|\mathbf{V}|}{\partial x1})\frac{d}{2}$$

$$F_{y1} = (T_u\frac{\partial|\mathbf{U}|}{\partial y1} + T_v\frac{\partial|\mathbf{V}|}{\partial y1})\frac{d}{2}$$

$$F_{z1} = (T_u\frac{\partial|\mathbf{U}|}{\partial z1} + T_v\frac{\partial|\mathbf{V}|}{\partial z1})\frac{d}{2}$$

$$F_{x2} = (T_u\frac{\partial|\mathbf{U}|}{\partial x2} + T_v\frac{\partial|\mathbf{V}|}{\partial x2})\frac{d}{2}$$

$$F_{y2} = (T_u\frac{\partial|\mathbf{U}|}{\partial y2} + T_v\frac{\partial|\mathbf{V}|}{\partial y2})\frac{d}{2}$$

$$F_{z2} = (T_u\frac{\partial|\mathbf{U}|}{\partial z2} + T_v\frac{\partial|\mathbf{V}|}{\partial z2})\frac{d}{2}$$

$$F_{x3} = (T_u\frac{\partial|\mathbf{U}|}{\partial x3} + T_v\frac{\partial|\mathbf{V}|}{\partial x3})\frac{d}{2}$$

$$F_{y3} = (T_u \frac{\partial|\mathbf{U}|}{\partial y3} + T_v \frac{\partial|\mathbf{V}|}{\partial y3}) \frac{d}{2}$$

$$F_{z3} = (T_u \frac{\partial|\mathbf{U}|}{\partial z3} + T_v \frac{\partial|\mathbf{V}|}{\partial z3}) \frac{d}{2}$$

The derivatives $\frac{\partial|U|}{\partial x1}$ ... $\frac{\partial|V|}{\partial z3}$ can be calculated, as the equations relating to U, V and X_i, Y_i, Z_i have already been described. This gives the following vectors force for the three vertices:

$$\mathbf{F_1} = (V_3 - V_2) T_u \frac{\mathbf{U}}{2|\mathbf{U}|} + (U_2 - U_3) T_v \frac{\mathbf{V}}{2|\mathbf{V}|}$$

$$\mathbf{F_2} = (V_1 - V_3) T_u \frac{\mathbf{U}}{2|\mathbf{U}|} + (U_3 - U_1) T_v \frac{\mathbf{V}}{2|\mathbf{V}|}$$

$$\mathbf{F_3} = (V_2 - V_1) T_u \frac{\mathbf{U}}{2|\mathbf{U}|} + (U_1 - U_2) T_v \frac{\mathbf{V}}{2|\mathbf{V}|}$$

The Newton-Raphson method, described earlier, requires the calculation of the stiffness matrix, which is calculated from the derivatives of effort with respect to the positions of the vertices of the triangular element. The 81 derivatives, that is to say, by 9 by 9 component coordinates, are then the following:

The stiffness matrix:

$$K = \begin{pmatrix} -\frac{\partial F_{x1}}{\partial x_1} & -\frac{\partial F_{x1}}{\partial y_1} & . & . & . & -\frac{\partial F_{x1}}{\partial z_3} \\ -\frac{\partial F_{y1}}{\partial x_1} & -\frac{\partial F_{y1}}{\partial y_1} & . & . & . & -\frac{\partial F_{y1}}{\partial z_3} \\ . & . & . & . & . & . \\ . & . & . & . & . & . \\ . & . & . & . & . & . \\ -\frac{\partial F_{z3}}{\partial x_1} & -\frac{\partial F_{z3}}{\partial y_1} & . & . & . & -\frac{\partial F_{z3}}{\partial z_3} \end{pmatrix}$$

The components are calculated as follows:

$$\frac{\partial F_{w1}}{\partial t} = \frac{EA_u(V_3 - V_2)}{2} \left[\frac{\partial U_w}{\partial t} \left(\frac{1}{n_0} - \frac{1}{|\mathbf{U}|} \right) + \frac{\partial|\mathbf{U}|}{\partial t} \frac{U_w}{|\mathbf{U}|^2} \right] + \frac{EA_v(U_2 - U_3)}{2} \left[\frac{\partial V_w}{\partial t} \left(\frac{1}{n_0} - \frac{1}{|\mathbf{V}|} \right) + \frac{\partial|\mathbf{V}|}{\partial t} \frac{V_w}{|\mathbf{V}|^2} \right]$$

$$\frac{\partial F_{w2}}{\partial t} = \frac{EA_u(V_1 - V_3)}{2} \left[\frac{\partial U_w}{\partial t} \left(\frac{1}{n_0} - \frac{1}{|\mathbf{U}|} \right) + \frac{\partial|\mathbf{U}|}{\partial t} \frac{U_w}{|\mathbf{U}|^2} \right] + \frac{EA_v(U_3 - U_1)}{2} \left[\frac{\partial V_w}{\partial t} \left(\frac{1}{n_0} - \frac{1}{|\mathbf{V}|} \right) + \frac{\partial|\mathbf{V}|}{\partial t} \frac{V_w}{|\mathbf{V}|^2} \right]$$

$$\frac{\partial F_{w3}}{\partial t} = \frac{EA_u(V_2 - V_1)}{2} \left[\frac{\partial U_w}{\partial t} \left(\frac{1}{n_0} - \frac{1}{|\mathbf{U}|} \right) + \frac{\partial|\mathbf{U}|}{\partial t} \frac{U_w}{|\mathbf{U}|^2} \right] + \frac{EA_v(U_1 - U_2)}{2} \left[\frac{\partial V_w}{\partial t} \left(\frac{1}{n_0} - \frac{1}{|\mathbf{V}|} \right) + \frac{\partial|\mathbf{V}|}{\partial t} \frac{V_w}{|\mathbf{V}|^2} \right]$$

With:
$w = x, y, z,$
$t = x1, y1, z1, x2, y2, z2, x3, y3, z3.$

The following derivatives are also required.
The derivatives of the components of $\mathbf{U}$ are as follows:

$$\frac{\partial U_x}{\partial x1} = \frac{\partial U_y}{\partial y1} = \frac{\partial U_z}{\partial z1} = \frac{V_2 - V_3}{d}$$

$$\frac{\partial U_x}{\partial x2} = \frac{\partial U_y}{\partial y2} = \frac{\partial U_z}{\partial z2} = \frac{V_3 - V_1}{d}$$

$$\frac{\partial U_x}{\partial x3} = \frac{\partial U_y}{\partial y3} = \frac{\partial U_z}{\partial z3} = \frac{V_1 - V_2}{d}$$
$$\frac{\partial U_x}{\partial yi} = \frac{\partial U_x}{\partial zi} = \frac{\partial U_y}{\partial zi} = \frac{\partial U_y}{\partial xi} = \frac{\partial U_z}{\partial xi} = \frac{\partial U_z}{\partial yi} = 0$$

The derivatives of the components of $\mathbf{V}$ are the following:

$$\frac{\partial V_x}{\partial x1} = \frac{\partial V_y}{\partial y1} = \frac{\partial V_z}{\partial z1} = \frac{U_3 - U_2}{d}$$
$$\frac{\partial V_x}{\partial x2} = \frac{\partial V_y}{\partial y2} = \frac{\partial V_z}{\partial z2} = \frac{U_1 - U_3}{d}$$
$$\frac{\partial V_x}{\partial x3} = \frac{\partial V_y}{\partial y3} = \frac{\partial V_z}{\partial z3} = \frac{U_2 - U_1}{d}$$
$$\frac{\partial V_x}{\partial yi} = \frac{\partial V_x}{\partial zi} = \frac{\partial V_y}{\partial zi} = \frac{\partial V_y}{\partial xi} = \frac{\partial V_z}{\partial xi} = \frac{\partial V_z}{\partial yi} = 0$$

The derivatives of $|\mathbf{U}|$ follow:

$$\frac{\partial |\mathbf{U}|}{\partial x1} = \frac{V_2 - V_3}{d^2}\left[(x_2 - x_1)(V_3 - V_1) - (x_3 - x_1)(V_2 - V_1)\right]$$
$$\frac{\partial |\mathbf{U}|}{\partial x2} = \frac{V_3 - V_1}{d^2}\left[(x_2 - x_1)(V_3 - V_1) - (x_3 - x_1)(V_2 - V_1)\right]$$
$$\frac{\partial |\mathbf{U}|}{\partial x3} = \frac{V_1 - V_2}{d^2}\left[(x_2 - x_1)(V_3 - V_1) - (x_3 - x_1)(V_2 - V_1)\right]$$

$$\frac{\partial |\mathbf{U}|}{\partial y1} = \frac{V_2 - V_3}{d^2}\left[(y_2 - y_1)(V_3 - V_1) - (y_3 - y_1)(V_2 - V_1)\right]$$
$$\frac{\partial |\mathbf{U}|}{\partial y2} = \frac{V_3 - V_1}{d^2}\left[(y_2 - y_1)(V_3 - V_1) - (y_3 - y_1)(V_2 - V_1)\right]$$
$$\frac{\partial |\mathbf{U}|}{\partial y3} = \frac{V_1 - V_2}{d^2}\left[(y_2 - y_1)(V_3 - V_1) - (y_3 - y_1)(V_2 - V_1)\right]$$

$$\frac{\partial |\mathbf{U}|}{\partial z1} = \frac{V_2 - V_3}{d^2}\left[(z_2 - z_1)(V_3 - V_1) - (z_3 - z_1)(V_2 - V_1)\right]$$
$$\frac{\partial |\mathbf{U}|}{\partial z2} = \frac{V_3 - V_1}{d^2}\left[(z_2 - z_1)(V_3 - V_1) - (z_3 - z_1)(V_2 - V_1)\right]$$
$$\frac{\partial |\mathbf{U}|}{\partial z3} = \frac{V_1 - V_2}{d^2}\left[(z_2 - z_1)(V_3 - V_1) - (z_3 - z_1)(V_2 - V_1)\right]$$

The derivatives of $|\mathbf{V}|$ are shown below:

$$\frac{\partial |\mathbf{V}|}{\partial x1} = \frac{U_2 - U_3}{d^2}\left[(x_2 - x_1)(U_3 - U_1) - (x_3 - x_1)(U_2 - U_1)\right]$$
$$\frac{\partial |\mathbf{V}|}{\partial x2} = \frac{U_3 - U_1}{d^2}\left[(x_2 - x_1)(U_3 - U_1) - (x_3 - x_1)(U_2 - U_1)\right]$$
$$\frac{\partial |\mathbf{V}|}{\partial x3} = \frac{U_1 - U_2}{d^2}\left[(x_2 - x_1)(U_3 - U_1) - (x_3 - x_1)(U_2 - U_1)\right]$$

$$\frac{\partial|\mathbf{V}|}{\partial y1} = \frac{U_2 - U_3}{d^2}\left[(y_2 - y_1)(U_3 - U_1) - (y_3 - y_1)(U_2 - U_1)\right]$$

$$\frac{\partial|\mathbf{V}|}{\partial y2} = \frac{U_3 - U_1}{d^2}\left[(y_2 - y_1)(U_3 - U_1) - (y_3 - y_1)(U_2 - U_1)\right]$$

$$\frac{\partial|\mathbf{V}|}{\partial y3} = \frac{U_1 - U_2}{d^2}\left[(y_2 - y_1)(U_3 - U_1) - (y_3 - y_1)(U_2 - U_1)\right]$$

$$\frac{\partial|\mathbf{V}|}{\partial z1} = \frac{U_2 - U_3}{d^2}\left[(z_2 - z_1)(U_3 - U_1) - (z_3 - z_1)(U_2 - U_1)\right]$$

$$\frac{\partial|\mathbf{V}|}{\partial z2} = \frac{U_3 - U_1}{d^2}\left[(z_2 - z_1)(U_3 - U_1) - (z_3 - z_1)(U_2 - U_1)\right]$$

$$\frac{\partial|\mathbf{V}|}{\partial z3} = \frac{U_1 - U_2}{d^2}\left[(z_2 - z_1)(U_3 - U_1) - (z_3 - z_1)(U_2 - U1)\right]$$

3.3.2 Twine tension in hexagonal mesh

The same technique for the diamond mesh netting is used for hexagonal ones. The triangular element dedicated to the hexagonal mesh netting has the same assumption as previously adopted: the three families of twines inside the element are parallel, i.e., **l**, **m**, and **n** twine vectors, are parallel (Figure 3.9).

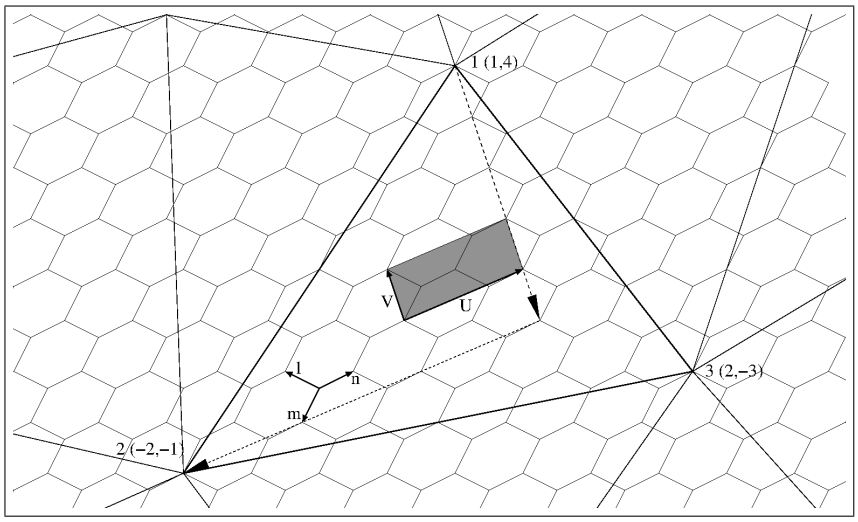

Figure 3.9: Triangular element dedicated to the hexagonal mesh nets. The twine vectors are **l**, **m**, and **n**. The number of meshes are noted for each vertex. The mesh base is in grey and is defined by vectors **U** and **V**.

The mesh base (shaded area in Figure 3.9) is first defined. This base mesh is defined as a parallelogram; its corners coincide with knots, and it includes two **l** twine vectors, two **m** twine vectors, and two **n** twine vectors. This base mesh is also used to quantify the number of meshes inside the triangular element. The vertices of the triangular element then have coordinates in base meshes ($U_1, U_2, U_3, V_1, V_2, V_3$; Figure 3.9).

Vectors **U** and **V** are the sides of the mesh base. There are linear relations between these two vectors and the sides of the triangular element (arrows on Figure 3.9):

$$\mathbf{12} = (U_2 - U_1)\mathbf{U} + (V_2 - V_1)\mathbf{V}$$
$$\mathbf{13} = (U_3 - U_1)\mathbf{U} + (V_3 - V_1)\mathbf{V}$$

The two previous equations give the following as in the case of diamond mesh (see section 3.2.1, page 32), namely:

$$\mathbf{U} = \frac{V_3 - V_1}{d}\mathbf{12} - \frac{V_2 - V_1}{d}\mathbf{13}$$
$$\mathbf{V} = \frac{U_3 - U_1}{d}\mathbf{12} - \frac{U_2 - U_1}{d}\mathbf{13}$$

With vectors of the sides of the mesh base:

$$\mathbf{12} = \left| \begin{array}{c} x_2 - x_1 \\ y_2 - y_1 \\ z_2 - z_1 \end{array} \right.$$

$$\mathbf{13} = \begin{vmatrix} x_3 - x_1 \\ y_3 - y_1 \\ z_3 - z_1 \end{vmatrix}$$

and

$$d = (U_2 - U_1)(V_3 - V_1) - (U_3 - U_1)(V_2 - V_1)$$

x_i, y_i, z_i: Cartesian coordinates of vertex i.

The number of base meshes in a triangular element is equal to $d/2$, the total number twine vectors is $3d$, the number of twine vectors $\mathbf{l}$, $\mathbf{m}$, or $\mathbf{n}$ is d, and the number of nodes is $2d$.

Tensions in twine vectors $\mathbf{l}$, $\mathbf{m}$, and $\mathbf{n}$ are now calculated. This is done by solving the force balance of the twines. This is solved by writing the following equations:

1) The base mesh definition leads to (Figure 3.9) :

$$\mathbf{U} = -\mathbf{m} + 2\mathbf{n} - \mathbf{l}$$

$$\mathbf{V} = -\mathbf{m} + \mathbf{l}$$

2) The amplitude of tension in the twines gives:

$$|\mathbf{T_l}| = EA_l \frac{|\mathbf{l}| - l_0}{l_0}$$

$$|\mathbf{T_m}| = EA_m \frac{|\mathbf{m}| - m_0}{m_0}$$

$$|\mathbf{T_n}| = EA_n \frac{|\mathbf{n}| - n_0}{n_0}$$

3) The balance of tensions leads to:

$$\mathbf{T_l} + \mathbf{T_m} + \mathbf{T_n} = \mathbf{0}$$

This gives six equations with six unknowns ($\mathbf{l}$, $\mathbf{m}$, $\mathbf{n}$, $\mathbf{T_l}$, $\mathbf{T_m}$, $\mathbf{T_n}$).

Equilibrium of the joint knot

The six previous equations can be reduced to the two that follow with two unknowns (m_x and m_y components of $\boldsymbol{m}$), since the triangular element has been turned in the plane XOY (Priour 2002, Priour 2006):

$$\begin{aligned}
& \frac{m_x + V_x}{\sqrt{(m_x + V_x)^2 + (m_y + V_y)^2}} \frac{E_l A_l}{l_o} \left[\sqrt{(m_x + V_x)^2 + (m_y + V_y)^2} - l_o \right] \\
+ \quad & \frac{m_x}{\sqrt{m_x^2 + m_y^2}} \frac{E_m A_m}{m_o} \left[\sqrt{m_x^2 + m_y^2} - m_o \right] \\
+ \quad & \frac{m_x + \frac{U_x + V_x}{2}}{\sqrt{(m_x + \frac{U_x + V_x}{2})^2 + (m_y + \frac{U_y + V_y}{2})^2}} \frac{E_n A_n}{n_o} \left[\sqrt{(m_x + \frac{U_x + V_x}{2})^2 + (m_y + \frac{U_y + V_y}{2})^2} - n_o \right] \\
= \quad & 0
\end{aligned}$$

$$\begin{aligned}
& \frac{m_y + V_y}{\sqrt{(m_x + V_x)^2 + (m_y + V_y)^2}} \frac{E_l A_l}{l_o} \left[\sqrt{(m_y + V_y)^2 + (m_y + V_y)^2} - l_o \right] \\
+ \quad & \frac{m_y}{\sqrt{m_x^2 + m_y^2}} \frac{E_m A_m}{m_o} \left[\sqrt{m_y^2 + m_y^2} - m_o \right] \\
+ \quad & \frac{m_y + \frac{U_y + V_y}{2}}{\sqrt{(m_x + \frac{U_x + V_x}{2})^2 + (m_y + \frac{U_y + V_y}{2})^2}} \frac{E_n A_n}{n_o} \left[\sqrt{(m_y + \frac{U_y + V_y}{2})^2 + (m_y + \frac{U_y + V_y}{2})^2} - n_o \right] \\
= \quad & 0
\end{aligned}$$

mx, my: components of m twine (m),
l_o, m_o, n_o: unstretched length of twines l, m, and n (m),
U_x, U_y, V_x, V_y: components of the sides of the mesh base (m; see Figure 3.9),
E_l, E_m, E_n: Young modulus of twines l, m, and n (Pa),
A_l, A_m, A_n: section of twines l, m, and n (m^2).

These two equations describe the equilibrium of the joint knot of three twines in a triangle, the sides of which are $\frac{\boldsymbol{U+V}}{2}$ and $\boldsymbol{V}$ (Figure 3.10). These equations are in newtons.

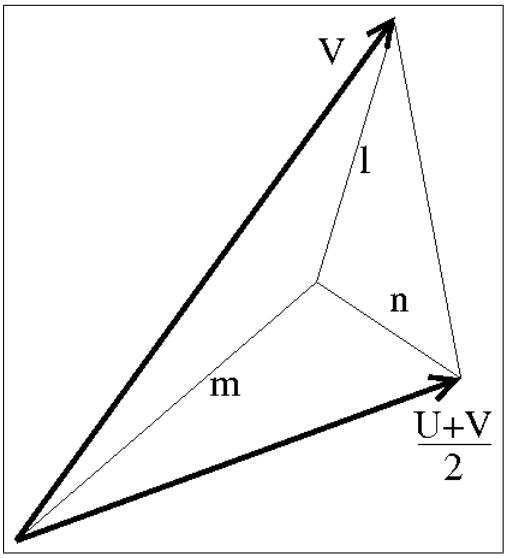

Figure 3.10: The three twines are in the triangle defined by $\frac{\boldsymbol{U+V}}{2}$ and $\boldsymbol{V}$ (cf. Figure 3.9).

Approximation of the equilibrium of the joint

The analytical solution of the two previous equations has not been found. Therefore, the following approximation has been made to simplify the equations. This approximation is acceptable because the stretched lengths of the twines are close to the unstretched length.

$$\frac{m_x}{|\boldsymbol{m}|} \approx \frac{m_x}{m_o}$$
$$\frac{m_y}{|\boldsymbol{m}|} \approx \frac{m_y}{m_o}$$

With this approximation the two previous equilibrium equations are reduced to the following:

$$\begin{aligned}(m_x + V_x)\tfrac{E_l A_l}{l_o^2}(\sqrt{(m_x+V_x)^2+(m_y+V_y)^2} - l_o) + m_x \tfrac{E_m A_m}{m_o^2}(\sqrt{m_x^2+m_y^2} - m_o) \quad + \\ (m_x + \tfrac{U_x+V_x}{2})\tfrac{E_n A_n}{n_o^2}(\sqrt{(m_x+\tfrac{U_x+V_x}{2})^2+(m_y+\tfrac{U_y+V_y}{2})^2} - n_o) \quad = 0\end{aligned}$$

$$\begin{aligned}(m_y + V_y)\tfrac{E_l A_l}{l_o^2}(\sqrt{(m_x+V_x)^2+(m_y+V_y)^2} - l_o) + m_y \tfrac{E_m A_m}{m_o^2}(\sqrt{m_x^2+m_y^2} - m_o) \quad + \\ (m_y + \tfrac{U_y+V_y}{2})\tfrac{E_n A_n}{n_o^2}(\sqrt{(m_x+\tfrac{U_x+V_x}{2})^2+(m_y+\tfrac{U_y+V_y}{2})^2} - n_o) \quad = 0\end{aligned}$$

They are the complete form of the following:

$$l_x \frac{E_l A_l}{l_o^2}(|\boldsymbol{l}| - l_o) + m_x \frac{E_m A_m}{m_o^2}(|\boldsymbol{m}| - m_o) + n_x \frac{E_n A_n}{n_o^2}(|\boldsymbol{n}| - n_o) = 0$$
$$l_y \frac{E_l A_l}{l_o^2}(|\boldsymbol{l}| - l_o) + m_y \frac{E_m A_m}{m_o^2}(|\boldsymbol{m}| - m_o) + n_y \frac{E_n A_n}{n_o^2}(|\boldsymbol{n}| - n_o) = 0$$

Newton-Raphson method

The previous approximation has not been sufficient to reach the analytical solution. The Newton-Raphson method is used to find a numerical solution (Deuflhard 2004).

For each iteration the displacement h is searched to find the equilibrium:

$$h_k = \frac{F(x_k)}{-F'(x_k)}$$
$$x_{k+1} = x_k + h_k$$

k: iteration number,

F: force on nodes,
x: position of nodes.
Here:

$$\boldsymbol{F} = \begin{cases} l_x \frac{E_l A_l}{l_o^2}(|\boldsymbol{l}| - l_o) + m_x \frac{E_m A_m}{m_o^2}(|\boldsymbol{m}| - m_o) + n_x \frac{E_n A_n}{n_o^2}(|\boldsymbol{n}| - n_o) = F_1 \\ l_y \frac{E_l A_l}{l_o^2}(|\boldsymbol{l}| - l_o) + m_y \frac{E_m A_m}{m_o^2}(|\boldsymbol{m}| - m_o) + n_y \frac{E_n A_n}{n_o^2}(|\boldsymbol{n}| - n_o) = F_2 \end{cases}$$

$$\boldsymbol{x} = \begin{cases} m_x \\ m_y \end{cases}$$

The derivative is:

$$F' = \begin{vmatrix} D_{11} & D_{12} \\ D_{21} & D_{22} \end{vmatrix}.$$

With:

$$D_{11} = -[\frac{EA_l}{l_o^2}(\boldsymbol{l} - l_o + \frac{l_x^2}{\boldsymbol{l}}) + \frac{EA_m}{m_o^2}(\boldsymbol{m} - m_o + \frac{m_x^2}{\boldsymbol{m}}) + \frac{EA_n}{n_o^2}(\boldsymbol{n} - n_o + \frac{n_x^2}{\boldsymbol{n}})]$$

$$D_{12} = D_{21} = -[\frac{EA_l}{l_o^2}\frac{l_x l_y}{\boldsymbol{l}} + \frac{EA_m}{m_o^2}\frac{m_x m_y}{\boldsymbol{m}} + \frac{EA_n}{n_o^2}\frac{n_x n_y}{\boldsymbol{n}}]$$

$$D_{22} = -[\frac{EA_l}{l_o^2}(\boldsymbol{l} - l_o + \frac{l_y^2}{\boldsymbol{l}}) + \frac{EA_m}{m_o^2}(\boldsymbol{m} - m_o + \frac{m_y^2}{\boldsymbol{m}}) + \frac{EA_n}{n_o^2}(\boldsymbol{n} - n_o + \frac{n_y^2}{\boldsymbol{n}})]$$

With the previous conditions the displacement ($\boldsymbol{h}$) can be calculated:

$$\boldsymbol{h} = \begin{cases} \frac{D_{22}F_1 - D_{12}F_2}{D_{22}D_{11} - D_{12}D_{21}} \\ \frac{D_{22}F_2 - D_{21}F_1}{D_{22}D_{11} - D_{12}D_{21}} \end{cases}$$

Forces on nodes

The forces on the sides of the triangular element are calculated from the twine tension. These forces are related to the number of twines through the sides of the triangle. This number of twines through each side can be calculated based on the number of base mesh of each vertex.

The effort on the side along **U** of the base mesh (Figure 3.9) is

$$\mathbf{F_U} = \mathbf{T_l} - \mathbf{T_m}$$

The effort along **V** is

$$\mathbf{F_V} = -\mathbf{T_n}$$

Under these conditions, the effort on each side of the triangle can be deduced:

$$\mathbf{T_{12}} = (U_2 - U_1)(\mathbf{T_l} - \mathbf{T_m}) + (V_2 - V_1)(-\mathbf{T_n})$$
$$\mathbf{T_{23}} = (U_3 - U_2)(\mathbf{T_l} - \mathbf{T_m}) + (V_3 - V_2)(-\mathbf{T_n})$$
$$\mathbf{T_{31}} = (U_1 - U_3)(\mathbf{T_l} - \mathbf{T_m}) + (V_1 - V_3)(-\mathbf{T_n})$$

Here, $\mathbf{T_{ij}}$ is the effort on the side **ij** of the triangular element.

Each side effort is distributed on each end of this side as the twines are evenly distributed along the sides of the triangle:

$$\mathbf{F_1} = \frac{\mathbf{T_{12}} + \mathbf{T_{31}}}{2}$$
$$\mathbf{F_2} = \frac{\mathbf{T_{23}} + \mathbf{T_{12}}}{2}$$
$$\mathbf{F_3} = \frac{\mathbf{T_{31}} + \mathbf{T_{23}}}{2}$$

$\mathbf{F_1}$, $\mathbf{F_2}$, and $\mathbf{F_3}$ are the forces on the three vertices of the triangular element due to the tension in the twines.

The contribution of the stiffness matrix is not described here.

3.3.3 Hydrodynamic drag

Introduction

The drag force on the netting is calculated in this model as the sum of the drag force on each twine (**U** and **V**). This assumption is probably questionable, because the drag on a twine alone is surely not exactly the same as the drag on this twine among other twines as it is the case in a netting. Anyway, this assumption leads to the calculation of the drag of each triangular element because for each the twines vectors are known, as described earlier. The formulation for the twine vector drag is based on the assumptions of Morrison adapted by Landweber and Richtmeyer (Landweber and Protter 1947, Richtmeyer 1941).

The drag amplitudes on the U twines used in the model (Figure 3.11) are:

$$|\mathbf{F}| = \frac{1}{2}\rho C_d D l_0 \left[|\mathbf{c}| sin(\alpha)\right]^2 \frac{d}{2}$$

$$|\mathbf{T}| = f\frac{1}{2}\rho C_d D l_0 \left[|\mathbf{c}| cos(\alpha)\right]^2 \frac{d}{2}$$

The directions of the drag on the **U** twine vectors are:

$$\frac{\mathbf{F}}{|\mathbf{F}|} = \frac{\mathbf{U} \wedge (\mathbf{c} \wedge \mathbf{U})}{|\mathbf{U} \wedge (\mathbf{c} \wedge \mathbf{U})|}$$

$$\frac{\mathbf{T}}{|\mathbf{T}|} = \frac{\mathbf{F} \wedge (\mathbf{c} \wedge \mathbf{F})}{|\mathbf{F} \wedge (\mathbf{c} \wedge \mathbf{F})|}$$

F: normal drag (N) on the U twines, following the assumptions of Landweber,
T: tangential drag (N) on the U twines, Richtmeyer hypothesis,
ρ: density of water (kg/m^3),
C_d: normal drag coefficient,
f: tangential drag coefficient,
D: diameter of twine (m),
l_0: length of twine vector (m),
c: water velocity relative to the twine (m/s),
α: angle between the U twine and the water velocity ($radians$),
$d/2$: number of U twine vectors in the triangular element.

In the equations of drag amplitude, the expressions $|\mathbf{c}|sin(\alpha)$ and $|\mathbf{c}|cos(\alpha)$ are the normal and tangential projections on **c** along the U twine vector.

The drag on V twines for a triangular element are similar: **U** is replaced by **V** and α by β.

The length of twine vectors used in the formulation of drag amplitude can be assessed by $|\mathbf{U}|$ for the U twines and by $|\mathbf{V}|$ for the V twines. That would mean it takes into account the twine elongation. Generally speaking, a twine elongation is associated with a diameter D reduction by the Poisson coefficient. Because this Poisson coefficient is not taken into account in the present modelling, the twine surface is approximated by Dl_0, where D is the diameter of the twines and l_0 is the unstretched length of the twine vectors.

All parameters, including the angles α and β, are constant and known for each triangular element. Therefore, the drag can be calculated for each triangular element. The drag force for a triangular element is spread over the three vertices of the element at 1/3 per vertex.

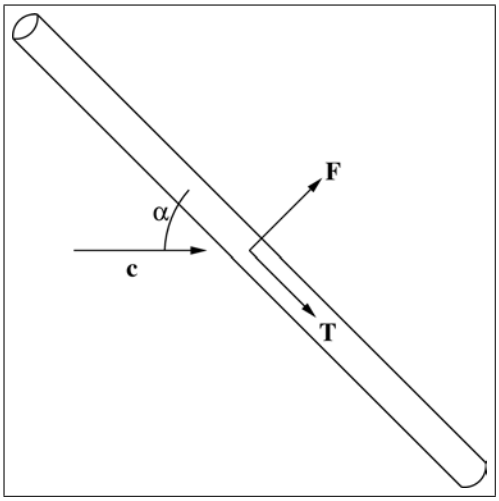

Figure 3.11: Normal (**F**) and tangential (**T**) forces on a twine due to the relative velocity of water (**c**).

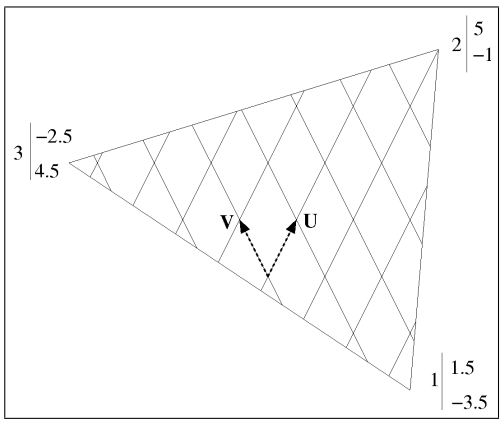

Figure 3.12: Example of triangular element. The drag forces are calculated for U twines and for V twines. The twine coordinates are noted in this example.

Definitions of the variables

The Cartesian coordinates of the three nodes (1, 2, 3) of the triangular element (cf. Figure 3.12) follow:

$$\mathbf{1} = \begin{vmatrix} x_1 \\ y_1 \\ z_1 \end{vmatrix}$$

$$\mathbf{2} = \begin{vmatrix} x_2 \\ y_2 \\ z_2 \end{vmatrix}$$

$$\mathbf{3} = \left| \begin{array}{l} x_3 \\ y_3 \\ z_3 \end{array} \right.$$

The twine coordinates of the three nodes (1, 2, 3) of the triangular element are as follows:

$$\mathbf{1} = \left| \begin{array}{l} U_1 \\ V_1 \end{array} \right.$$

$$\mathbf{2} = \left| \begin{array}{l} U_2 \\ V_2 \end{array} \right.$$

$$\mathbf{3} = \left| \begin{array}{l} U_3 \\ V_3 \end{array} \right.$$

The vector current is

$$\mathbf{c} = \left| \begin{array}{l} c_x \\ c_y \\ c_z \end{array} \right.$$

Generally speaking, c_z is null.
It has been seen previously:

$$\mathbf{U} = \frac{V_3 - V_1}{d}\mathbf{12} - \frac{V_2 - V_1}{d}\mathbf{13}$$

$$\mathbf{V} = \frac{U_2 - U_1}{d}\mathbf{13} - \frac{U_3 - U_1}{d}\mathbf{12}$$

with sides vectors:

$$\mathbf{12} = \left| \begin{array}{l} x_2 - x_1 \\ y_2 - y_1 \\ z_2 - z_1 \end{array} \right.$$

$$\mathbf{13} = \left| \begin{array}{l} x_3 - x_1 \\ y_3 - y_1 \\ z_3 - z_1 \end{array} \right.$$

and

$$d = (U_2 - U_1)(V_3 - V_1) - (U_3 - U_1)(V_2 - V_1)$$

The components of U twine vectors are as follows:

$$\mathbf{U} = \left| \begin{array}{l} U_x \\ U_y \\ U_z \end{array} \right.$$

$$\mathbf{U} = \left| \begin{array}{l} \frac{1}{d}\left[(V_3 - V_1)(x_2 - x_1) - (V_2 - V_1)(x_3 - x_1)\right] \\ \frac{1}{d}\left[(V_3 - V_1)(y_2 - y_1) - (V_2 - V_1)(y_3 - y_1)\right] \\ \frac{1}{d}\left[(V_3 - V_1)(z_2 - z_1) - (V_2 - V_1)(z_3 - z_1)\right] \end{array} \right.$$

The angle between current and U is

$$cos(\alpha) = \frac{\mathbf{c}.\mathbf{U}}{|\mathbf{c}||\mathbf{U}|}$$

The components of V twine vectors are as follows:

$$\mathbf{V} = \left| \begin{array}{l} V_x \\ V_y \\ V_z \end{array} \right.$$

$$\mathbf{V} = \left| \begin{array}{l} \frac{1}{d}\left[(U_2 - U_1)(x_3 - x_1) - (U_3 - U_1)(x_2 - x_1)\right] \\ \frac{1}{d}\left[(U_2 - U_1)(y_3 - y_1) - (U_3 - U_1)(y_2 - y_1)\right] \\ \frac{1}{d}\left[(U_2 - U_1)(z_3 - z_1) - (U_3 - U_1)(z_2 - z_1)\right] \end{array} \right.$$

The angle between current and V is

$$cos(\beta) = \frac{\mathbf{c}.\mathbf{V}}{|\mathbf{c}||\mathbf{V}|}$$

Evaluations for the stiffness of the normal force on the U twines

The normal force on U twines is

$$\mathbf{F} = |\mathbf{F}| \frac{\mathbf{U} \wedge (\mathbf{c} \wedge \mathbf{U})}{|\mathbf{U} \wedge (\mathbf{c} \wedge \mathbf{U})|}$$

That means that the x y and z components are as follows:

$$\mathbf{F}_x = |\mathbf{F}| \frac{\mathbf{E}_x}{|\mathbf{E}|}$$

$$\mathbf{F}_y = |\mathbf{F}| \frac{\mathbf{E}_y}{|\mathbf{E}|}$$

$$\mathbf{F}_z = |\mathbf{F}| \frac{\mathbf{E}_z}{|\mathbf{E}|}$$

With:

$$\mathbf{E} = \mathbf{U} \wedge (\mathbf{c} \wedge \mathbf{U})$$

and

$$\mathbf{E} = \left| \begin{array}{l} E_x \\ E_y \\ E_z \end{array} \right.$$

The x component of the derivative is

$$\mathbf{F}'_x = |\mathbf{F}|' \frac{\mathbf{E}_x}{|\mathbf{E}|} + |\mathbf{F}| \frac{\mathbf{E}'_x |\mathbf{E}| - \mathbf{E}_x |\mathbf{E}|'}{|\mathbf{E}|^2}$$

Which gives for the x y and z components:

$$\mathbf{F}'_x = |\mathbf{F}|' \frac{\mathbf{E}_x}{|\mathbf{E}|} + \frac{|\mathbf{F}|}{|\mathbf{E}|^2} \left\{ \mathbf{E}'_x |\mathbf{E}| - \frac{\mathbf{E}_x}{|\mathbf{E}|} (\mathbf{E}_x \mathbf{E}'_x + \mathbf{E}_y \mathbf{E}'_y + \mathbf{E}_z \mathbf{E}'_z) \right\}$$

$$\mathbf{F}'_y = |\mathbf{F}|' \frac{\mathbf{E}_y}{|\mathbf{E}|} + \frac{|\mathbf{F}|}{|\mathbf{E}|^2} \left\{ \mathbf{E}'_y |\mathbf{E}| - \frac{\mathbf{E}_y}{|\mathbf{E}|} (\mathbf{E}_x \mathbf{E}'_x + \mathbf{E}_y \mathbf{E}'_y + \mathbf{E}_z \mathbf{E}'_z) \right\}$$

$$\mathbf{F}'_z = |\mathbf{F}|'\frac{\mathbf{E}_z}{|\mathbf{E}|} + \frac{|\mathbf{F}|}{|\mathbf{E}|^2}\left\{\mathbf{E}'_z|\mathbf{E}| - \frac{\mathbf{E}_z}{|\mathbf{E}|}(\mathbf{E}_x\mathbf{E}'_x + \mathbf{E}_y\mathbf{E}'_y + \mathbf{E}_z\mathbf{E}'_z)\right\}$$

For this assessment the derivative of $\mathbf{E}$ is required:

$$\mathbf{E}' = \mathbf{U}' \wedge (\mathbf{c} \wedge \mathbf{U}) + \mathbf{U} \wedge (\mathbf{c} \wedge \mathbf{U}')$$

This leads to:

$$\mathbf{E}' = 2(\mathbf{U}'.\mathbf{U})\mathbf{c} - (\mathbf{U}'.\mathbf{c})\mathbf{U} - (\mathbf{U}.\mathbf{c})\mathbf{U}'$$

Which is:

$$\mathbf{E}'_x = 2(\mathbf{U}'.\mathbf{U})\mathbf{c}_x - (\mathbf{U}'.\mathbf{c})\mathbf{U}_x - (\mathbf{U}.\mathbf{c})\mathbf{U}'_x$$
$$\mathbf{E}'_y = 2(\mathbf{U}'.\mathbf{U})\mathbf{c}_y - (\mathbf{U}'.\mathbf{c})\mathbf{U}_y - (\mathbf{U}.\mathbf{c})\mathbf{U}'_y$$
$$\mathbf{E}'_z = 2(\mathbf{U}'.\mathbf{U})\mathbf{c}_z - (\mathbf{U}'.\mathbf{c})\mathbf{U}_z - (\mathbf{U}.\mathbf{c})\mathbf{U}'_z$$

With:

$$\mathbf{U}'.\mathbf{U} = \mathbf{U}_x\mathbf{U}'_x + \mathbf{U}_y\mathbf{U}'_y + \mathbf{U}_z\mathbf{U}'_z$$
$$\mathbf{U}'.\mathbf{c} = \mathbf{c}_x\mathbf{U}'_x + \mathbf{c}_y\mathbf{U}'_y + \mathbf{c}_z\mathbf{U}'_z$$
$$\mathbf{U}.\mathbf{c} = \mathbf{U}_x\mathbf{c}_x + \mathbf{U}_y\mathbf{c}_y + \mathbf{U}_z\mathbf{c}_z$$

The derivative of the amplitude of the normal force is

$$|\mathbf{F}|' = \frac{1}{2}\rho C_d D l_0 |\mathbf{c}|^2 \left([sin(\alpha)]^2\right)' \frac{d}{2}$$

which is

$$|\mathbf{F}|' = \frac{d}{2}\rho C_d D l_0 |\mathbf{c}|^2 cos(\alpha) sin(\alpha)\alpha'$$

The derivative of α is

$$\alpha' = \frac{-1}{\sqrt{1 - (\frac{\mathbf{c}.\mathbf{U}}{|\mathbf{c}||\mathbf{U}|})^2}}\left[\frac{\mathbf{c}.\mathbf{U}}{|\mathbf{c}||\mathbf{U}|}\right]'$$

That gives

$$\alpha' = \frac{-1}{\sqrt{1 - (\frac{\mathbf{c}.\mathbf{U}}{|\mathbf{c}||\mathbf{U}|})^2}}\left[\frac{\mathbf{c}}{|\mathbf{c}|}.\left(\frac{\mathbf{U}}{|\mathbf{U}|}\right)'\right]$$

The derivative of the U twine direction is

$$\left(\frac{\mathbf{U}}{|\mathbf{U}|}\right)' = \frac{\mathbf{U}'|\mathbf{U}| - \mathbf{U}|\mathbf{U}|'}{|\mathbf{U}|^2}$$

That means that the derivative of α is

$$\alpha' = \frac{-1}{\sqrt{1 - (\frac{\mathbf{c}.\mathbf{U}}{|\mathbf{c}||\mathbf{U}|})^2}}\left(\frac{\mathbf{c}}{|\mathbf{c}|}\right).\left(\frac{\mathbf{U}'|\mathbf{U}| - \mathbf{U}|\mathbf{U}|'}{|\mathbf{U}|^2}\right)$$

or

$$\alpha' = \frac{-1}{|\mathbf{U}|^2|\mathbf{c}|\sin\alpha}\left\{|\mathbf{U}|\left[c_x\mathbf{U}'_x + c_y\mathbf{U}'_y + c_z\mathbf{U}'_z\right] - (\mathbf{c}.\mathbf{U})|\mathbf{U}|'\right\}$$

In this case $\mathbf{U}'_x$ is the component along x of $\mathbf{U}'$.
The derivative of vector $\mathbf{U}$ is

$$\mathbf{U}' = \left|\begin{array}{c}\mathbf{U}'_x\\ \mathbf{U}'_y\\ \mathbf{U}'_z\end{array}\right.$$

Which is

$$\frac{\partial U_x}{\partial x_1} = \frac{\partial U_y}{\partial y_1} = \frac{\partial U_z}{\partial z_1} = \frac{1}{d}(V_2 - V_3)$$
$$\frac{\partial U_x}{\partial x_2} = \frac{\partial U_y}{\partial y_2} = \frac{\partial U_z}{\partial z_2} = \frac{1}{d}(V_3 - V_1)$$
$$\frac{\partial U_x}{\partial x_3} = \frac{\partial U_y}{\partial y_3} = \frac{\partial U_z}{\partial z_3} = \frac{1}{d}(V_1 - V_2)$$
$$\frac{\partial U_x}{\partial y_1} = \frac{\partial U_x}{\partial y_2} = \frac{\partial U_x}{\partial y_3} = \frac{\partial U_x}{\partial z_1} = \frac{\partial U_x}{\partial z_2} = \frac{\partial U_x}{\partial z_3} = 0$$
$$\frac{\partial U_y}{\partial z_1} = \frac{\partial U_y}{\partial z_2} = \frac{\partial U_y}{\partial z_3} = \frac{\partial U_y}{\partial x_1} = \frac{\partial U_y}{\partial x_2} = \frac{\partial U_y}{\partial x_3} = 0$$
$$\frac{\partial U_z}{\partial x_1} = \frac{\partial U_z}{\partial x_2} = \frac{\partial U_z}{\partial x_3} = \frac{\partial U_z}{\partial y_1} = \frac{\partial U_z}{\partial y_2} = \frac{\partial U_z}{\partial y_3} = 0$$

On vector form and for the nine coordinates of the triangular element it is:

$$\frac{\partial \mathbf{U}}{\partial x_1} = \left|\begin{array}{c}\frac{V_2-V_3}{d}\\ 0\\ 0\end{array}\right.$$

$$\frac{\partial \mathbf{U}}{\partial y_1} = \left|\begin{array}{c}0\\ \frac{V_2-V_3}{d}\\ 0\end{array}\right.$$

$$\frac{\partial \mathbf{U}}{\partial z_1} = \left|\begin{array}{c}0\\ 0\\ \frac{V_2-V_3}{d}\end{array}\right.$$

$$\frac{\partial \mathbf{U}}{\partial x_2} = \left|\begin{array}{c}\frac{V_3-V_1}{d}\\ 0\\ 0\end{array}\right.$$

$$\frac{\partial \mathbf{U}}{\partial y_2} = \left|\begin{array}{c}0\\ \frac{V_3-V_1}{d}\\ 0\end{array}\right.$$

$$\frac{\partial \mathbf{U}}{\partial z_2} = \left|\begin{array}{c}0\\ 0\\ \frac{V_3-V_1}{d}\end{array}\right.$$

$$\frac{\partial \mathbf{U}}{\partial x_3} = \begin{vmatrix} \frac{V_1 - V_2}{d} \\ 0 \\ 0 \end{vmatrix}$$

$$\frac{\partial \mathbf{U}}{\partial y_3} = \begin{vmatrix} 0 \\ \frac{V_1 - V_2}{d} \\ 0 \end{vmatrix}$$

$$\frac{\partial \mathbf{U}}{\partial z_3} = \begin{vmatrix} 0 \\ 0 \\ \frac{V_1 - V_2}{d} \end{vmatrix}$$

The derivative of the norm of vector $\mathbf{U}$ is

$$|\mathbf{U}|' = \frac{U_x U_x' + U_y U_y' + U_z U_z'}{|\mathbf{U}|}$$

This gives for the nine coordinates of the triangular element:

$$\frac{\partial |\mathbf{U}|}{\partial x_1} = \frac{U_x(V_2 - V_3)}{d|\mathbf{U}|}$$

$$\frac{\partial |\mathbf{U}|}{\partial y_1} = \frac{U_y(V_2 - V_3)}{d|\mathbf{U}|}$$

$$\frac{\partial |\mathbf{U}|}{\partial z_1} = \frac{U_z(V_2 - V_3)}{d|\mathbf{U}|}$$

$$\frac{\partial |\mathbf{U}|}{\partial x_2} = \frac{U_x(V_3 - V_1)}{d|\mathbf{U}|}$$

$$\frac{\partial |\mathbf{U}|}{\partial y_2} = \frac{U_y(V_3 - V_1)}{d|\mathbf{U}|}$$

$$\frac{\partial |\mathbf{U}|}{\partial z_2} = \frac{U_z(V_3 - V_1)}{d|\mathbf{U}|}$$

$$\frac{\partial |\mathbf{U}|}{\partial x_3} = \frac{U_x(V_1 - V_2)}{d|\mathbf{U}|}$$

$$\frac{\partial |\mathbf{U}|}{\partial y_3} = \frac{U_y(V_1 - V_2)}{d|\mathbf{U}|}$$

$$\frac{\partial |\mathbf{U}|}{\partial z_3} = \frac{U_z(V_1 - V_2)}{d|\mathbf{U}|}$$

This leads to the derivatives of α (angle between c and U):

$$\frac{\partial \alpha}{\partial x_1} = \frac{V_3 - V_2}{d|\mathbf{U}|^2|\mathbf{c}|\sqrt{1 - \left(\frac{\mathbf{c}.\mathbf{U}}{|\mathbf{c}||\mathbf{U}|}\right)^2}} \left[c_x|\mathbf{U}| - \frac{U_x}{|\mathbf{U}|}\mathbf{c}.\mathbf{U}\right]$$

$$\frac{\partial \alpha}{\partial y_1} = \frac{V_3 - V_2}{d|\mathbf{U}|^2|\mathbf{c}|\sqrt{1 - \left(\frac{\mathbf{c}.\mathbf{U}}{|\mathbf{c}||\mathbf{U}|}\right)^2}} \left[c_y|\mathbf{U}| - \frac{U_y}{|\mathbf{U}|}\mathbf{c}.\mathbf{U}\right]$$

$$\frac{\partial\alpha}{\partial z_1} = \frac{V_3 - V_2}{d|\mathbf{U}|^2|\mathbf{c}|\sqrt{1-\left(\frac{\mathbf{c}.\mathbf{U}}{|\mathbf{c}||\mathbf{U}|}\right)^2}}\left[c_z|\mathbf{U}| - \frac{U_z}{|\mathbf{U}|}\mathbf{c}.\mathbf{U}\right]$$

$$\frac{\partial\alpha}{\partial x_2} = \frac{V_1 - V_3}{d|\mathbf{U}|^2|\mathbf{c}|\sqrt{1-\left(\frac{\mathbf{c}.\mathbf{U}}{|\mathbf{c}||\mathbf{U}|}\right)^2}}\left[c_x|\mathbf{U}| - \frac{U_x}{|\mathbf{U}|}\mathbf{c}.\mathbf{U}\right]$$

$$\frac{\partial\alpha}{\partial y_2} = \frac{V_1 - V_3}{d|\mathbf{U}|^2|\mathbf{c}|\sqrt{1-\left(\frac{\mathbf{c}.\mathbf{U}}{|\mathbf{c}||\mathbf{U}|}\right)^2}}\left[c_y|\mathbf{U}| - \frac{U_y}{|\mathbf{U}|}\mathbf{c}.\mathbf{U}\right]$$

$$\frac{\partial\alpha}{\partial z_2} = \frac{V_1 - V_3}{d|\mathbf{U}|^2|\mathbf{c}|\sqrt{1-\left(\frac{\mathbf{c}.\mathbf{U}}{|\mathbf{c}||\mathbf{U}|}\right)^2}}\left[c_z|\mathbf{U}| - \frac{U_z}{|\mathbf{U}|}\mathbf{c}.\mathbf{U}\right]$$

$$\frac{\partial\alpha}{\partial x_3} = \frac{V_2 - V_1}{d|\mathbf{U}|^2|\mathbf{c}|\sqrt{1-\left(\frac{\mathbf{c}.\mathbf{U}}{|\mathbf{c}||\mathbf{U}|}\right)^2}}\left[c_x|\mathbf{U}| - \frac{U_x}{|\mathbf{U}|}\mathbf{c}.\mathbf{U}\right]$$

$$\frac{\partial\alpha}{\partial y_3} = \frac{V_2 - V_1}{d|\mathbf{U}|^2|\mathbf{c}|\sqrt{1-\left(\frac{\mathbf{c}.\mathbf{U}}{|\mathbf{c}||\mathbf{U}|}\right)^2}}\left[c_y|\mathbf{U}| - \frac{U_y}{|\mathbf{U}|}\mathbf{c}.\mathbf{U}\right]$$

$$\frac{\partial\alpha}{\partial z_3} = \frac{V_2 - V_1}{d|\mathbf{U}|^2|\mathbf{c}|\sqrt{1-\left(\frac{\mathbf{c}.\mathbf{U}}{|\mathbf{c}||\mathbf{U}|}\right)^2}}\left[c_z|\mathbf{U}| - \frac{U_z}{|\mathbf{U}|}\mathbf{c}.\mathbf{U}\right]$$

Evaluation for the stiffness of the tangential force on the U twines

The tangential force on U twines is

$$\mathbf{T} = |\mathbf{T}|\frac{\mathbf{F}\wedge(\mathbf{c}\wedge\mathbf{F})}{|\mathbf{F}\wedge(\mathbf{c}\wedge\mathbf{F})|}$$

Following the definition of $\mathbf{F}_1$:

$$\mathbf{T} = |\mathbf{T}|\frac{[\mathbf{U}\wedge(\mathbf{c}\wedge\mathbf{U})]\wedge\{\mathbf{c}\wedge[\mathbf{U}\wedge(\mathbf{c}\wedge\mathbf{U})]\}}{|\,[\mathbf{U}\wedge(\mathbf{c}\wedge\mathbf{U})]\wedge\{\mathbf{c}\wedge[\mathbf{U}\wedge(\mathbf{c}\wedge\mathbf{U})]\}\,|}$$

It follows that

$$\mathbf{T} = |\mathbf{T}|\frac{[(\mathbf{U}.\mathbf{U})(\mathbf{c}.\mathbf{c}) - (\mathbf{U}.\mathbf{c})^2](\mathbf{U}.\mathbf{c})\mathbf{U}}{|[(\mathbf{U}.\mathbf{U})(\mathbf{c}.\mathbf{c}) - (\mathbf{U}.\mathbf{c})^2](\mathbf{U}.\mathbf{c})\mathbf{U}|}$$

or

$$\mathbf{T} = |\mathbf{T}|\frac{[|\mathbf{U}|^2|\mathbf{c}|^2 - (|\mathbf{U}||\mathbf{c}|cos\alpha)^2]|\mathbf{U}||\mathbf{c}|cos\alpha\mathbf{U}}{|[|\mathbf{U}|^2|\mathbf{c}|^2 - (|\mathbf{U}||\mathbf{c}|cos\alpha)^2]|\mathbf{U}||\mathbf{c}|cos\alpha\mathbf{U}|}$$

and

$$\mathbf{T} = |\mathbf{T}|\frac{\cos\alpha\mathbf{U}}{|\cos\alpha||\mathbf{U}|}$$

The x y and z components are as follows:

$$\mathbf{T}_x = |\mathbf{T}|\frac{\cos\alpha\mathbf{U}_x}{|\cos\alpha||\mathbf{U}|}$$
$$\mathbf{T}_y = |\mathbf{T}|\frac{\cos\alpha\mathbf{U}_y}{|\cos\alpha||\mathbf{U}|}$$
$$\mathbf{T}_z = |\mathbf{T}|\frac{\cos\alpha\mathbf{U}_z}{|\cos\alpha||\mathbf{U}|}$$

The derivative of $\mathbf{T}_x$ is:

$$\mathbf{T}'_x = |\mathbf{T}|'\frac{\cos\alpha\mathbf{U}_x}{|\cos\alpha||\mathbf{U}|} + |\mathbf{T}|\frac{(\cos\alpha\mathbf{U}_x)'|\cos\alpha||\mathbf{U}| - \cos\alpha\mathbf{U}_x(|\cos\alpha||\mathbf{U}|)'}{(|\cos\alpha||\mathbf{U}|)^2}$$

$$\begin{aligned}\mathbf{T}'_x &= |\mathbf{T}|'\frac{\cos\alpha\mathbf{U}_x}{|\cos\alpha||\mathbf{U}|}\\ &+ \frac{|\mathbf{T}|}{|\cos\alpha||\mathbf{U}|}(\cos\alpha\mathbf{U}'_x - \sin\alpha\alpha'\mathbf{U}_x)\\ &- \frac{|\mathbf{T}|\cos\alpha\mathbf{U}_x}{(|\cos\alpha||\mathbf{U}|)^2}\left[|\cos\alpha|\frac{\mathbf{U}_x\mathbf{U}'_x + \mathbf{U}_y\mathbf{U}'_y + \mathbf{U}_z\mathbf{U}'_z}{|\mathbf{U}|} - \frac{\cos\alpha}{|\cos\alpha|}\sin\alpha\alpha'|\mathbf{U}|\right]\end{aligned}$$

$$\begin{aligned}\mathbf{T}'_x &= |\mathbf{T}|'\frac{\mathbf{T}_x}{|\mathbf{T}|} + \frac{|\mathbf{T}|}{|\cos\alpha||\mathbf{U}|}(\cos\alpha\mathbf{U}'_x - \sin\alpha\alpha'\mathbf{U}_x)\\ &- \frac{\mathbf{T}_x}{|\cos\alpha||\mathbf{U}|}\left[|\cos\alpha|\frac{\mathbf{U}_x\mathbf{U}'_x + \mathbf{U}_y\mathbf{U}'_y + \mathbf{U}_z\mathbf{U}'_z}{|\mathbf{U}|} - \frac{\cos\alpha}{|\cos\alpha|}\sin\alpha\alpha'|\mathbf{U}|\right]\end{aligned}$$

$$\begin{aligned}\mathbf{T}'_y &= |\mathbf{T}|'\frac{\mathbf{T}_y}{|\mathbf{T}|} + \frac{|\mathbf{T}|}{|\cos\alpha||\mathbf{U}|}(\cos\alpha\mathbf{U}'_y - \sin\alpha\alpha'\mathbf{U}_y)\\ &- \frac{\mathbf{T}_y}{|\cos\alpha||\mathbf{U}|}\left[|\cos\alpha|\frac{\mathbf{U}_x\mathbf{U}'_x + \mathbf{U}_y\mathbf{U}'_y + \mathbf{U}_z\mathbf{U}'_z}{|\mathbf{U}|} - \frac{\cos\alpha}{|\cos\alpha|}\sin\alpha\alpha'|\mathbf{U}|\right]\end{aligned}$$

$$\begin{aligned}\mathbf{T}'_z &= |\mathbf{T}|'\frac{\mathbf{T}_z}{|\mathbf{T}|} + \frac{|\mathbf{T}|}{|\cos\alpha||\mathbf{U}|}(\cos\alpha\mathbf{U}'_z - \sin\alpha\alpha'\mathbf{U}_z)\\ &- \frac{\mathbf{T}_z}{|\cos\alpha||\mathbf{U}|}\left[|\cos\alpha|\frac{\mathbf{U}_x\mathbf{U}'_x + \mathbf{U}_y\mathbf{U}'_y + \mathbf{U}_z\mathbf{U}'_z}{|\mathbf{U}|} - \frac{\cos\alpha}{|\cos\alpha|}\sin\alpha\alpha'|\mathbf{U}|\right]\end{aligned}$$

The derivative of the amplitude of the tangential force is

$$|\mathbf{T}|' = f\frac{1}{2}\rho C_d D l_0 |\mathbf{c}|^2 \left([cos(\alpha)]^2\right)' \frac{d}{2}$$

which is

$$|\mathbf{T}|' = -\frac{d}{2} f\rho C_d D l_0 |\mathbf{c}|^2 cos(\alpha) sin(\alpha)\alpha'$$

Evaluations for the stiffness of the normal and tangential forces on the V twines

This evaluations are identical to the previous, but with V and β used in place of U and α.

3.3.4 Twine flexion in Netting plane

The resistance to twine bending in the plane of the net is also called the mesh opening stiffness (Figure 3.13). In a first approximation, this stiffness is neglected, but the use of steeper nets makes it necessary to take this mechanical phenomenon into account in numerical models. Currently, only O'Neill (1994, 2004) and the present model take this mesh opening stiffness into account.

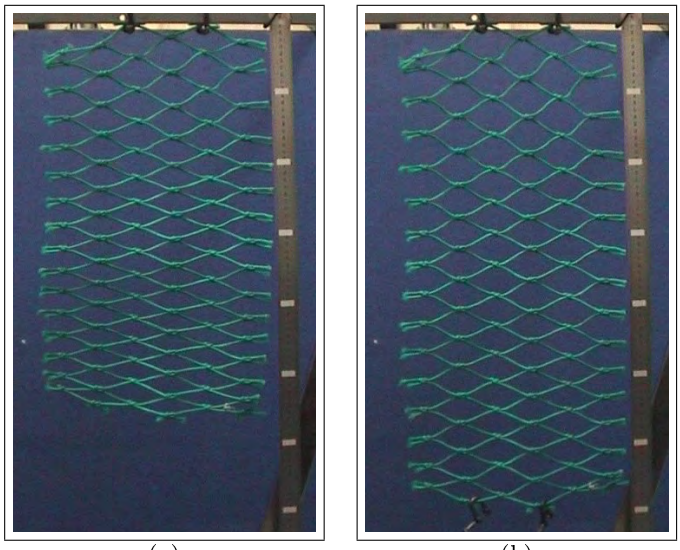

(a) (b)

Figure 3.13: Demonstration of mesh opening stiffness. Deformation remains limited despite the weight added to the bottom of the net on (b).

In the present model, the half angle (α) between the twine vectors (**U** and **V**) could lead to a couple between twine vectors (**U** and **V**). This angle is calculated by

$$\alpha = \frac{1}{2} acos(\frac{\mathbf{U}.\mathbf{V}}{|\mathbf{U}||\mathbf{V}|})$$

The couple on a knot due to the U twine is equilibrated by the couple of the V twine; otherwise the knot would not be in equilibrium. These couples are approximated in the model by

$$C_u = -C_v = H(\alpha - \alpha_0)$$

where α_0 is the angle between the unstressed twines (without couple on twines) and H is the mesh opening stiffness ($N.m/Rad$).

This couple varies linearly with the angle. O'Neill (1994, 2004) suggests another formulation, since he models the twines as beams.

Forces at the vertices of the triangular element, mechanically equivalent to the mesh opening stiffness, are calculated using the principle of virtual work:

If ∂x_1 is a virtual displacement along the x axis of vertex 1, then the external work (W_e) is

$$W_e = F x_1 \partial x_1$$

where Fx_1 is the effort along the x axis at vertex 1 of a triangular element.

This displacement creates a change in angle α, and therefore an internal work (W_i):

$$W_i = \frac{d}{2}(C_u \partial\alpha + C_v \partial\alpha)$$

$$d = (U_2 - U_1)(V_1 - V_3) - (U_3 - U_1)(V_1 - V_2)$$

where $d/2$ is the number of nodes in a triangular element.

Since the internal work is equal to the external work,

$$Fx_1 = C_u d \frac{\partial\alpha}{\partial x_1}$$

This gives, for all the force components at the vertices of the triangular element,

$$Fw_i = H(\alpha - \alpha_0) d \frac{\partial\alpha}{\partial w_i}$$

where $w = x$, y, and z, and $i = 1$, 2, and 3.

The derivative $\frac{\partial\alpha}{\partial w_i}$ of α relative to the coordinates w_i of vertices, which is necessary for calculating the forces, is

$$\frac{\partial\alpha}{\partial w_i} = \frac{\mathbf{V}_w v_i - \mathbf{U}_w u_i - \frac{\mathbf{U}_w(\mathbf{U}.\mathbf{V})v_i}{|\mathbf{U}|^2} - \frac{\mathbf{V}_w(\mathbf{U}.\mathbf{V})u_i}{|\mathbf{V}|^2}}{2dsin(\alpha)|\mathbf{U}||\mathbf{V}|}$$

where $w = x$, y, and z, and $i = 1$, 2, and 3.

The stiffness matrix ($-\mathbf{F}'(\mathbf{X})$) is completed by calculating the derivative component of efforts related to the coordinates of the vertices of the triangular element:

$$-\frac{\partial F_w i}{\partial t j}$$

where as above, $w = x$, y, and z, and $i = 1$, 2, and 3, and $t = x$, y, and z, and $j = 1$, 2, and 3.

3.3.5 Twine flexion outside the netting plane

Figure 3.14: The net bends under its own weight, which highlights the bending stiffness of the net.

To our knowledge, no numerical model, except the present one, takes into account this mechanical property of the nets (Figure 3.14). The angle between the U twine of a triangle ($\mathbf{U}_a$ in Figure 3.15) and its neighbour ($\mathbf{U}_b$) is constant along the side common to the two triangular elements. This angle quantifies the bending of the twine.

The bending stiffness of the U twine tends to keep the twine straight. The equation governing the bending is as follows:

$$C = \frac{EI}{\rho}$$

C: bending couple on the U twine (Nm),
EI: flexural stiffness, which is Young's modulus by inertia (Nm^2),
ρ: radius of curvature of the U twine (m).

This couple is generated, in the present modelling, when two successive triangular elements are bent or, more precisely, when the U twine is bent to the passage of a triangular element with its neighbour. The couple will then generate forces on the vertices (1, 2, 3, 4 in Figure 3.15) on the two adjacent triangular elements. Obviously the bending of the V twines also leads to a couple. In the following only the effect of bending on the U twines is described; the bending on V twines has to be taken into account in the same way.

The radius of the curvature is estimated from the average lengths of twine U in each triangular element (Figure 3.16). These average lengths are calculated using the average number of twine

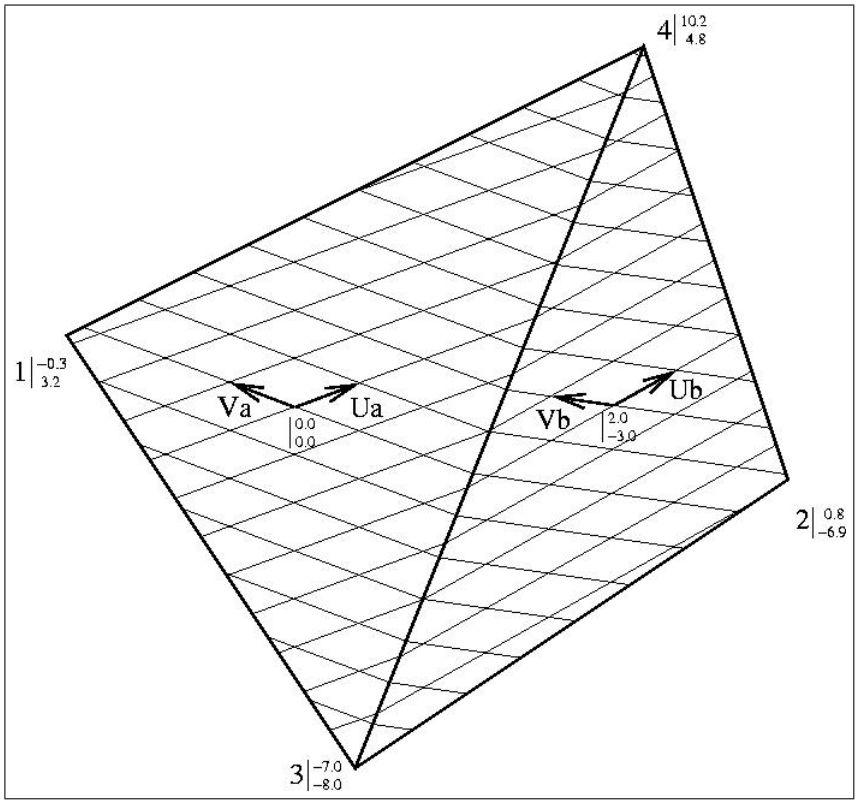

Figure 3.15: Two triangular elements (134 and 243), the coordinates of which, in number of twines, are noted. The angle between the twine vectors $\mathbf{U_a}$ and $\mathbf{U_b}$ leads to a bending couple between the two triangular elements.

vectors ($\mathbf{U_a}$ and $\mathbf{U_b}$) by the U twine in the two triangular elements (n_a and n_b).

The twine vectors of the two triangular elements (see section 3.2.1 page 32) are as follows:

$$\mathbf{U_a} = \frac{V_4 - V_1}{d_a}\mathbf{13} - \frac{V_3 - V_1}{d_a}\mathbf{14}$$

$$\mathbf{V_a} = \frac{U_4 - U_1}{d_a}\mathbf{13} - \frac{U_3 - U_1}{d_a}\mathbf{14}$$

$$\mathbf{U_b} = \frac{V_3 - V_2}{d_b}\mathbf{24} - \frac{V_4 - V_2}{d_b}\mathbf{23}$$

$$\mathbf{V_b} = \frac{U_3 - U_2}{d_b}\mathbf{24} - \frac{U_4 - U_2}{d_b}\mathbf{23}$$

U_i, V_i: coordinates of vertex i in number of twines (twine coordinates).

With side vectors:

$$\mathbf{13} = \begin{vmatrix} x_3 - x_1 \\ y_3 - y_1 \\ z_3 - z_1 \end{vmatrix}$$

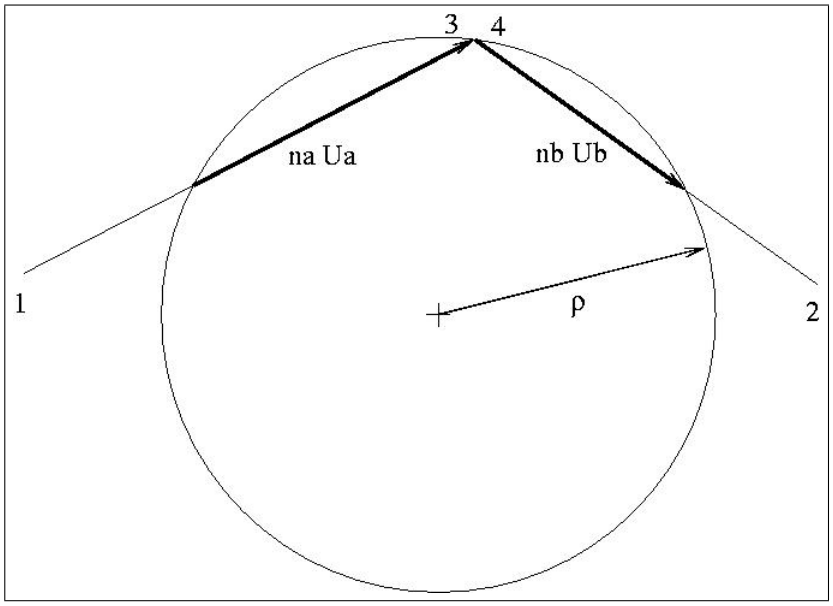

Figure 3.16: Profile view of the two triangular elements. The radius of curvature (ρ) is estimated from the average length of twine vectors $\mathbf{U}$ in each triangle : $n_a\mathbf{U_a}$ and $n_b\mathbf{U_b}$.

$$\mathbf{24} = \begin{vmatrix} x_4 - x_2 \\ y_4 - y_2 \\ z_4 - z_2 \end{vmatrix}$$

The numbers of twine vectors ($\mathbf{U_a}$ and $\mathbf{U_b}$) for the U twines in the two triangular elements are

$$d_a = (U_3 - U_1)(V_4 - V_1) - (U_4 - U_1)(V_3 - V_1)$$
$$d_b = (U_4 - U_2)(V_3 - V_2) - (U_3 - U_2)(V_4 - V_2)$$

The average numbers of twine vectors ($\mathbf{U_a}$ and $\mathbf{U_b}$) by U twine are calculated from the number of twine vectors in the triangular elements and the length of the common side in twine coordinates ($V_3 - V_4$):

$$n_a = \frac{d_a}{2|V_3 - V_4|}$$
$$n_b = \frac{d_b}{2|V_3 - V_4|}$$

The radius of the curvature (ρ) is calculated from the circumscribed circle in the triangle of sides $na\mathbf{U_a}$, $nb\mathbf{U_b}$ and $na\mathbf{U_a} + nb\mathbf{U_b}$, as shown in Figure 3.16. The side lengths of the triangle are

$$A = |n_a\mathbf{U_a}|$$
$$B = |n_b\mathbf{U_b}|$$
$$C = |n_a\mathbf{U_a} + n_b\mathbf{U_b}|$$

The equations of the triangle, which can be obtained in a mathematical compendium, give the radius of curvature:

$$\rho = \frac{ABC}{4S}$$

where S and p, the surface and the half perimeter of the triangle, are

$$S = \sqrt{p(p-A)(p-B)(p-C)}$$
$$p = \frac{A+B+C}{2}$$

The forces on the vertices (1, 2, 3 and 4) of the two triangular elements due to the twine bending are calculated using the principle of virtual work. In case of the X component of the force on vertex 1 (F_{x1}), a displacement ($\partial x1$) is defined along X axis of vertex 1. This displacement generates an external work:

$$W_e = F_{x1}\partial x1$$

This movement also causes a variation of angle ($\partial\alpha$) between the twine vectors ($\mathbf{U_a}$ and $\mathbf{U_b}$) of the two triangular elements. This variation induces an internal work:

$$W_i = C\partial\alpha(V_3 - V_4)$$

According to the principle of virtual work, these works are equal, which gives the following:

$$F_{wi} = \frac{EI}{\rho}\frac{\partial\alpha}{\partial wi}(V_3 - V_4)$$

w: directions x, y, and z,
i: vertices 1, 2, 3, and 4,
$V_3 - V_4$: number of twines involved in the bending.

The angle α between the two twine vectors ($\mathbf{U_a}$ and $\mathbf{U_b}$) of the two triangular elements is calculated with the dot product of twine vectors (Figure 3.16):

$$cos(\alpha) = \frac{\mathbf{U_a}.\mathbf{U_b}}{|\mathbf{U_a}||\mathbf{U_b}|}$$

The 12 derivatives of α relative to the coordinates of the vertices of the two triangular elements ($\frac{\partial\alpha}{\partial wi}$) are therefore required to calculate the effort on the vertices. They are as follows:

$$\frac{\partial\alpha}{\partial w1} = (V_3 - V_4)\frac{(\mathbf{U_a}.\mathbf{U_b})U_{aw} - U_{bw}|\mathbf{U_a}|^2}{|\mathbf{U_a}|^3|\mathbf{U_b}|d_a sin(\alpha)}$$

$$\frac{\partial\alpha}{\partial w2} = (V_4 - V_3)\frac{(\mathbf{U_a}.\mathbf{U_b})U_{bw} - U_{aw}|\mathbf{U_b}|^2}{|\mathbf{U_b}|^3|\mathbf{U_a}|d_b sin(\alpha)}$$

$$\frac{\partial\alpha}{\partial w3} = (V_4 - V_1)\frac{(\mathbf{U_a}.\mathbf{U_b})U_{aw} - U_{bw}|\mathbf{U_a}|^2}{|\mathbf{U_a}|^3|\mathbf{U_b}|d_a sin(\alpha)} + (V_2 - V_4)\frac{(\mathbf{U_a}.\mathbf{U_b})U_{bw} - U_{aw}|\mathbf{U_b}|^2}{|\mathbf{U_b}|^3|\mathbf{U_a}|d_b sin(\alpha)}$$

$$\frac{\partial\alpha}{\partial w4} = (V_1 - V_3)\frac{(\mathbf{U_a}.\mathbf{U_b})U_{aw} - U_{bw}|\mathbf{U_a}|^2}{|\mathbf{U_a}|^3|\mathbf{U_b}|d_a sin(\alpha)} + (V_3 - V_2)\frac{(\mathbf{U_a}.\mathbf{U_b})U_{bw} - U_{aw}|\mathbf{U_b}|^2}{|\mathbf{U_b}|^3|\mathbf{U_a}|d_b sin(\alpha)}$$

Here, U_{aw} is the component along the w axis of $\mathbf{U_a}$. In this case w is the axis consisting of x, y, and z. Obviously, U_{bw} is the component along the w axis of $\mathbf{U_b}$.

The efforts on the four vertices of the two triangular elements due to the bending of the U twine between these two elements have been previously calculated.

The stiffness matrix $(-F'(X))$ is completed by calculating the derivative of the 12 components of the forces relative to the 12 coordinates of the vertices of the two triangular elements. The 144 components of this matrix are

$$-\frac{\partial F_{wi}}{\partial tj}$$

With, as above:
w: x, y, and z.
i: 1, 2, 3, and 4.

And more:
t: x, y, and z,
j: 1, 2, 3, and 4.

3.3.6 Fish catch pressure

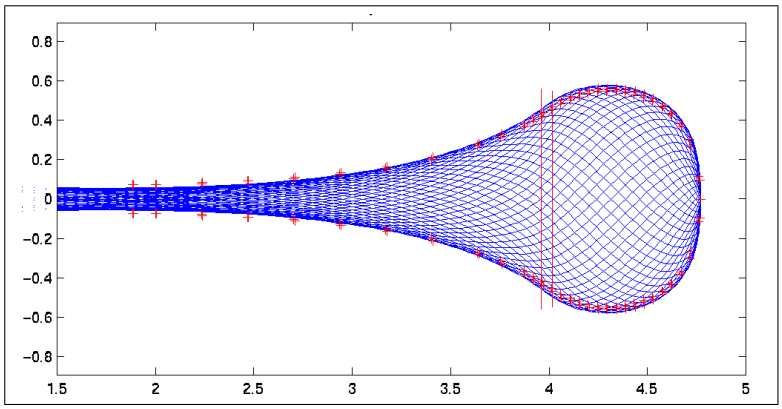

Figure 3.17: Measurement in a flume tank tests (cross) and numerical modelling (mesh) for a scale (1/3) model of North Sea cod-end with 300kg of catch.

The mechanical effect of caught fish (Figure 3.17) in a net is estimated by a pressure (Anon 1999). This pressure is exerted directly on the triangular elements in contact with the fish. In the case of water speed relative to that catch:

$$p = \frac{1}{2}\rho C_d v^2$$

p: pressure of the catch on the net (Pa),
ρ: density of water (kg/m^3),
C_d: drag coefficient,
v: current amplitude (m/s).

This pressure is then applied to the surface of the triangular element ($\frac{\mathbf{12}\wedge\mathbf{13}}{2}$). The resultant force is directed perpendicular to the triangular element. The effort on each vertex is that force by 1/3.

$$\mathbf{F}_1 = \frac{\mathbf{12}\wedge\mathbf{13}}{2}\frac{p}{3}$$

$$\mathbf{F}_2 = \frac{\mathbf{12}\wedge\mathbf{13}}{2}\frac{p}{3}$$

$$\mathbf{F}_3 = \frac{\mathbf{12}\wedge\mathbf{13}}{2}\frac{p}{3}$$

With sides vectors:

$$\mathbf{12} = \begin{vmatrix} x_2 - x_1 \\ y_2 - y_1 \\ z_2 - z_1 \end{vmatrix}$$

$$\mathbf{13} = \begin{vmatrix} x_3 - x_1 \\ y_3 - y_1 \\ z_3 - z_1 \end{vmatrix}$$

That gives:

$$\mathbf{F}_{1x} = \frac{p}{6}\left[(y_2 - y_1)(z_3 - z_1) - (z_2 - z_1)(y_3 - y_1)\right]$$

$$\mathbf{F}_{1y} = \frac{p}{6}\left[(z_2 - z_1)(x_3 - x_1) - (x_2 - x_1)(z_3 - z_1)\right]$$

$$\mathbf{F}_{1z} = \frac{p}{6}\left[(x_2 - x_1)(y_3 - y_1) - (y_2 - y_1)(x_3 - x_1)\right]$$

The contribution of this effect to the stiffness matrix is calculated through the derivatives of the forces. The derivatives of $\mathbf{F}_1$ is

$$\mathbf{F}_1' = (\mathbf{12}' \wedge \mathbf{13} + \mathbf{12} \wedge \mathbf{13}')\frac{p}{6}$$

The derivatives of $\mathbf{F}_1$, $\mathbf{F}_2$, and $\mathbf{F}_3$ are identical:

$$\frac{\partial \mathbf{F}_1}{\partial x_1} = \frac{p}{6}\begin{vmatrix} 0 \\ z_3 - z_2 \\ y_2 - y_3 \end{vmatrix}$$

$$\frac{\partial \mathbf{F}_1}{\partial y_1} = \frac{p}{6}\begin{vmatrix} z_2 - z_3 \\ 0 \\ x_3 - x_2 \end{vmatrix}$$

$$\frac{\partial \mathbf{F}_1}{\partial z_1} = \frac{p}{6}\begin{vmatrix} y_3 - y_2 \\ x_2 - x_3 \\ 0 \end{vmatrix}$$

$$\frac{\partial \mathbf{F}_1}{\partial x_2} = \frac{p}{6}\begin{vmatrix} 0 \\ z_1 - z_3 \\ y_3 - y_1 \end{vmatrix}$$

$$\frac{\partial \mathbf{F}_1}{\partial y_2} = \frac{p}{6}\begin{vmatrix} z_3 - z_1 \\ 0 \\ x_1 - x_3 \end{vmatrix}$$

$$\frac{\partial \mathbf{F}_1}{\partial z_2} = \frac{p}{6}\begin{vmatrix} y_1 - y_3 \\ x_3 - x_1 \\ 0 \end{vmatrix}$$

$$\frac{\partial \mathbf{F}_1}{\partial x_3} = \frac{p}{6}\begin{vmatrix} 0 \\ z_2 - z_1 \\ y_1 - y_2 \end{vmatrix}$$

$$\frac{\partial \mathbf{F}_1}{\partial y_3} = \frac{p}{6}\begin{vmatrix} z_1 - z_2 \\ 0 \\ x_2 - x_1 \end{vmatrix}$$

$$\frac{\partial \mathbf{F}_1}{\partial z_3} = \frac{p}{6}\begin{vmatrix} y_2 - y_1 \\ x_1 - x_2 \\ 0 \end{vmatrix}$$

3.3.7 Dynamic: force of inertia

The force of inertia is related to accelerations of the net and of the water particles just around the net. The calculation is done for each triangular element in three parts, one for each vertex, since the acceleration is not constant over the entire surface of each triangular element. Under these conditions, the parameters are local parameters at each vertex, including the acceleration and the mass. The mass per vertex is considered the third of the total mass of netting of the triangular element.

The force of inertia on each vertex of a triangular element mesh is estimated by (Hallam 1977):

$$\mathbf{F_i} = M_a(\boldsymbol{\gamma_h} - \boldsymbol{\gamma}) + \rho V \boldsymbol{\gamma_h} - M\boldsymbol{\gamma}$$

$\mathbf{F_i}$: inertial force on the vertex i (N),
M_a: added mass (kg) of 1/3 of the triangular element,
M: mass of 1/3 of the net (kg),
V: volume of 1/3 of the net (m^3),
ρ : density of water (kg/m^3),
$\boldsymbol{\gamma}$: acceleration of the vertex (m/s^2),
$\boldsymbol{\gamma_h}$: acceleration of the water around the vertex (m/s^2).

The vertex speed is calculated as follows:

$$\mathbf{v} = \frac{\mathbf{x_1} - \mathbf{x}}{\Delta t}$$

The acceleration of the vertex is

$$\boldsymbol{\gamma} = \frac{\mathbf{v_1} - \mathbf{v}}{\Delta t}$$

which gives

$$\boldsymbol{\gamma} = \frac{\mathbf{x_2} - 2\mathbf{x_1} + \mathbf{x}}{\Delta t^2}$$

In this case, the contribution to the stiffness matrix, from the derivative of this inertia, is calculated by

$$-F' = -\frac{\partial \mathbf{F_i}}{\partial \mathbf{x}}$$

which leads to

$$-F' = (M + M_a)\frac{\partial \boldsymbol{\gamma}}{\partial \mathbf{x}}$$

and

$$-F' = \frac{M + M_a}{\Delta t^2}$$

With: $\mathbf{x}$: position at t (m),
$\mathbf{x_1}$: position at $t - \Delta t$ (m),
$\mathbf{x_2}$: position at $t - 2\Delta t$ (m),
F': derivative of the force of inertia relative to the position(N/m),
Δt: time step (s).

3.3.8 Dynamic: drag force

The drag is related to the net and the relative speed of water particles just around the net. The calculation is done for each triangular element in three parts, one for each vertex, since this speed is not constant over the entire surface of each triangular element. Under these conditions the local parameters at each vertex are the vertex speed and one third of the number of twine vectors for the triangular element. The calculation is done for twines U and V.

The formulation for the twine drag is based on the assumptions of Landweber and Richtmeyer, as described earlier (section 3.3.3, page 47). The drag on the U twines applied on vertex i of the triangular element takes into account $1/3$ of the number of U twine vectors in the triangular element. This drag is as follows:

$$|\mathbf{F_i}| = \frac{d}{6}\frac{1}{2}\rho C_d D l_o (|\mathbf{c_i}| sin(\theta))^2$$

$$|\mathbf{T_i}| = \frac{d}{6} f \frac{1}{2}\rho C_d D l_o (|\mathbf{c_i}| cos(\theta))^2$$

F_i: normal force to the twines (N) on vertex i, this expression coming from the assumptions of Landweber,
T_i: tangential force (N) on vertex i, from Richtmeyer's assumption,
ρ: density of water (kg/m^3),
Cd: normal drag coefficient,
f: tangential coefficient,
D: diameter of twines U (m),
l_o: length of twine vectors U (m),
c_i: amplitude of the relative velocity of the water at vertex i (m/s),
θ: angle between the twine vectors U and the relative velocity ($radians$),
$\frac{d}{6}$: one third of the number of twine vectors U in the triangular element.

The angle θ between the twine vector $\mathbf{U}$ and the relative velocity is calculated by

$$cos(\theta) = \frac{\mathbf{c}_i \mathbf{U}}{|\mathbf{c}_i||\mathbf{U}|}$$

The directions of the drag in case of twine vector $\mathbf{U}$ are as follows:

$$\frac{\mathbf{F_i}}{|\mathbf{F_i}|} = \frac{\mathbf{U}}{|\mathbf{U}|} \wedge \frac{\mathbf{c_i} \wedge \mathbf{U}}{|\mathbf{c_i}||\mathbf{U}|}$$

$$\frac{\mathbf{T_i}}{|\mathbf{T_i}|} = \frac{\mathbf{F_i}}{|\mathbf{F_i}|} \wedge \frac{\mathbf{c_i} \wedge \mathbf{U}}{|\mathbf{c_i}||\mathbf{U}|}$$

The drag amplitude on twines V is calculated following the same scheme.

3.3.9 Buoyancy and weight

Buoyancy and weight are vertical forces (along the z axis, if it is the vertical axis). Their expression is summed in the following:

$$F_z = d\pi \frac{D^2}{4} l_0 (\rho_{netting} - \rho) g$$

F_z: weight of the net once immersed (N),
d: number of twine vectors $\mathbf{U}$ and twine vectors $\mathbf{V}$ per triangular element,
ρ: water density (kg/m^3),
$\rho_{netting}$: net density (kg/m^3),
D: diameter of twines (m),
g: gravity of the Earth (around $9.81 m/s^2$),
l_0: length of twine vectors (m).

The length of the twine vectors is approximated by the unstretched twine vector l_0, since the elongation is generally quite small.

There is a contribution of this force to the stiffness matrix when the netting crosses the water surface. In this case there is a variation of force with the immersion. This contribution is not described here.

Contact between knots

It happens quite frequently that the nets are so close that the nodes come into contact with each other. This contact limits the closing of mesh (Figure 3.18).

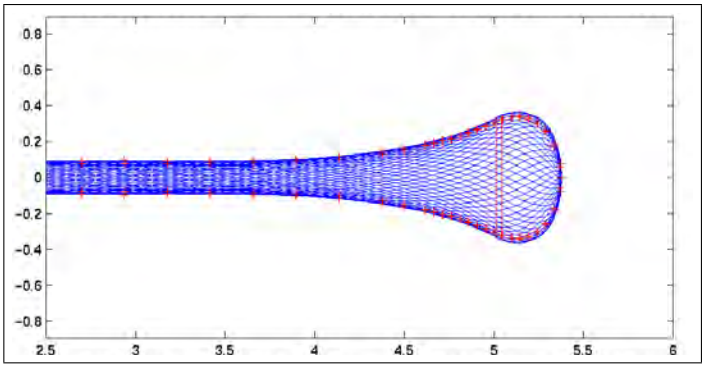

Figure 3.18: Comparison between simulations (net) and flume tank tests (crosses) of trawl cod-ends (Anon 1999). Between 2.5 and 3.5 m the diameter is constant. This is due to contact between the nodes of the net.

An effort similar to that described in section 3.3.4 (page 56) has been introduced to take into account this feature. This effort appears only when the twines are close enough, that is, when the angle between U and V twines is below a critical angle (α_{mini}). This angle is related to the node size and mesh side as follows (Figure 3.18):

$$\alpha_{mini} = 2 \arcsin \left[\frac{knot_{size}}{2mesh_{side}} \right]$$

α_{mini}: limit angle of contact between twines (rad),
$knot_{size}$: size of the node (m),
$mesh_{side}$: side of the mesh or length of twine vectors (m).

The $mesh_{side}$ could be the length of the twine vector along the U twine ($|\mathbf{U}|$) or the length of the twine vector along the V twine ($|\mathbf{V}|$). To avoid this choice (between $|\mathbf{U}|$ and $|\mathbf{V}|$), this length can be approximated by the unstretched length l_0 of the twine vector.

A couple is generated between the twines if the angle between them is less than the minimal angle:

$$\begin{cases} C = & H(\alpha - \alpha_{mini}) & if & \alpha <= \alpha_{mini} \\ C = & 0 & if & \alpha > \alpha_{mini} \end{cases}$$

C: couple between the twines due to the contact between knots (Nm),
α: angle between twines U and V (rad),
H: stiffness (Nm/Rad).

This stiffness is not well known. Therefore, arbitrary values can be used, such as the following, proportional to the elongation stiffness of the twine (EA):

$$H = \frac{1}{100} \frac{mesh_{side}^2 EA}{knot_{size}}$$

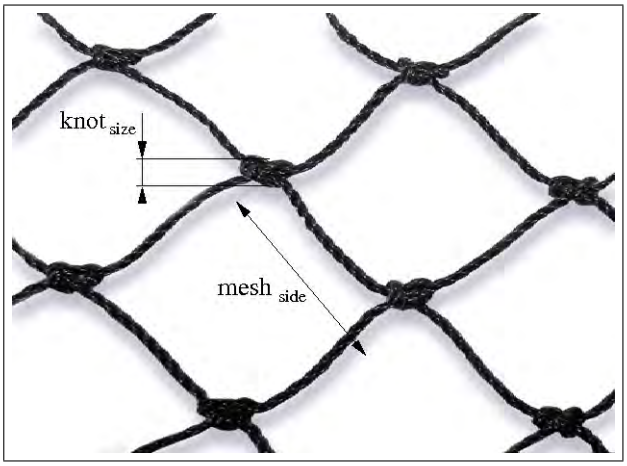

Figure 3.19: The size of the knot limits the closure of the mesh. The minimal angle between twines is due to the size of the knot and the side of the mesh (which is also the length of twine vector).

A: section of the twine (m^2),
E: Young's modulus (Pa).

The forces on the vertices of triangular elements and the stiffness use the same expressions as those described in section 3.3.4 (page 56).

Chapter 4

The bar finite element for cable

4.1 Principle

The cables are split into bar elements (Figure 4.1). The greater the number of bars, the better the representation of the curvature.

From the position **X** of the extremities of the bar elements the forces **F** on these extremities are calculated. The bar elements, in the present modelling, respect a couple of hypotheses. The first is that the bar element is straight. The second is that the bar element is elastic. These hypotheses make possible the calculation of forces on the extremities of the bar element.

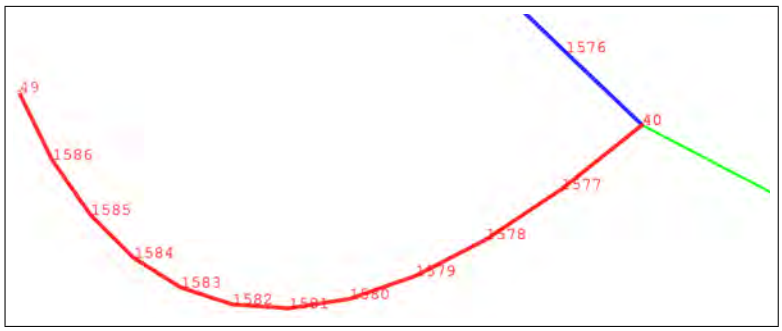

Figure 4.1: View of three cables split into bar elements. The nodes number are noted.

4.2 Tension on bars

4.2.1 Force vector

The forces on the extremities of the bar elements are due to the tension in the bar (Figure 4.2).

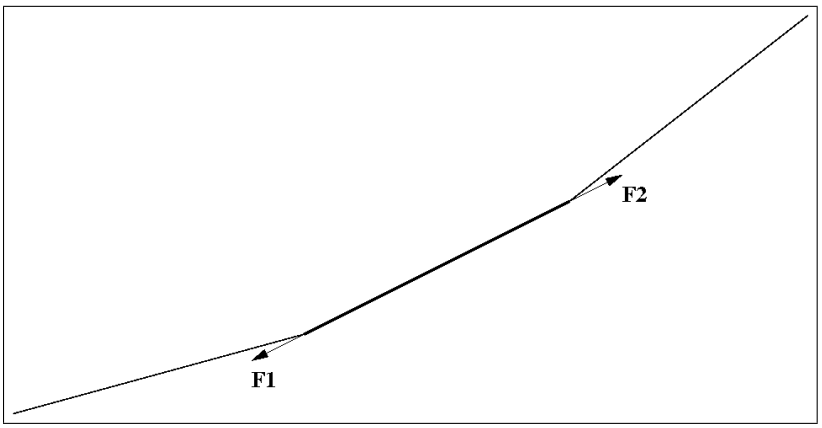

Figure 4.2: Tension forces **F1** and **F2** on the extremities of the bar due to its tension.

If the position of the extremities are noted 1 and 2, the length of the bar is:

$$l = \sqrt{\mathbf{12}.\mathbf{12}}$$

With:

$$\mathbf{12} = \begin{vmatrix} x_2 - x_1 \\ y_2 - y_1 \\ z_2 - z_1 \end{vmatrix}$$

The tension in the bar is:

$$|\mathbf{F}| = \frac{l - l_0}{l_0} EA$$

E : Young's modulus of the material (N/m^2),
A : mechanical section of the cable (m^2),
l_o : unstretched length of the bar element (m).

The force vectors on the two extremities of the bar are

$$\mathbf{F}_1 = |\mathbf{F}| \frac{\mathbf{21}}{l}$$

$$\mathbf{F}_2 = |\mathbf{F}| \frac{\mathbf{12}}{l}$$

The components of these forces are:

$$\mathbf{F}_{1x} = |\mathbf{F}| \frac{x_1 - x_2}{l}$$

$$\mathbf{F}_{1y} = |\mathbf{F}| \frac{y_1 - y_2}{l}$$

$$\mathbf{F}_{1z} = |\mathbf{F}|\frac{z_1 - z_2}{l}$$
$$\mathbf{F}_{2x} = |\mathbf{F}|\frac{x_2 - x_1}{l}$$
$$\mathbf{F}_{2y} = |\mathbf{F}|\frac{y_2 - y_1}{l}$$
$$\mathbf{F}_{2z} = |\mathbf{F}|\frac{z_2 - z_1}{l}$$

4.2.2 Stiffness matrix

The stiffness matrix is as follows:

$$K = \begin{pmatrix} -\frac{\partial F_{1x}}{\partial x_1} & -\frac{\partial F_{1x}}{\partial y_1} & -\frac{\partial F_{1x}}{\partial z_1} & -\frac{\partial F_{1x}}{\partial x_2} & -\frac{\partial F_{1x}}{\partial y_2} & -\frac{\partial F_{1x}}{\partial z_2} \\ -\frac{\partial F_{1y}}{\partial x_1} & -\frac{\partial F_{1y}}{\partial y_1} & -\frac{\partial F_{1y}}{\partial z_1} & -\frac{\partial F_{1y}}{\partial x_2} & -\frac{\partial F_{1y}}{\partial y_2} & -\frac{\partial F_{1y}}{\partial z_2} \\ -\frac{\partial F_{1z}}{\partial x_1} & -\frac{\partial F_{1z}}{\partial y_1} & -\frac{\partial F_{1z}}{\partial z_1} & -\frac{\partial F_{1z}}{\partial x_2} & -\frac{\partial F_{1z}}{\partial y_2} & -\frac{\partial F_{1z}}{\partial z_2} \\ -\frac{\partial F_{2x}}{\partial x_1} & -\frac{\partial F_{2x}}{\partial y_1} & -\frac{\partial F_{2x}}{\partial z_1} & -\frac{\partial F_{2x}}{\partial x_2} & -\frac{\partial F_{2x}}{\partial y_2} & -\frac{\partial F_{2x}}{\partial z_2} \\ -\frac{\partial F_{2y}}{\partial x_1} & -\frac{\partial F_{2y}}{\partial y_1} & -\frac{\partial F_{2y}}{\partial z_1} & -\frac{\partial F_{2y}}{\partial x_2} & -\frac{\partial F_{2y}}{\partial y_2} & -\frac{\partial F_{2y}}{\partial z_2} \\ -\frac{\partial F_{2z}}{\partial x_1} & -\frac{\partial F_{2z}}{\partial y_1} & -\frac{\partial F_{2z}}{\partial z_1} & -\frac{\partial F_{2z}}{\partial x_2} & -\frac{\partial F_{2z}}{\partial y_2} & -\frac{\partial F_{2z}}{\partial z_2} \end{pmatrix}$$

The stiffness matrix is calculated through the derivatives of force components. For the first component that gives:

$$-\frac{\partial F_{1x}}{\partial x_1} = -\frac{\left[\frac{EA}{l_0}\frac{\partial l}{\partial x_1}(x_1 - x_2) + |\mathbf{F}|\frac{\partial (x_1 - x_2)}{\partial x_1}\right] l - |\mathbf{F}|(x_1 - x_2)\frac{\partial l}{\partial x_1}}{l^2}$$

with

$$\frac{\partial l}{\partial x_1} = \frac{x_2 - x_1}{l}$$

That gives for the 36 components:

$$-\frac{\partial F_{1x}}{\partial x_1} = \frac{\partial F_{1x}}{\partial x_2} = \frac{\partial F_{2x}}{\partial x_1} = -\frac{\partial F_{2x}}{\partial x_2} = \frac{EA}{l^3 lo}\left[l^3 - l^2 lo + lo(x_2 - x_1)^2\right]$$
$$-\frac{\partial F_{1y}}{\partial y_1} = \frac{\partial F_{1y}}{\partial y_2} = \frac{\partial F_{2y}}{\partial y_1} = -\frac{\partial F_{2y}}{\partial y_2} = \frac{EA}{l^3 lo}\left[l^3 - l^2 lo + lo(y_2 - y_1)^2\right]$$
$$-\frac{\partial F_{1z}}{\partial z_1} = \frac{\partial F_{1z}}{\partial z_2} = \frac{\partial F_{2z}}{\partial z_1} = -\frac{\partial F_{2z}}{\partial z_2} = \frac{EA}{l^3 lo}\left[l^3 - l^2 lo + lo(z_2 - z_1)^2\right]$$

$$-\frac{\partial F_{1x}}{\partial y_1} = -\frac{\partial F_{1y}}{\partial x_1} = -\frac{\partial F_{2y}}{\partial x_2} = -\frac{\partial F_{2x}}{\partial y_2} = \frac{\partial F_{2y}}{\partial x_1} = \frac{\partial F_{2x}}{\partial y_1} = \frac{\partial F_{1y}}{\partial x_2} = \frac{\partial F_{1x}}{\partial y_2} = \frac{EA}{l^3}\left[(x_2 - x_1)(y_2 - y_1)\right]$$

$$-\frac{\partial F_{1x}}{\partial z_1} = -\frac{\partial F_{1z}}{\partial x_1} = -\frac{\partial F_{2z}}{\partial x_2} = -\frac{\partial F_{2x}}{\partial z_2} = \frac{\partial F_{2z}}{\partial x_1} = \frac{\partial F_{2x}}{\partial z_1} = \frac{\partial F_{1z}}{\partial x_2} = \frac{\partial F_{1x}}{\partial z_2} = \frac{EA}{l^3}\left[(x_2 - x_1)(z_2 - z_1)\right]$$

$$-\frac{\partial F_{1y}}{\partial z_1} = -\frac{\partial F_{1z}}{\partial y_1} = -\frac{\partial F_{2z}}{\partial y_2} = -\frac{\partial F_{2y}}{\partial z_2} = \frac{\partial F_{2z}}{\partial y_1} = \frac{\partial F_{2y}}{\partial z_1} = \frac{\partial F_{1z}}{\partial y_2} = \frac{\partial F_{1y}}{\partial z_2} = \frac{EA}{l^3}\left[(y_2 - y_1)(z_2 - z_1)\right]$$

4.3 Bending of cables

Cables could have a resistance in bending, such as beams. Beam deformation relates the curvature of the beam to the couple, such as:

$$C_o = \frac{EI}{R}$$

C_o: the couple on any point of the cable ($N.m$),
EI: the bending rigidity of the cable ($N.m^2$),
R: the radius of the cable at the point (m).

To take into account this behaviour in the numerical model, the cables are split into bar elements (Figure 4.3). In case of bending stiffness, there is a couple C_o between consecutive bar elements (Figure 4.4). This couple leads to forces on the extremities of theses two elements.

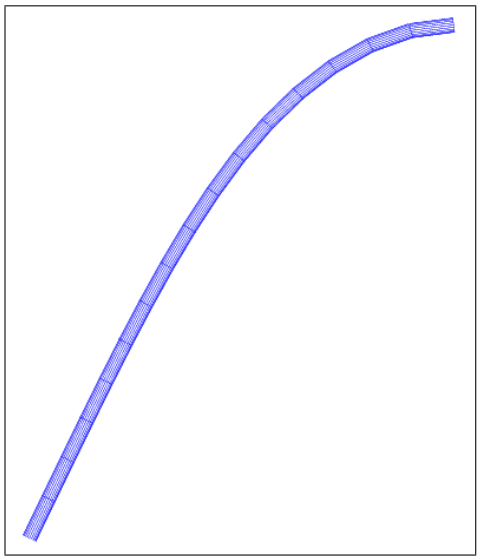

Figure 4.3: The cable is embedded at top right. It is modelled with bar elements. Each bar is straight and articulated with its neighbour.

4.3.1 Force vector

The forces on the extremities of two consecutive bar elements are due to the bending between the bar elements (Figure 4.4).

The curvature is approximated by the circle passing by the extremities of the two bar elements. The positions of the extremities of the bars allow assessment of this radius (Figure 4.5). From this radius, and if the bending rigidity is known, the model is able to calculate the couple:

$$C_o = \frac{EI}{R}$$

The radius (R) is calculated from the position of the extremities:

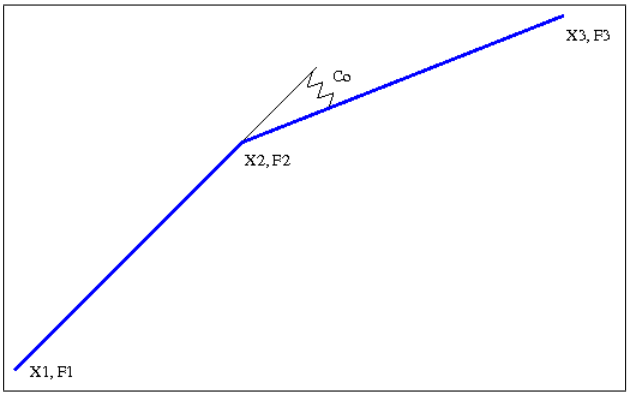

Figure 4.4: Representation of two consecutive bars. A couple is introduced to take into account the bending rigidity of the cable. The spring symbolizes the couple.

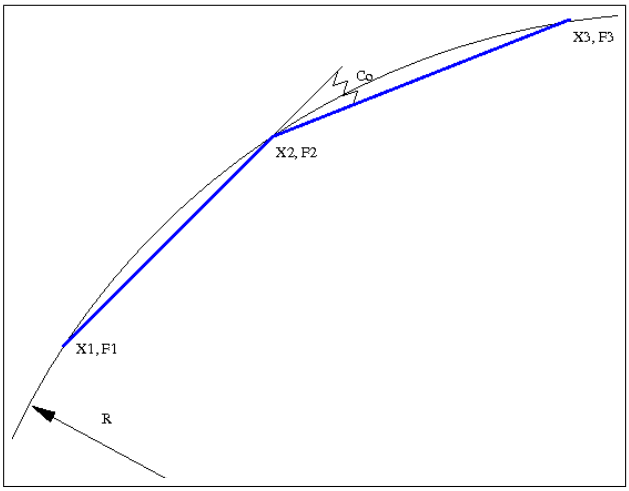

Figure 4.5: The radius of the curvature is assessed by the circle passing by the extremities of the two bar elements.

$$R = \frac{ABC}{4\sqrt{p(p-A)(p-B)(p-C)}}$$

A (B): length of the first (second) bar (m),
C: distance between the extremities 1 and 3 in Figure 4.5 (m),
p: the half perimeter (m), where

$$p = \frac{A+B+C}{2}$$

Once the couple C_o is calculated, the model assesses the forces on the extremities of the bars using the virtual work principle.

The force component along X on the extremity 1 of the first bar element is estimated by considering a virtual displacement ($\partial x1$) along the axis x of the extremity 1 (Figure 4.6). This

displacement leads to an external work, considering $\partial x1$ small and consequently F_{x1} constant:

$$W_e = F_{x1}\partial x1$$

This virtual displacement also induces a change in the angle (α) between bar elements.

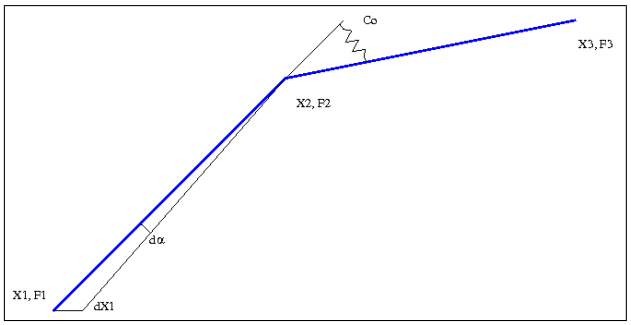

Figure 4.6: A virtual displacement ($\partial x1$) leads to an external work ($F_{x1}\partial x1$) equal to the internal work ($C_o\partial\alpha$).

This virtual displacement leads to a variation of angle between bars ($\partial\alpha$), and this variation of angle generates an internal work. If $\partial x1$ is small, $\partial\alpha$ is small and consequently C_o is constant. That gives

$$W_i = C_o\partial\alpha$$

Because the forces on the extremities of the two bar elements represent the couple C_o there is equality between the works. That leads to:

$$\begin{array}{lll} F_{x1} = C_o\frac{\partial\alpha}{\partial x1} & F_{x2} = C_o\frac{\partial\alpha}{\partial x2} & F_{x3} = C_o\frac{\partial\alpha}{\partial x3} \\ F_{y1} = C_o\frac{\partial\alpha}{\partial y1} & F_{y2} = C_o\frac{\partial\alpha}{\partial y2} & F_{y3} = C_o\frac{\partial\alpha}{\partial y3} \\ F_{z1} = C_o\frac{\partial\alpha}{\partial z1} & F_{z2} = C_o\frac{\partial\alpha}{\partial z2} & F_{z3} = C_o\frac{\partial\alpha}{\partial z3} \end{array}$$

These forces components are:

$$F_{x1} = \frac{EI}{R\sin\alpha}\left[\frac{(x2-x1)\mathbf{AB}}{A^3B} + \frac{x2-x3}{AB}\right]$$

$$F_{y1} = \frac{EI}{R\sin\alpha}\left[\frac{(y2-y1)\mathbf{AB}}{A^3B} + \frac{y2-y3}{AB}\right]$$

$$F_{z1} = \frac{EI}{R\sin\alpha}\left[\frac{(z2-z1)\mathbf{AB}}{A^3B} + \frac{z2-z3}{AB}\right]$$

$$F_{x2} = \frac{EI}{R\sin\alpha}\left[\frac{(x1-x2)\mathbf{AB}}{A^3B} + \frac{(x3-x2)\mathbf{AB}}{AB^3} + \frac{x3-2x2+x1}{AB}\right]$$

$$F_{y2} = \frac{EI}{R\sin\alpha}\left[\frac{(y1-y2)\mathbf{AB}}{A^3B} + \frac{(y3-y2)\mathbf{AB}}{AB^3} + \frac{y3-2y2+y1}{AB}\right]$$

$$F_{z2} = \frac{EI}{R\sin\alpha}\left[\frac{(z1-z2)\mathbf{AB}}{A^3B} + \frac{(z3-z2)\mathbf{AB}}{AB^3} + \frac{z3-2z2+z1}{AB}\right]$$

$$F_{x3} = \frac{EI}{R\sin\alpha}\left[\frac{(x2-x3)\mathbf{AB}}{AB^3} + \frac{x2-x1}{AB}\right]$$

$$F_{y3} = \frac{EI}{R\sin\alpha}\left[\frac{(y2-y3)\mathbf{AB}}{AB^3} + \frac{y2-y1}{AB}\right]$$
$$F_{z3} = \frac{EI}{R\sin\alpha}\left[\frac{(z2-z3)\mathbf{AB}}{AB^3} + \frac{z2-z1}{AB}\right]$$

On vectorial form:

$$\mathbf{F}_1 = \frac{EI}{ABR\sin\alpha}\left[\frac{\mathbf{A}.\mathbf{AB}}{A^2} - \mathbf{B}\right]$$
$$\mathbf{F}_2 = \frac{EI}{ABR\sin\alpha}\left[-\frac{\mathbf{A}.\mathbf{AB}}{A^2} + \frac{\mathbf{B}.\mathbf{AB}}{B^2} + \mathbf{B} - \mathbf{A}\right]$$
$$\mathbf{F}_3 = \frac{EI}{ABR\sin\alpha}\left[-\frac{\mathbf{B}.\mathbf{AB}}{B^2} + \mathbf{A}\right]$$

With:
$\mathbf{F}_1$ ($\mathbf{F}_2$, $\mathbf{F}_3$): force on the node 1 (2, 3),
AB: scalar product between the two bar vectors,
A (**B**): vector along the first (second) bar element,
A (B): length of the first (second) bar element (m),
$x1$ to $z3$: the Cartesian coordinates of the three extremities of the two bar elements (m).

4.3.2 Stiffness matrix

The stiffness matrix is calculated with the derivatives of the force components (F_{x1} to F_{z3}) relative to the positions ($x1$ to $z3$). This means that the stiffness matrix has 81 components.

4.4 Drag on cables

Introduction

The drag force on cables is calculated in this model as the contribution of the drag force on each bar elements. The formulation for the drag is based on the assumptions of Morrison, as adapted by Landweber and Richtmeyer (see section 3.3.3 page 47).

The drag amplitudes on bar element used in the model (Figure 4.7) are

$$|\mathbf{F}| = \frac{1}{2}\rho C_d D l_0 \left[|\mathbf{c}| sin(\alpha)\right]^2$$

$$|\mathbf{T}| = f\frac{1}{2}\rho C_d D l_0 \left[|\mathbf{c}| cos(\alpha)\right]^2$$

The directions of the drag are as follows:

$$\frac{\mathbf{F}}{|\mathbf{F}|} = \frac{\mathbf{B} \wedge (\mathbf{c} \wedge \mathbf{B})}{|\mathbf{B} \wedge (\mathbf{c} \wedge \mathbf{B})|}$$

$$\frac{\mathbf{T}}{|\mathbf{T}|} = \frac{\mathbf{F} \wedge (\mathbf{c} \wedge \mathbf{F})}{|\mathbf{F} \wedge (\mathbf{c} \wedge \mathbf{F})|}$$

$\mathbf{F}$: normal drag (N), following the assumptions of Landweber,
$\mathbf{T}$: tangential drag (N), Richtmeyer hypothesis,
$\mathbf{B}$: bar element vector,
ρ: density of water (kg/m^3),
C_d: normal drag coefficient,
f: tangential drag coefficient,
D: diameter of the bar element (m),
l_0: length of the bar element (m),
$\mathbf{c}$: water velocity relative to the bar element (m/s),
α: angle between the bar element and the water velocity ($radians$).

In the equations of drag amplitude, the expressions $|\mathbf{c}|sin(\alpha)$ and $|\mathbf{c}|cos(\alpha)$ are the normal and tangential projections on $\mathbf{c}$ along the bar element vector.

The length of the bar element used in the formulation of drag amplitude could be assessed by $|\mathbf{B}|$. That would mean it takes into account the bar element elongation. Generally speaking, a bar elongation is associated with a diameter D reduction by the Poisson coefficient. Because this Poisson coefficient is not taken into account in the present modelling, the bar element surface is approximated by Dl_0, where D is the diameter of the bar and l_0 is the unstretched length of the bar element vectors.

All parameters, including the angle α are constant and known for each bar element. Therefore, the drag can be calculated for each bar element. The drag force for a bar element is spread over the two vertices of the element at 1/2 per vertex.

Definitions of the variables

The Cartesian coordinates of the two nodes (1, 2) of the bar element are the following:

$$\mathbf{1} = \left| \begin{array}{l} x_1 \\ y_1 \\ z_1 \end{array} \right.$$

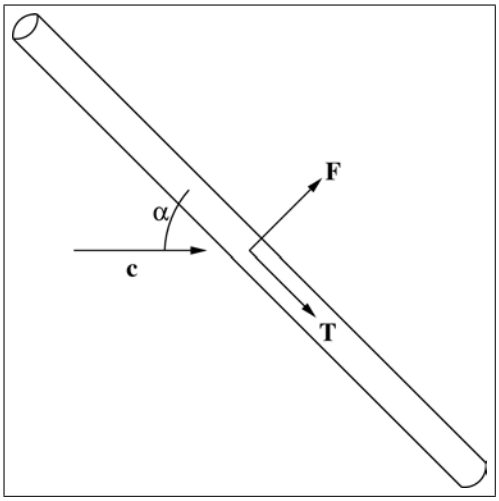

Figure 4.7: Normal (**F**) and tangential (**T**) forces on a bar element due to the velocity of water (**c**).

$$\mathbf{2} = \left| \begin{array}{l} x_2 \\ y_2 \\ z_2 \end{array} \right.$$

The vector bar element is as follows:

$$\mathbf{B} = \left| \begin{array}{l} x_2 - x_1 \\ y_2 - y_1 \\ z_2 - z_1 \end{array} \right.$$

The vector current is

$$\mathbf{c} = \left| \begin{array}{l} c_x \\ c_y \\ c_z \end{array} \right.$$

Generally speaking, c_z is null.
The angle between current and B is

$$cos(\alpha) = \frac{\mathbf{c}.\mathbf{B}}{|\mathbf{c}||\mathbf{B}|}$$

Evaluation for the stiffness of the normal force

The normal force on B is

$$\mathbf{F} = |\mathbf{F}| \frac{\mathbf{B} \wedge (\mathbf{c} \wedge \mathbf{B})}{|\mathbf{B} \wedge (\mathbf{c} \wedge \mathbf{B})|}$$

That means that the x y and z components are:

$$\mathbf{F}_x = |\mathbf{F}| \frac{\mathbf{E}_x}{|\mathbf{E}|}$$

$$\mathbf{F}_y = |\mathbf{F}|\frac{\mathbf{E}_y}{|\mathbf{E}|}$$

$$\mathbf{F}_z = |\mathbf{F}|\frac{\mathbf{E}_z}{|\mathbf{E}|}$$

With:

$$\mathbf{E} = \mathbf{B} \wedge (\mathbf{c} \wedge \mathbf{B})$$

and

$$\mathbf{E} = \left| \begin{array}{l} E_x \\ E_y \\ E_z \end{array} \right.$$

The x component of the derivative is

$$\mathbf{F}'_x = |\mathbf{F}|'\frac{\mathbf{E}_x}{|\mathbf{E}|} + |\mathbf{F}|\frac{\mathbf{E}'_x|\mathbf{E}| - \mathbf{E}_x|\mathbf{E}|'}{|\mathbf{E}|^2}$$

Which gives for the x y and z components:

$$\mathbf{F}'_x = |\mathbf{F}|'\frac{\mathbf{E}_x}{|\mathbf{E}|} + \frac{|\mathbf{F}|}{|\mathbf{E}|^2}\left\{\mathbf{E}'_x|\mathbf{E}| - \frac{\mathbf{E}_x}{|\mathbf{E}|}(\mathbf{E}_x\mathbf{E}'_x + \mathbf{E}_y\mathbf{E}'_y + \mathbf{E}_z\mathbf{E}'_z)\right\}$$

$$\mathbf{F}'_y = |\mathbf{F}|'\frac{\mathbf{E}_y}{|\mathbf{E}|} + \frac{|\mathbf{F}|}{|\mathbf{E}|^2}\left\{\mathbf{E}'_y|\mathbf{E}| - \frac{\mathbf{E}_y}{|\mathbf{E}|}(\mathbf{E}_x\mathbf{E}'_x + \mathbf{E}_y\mathbf{E}'_y + \mathbf{E}_z\mathbf{E}'_z)\right\}$$

$$\mathbf{F}'_z = |\mathbf{F}|'\frac{\mathbf{E}_z}{|\mathbf{E}|} + \frac{|\mathbf{F}|}{|\mathbf{E}|^2}\left\{\mathbf{E}'_z|\mathbf{E}| - \frac{\mathbf{E}_z}{|\mathbf{E}|}(\mathbf{E}_x\mathbf{E}'_x + \mathbf{E}_y\mathbf{E}'_y + \mathbf{E}_z\mathbf{E}'_z)\right\}$$

For this assessment the derivative of $\mathbf{E}$ is required:

$$\mathbf{E}' = \mathbf{B}' \wedge (\mathbf{c} \wedge \mathbf{B}) + \mathbf{B} \wedge (\mathbf{c} \wedge \mathbf{B}')$$

This leads to

$$\mathbf{E}' = 2(\mathbf{B}'.\mathbf{B})\mathbf{c} - (\mathbf{B}'.\mathbf{c})\mathbf{B} - (\mathbf{B}.\mathbf{c})\mathbf{B}'$$

which is

$$\mathbf{E}'_x = 2(\mathbf{B}'.\mathbf{B})\mathbf{c}_x - (\mathbf{B}'.\mathbf{c})\mathbf{B}_x - (\mathbf{B}.\mathbf{c})\mathbf{B}'_x$$
$$\mathbf{E}'_y = 2(\mathbf{B}'.\mathbf{B})\mathbf{c}_y - (\mathbf{B}'.\mathbf{c})\mathbf{B}_y - (\mathbf{B}.\mathbf{c})\mathbf{B}'_y$$
$$\mathbf{E}'_z = 2(\mathbf{B}'.\mathbf{B})\mathbf{c}_z - (\mathbf{B}'.\mathbf{c})\mathbf{B}_z - (\mathbf{B}.\mathbf{c})\mathbf{B}'_z$$

with

$$\mathbf{B}'.\mathbf{B} = \mathbf{B}_x\mathbf{B}'_x + \mathbf{B}_y\mathbf{B}'_y + \mathbf{B}_z\mathbf{B}'_z$$
$$\mathbf{B}'.\mathbf{c} = \mathbf{c}_x\mathbf{B}'_x + \mathbf{c}_y\mathbf{B}'_y + \mathbf{c}_z\mathbf{B}'_z$$
$$\mathbf{B}.\mathbf{c} = \mathbf{B}_x\mathbf{c}_x + \mathbf{B}_y\mathbf{c}_y + \mathbf{B}_z\mathbf{c}_z$$

The derivative of the amplitude of the normal force is

$$|\mathbf{F}|' = \frac{1}{2}\rho C_d D l_0 |\mathbf{c}|^2 \left([sin(\alpha)]^2\right)'$$

which is

$$|\mathbf{F}|' = \rho C_d D l_0 |\mathbf{c}|^2 cos(\alpha) sin(\alpha) \alpha'$$

The derivative of α is

$$\alpha' = \frac{-1}{\sqrt{1-(\frac{\mathbf{c}.\mathbf{B}}{|\mathbf{c}||\mathbf{B}|})^2}} \left[\frac{\mathbf{c}.\mathbf{B}}{|\mathbf{c}||\mathbf{B}|}\right]'$$

That gives

$$\alpha' = \frac{-1}{\sqrt{1-(\frac{\mathbf{c}.\mathbf{B}}{|\mathbf{c}||\mathbf{B}|})^2}} \left[\frac{\mathbf{c}}{|\mathbf{c}|}.\left(\frac{\mathbf{B}}{|\mathbf{B}|}\right)'\right]$$

The derivative of the bar element direction is

$$\left(\frac{\mathbf{B}}{|\mathbf{B}|}\right)' = \frac{\mathbf{B}'|\mathbf{B}| - \mathbf{B}|\mathbf{B}|'}{|\mathbf{B}|^2}$$

That means that the derivative of α is

$$\alpha' = \frac{-1}{\sqrt{1-(\frac{\mathbf{c}.\mathbf{B}}{|\mathbf{c}||\mathbf{B}|})^2}} \left(\frac{\mathbf{c}}{|\mathbf{c}|}\right).\left(\frac{\mathbf{B}'|\mathbf{B}| - \mathbf{B}|\mathbf{B}|'}{|\mathbf{B}|^2}\right)$$

or

$$\alpha' = \frac{-1}{|\mathbf{B}|^2|\mathbf{c}|\sin\alpha} \left\{|\mathbf{B}|\left[c_x\mathbf{B}'_x + c_y\mathbf{B}'_y + c_z\mathbf{B}'_z\right] - (\mathbf{c}.\mathbf{B})|\mathbf{B}|'\right\}$$

In this case $\mathbf{B}'_x$ is the component along x of $\mathbf{B}'$.
The derivative of vector $\mathbf{B}$ is

$$\mathbf{B}' = \left|\begin{array}{l} \mathbf{B}'_x \\ \mathbf{B}'_y \\ \mathbf{B}'_z \end{array}\right.$$

which is

$$\frac{\partial B_x}{\partial x_1} = \frac{\partial B_y}{\partial y_1} = \frac{\partial B_z}{\partial z_1} = -1$$

$$\frac{\partial B_x}{\partial x_2} = \frac{\partial B_y}{\partial y_2} = \frac{\partial B_z}{\partial z_2} = 1$$

$$\frac{\partial B_x}{\partial y_1} = \frac{\partial B_x}{\partial y_2} = \frac{\partial B_x}{\partial z_1} = \frac{\partial B_x}{\partial z_2} = 0$$

$$\frac{\partial B_y}{\partial z_1} = \frac{\partial B_y}{\partial z_2} = \frac{\partial B_y}{\partial x_1} = \frac{\partial B_y}{\partial x_2} = 0$$

$$\frac{\partial B_z}{\partial x_1} = \frac{\partial B_z}{\partial x_2} = \frac{\partial B_z}{\partial y_1} = \frac{\partial B_z}{\partial y_2} = 0$$

On vector form and for the nine coordinates of the triangular element it is

$$\frac{\partial \mathbf{B}}{\partial x_1} = \begin{vmatrix} -1 \\ 0 \\ 0 \end{vmatrix}$$

$$\frac{\partial \mathbf{B}}{\partial y_1} = \begin{vmatrix} 0 \\ -1 \\ 0 \end{vmatrix}$$

$$\frac{\partial \mathbf{B}}{\partial z_1} = \begin{vmatrix} 0 \\ 0 \\ -1 \end{vmatrix}$$

$$\frac{\partial \mathbf{B}}{\partial x_2} = \begin{vmatrix} 1 \\ 0 \\ 0 \end{vmatrix}$$

$$\frac{\partial \mathbf{B}}{\partial y_2} = \begin{vmatrix} 0 \\ 1 \\ 0 \end{vmatrix}$$

$$\frac{\partial \mathbf{B}}{\partial z_2} = \begin{vmatrix} 0 \\ 0 \\ 1 \end{vmatrix}$$

The derivative of the norm of vector $\mathbf{B}$ is

$$|\mathbf{B}|' = \frac{B_x B'_x + B_y B'_y + B_z B'_z}{|\mathbf{B}|}$$

Which gives for the nine coordinates of the triangular element:

$$\frac{\partial |\mathbf{B}|}{\partial x_1} = \frac{-B_x}{|\mathbf{B}|}$$

$$\frac{\partial |\mathbf{B}|}{\partial y_1} = \frac{-B_y}{|\mathbf{B}|}$$

$$\frac{\partial |\mathbf{B}|}{\partial z_1} = \frac{-B_z}{|\mathbf{B}|}$$

$$\frac{\partial |\mathbf{B}|}{\partial x_2} = \frac{B_x}{|\mathbf{B}|}$$

$$\frac{\partial |\mathbf{B}|}{\partial y_2} = \frac{B_y}{|\mathbf{B}|}$$

$$\frac{\partial |\mathbf{B}|}{\partial z_2} = \frac{B_z}{|\mathbf{B}|}$$

Evaluation for the stiffness of the tangential force

The tangential force on the bar element is

$$\mathbf{T} = |\mathbf{T}|\frac{\mathbf{F} \wedge (\mathbf{c} \wedge \mathbf{F})}{|\mathbf{F} \wedge (\mathbf{c} \wedge \mathbf{F})|}$$

Following the definition of $\mathbf{F}$:

$$\mathbf{T} = |\mathbf{T}|\frac{[\mathbf{B} \wedge (\mathbf{c} \wedge \mathbf{B})] \wedge \{\mathbf{c} \wedge [\mathbf{B} \wedge (\mathbf{c} \wedge \mathbf{B})]\}}{|\,[\mathbf{B} \wedge (\mathbf{c} \wedge \mathbf{B})] \wedge \{\mathbf{c} \wedge [\mathbf{B} \wedge (\mathbf{c} \wedge \mathbf{B})]\}\,|}$$

It follows:

$$\mathbf{T} = |\mathbf{T}|\frac{[(\mathbf{B}.\mathbf{B})(\mathbf{c}.\mathbf{c}) - (\mathbf{B}.\mathbf{c})^2](\mathbf{B}.\mathbf{c})\mathbf{B}}{|[(\mathbf{B}.\mathbf{B})(\mathbf{c}.\mathbf{c}) - (\mathbf{B}.\mathbf{c})^2](\mathbf{B}.\mathbf{c})\mathbf{B}|}$$

or

$$\mathbf{T} = |\mathbf{T}|\frac{[|\mathbf{B}|^2|\mathbf{c}|^2 - (|\mathbf{B}||\mathbf{c}|cos\alpha)^2]|\mathbf{B}||\mathbf{c}|cos\alpha\mathbf{B}}{|[|\mathbf{B}|^2|\mathbf{c}|^2 - (|\mathbf{B}||\mathbf{c}|cos\alpha)^2]|\mathbf{B}||\mathbf{c}|cos\alpha\mathbf{B}|}$$

and

$$\mathbf{T} = |\mathbf{T}|\frac{\cos\alpha\mathbf{B}}{|\cos\alpha||\mathbf{B}|}$$

The x y and z components are:

$$\mathbf{T}_x = |\mathbf{T}|\frac{\cos\alpha\mathbf{B}_x}{|\cos\alpha||\mathbf{B}|}$$

$$\mathbf{T}_y = |\mathbf{T}|\frac{\cos\alpha\mathbf{B}_y}{|\cos\alpha||\mathbf{B}|}$$

$$\mathbf{T}_z = |\mathbf{T}|\frac{\cos\alpha\mathbf{B}_z}{|\cos\alpha||\mathbf{B}|}$$

The derivative of $\mathbf{T}_x$ is:

$$\mathbf{T}'_x = |\mathbf{T}|'\frac{\cos\alpha\mathbf{B}_x}{|\cos\alpha||\mathbf{B}|} + |\mathbf{T}|\frac{(\cos\alpha\mathbf{B}_x)'|\cos\alpha||\mathbf{B}| - \cos\alpha\mathbf{B}_x(|\cos\alpha||\mathbf{B}|)'}{(|\cos\alpha||\mathbf{B}|)^2}$$

$$\begin{aligned}
\mathbf{T}'_x &= |\mathbf{T}|'\frac{\cos\alpha\mathbf{B}_x}{|\cos\alpha||\mathbf{B}|} \\
&+ \frac{|\mathbf{T}|}{|\cos\alpha||\mathbf{B}|}(\cos\alpha\mathbf{B}'_x - \sin\alpha\alpha'\mathbf{B}_x) \\
&- \frac{|\mathbf{T}|\cos\alpha\mathbf{B}_x}{(|\cos\alpha||\mathbf{B}|)^2}\left[|\cos\alpha|\frac{\mathbf{B}_x\mathbf{B}'_x + \mathbf{B}_y\mathbf{B}'_y + \mathbf{B}_z\mathbf{B}'_z}{|\mathbf{B}|} - \frac{\cos\alpha}{|\cos\alpha|}\sin\alpha\alpha'|\mathbf{B}|\right]
\end{aligned}$$

$$\begin{aligned}
\mathbf{T}'_x &= |\mathbf{T}|'\frac{\mathbf{T}_x}{|\mathbf{T}|} + \frac{|\mathbf{T}|}{|\cos\alpha||\mathbf{B}|}(\cos\alpha\mathbf{B}'_x - \sin\alpha\alpha'\mathbf{B}_x) \\
&- \frac{\mathbf{T}_x}{|\cos\alpha||\mathbf{B}|}\left[|\cos\alpha|\frac{\mathbf{B}_x\mathbf{B}'_x + \mathbf{B}_y\mathbf{B}'_y + \mathbf{B}_z\mathbf{B}'_z}{|\mathbf{B}|} - \frac{\cos\alpha}{|\cos\alpha|}\sin\alpha\alpha'|\mathbf{B}|\right]
\end{aligned}$$

$$\begin{aligned}\mathbf{T}'_y &= |\mathbf{T}|'\frac{\mathbf{T}_y}{|\mathbf{T}|} + \frac{|\mathbf{T}|}{|\cos\alpha||\mathbf{B}|}(\cos\alpha\mathbf{B}'_y - \sin\alpha\alpha'\mathbf{B}_y) \\ &- \frac{\mathbf{T}_y}{|\cos\alpha||\mathbf{B}|}\left[|\cos\alpha|\frac{\mathbf{B}_x\mathbf{B}'_x + \mathbf{B}_y\mathbf{B}'_y + \mathbf{B}_z\mathbf{B}'_z}{|\mathbf{B}|} - \frac{\cos\alpha}{|\cos\alpha|}\sin\alpha\alpha'|\mathbf{B}|\right]\end{aligned}$$

$$\begin{aligned}\mathbf{T}'_z &= |\mathbf{T}|'\frac{\mathbf{T}_z}{|\mathbf{T}|} + \frac{|\mathbf{T}|}{|\cos\alpha||\mathbf{B}|}(\cos\alpha\mathbf{B}'_z - \sin\alpha\alpha'\mathbf{B}_z) \\ &- \frac{\mathbf{T}_z}{|\cos\alpha||\mathbf{B}|}\left[|\cos\alpha|\frac{\mathbf{B}_x\mathbf{B}'_x + \mathbf{B}_y\mathbf{B}'_y + \mathbf{B}_z\mathbf{B}'_z}{|\mathbf{B}|} - \frac{\cos\alpha}{|\cos\alpha|}\sin\alpha\alpha'|\mathbf{B}|\right]\end{aligned}$$

The derivative of the amplitude of the tangential force is

$$|\mathbf{T}|' = f\frac{1}{2}\rho C_d D l_0 |\mathbf{c}|^2 \left([cos(\alpha)]^2\right)' \frac{d}{2}$$

which is

$$|\mathbf{T}|' = -\frac{d}{2} f\rho C_d D l_0 |\mathbf{c}|^2 cos(\alpha) sin(\alpha)\alpha'$$

Chapter 5

The node element

5.1 Principle

The contact of a marine structure with the sea bed has to be taken into account. It is of great importance for structures such as chains lying on the sea-bed or bottom trawls.

In the following sections a few forces related to this contact are described.

5.2 Contact on bottom

In this model, the main hypothesis for these contact forces is that the bottom is elastic. That means that if a node is in contact with the bottom, the force reaction (N) is equal to the product of the node depth (m) in the soil by the soil stiffness (N/m).

5.2.1 Force vector

The vertical force on a node due to its potential contact with the bottom is

$$\begin{aligned} if z < Z_b \quad F_z &= \quad B_k(Z_b - z) \\ if z \geq Z_b \quad F_z &= \quad 0 \end{aligned}$$

With:
F_z: the vertical force on the node (N),
B_k: the bottom stiffness (N/m),
Z_b: the vertical position of the bottom (m),
z: the vertical position of the node (m).

5.2.2 Stiffness matrix

$$\begin{aligned} if z < Z_b \quad -\frac{\partial F_z}{\partial z} &= \quad B_k \\ if z \geq Z_b \quad -\frac{\partial F_z}{\partial z} &= \quad 0 \end{aligned}$$

5.3 Drag on bottom

Contact of a node with the bottom could lead to a wearing force. This force is taken into account when there is a movement of the structure on the bottom. This wearing depends on the depth on which the node digs the bottom, on the bottom stiffness, and on the node speed displacement on the bottom.

5.3.1 Force vector

As mentioned earlier (section 5.2, page 89), the vertical force on a node due to its contact ($z < Z_b$) to the bottom is:

$$F_c = B_k(Z_b - z)$$

With:
F_c: the vertical force on the node (N),
B_k: the bottom stiffness (N/m),
Z_b: the vertical position of the bottom (m),
z: the vertical position of the node (m).

The drag force on the bottom has been modelled as a function of the displacement speed of the node on the bottom. Figure 5.1 shows this relation.

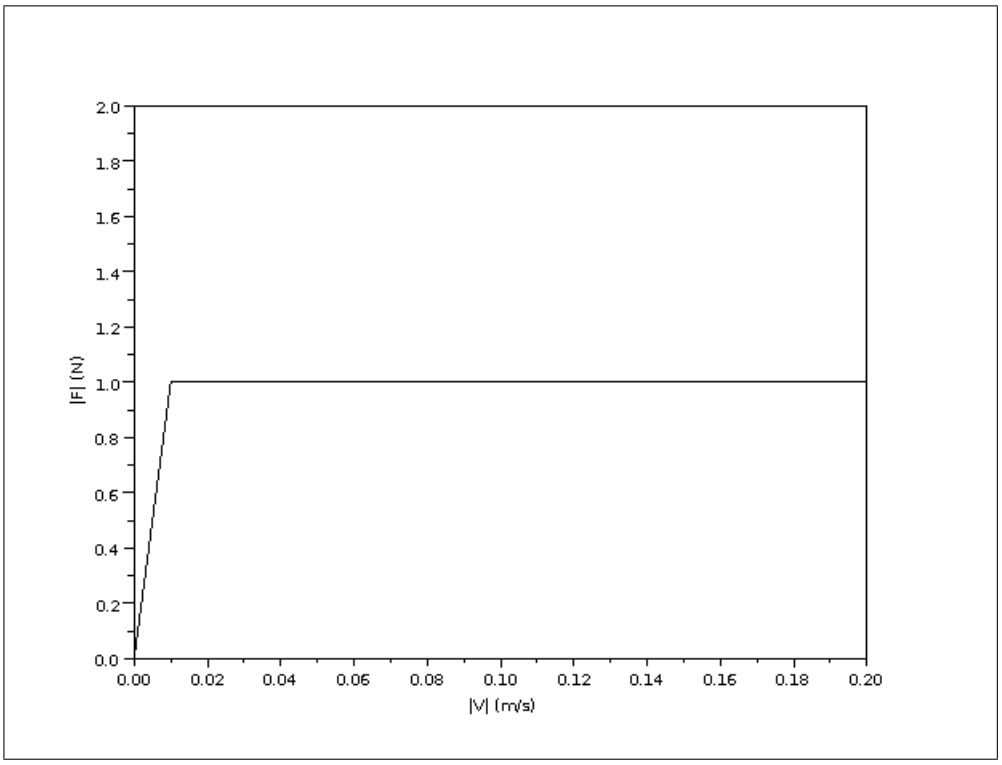

Figure 5.1: Example of amplitude of wearing force $|\mathbf{F}|$ depending on the node displacement speed on the bottom $|\mathbf{V}|$.

$$if|\mathbf{V}| < V_l \quad |\mathbf{F}| = \quad F_c B_f \frac{|\mathbf{V}|}{V_l}$$
$$if|\mathbf{V}| \geq V_l \quad |\mathbf{F}| = \quad F_c B_f$$

With:

$$\mathbf{V} = \left| \begin{array}{l} V_x \\ V_y \\ V_z \end{array} \right.$$

The components of speed are calculated as follows:

$$V_x = \frac{x - x_p}{\Delta t}$$
$$V_y = \frac{y - y_p}{\Delta t}$$
$$V_z = \frac{z - z_p}{\Delta t}$$

V_x (V_y, V_z): component of the speed of the node along the x (y, z) axis (m/s),
x (y, z): coordinate of the node along the x (y, z) axis (m) calculated at time t,
x_p (y_p, z_p): previous coordinate of the node along the x (y, z) axis (m) calculated at time $t - \Delta t$.

Two cases are defined: a high-speed case ($|\mathbf{V}| \geq V_l$) and a low-speed case ($|\mathbf{V}| < V_l$). The wearing force is calculated in the two cases such as there is continuity between the two cases (at $|\mathbf{V}| = V_l$).

High-speed

In this case, $|\mathbf{V}| \geq V_l$.
That means that the components of this force are the following:

$$F_x = -F_c B_f \frac{V_x}{|\mathbf{V}|}$$
$$F_y = -F_c B_f \frac{V_y}{|\mathbf{V}|}$$
$$F_z = -F_c B_f \frac{V_z}{|\mathbf{V}|}$$

Low-speed

In this case, $|\mathbf{V}| < V_l$.
That means that the components of this force are the following:

$$F_x = -F_c B_f \frac{V_x}{V_l}$$
$$F_y = -F_c B_f \frac{V_y}{V_l}$$
$$F_z = -F_c B_f \frac{V_z}{V_l}$$

5.3.2 Stiffness matrix

High-speed

$$\frac{\partial F_x}{\partial x} = -\frac{F_c B_f}{|\mathbf{V}|^2}\frac{\partial V_x}{\partial x}\left[|\mathbf{V}| - \frac{V_x^2}{|\mathbf{V}|}\right]$$

$$\frac{\partial F_x}{\partial y} = -\frac{F_c B_f}{|\mathbf{V}|^2}\frac{\partial V_y}{\partial y}\left[-\frac{V_x V_y}{|\mathbf{V}|}\right]$$

$$\frac{\partial F_x}{\partial z} = B_k B_f \frac{V_x}{|\mathbf{V}|} - \frac{F_c B_f}{|\mathbf{V}|^2}\left[-\frac{V_x V_z}{|\mathbf{V}|}\frac{\partial V_z}{\partial z}\right]$$

$$\frac{\partial F_y}{\partial x} = \frac{F_c B_f}{|\mathbf{V}|^2}\left[\frac{V_x V_y}{|\mathbf{V}|}\frac{\partial V_x}{\partial x}\right]$$

$$\frac{\partial F_y}{\partial y} = -\frac{F_c B_f}{|\mathbf{V}|^2}\frac{\partial V_y}{\partial y}\left[|\mathbf{V}| - \frac{V_y^2}{|\mathbf{V}|}\right]$$

$$\frac{\partial F_y}{\partial z} = B_k B_f \frac{V_y}{|\mathbf{V}|} - \frac{F_c B_f}{|\mathbf{V}|^2}\left[-\frac{V_x V_z}{|\mathbf{V}|}\frac{\partial V_z}{\partial z}\right]$$

$$\frac{\partial F_z}{\partial x} = \frac{F_c B_f}{|\mathbf{V}|^2}\left[\frac{V_x V_z}{|\mathbf{V}|}\frac{\partial V_x}{\partial x}\right]$$

$$\frac{\partial F_z}{\partial y} = \frac{F_c B_f}{|\mathbf{V}|^2}\left[\frac{V_y V_z}{|\mathbf{V}|}\frac{\partial V_y}{\partial y}\right]$$

$$\frac{\partial F_z}{\partial z} = B_k B_f \frac{V_z}{|\mathbf{V}|} - \frac{F_c B_f}{|\mathbf{V}|^2}\left[\frac{\partial V_z}{\partial z}|\mathbf{V}| - \frac{V_z^2}{|\mathbf{V}|}\frac{\partial V_z}{\partial z}\right]$$

With:

$$\frac{\partial V_x}{\partial x} = \frac{1}{\Delta t}$$

$$\frac{\partial V_y}{\partial y} = \frac{1}{\Delta t}$$

$$\frac{\partial V_z}{\partial z} = \frac{1}{\Delta t}$$

The stiffness matrix becomes:

$$K = -\frac{B_f F_c}{|\mathbf{V}|^2 \Delta t}\begin{pmatrix} \frac{V_x^2}{|\mathbf{V}|} - |\mathbf{V}| & \frac{V_x V_y}{|\mathbf{V}|} & \frac{V_x V_z}{|\mathbf{V}|} \\ \frac{V_x V_y}{|\mathbf{V}|} & \frac{V_y^2}{|\mathbf{V}|} - |\mathbf{V}| & \frac{V_y V_z}{|\mathbf{V}|} \\ \frac{V_x V_z}{|\mathbf{V}|} & \frac{V_y V_z}{|\mathbf{V}|} & \frac{V_z^2}{|\mathbf{V}|} - |\mathbf{V}| \end{pmatrix} - \frac{B_f B_k}{|\mathbf{V}|}\begin{pmatrix} 0 & 0 & V_x \\ 0 & 0 & V_y \\ 0 & 0 & V_z \end{pmatrix}$$

Low-speed

$$\frac{\partial F_x}{\partial x} = -\frac{F_c B_f}{V_l}\frac{\partial V_x}{\partial x}$$
$$\frac{\partial F_x}{\partial y} = 0$$
$$\frac{\partial F_x}{\partial z} = B_k B_f \frac{V_x}{V_l}$$
$$\frac{\partial F_y}{\partial x} = 0$$
$$\frac{\partial F_y}{\partial y} = -\frac{F_c B_f}{V_l}\frac{\partial V_y}{\partial y}$$
$$\frac{\partial F_y}{\partial z} = B_k B_f \frac{V_y}{V_l}$$
$$\frac{\partial F_z}{\partial x} = 0$$
$$\frac{\partial F_z}{\partial y} = 0$$
$$\frac{\partial F_z}{\partial z} = B_k B_f \frac{V_z}{V_l} - \frac{F_c B_f}{V_l}\frac{\partial V_z}{\partial z}$$

The stiffness matrix becomes:

$$K = \frac{B_f}{V_l}\begin{pmatrix} \frac{F_c}{\Delta t} & 0 & -B_k V_x \\ 0 & \frac{F_c}{\Delta t} & -B_k V_y \\ 0 & 0 & -B_k V_z + \frac{F_c}{\Delta t} \end{pmatrix}$$

Chapter 6

Validation

Several simulations are presented here. They are compared with flume tank tests, sea trials, and other models.

6.1 Tractrix

The shape of the meridian of a cylinder of netting of inextensible twines held between two circular rings is a tractrix.

In the case of a cylinder of stretched netting of 100 meshes around, 50 meshes along, a radius of $1m$ at one extremity and $0.048599m$ at the other, and a mesh side of $0.05m$, the shape is as displayed in Figure 6.1 (O'Neill and Priour, 2009).

The accuracy of the model depends on the number of nodes used (Table 6.1). The model uses 32 to 662 nodes and two planes of symmetry.

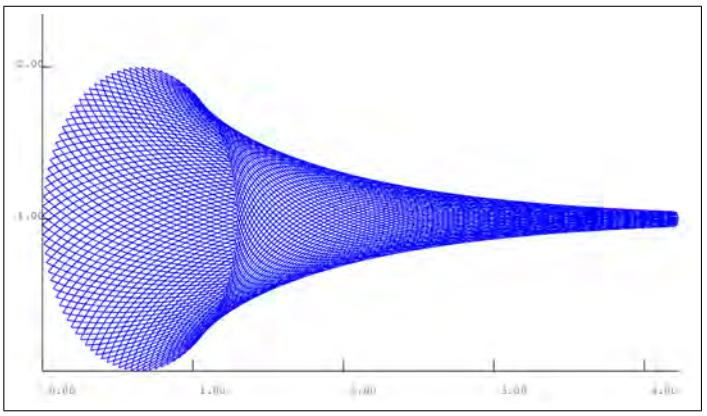

Figure 6.1: Cylinder of inextensible netting held between two circular rings.

Table 6.1: Tractrix shape and accuracy of the model, where x and y are the analytical solution; x is along the axis and y is radial. The accuracy on y depends on the number of nodes in the model (from 32 to 662).

x (m)	y (m)	662	298	84	32
0	1				
0.403501	0.739032	0.02%	0.22%	1.4%	-1.1%
0.844094	0.546168	0.00%	0.19%	1.2%	-2.7%
1.303628	0.403636	-0.01%	0.14%	1.0%	-1.8%
1.773173	0.2983	0.00%	0.19%	1.5%	-2.3%
2.248093	0.220453	-0.02%	0.17%	1.3%	-2.4%
2.725923	0.162922	-0.03%	0.15%	1.0%	-3.6%
3.205334	0.120404	-0.07%	0.18%	1.0%	-2.8%
3.685607	0.088983	-0.11%	0.17%	0.6%	-3.2%
4.166349	0.065761	-0.15%	0.16%	0.2%	-1.9%
4.647348	0.048599				

6.2 Diamond mesh netting stretched by its weight

This check is done by comparing the results of the model based on triangular elements with a model where each twine is modelled by an elastic bar. This comparison is taken from Priour (1999).

The mesh panel is square and consists of 1600 meshes. The elongation rigidity (EA)of the twines is $10000N$, their diameter is $0.01m$, the side of the mesh is $1.2m$, the length of the upper edge is $32m$, and the density of the net is $2000kg/m^3$.

The model uses 1050 triangular elements and 512 nodes with a vertical plane of symmetry (Figures 6.2 and 6.3b). The comparison is made with a reference model where each side of mesh (twine vector) is modelled with an elastic bar (Figure 6.3a). This reference model uses 3136 bars and 1625 nodes with a plane of symmetry. The forms calculated by the two models are quite similar (Figure 6.3).

The forces involved here are the netting weight and the twine tension (sections 3.3.9 page 67 and 3.3 page 37).

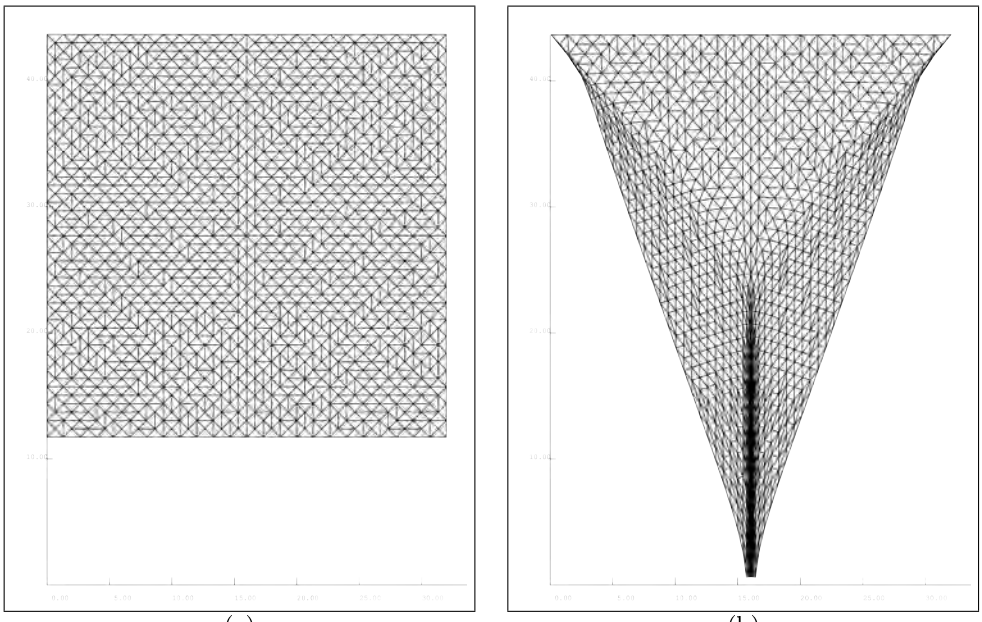

(a) (b)

Figure 6.2: Calculation of the shape of a net held by its top border. The initial shape of the model is unbalanced (a) and the final one is balanced (b). Only the triangular elements are represented.

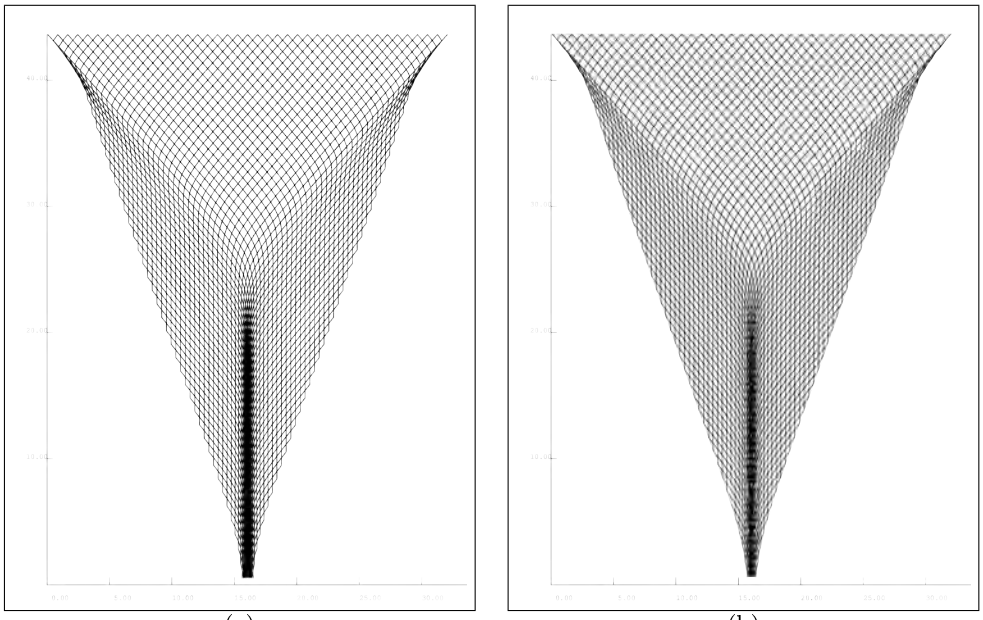

(a) (b)

Figure 6.3: Equilibrium of a net held by its top edge and stretched by its own weight: (a) model where each twine is modelled as an elastic bar; (b) model using triangular elements, with only the twines drawn.

6.3 Hexagonal mesh net held vertically in the current

The results of the model using triangular elements for netting with hexagonal meshes are compared with those of a model using bar elements for each twine. The mesh panel is square and consists of 18 by 33 meshes and 3564 twines. The elongation rigidity of the twines is $3000N$ and $0.0003N$ in compression. The diameter of the twines is $1mm$, and their length is $19mm$. The length of each edge is $1m$. The density of the material is considered equal to that of sea water ($1025kg/m^3$). The net is held by its four edges perpendicular to a current of $1m/s$ of sea water.

The first model uses 924 triangular elements and 495 nodes (Figures 6.4a and 6.4b), whereas the second model uses 3564 bars and 2446 nodes (Figure 6.4c).

The results of the two models are similar. The maximum displacement is $0.182m$ for the first model and $0.184m$ for the second. The drag force is $54.10N$ for the first and $54.04N$ for the second.

Convergence is obtained in 29 iterations with the first model compared with 296 iterations for the second model. This acceleration is related to the reduction in the number of nodes in the model using triangular elements.

This comparison is based on Priour (2002).

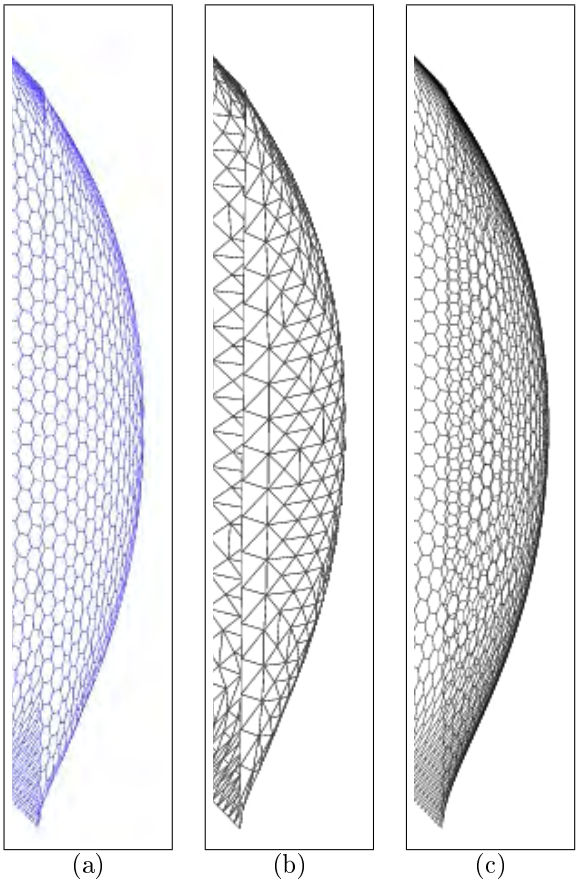

Figure 6.4: Equilibrium of a net held by its four edges in a current perpendicular: (a) the twines in the model using triangular elements; (b) the triangular elements; (c) the twines in the model using bar elements. The shapes are similar.

6.4 Hydrostatic pressure

The results of the model using triangular elements are compared with measurements made by O'Neill and O'Donoghue (1997). These measures involve a net bag partially filled with water bags (Figure 6.5). The pressure from the weight of the bags is implemented as in section 3.3.6 (page 63), but in this case the pressure is modelled as a hydrostatic pressure:

$$p = \rho g h$$

p: pressure exerted by the catch on the net (Pa),
ρ : density of water (kg/m^3),
g: gravity $(9.81m/s^2)$,
h: height in relation to the upper limit of the catch (m).
The test conditions are as follows:
Mesh size: $37.2mm$,
Number of meshes around: 50,
Number of meshes along: 50,
Catch volume: $0.0265m^3$,
Catch density (ρ): $1000kg/m^3$,
Radius of the hoop above: $0.25m$
The model uses 742 nodes, 1360 triangular elements, one bar for closing the netting at the bottom, and two symmetry planes. This comparison comes from Priour (2005).

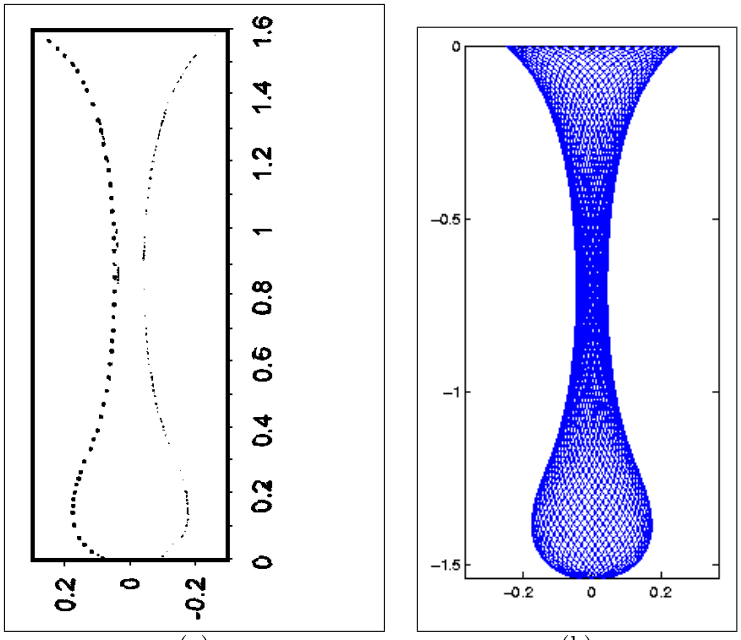

(a) (b)

Figure 6.5: Bag of netting with $26.5kg$ of water. Comparison between measurements (a) and the model using triangular elements (b). Only twines are shown in (b)

6.5 Cod-end with catch in the current

A cod-end is the backmost part of a trawl where the catch of fish builds up. The results of the model are compared with measurements made in test tank on cod-ends partially filled with water (Anon. 1999). The pressure of the catch is implemented here as follows (see section 3.3.6, page 63):

$$p = \frac{1}{2}\rho C_d v^2$$

p: catch pressure on the net (Pa),
ρ : density of water (kg/m^3),
C_d: drag coefficient (1.4),
v: current amplitude (m/s).

The distance between the front of the catch and the extremity of the cod-end is inserted into the model as data because this distance was measured during the tests. Figure 6.6 shows the model output (net) and the flume tank measurements (cross). The comparison shows that the model gives a pretty good description of the cod-end with the catch.

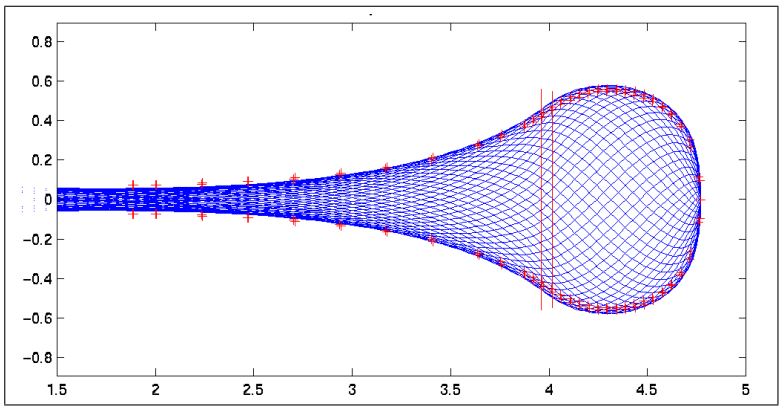

Figure 6.6: Comparison of flume tank tests (cross) and the numerical model outputs (mesh) for a scale (1/3) model of North Sea cod-end with 300kg of catch.

6.6 Full cod-end

A long and full cod-end subject to constant internal pressure presents a maximal diameter. This maximal diameter depends on the number of meshes around N and the mesh side m by the following analytical equation (O'Neill and Priour 2009):

$$D_{max} = 4\frac{Nm}{\pi\sqrt{6}}$$

In the case of a cod-end close at one extremity of 100 meshes around, 100 meshes along (N), and a mesh side of $0.05m$ (m), the shape is as displayed in Figure 6.7.

The accuracy of the model on the maximal diameter is 0.015%.

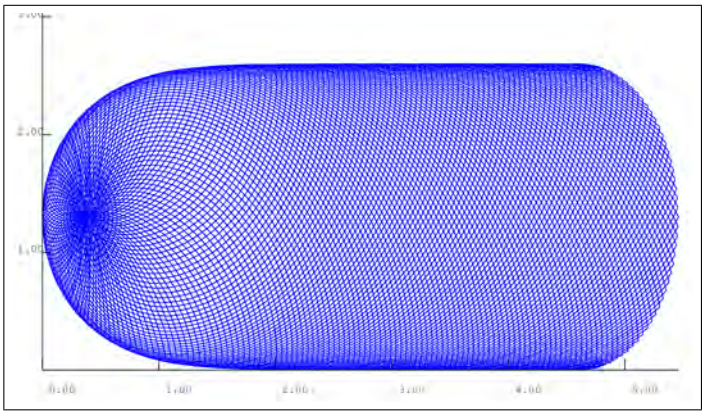

Figure 6.7: Cod-end of netting subject to constant internal pressure.

6.7 Bottom trawl

Several series of measurements on a bottom trawl were carried out during a sea trial on a French vessel. The results of the numerical model were compared with these measurements (Priour 2012; Figure 6.8, Table 6.2).

The vessel was equipped with measurement systems suitable for trawling. Several measurements were carried out:

- the position of the doors (immersion and distance),
- the distance between the headline and the bottom,
- the speed over ground and speed relative to the water,
- the warps and bridles tension.

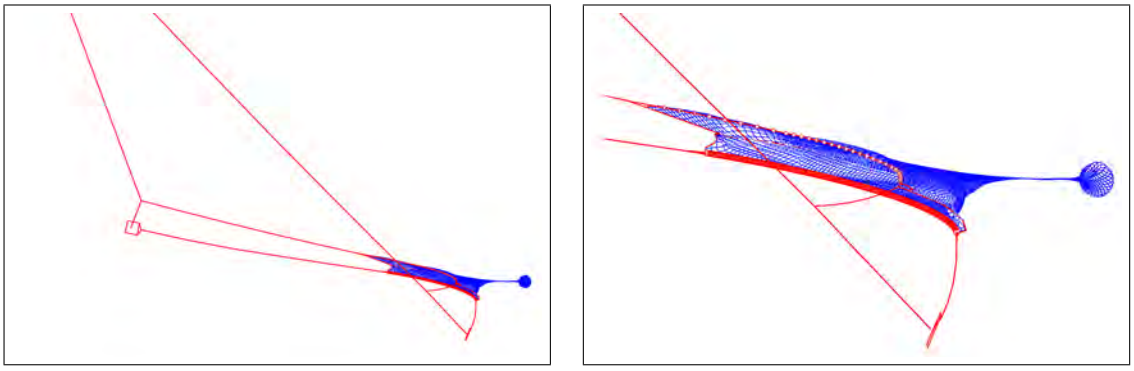

Figure 6.8: Shape of the bottom trawl assessed by the model. Only 1 twine on 5 is drawn.

Table 6.2: Differences between tests at sea and simulation. SD: standard deviation.

	Mean-SD	Mean+SD	Simulation
Warp tension (kg)	1966	3121	2300
Top bridle tension (kg)	864	1370	980
Bottom bridle tension (kg)	609	972	830
Vertical opening (m)	3.5	4.3	3.4

Measurements on the trawl are highly variable. The results of model calculation are generally close to measured quantities.

6.8 Cubic fish cage

Tests were carried out on models of a fish cage in the flume tank of Boulogne/mer (Répécaud and Rodier 1993). The cage consisted of 4 side panels of 23 horizontal by 26 vertical meshes and a bottom panel of 23 by 23 meshes. The net had a mesh side of $35mm$ and a twine diameter of $2.2mm$. The four bottom corners were tightened with $3kg$ of lead sinkers. The size of the cage top was $1m$ by $1m$. The water speed was $0.5m/s$. Figure 6.9 compares the flume tank test and the simulation.

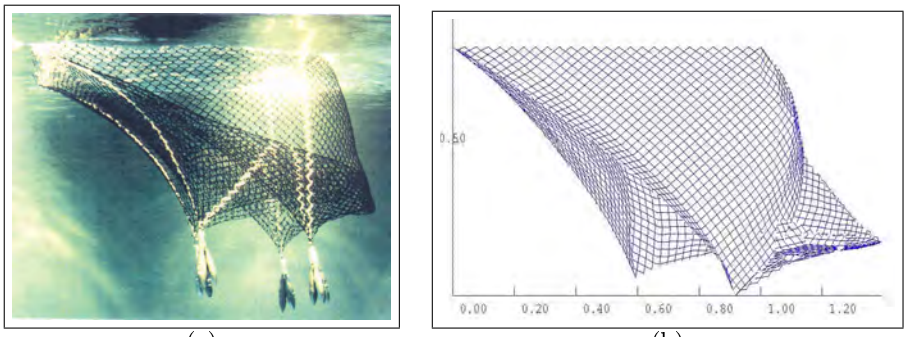

(a) (b)

Figure 6.9: Qualitative comparison between the deformation of a cubic cage in a flume tank (a) and simulation (b).

6.9 Bending of cable

The model of bending of cables (section 4.3, page 75) is compared with a beam deformation (Figure 6.10) in the thin beam theory. In this case the deflection is well known. In case of a cantilever the analytical equation of the deflection is as follows:

$$y = \frac{-Wl^4}{8EI}$$

y: the vertical deflection of the free extremity of the cantilever (m),
l: the length of the cantilever (m),
w: the linear weight of the cantilever (N/m),
EI: the bending rigidity $(N.m^2)$.

In case of a beam $1m$ long (l), with a density of iron $(7800kg/m^3)$, a diameter of $2cm$, and a rigidity (EI) of $164.93N.m^2$, the deflection is $18.2mm$.

Table 6.3 and Figure 6.11 show the vertical deflection of the beam calculated with the model in function of bar element number. The model is shown to be valid. The larger the number of bar elements, the smaller the error.

Table 6.3: Vertical deflection of the beam deflection calculated with the model in function of bar elements number and error relative to the analytical deflection $(18.2mm)$

Number of bars	5	8	10	12	16	20	30	40
Simulated deflection (mm)	18.9	18.5	18.4	18.3	18.3	18.3	18.2	18.2
Error %	4.0	1.5	0.97	0.67	0.36	0.23	0.082	0.039

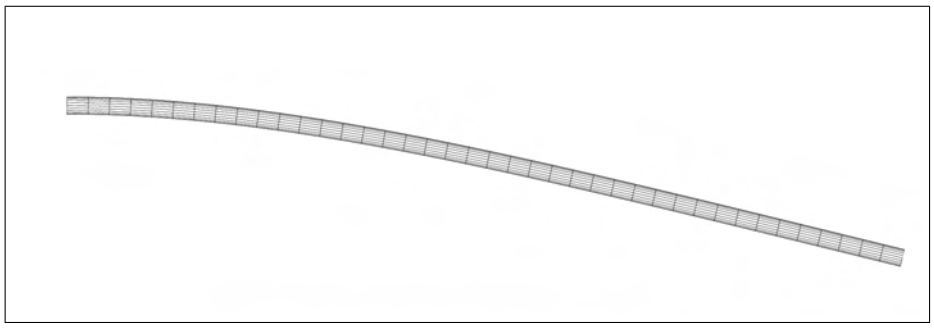

Figure 6.10: Vertical deflection of a beam calculated with the model. The beam is fixed on the left and free to bend on its own weight on the right. The conditions are the same as in the text except for the bending rigidity, which is $(EI = 16.493N.m^2)$, ten times less than the case of Table 6.3 and Figure 6.11 to highlight the deformation.

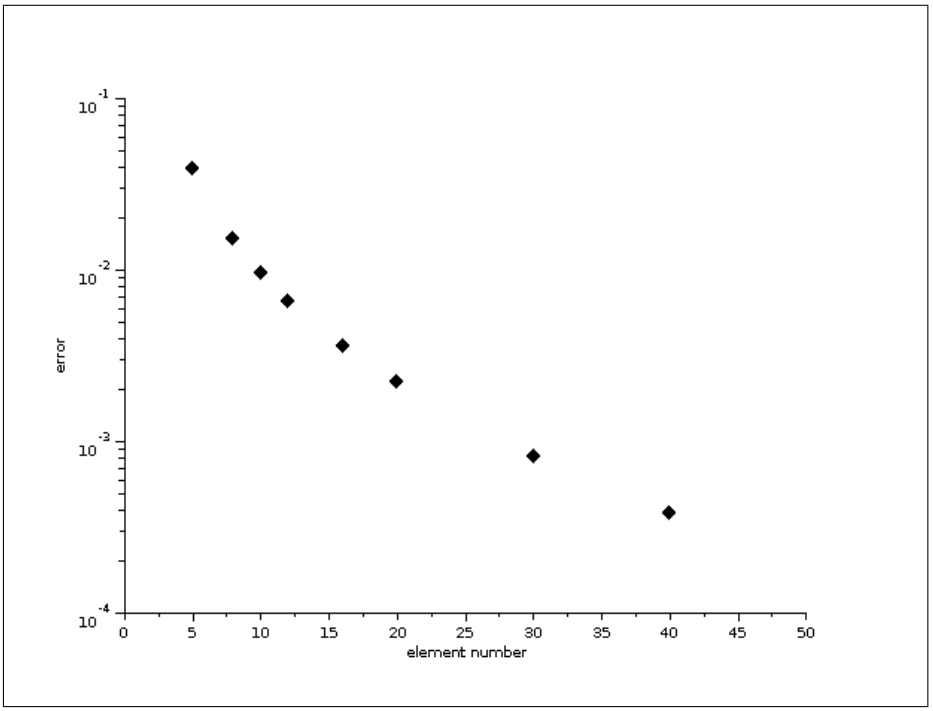

Figure 6.11: Error of the model relative to the analytical deflection in function of the number of bar elements.

Chapter 7

References

Anon., 1999. PREMECS FAIR Program CT96 1555, Final report – 1st December 1996 – 31st November 1999

Bessonneau, J.S., and Marichal, D., 1998. Study of the dynamics of submerged supple nets. Ocean Engineering 27 (7).

Chang S.Y., 2004. Studies of Newmark method for solving non linear systems: (I) Basic analysis. Journal of the Chinese institute of engineers, Vol.27, No.5, pp. 651-662.

Deuflhard, P., 2004. Newton methods for non-linear problems, Affine invariance and adaptive algorithms. Springer series in computational mathematics. ISSN 0 179-3632. ISBN 3-540-21099-7.

Desai, C.S., and Abel, J.F., 1972. Introduction to the finite element method: a numerical method for engineering analysis, Van Nostrand Reinhold.

Ferro, R.S.T., 1988. Computer simulation of trawl gear shape and loading. In: Proceedings of Word Symposium on Fishing Gear and Fishing Vessel Design. Marine Institute, Saint John's, pp. 259–262.

Hallam, M.G., Heaf, N.J., and Wootton, L.R., 1977. Dynamics of marine structures, CIRIA Underwater Engineering Group, Londres.

Landweber, L., and Protter, M.H., 1947. The shape and tension of a light flexible cable in a uniform current. Journal of applied mechanics. June 1947. pp. 121-126.

Le Dret, H., Priour, D., Lewandowski, R., and Chagneau, F., 2004. Numerical simulation of a cod end net. Part 1. Equilibrium in a uniform flow. Journal of Elasticity 76 (2), pp. 139–162.

Lee, C.-W., Lee, J.-H., Cha, B.-J., Kim, H.-Y., and Lee, J.-H., 2005. Physical modeling for underwater flexible systems dynamic simulation. Ocean Engineering 32, pp. 331–347.

Niedzwiedz, G., and Hopp, M., 1998. Rope and net calculations applied to problems in marine engineering and fisheries research. Archive of Fishery and Marine Research 46, pp. 125–138.

O'Neill, F.G., 2004. The influence of bending stiffness on the deformation of axi-symmetric networks, Proceedings of OMAE'04, June 20-25, 2004, Vancouver Canada.

O'Neill, F.G., and O'Donoghue, T., 1997. The fluid dynamic loading on catch and the geometry of trawl cod-ends. Proceedings of the Royal Society of London, Series A: Mathematics and Physical Sciences 1997;453: pp. 1631-1648.

O'Neill, F.G., and Priour, D., 2009. Comparison and validation of two models of netting deformation. Journal of Applied Mechanics, 76(5), pp. 1-7.

O'Neill, F.G., and Xu, L., 1994. Twine flexural rigidity and mesh resistance to opening, ICES CM/B:31.

Priour, D., 1999. Calculation of net shapes by the finite element method with triangular elements. Commun. Numer. Meth. Engng, 15, pp. 755-763.

Priour, D., 2002. Analysis of nets with hexagonal mesh using triangular elements, Int. J. Numer. Meth. Engng., 56, pp. 1721-1733. DOI: 10.1002/nme.635.

Priour, D., 2005. FEM modelling of flexible structures made of cables, bars and nets. Proceedings of the IMAM Conference: Guedes Soares, Garbatov and Fonseca, eds. Maritime Transportation and Exploitation of Ocean and Coastal Resources. London: Taylor and Francis Group, pp. 1285-1292.

Priour, D., 2006. Twines equilibrium in a finite element dedicated to hexagonal mesh netting (ESAIM: PROCEEDINGS, October 2007, Vol. 22, pp. 140-149).

Priour, D., 2012. Rapport final du projet EFFICHALUT , Rapport Ifremer/DCB/RDT/HO/R12-001.

Répécaud, M., and Rodier, P., 1993. Note interne IFREMER, Compte rendu d'essais: Cages pour l'élevage du poisson en mer, DITI/NPA/93.020.

Richtmyer, R.D., 1941. Design and operation of mark IV magnetic mine sweeping gear. Bureau of ships scientific group report No12. January 1941.

Rivlin, R.S., 1955. Plane Strain of a Net Formed by Inextensible Cords, Indiana Univ. Math. J., pp. 951-974.

Tsukrov, I., Eroshkin, O., Fredriksson, D., Swift, M.R., and Celikkol, B., 2003. Finite element modeling of net panels using a consistent net element. Ocean Engineering 30 (February (2)), pp. 251-270.

Zienkiewicz, O.C., and Taylor, R.L., 2000. Finite Element Method (5th Edition), Volume 1 - The Basis, Elsevier.

Appendix A8

Scottish seine net selectivity and catch comparison data

Scottish seine net selectivity and catch comparison data

Barry O’Neill

marinescotland

Sea trials

- Harmony NAFC
  - 110mm codend,
  - 110mm codend with 90mm smp
  - 120mm codend
  - compared with 100mm codend with 90 smp fitted @ 6 – 9m
- Harmony FRS
  - 100mm codend,
  - 100mm codend with 90mm smp @ 3 – 6m
  - 100mm codend with 90mm smp @ 9 - 12m
  - Compared with a 40mm codend
- Boy Andrew
  - 100mm codend with a 90 smp fitted 9 – 12m
  - 100mm codend with a 90 smp fitted 7 – 10m
  - Compared with a 100mm codend.

marinescotland

Analysis

- Most studies of seine net selectivity use the alternate shot method
- this allows trials to resemble commercial practices as much as possible
- the temporal and spatial difference between shots can
  - lead to high variability,
  - data which does not conform to any standard selection curve and/or
  - data for which there is insufficient information to estimate both the selection parameters and the ‘split’ parameter
- Hence, it has often been difficult to fit parametric selection curves to seine net data and assess the relative catch rate of the test and control gears

marinescotland

Analysis

- mixed model smoothing methodology of Fryer et al. (2003) to estimate the catch rate
- This methodology makes no prior assumptions on the nature of the relative catch rates and is underpinned by the SELECT model of Millar (1992).
- Haddock and whiting

marinescotland

Harmony NAFC

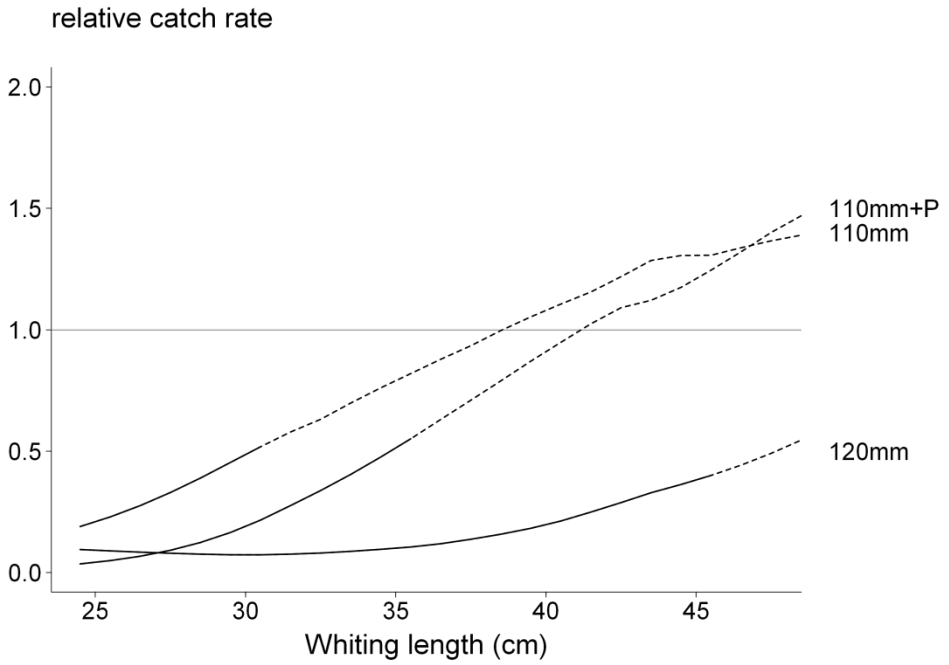

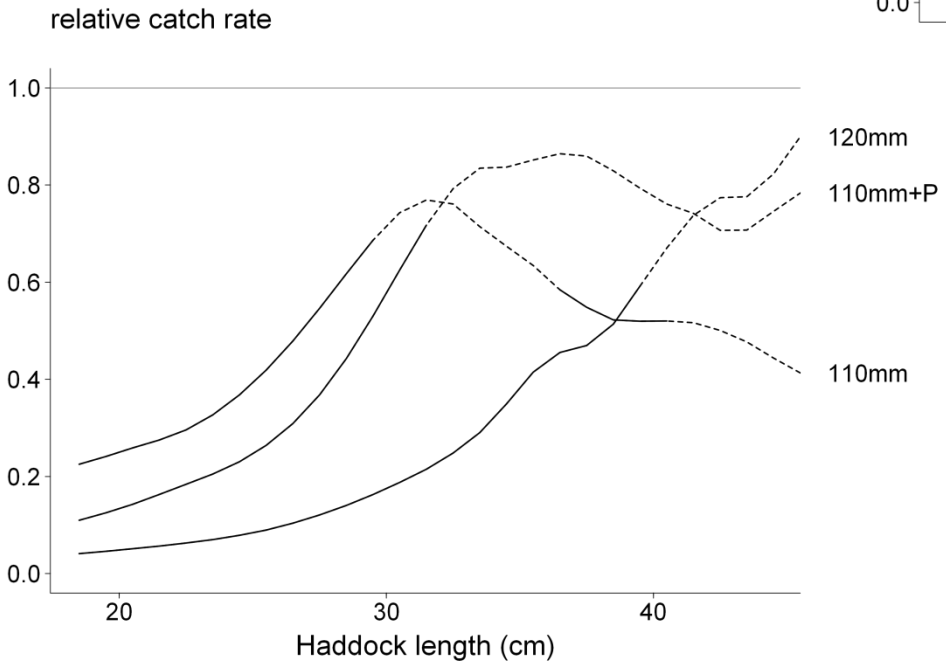

marinescotland

Harmony FRS

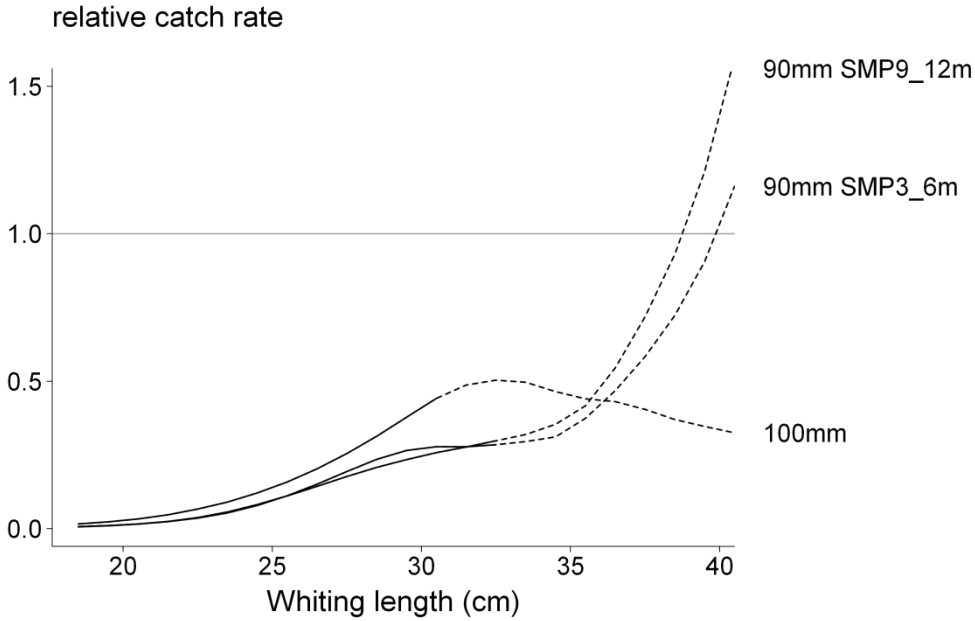

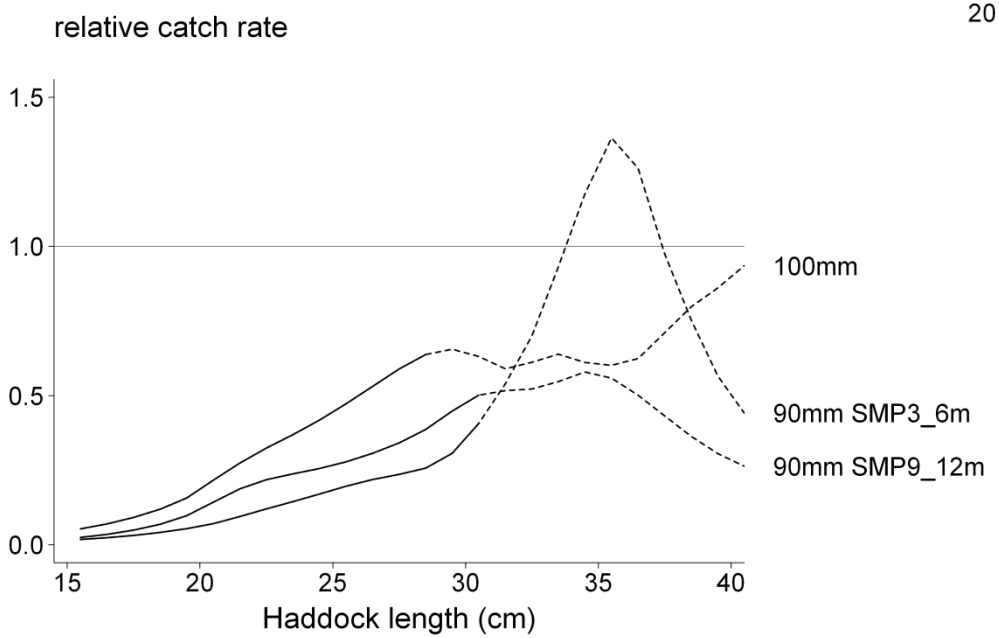

marinescotland

Boy Andrew

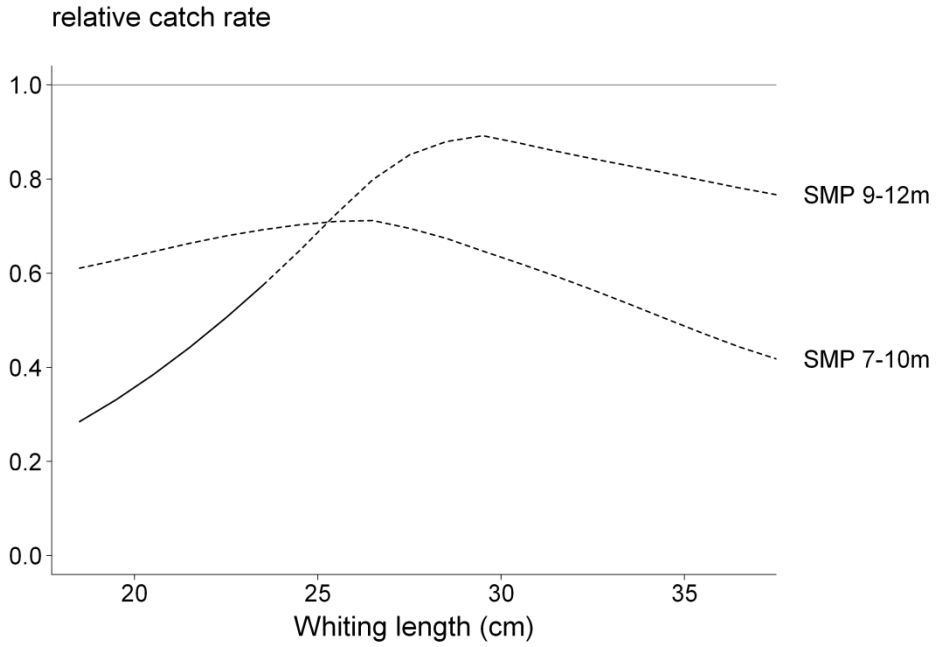

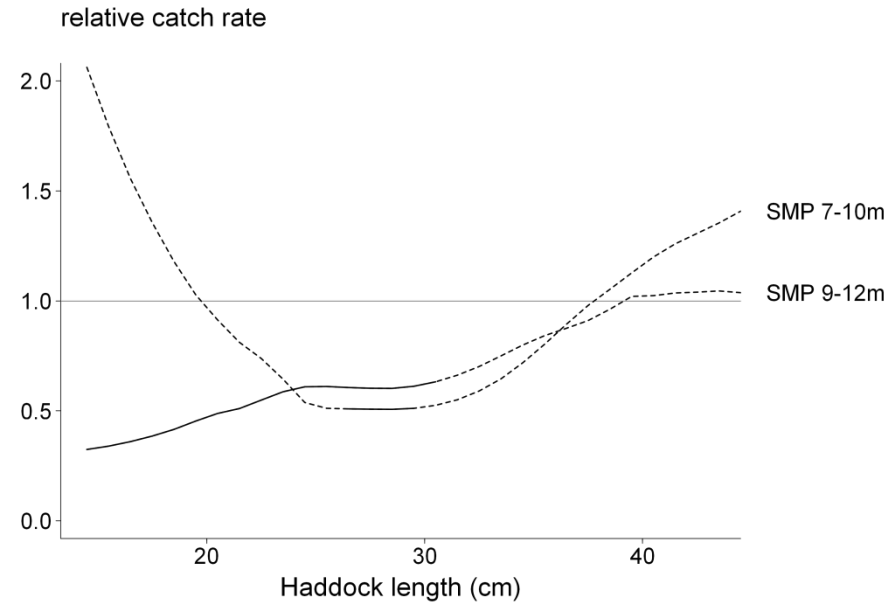

marinescotland

Comparison with trawl data

- Harmony FRS seine net trials – 40mm control codend

- trawl selectivity model of Madsen and Ferro in the EU Expert Meeting report of April/May 2003.
- haddock selectivity data from 512 selectivity hauls on 8 commercial and 2 research vessel cruises

marinescotland

Comparison with trawl data

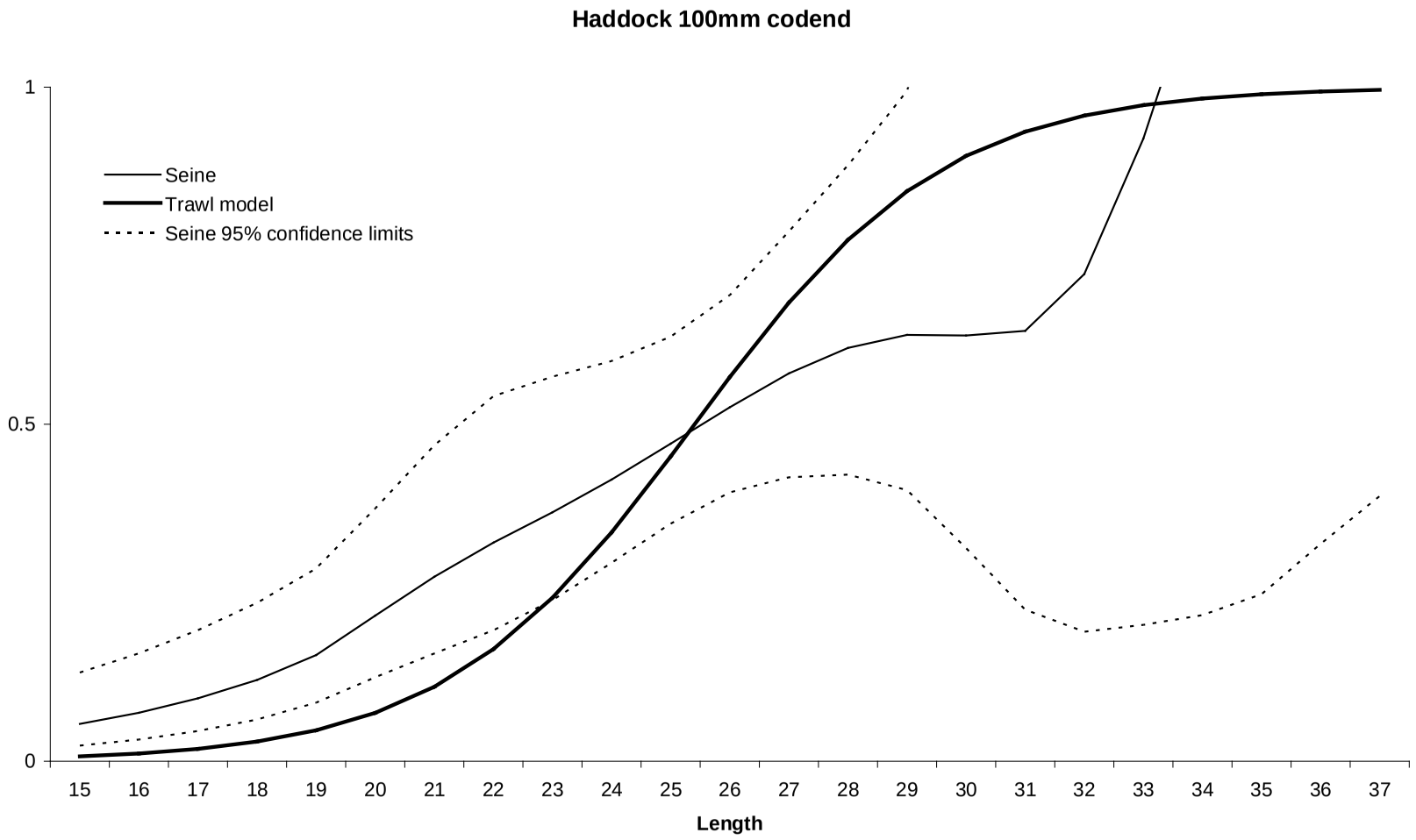

marinescotland

Comparison with trawl data

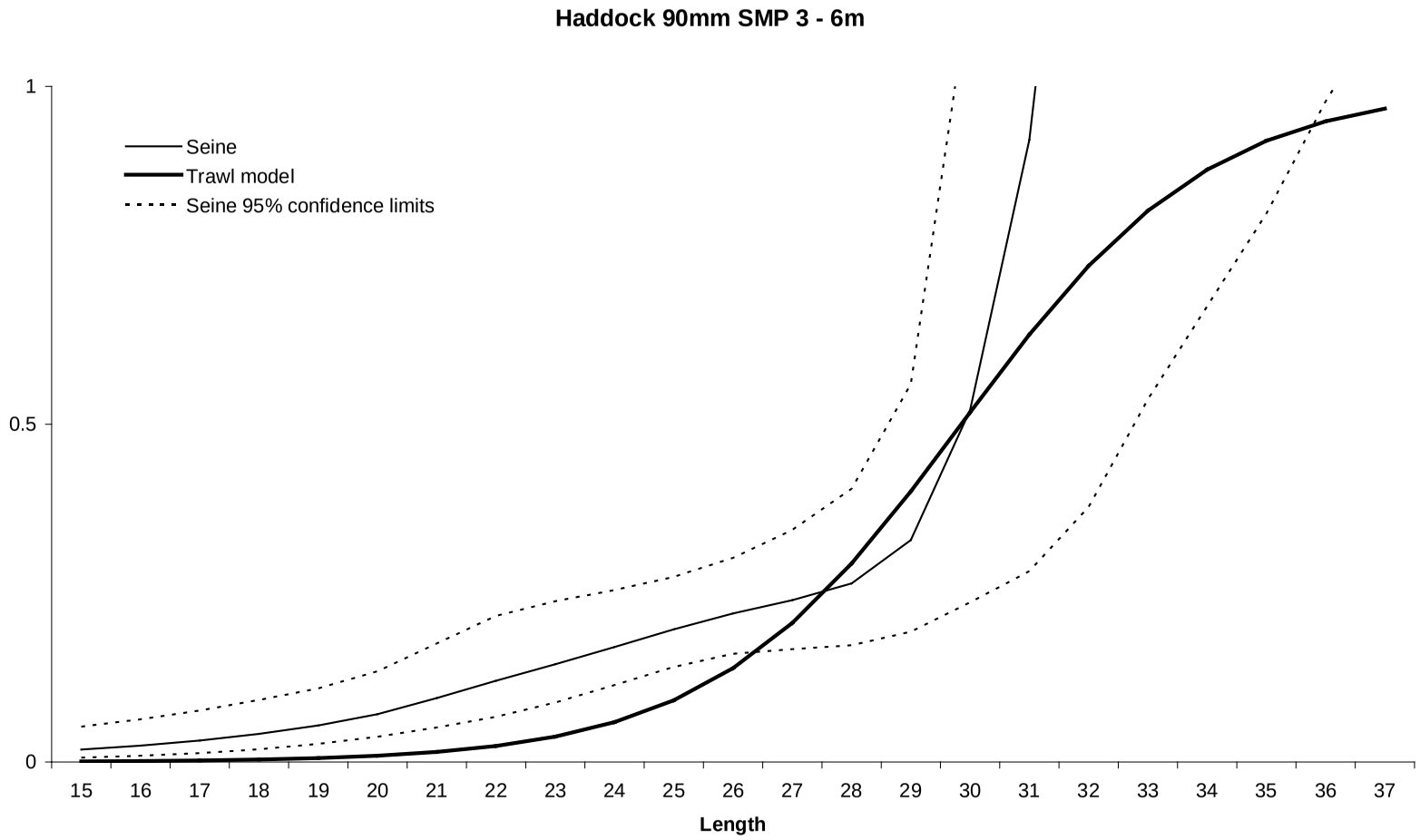

marinescotland

Comparison with trawl data

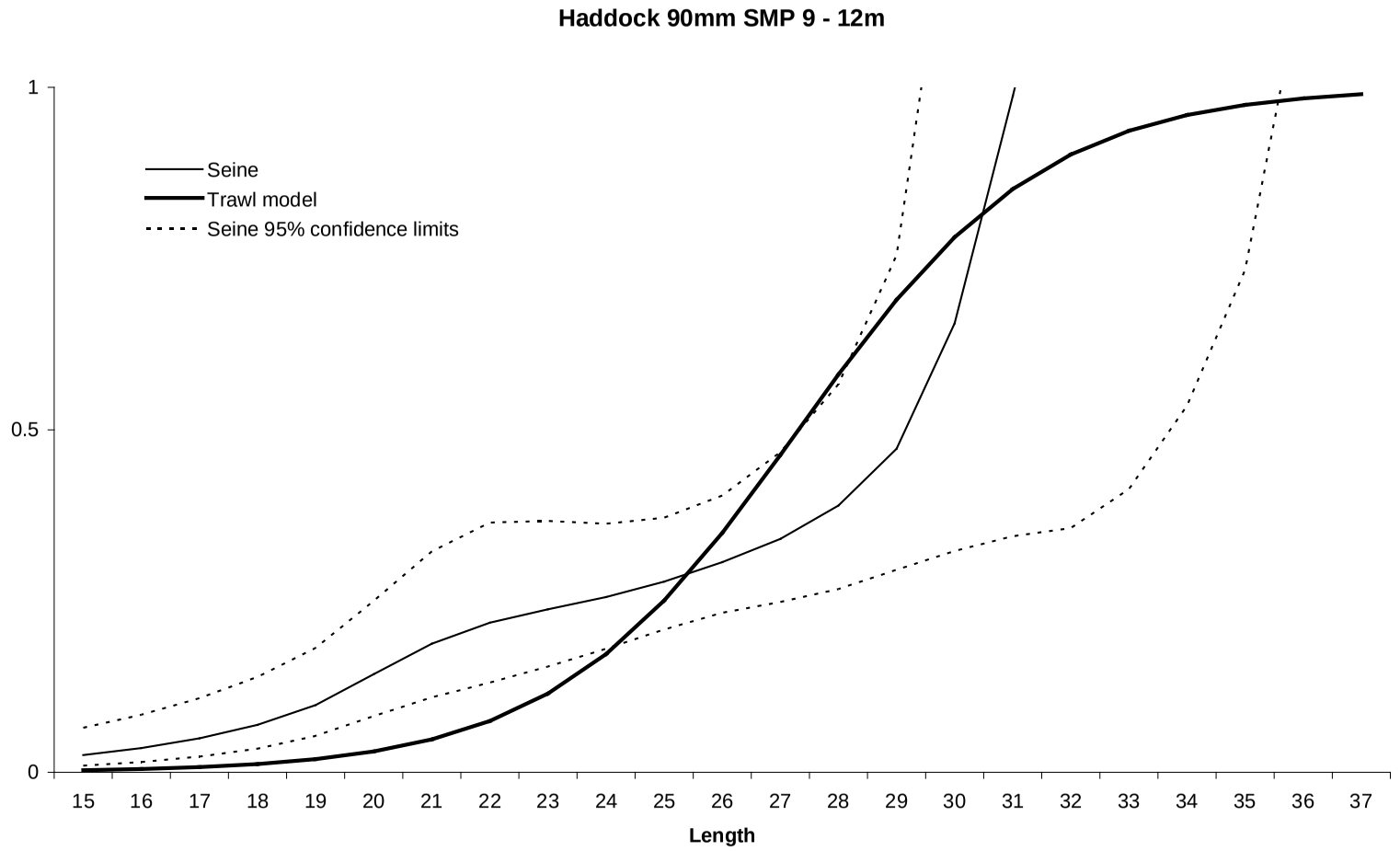

marinescotland

Comparison with trawl data

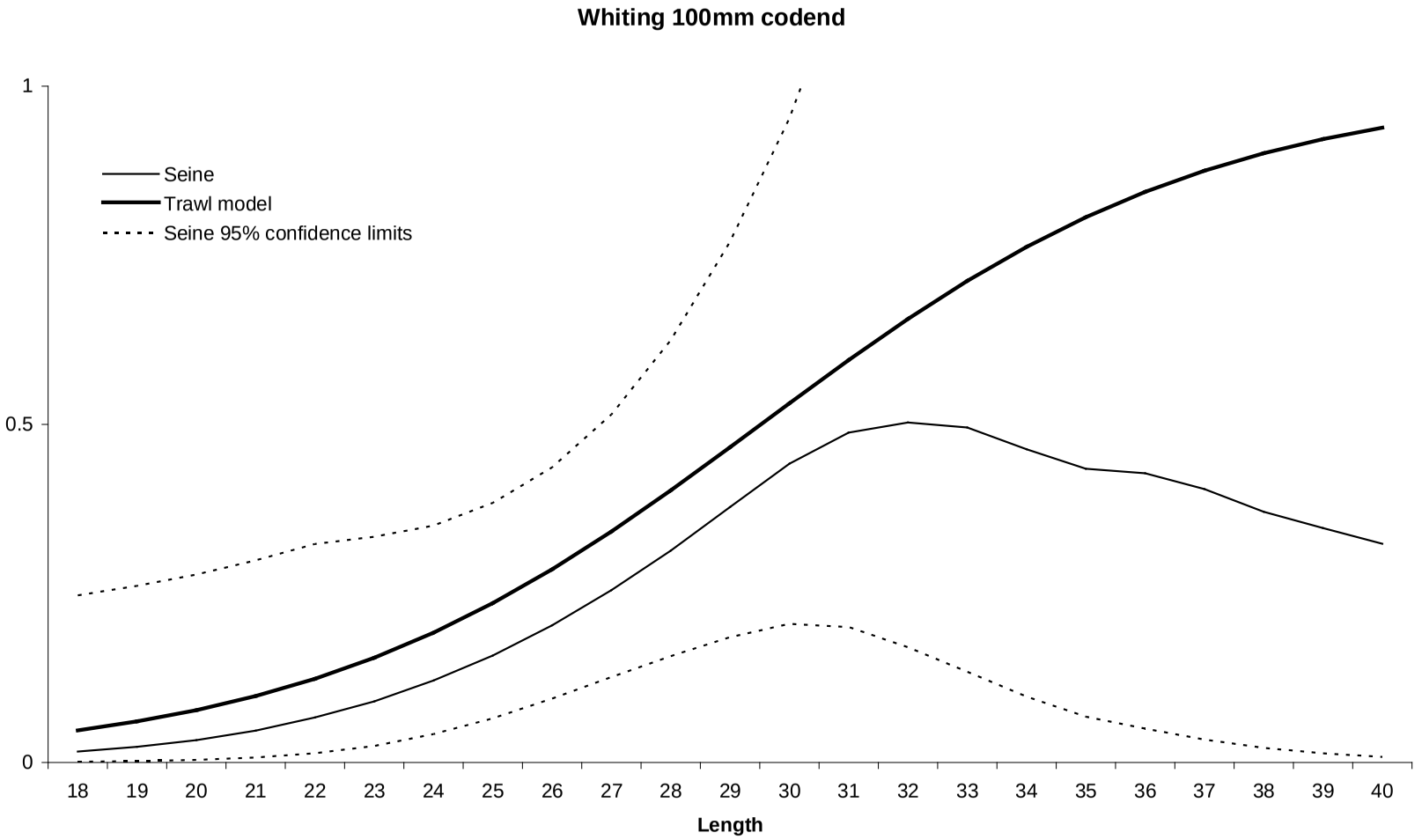

marinescotland

Comparison with trawl data

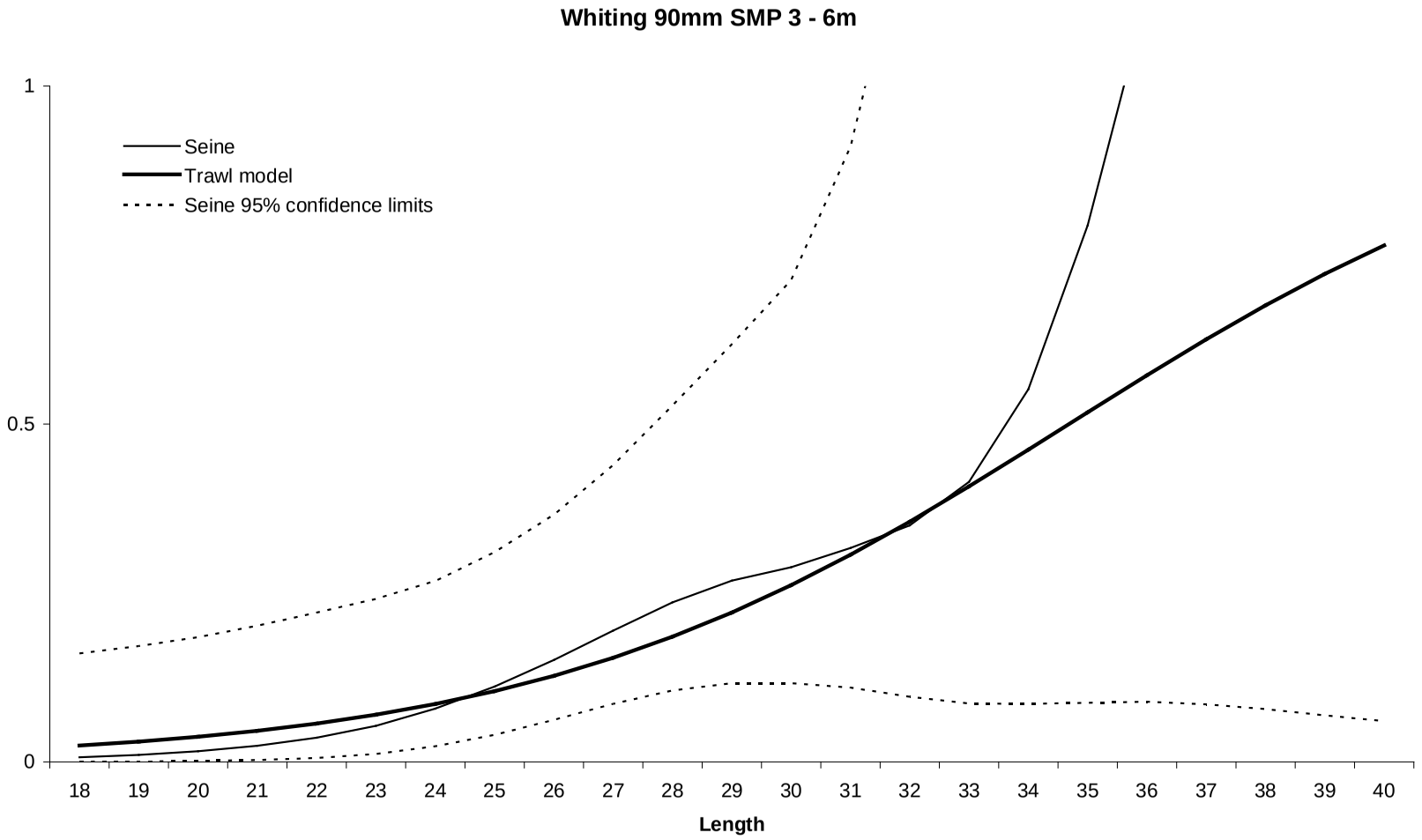

marinescotland

Comparison with trawl data

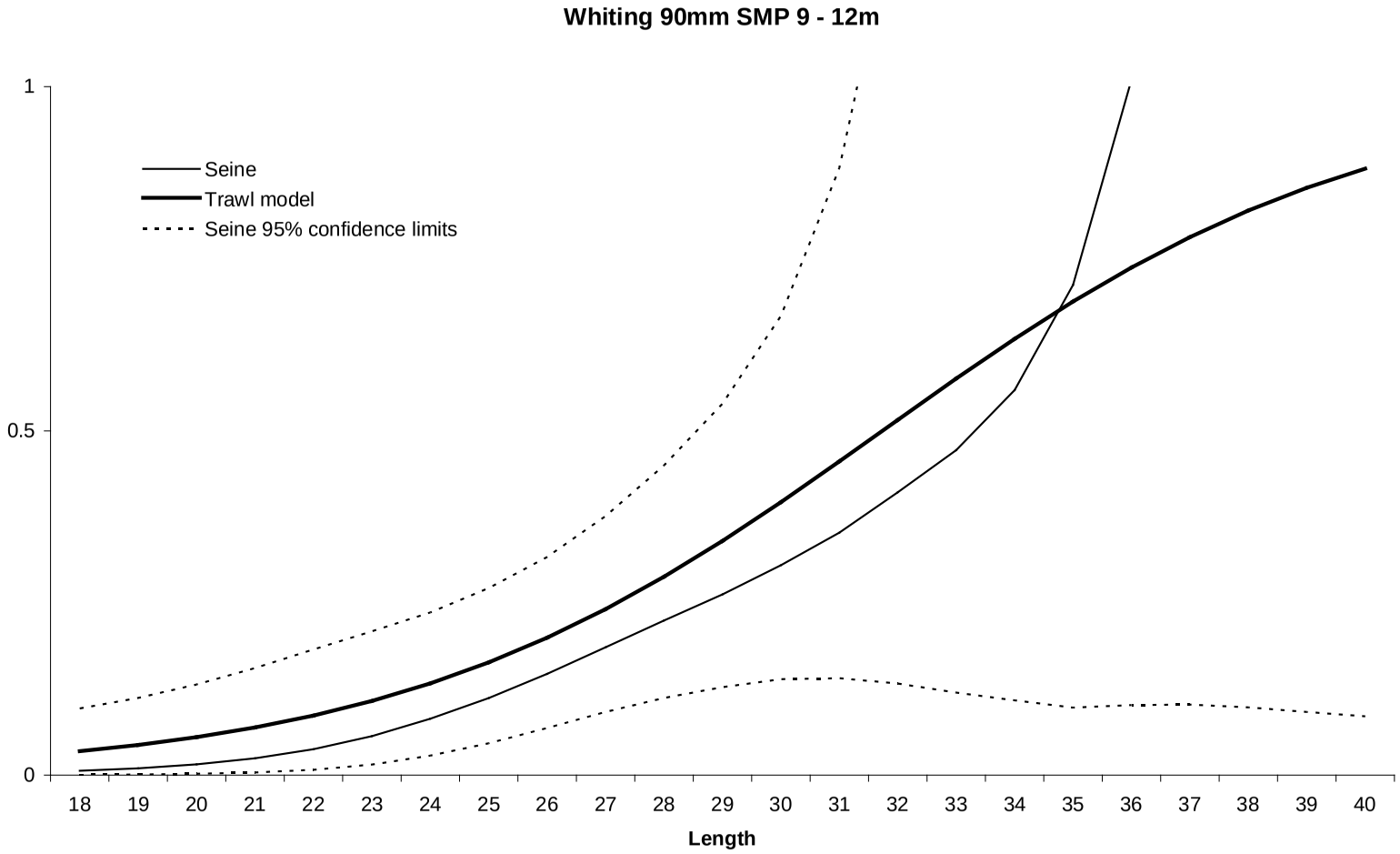

marinescotland

In summary

- mixed model smoothing methodology of Fryer et al. (2003) to estimate the catch rate
- No evidence of a difference between the selectivity of seine and trawl gears – influence of mesh size and smps appear to be the same

marinescotland

Appendix A9

A comparative analysis of legislated and modified Baltic Sea trawlcodends for simultaneously improving the size selection ofcod (Gadus morhua) and plaice (Pleuronectes platessa)

A comparative analysis of legislated and modified Baltic Sea trawlcodends for simultaneously improving the size selection ofcod (Gadus morhua) and plaice (Pleuronectes platessa)Harald

Harald Wienbeck
Bent Herrmann
Jordan P. Feekings
Daniel Stepputtis
Waldemar Moderhak

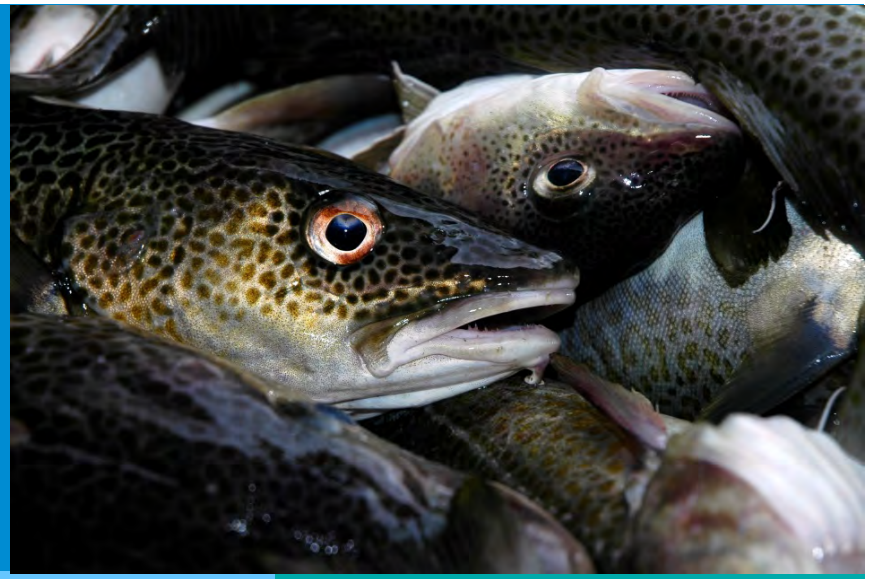

WGFTB
New Bedford 07.05.2014

goal

Assessment of different **modified codends** for their utility in **simultaneously** improving the size selectivity of **cod** (Gadus morhua) and **plaice** (Pleuronectes platessa) in the Baltic Sea

codends

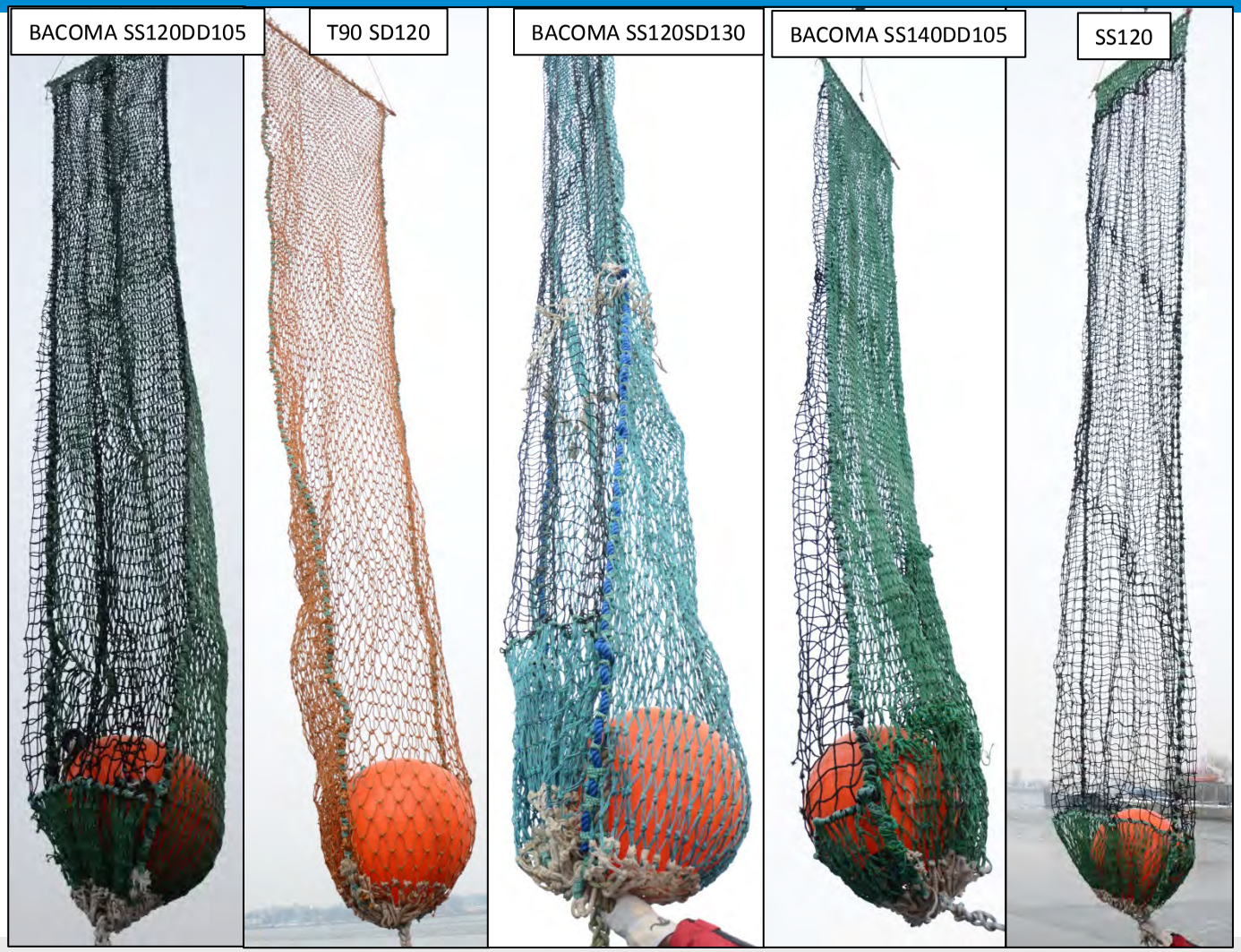

THÜNEN

cod

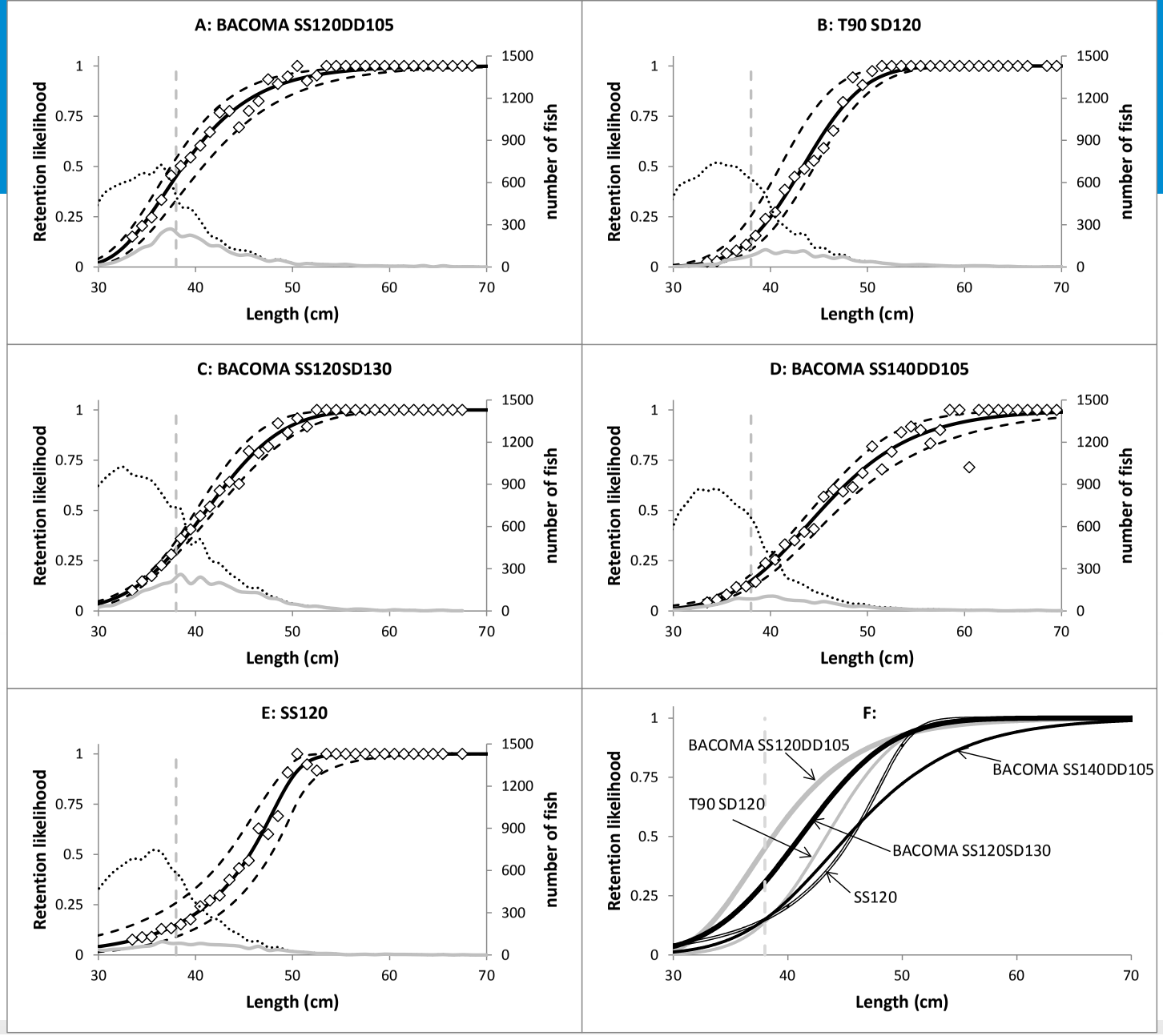
A: BACOMA SS120DD105
B: T90 SD120
C: BACOMA SS120SD130
D: BACOMA SS140DD105
E: SS120
F:
Retention likelihood
number of fish
Length (cm)
BACOMA SS120DD105
T90 SD120
BACOMA SS120SD130
SS120
BACOMA SS140DD105

THÜNEN

cod

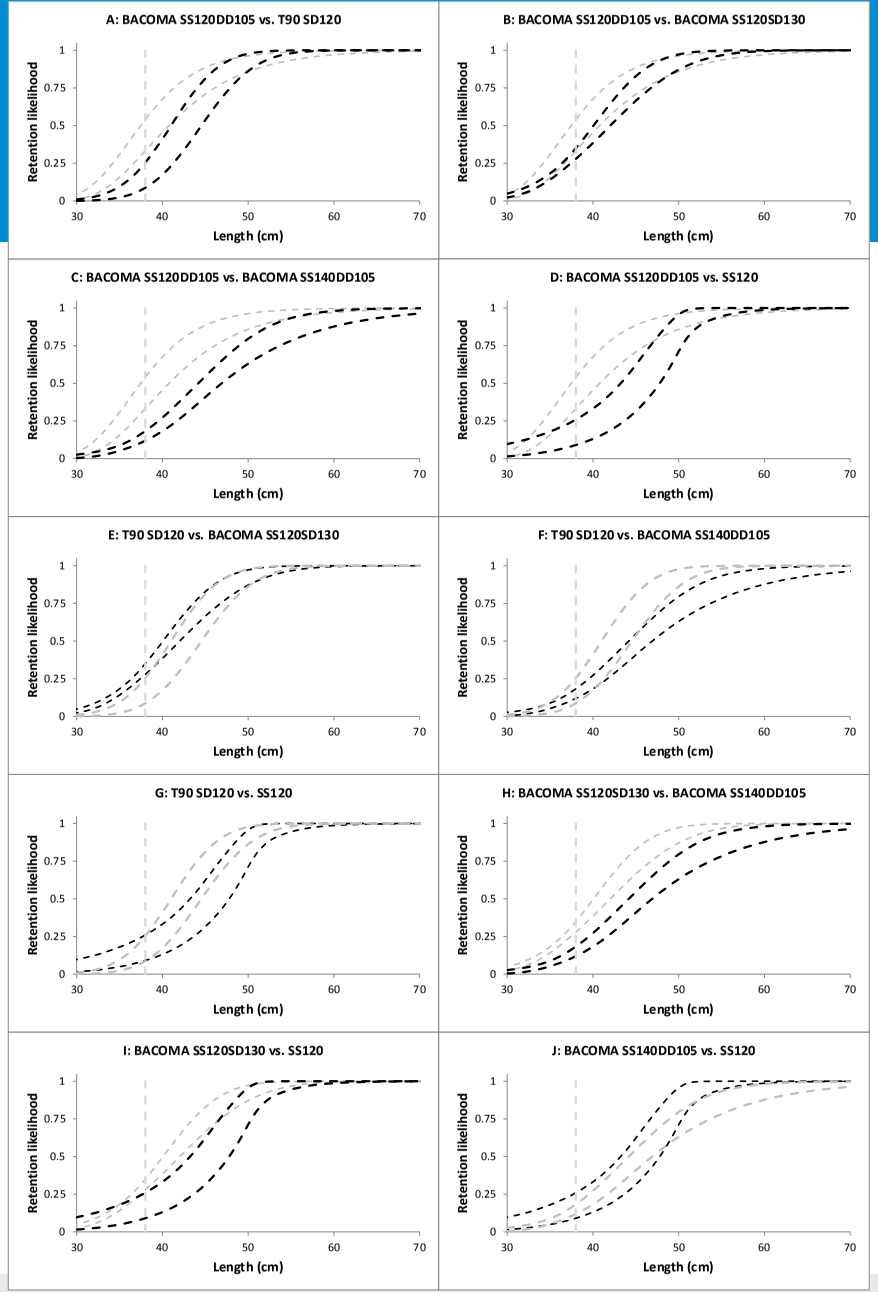
A: BACOMA SS120DD105 vs. T90 SD120
B: BACOMA SS120DD105 vs. BACOMA SS120SD130
C: BACOMA SS120DD105 vs. BACOMA SS140DD105
D: BACOMA SS120DD105 vs. SS120
E: T90 SD120 vs. BACOMA SS120SD130
F: T90 SD120 vs. BACOMA SS140DD105
G: T90 SD120 vs. SS120
H: BACOMA SS120SD130 vs. BACOMA SS140DD105
I: BACOMA SS120SD130 vs. SS120
J: BACOMA SS140DD105 vs. SS120
Retention likelihood
Length (cm)
0
0.25
0.5
0.75
1
30
40
50
60
70

cod

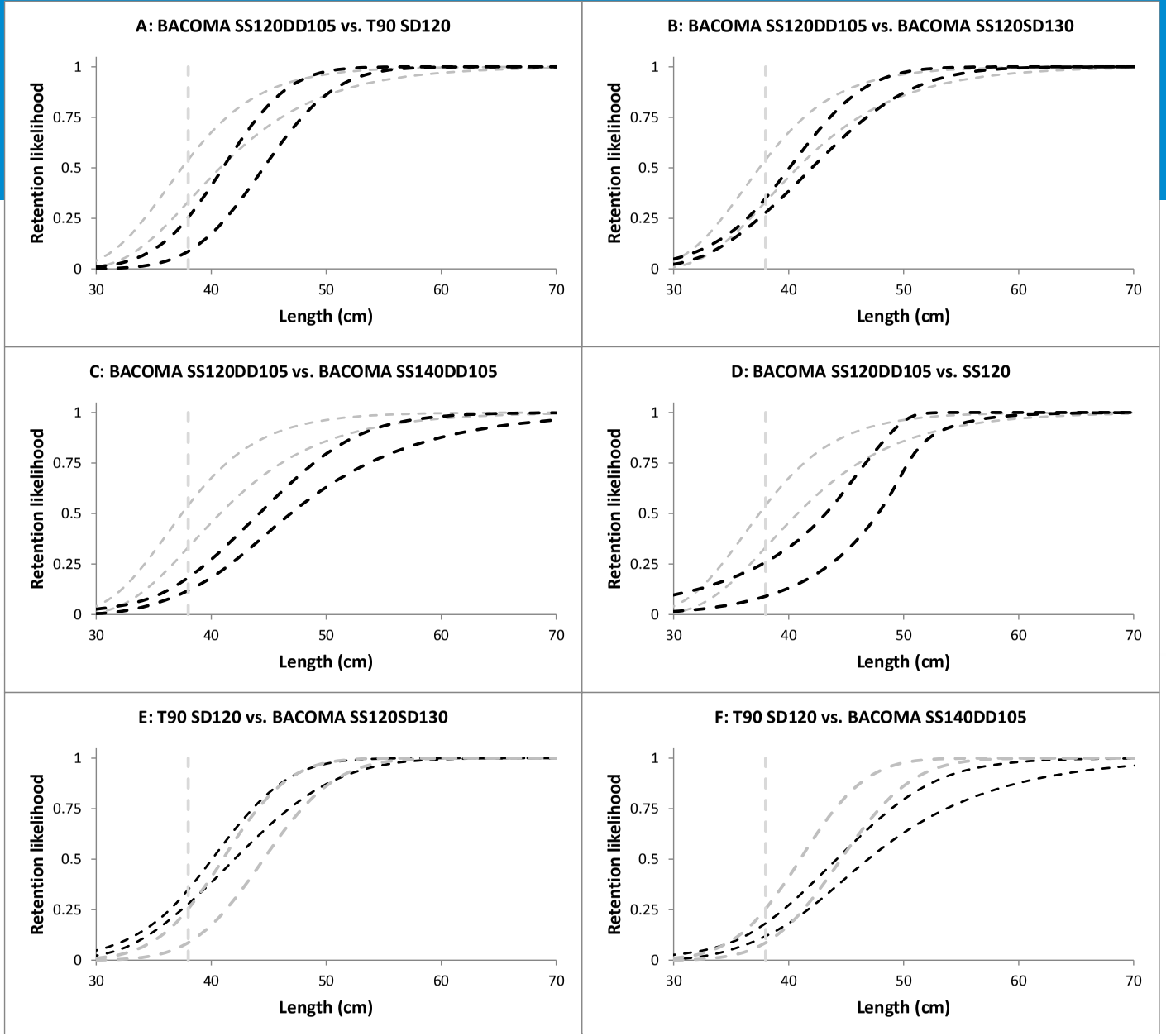
A: BACOMA SS120DD105 vs. T90 SD120
B: BACOMA SS120DD105 vs. BACOMA SS120SD130
C: BACOMA SS120DD105 vs. BACOMA SS140DD105
D: BACOMA SS120DD105 vs. SS120
E: T90 SD120 vs. BACOMA SS120SD130
F: T90 SD120 vs. BACOMA SS140DD105
Retention likelihood
0
0.25
0.5
0.75
1
30
40
50
60
70
Length (cm)

THÜNEN

cod

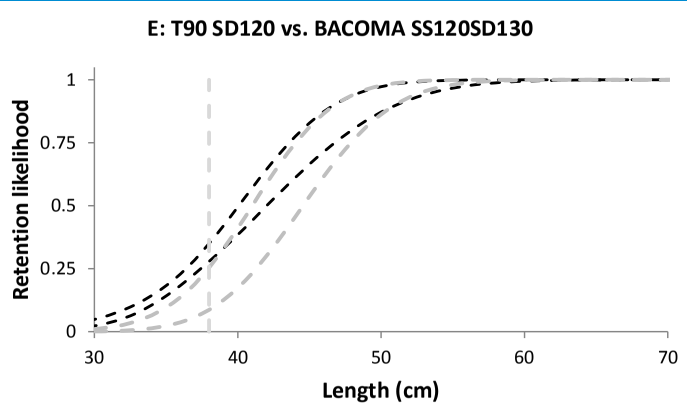
E: T90 SD120 vs. BACOMA SS120SD130
Retention likelihood
1
0.75
0.5
0.25
0
30
40
50
60
70
Length (cm)

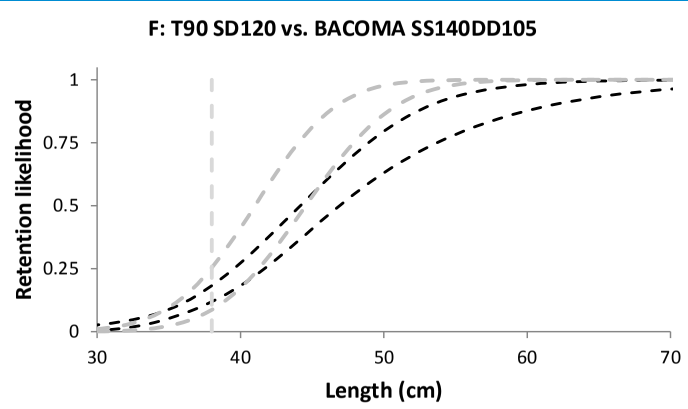
F: T90 SD120 vs. BACOMA SS140DD105
Retention likelihood
1
0.75
0.5
0.25
0
30
40
50
60
70
Length (cm)

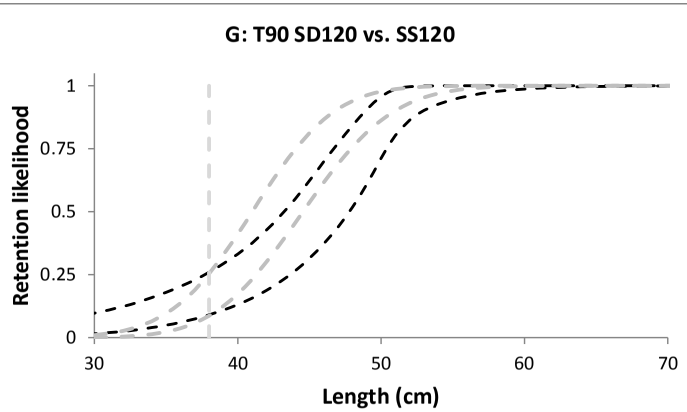
G: T90 SD120 vs. SS120
Retention likelihood
1
0.75
0.5
0.25
0
30
40
50
60
70
Length (cm)

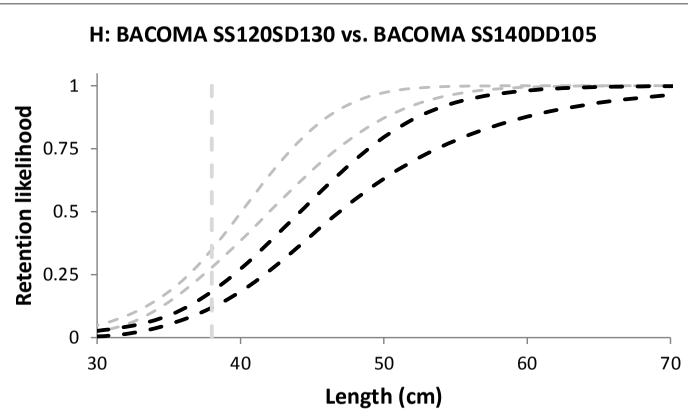
H: BACOMA SS120SD130 vs. BACOMA SS140DD105
Retention likelihood
1
0.75
0.5
0.25
0
30
40
50
60
70
Length (cm)

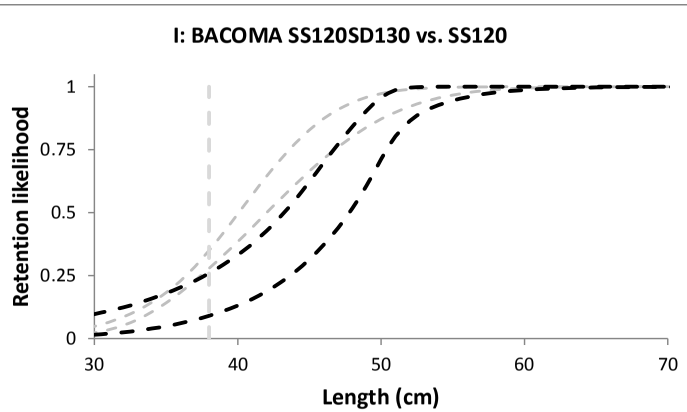
I: BACOMA SS120SD130 vs. SS120
Retention likelihood
1
0.75
0.5
0.25
0
30
40
50
60
70
Length (cm)

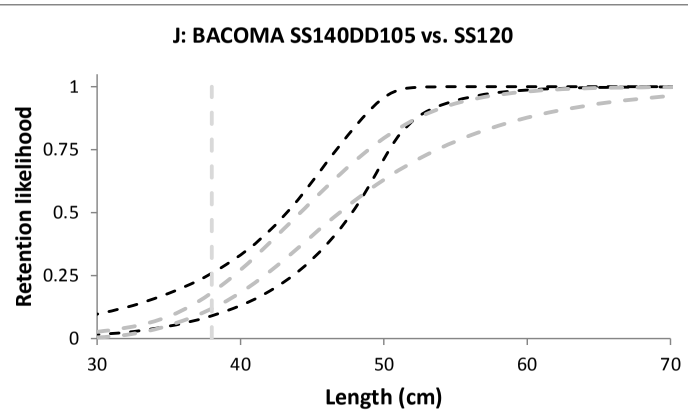
J: BACOMA SS140DD105 vs. SS120
Retention likelihood
1
0.75
0.5
0.25
0
30
40
50
60
70
Length (cm)

plaice

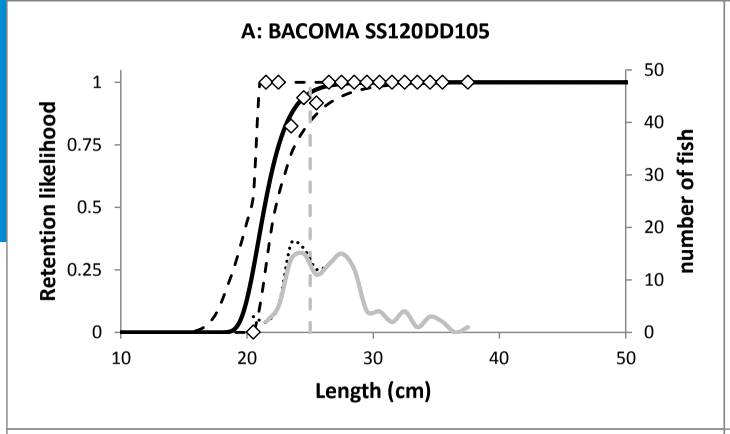

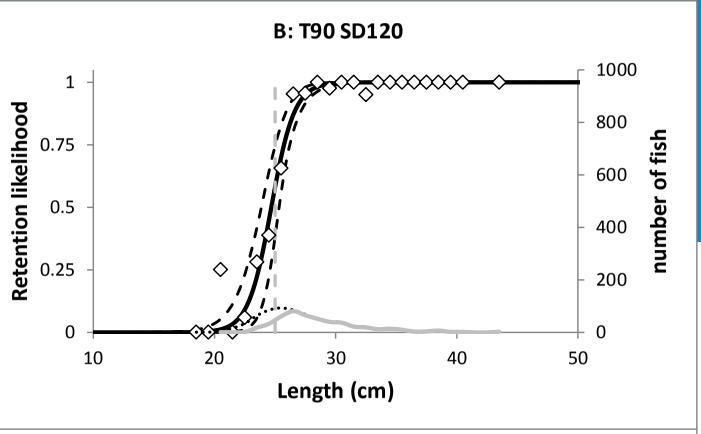

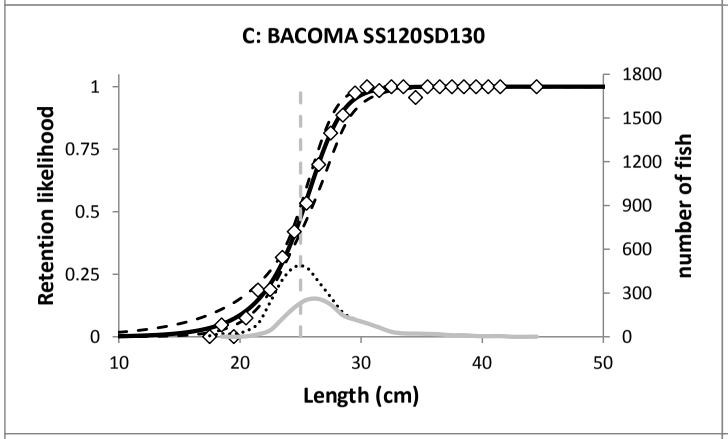

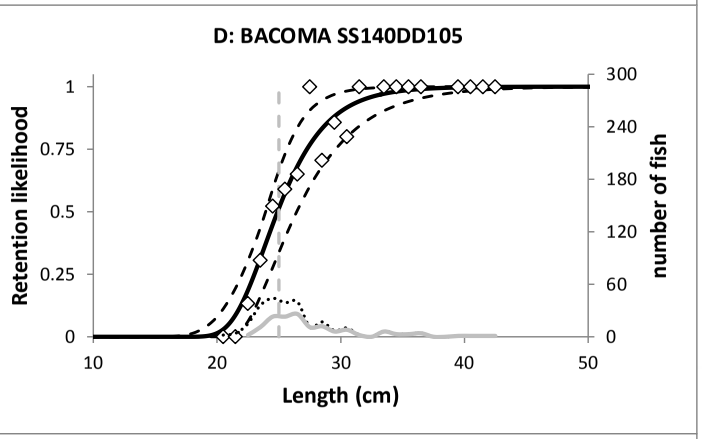

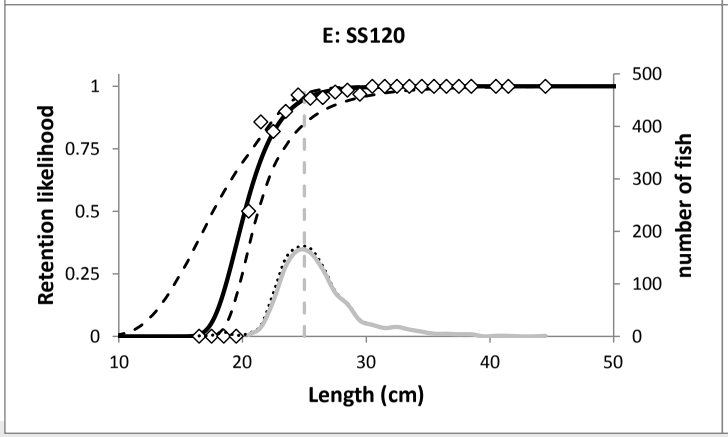

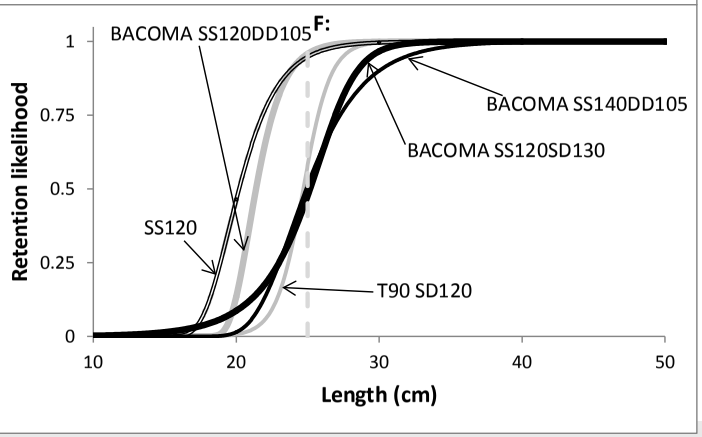

THÜNEN

plaice

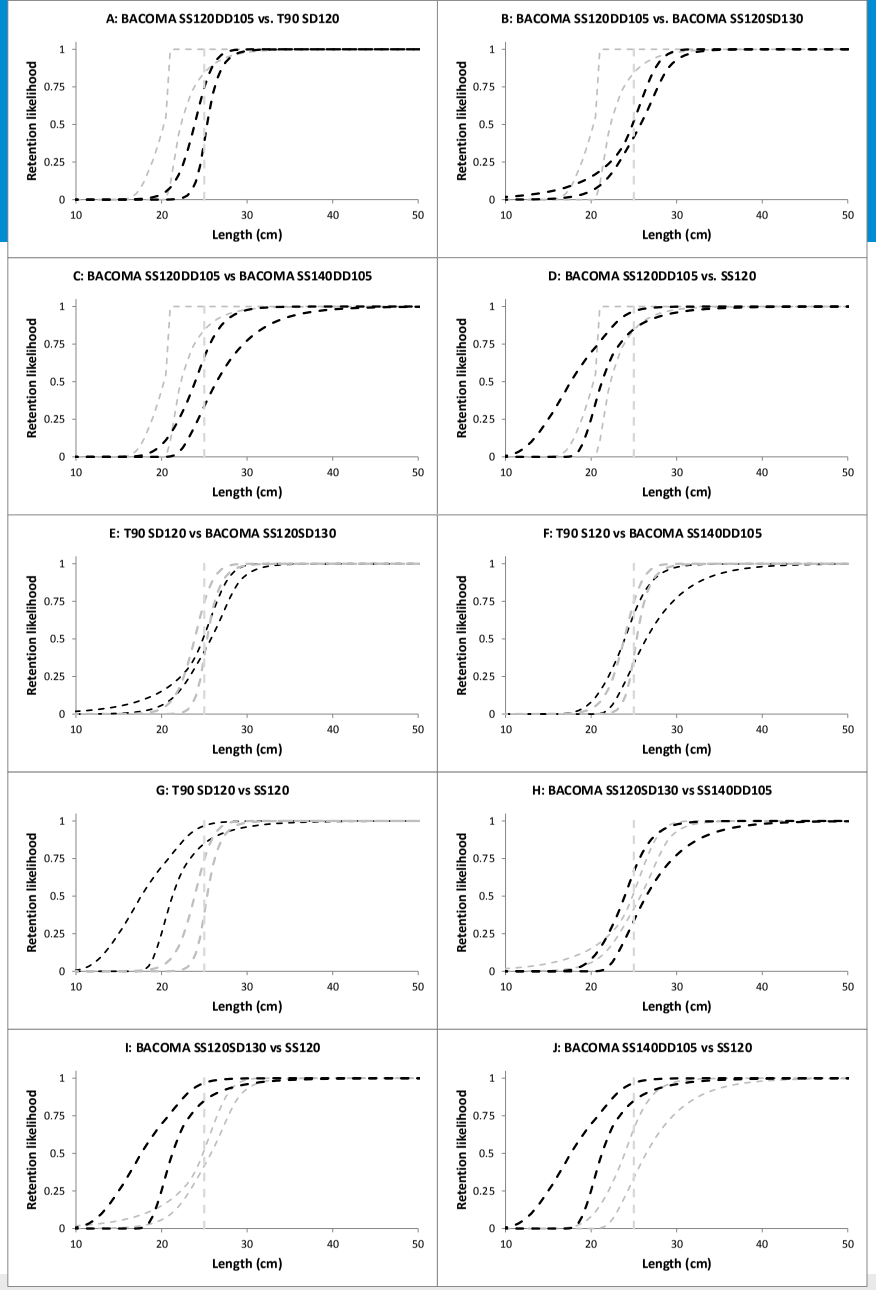
A: BACOMA SS120DD105 vs. T90 SD120
B: BACOMA SS120DD105 vs. BACOMA SS120SD130
C: BACOMA SS120DD105 vs BACOMA SS140DD105
D: BACOMA SS120DD105 vs. SS120
E: T90 SD120 vs BACOMA SS120SD130
F: T90 S120 vs BACOMA SS140DD105
G: T90 SD120 vs SS120
H: BACOMA SS120SD130 vs SS140DD105
I: BACOMA SS120SD130 vs SS120
J: BACOMA SS140DD105 vs SS120
Retention likelihood
Length (cm)
0
0.25
0.5
0.75
1
10
20
30
40
50

plaice

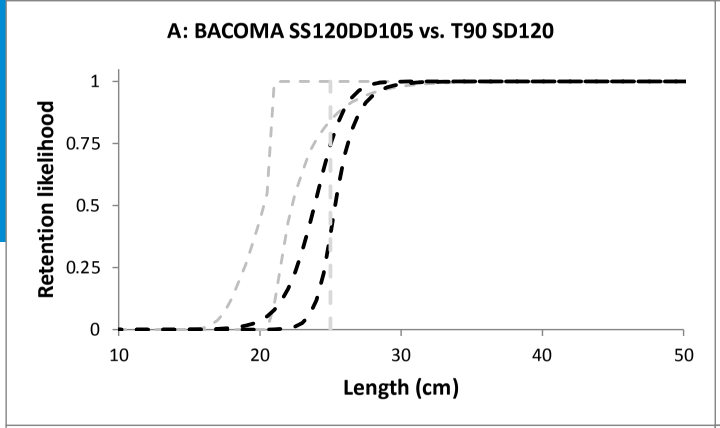
A: BACOMA SS120DD105 vs. T90 SD120
Retention likelihood
1
0.75
0.5
0.25
0
10
20
30
40
50
Length (cm)

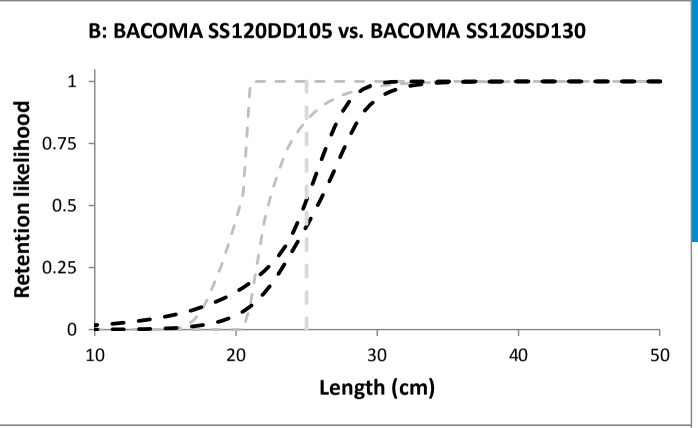
B: BACOMA SS120DD105 vs. BACOMA SS120SD130
Retention likelihood
1
0.75
0.5
0.25
0
10
20
30
40
50
Length (cm)

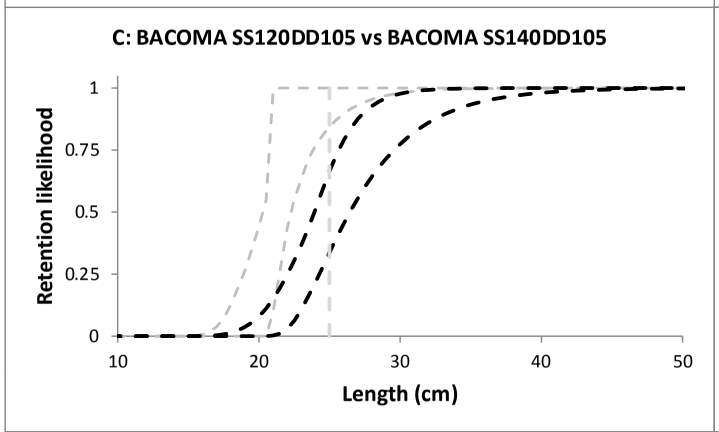
C: BACOMA SS120DD105 vs BACOMA SS140DD105
Retention likelihood
1
0.75
0.5
0.25
0
10
20
30
40
50
Length (cm)

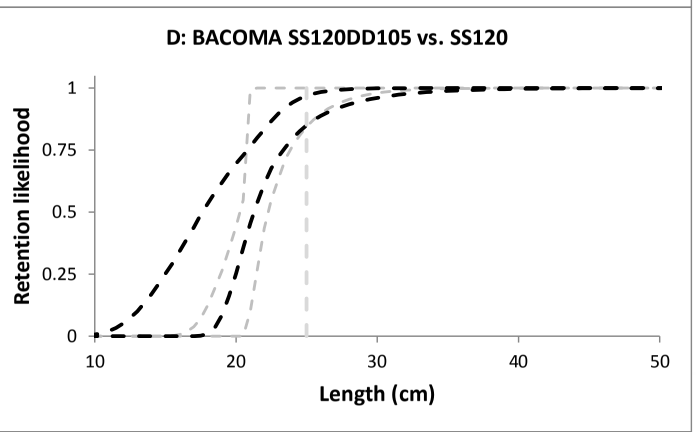
D: BACOMA SS120DD105 vs. SS120
Retention likelihood
1
0.75
0.5
0.25
0
10
20
30
40
50
Length (cm)

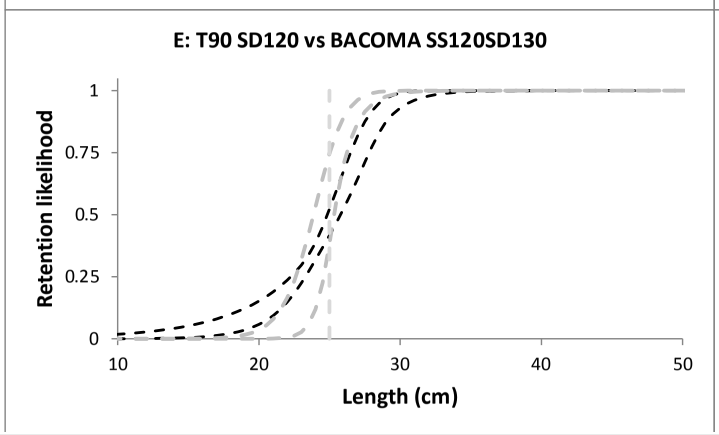
E: T90 SD120 vs BACOMA SS120SD130
Retention likelihood
1
0.75
0.5
0.25
0
10
20
30
40
50
Length (cm)

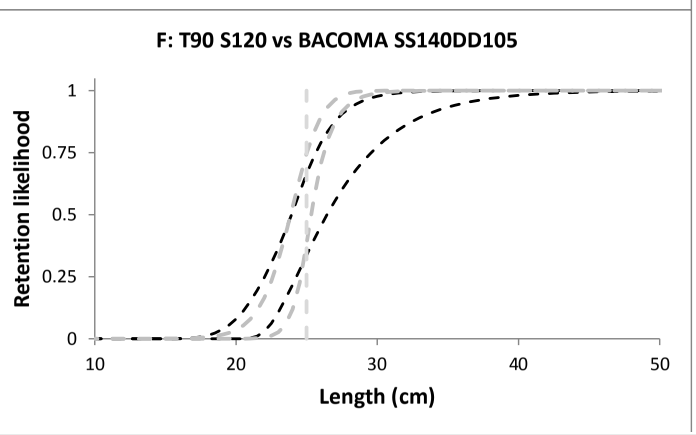
F: T90 S120 vs BACOMA SS140DD105
Retention likelihood
1
0.75
0.5
0.25
0
10
20
30
40
50
Length (cm)

plaice

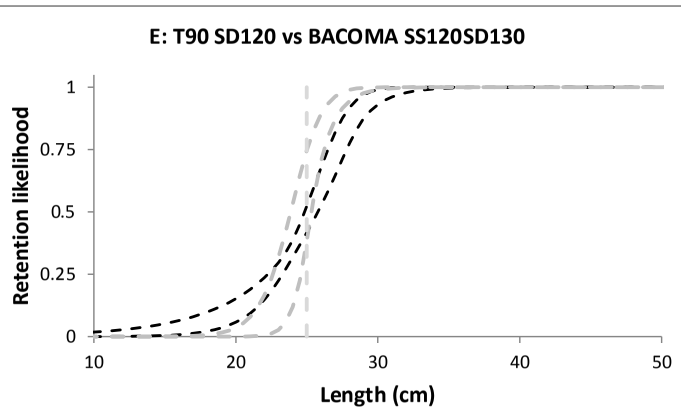
E: T90 SD120 vs BACOMA SS120SD130
Retention likelihood
1
0.75
0.5
0.25
0
10
20
30
40
50
Length (cm)

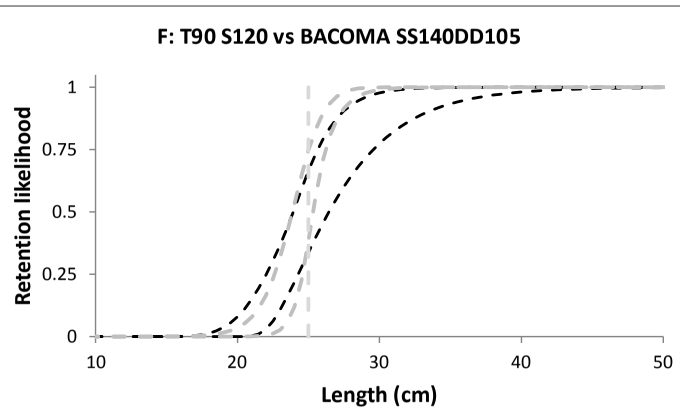
F: T90 S120 vs BACOMA SS140DD105
Retention likelihood
1
0.75
0.5
0.25
0
10
20
30
40
50
Length (cm)

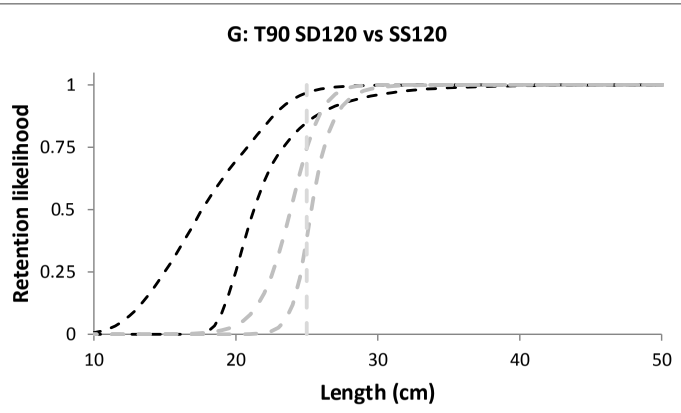
G: T90 SD120 vs SS120
Retention likelihood
1
0.75
0.5
0.25
0
10
20
30
40
50
Length (cm)

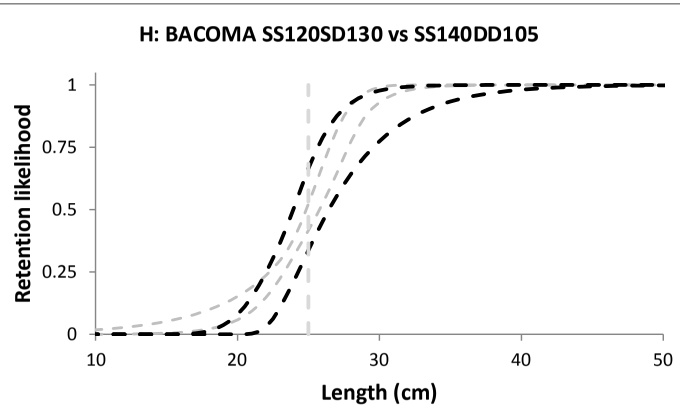
H: BACOMA SS120SD130 vs SS140DD105
Retention likelihood
1
0.75
0.5
0.25
0
10
20
30
40
50
Length (cm)

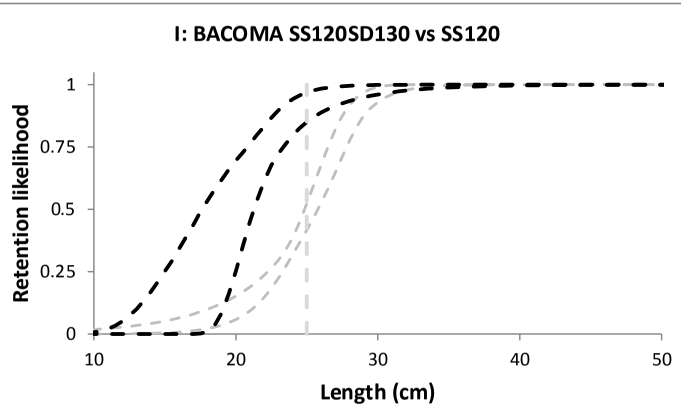
I: BACOMA SS120SD130 vs SS120
Retention likelihood
1
0.75
0.5
0.25
0
10
20
30
40
50
Length (cm)

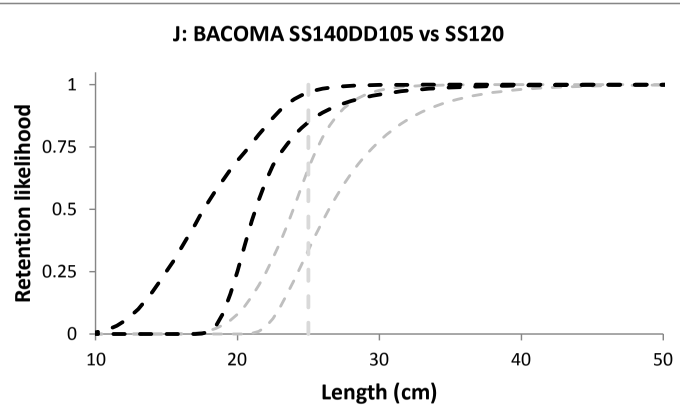
J: BACOMA SS140DD105 vs SS120
Retention likelihood
1
0.75
0.5
0.25
0
10
20
30
40
50
Length (cm)

Appendix A10

Warum funktioniert das Bacoma?

Warum funktioniert das Bacoma?

Thünen-Institut für Ostseefischerei

Dr. Daniel Stepputtis,
Dr. Bent Herrmann (DK)
Harald Wienbeck
Junita Karlsen (DK)

Rendsburg 30.01.2014

Quadratmaschen

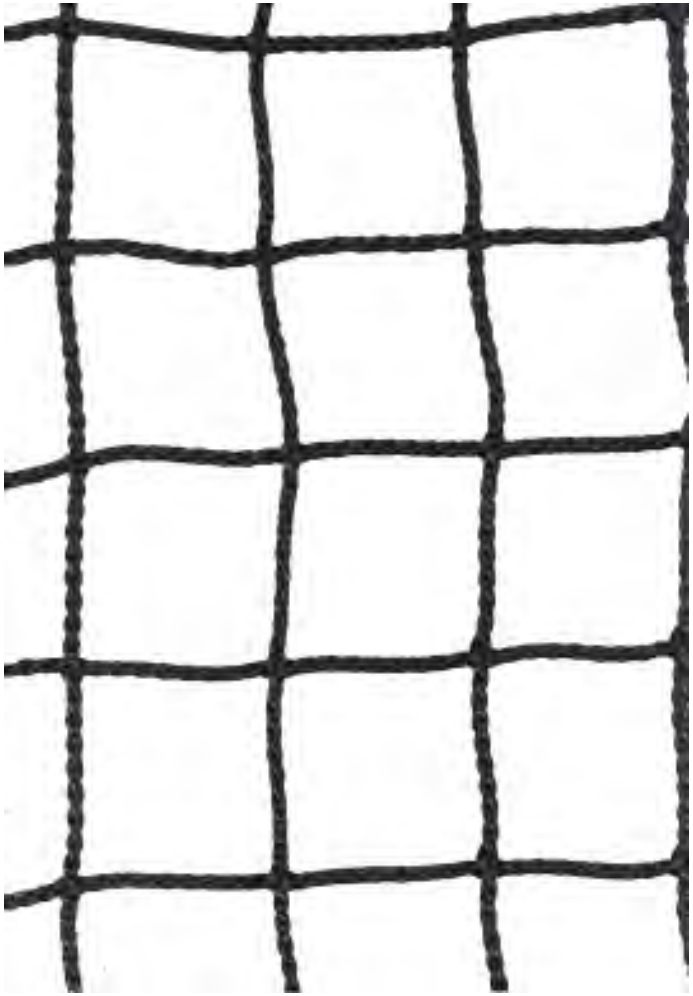

Bacoma

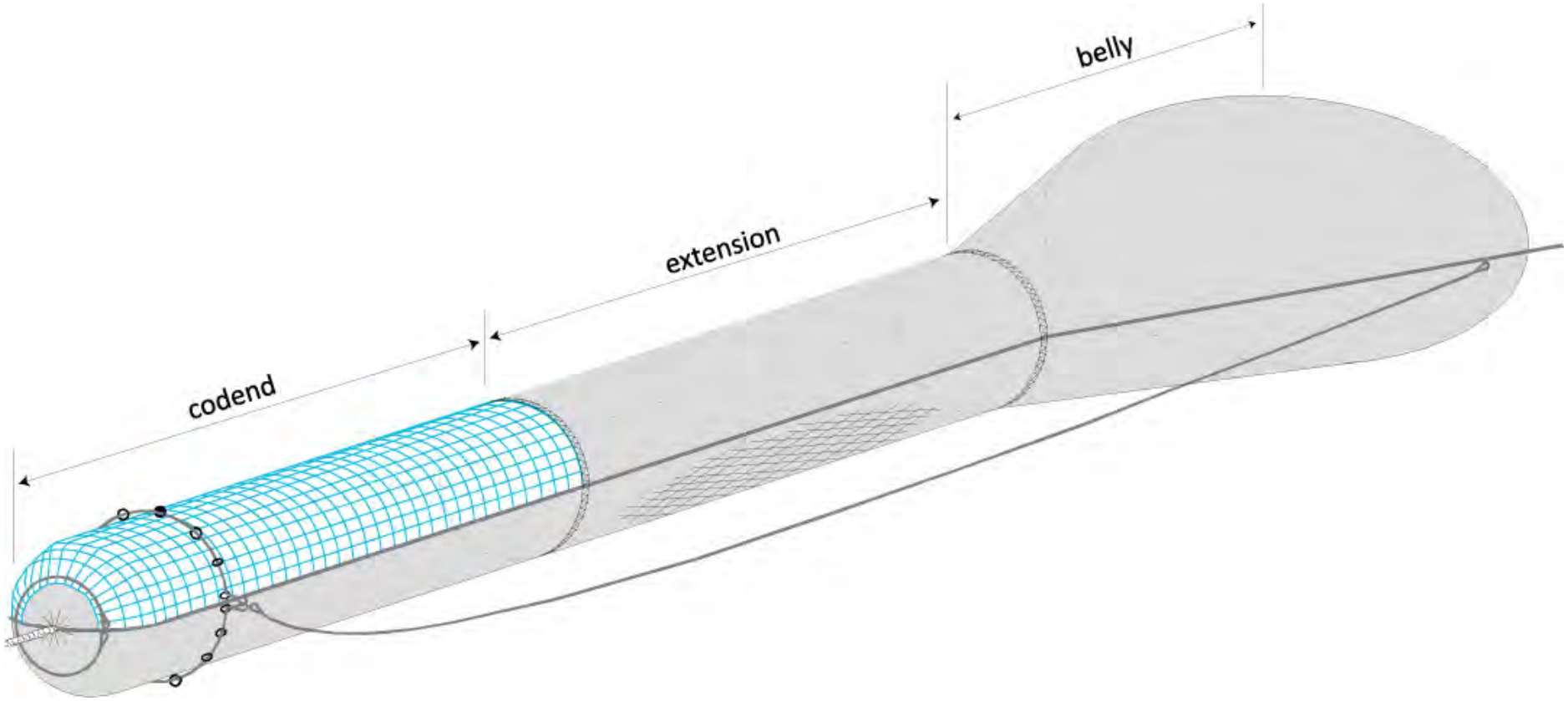

THÜNEN

Bacoma

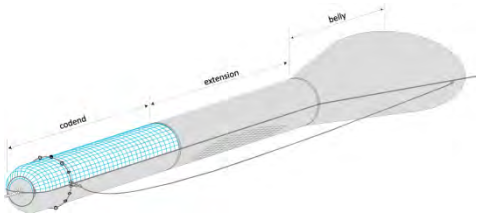

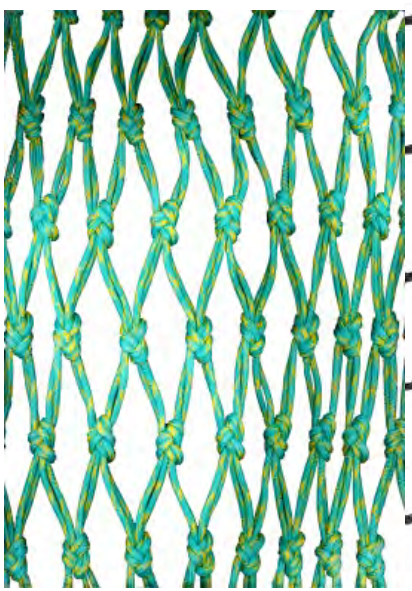

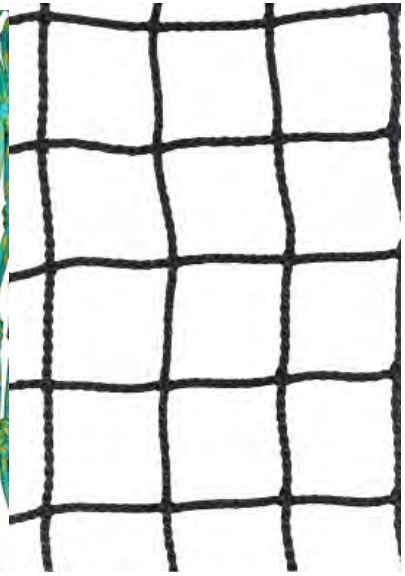

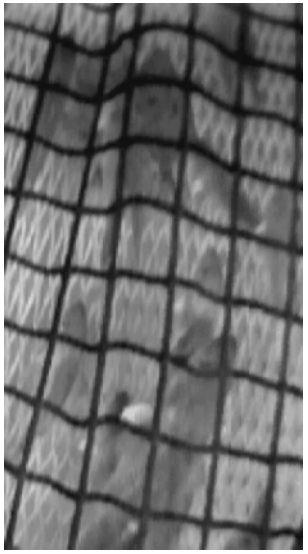

THÜNEN

Test

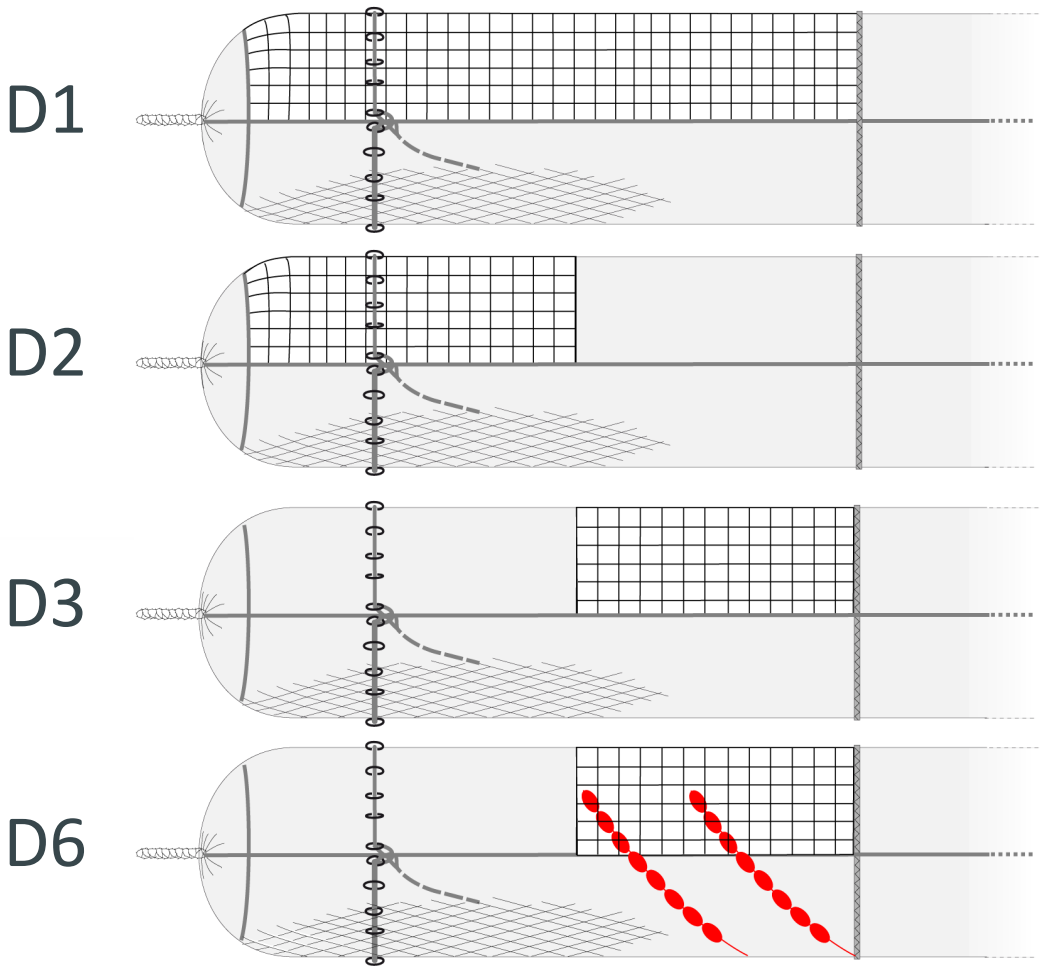

Test

Test

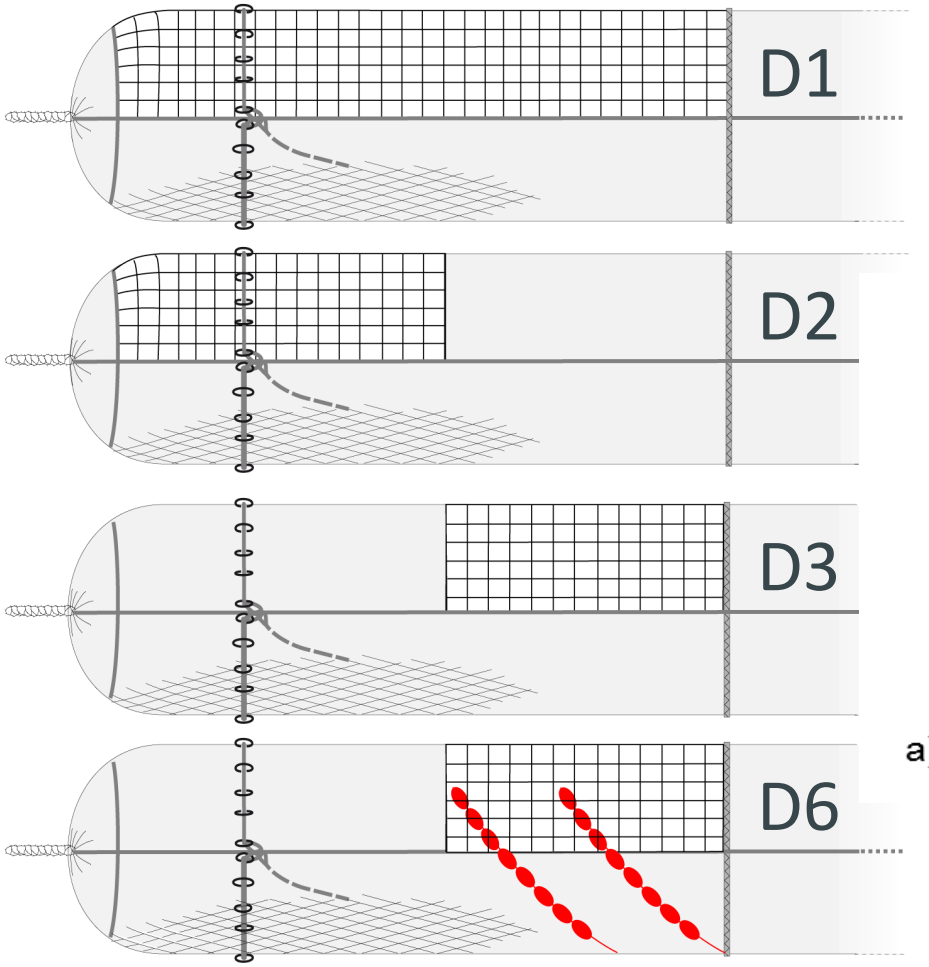

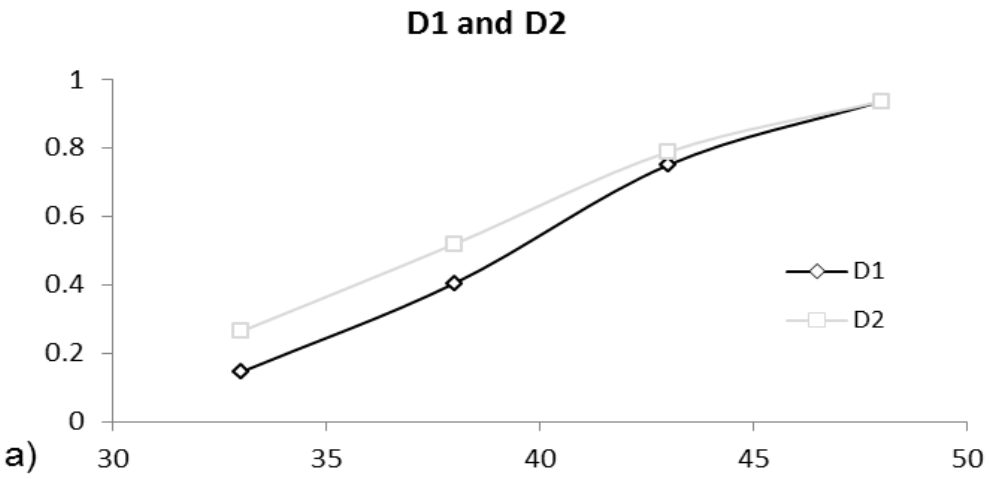

a)

THÜNEN

Test

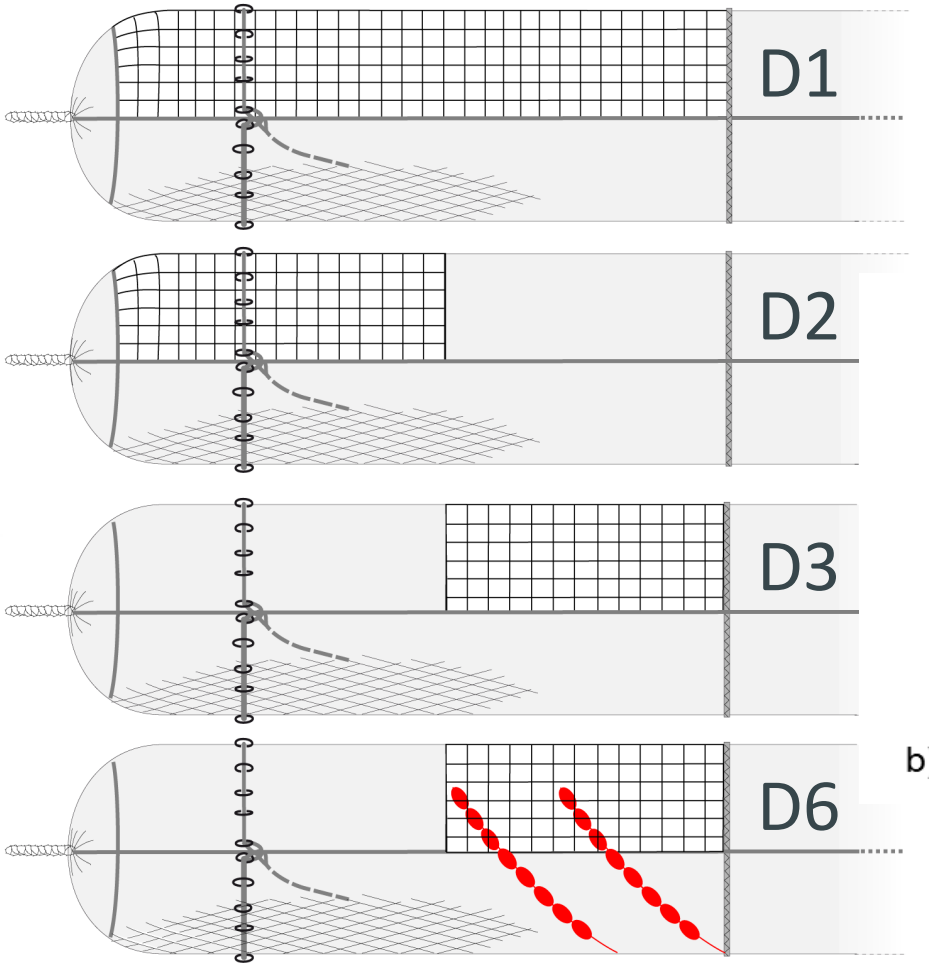

b)

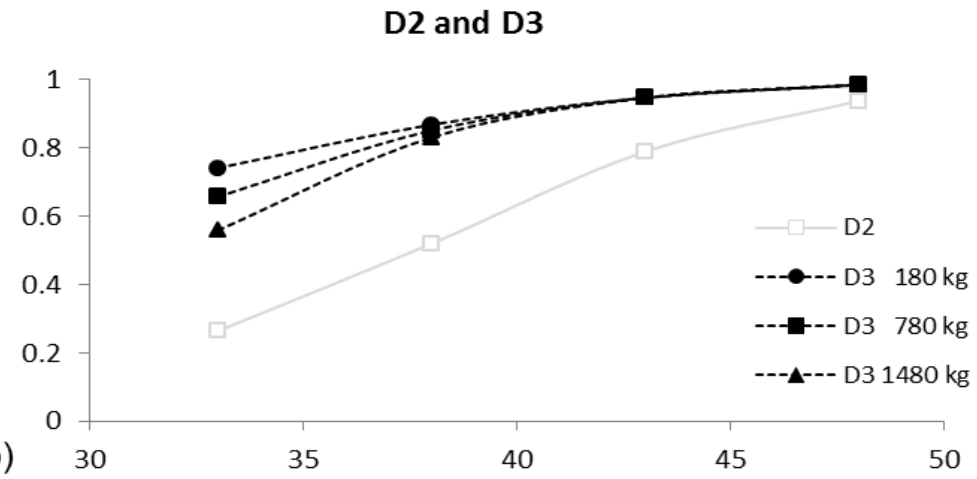

THÜNEN

Test

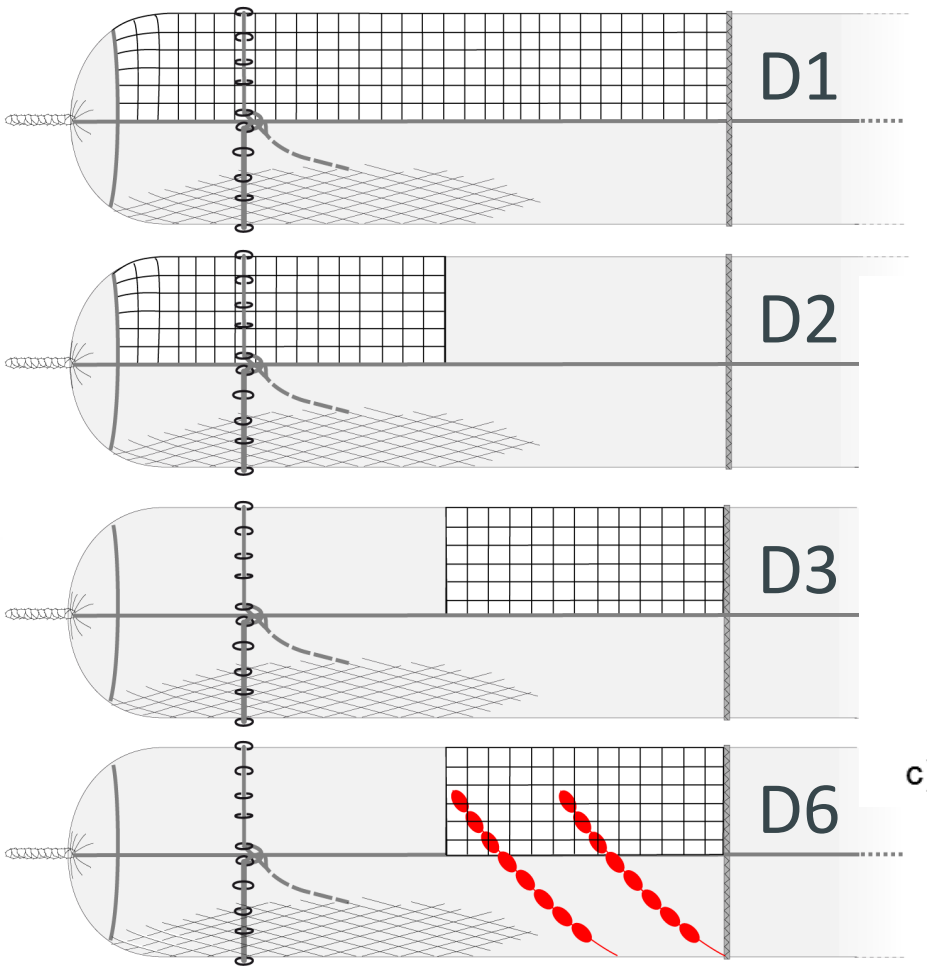

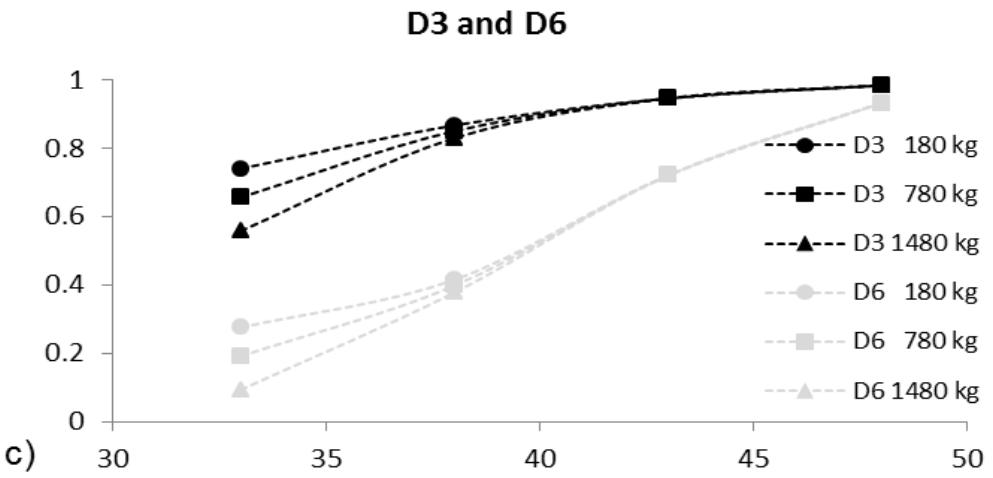

c)

THÜNEN

Test

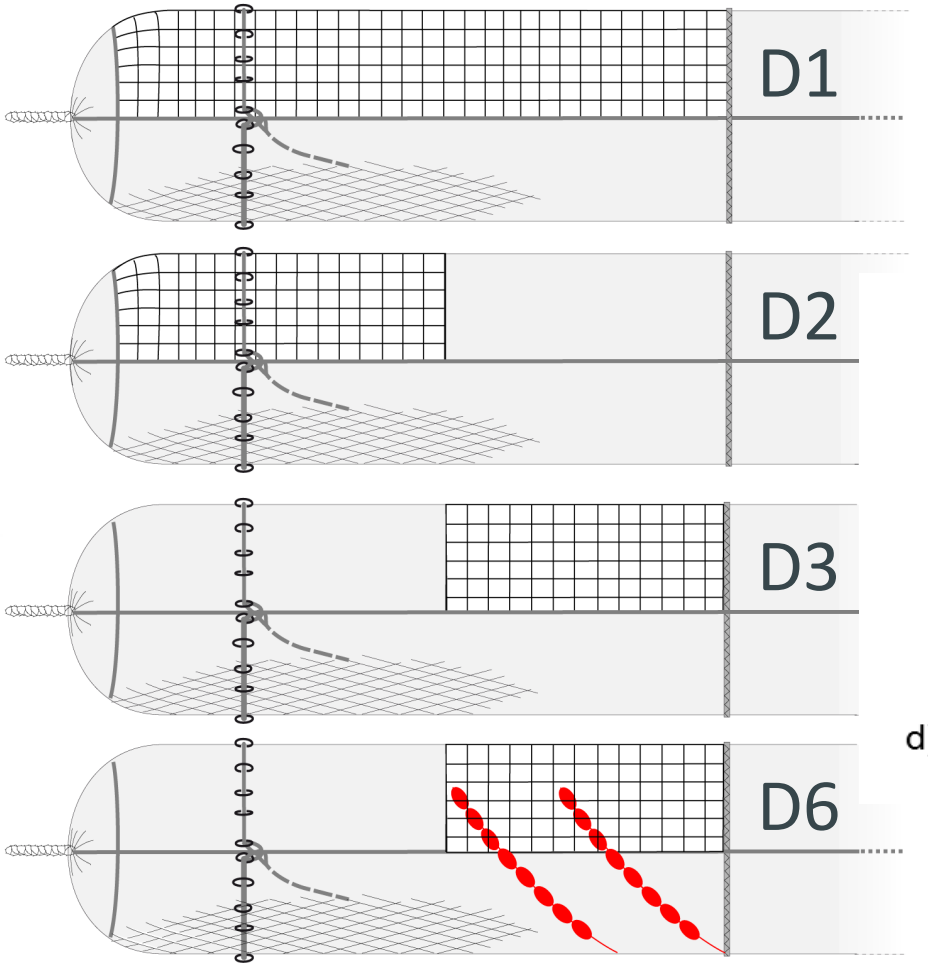

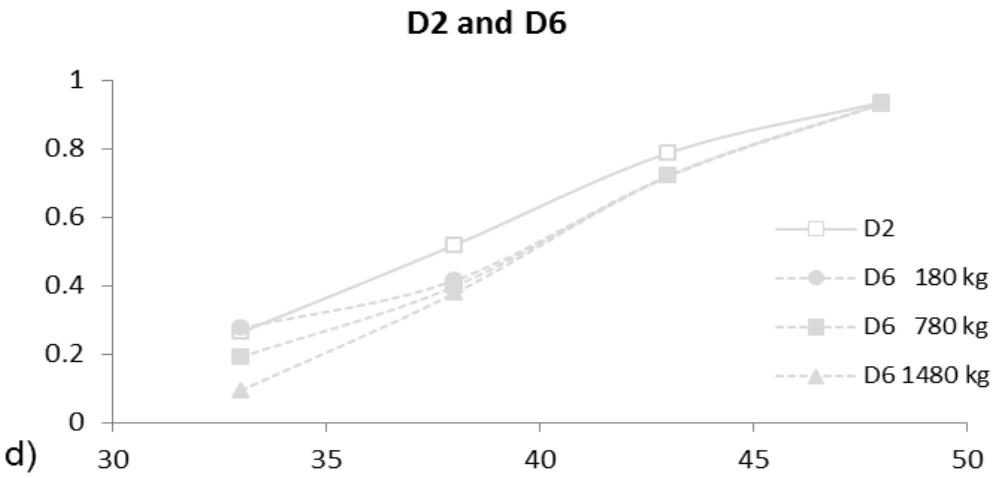

d)

THÜNEN

Test

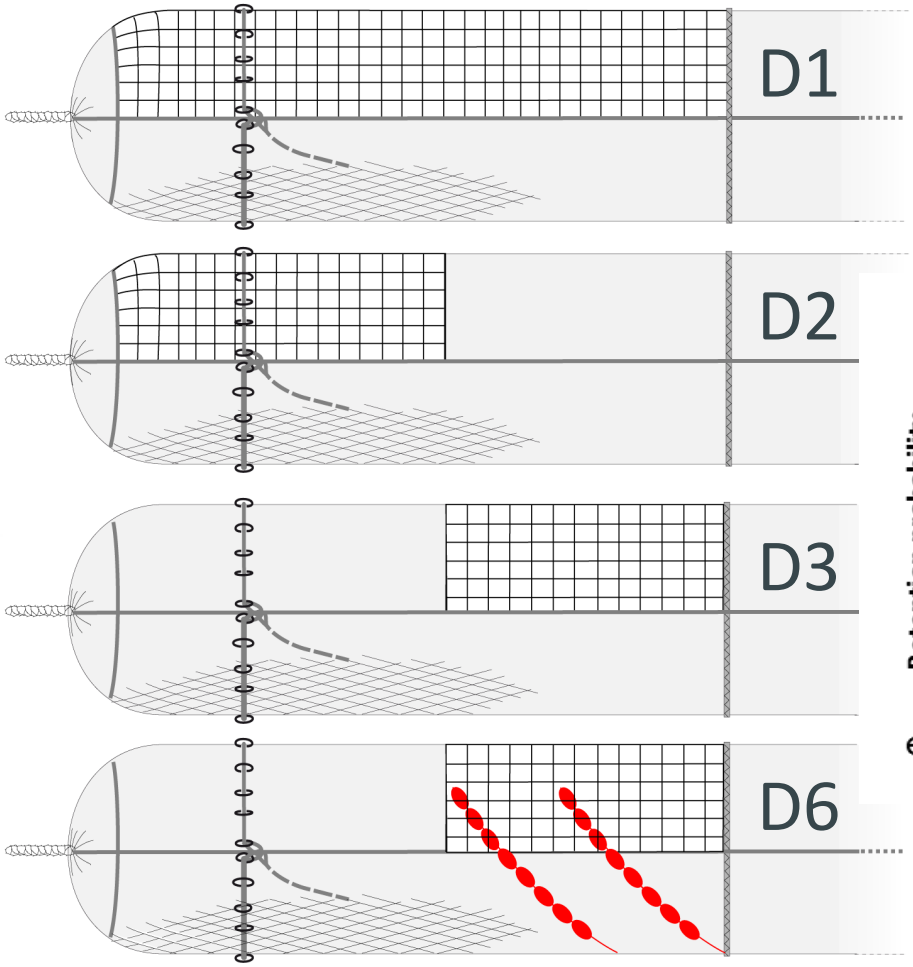

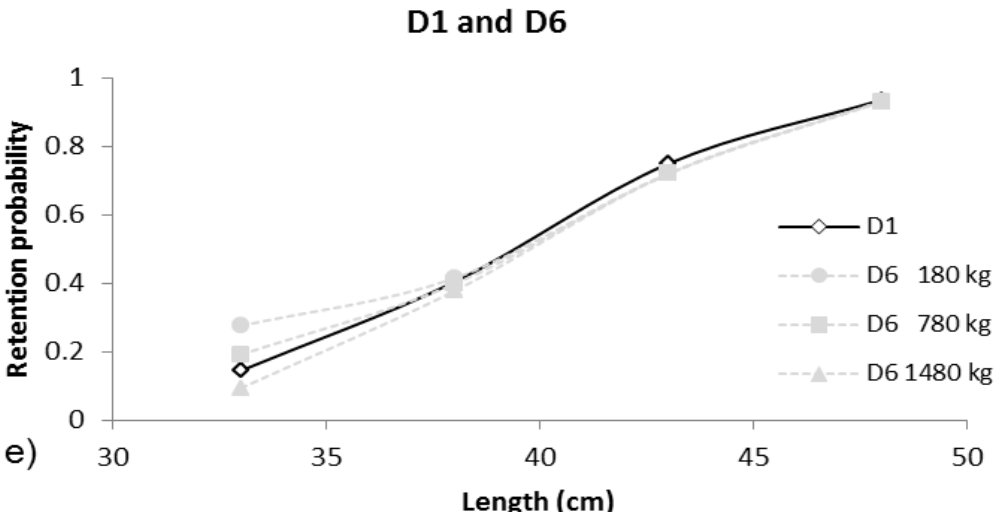

e)

THÜNEN

Test

Appendix A11

German pictures for roundfish escapement through square meshes of codends

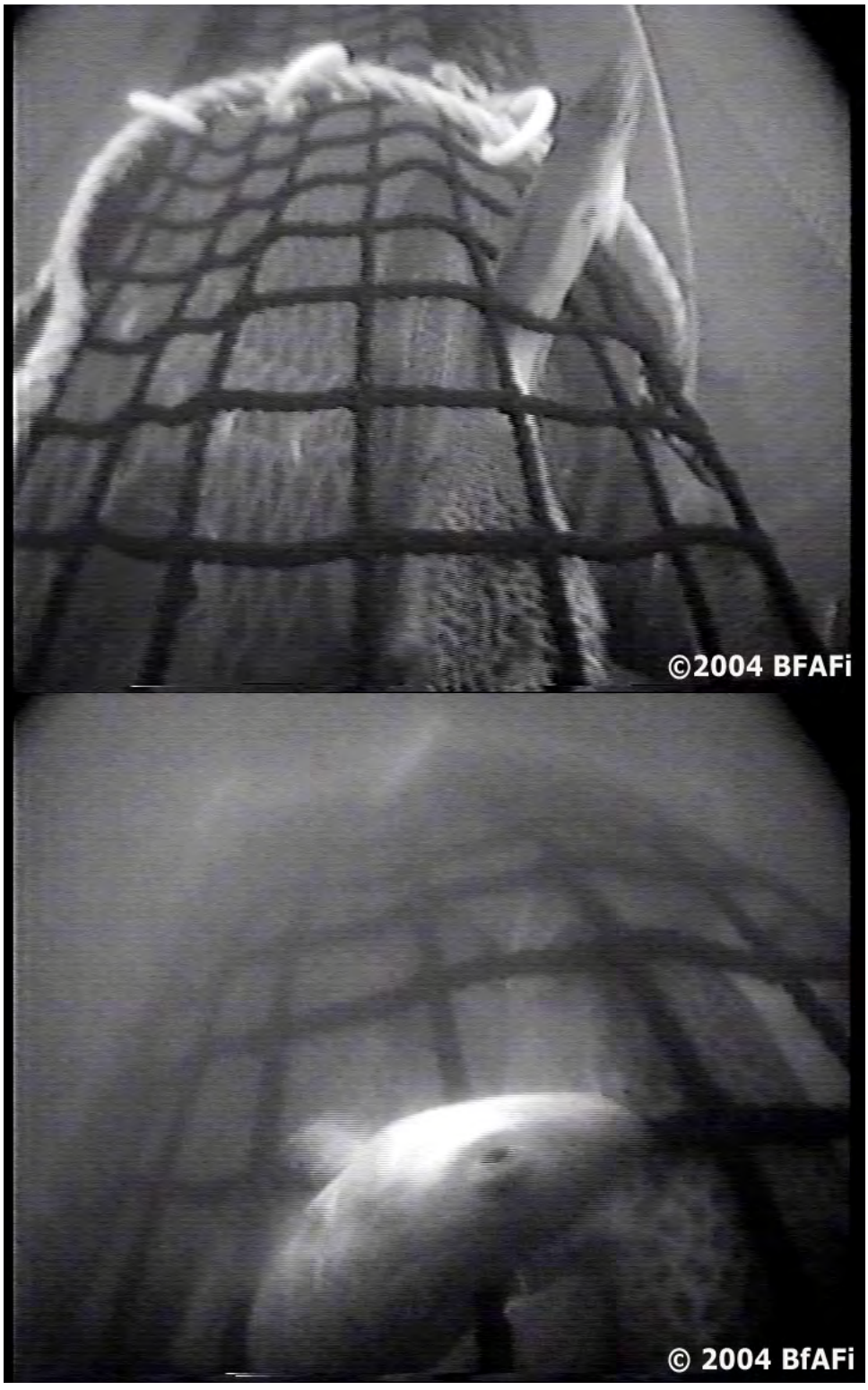
©2004 BFAFi
© 2004 BfAFi


©2004 BFAFi


©2004 BFAFi

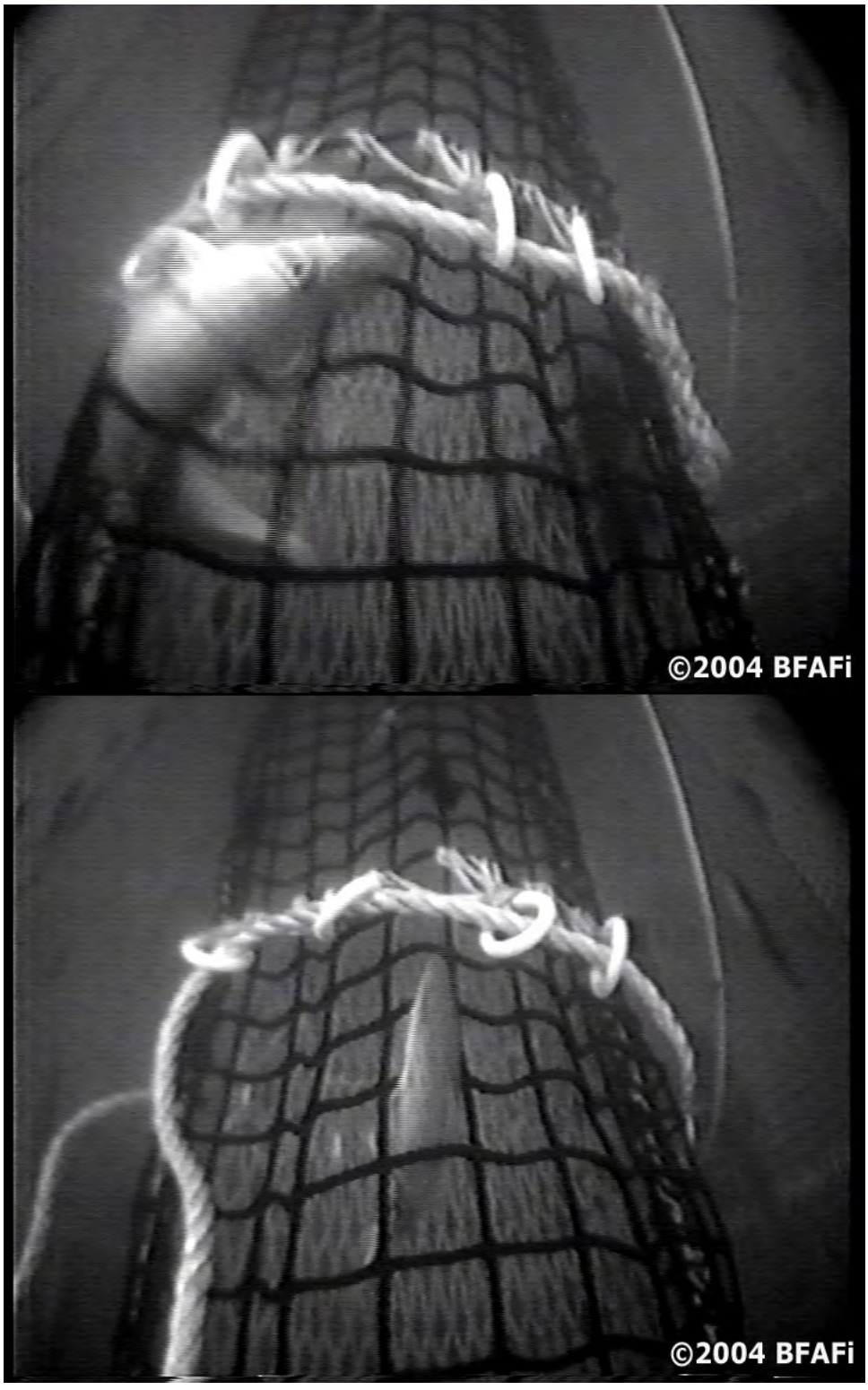
©2004 BFAFi
©2004 BFAFi

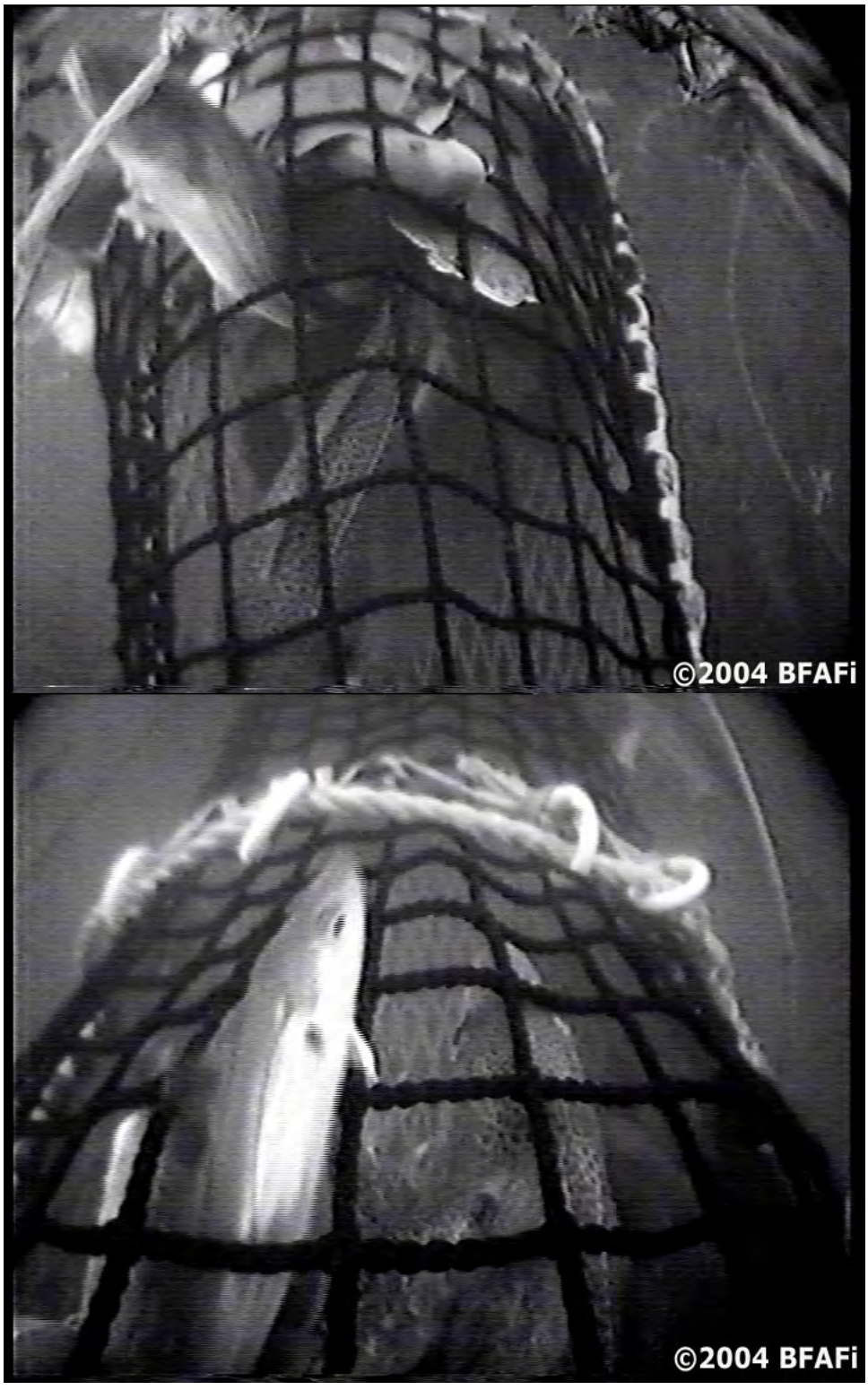
©2004 BFAFi
©2004 BFAFi

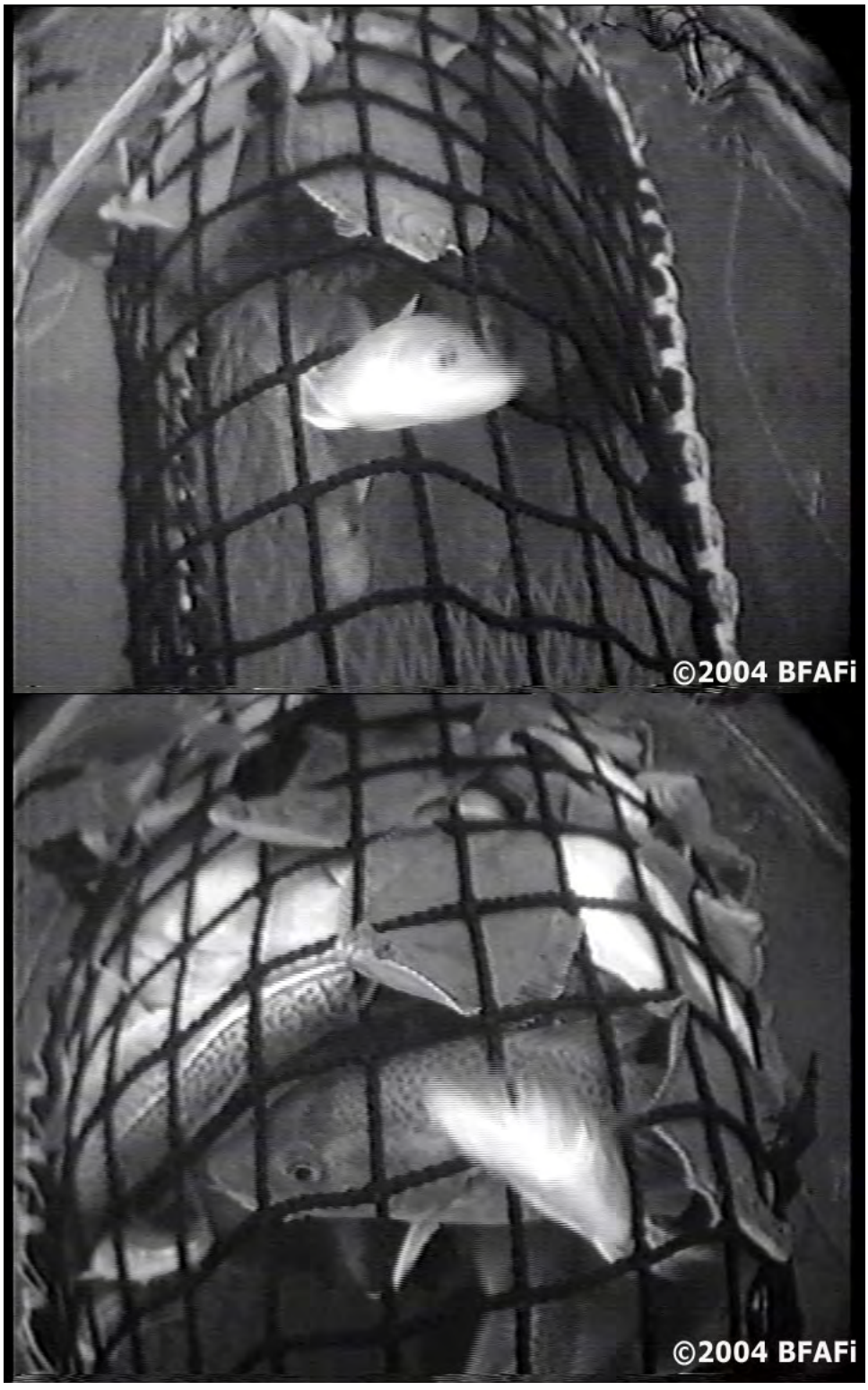
©2004 BFAFi
©2004 BFAFi

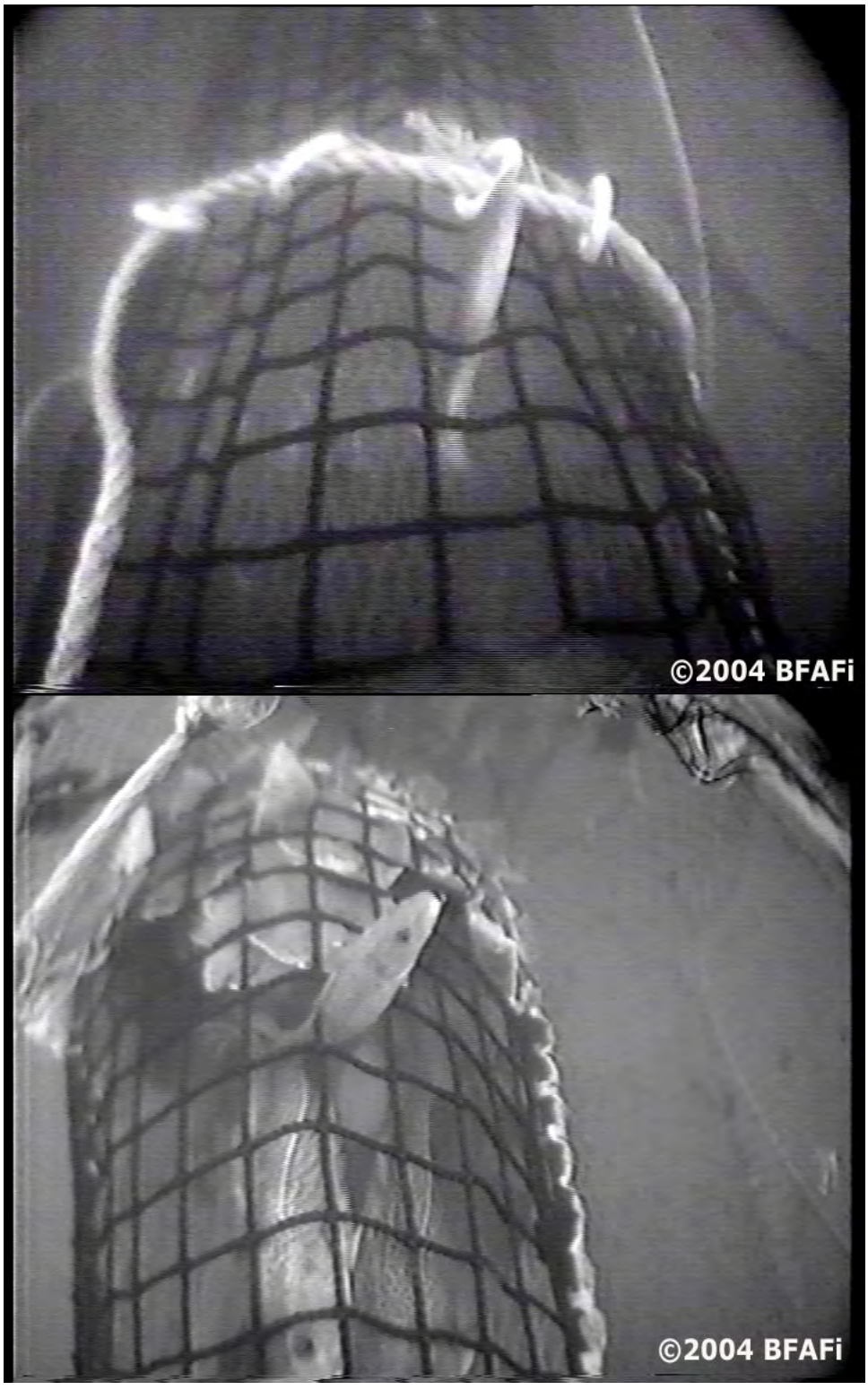
©2004 BFAFi
©2004 BFAFi

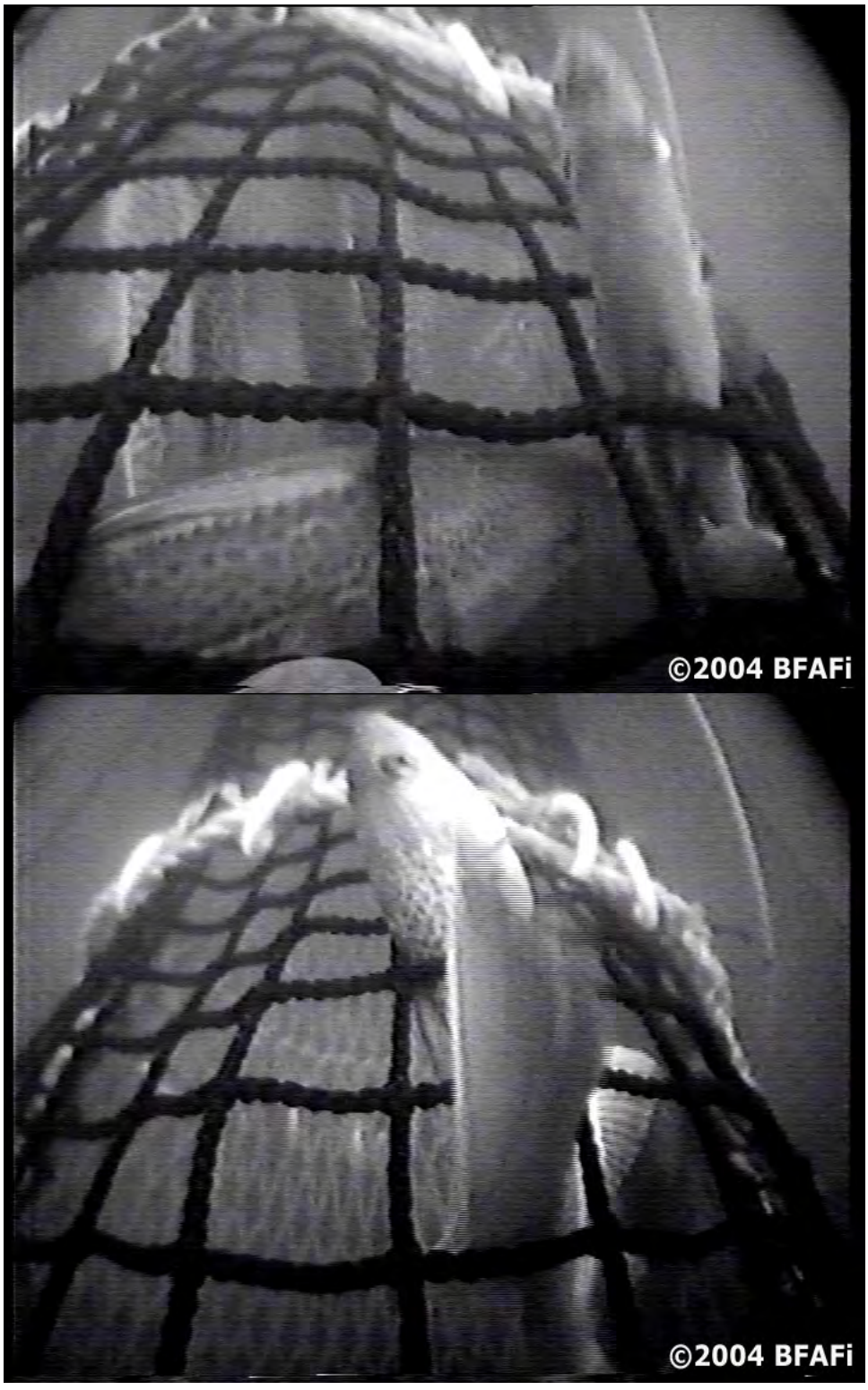
©2004 BFAFi
©2004 BFAFi

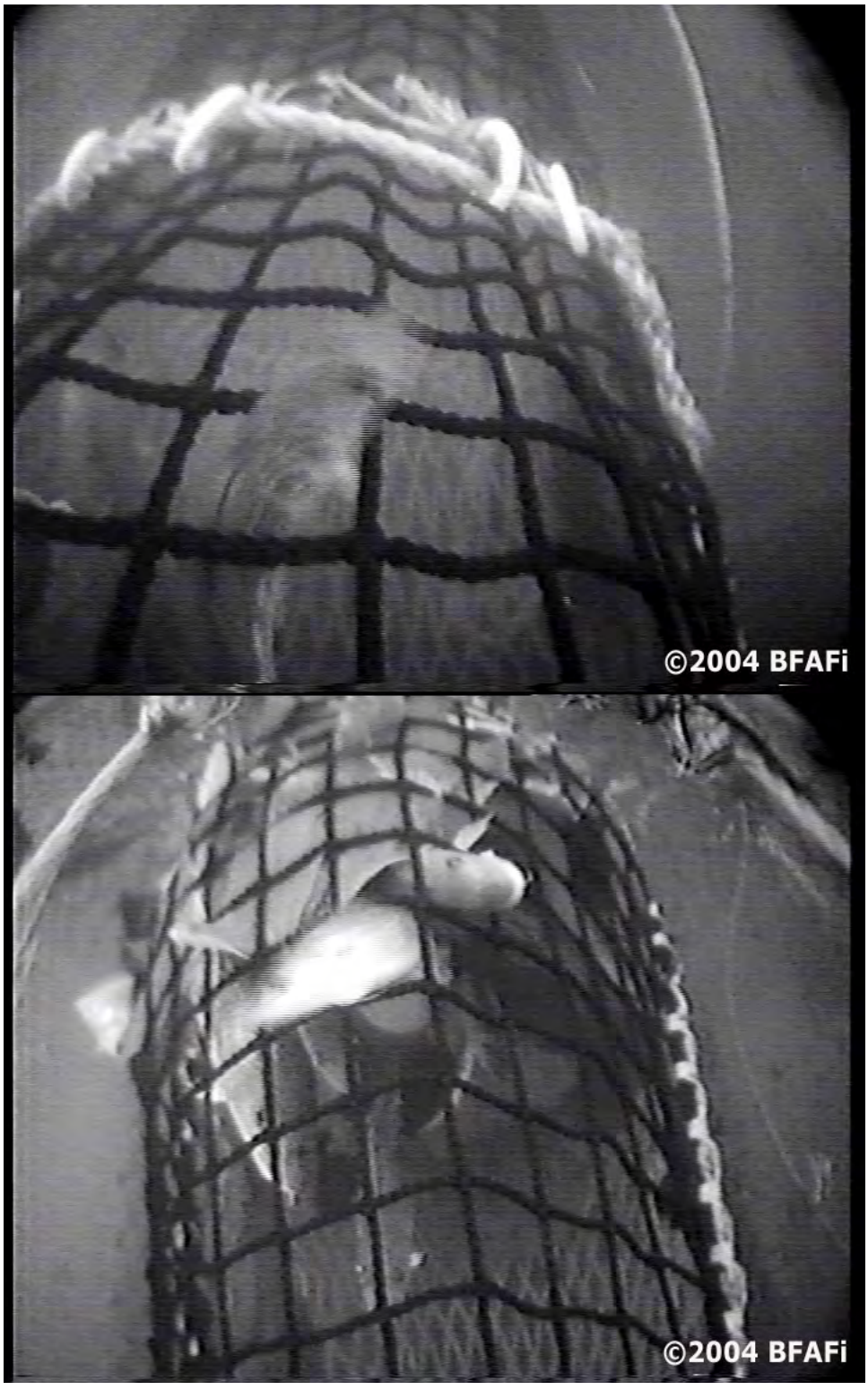
©2004 BFAFi
©2004 BFAFi

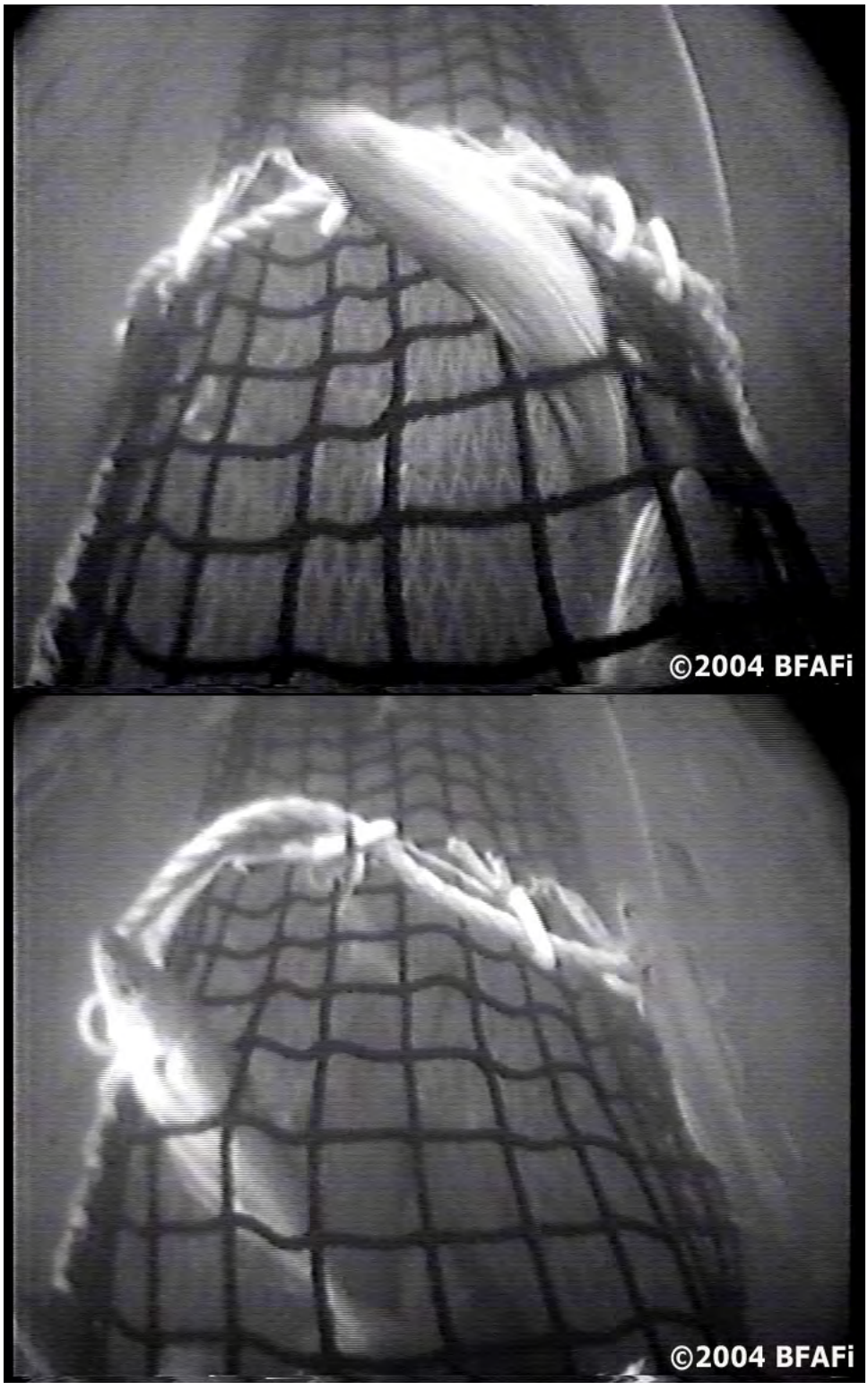
©2004 BFAFi
©2004 BFAFi

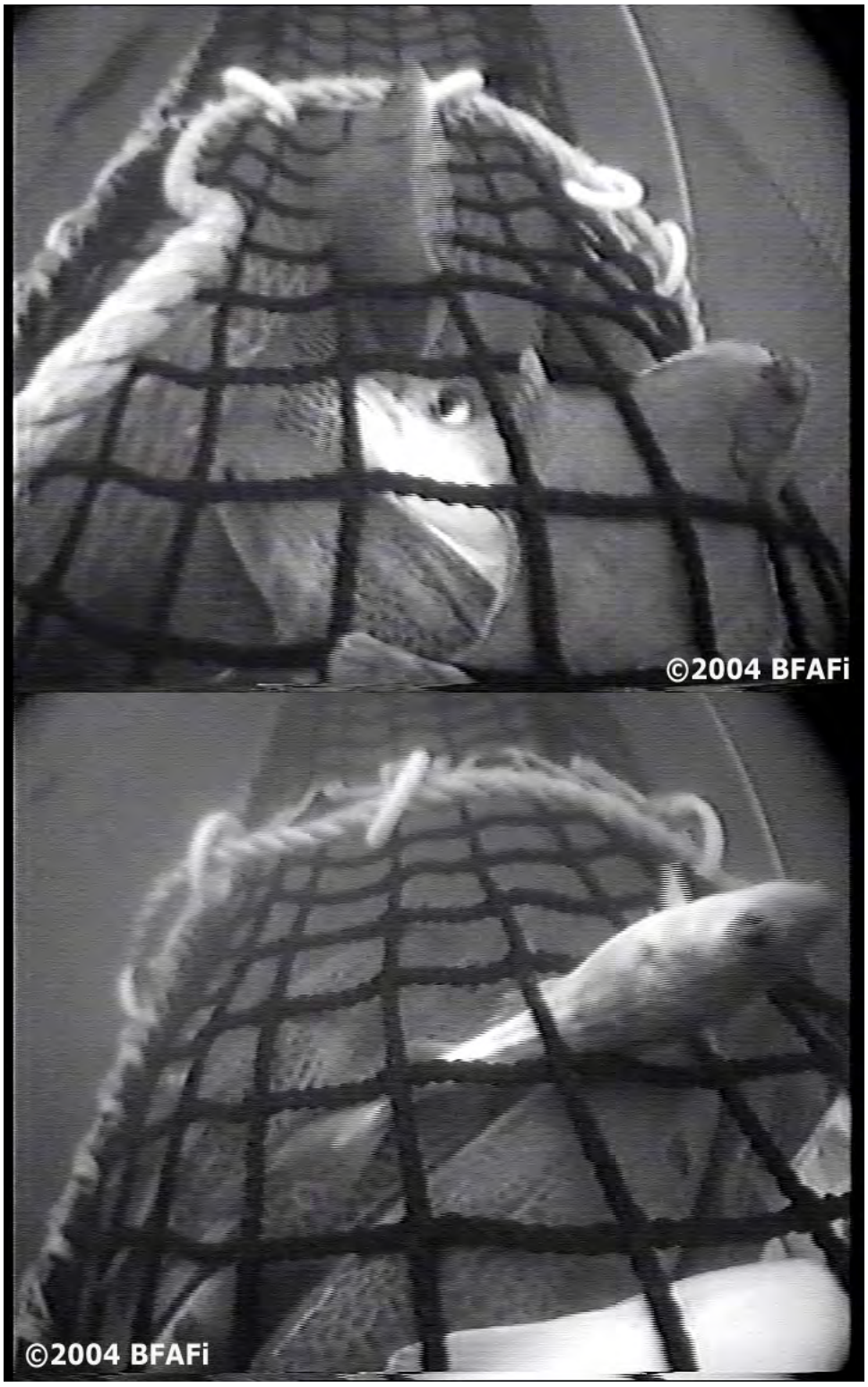
©2004 BFAFi
©2004 BFAFi

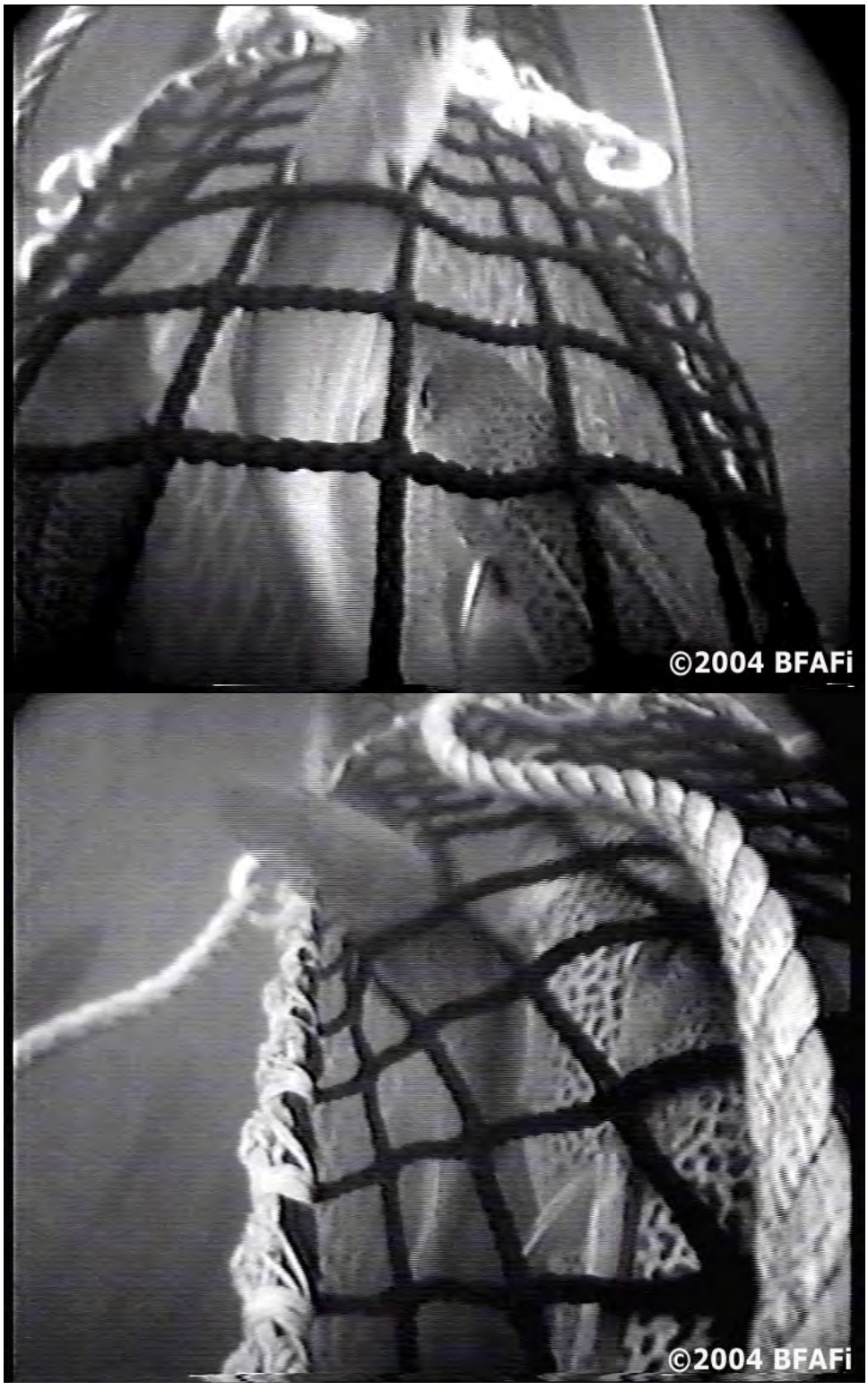
©2004 BFAFi
©2004 BFAFi

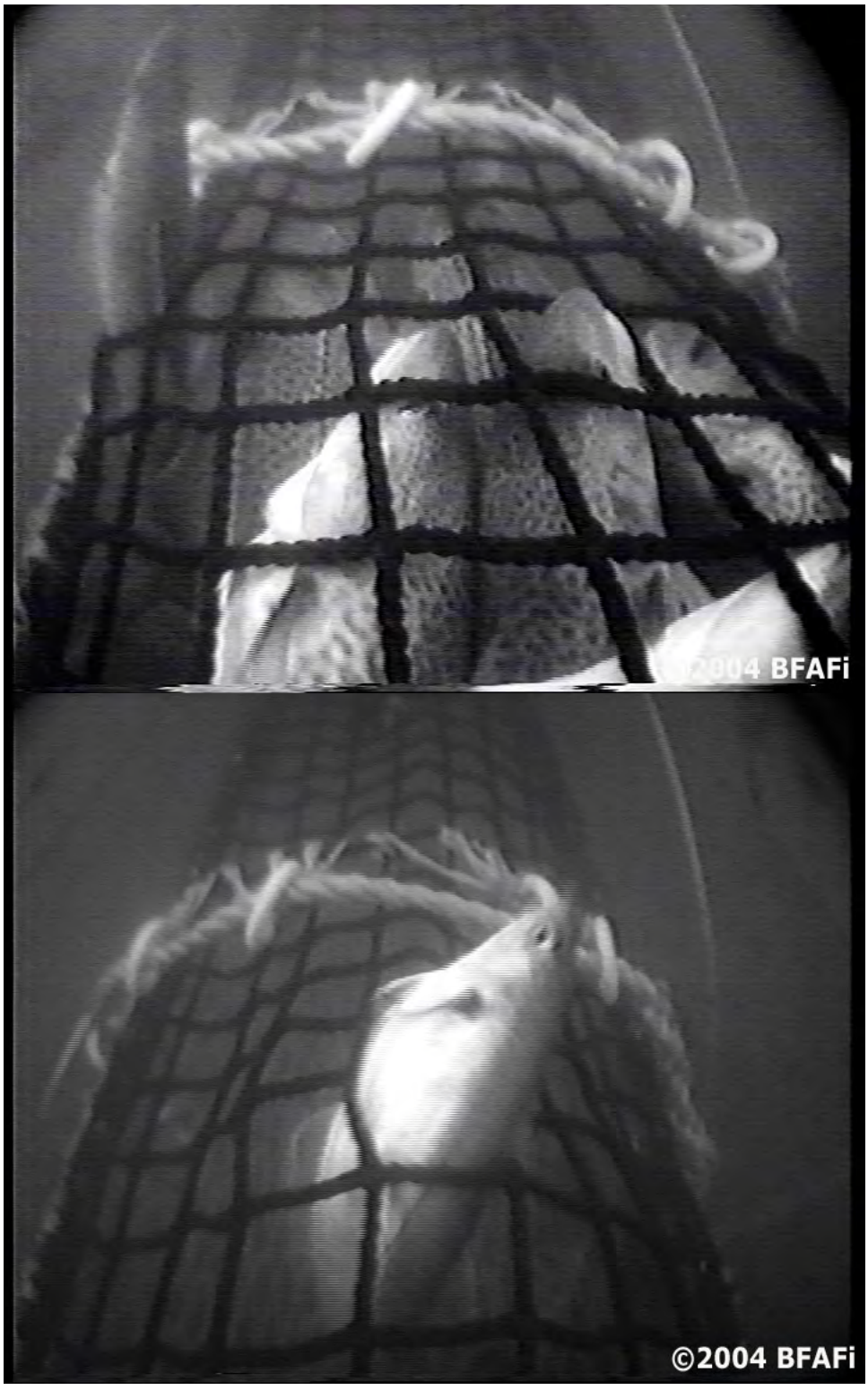
©2004 BFAFi

Appendix A12

FISKE MED SNURREVAD

MTE- 2001 FISKE MED SNURREVAD #1

Fangstprinsippet (fly-shooting)

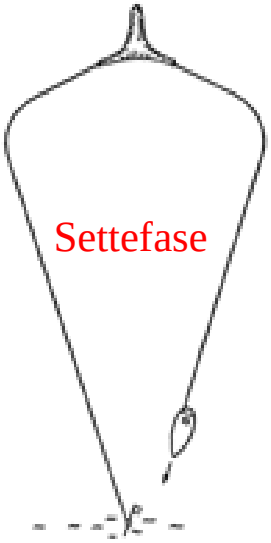

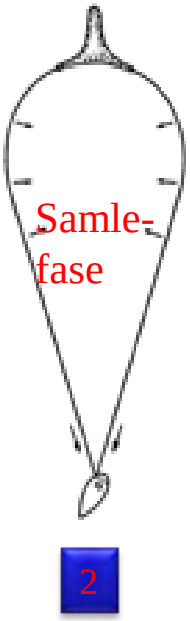

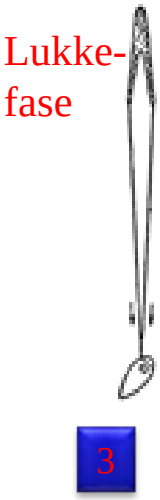

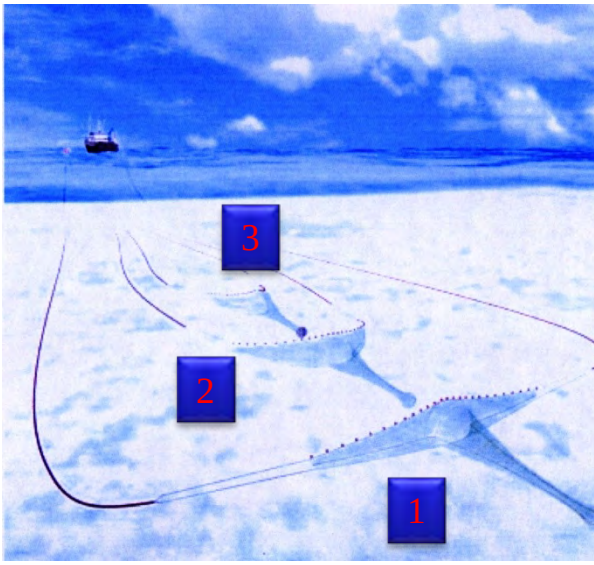

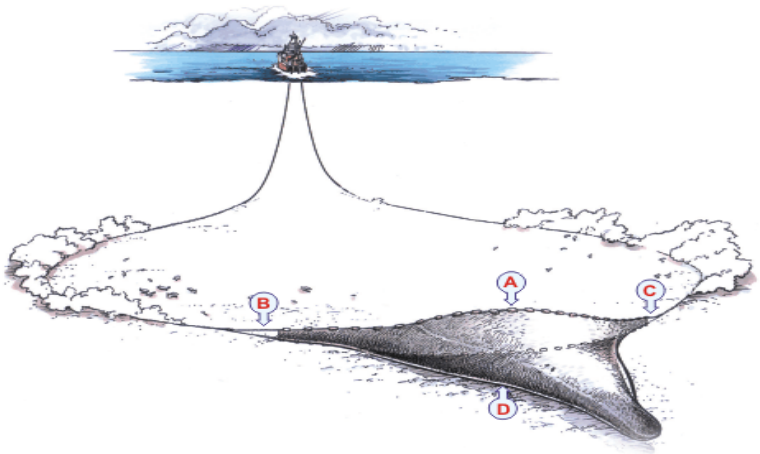

RB Larsen, NFH-UiTø

MTE- 2001 FISKE MED SNURREVAD #2

TAU/ARMER: Det brukes utelukkende kombinasjonstau av polypropylen (syntetfiber) med kjerner av stål i norsk fiske. Dimensjonene varierer fra 20-44 mm (diam.), med de tyngste tauene nærmest nota (vekt på opp mot 1.5 kg/m).

Ø 44 = 320 kg/kveil

Ø 42 = 280 kg/kveil

Ø 40 = 260 kg/kveil

Ø 36 = 225 kg/kveil

Ø 28 = 150 kg/kveil

* 1 kveil tau = 120 favner (220 m)

- På 40 - 50 fv. dyp brukes 4-5 kveiler tau,
- på 150-200 fv. brukes 8-10 kveiler.

Meydam combination rope - Breaking load

Diameter	kg / 220m	Load / kg	Max length
20mm	90	6900	
22mm	110	7800	2450
24mm	110	9000	1980
26mm	125	10000	1980
28mm	135	16800	1540
30mm	152	17500	1320
32mm	185	18000	1320
34mm	185	18500	1100
36mm	225	18800	880
40mm	260	20000	880
42mm	280	22000	880
44mm	320	24000	770
50mm	405	29000	770
60mm	480	35000	525

Snurrevadtau kan leveres i forskjellig vekt for alle dimensjoner.

MTE- 2001 FISKE MED SNURREVAD #3

NOTA: **Nota (i norsk fiske) er sammensatt av 4 like paneler og forlenget med relativt lange og høye vinger. Norske snurrevad har ikke tak (slik som trål har). Nota lages av PE, mens vinger kan være av PA. Sekken er (nesten alltid) av PA. Vi deler snurrevadnota inn i:**

- **Vingetamper (20-30 m) + børtre + tauarm**
- **Vinger**
- **Lask**
- **Belg**
- **Overgang (12-metring) og pose/fiskeløft**

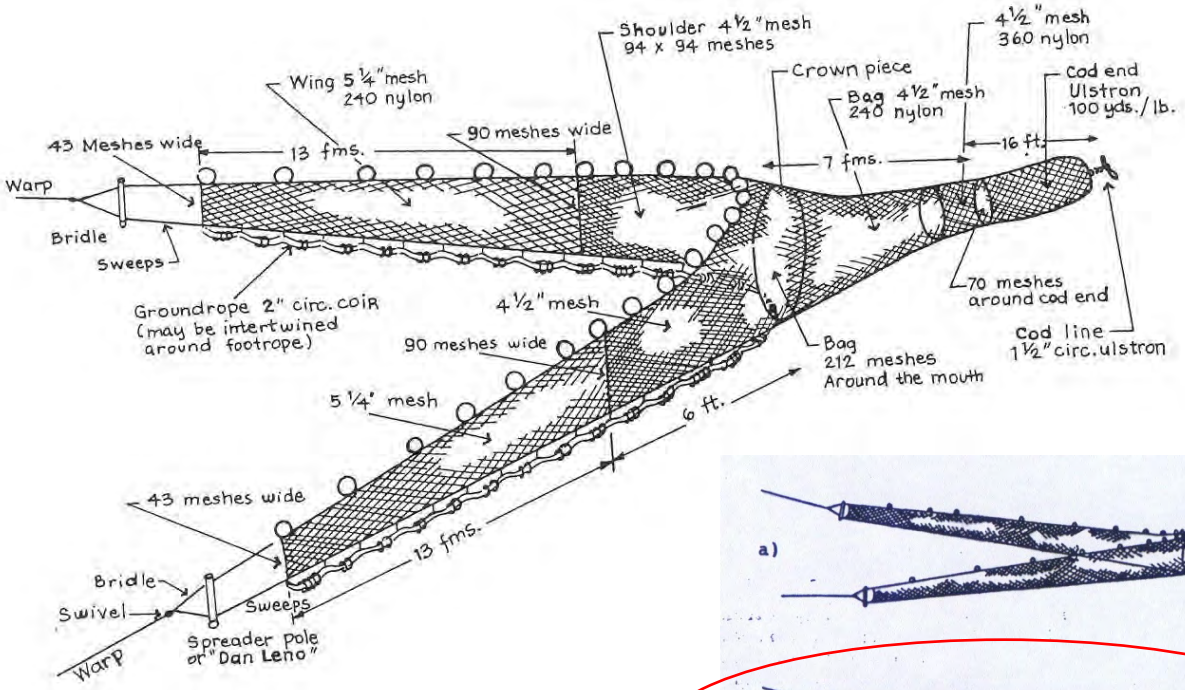

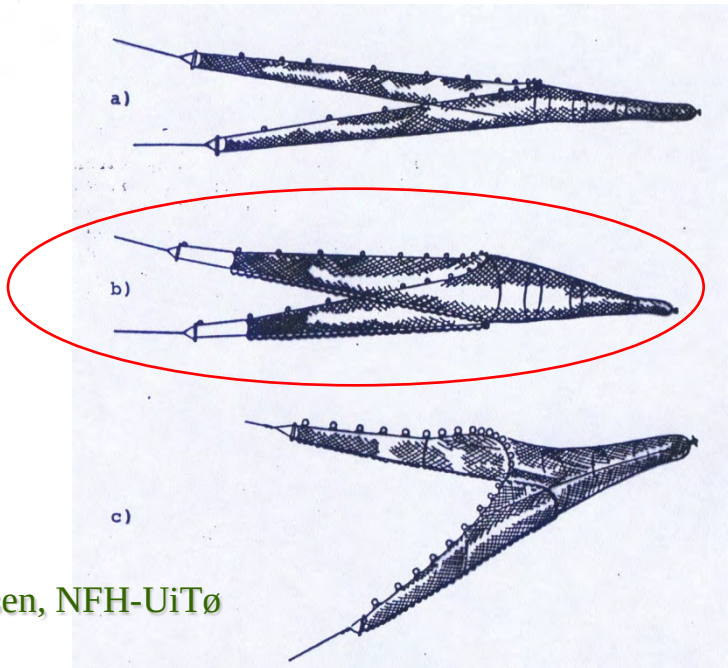

MTE- 2001 FISKE MED SNURREVAD #4

NOTSTØRRELSE: Det er mest vanlig å beskrive snurrevadets størrelse som antall masker (300 mm) i vingehøyde (ved overgang til lasken). Alternativt kan lengden på telnene brukes. Ved en antatt maskeåpning på θ= 0.4, vil følgende masketall (300 mm) gi vingehøyde på:

116# ≈14 m
180# ≈22 m
210# ≈25 m
240# ≈29 m
260# ≈31 m
280# ≈34 m

TELNER: Over- og undertelne (i norsk snurrevad) er like lange (i.e. intet tak). Standard lengde på telnene er 60-65 fv. (110-120 m).

*** Unntak: Lofotbestemmelser om maksimale størrelser:**

1) Telner: Ikke over 67 fv. (123 m)

2) Omkrets: 144 m strukket lengde (=480# x 300 mm)

*** Lokale reguleringer**

RB Larsen, NFH-UiTø

MTE- 2001 FISKE MED SNURREVAD #5

MASKESTØRRELSE: Panelene bygges av lett PE fiber Ø1.8-2.5.

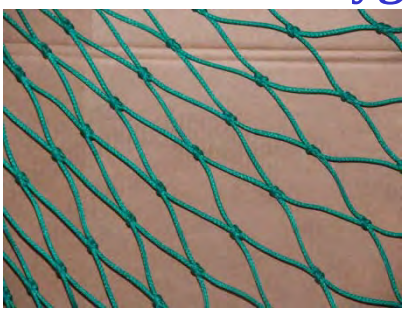

1) Vingene: 300 mm (600 mm, eller langsgående tau)
2) Lasken: 200 mm
3) Belgen/forlengelsen: 150 mm
4) Posen og fiskeløft:
   * Nord av 64°N: 130 mm (125 mm i kvadratmaske)
   * Sør av 64°N: 100 mm
   * I Skagerak: 90 mm

FLØYT/SYNK: Snurrevaden må ha en relativt stor netto underflotasjon;

* Små nøter ≈ 15-20 kg
* Større nøter ≈ 40-60++ kg

Moderne rigginger omfatter tyngre ”skjørt” for å sikre bunnkontakt og å unngå slitasje på nota.

MTE- 2001 FISKE MED SNURREVAD #6

Konstruksjonstegning av en standard 180# snurrevad-not. Gjengitt med tillatelse av NOFI og hentet fra kandidatoppgaven til J. Vollstad (2003).

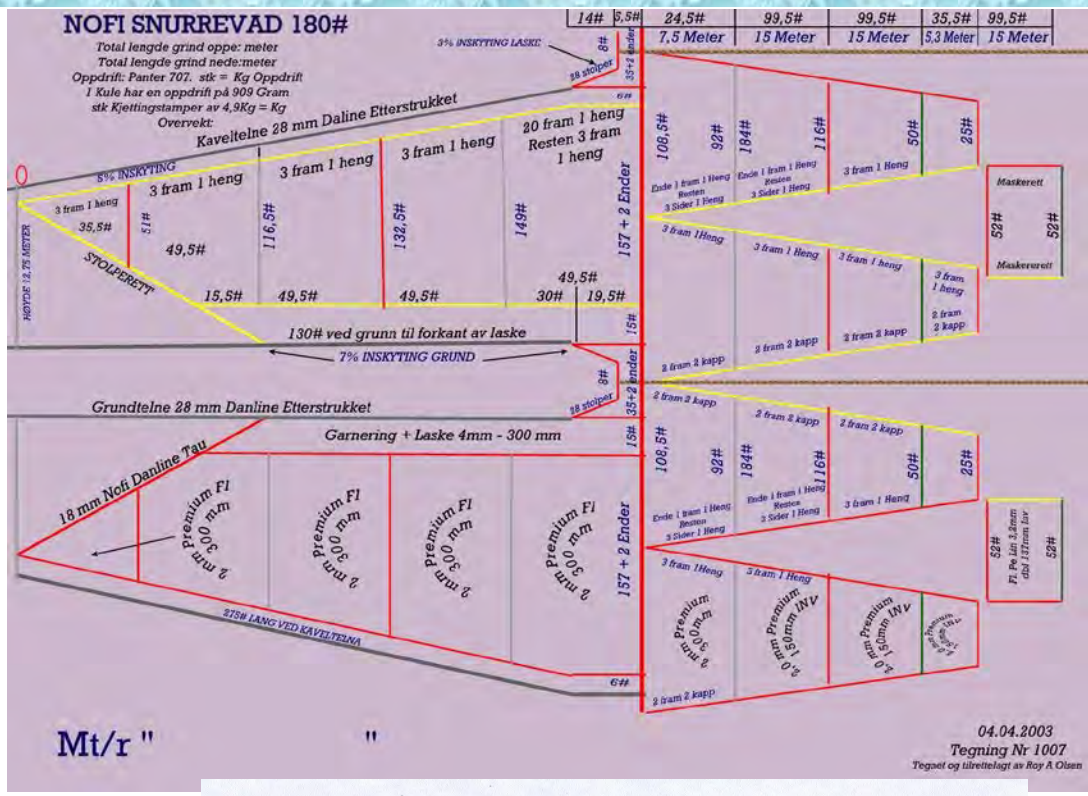

Konstruksjonstegning av en 116# Lofotnot (tegning fra 1980-tallet).

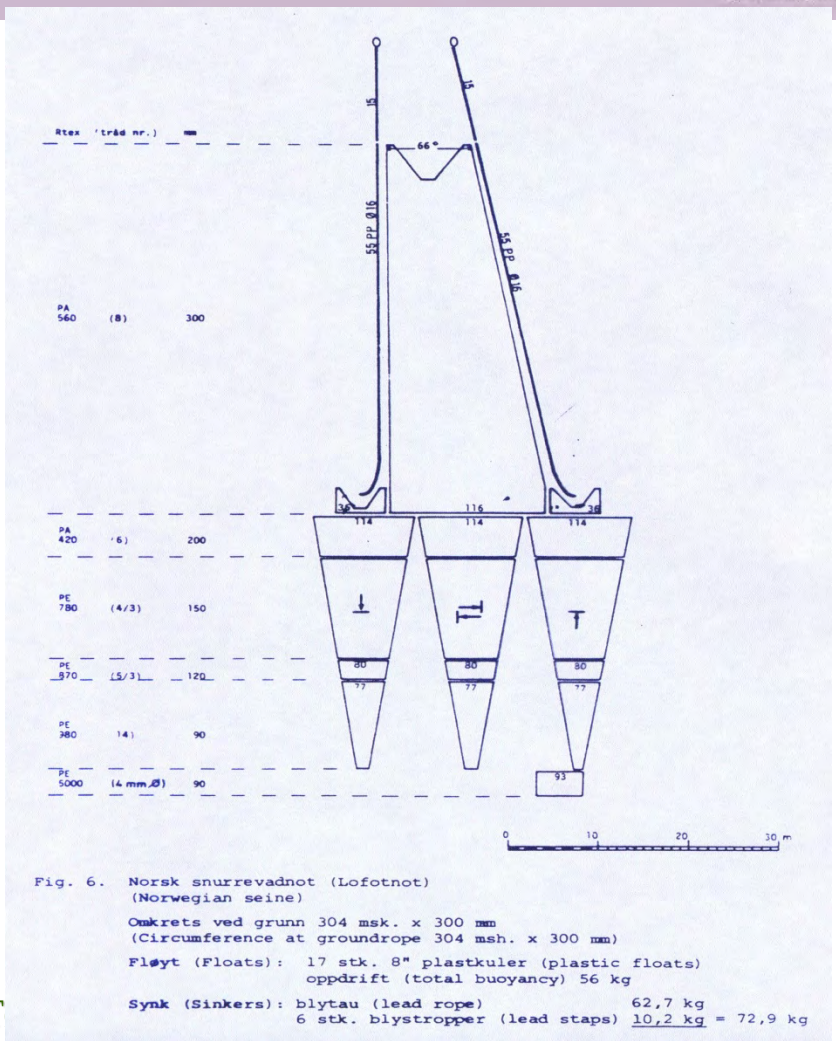

Fig. 6. Norsk snurrevadnot (Lofotnot)
(Norwegian seine)

Omkrets ved grunn 304 msk. x 300 mm
(Circumference at groundrope 304 msh. x 300 mm)

Fløyt (Floats): 17 stk. 8" plastkuler (plastic floats)
oppdrift (total buoyancy) 56 kg

Synk (Sinkers): blytau (lead rope) 62,7 kg
6 stk. blystropper (lead staps) 10,2 kg = 72,9 kg

MTE- 2001 FISKE MED SNURREVAD #7

plaice
smooth ground
Scotland

à plie
fond doux
Ecosse

para solla
fondo limpio
Escocia

REFERENCE
J. Gundry and Co. Ltd.
Bridport
United Kingdom

VESSEL	BATEAU	BARCO	
Loa	Lht	Et	17–21 m
GT	TJB	TB	20–60
hp	ch	cv	100–200

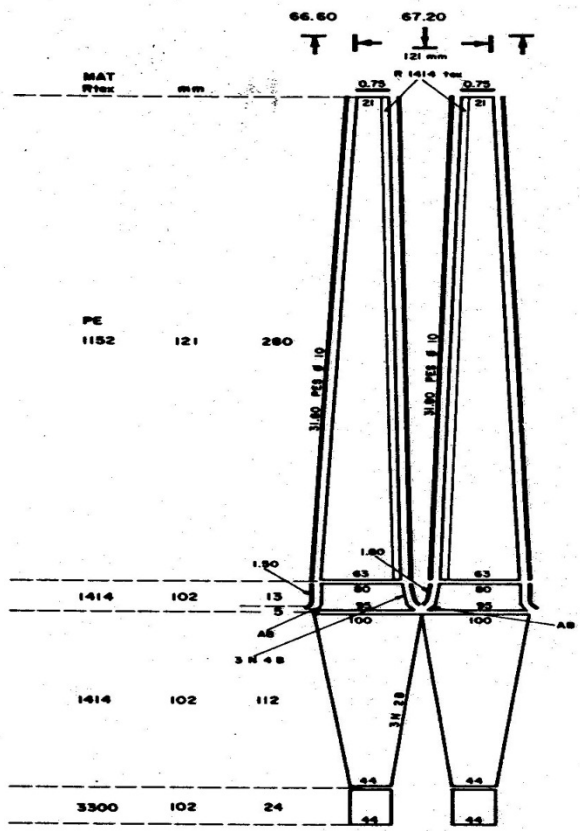

Den norske snurrevadnota har karakteristisk høge, relativt langer vinger.

Belgen bygges av lett materiale (PE) og er alltid sammensatt av 4 paneler (selv om konstruksjonstegninga viser bare 2 sider)

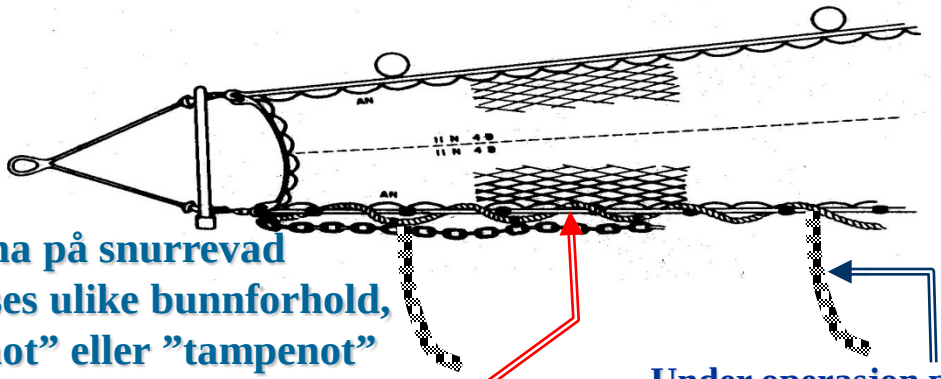

Grunntelna på snurrevad må tilpasses ulike bunnforhold, som ”klenot” eller ”tampenot”

Kle av kjetting eller naturfiber med blylodd brukes på fin sandbunn for å få fiskelinen helt ned til bunnen

Under operasjon på de fleste fiskefelt (for torskefisk) må fiskelinen løftes et stykke fra bunnen vha av tamper ca. 1 favn lang (kjetting eller blytau-tamp)

RB Larsen, NFH-UiTø

MTE- 2001 FISKE MED SNURREVAD #8

Eksempel på en norsk snurrevad (260#x300 vingehøyde) med alle detaljer for konstruksjon og montering kopiert fra RHS, Roy Olsen på Gibostad

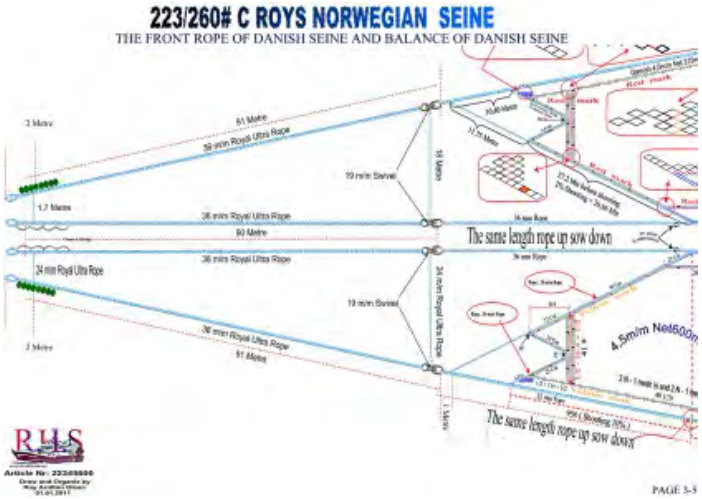

ROYS HAVBRUKSERVICE

Snurrevadens høyde på midten blir ca 30 meter med 1,7 knop.
Snurrevadens totale vekt er ca 1880 Kg.

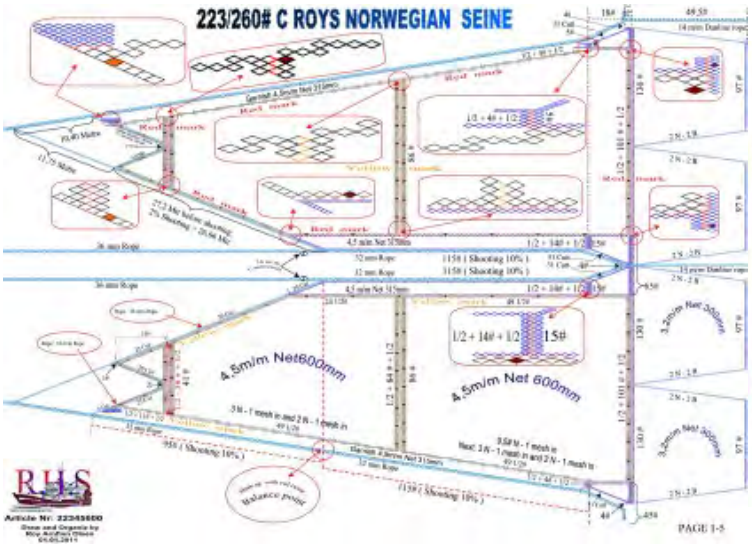

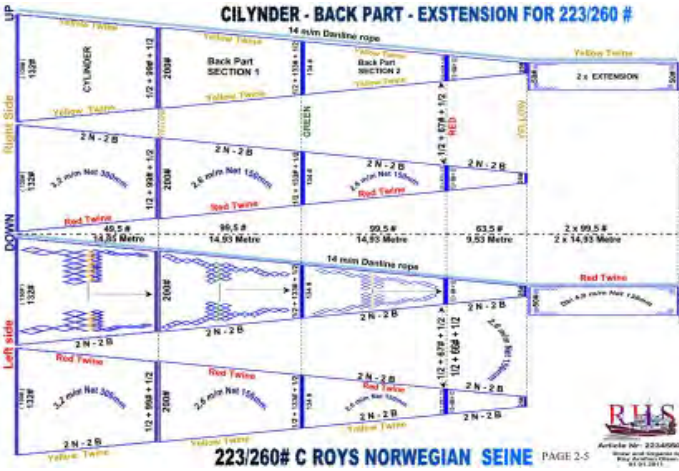

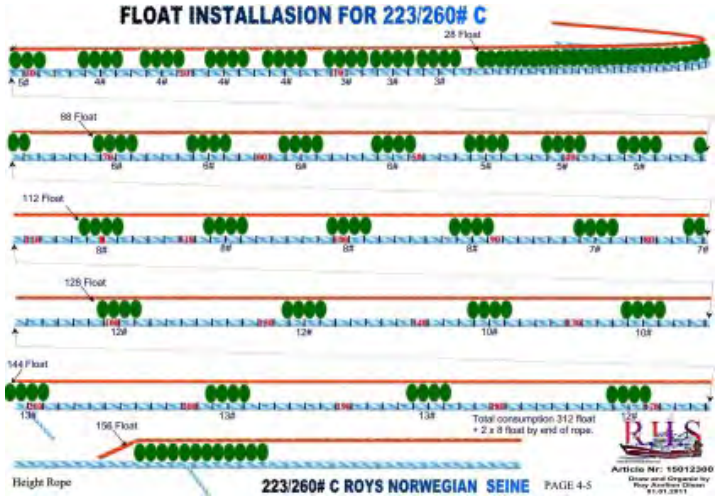

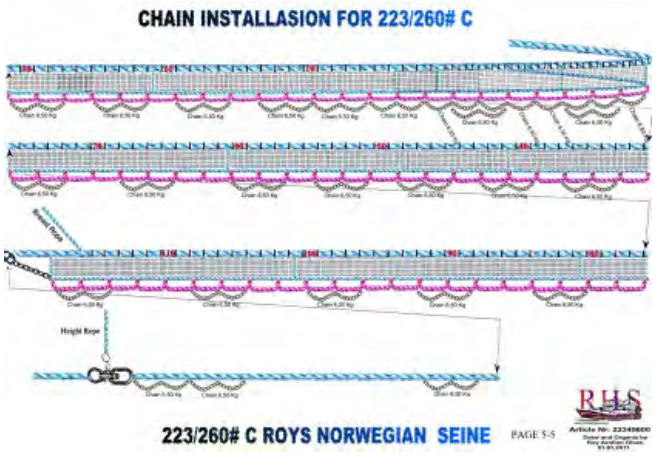

RB Larsen, NFH-UiTø

MTE- 2001 FISKE MED SNURREVAD #9

Arrangement (2004) på et vanlig kystfiskefartøy

RB Larsen, NFH-UiTø

MTE- 2001 FISKE MED SNURREVAD #10

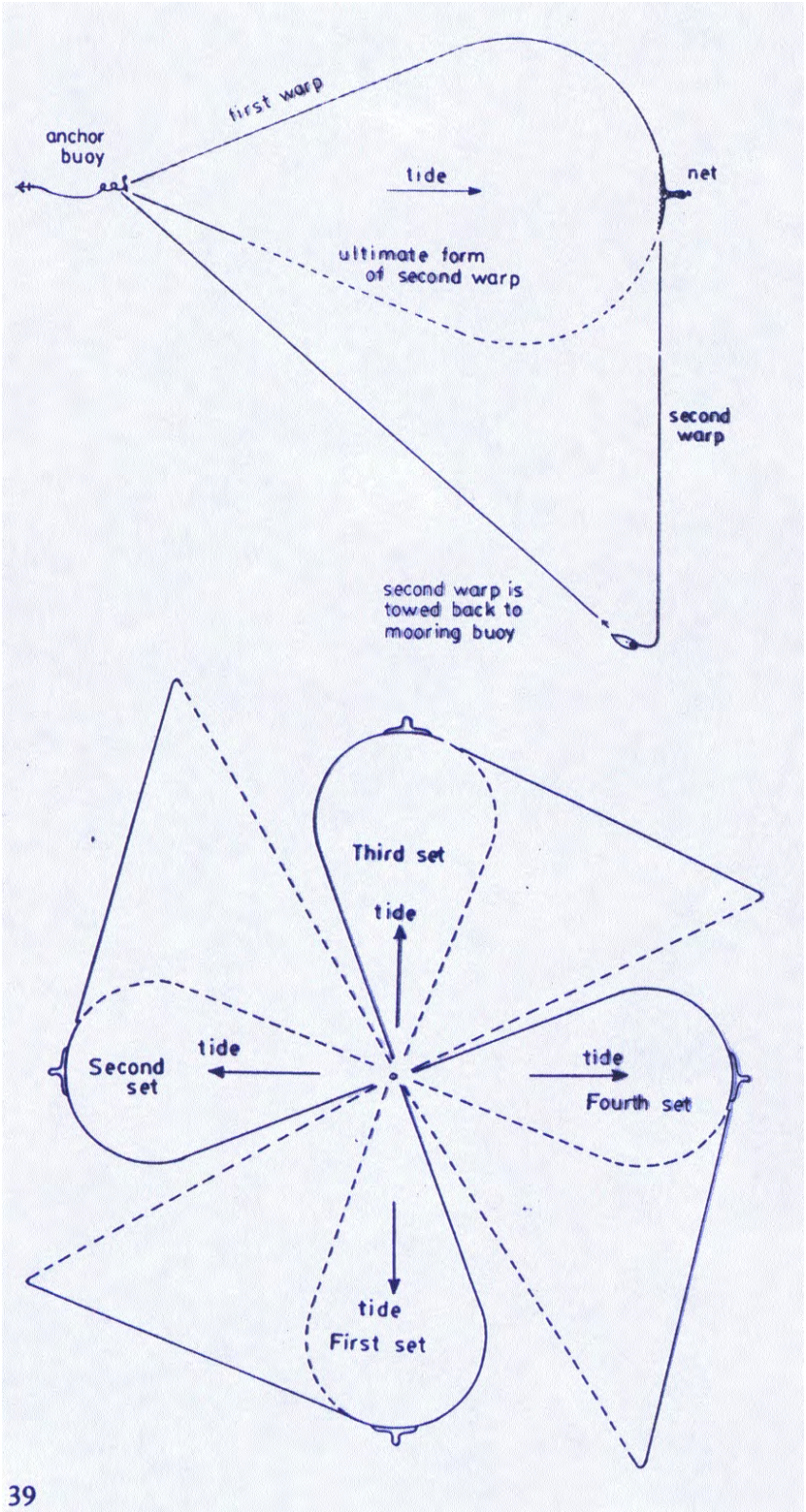

Den opprinnelige formen av snurrevad blir gjort ved at fartøyet ligger for anker under fangstoperasjonen. Bildet t.v. viser anker-seining og operasjon i løpet av døgnet med skiftende strømretning.

Den norske varianten av snurrevad opereres etter det skotske fly-shooting prinsippet: Første arm festes til en blåse og drivanker og armer og not samles ved å sige fartøyet framover samtidig som armene (og not) tromles inn.

I Skottland hales nota motstrøms, mens vi i Norge haler medstrøms. Med medstrøms haling kan vi bruke større redskap.

Eksempel på par-snurrevad

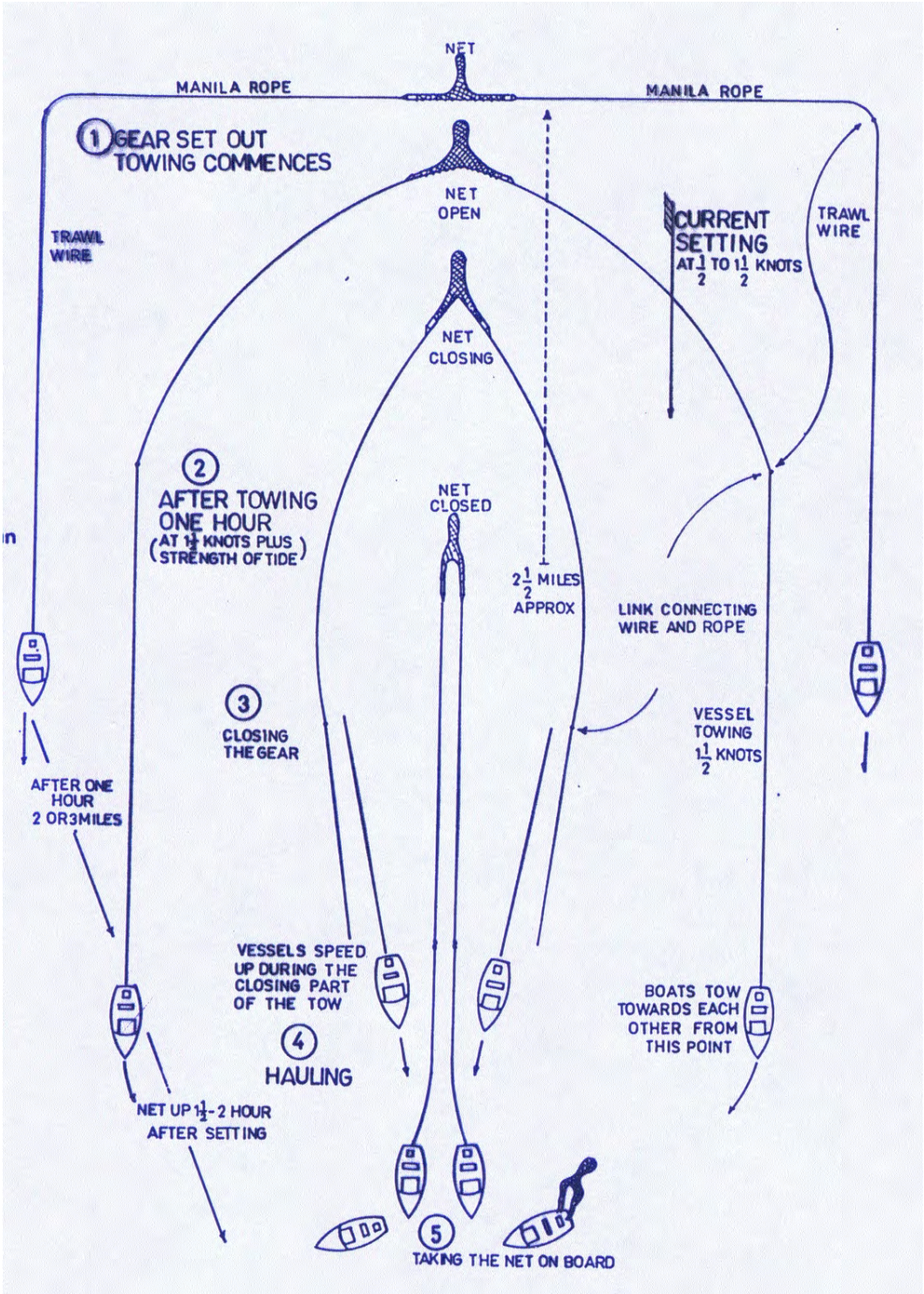

MTE- 2001 FISKE MED SNURREVAD #12

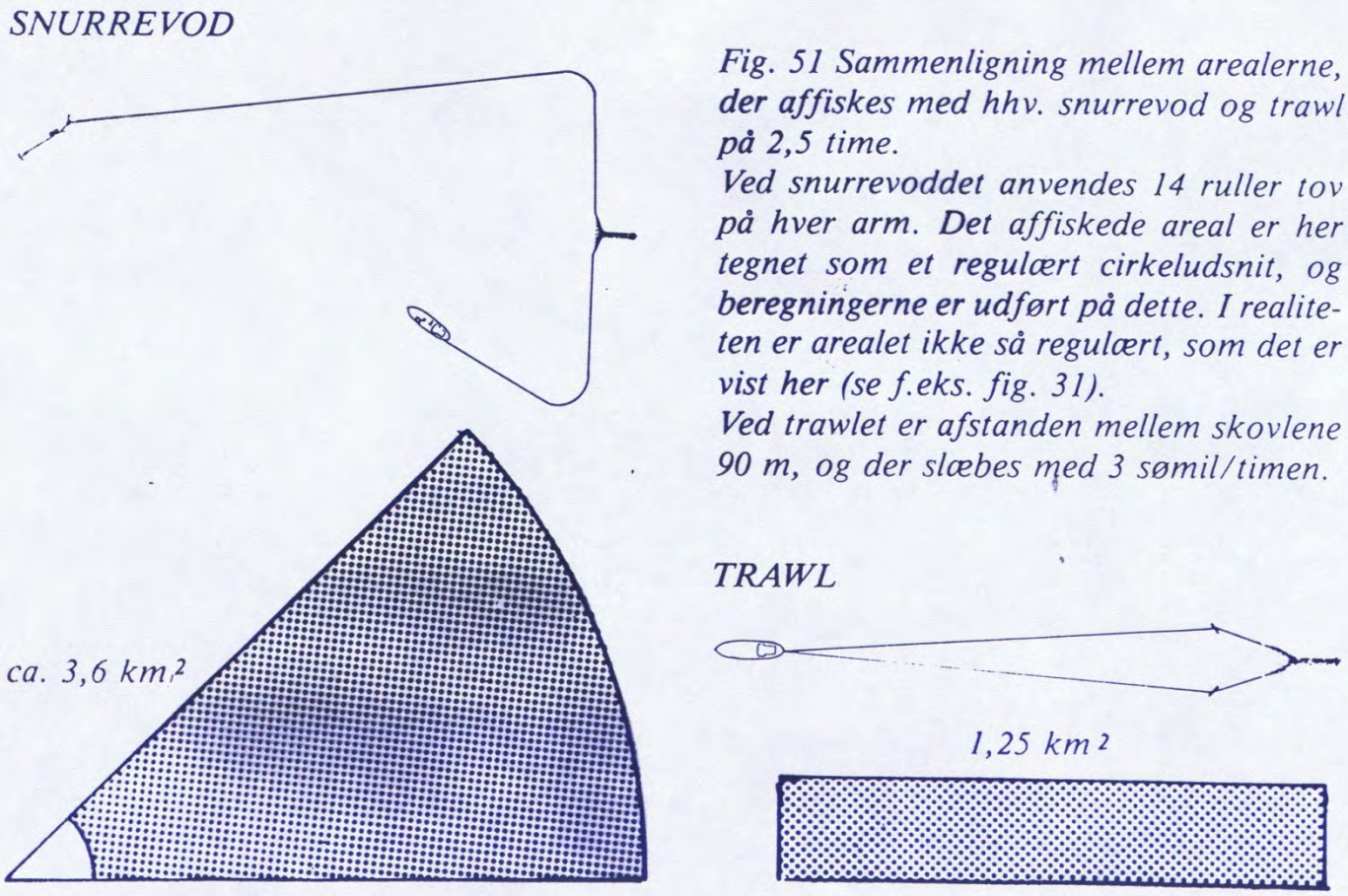

Fig. 51 Sammenligning mellem arealerne, der affiskes med hhv. snurrevod og trawl på 2,5 time.
Ved snurrevoddet anvendes 14 ruller tov på hver arm. Det affiskede areal er her tegnet som et regulært cirkeludsnit, og beregningerne er udført på dette. I realiteten er arealet ikke så regulært, som det er vist her (se f.eks. fig. 31).
Ved trawlet er afstanden mellem skovlene 90 m, og der slæbes med 3 sømil/timen.

Figuren over viser hvilket areal over bunn snurrevad og bunntrål ville dekke i løpet av 2,5 timer. Under forutsetning av fisk var uniformt fordelt og at sveipe-effekten (sveiper og tau) var 100%, så ville snurrevaden være nærmere 3 ganger så effektiv som bunntrålen.

Det er ingen tvil om at snurrevad under gitte betingelser er et meget effektivt fiskeredskap. Hos oss er det primært i fangst av torsk og hyse vi bruker snurrevad. Opprinnelig ble snurrevaden konstruert (i Danmark 1848) for fangst av rødspette. Det finnes eksempler på at snurrevad brukes til fangst av sei, sild og blåkveite (på store dyp)

RB Larsen, NFH-UiTø

MTE- 2001 FISKE MED SNURREVAD #13

Hvorfor fanger snurrevaden mer selektivt på art og størrelse av fisk enn fisketrål?

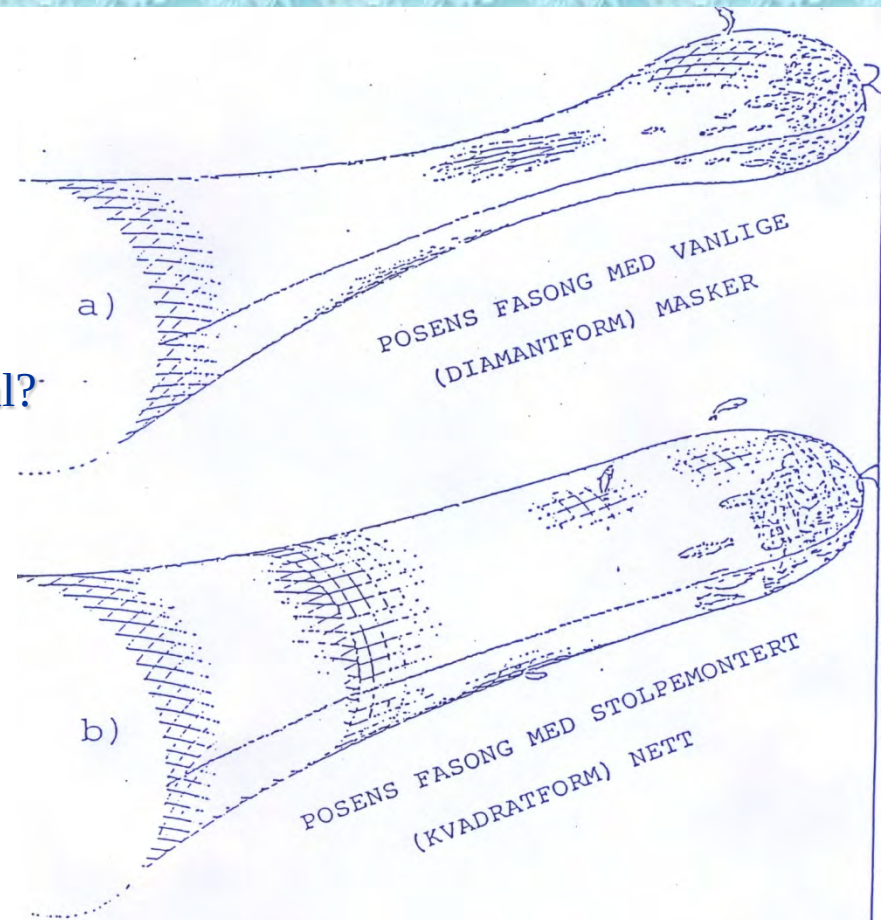

Denne snurrevad-posen er i deler av året påbudt i fisket i de nordlige områder

FISKERIDIREKTORATET
Strandgaten 229, Boks 185 Sentrum, 5804 BERGEN
Telex 42 151 * Telefax 55 23 80 90 * Tlf. 55 23 80 00

SNURREVADPOSE MED KVADRATISKE MASKER

TYPE I: Underpanel + Overpanel TYPE II: Underpanel + Overpanel + to sidepanel

OVER- OG UNDERPANEL identiske
Spesifikasjon gitt for ett panel

MATERIALE:	Polyethylene knutelin	Knuteløst, flettet materiale (PA, PE, PP, PES)	Polyethylene knutelin
TRÅD:	Maks 2x5 mm (alt. 3x3,2 mm)	Maks 7,5 mm diameter	Maks 2x5 mm
MASKEVIDDE:	Min 135 mm	Min 125 mm	Min 150 mm
LENGDE:	5-8 #	Min 12,5 meter	Maks 4 # mellom løftestropp og ## sylinder. Ellers fritt
BREDDE:	Maks 50 "frie" masker	Maks 50 "frie" masker	Maks 40 "frie" masker

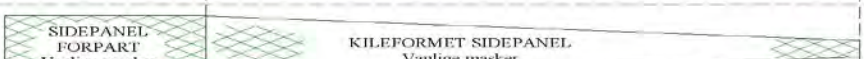

KILEFORMET SIDEPANEL
Spesifikasjon gitt for ett panel

MATERIALE:	Polyethylene knutelin	Samme som i seksjon med kvadratiske masker	
TRÅD:	Maks 2x5 mm (alt. 3x3,2 mm)	Maks 2x5 mm (alt. 3x3,2 mm)	
MASKEVIDDE:	Min 135 mm	Min 135 mm	
LENGDE:	Som forpart på over-/under-panel	Strekt lengde – lengde seksjon med kvadratiske masker	
BREDDE:	21 "frie" masker (25 tot)	Foran: 21 "frie" masker (25 tot)	Bak: 0-1 "frie masker (4 tot)

NORGES FISKERIHØGSKOLE
UNIVERSITETET I TROMSØ

MTE- 2001 FISKE MED SNURREVAD #14

FISKERIDIREKTORATET
Strandgaten 229, Pb. 185, Sentrum, 5804 Bergen
Faks 55 23 80 90* Tlf. 03495

Forskrift om utøvelse av fisket i sjøen

(utdrag om bestemmelser for snurrevad pr J-154-2013):

MELDING FRA FISKERIDIREKTØREN
J-154-2013
(J-148-2013 UTGÅR)

Bergen, 3.7.2013
TO/EW

Forskrift om endring av forskrift om utøvelse av fisket i sjøen

Fiskeri- og kystdepartementet har 2. juli 2013 med hjemmel i lov 6. juni 2008 nr. 37 om forvaltning av viltlevande marine ressursar §§ 16, 36 og 37 fastsatt følgende forskrift:

§ 3 Maskevidde i stormasket trål og snurrevad

Det er forbudt å bruke trål eller snurrevad dersom det i noen del av redskapet er mindre maskevidde enn fastsatt nedenfor.

1. Nord for 64°N.

a) 130 mm.

b) Ved bruk av snurrevad er det kun tillatt å benytte fiskepose med kvadratmasker med en minste maskevidde på 125 mm i et område nord og øst av en linje trukket gjennom følgende posisjoner:

§ 15 Begrensninger i bruk av stormasket trål og snurrevad

a) Snurrevad.

(1) Det er forbudt å bruke fiskepose i snurrevad som er laget av tvunnet eller flettet diamantmasket knuteløst nett.

(2) Ved fiske med snurrevad i området innenfor 4 nm fra grunnlinjene er det forbud å bruke snurrevad som har:

- En kuletelne eller grunntelne som er lengre enn 123 meter fra vingespiss til vingespiss.
- En total omkrets i åpningen større enn 156 meter målt på strukket maske.
- Mer enn 2000 meter taulengde (9 kveiler à 220 meter).

(3) Innenfor Lofoten oppsynsområde er det forbudt å bruke mer enn 1100 meter taulengde (5 kveiler à 220 meter) i den tiden oppsynet er satt.

POLAR SNURREVAD

Stor, moderne snurrevad under bygging på fabrikk

Setting av not

Triplex erstatter kraftblokk under haling

RB Larsen, NFH-UiTø

MTE- 2001 FISKE MED SNURREVAD #16

Moderne snurrevad med kraftige skjørt langs fiskeline

Hva med fangstbehandling og kvalitet på slike fangster?

RB Larsen, NFH-UiTø

Bilder fra SINTEF F&H 2010: ***Et utvalg av typiske snurrevadfartøyer***

M/S Karl Wilhelm

M/S Ranton

M/S Ole Elvan

M/S Kloegga

M/S Olagutt

M/S Myrebuen

M/S Gunnar K

M/S Heroyfisk (tidligere Stålegg)

MTE- 2001 FISKE MED SNURREVAD #18

Bilde 3-4 Bilder av fangstoperasjoner. A) Ombordtaking ved hjelp av sekking, ca 500 kg sløyd fisk pr sekk, B) ombordtaking i tørbinge i storm, C) inntak av snurrevadnota.

Bilder: SINTEF F&H 2010

Bilde 6-6 Kombinasjonsvinsjer – 12 tonn - for snurrevad, not og evt. trål (foto: SINTEF Fiskeri og havbruk)

Dimensjon og vekt på de to tautromlene vil begrense hvor stor taumengde som kan brukes: Jo tykkere tau, desto kortere lengde vil kunne spoles inn. (Maks. lengde på armene/tauene er nå 2000 m pr side).

Stadig flere snurrevadbåter monterer Triplex (kraftblokk) for sikrere innhaling av nota. Alternativet er ordinær to-skivet kraftblokk montert på bom på hekket

Bilde 6-10 Tørking av snurrevadsekk ved bruk av kraftblokk (notvinsj) (foto: SINTEF Fiskeri og havbruk)

RB Larsen, NFH-UiTø

MTE- 2001 FISKE MED SNURREVAD #19

Greiing av nota under inntak (må skille vingene og grunntelne med tamper fra overtelna)

Stor fangst og mange timers arbeid

RB Larsen, NFH-UiTø

MTE- 2001 FISKE MED SNURREVAD #20

15-20% av den norske torskekvoten tas med snurrevad – og andelen er økende på bekostning av line og garn. Begrensede fangster med snurrevad gir fisk av ypperste kvalitet dersom den blir fortløpende bløgget. Utfordringene oppstår når fangstene blir for store!

(Kilde: Akse et al 2004)

Ubløgget torsk fotografert 5 minutter (venstre) og 24 timer (høyre) etter opptak.

Bilde 3. Filetene til venstre kommer fra fisk som er bløgget <5 minutter etter opptak og utblødd 60 min. i rennende sjøvann. Filetene til høyre kommer fra ubløgget råstoff

RB Larsen, NFH-UiTø

MTE- 2001 FISKE MED SNURREVAD #21

Moderate fangster med snurrevad er velegnet til føring og lagring av levende fisk.

Fangstbegrensning vil være er en av de store utfordringer med hensyn til overlevelse og kvalitet.

Teknologien for skånsom om bord-Taking av fisk ble utviklet på tidlig 2000-tall. Bakre del av sekken er utstyrt med et vannfylt lerretsløft.

Når fisken er kommet om bord blir Den sortert. Levedyktig fisk lagres i lasterommet rommet. Det må være nok volum og god oksygentilførsel (utskifting av vann).

SINTEF F&H 2010: Automatisering i snurrevadflåten

Automatisk bløgging om bord vil høyne kvaliteten på hvitfisk fra snurrevadflåten og fjerne tunge arbeidsbelastninger for fiskerne. Hensikten med prosjektet var å kartlegge teknologiske utfordringer og muligheter i snurrevadfisket, og da knyttet til fangstbehandling og HMS.

- For lav kapasitet i bløgge/sløyetrinnet på fartøyene er vanlig. Automatiseringsgraden ombord bør derfor økes, både for å forbede fangstbehandlingen og av hensyn til fiskernes helse, miljø og sikkerhet. Viktigst blir det å utvikle nye automatiserte løsninger for bløgging (inkl. mottakstank, bedøving før bløgging og automatisk bløgging) og sortering av hvitfisk (anbefaler utvikling av veiesystem om bord for snurrevadfanget fisk).

  Fangstbegrensning/fangstkontroll ble pekt på som en hovedutfordring innen snurrevadfiske under en workshop med næringen i november 2009.

- Ombordtaking av snurrevadfanget fisk bør gjøres mer effektiv og skånsom (interessant også å vurdere helt andre løsninger for ombordtaking enn de tradisjonelle som benyttes i dag).

- Det er behov for mer optimal nedkjøling og kjølelagring av snurrevadfanget fisk. Temperaturen i fisken varierte fra 0,3 til 5,6oC ved landing. Kjøling av fangsten med sjøvann ga ikke tilfredsstillende temperaturer i fisken.

- Risikofaktorer som har betydning for sikkerheten til fiskerne bør reduseres. Hyppigere bruk av riktig verneutstyr anbefales. Hele en av tre snurrevadfiskere sier at de sjelden bruker påbudt personlig verneutstyr, selv om utstyret er tilgjengelig. Også bedre sklisikring anbefales på gangbaner og ståplasser hvor fangstbehandling foregår.

MTE- 2001 FISKE MED SNURREVAD #23

Seniorforsker Bjørnar Isaksen ved HI, Bergen, har gjennom de siste 20 år ledet forskning på snurrevad. HI har flere prosjekter mot bl.a. fangstbegrensning, med finansiering fra bl.a. FHF (Fiskeri og havbruksnæringens forskningsfond).

I de siste 20 årene er det stadig flere kystfiskefartøy som har lagt om redskapsbruken fra garn og line til snurrevad. I dag er det over 300 fartøy som tar hele eller deler av sin kvote med snurrevad (Odd Olsen Råfisklaget, 2009, personlig meddelelse). I kystflåten er det bare fartøy som fisker med garn som bringer på land mer fisk enn snurrevadflåten. Og stadig foregår det en konvertering fra line og garn til snurrevad.

Samtidig med økt effektivitet, hører en ofte om store snurrevadhal, og om dårlig kvalitet på fisk som bringes på land. Dette skyldes ikke de store halene i seg selv, for kvaliteten på fisken er helt på topp idet fangsten hales inn mot fartøyside. Det er fra dette stadiet og den påfølgende behandling av fangst som medfører en kvalitetsreduksjon. Snurrevadfartøy generelt har ikke mottaks- og produksjonskapasitet som står i forhold til den fangstkapasiteten som kombinasjon av fartøy og redskap til tider viser. Fangstene sekkes ofte direkte om bord, og bløgges eller aller helst direktesløyes med dårlig utblødning som resultat. Med mannskap på 6 til 7 personer, vil store fangster ofte ikke være ferdig bearbeidet, dvs bløgget og sløyd før etter seks til åtte timer. Dette gir uvilkårlig en redusert kvalitet på ilandbrakt fangst. Dette er spesielt iøynefallende i hysefisket.

Under fangst av levende fisk forsøker fartøyene å unngå fangster større en ca ti tonn. Store fangster fører til mange sekkinger, med flytting av fisk fram og tilbake i forlengelse og sekk flere titals ganger, og rygg- og bukfinner blir oppfliset (Isaksen & Midling 1995). Skinn utsettes for slitasje, og hinnen over øyene på fisken mattes ned. Store fangster medfører også dårlig kontroll med oppstigingshastigheten til snurrevadposen. Ofte kommer store fangster opp fortere enn middels store og små fangster. Dette medfører at en mindre del av fisken har klart å kvitte seg med svømmeblæregass fra bukhulen og fangsten består da av flere “flytere”, det vil si fisk med gass i bukhulen når den kommer til overflata. Denne fisken er svært dårlig egnet til innsetting i merd.

I takt med konvertering av garn- og linefartøy til snurrevad, er det stadig flere mindre fartøy som legger om til snurrevad. Dersom signalene fra Fiskeri- og kystdepartementet om et friere redskapsvalg følges opp og blir en realitet, er det ikke utenkelig at den mindre flåte under f.eks. 15 meter vil få anledning til to-båts snurrevad. Dette vil gi denne flåten det nødvendige løft med hensyn til fangsteffektivitet, men samtidig en risiko for enkel tilfeller av store hal. På små fartøy vil store hal, og spesielt med “synkesekker” under dårlig vær, kunne være en risikofaktor, og fangstmengden bør derfor kunne reguleres.

RB Larsen, NFH-UiTø

Appendix A13

A review on the application and selectivity of square mesh netting in trawls and seines

low survival rate on escaping fish, especially on the haddock, is measured when using the diamond mesh codends. Through comparisons between square mesh and diamond mesh codends, promising results with respect to the survival of escaping fish when using square mesh codends are obtained. The observation techniques used may be further and continously discussed, and improvements may be found in order to achieve more valid results. The importance of this issue is, however, indisputable.

If the official purpose is to reduce the bycatch of juvinile fish to assure the recruitment to stocks, the findings with respect to survival rates should certainly favour the introduction of square mesh codends. In this point of viev, the use of square mesh codends should be a good alternative to the proposed increasement of the mesh size of normal, diamond mesh netting. Several other factors, mentioned earlier, should also favour the use of the square mesh codends.

Further experiments when using the square mesh netting is needed, and one of the important questions to be answered is how increasing catchsizes affects the selectivity in these types of codends. With respect to the selectivity of juvinile shrimps, our results gave evidences for a reduced selectivity as the catch sizes grew. Will the selectivity drop at increasing catches when using square mesh codends in ordinary white fish trawls and Danish seines, and will it be possible to solve such problems?

Preliminary results given by the Institute of Fishery Technology Research, when testing a normal, diamond meshed codend, equipped with relatively short lacing ropes, shows comparable improvements of the selectivity (at lower catch rates) as obtained when using the square mesh codends. This improved selectivity is explained by more open meshes in the codend as the short lacing ropes causes a slacker netting all along the codend. If this finding is significant, this method should be considered as an altenative to the square mesh codend method.

Valid conclusions may be difficult to drav from these first years of testing the square mesh codends. At the present stage, however, one single, but important, advice could be given: In the further work on codend selectivity it should be stressed that constructional changes of the codends are needed if a significant improvement with respect to size selectivity shall be obtained.

Trivat kopi.

WORKSHOP ON THE APLLICATION AND SELECTIVITY OF SQUARE NETTING IN THE CODEND OF TRAWLS AT THE WORLD SYMPOSIUM ON FISHING GEAR AND FISHING VESSEL DESIGN

FRIDAY NOVEMBER 25. 1988

INSTITUTE OF FISHERIES AND MARINE TECHNOLOGY
ST. JOHN'S, NEWFOUNDLAND, CANADA

"A review on the application and selectivity of square mesh netting in trawls & seines".

by

Roger B. Larsen

The Norwegian College of Fishery Science
University of Tromso

P.O.Box 3083, Guleng, N-9001 Tromso

PREFACE

The square mesh netting in the codends of fishing gears like the travls, may be very useful with respect to increased selectivity of this type of gears, and for the saving of the juvinile fish of commercial important species.

Through several years of experiments with square mesh codends, a lot of information about improved selectivity have been obtained by research institutes on a global bases.

In spite of the convincing selectivity results found, more information on the practical field, and the application of these types of codends, is needed.

The initiative taken by the "square mesh codend" committee should be acknowledged, and this workshop will hopefully give ideas, new arguments and practical guidelines for the further development of some new, and really selective codend constructions.

Most of the work on square mesh codends in fish travls and in the Danish seine done in Norway, have been made by the Institute of Fishery Technology Research. This paper is, however, written as a review on square mesh codend selection experiments the Norvegian College of Fishery Science has been involved with, and will thus give information about a rather small part of all the experiments made in Norway during the period 1983 - 1988.

No references are given in the paper, but most of the results are already published by Karlsen & Larsen (1988)* and by Isaksen & Larsen (1988)**.

* Karlsen, L. & Larsen, R.B. 1988: Progress in the Selective Shrimp Travl Development in Norway. World Symposium on Fishing Gear and Fishing Vessel Design. St. John's, Newfoundland, Canada. November 21.-24. 1988.

** Isaksen, B. & Larsen, R.B. 1988: Codend Selectivity of the Danish seine investigated by the Trouser Travl Method. Coun. Meet. int. Coun. Explor. Sea. 1988. B: 28.

The experiments when using the square mesh codends have shown the need for a reduction of the mesh sizes (compared to diamond mesh size) in travls and seines, to achieve an acceptable selectivity, i.e. to avoid too high losses of the commercially utilizable fish (and shrimps).

It seems very difficult to explain, and to have an acception for, a reduction of the mesh size, when discussing the case with both biologists and administration staffs. This may delay (or even undermine) the introduction of square mesh codends to the practical fishing.

At the present stage, a few practical problems have to be solved before the introduction of the square mesh codends. The choice of material (PA, PES, PE or PP) may be important. So far we've made all our experiments using nylon (PA), which is strong and thus can allow a thinner twine than as for most of the other materials. Both knotted and knotless square mesh netting is tested (by other institutes), but the differences with respect to selectivity are yet not clear.

Testing have stated a reduction of the knot breaking strength of knotted square mesh netting compared to knotted diamond netting in the order of 15 - 25%. This reduction of the breaking strength will favour the use of knotless netting. On the other hand, no practical problems are discovered in using knotted square meshed netting, and besides knotted netting is preferable with respect to repairing of broken meshes. To compensate for the reduced knot breaking strength, we've used lengthwise lacing ropes and "round-straps" (instead of increased twine thickness) as a reinforcement of the square mesh codends.

As already mentioned, the fishermen have developed many sophisticated systems to reduce or prevent codend selectivity when using the normal, diamond mesh codends. If the use of square mesh codends is introduced by law, fishermen will have less possibilities for developing systems which reduces the codend selectivity, and it may be easier to control the legality of a square mesh codend than of a diamond mesh codend.

One of the most interesting findings, and also (one of) the most important findings, when using the square mesh codends, is the drastic difference with respect to survival of escaping fish when comparing square mesh netting to diamond mesh netting. Due to the preliminary reports from DAFS (Scotland) and PINRO (USSR), a very

DISCUSSION

Square mesh codends are shown to be superior compared to diamond mesh codends with respect to the size selectivity of fish. Using the square mesh netting in the codends, the selection factor will normally be increased, but more interesting is the decrease of the selection range, followed by a sharper selection curve.

If the retention length is adjusted to the legal minimum (catchable) size of the species through the choice of the mesh size in the square mesh codend, two important considerations are achieved at a sharper selection curve: Less juvinile fish will be retained in the catch, and more of the commercially utilizable fish (above the legal minimum size) is caught, thus pleasing both biologists and fishermen.

Several groups of biologists, fishermen and their organizations, and environmental organizations, are claiming an increase of the mesh sizes of fishing gears like the trawls, to prevent catch of the juvinile fish of important species. In the northern waters of Norway, this will implicate an increase of the mesh size for fish trawls (and Danish seines?) from today's 135 mm to 155 mm, using PA or PES materials in the codend.

Such increasements of the mesh sizes will most likely not affect the shapes of the selection curves, but move the curves more to the right side (of the fish-length scale). Using the normal, diamond mesh, codends and even a mesh size as high as 155 mm, still huge amounts of juvinile fish may be caught, especially at higher catch rates. Additionally fishermen will note, and react upon, the considerable loss of commercially valuable fish an increase of the mesh size will cause.

The effects upon selectivity caused by a diamond mesh codend, i.e. a wide selection range, will in case of a increased mesh size to 155 mm, cause many "law breakers", as fishermen will develop systems for reducing or avoiding selectivity on commercially utilizable fish. A paradox may be that such attempts of avoiding selectivity will be more often seen, and obviously more damaging, in times when strict (quota) regulations are needed, as a result of over-exploited stocks, than seen under conditions with plenty of fish (and less concerns about catch of juvinile fish).

INTRODUCTION

The bycatch problems:

For any type of active fishing gear, like trawls, the bycatch of juvinile fish has always been a considerable problem. By active fishing gears we primarily think of the gears like purse seines, trawls and (Scottish or Danish) seines. These groups of fishing gears are all characterized by their rather low selectivity. An exception, though, should be made for the purse seines, which are normally used on dense shoals of one species of fish, uniform in size. As the capacity and effeciency of the fishing fleet using active fishing gears has increased during the past decades, by-catches of juvinile fish may be one of several factors explaining the drastic decline of many commercially important species.

Since the early sixties it has been investigated and (well) understood why a fishing gear like the trawl and the seine necessarily will catch high numbers of small fish when fishing in an area with mixed size groups. In spite of the effects caused by different materials used, twine thickness and stiffness, catch size, towing time, etc., this is mainly due to the construction of the codend itself and the use of the normal, diamond shaped meshes.

A lot of effort has been put into the work to establish selection factors, retention lengths and selection ranges, when changing parametres as for example twine material, twine thickness, towing time, catch sizes and mesh sizes. The value of all these experiments and the huge amounts of data may be discussed.

Biologists and administration staffs seems to be very concerned about the selection factors and retention lengths obtained by the gears. In their aim for fitting the retention length (for a given species) to the legal, catchable size of the fish, they "forget" to discuss the more important selection ranges.

Calculation of a theoretical retention length of a given species of fish by using the selection factor and a given mesh size, is simple mathematics. It will, however, have very limited value as long as no information about the selection ranges is given, i.e. how big proportions of undersized fish will be taken, and how big proportions of oversized fish will be lost around the retention length ($L_{50\%}$) when fishing in an area with fish of mixed sizes.

During the past 20 years the mesh size for cod trawling in the northern parts of Norway (above 64°N), has been gradually increased from 120 mm, to 125 mm and to 135 mm, which is the legal mesh size today. For the last two years, again a discussion about the mesh size in cod trawling has arisen, and the idea is to increase the legal mesh size to 155 mm.

Codend selectivity

It is commonly known that almost all of the selection in a normal bottom trawl will take place in a very small area of the codend, i.e. over a few meshes in length and through the upper panel of the codend, where the meshes will be squeezed open just in front of the growing catch. In most of the codend, especially in the sentral parts of it, the meshes will elongate and become nearly closed as the catch grows and/or when the towing speed is increased, thus leaving almost no possibilty for small fish to escape.

Only by changing the construction of the codends, will it be possible to delvelop a really selective trawl codend. At the moment it seems to be two realistic ways of increasing selectivity in a trawl codend. The easiest, and also the cheapest way is to by law introduce lacing ropes along the normal, diamond mesh codend. The lacing ropes must be shorter (10-15%) than the netting, in order to achieve slacker netting and thus getting open meshes along the whole codend piece. The other, and more complicated, method is to by law introduce square mesh netting in the whole codend. This latter method is complicated by a number of factors, and among these are: Reduction of the mesh size in the codend, a reduced breaking strength of the twine and handling problems with this type of codend in cases with bigger catches.

Whenever a new construction of a codend is to be introduced, it should be kept in mind that the fishermen are among the worlds leading "gear technologists". A lot of sophisticated systems are developed by fishermen to reduce and avoid selectivity in the codends. Using the normal, diamond meshed, codends, several methods are known to effectivily reduce the codend selectivity, and among these methods are: Use of round straps, use of a shorter overpanel than lover panel in the codend, seving up the meshes of the overpanel with a thin twine (which will break either in the sea at a big catch in the codend or as the catch is hauled on board), etc.

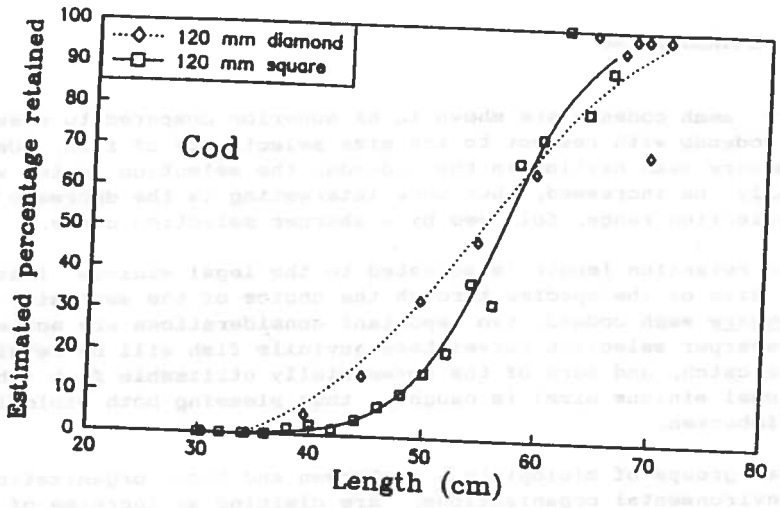

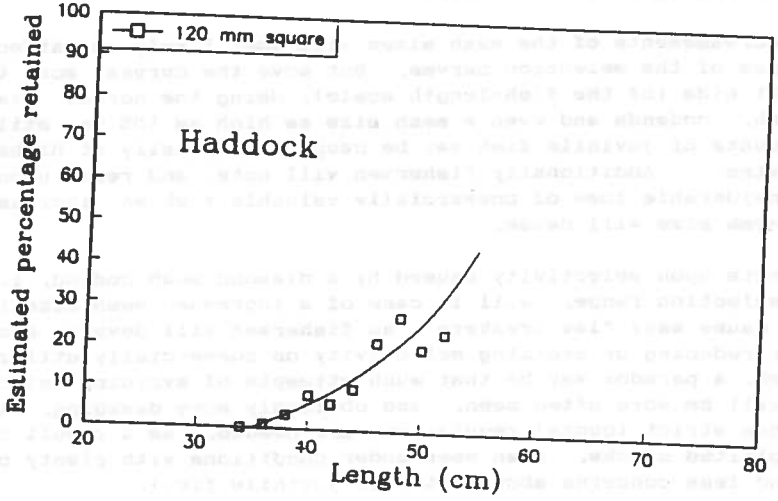

Figure 10: Selection curves for cod (Gadus morhua) and haddock (Melanogrammus aeglefinus) comparing the 120 mm square mesh codend to the 120 mm diamond mesh codend. Results from the Danish seine experiments May 1986.

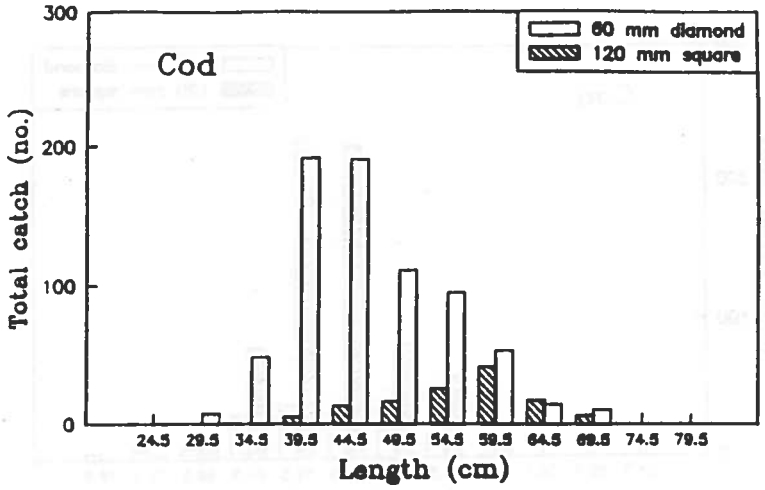

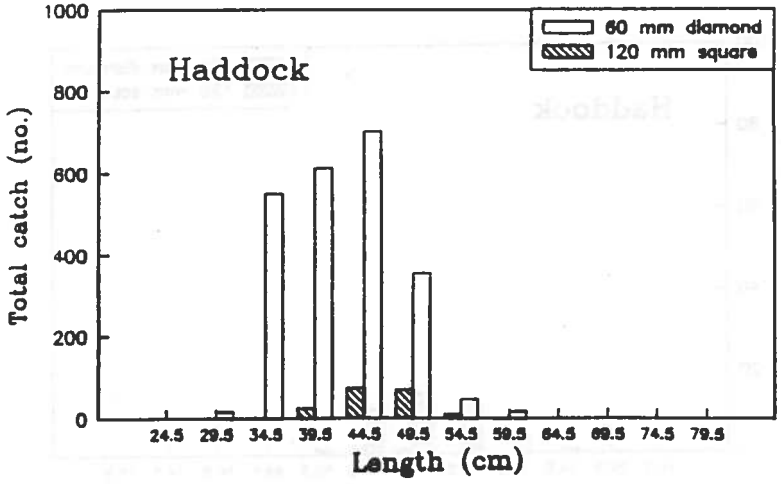

Figure 9: Catch distribution (no.) for cod (Gadus morhua) and haddock (Melanogrammus aeglefinus) found by the "twin codend method", using a 120 mm square mesh and a 60 mm diamond mesh codend. Results from the Danish seine experiments May 1986.

Experimental works:

Since 1983 the Norvegian College of Fishery Science has been involved in the selectivity experiments using square mesh codends. Almost all of these experiments are carried as cooperations with other institutes in Norway. Most of the selectivity experiments with Danish seines have been made together with the Institute of Fishery Technology Research (Bergen). The experiments using the square mesh netting in shrimp trawl codends have been carried out in cooperation with the Institute of Marine System Design (Trondheim). Experiments when using square mesh codends in cod trawls have so far been tested only once (March 1988) by us, while the Institute of Fishery Technology Research has for several years made experiments with these types of codends.

The ambitious aim of these trials has been to reduce the catch of juvinile fish of commercial important species, primarily on cod (Gadus morhua) and haddock (Melanogrammus aeglefinus). Additionaly it is most desirable to achieve a sharper selection, i.e. a narrower selection range, when using the square meshed codends.

In 1983 the mesh size for the Danish seine was increased from 110 to 135 mm (using PA or PES, and to 145 mm using PE or PP). The fishermen reported for several years about decreasing catches and very high losses of commercially utilizable fish when using the 135 mm codends, and have argued for a meshsize reduction. In 1988 the mesh size for the Danish seine was reduced to 125 mm (PA/PES). Contrary to the advices given, as a result of the fishing trials made, the square mesh codend constructions were not taken into practical use (in Norway).

With respect to the shrimp trawls, our aims have been to develop a system which reduces the bycatch of undersized deep sea shrimps (Pandalus borealis), less than 6 cm total length, and which will release (remove) small and particularly slim bodied species. The square mesh codend experiments are often combined to experiments when using the sorting panel, which will effectivily remove and release fish (bigger than 20-25 cm) from the catch during shrimp trawling. As shown in Table 1, more than 40 species of fish are regularly taken as bycatch by shrimp trawls in norvegian waters.

Normally, all the fish are dead or dying when taken on board the vessel, and the juvinile fish will together with the "worthless" species, be discharged after sorting the catches - no matter the laws given.

Table 1: Common species of fish caught as bycatches during shrimp trawling on commercially exploited fishing grounds along the coast of Northern Norway and in the Spitzbergen area.

SPECIES NORMALLY FOUND IN THE SHRIMP CATCHES	MOST COMMON SIZE RANGE	REGARDED AS VALUABLE AND SALEABLE FISH BY SHRIMPERS	SORTING EFFECT WHEN USING THE HH-SORTING PANEL
Cod (Gadus morhua)	15-70 cm	yes, above 42 cm	high
Haddock (Melanogrammus aeglefinus)	15-50 cm	yes, above 39 cm	high
Saithe (Pollachius virens)	25-50 cm	yes, above 35 cm	very high
Plaice (Pleuronectes platessa)	25-55 cm	yes, above 29 cm	very high
Tusk (Brosme brosme)	40-60 cm	yes	very high
Greenland halibut (Reinhardtius hippoglossoides)	20-60 cm	yes	high
Spotted catfish (Anarhichas minor)	30-60 cm	yes	very high
Red-fish (Sebastes sp.)	6-45 cm	no	low
Long rough dab (Hippoglossoides platessoides)	12-45 cm	no	partly high
Witch (Glyptocephalus cynoglossus)	20-45 cm	no	high
Common dab (Limanda limanda)	15-35 cm	no	partly high
Flounder (Platichthys flesus)	20-35 cm	no	partly high
Thornback ray (Raja clavata)	10-55 cm	no	high
Blue whiting (Micromesistius poutassou)	20-30 cm	no	partly low
Norway pout (Boreogadus esmarkii)	12-30 cm	no	low
Polar cod (Boreogadus saida)	15-25 cm	no	low
Lumpfish (Cyclopterus lumpus)	30-45 cm	no	very high
Herring (Clupea harengus)	15-30 cm	no	low
Capelin (Mallotus villosus)	10-16 cm	no	very low
Snake blenny (Lumpenus lampretaeformis)	10-25 cm	no	very low

More than 20 other species of fish are regularly found as bycatch in the shrimp trawl.

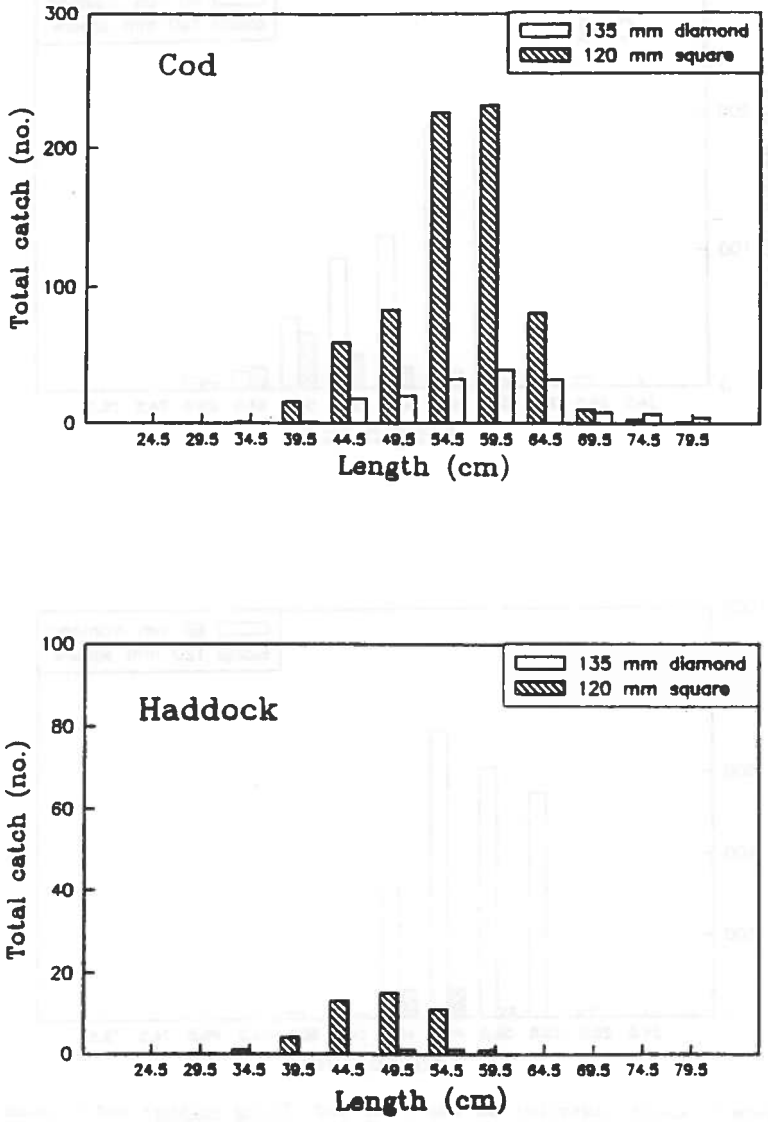

Figure 8: Catch distribution (no.) for cod (Gadus morhua) and haddock (Melanogrammus aeglefinus) found by the "twin codend method", using a 120 mm square mesh and a 135 mm diamond mesh codend. Results from the Danish seine experiments May 1986.

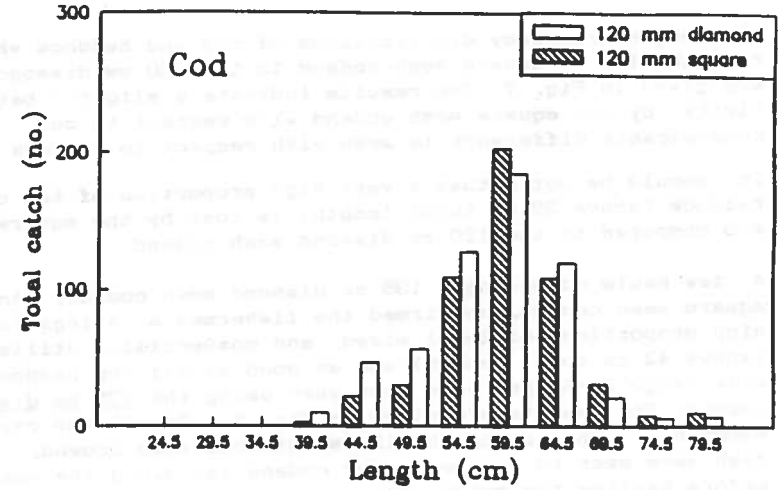

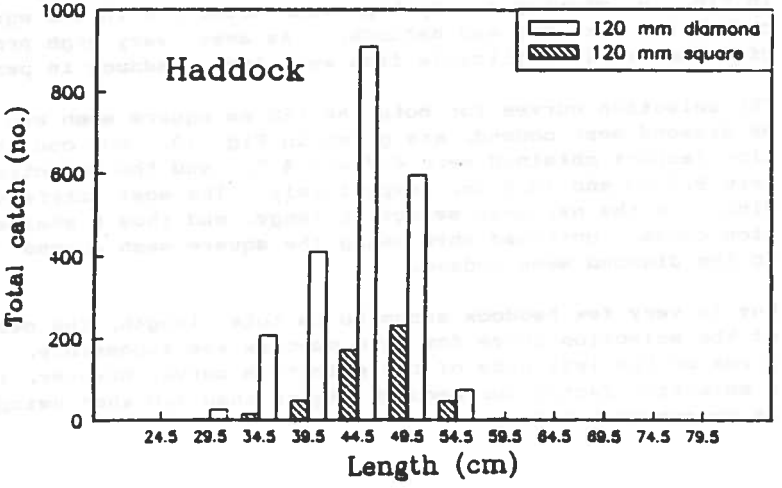

Figure 7: Catch distribution (no.) for cod (Gadus morhua) and haddock (Melanogrammus aeglefinus) found by the "twin codend method", using a 120 mm square mesh and a 120 mm diamond mesh codend. Results from the Danish seine experiments May 1986.

MATERIALS AND METHODS

Cod trawl:

The experiments were carried out during March 1988 on board the 33 m R/V "Johan Ruud" (University of Tromsoe) on a commercially exploited fishing ground off the coast of Finnmark, Northern Norway. The fishing trials were made with a small (360 meshes) cod trawl, on depths of 250 - 350 m, and the towing times were varied from 1 to 3 hours.

Throughout the test period a 120 mm square mesh codend was used, and the catches with this codend were compared to catches with a 125 mm diamond meshed codend. As an attempt to solve the handling problems when using the (overall) square mesh netting, the codend was fitted with a 5 m piece of 125 mm diamond mesh netting in the rear part of it. A small meshed (70 mm) funnel was placed in the middle of the 9 m long square mesh section of the codend. The intended function of the funnel was to delay fish in entering the diamond mesh part of the codend. The square mesh section of the codend was reinforced with two 24 mm PP lacing ropes. The construction, and a principal sketch, of the square mesh codend is given in Fig. 1.

Shrimp trawl:

Since 1984 several experiments when using different constructions of the square mesh codends have been made in the Spitzbergen area. All the experiments have been carried out on board the R/V "Johan Ruud" (University of Tromsoe), using a 1300 mesh shrimp trawl, on commercially exploited shrimp grounds. The fishing depths were in the order of 300-400 m, and the towing times were 1 - 4 hours.

Most of the fishing trials have been made when using a 16 m long square mesh codend, made from 35 mm knotted PA netting. Comparisons of the results were made as "alternate hauls", using a 16 m long diamond mesh (35 mm knotted PA netting) codend. Fig. 2 gives the construction of the two codends.

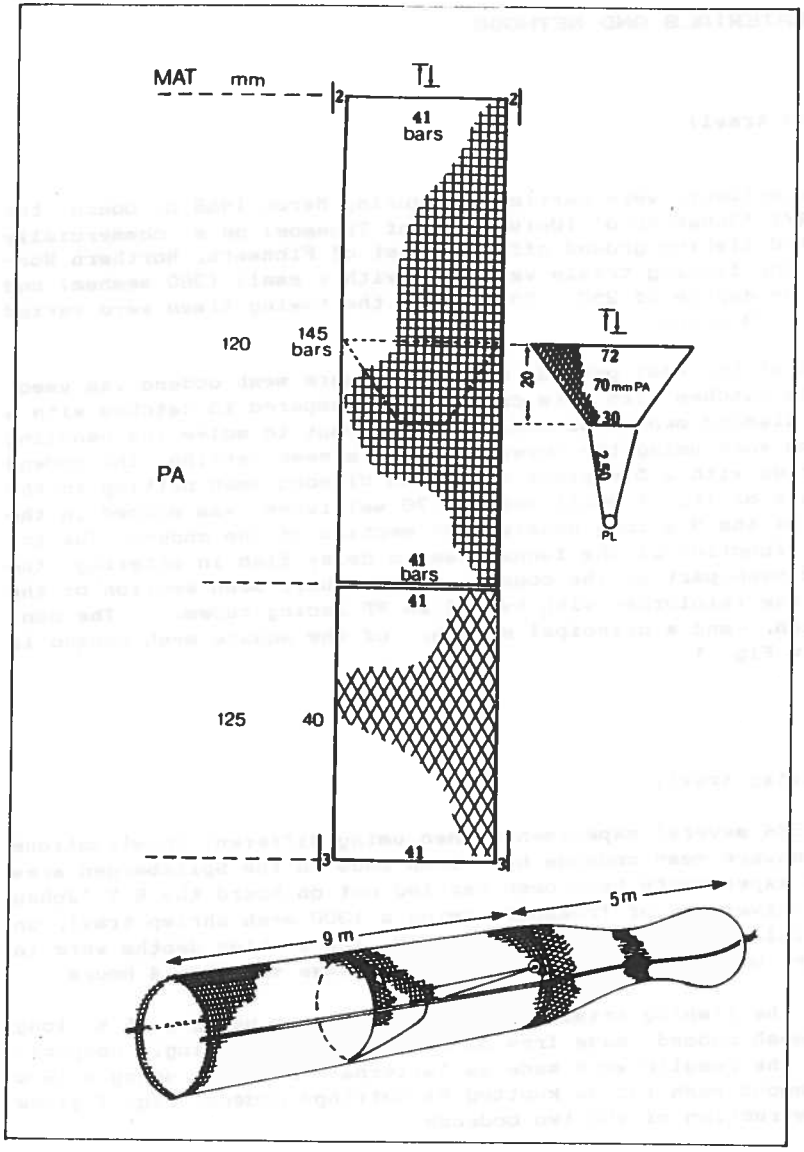

Figure 1: Construction of the 120 mm square mesh codend used during the cod trawl fishing trials off the coast of Finnmark, March 1988. A principal sketch of the shape of the codend (as observed by an u.w. vehicle) is given.

Danish seine:

The length-frequency distributions of cod and haddock when comparing the 120 mm square mesh codend to the 120 mm diamond codend, are given in Fig. 7. The results indicate a slightly better selectivity by the square mesh codend with respect to cod, whilst a considerable difference is seen with respect to haddock.

It should be noted that a very high proportion of the over sized haddock (above 39 cm total length) is lost by the square mesh codend compared to the 120 mm diamond mesh codend.

A few hauls comparing a 135 mm diamond mesh codend, to a 120 mm square mesh codend, confirmed the fishermen's allegations: Very high proportions of legal sized, and commercially utilizable, cod (above 42 cm total length) and as good as all the haddock (in the size range 30-60 cm) were lost when using the 135 mm diamond mesh codend. The results are given in Fig. 8. In all the experiments, especially when using the 135 mm diamond mesh codend, a lot of fish were seen to escape as the codend lay along the vessels side before hauling the catch on board.

Using the "twin codend method", a small meshed codend (60 mm) was used for establishing the selectivity of both the 120 mm square mesh and the 120 mm diamond mesh codend. Comparisons of length-frequency distributions between the different codends, are given in Fig. 9, showing a very high mesh selection in the square mesh codend for both cod and haddock. As seen, very high proportions of commercially utilizable fish were lost, haddock in particular.

The selection curves for both the 120 mm square mesh and the 120 mm diamond mesh codend, are given in Fig. 10. For cod the selection factors obtained were 4.7 and 4.5, and the selection ranges were 8.5 cm and 13.5 cm, respectively. The most interesting finding, is the narrower selection range, and thus a sharper selection curve, obtained when using the square mesh codend compared to the diamond mesh codend.

Due to very few haddock above 50 cm total length, the calculation of the selection curve for this species was impossible. The progress of the left side of the selection curve, however, indicates a selection factor for haddock higher than 4.0 when using the 120 mm square mesh codend.

Table 2: Sorting effects (%) upon shrimps and some species of fish when using the combined sorting system with the 70 mm HH-sorting panel and the 16 m square mesh codend. The results are given as a comparison between 8 different hauls (4 parallells) made during the test period in 1987, along the western side of Spitzbergen.

	SORTING EFFECTS BY THE 70 MM HH-SORTING PANEL			
COMPARISON	1	2	3	4
SPECIES:				
Shrimps (*Pandalus borealis*), size range: 9-26 mm carapace length. (loss by weight)	11%	9%	6%	8%
Cod (*Gadus morhua*), size range: 20-65 cm total length.	-	-	96%	93%
Polar cod (*Boreogadus saida*), size range: 8-20 cm total length.	28%	19%	33%	60%
Snake blenny (*Lumpenus lampretaeformis*), size range: 10-25 cm total length.	62%	17%	-	57%

	SORTING EFFECTS BY THE 16 M SQUARE MESH CODEND (Shrimps and fish passed through the sorting panel)			
COMPARISON	1	2	3	4
SPECIES:				
Shrimps (*Pandalus borealis*), size range: 9-15 mm carapace length.	81%	90%	66%	51%
Polar cod (*Boreogadus saida*), size range: 8-15 cm total length.	82%	90%	88%	79%
Snake blenny (*Lumpenus lampretaeformis*), size range: 10-25 cm total length.	97%	93%	-	87%

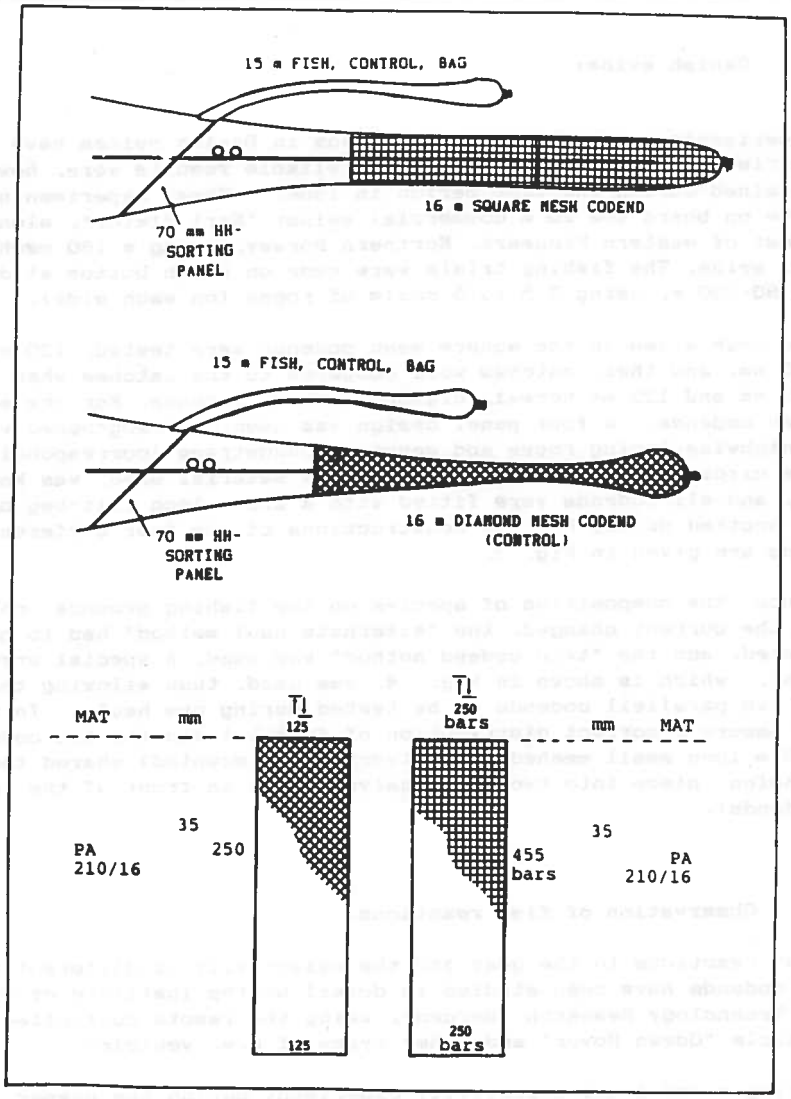

Figure 2: Construction of the two 35 mm (square and diamond) mesh codends used during shrimp trawl experiments along the coast of Spitzbergen, 1984-1988. A principal sketch of a combined sorting system, used during the experimental period in 1987, is given.

Danish seine:

Experiments with square mesh codends in Danish seines have been carried out since 1983. The most reliable results were, however, obtained during the test period in 1986. These experiments were made on board the 20 m commercial seiner "Karl Viktor", along the coast of eastern Finnmark, Northern Norway, using a 180 mesh (300 mm) seine. The fishing trials were made on rough bottom at depths of 80-230 m, using 3.5 to 5 coils of ropes (on each side).

Two mesh sizes in the square mesh codends were tested, 120 mm and 135 mm, and their catches were compared to the catches when using 120 mm and 135 mm normal, diamond meshed, codends. For the square mesh codends, a four panel design was used, strengthened with 4 lentghwise lacing ropes and several roundstraps (corresponding to the circumference of the codend). The material used, was knotted PE, and all codends were fitted with a 2.5 m long lift-bag of 110 mm knotted double PA. The constructions of the four different codends are given in Fig. 3.

Since the composition of species on the fishing grounds changed as the current changed, the "alternate haul method" had to be rejected, and the "twin codend method" was used. A special arrangement, which is shown in Fig. 4, was used, thus allowing the use of two parallell codends to be tested during one haul. In order to assure a correct distribution of fish between the two codends, a 8 m long small meshed panel (vertically mounted) shared the extension piece into two equal halves (well in front of the tested codends).

Observation of fish reactions:

Fish reactions to the gear and the selectivity of different types of codends have been studied in detail by the Institute of Fishery Technology Research (Bergen), using the remote controlled u.w. vehicle "Ocean Rover" and other types of u.w. vehicles.

During a cod trawl selectivity experiment during the summer 1988, fish reactions to the 120 mm square meshed codend with the small meshed funnel (see page 4), were studied.

Shrimp trawls:

The use of a 16 m long square meshed codend in shrimp trawls has been successful in a selectivity point of view. The calculated reduction of undersized shrimps (less than 6 cm) varied from 30% to 90%, comparing the 35 mm square mesh codend to the 35 mm diamond mesh codend. The selectivity will be dependent upon the size distribution of shrimps and the catch size, i.e. reduced selectivity at increasing catches.

The fishing trials have also stated that small and in particular slim bodied species of fish, will effectively be removed from the shrimp catches, thus saving time-consuming sorting work on board the vessels. The most common, and most numerous, species of fish in the shrimp catches in the Spitzbergen area, are snake blenny (Lumpenus lampretaeformis), polar cod (Boreogadus saida) and redfish species (Sebastes sp.). The mesh selection on snake blenny is close to 90%, while the polar cod and the red fish species are more difficult to sort out through the 35 mm meshes. In the size range 8-20 cm, however, more than 80% of the polar cod was sorted out. Results when using a combination with a 70 mm sorting panel and a 16 m long 35 mm square mesh codend, are given in Table 2.

A comparable construction of the square mesh codend, as described for the cod trawl experiments, has been tested in shrimp trawls. The best results are undoubtedly obtained if the entrance to the last section of diamond meshes (8 m long) is closed (by a codline) during the fishing operation. The "codline" is opened as the codend is hauled on board, and the catch will slide from the square mesh part into the diamond mesh part of the codend.

In spite of several years of testing, no handling problems or constructional problems are seen when using the square mesh codends in (deep sea) shrimp trawling.

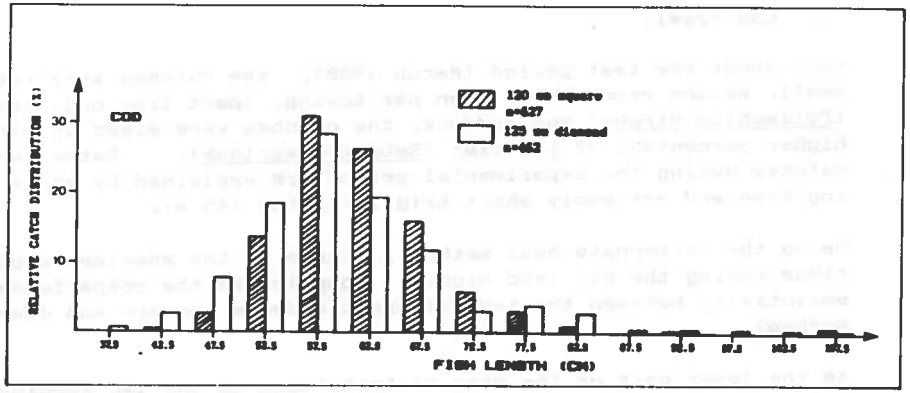

Figure 5: Relative catch distribution (%) for cod (Gadus morhua) in a 120 mm square mesh and a 125 mm diamond mesh codend found during the cod trawl experiments March 1988.

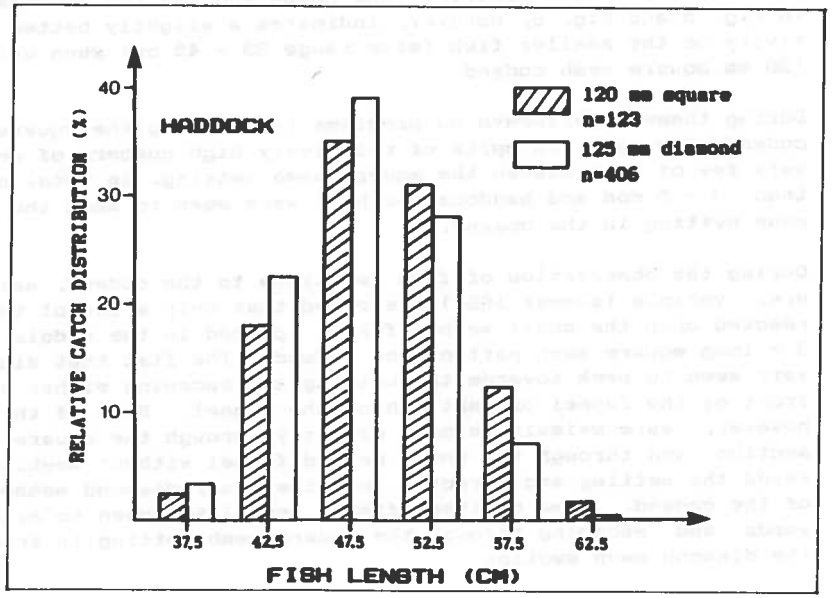

Figure 6: Relative catch distribution (%) for haddock (Melanogrammus aeglefinus) in a 120 mm square mesh and a 125 mm diamond mesh codend found during the cod trawl experiments March 1988.

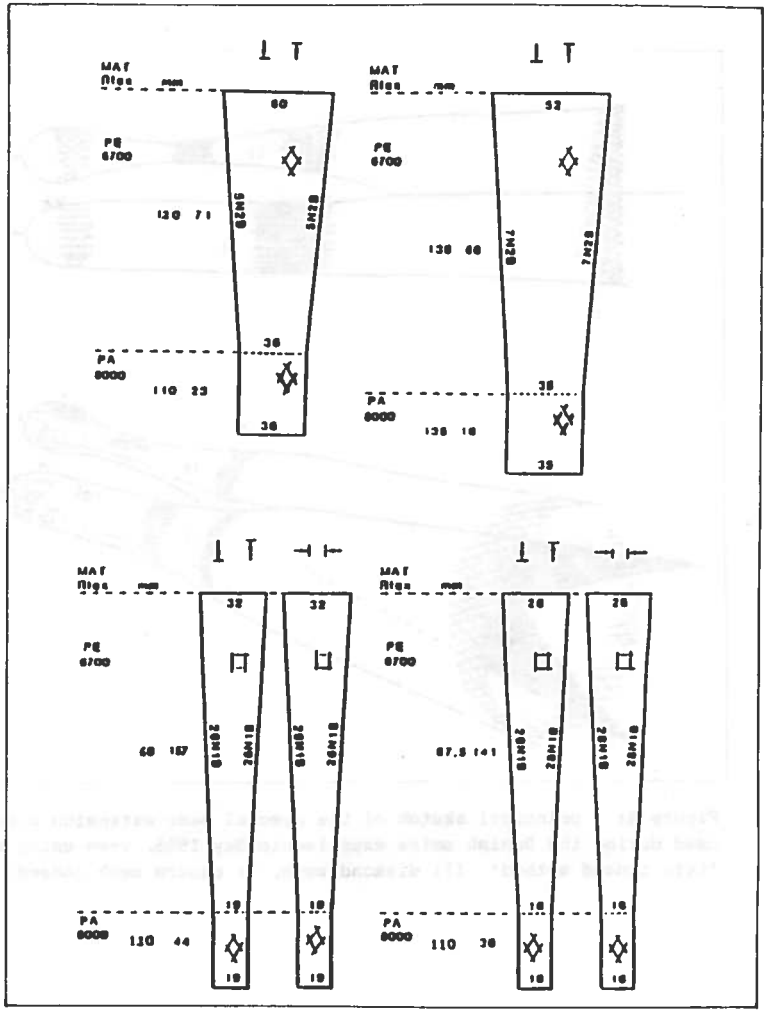

Figure 3: Construction of the four different codends used during the Danish seine experiments along the coast of Finnmark, May 1986. The diamond mesh codends (120 and 135 mm) are of a two-panel design, whilst the square mesh codends (120 and 135 mm) are of a four-panel design. All codends were equipped with a 110 mm (PA) lift-bag.

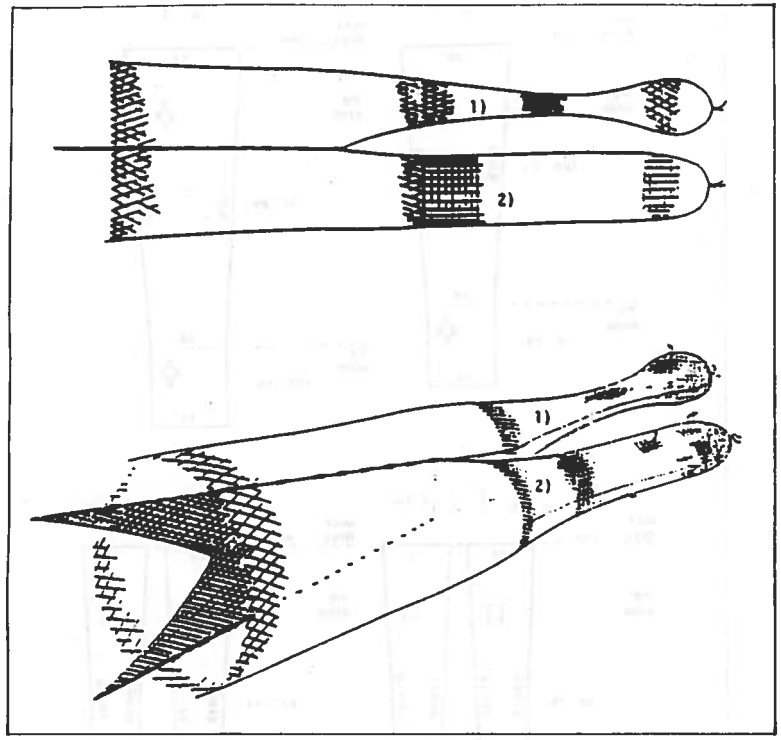

Figure 4: A principal sketch of the special made extension piece used during the Danish seine experiments May 1986, when using the "twin codend method". (1: diamond mesh, 2: square mesh codend).

RESULTS

Cod trawl:

Throughout the test period (March 1988), the catches were rather small, seldom exceeding 1 tonn per towing. Apart from cod, saithe (Pollachius virens) and haddock, the catches were mixed up with a higher percentage of red fish (Sebastes marinus). Rather small catches during the experimental period are explained by short towing time and extremely short bridle lengths (45 m).

Using the "alternate haul method", change of the species compositions during the day (and night), complicated the comparisons of selectivity between the two different codends (square and diamond meshes).

As the lower part of the size distributions of the two species of interest, cod and haddock, were close to the legal minimum size, i.e. 42 cm and 39 cm respectively, it was difficult to find the big differences between the codends with respect to selectivity.

The relative length distributions comparing the two codends given in Fig. 5 and Fig. 6, however, indicates a slightly better selectivity on the smaller fish (size range 35 - 45 cm) when using the 120 mm square mesh codend.

During these experiments no problems in handling the square mesh codend were seen. In spite of relatively high numbers of red fish, very few of them masked the square mesh netting. In total no more than 3 - 5 cod and haddock per haul were seen to mask the square mesh netting in the codend.

During the observation of fish reactions to the codend, using the u.w. vehicle (summer 1988), revealed that only a few of the fish reacted upon the small meshed funnel (placed in the middle of the 9 m long square mesh part of the codend). The fish that did react, were seen to seek towards the netting and escaping either just in front of the funnel or just behind the funnel. Most of the fish, however, were swimming almost directly through the square meshed section and through the small meshed funnel without seeking towards the netting and directly into the rear, diamond meshed part of the codend. Some of these fishes were later seen to swim forwards and escaping through the square mesh netting in front of the diamond mesh section.

Appendix A14

Foreløbige resultater for snurrevad

DEL I:

FORELØPIGE RESULTATER, SNURREVAD
ØST-FINNMARK, 17. TIL 22. JUNI 1991

FORSØK MED M/S "HEIDI ANITA" T-100-T
135 mm PE poser versus
55 mm sorteringsrist

TOKTDELTAKERE:
Bjørnar Isaksen, Roger Larsen,
Svein Løkkeborg & Oddvar Chruickshank

KOMMENTARER TIL FORSØK MED SORTERINGSRIST I SNURREVAD, ØST-FINNMARK I JUNI 1991:

Fartøy, utstyr og fangstområde:

Forsøkene ble utført med snurrevadfartøyet M/S "Heidi Anita", som er 19.9 m lang, 6.4 m bred og har en 523 BHk Bos/Merzedes hovedmotor. Fartøyet er spesialrigget for effektivt snurrevadfiske. Begge tautromler er plassert på båtdekket (bak rorhuset) og fartøyet har 2 hiab-kraner for håndtering av bruk og fangst. Fangsten blir tatt ned på arbeidsdekket gjennom inntaksbinge fra båtdekket. Fisken blir sløyd for hånd, vasket og kjørt ned i CSW-tanker i rommet.

Under seleksjonsforsøkene ble det benyttet en standard Brd. Selstad tampenot (180 msk. x 300 mm) med tauvinger, og det ble i regelen gått ut 5 kveiler tau (à 120 fv) på hver arm. Forsøkene ble utført i områdene øst av Makkaur, nærmere bestemt ved Syltefjord-stauran og inne på Gambukta, på dybder mellom 30 og 50 fv. Under forsøksperioden gikk fisk (torsk og hyse) og beitet på sil (tobis). Det ble funnet torsk i størrelsene 25 til 80 cm, med hovedtyngden på undermåls fisk. Hyse ble funnet i størrelsene 25 til 68 cm, størstedelen under minstemål. I enkelte hal med standard snurrevad og 135 mm PE pose (under RCTV-observasjoner) var innblandingsprosenten av undermåls fisk på disse feltene 70-90%!

Seleksjonsforsøk med 55 mm sorteringsrist:

I fremste del (ca. 10 m foran cod-end) av den ordinære 135 mm PE posen ble det montert inn 3 stk. 70 x 70 cm rister av rustfritt stål (ST 18.8) med 55 mm spileavstand. Tilsammen 12 stk. 8" PL-kuler ble brukt for å nøytralisere vekten av ristene, plassert på en slik måte at ristene fikk en viss angrepsvinkel.

For å fange opp fisk som ble sortert ut gjennom ristene ble det benyttet en finmasket oppsamlingspose, kfr. skisse av forsøksoppsettet. **Det ble ikke gjort "blinding" av hovedsekken.**

Håndtering og praktiske erfaringer:

Det ble under disse forsøkene ikke avdekket vansker med håndtering av utstyret, selv om det ble brukt en stor oppsamlingspose. Praksis for utsetting og haling ble gjort identisk med vanlig, ordinært fiske, men det ble naturligvis sørget for at pose med rister og oppsamlingspose gikk riktig ut. Når avstand mellom ristseksjonen og codend var riktig, oppstod det ikke problemer med "tørking" og tømming av sekkene. I alle

tre seleksjonshalene var det 4-5 sekker fisk i oppsamlingsposen og 2-4 sekker i hovedposen. "Heidi Anita" er et fartøy med høy hekk, og ventelig blir "vanskene" med å håndtere sorteringsrist i snurrevad enda mer uproblematisk (om mulig?) på et mindre fartøy hvor hekket er nærmere vannspeilet.

Resultater fra seleksjonsforsøkene:

Resultatene fra forsøkene er svært oppløftende, det er oppnådd meget stor grad av utsortering på yngel og undermåls fisk på tross av en "rimelig" middelseleksjon for torsk og hyse. Det er oppnådd skarp seleksjon med hensyn til fiskestørrelse, med seleksjonsintervall på henholdsvis 5.2 cm og 5.1 cm for torsk og hyse.

Det kan ikke trekkes noen konklusjoner eller gis noen anbefalinger ut fra dette materialet!. Årsaken til dette ligger i at det er gjort kun tre hal, og at det ikke ble benyttet finmasket innernett i hovedposen. Dermed er eventuell maskeseleksjon i hovedposen ikke kontrollert. Det nærmeste vi kan komme et svar på dette i denne omgang, er gjennom sammenligningen mellom hal 12 og hal 14 beskrevet i det understående.

Det er gjort en sammenligning, gjennom kumulert prosent-fordeling, av resultatene fra snurrevad med ordinær 135 mm PE pose (hal 12) og snurrevad med 55 mm sorteringsrist, hvor effektene av sorteringsristen kommer klart til uttrykk.

Sluttord:

Gjennom disse innledende forsøk til utvikling av en sorteringsrist for snurrevad ble det oppnådd resultater og erfaringer langt over det forventede. Idèen bak forsøket var i hovedsak å få svar på den praktiske siden ved håndtering av rister og oppsamlingspose på et snurrevadfartøy. Dette forklarer hvorfor forsøkene ikke ble lagt opp som kontrollerte forsøk med "blindet" hovedsekk.

På tross av dette, så er det allerede nå helt tydelig at sorteringsristen vil kunne fungere svært godt i snurrevad. Forskjellene mellom fangstsammensetningen i et snurrevadhal med ordinær pose (135 mm PE) sammenlignet med et snurrevadhal hvor det brukes sorteringsrist + 135 mm PE pose, er som dag og natt.

Tromsø, den 21.09.1991

Bjørnar Isaksen & Roger B. Larsen

VEDLEGG:

Snurrevad med 55 mm sorteringsrist

Forsøksoppsettet, sett fra siden

Forsøkene ble gjort med en standard 180x300 mm

Brd. Selstad tampenot m/tauvinger & 5 kveiler armer

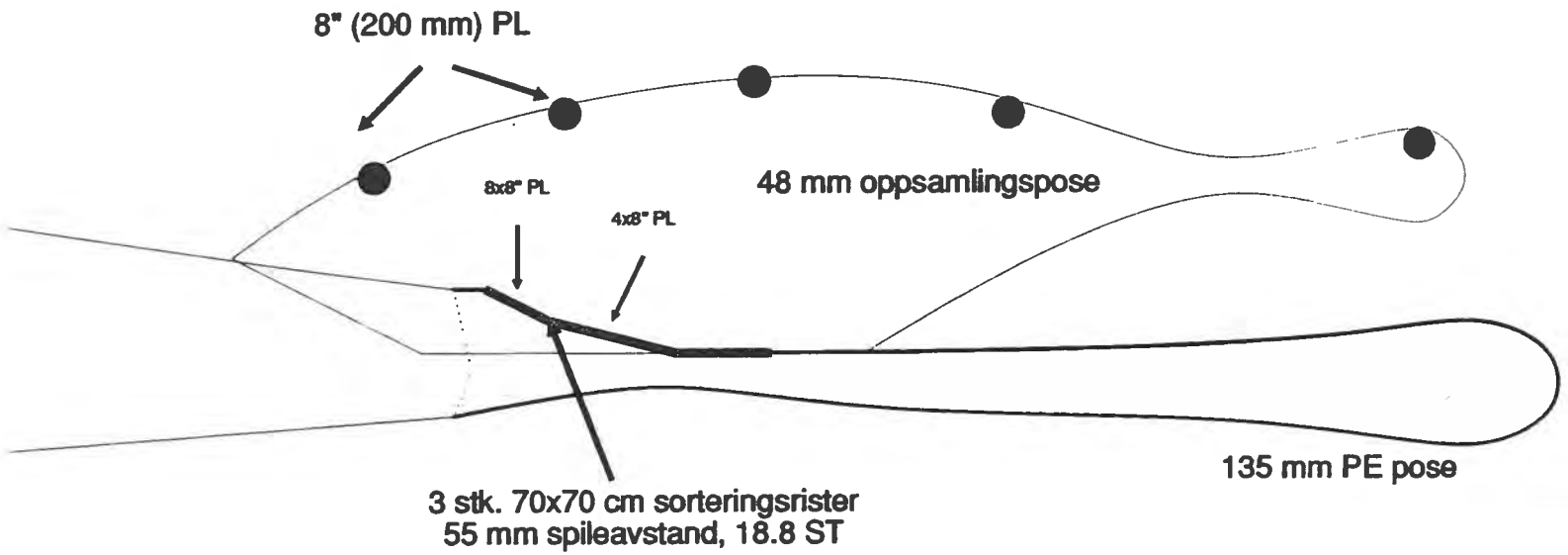

Isaksen & Larsen 1991

Lengde-frekvens fordeling for torsk

55 mm sorteringrist hal 13+14+15

M/S "Heidi Anita" T-100-T, 21. Juni 1991

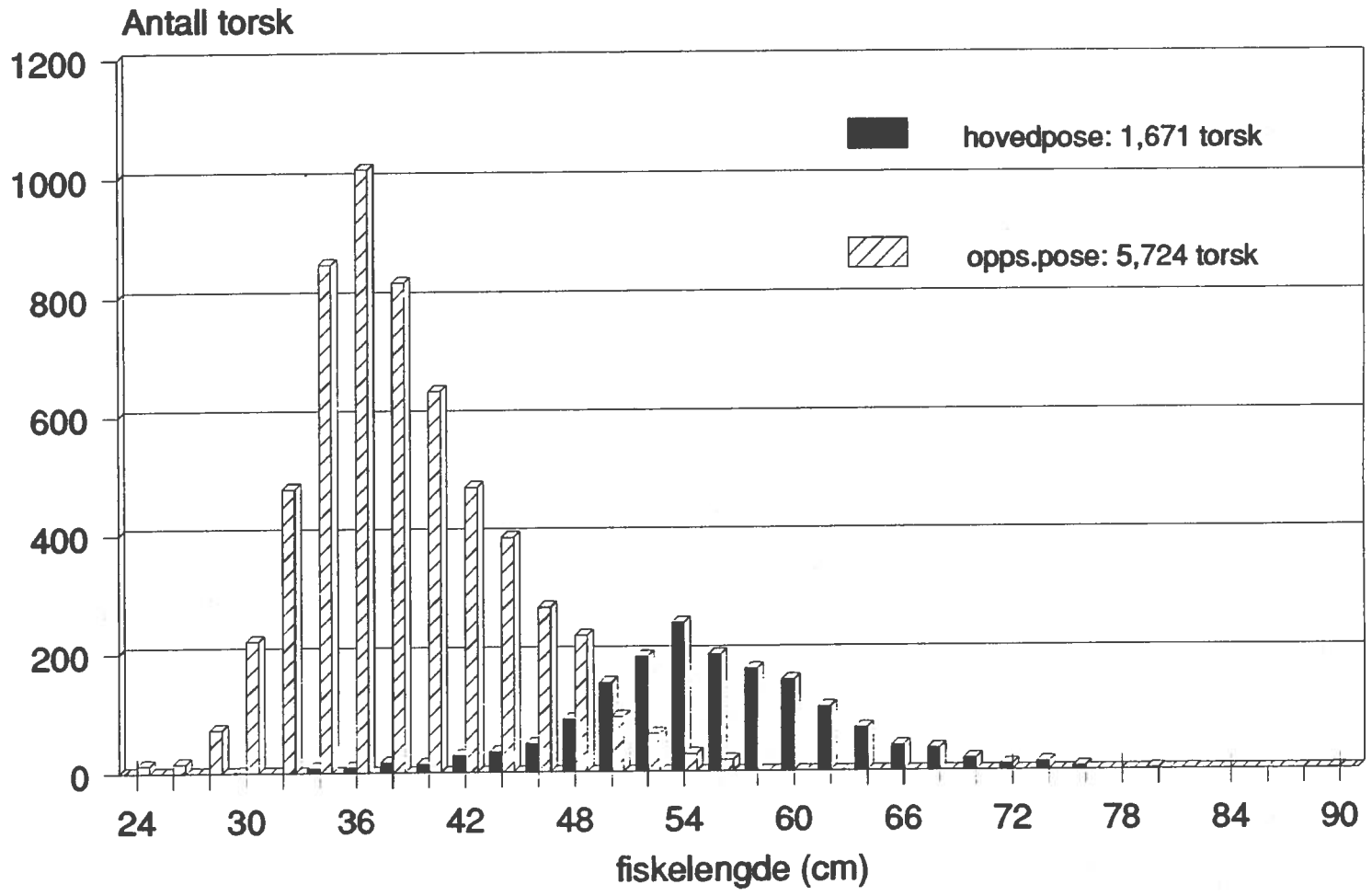

Isaksen & Larsen 1991

Seleksjonskurve for torsk hal 13-15

55 mm sorteringsrist

M/S "Heidi Anita" T-100-T, 21. Juni 1991

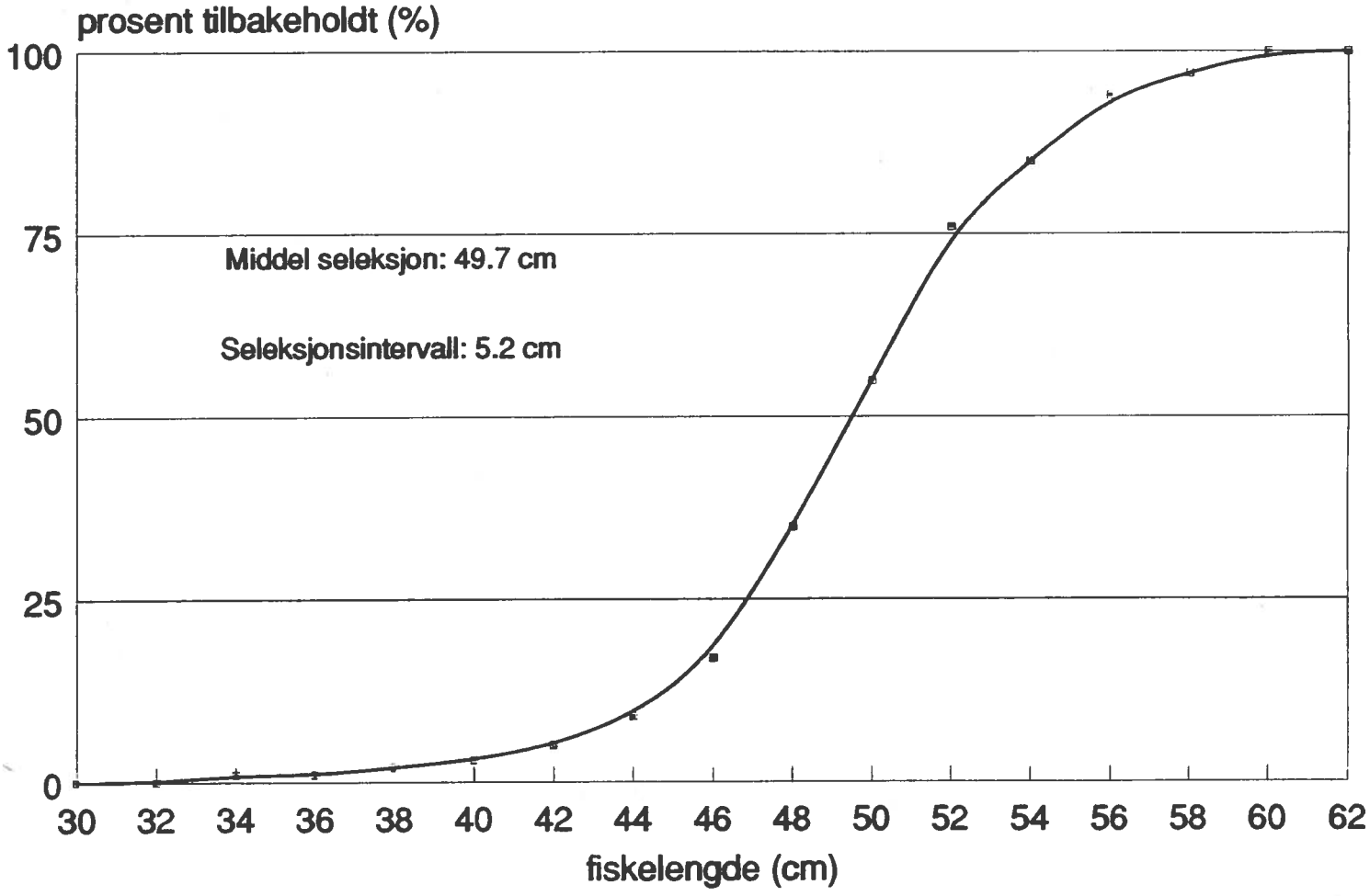

Isaksen & Larsen 1991

Seleksjonskurve for hyse hal 13-15

55 mm sorteringsrist i snurrevad

M/S "Heidi Anita" T-100-T, 21. Juni 1991

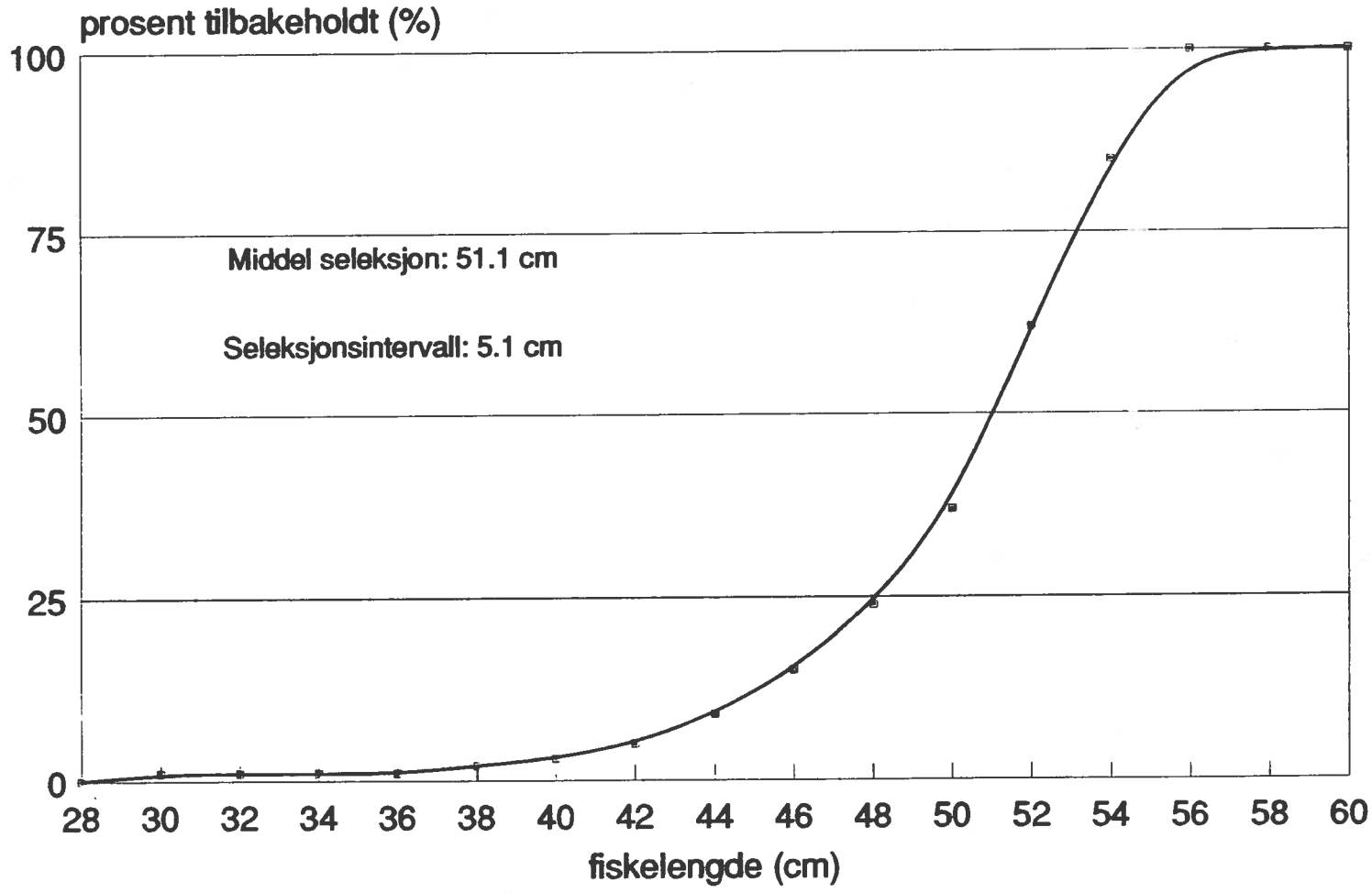

Isaksen & Larsen 1991

Lengde-frekvens fordeling for hyse

55 mm sorteringrist hal 13+14+15

M/S "Heidi Anita" T-100-T Juni 1991

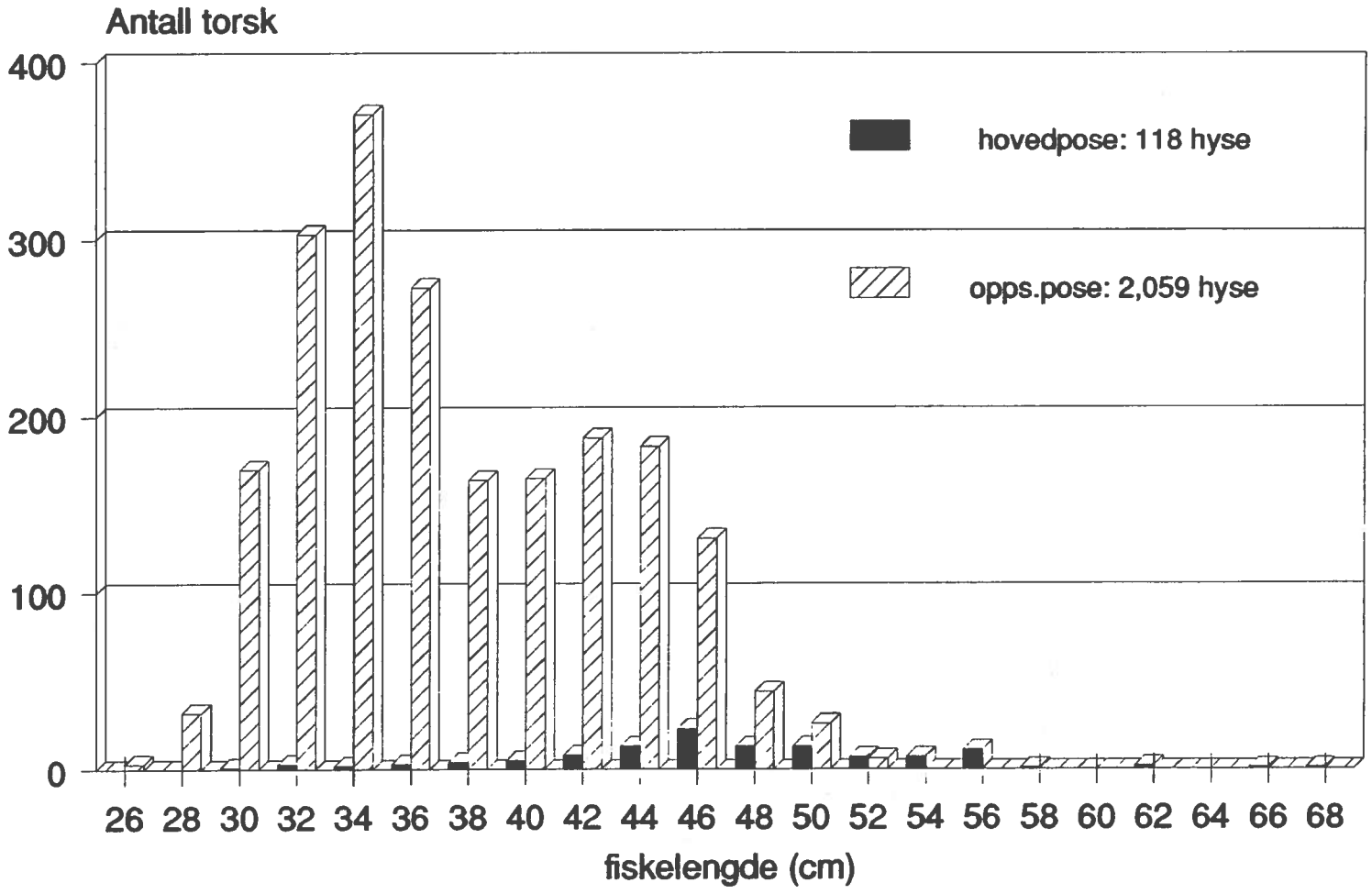

Isaksen & Larsen 1991

Seleksjonskurve for torsk hal 13

55 mm sorteringsrist

M/S "Heidi Anita" T-100-T Juni 1991

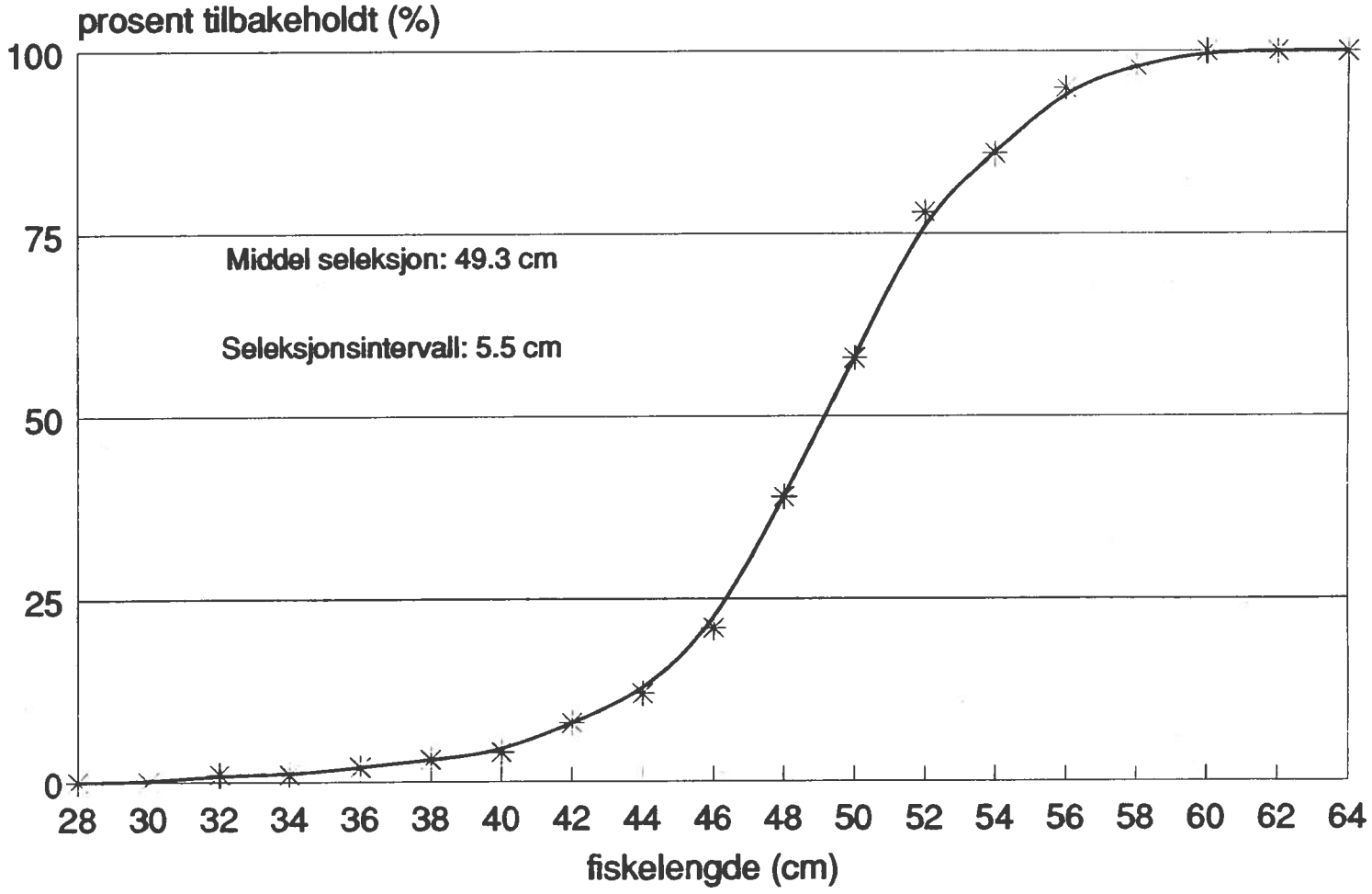

Lengde-frekvens fordeling for torsk

55 mm sorteringrist hal 13

M/S "Heidi Anita" T-100-T Juni 1991

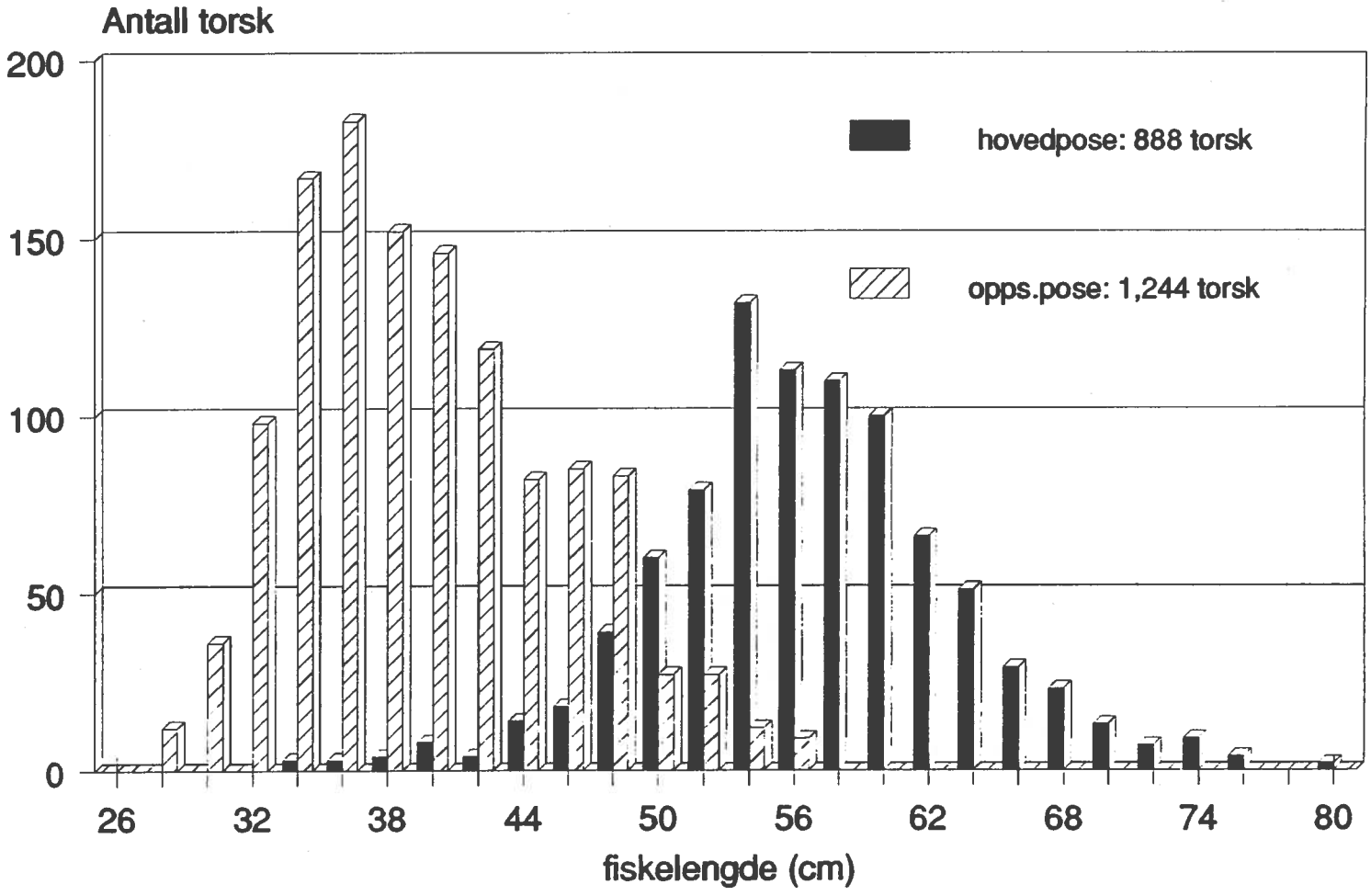

Seleksjonskurve for torsk hal 14

55 mm sorteringsrist

M/S "Heidi Anita" T-100-T Juni 1991

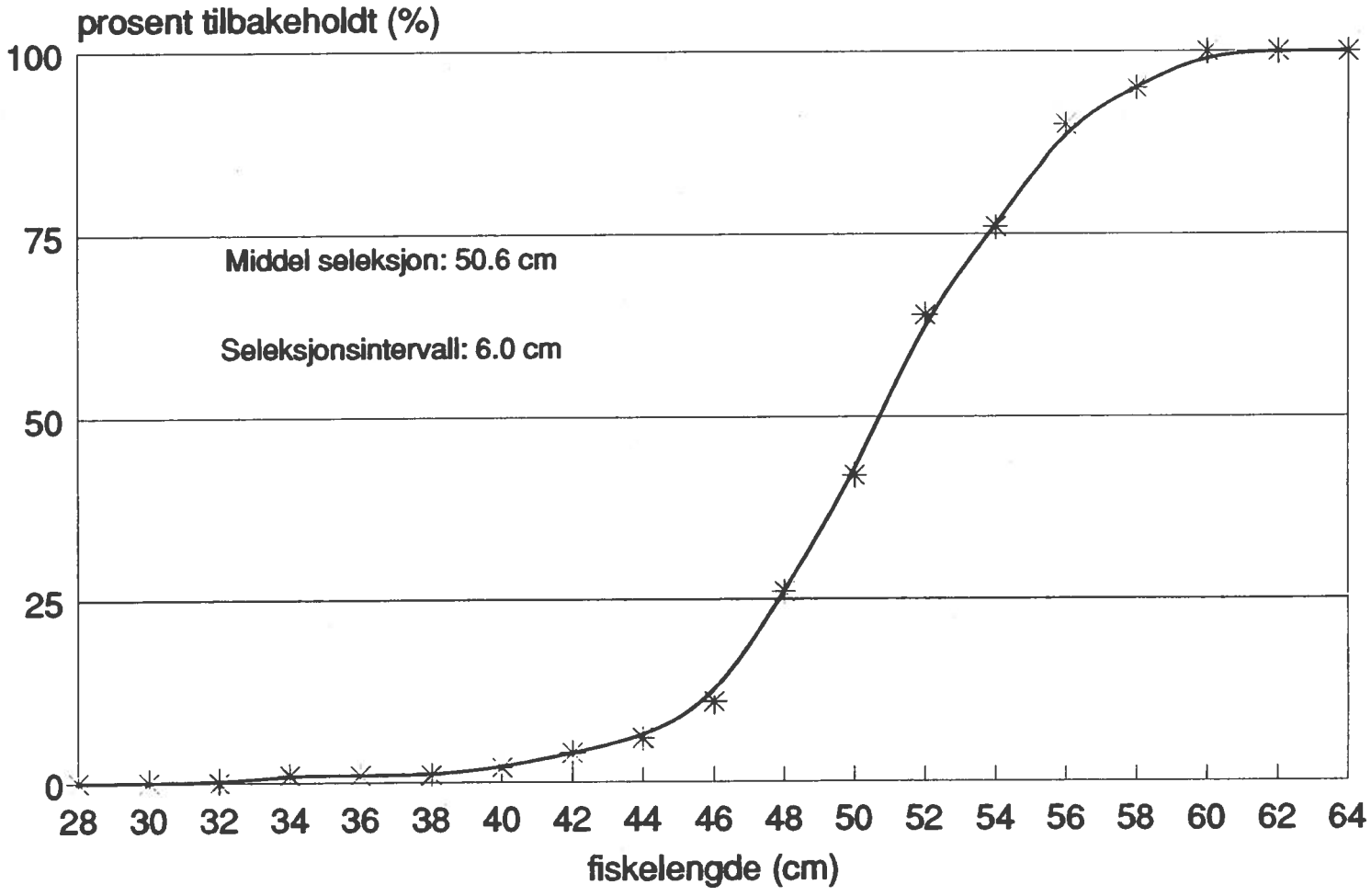

Lengde-frekvens fordeling for torsk

55 mm sorteringrist hal 14

M/S "Heidi Anita" T-100-T Juni 1991

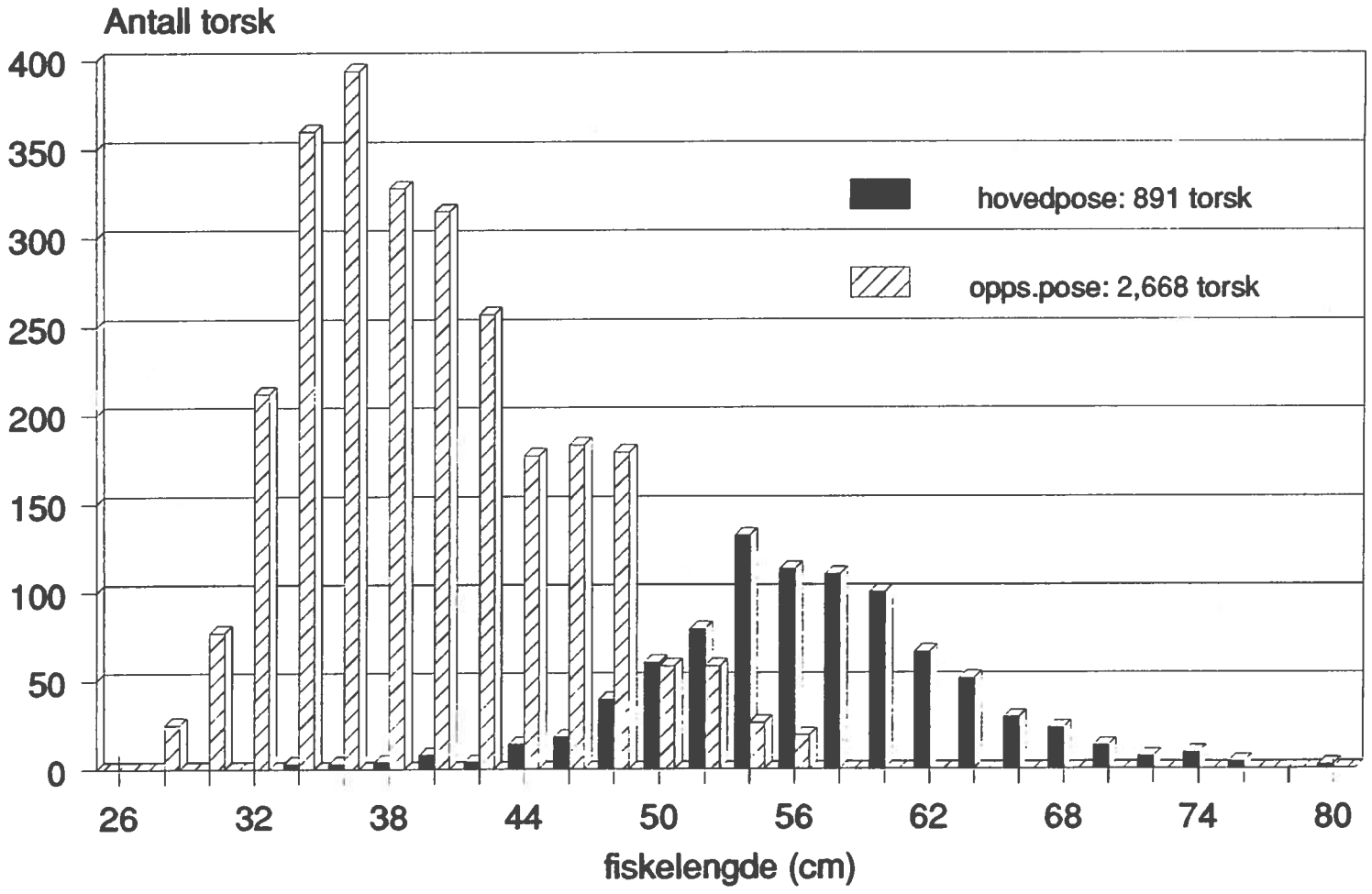

Seleksjonskurve for torsk hal 15

55 mm sorteringsrist

M/S "Heidi Anita" T-100-T Juni 1991

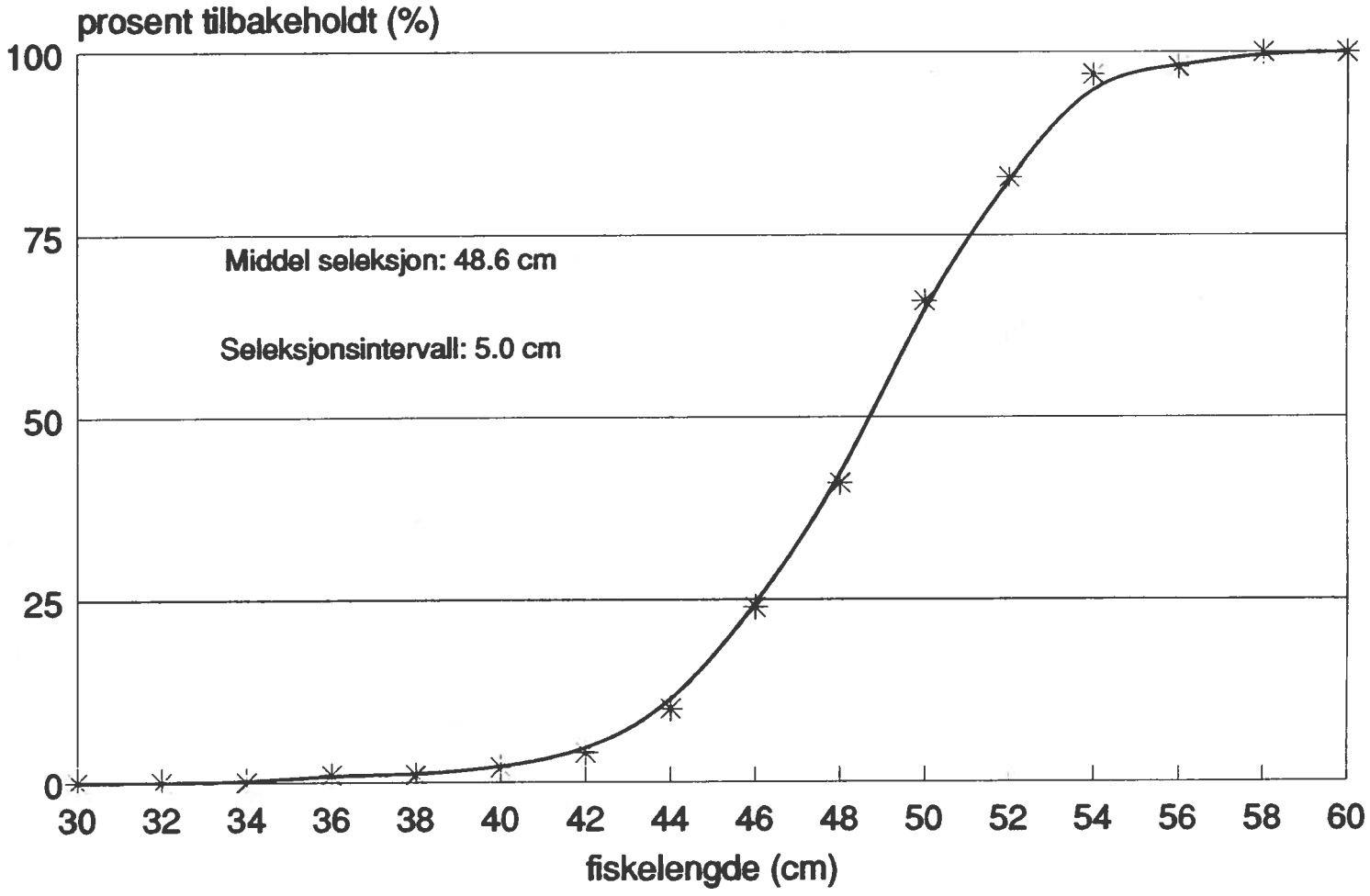

Lengde-frekvens fordeling for torsk

55 mm sorteringrist hal 15

M/S "Heidi Anita" T-100-T Juni 1991

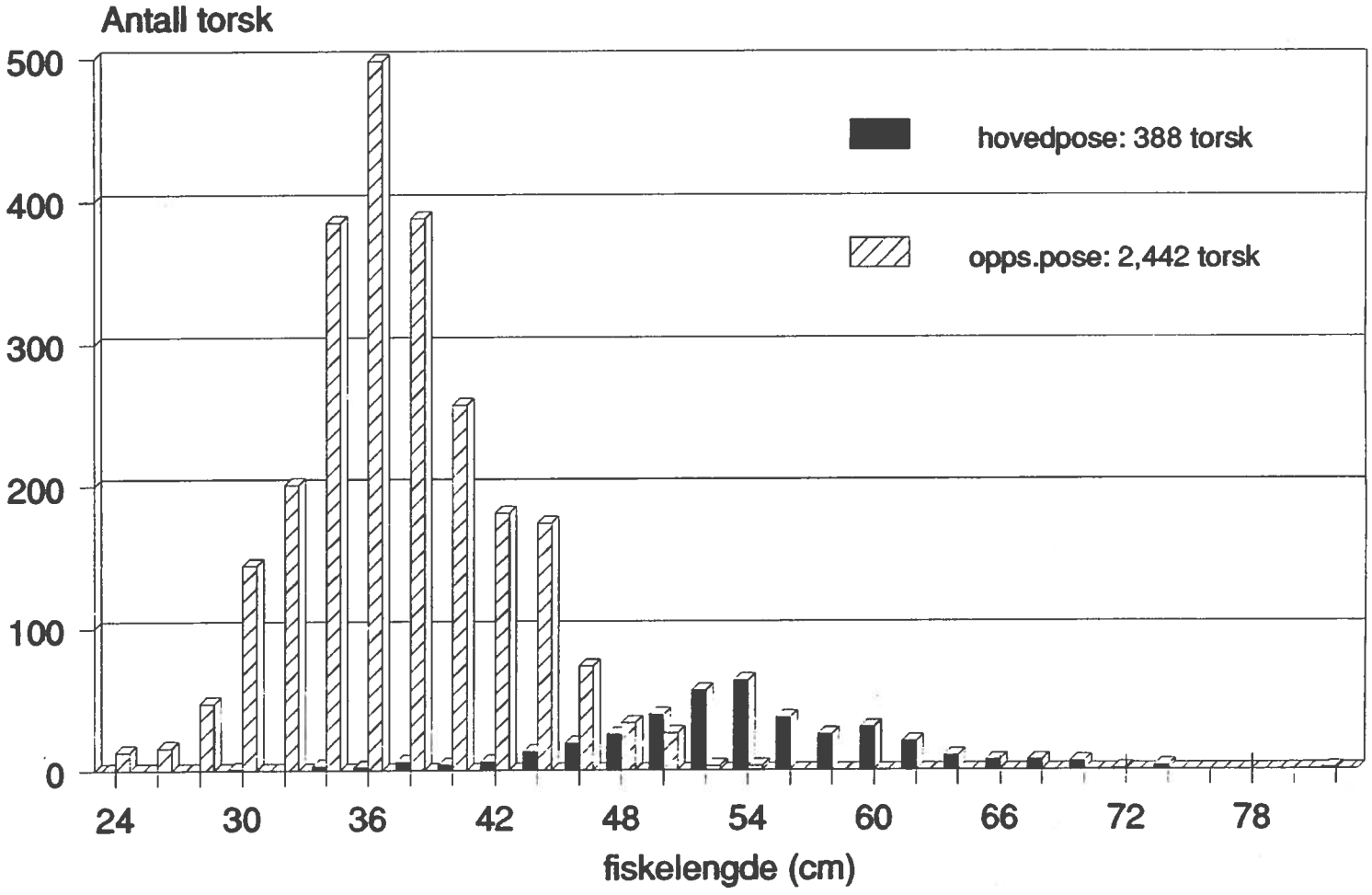

Seleksjonskurve for hyse hal 13

55 mm sorteringsrist

M/S "Heidi Anita" T-100-T Juni 1991

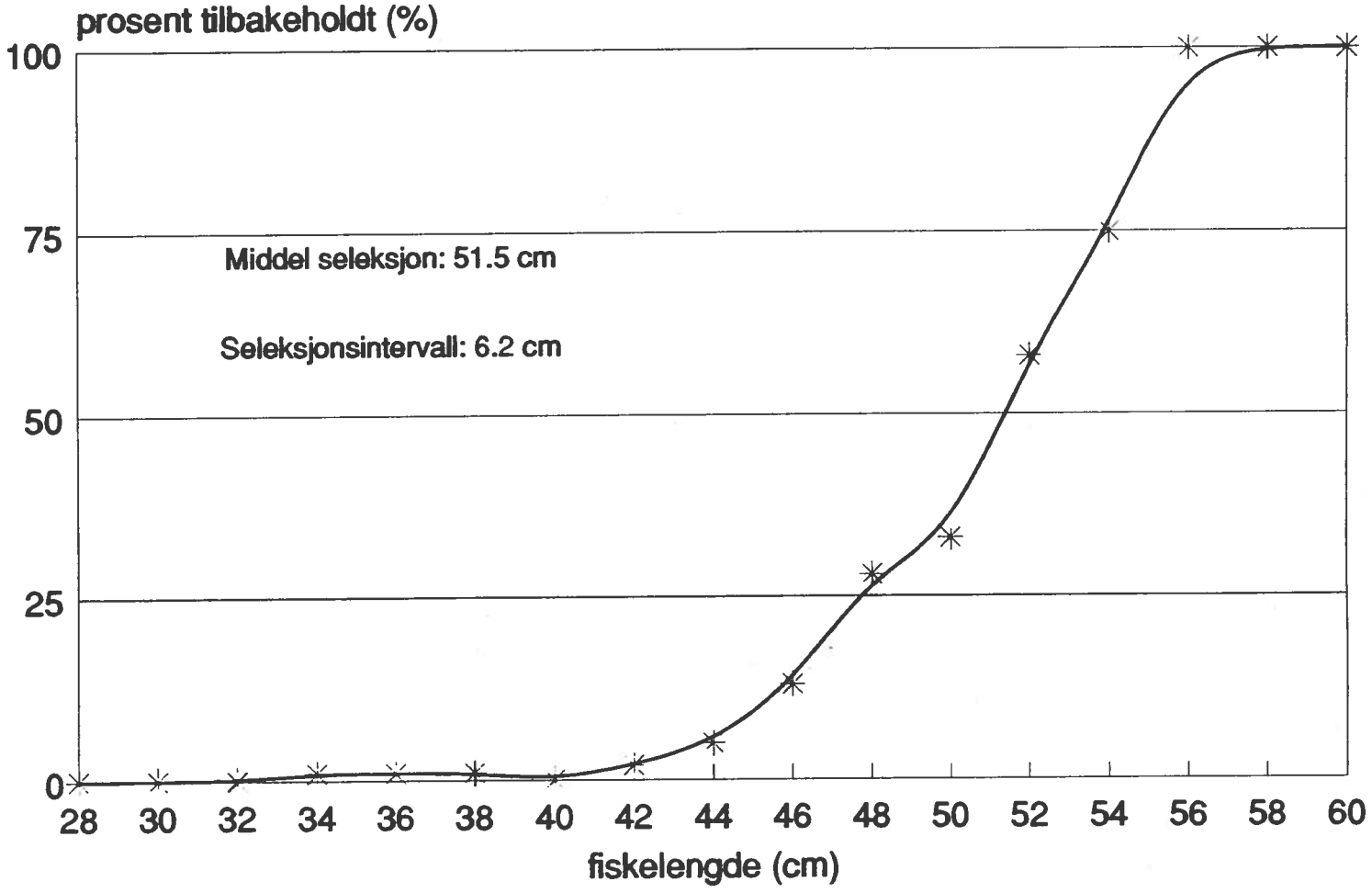

Lengde-frekvens fordeling for hyse

55 mm sorteringrist hal 13

M/S "Heidi Anita" T-100-T Juni 1991

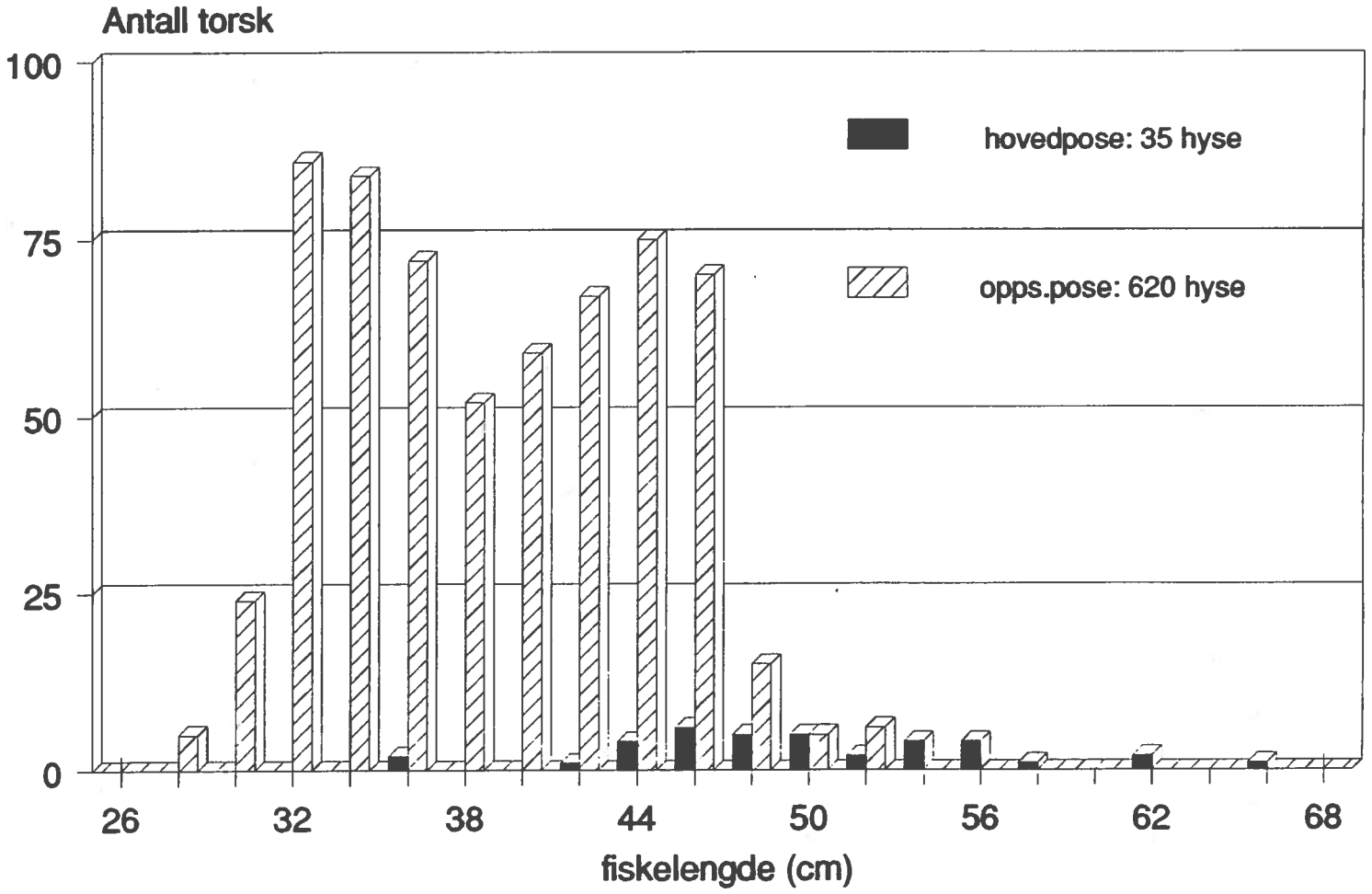

Seleksjonskurve for hyse hal 14

55 mm sorteringsrist

M/S "Heidi Anita" T-100-T Juni 1991

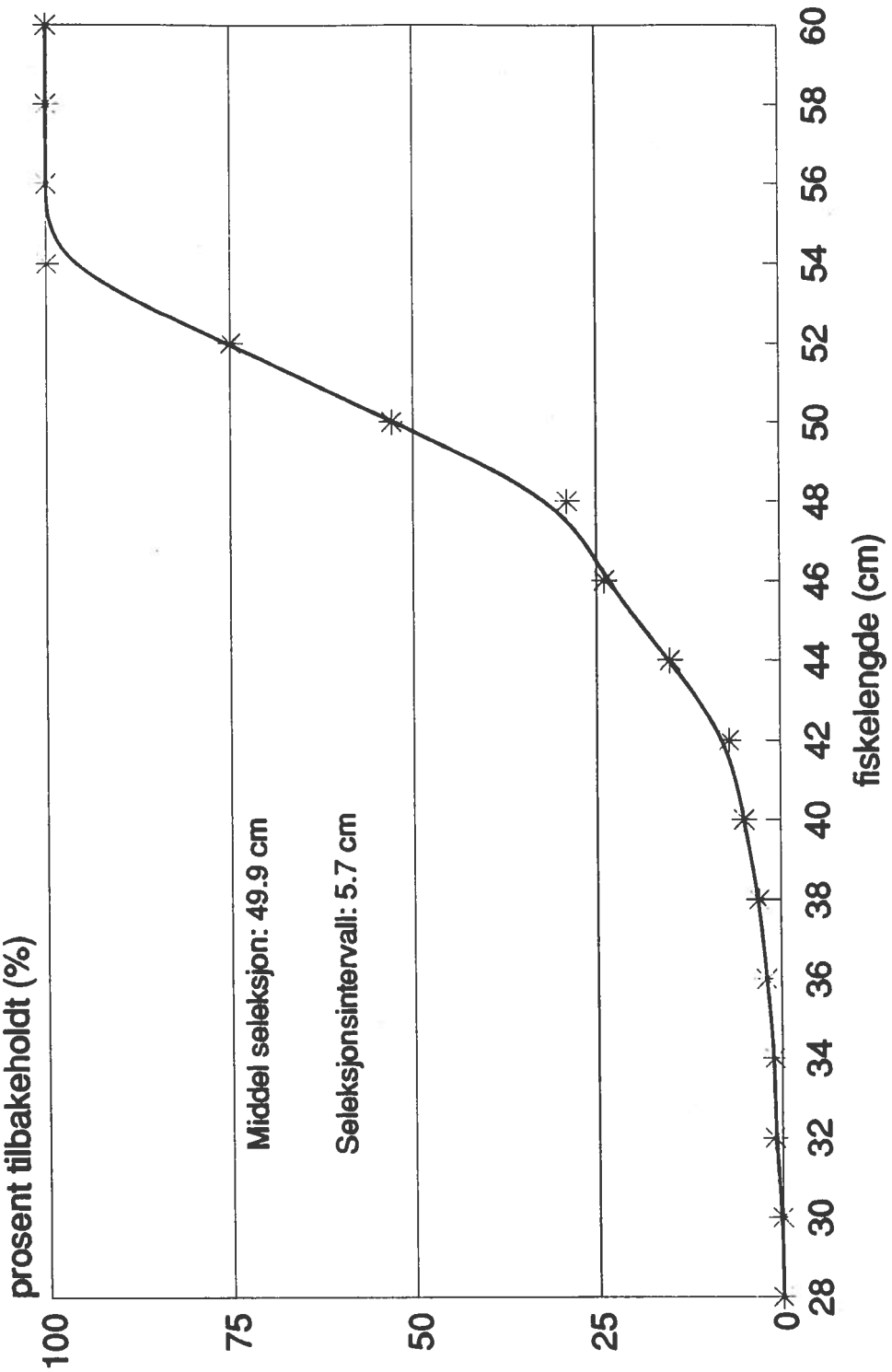

Lengde-frekvens fordeling for hyse

55 mm sorteringrist hal 14

M/S "Heidi Anita" T-100-T Juni 1991

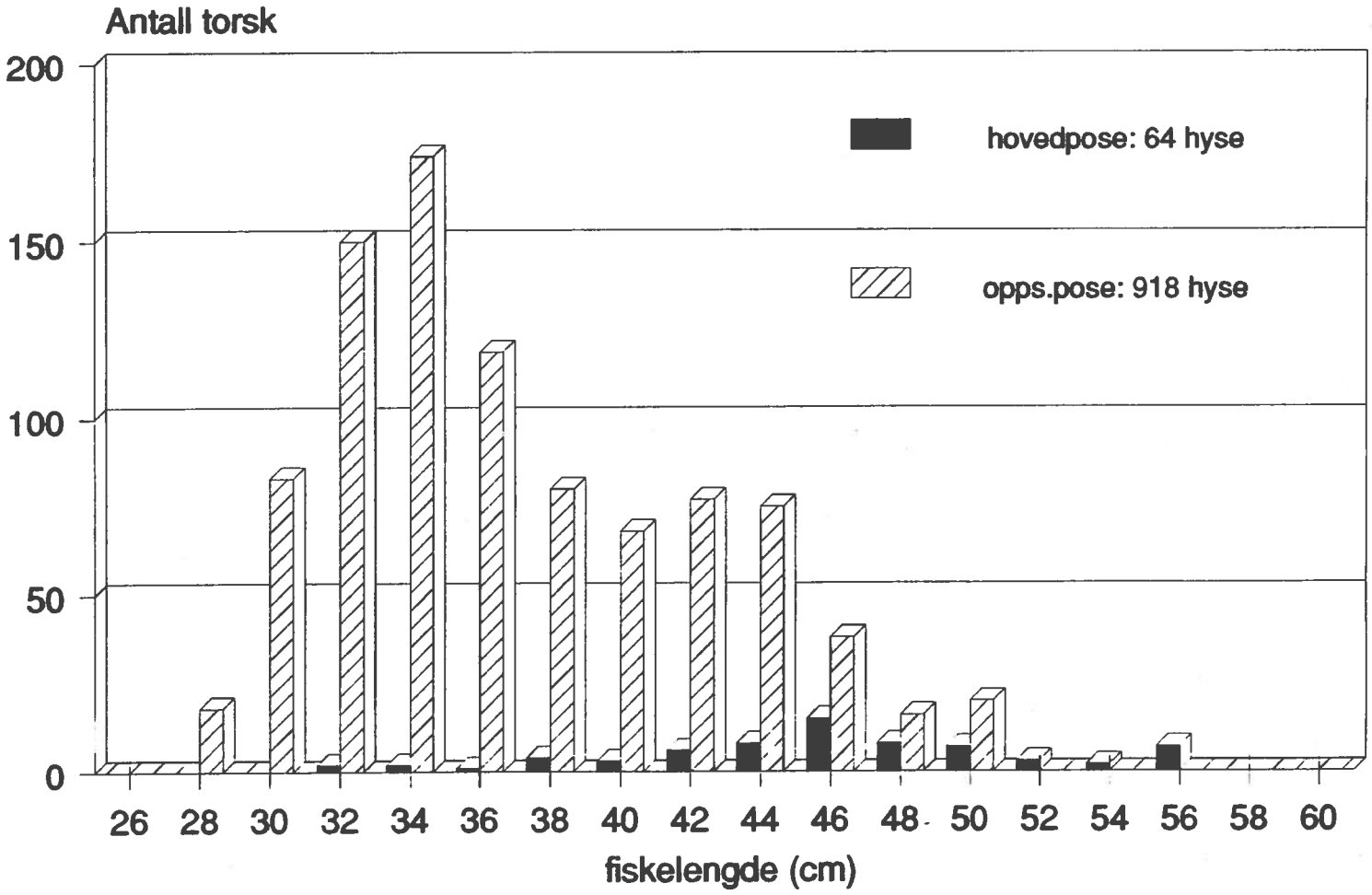

Seleksjonskurve for hyse hal 15

55 mm sorteringsrist

M/S "Heidi Anita" T-100-T Juni 1991

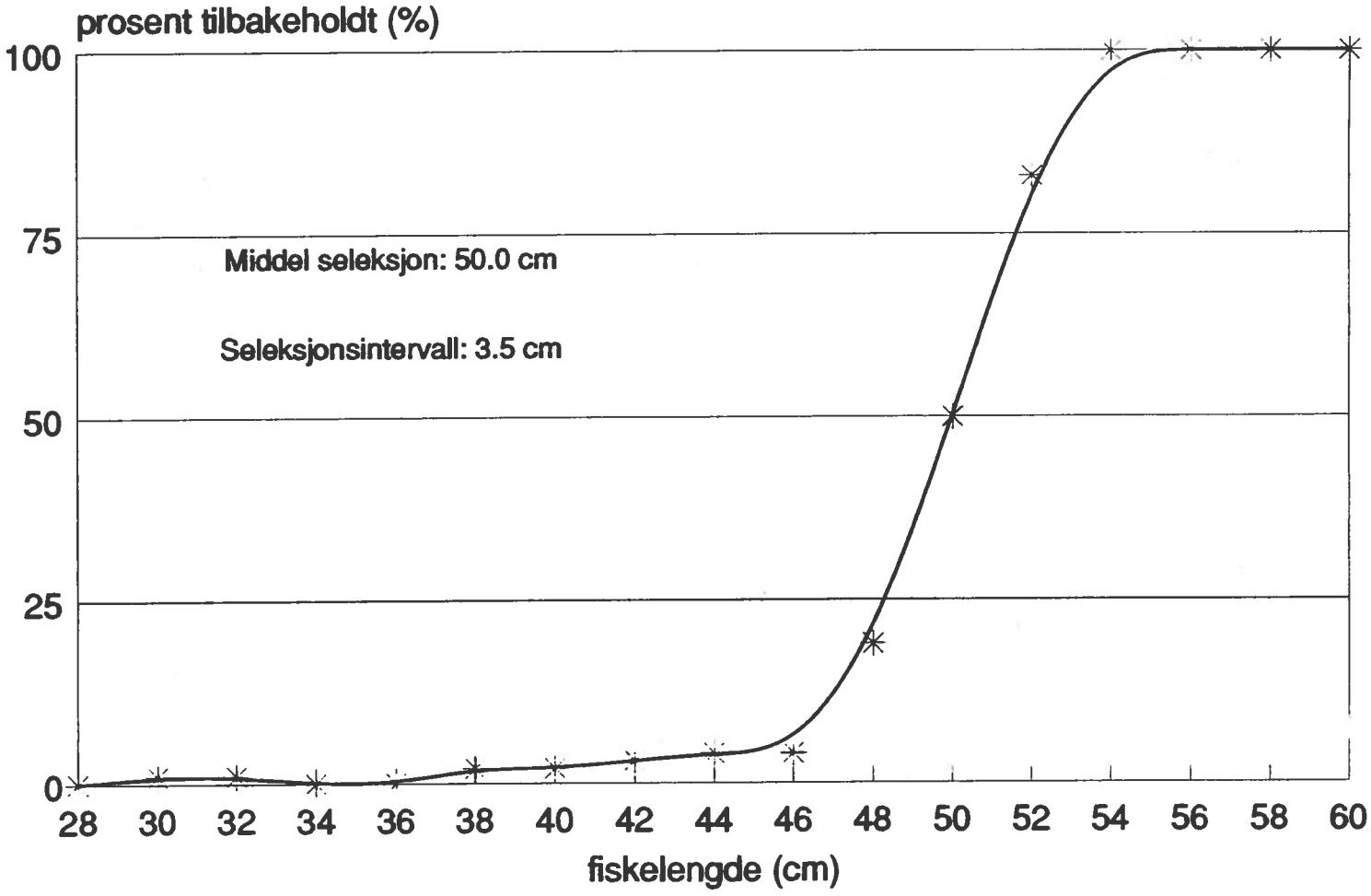

Lengde-frekvens fordeling for hyse

55 mm sorteringrist hal 15

M/S "Heidi Anita" T-100-T Juni 1991

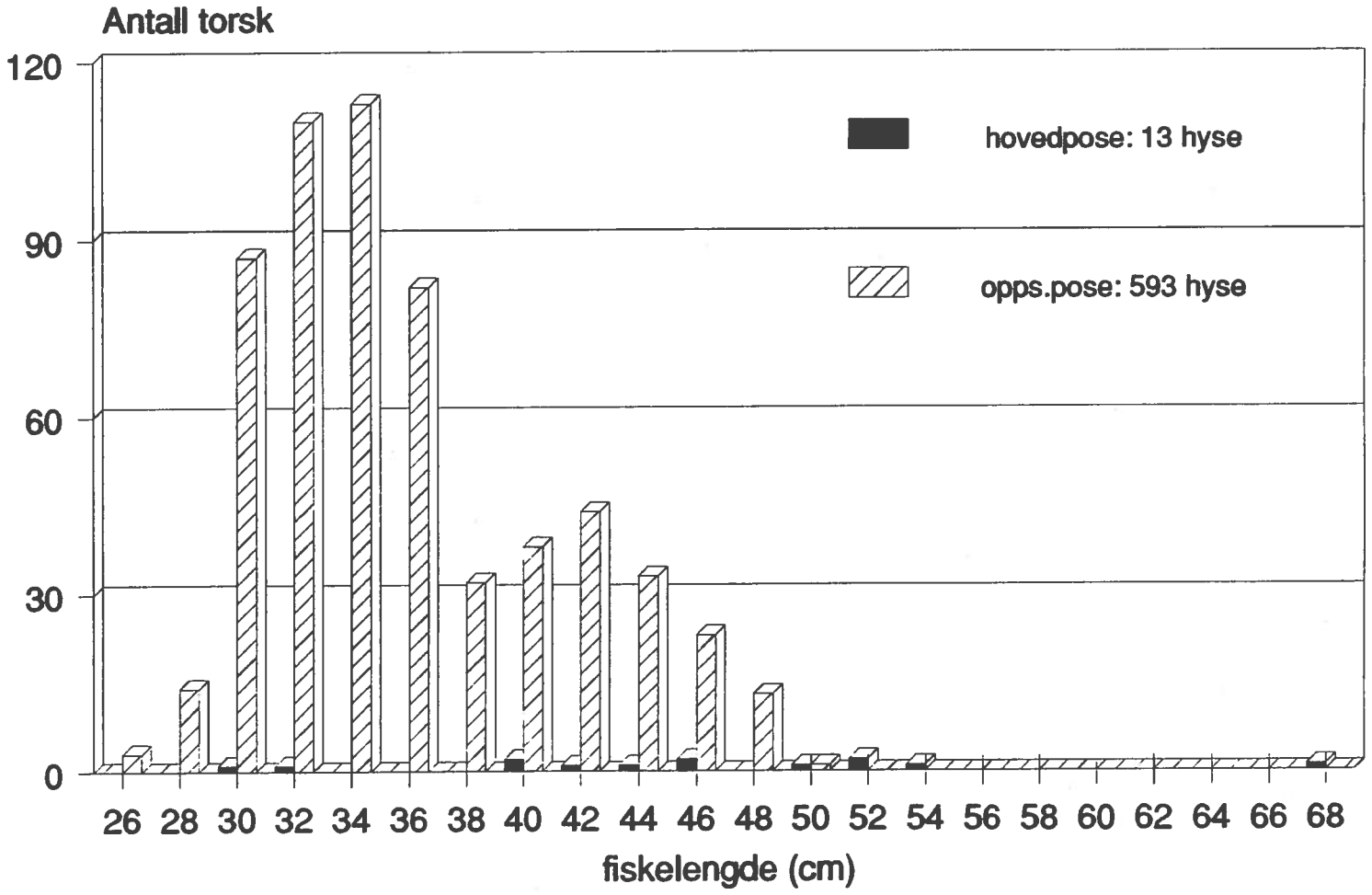

Kumulert prosent fordeling for torsk

Snurrevadforsøk, juni 1991, Heidi Anita

135 mm PE pose vs. 55 mm sort.rist

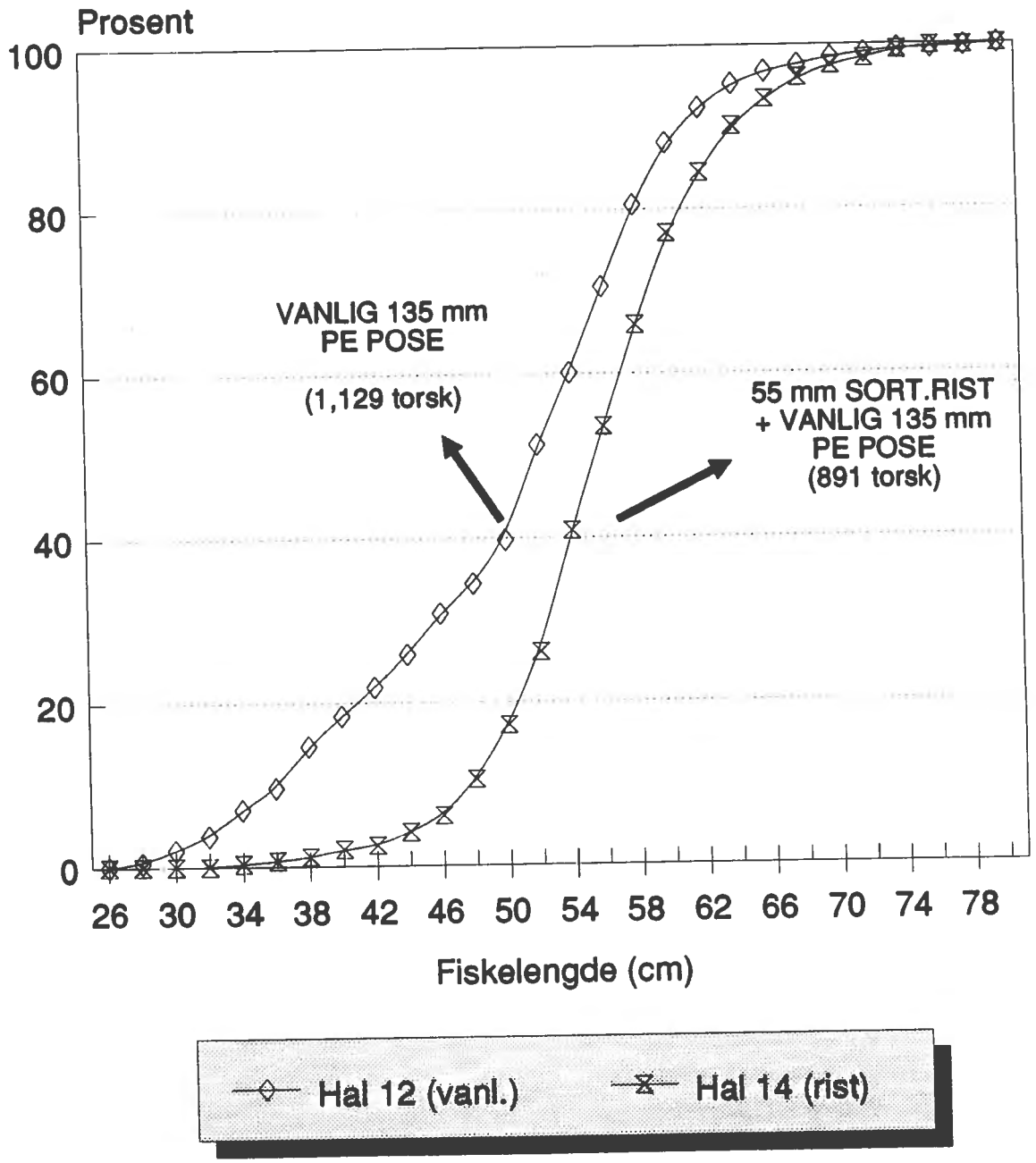

Isaksen & Larsen 1991

Kumulert prosent fordeling for hyse

Snurrevadforsøk, juni 1991, Heidi Anita

135 mm PE pose vs. 55 mm sort.rist

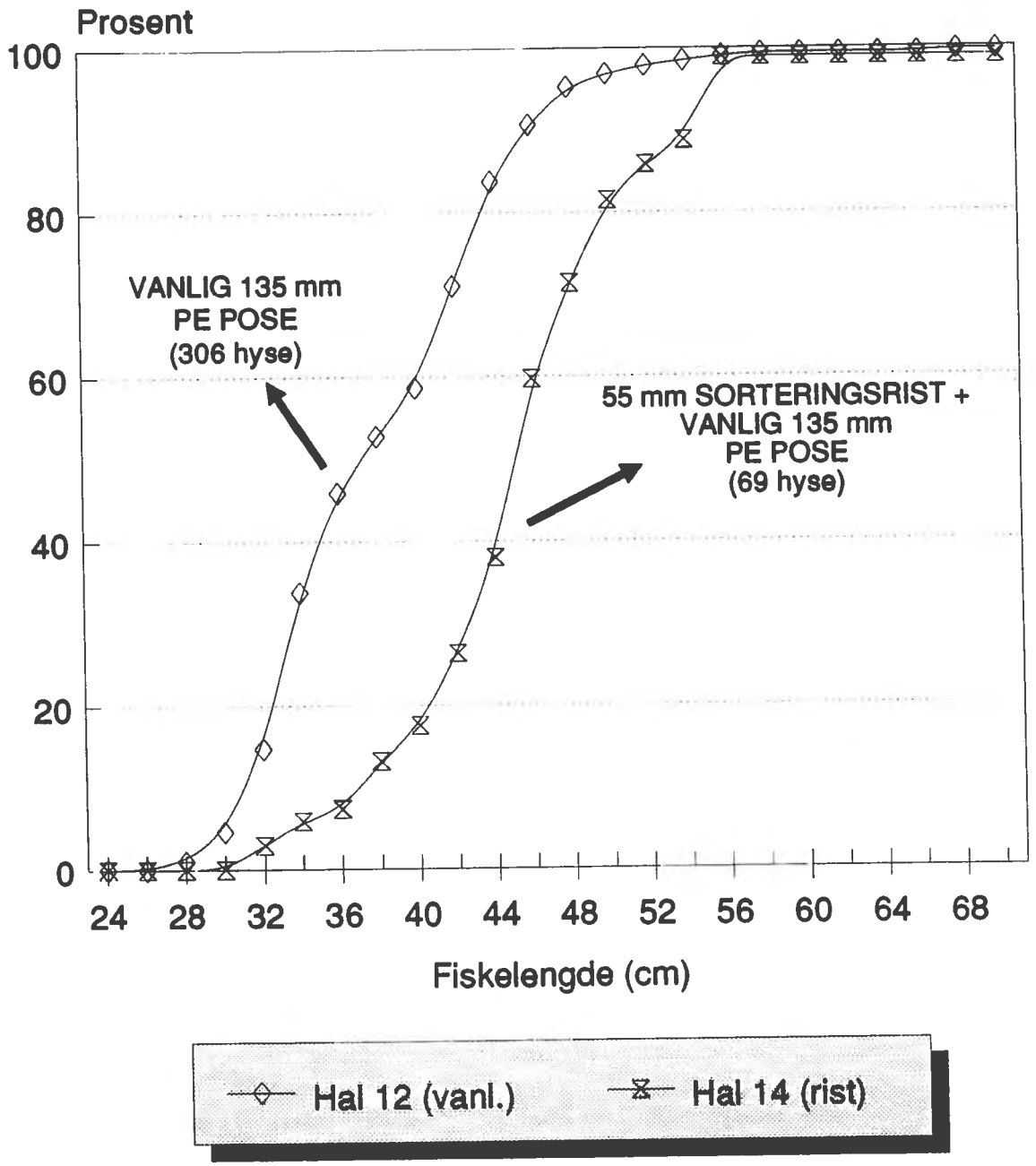

Isaksen & Larsen 1991

Størrelses-fordeling for torsk

Snurrevad med 55 mm sort.rist, hal 13-15

M/S "Heidi Anita" T-100-T 21. Juni 1991

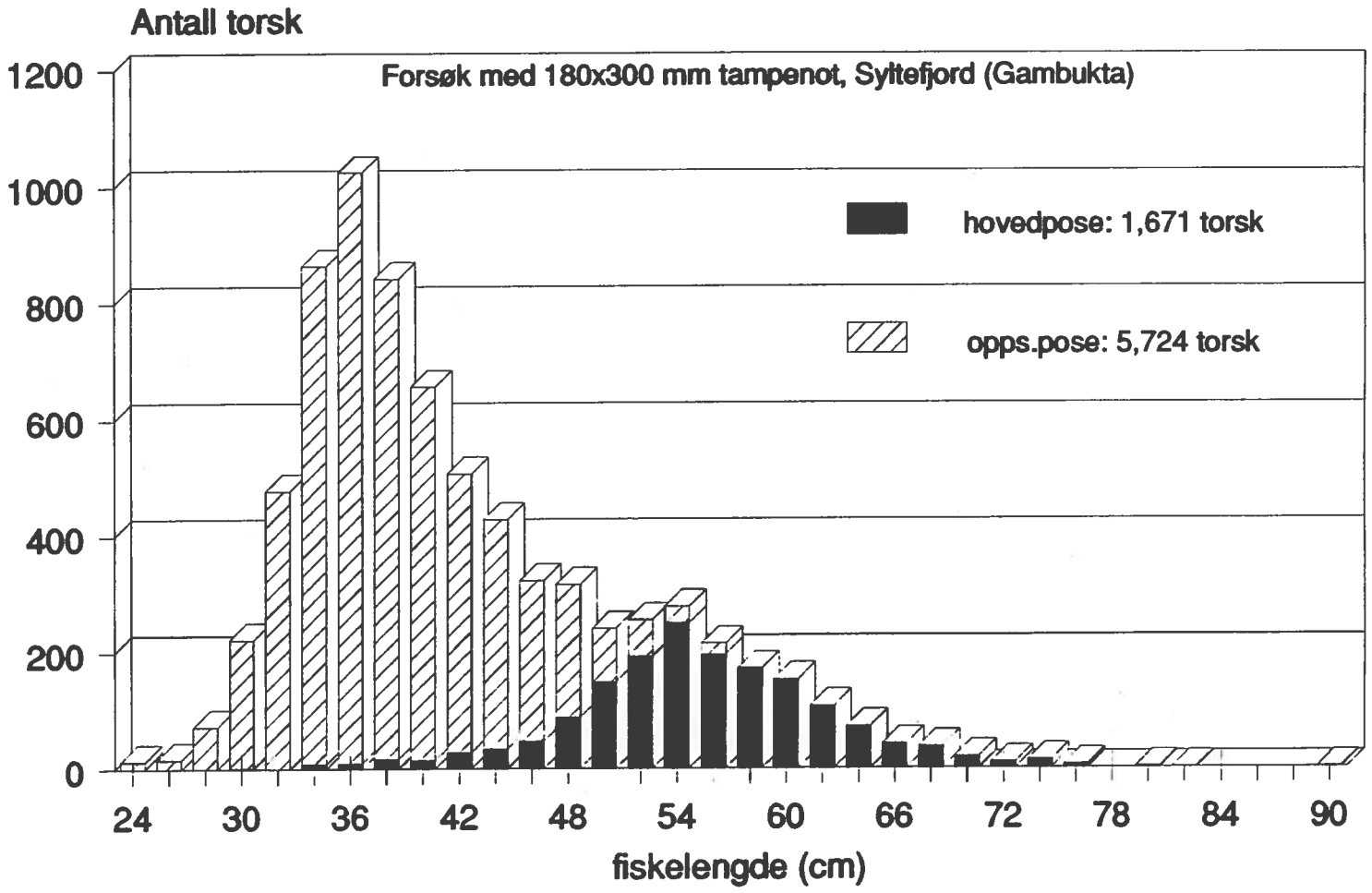

Isaksen & Larsen 1991

Størrelses-fordeling for hyse

Snurrevad med 55 mm sort.rist, hal 13-15

M/S "Heidi Anita" T-100-T, 21. Juni 1991

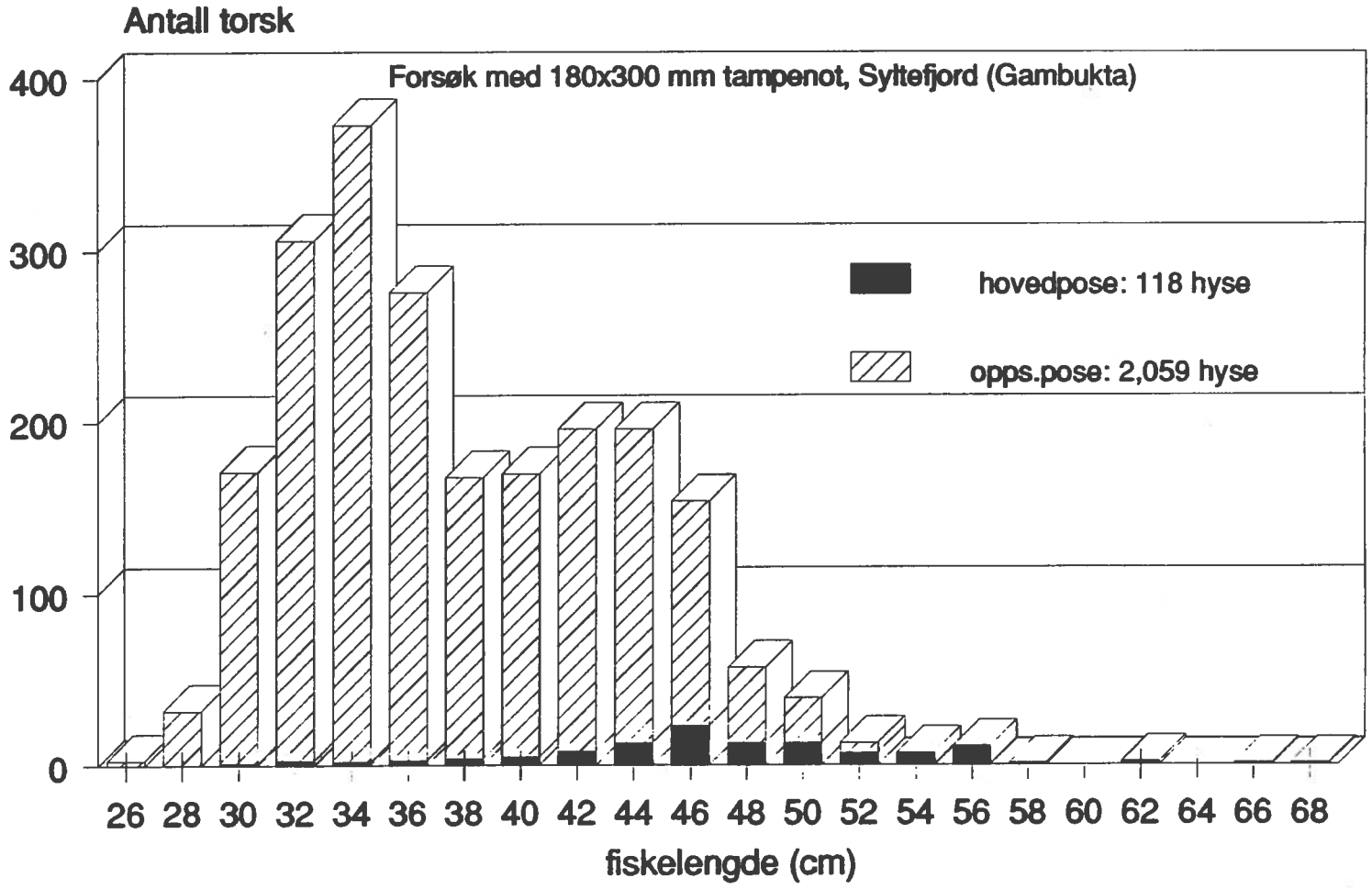

Isaksen & Larsen 1991

Lengde-frekvens fordeling for torsk
Snurrevadforsøk, 17. juni 1991
M/S "Heidi Anita"

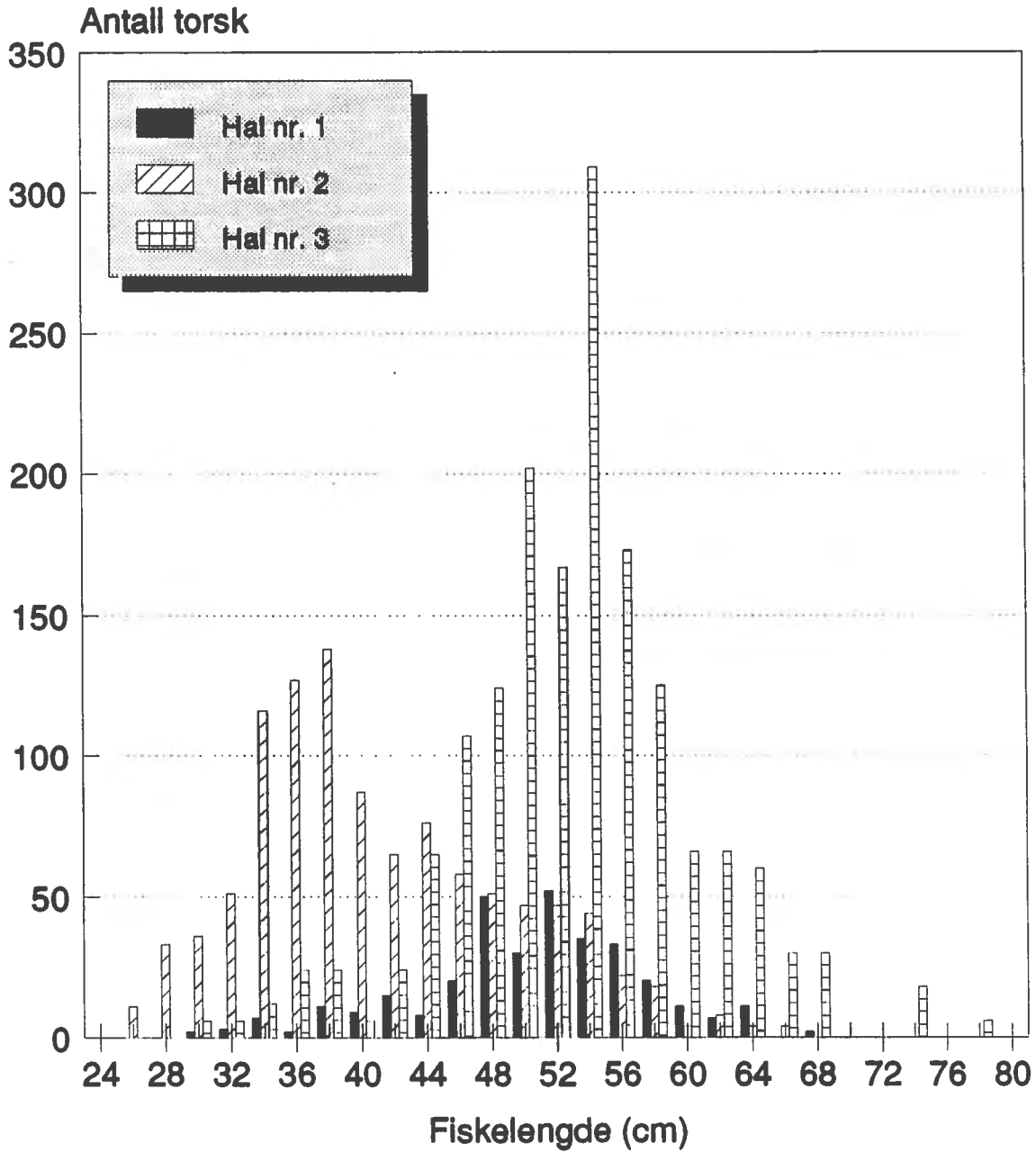

Lengde-frekvens fordeling for torsk
Snurrevadforsøk, 20. juni 1991
M/S "Heidi Anita"

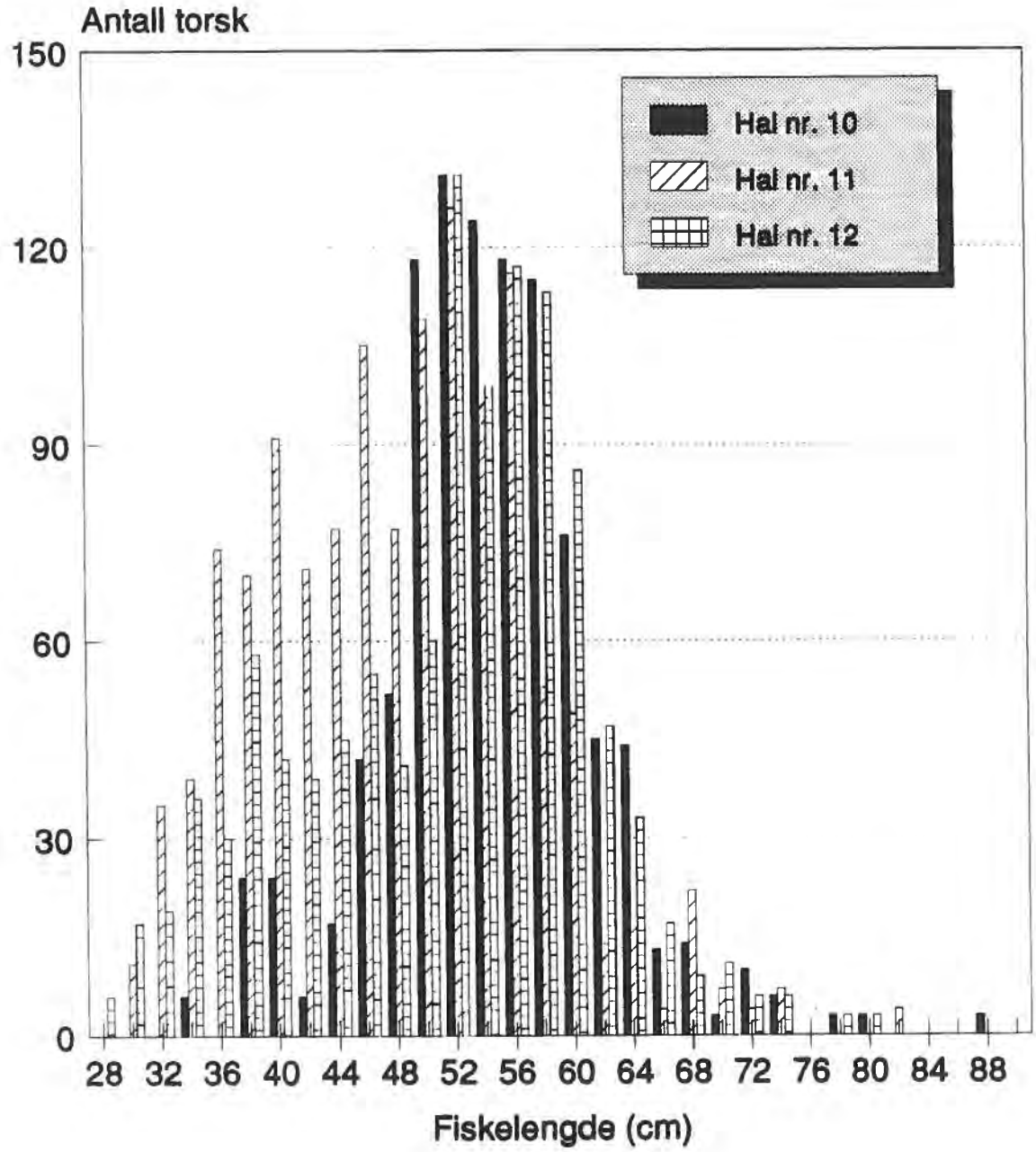

Appendix A15

The physical impact of trawl gears

The physical impact of trawl gears.

marinescotland science

Barry O’Neill and Keith Summerbell

The impact of towed fishing gears on the sea bed

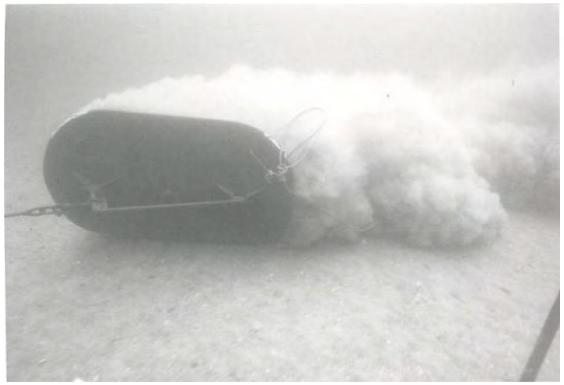

- Physical processes

- Hydrodynamic
  - sediment mobilisation

- Geotechnical
  - Penetration into the seabed
  - Forces acting on the seabed

Sediment mobilisation

- Sediment put into water column related to the hydrodynamic drag of the gear component

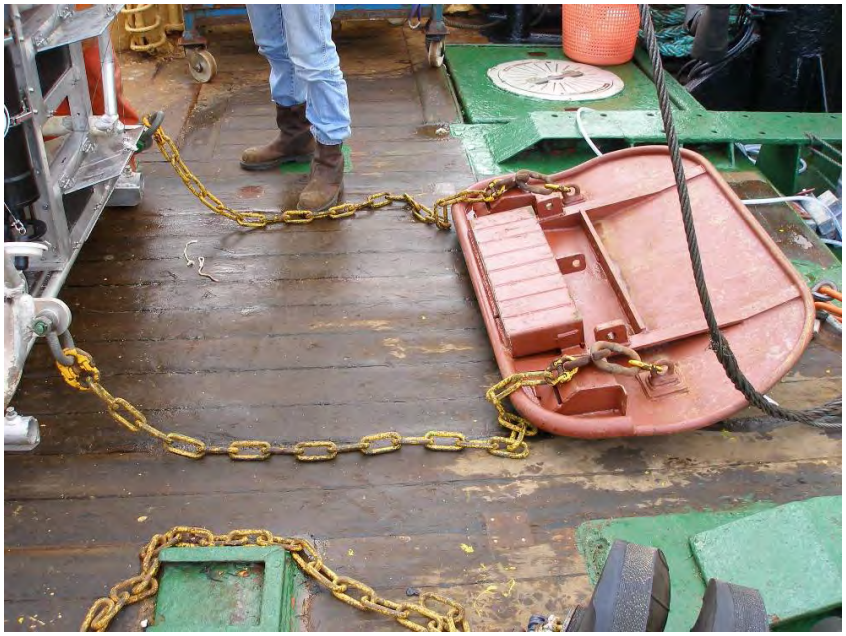

Sediment mobilisation

- The greater the drag the greater the amount of sediment mobilised
- the finer the sediment type the greater the amount mobilised

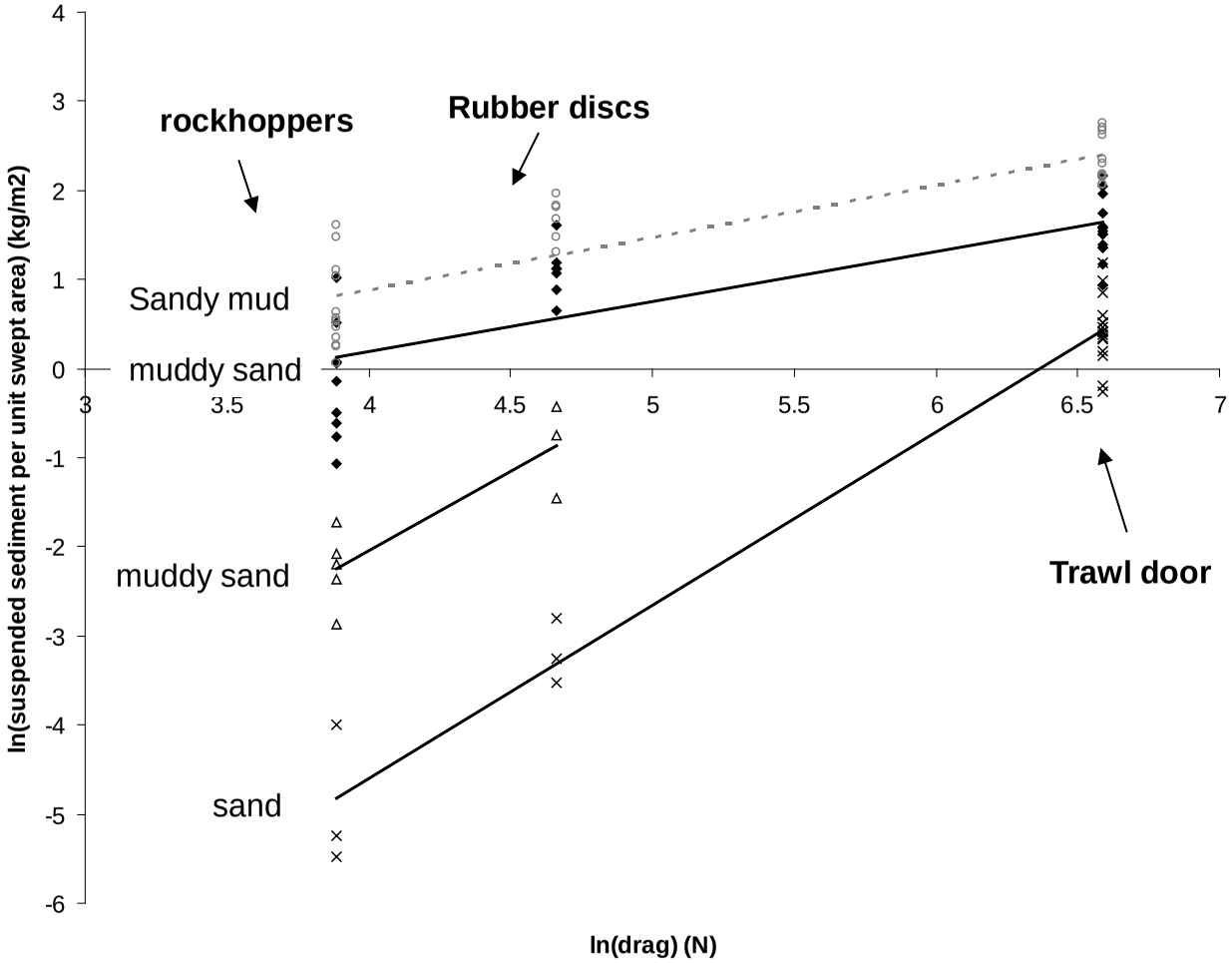

- sea trials Alba na Mara 3 -14 October
- Gear components on a towed sledge
- Measuring
  - suspension of sediment behind gear components
  - drag forces
- Investigate relationship between drag and mobilised sediment

Towing faster more sediment mobilised

Weight and penetration does not influence quantity of sediment mobilised

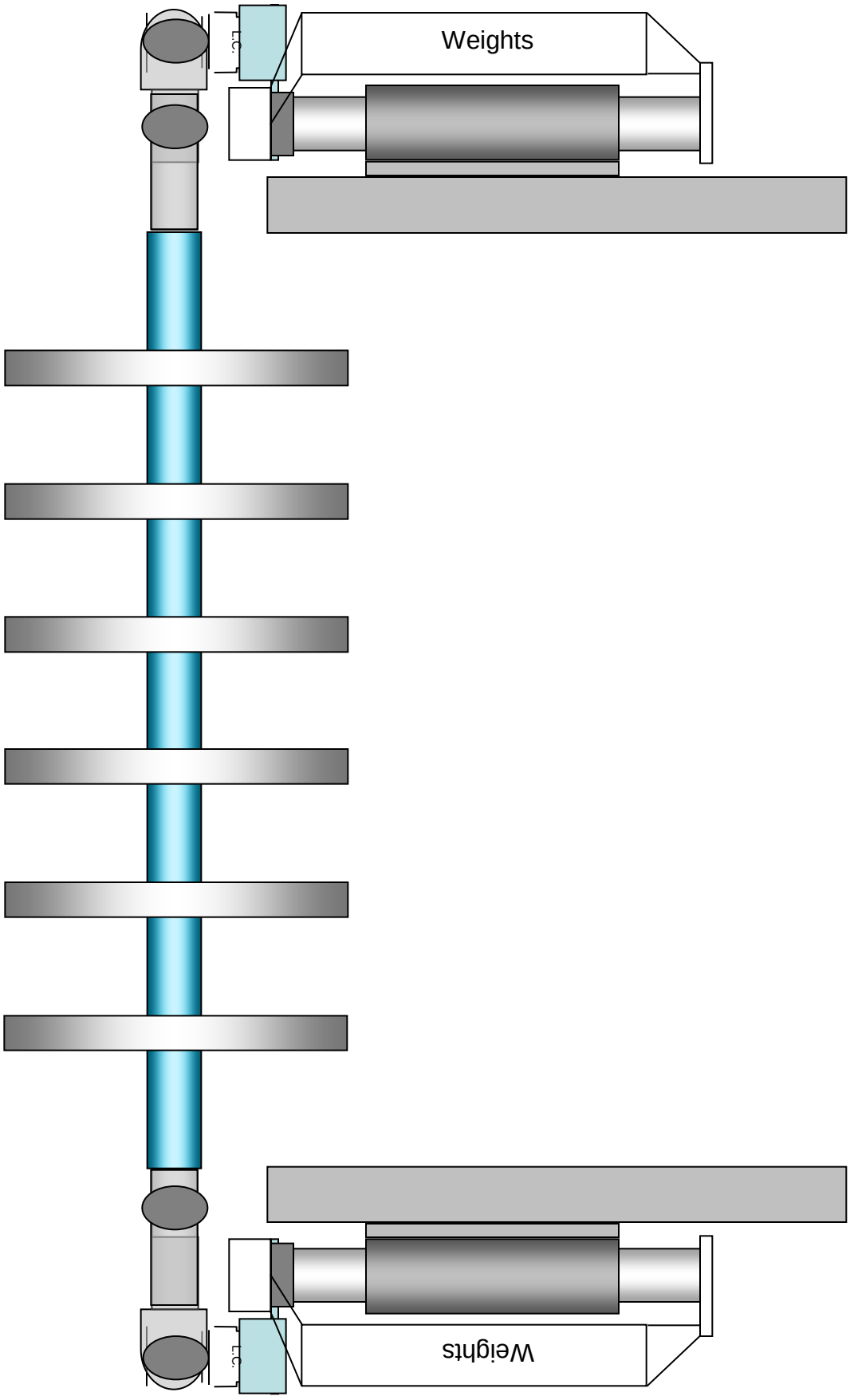
Weights
Weights

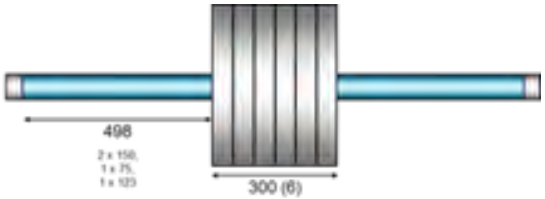
498
2 x 150,
1 x 75,
1 x 123
300 (6)

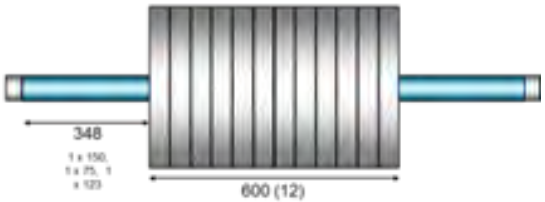
348
1 x 150,
1 x 75, 1
x 123
600 (12)


63

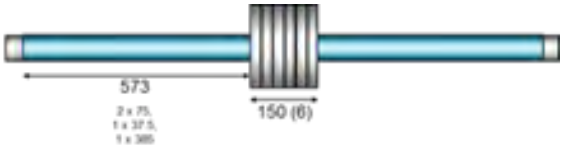
573
2 x 75,
1 x 37.5,
1 x 385
150 (6)

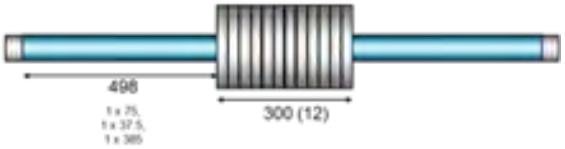
498
1 x 75,
1 x 37.5,
1 x 385
300 (12)

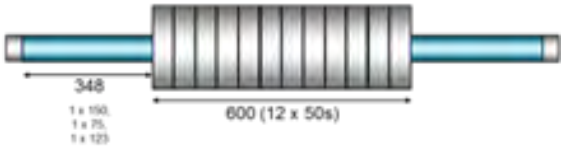
348
1 x 150,
1 x 75,
1 x 123
600 (12 x 50s)

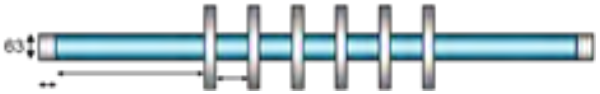
63

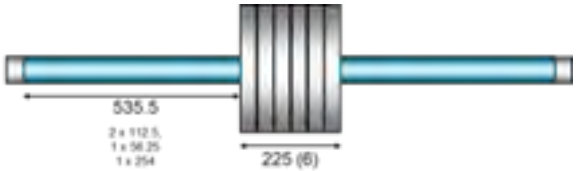
535.5
2 x 112.5,
1 x 56.25
1 x 254
225 (6)

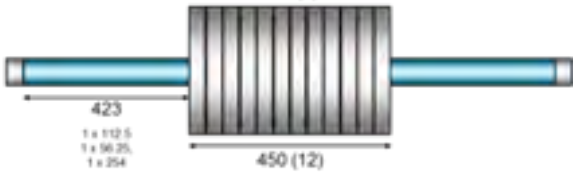
423
1 x 112.5
1 x 56.25,
1 x 254
450 (12)

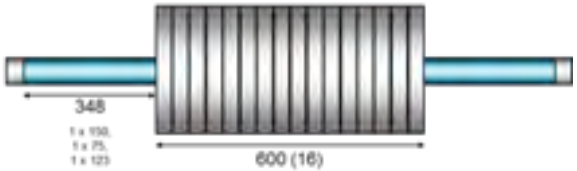
348
1 x 150,
1 x 75,
1 x 123
600 (16)

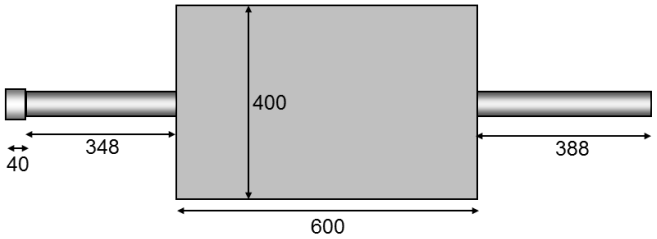
400
348
388
40
600

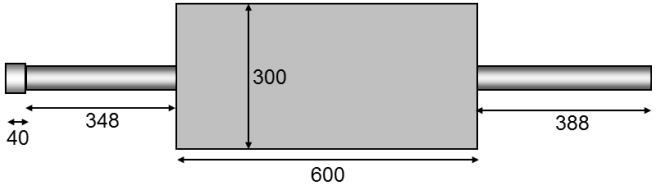
300
348
388
40
600

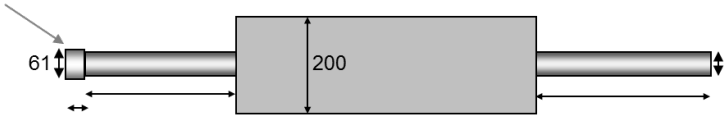
61
200

- Not touching the sea bed (tied up)
  - Hydrodynamic only
- Three different weights
  - ~ 60, 120, 180kg
  - Hydrodynamic and geotechnical
- Range of speeds
  - ~ 1 – 2 ms^{-1}
- Fixed and rolling
- sediment in wake and drag

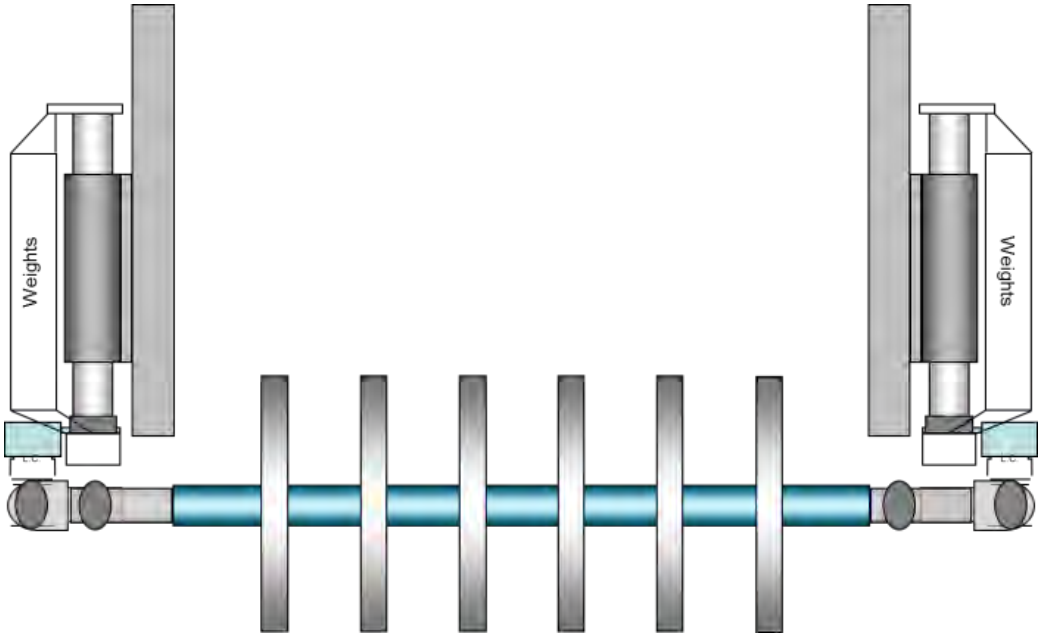


10/10/11
16:41:31

- Not touching the sea bed (tied up)
  - Hydrodynamic drag
- Touching the sea bed
  - ~ 60, 120, 180kg
  - Combined hydrodynamic and geotechnical drag
  - Sediment in the water column
- Relate hydrodynamic drag to sediment in the plume
- Relate geotechnical drag to weight

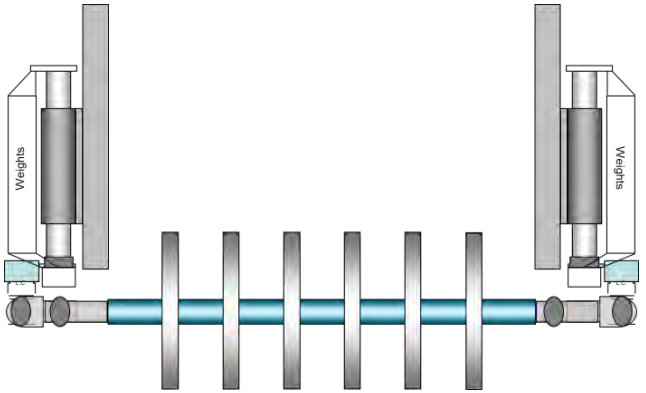

Hydrodynamics and mobilisation of sediment

- Hydrodynamic drag

- 10 sec averaged measurements
  - –Speeds 1 – 2 ms^{-1}
  - –8 configurations for cylindrical block
  - –3 configurations for spaced disks
  - –3 configurations for rectangular doors

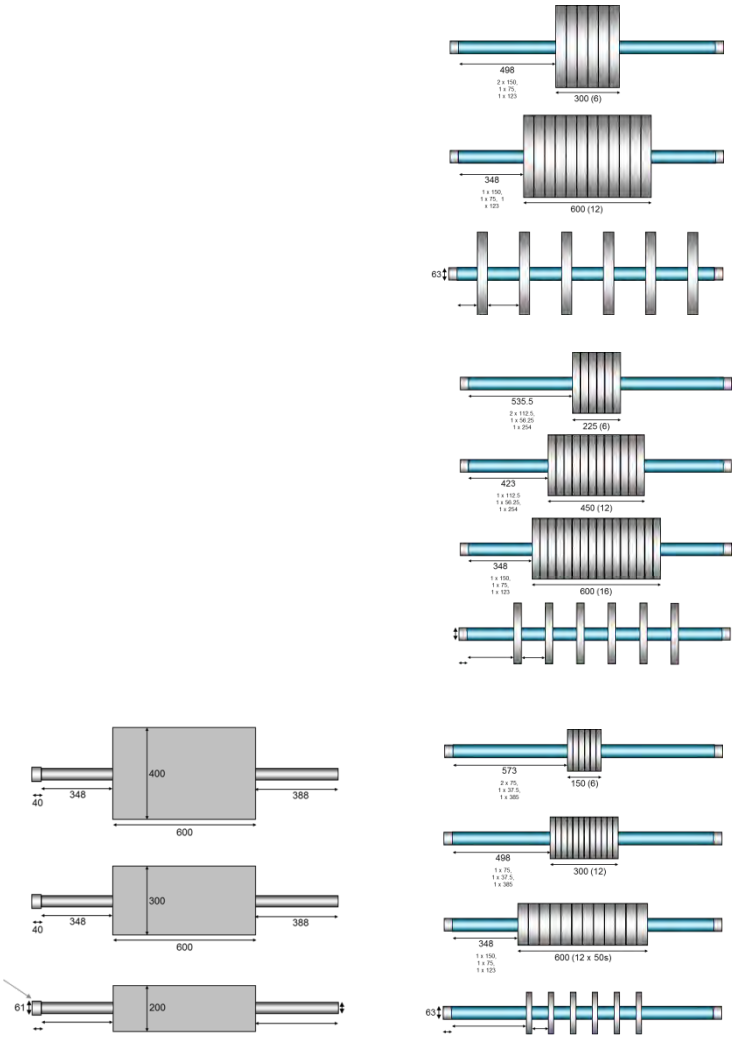

Hydrodynamic drag vs speed

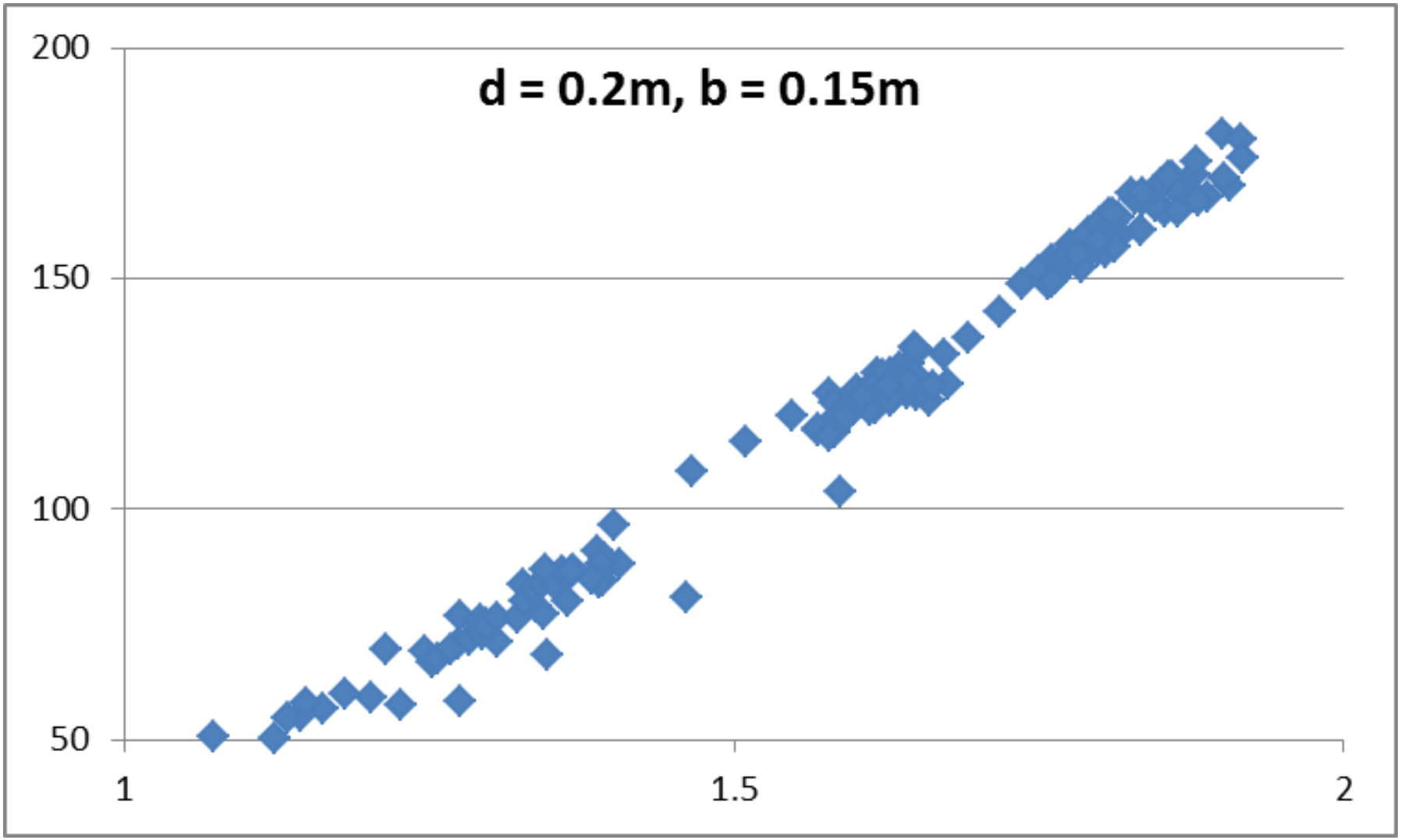

Hydrodynamic drag

$$D = 0.5\rho C_d A U^2$$

C_d – hydrodynamic drag coefficient

$$D = 0.5\rho C_d A_d U^2 + 0.5\rho C_{axel} A_{axel} U^2$$

C_{cyl} C_{disk} C_{door} C_{axel}

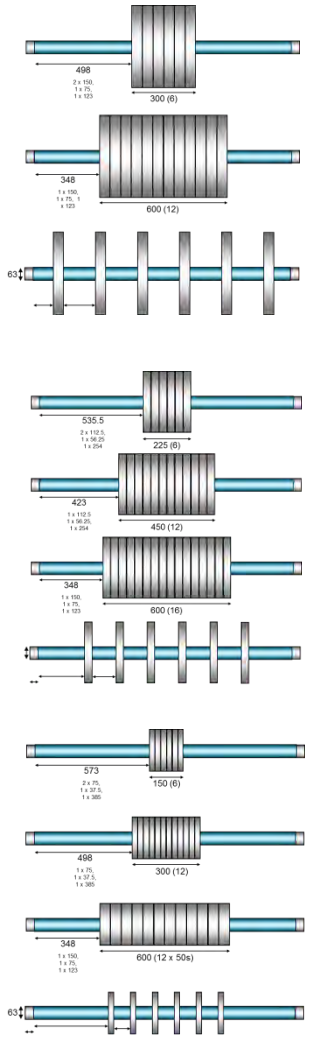

Hydro drag vs speed cylindrical blocks

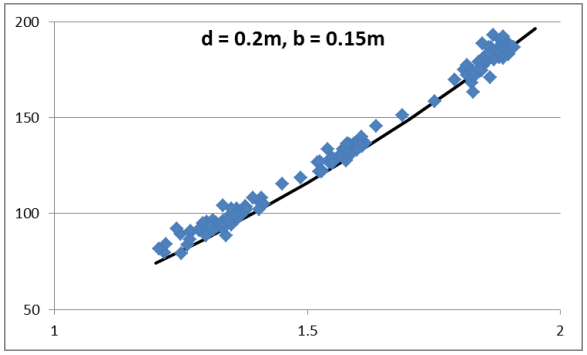

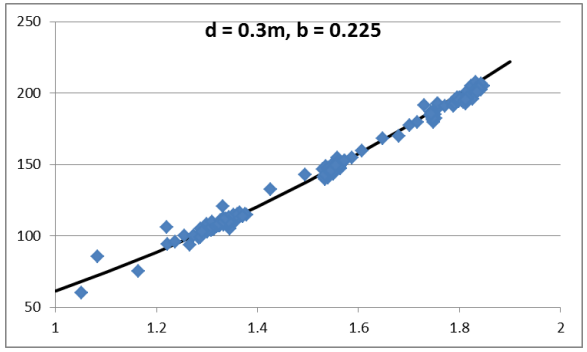

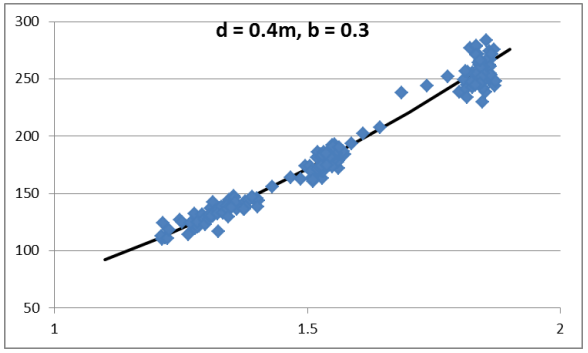

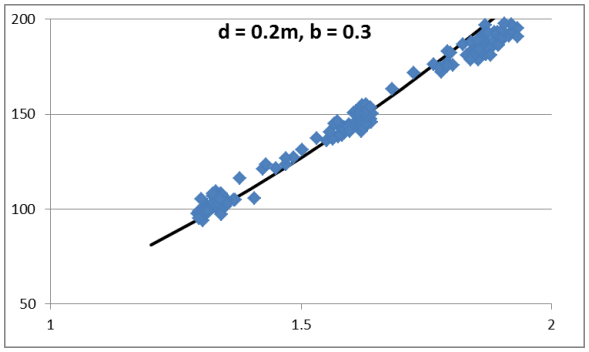

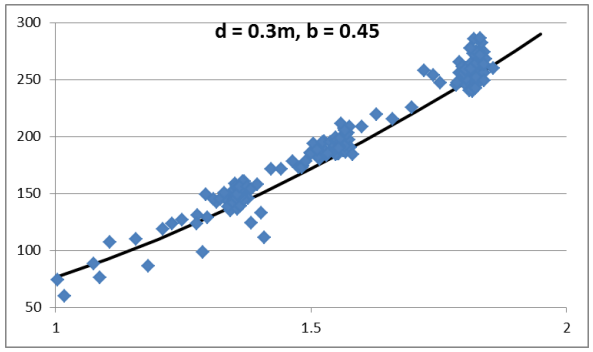

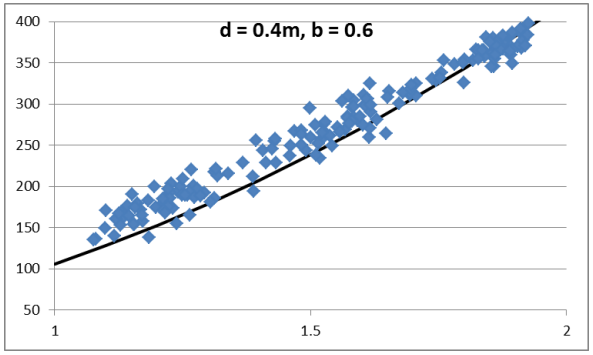

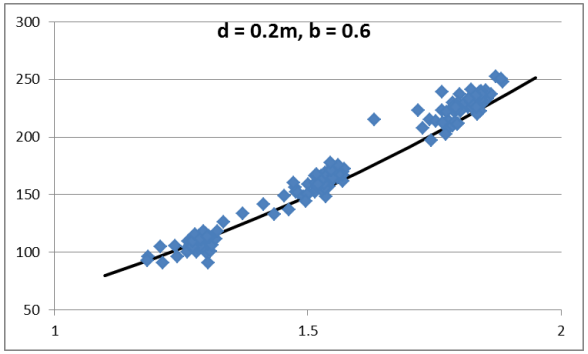

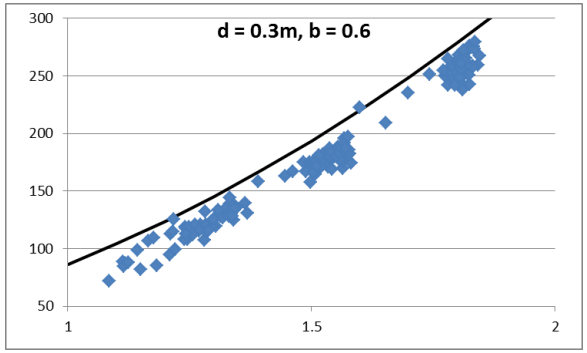

Hydrodynamic drag

marinescotland science

- Drag coefficient values very similar to what is in the engineering literature
- Confidence in assumptions made in previous studies
- Confidence in methodology and load cells

Hydrodynamics and mobilisation of sediment

marinescotland science

LISST 100X

- Particle size analyser
- Laser diffraction principle
- Volume concentration of 32 particle size bins between 2.5 and 500 microns
- In situ readings @ 1Hz

Hydrodynamics and mobilisation of sediment

marinescotland science

The greater the hydrodynamic drag the greater the amount of sediment mobilised

Weight and penetration does not influence quantity of sediment Mobilised

Weights ~ 60, 120 and 180kg
Speeds ~ 1 – 2 ms^{-1}

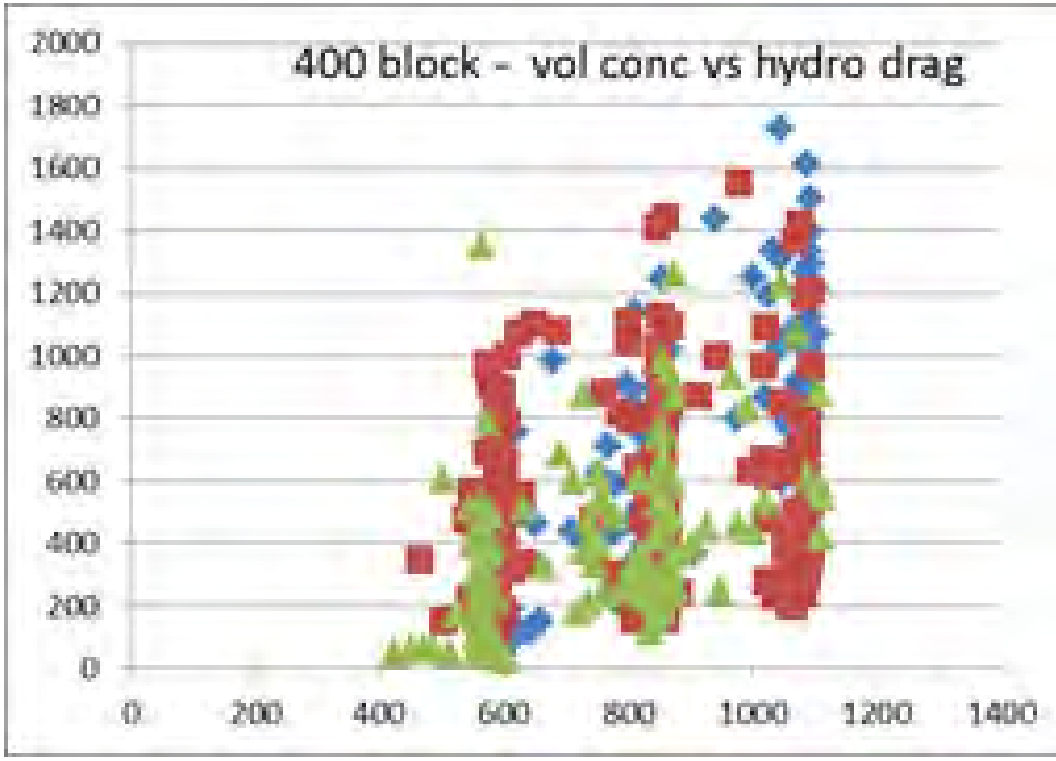

Hydrodynamics and mobilisation of sediment

marinescotland science

Concentration vs hydro drag

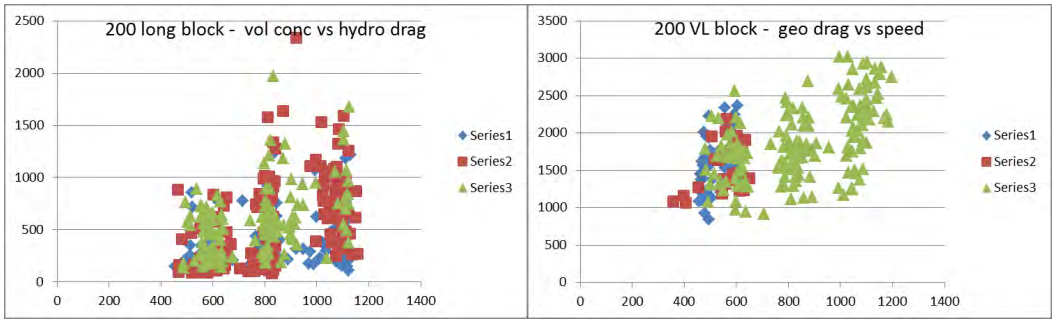

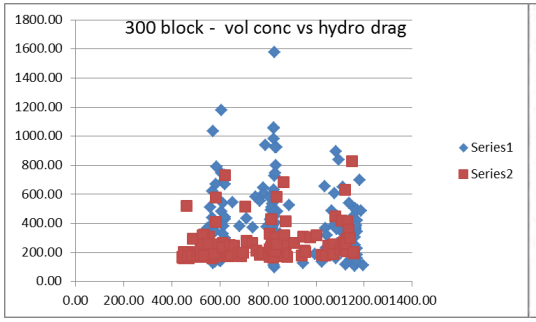

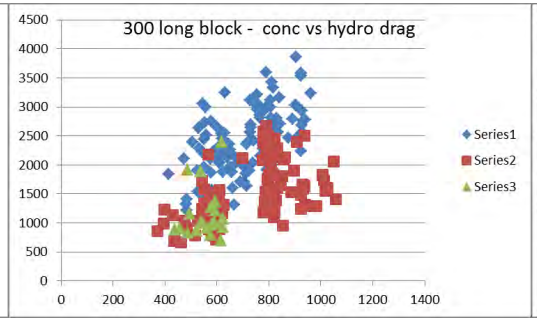

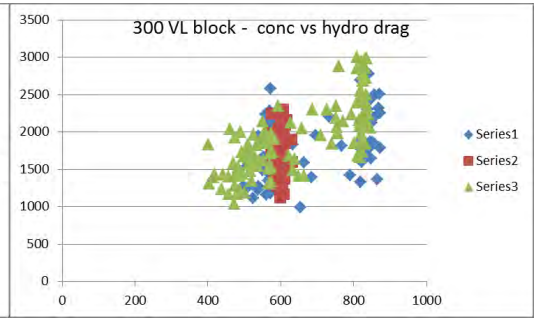

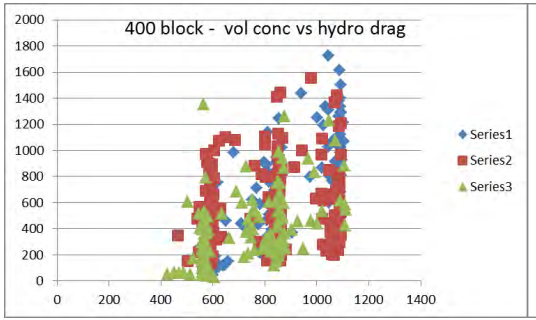

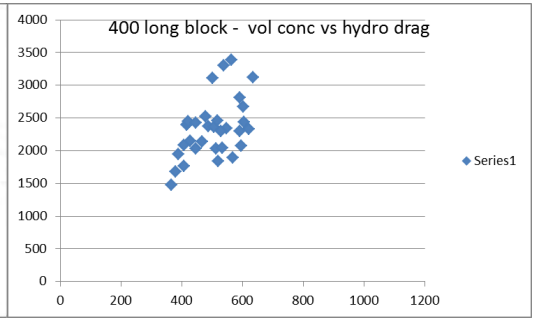

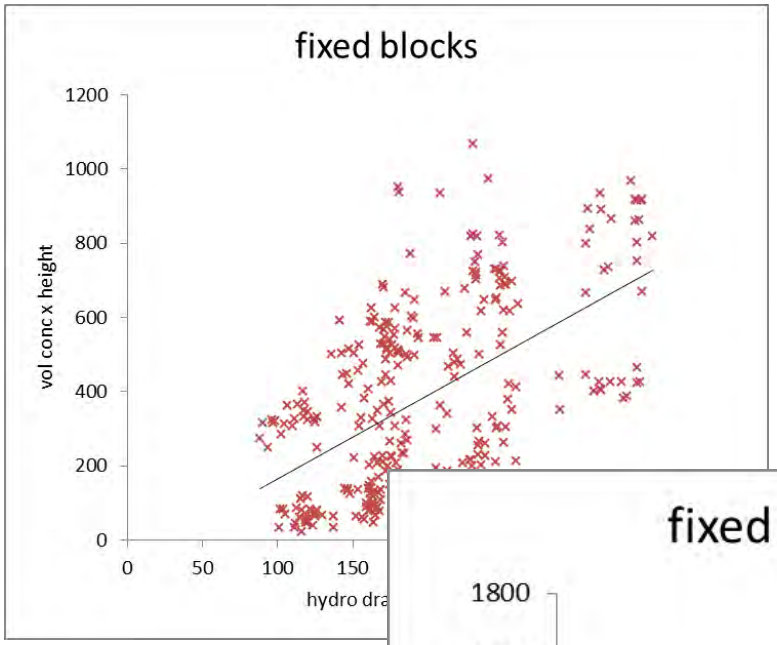
fixed blocks
vol conc x height
0
200
400
600
800
1000
1200
0
50
100
150
hydro dra

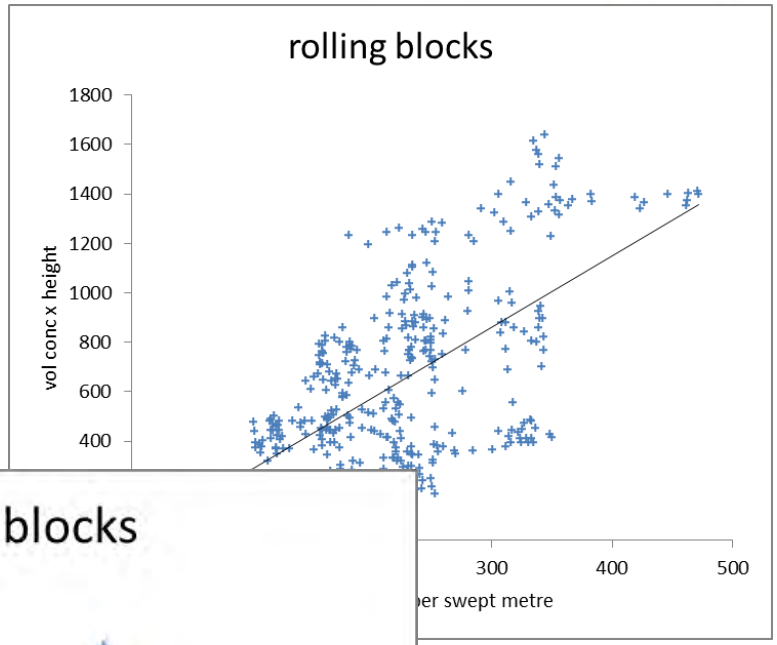
rolling blocks
vol conc x height
400
600
800
1000
1200
1400
1600
1800
300
400
500
er swept metre

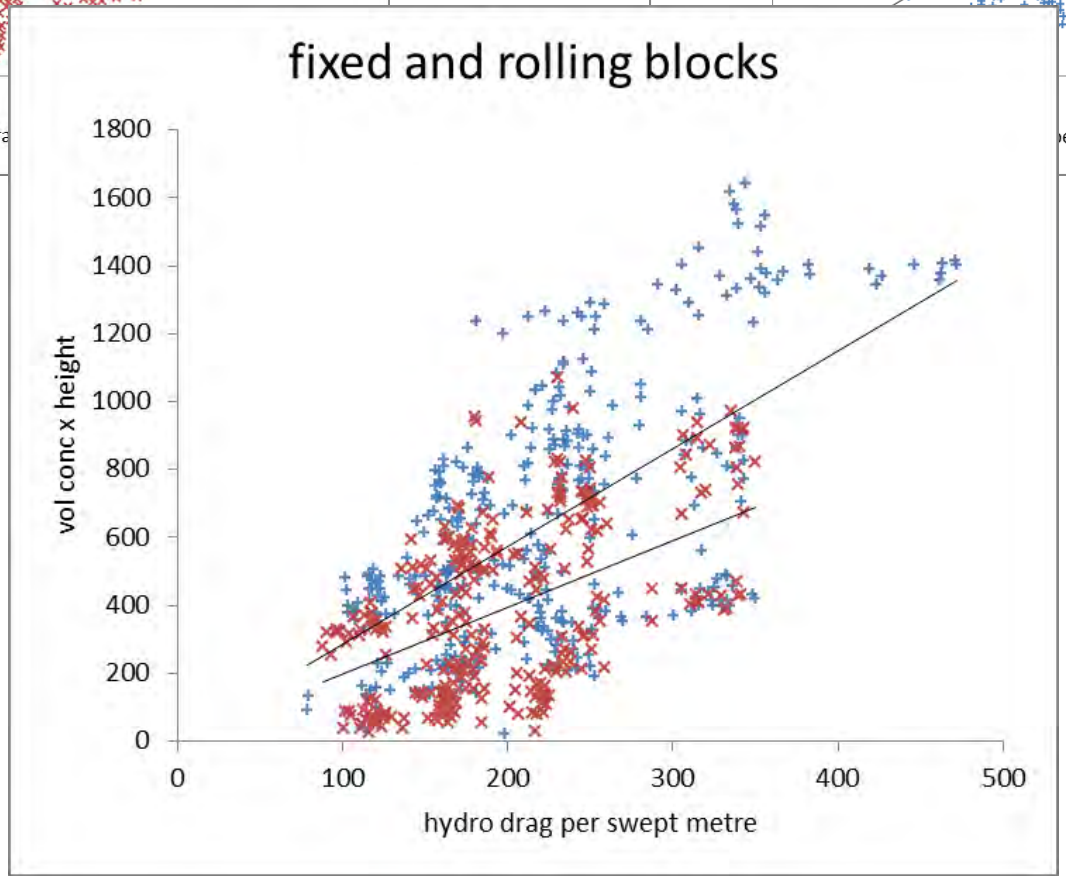
fixed and rolling blocks
vol conc x height
0
200
400
600
800
1000
1200
1400
1600
1800
0
100
200
300
400
500
hydro drag per swept metre

Geotechnical drag

- Drag = geotechniclal drag + hydrodynamic drag
  - Weights ~ 60, 120 and 180kg
- 10 sec averaged measurements
  - Weights ~ 60, 120 and 180kg
  - Speeds 1 – 2 ms^{-1}
  - 8 configurations for cylindrical block
  - 3 configurations for spaced disks
  - 3 configurations for rectangular doors
  - Fixed and rolling

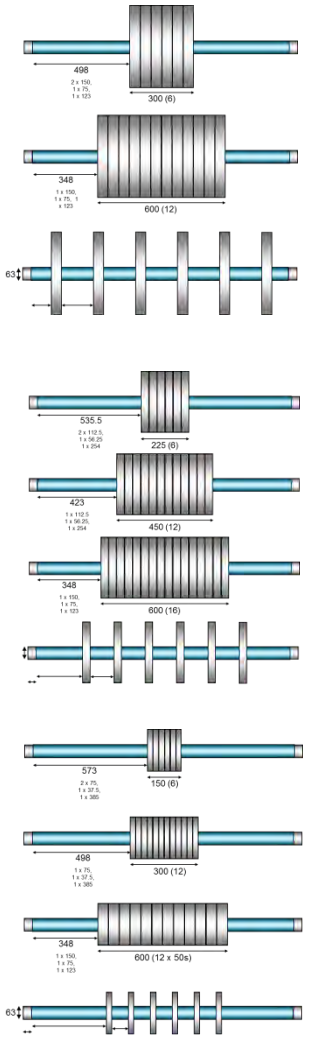

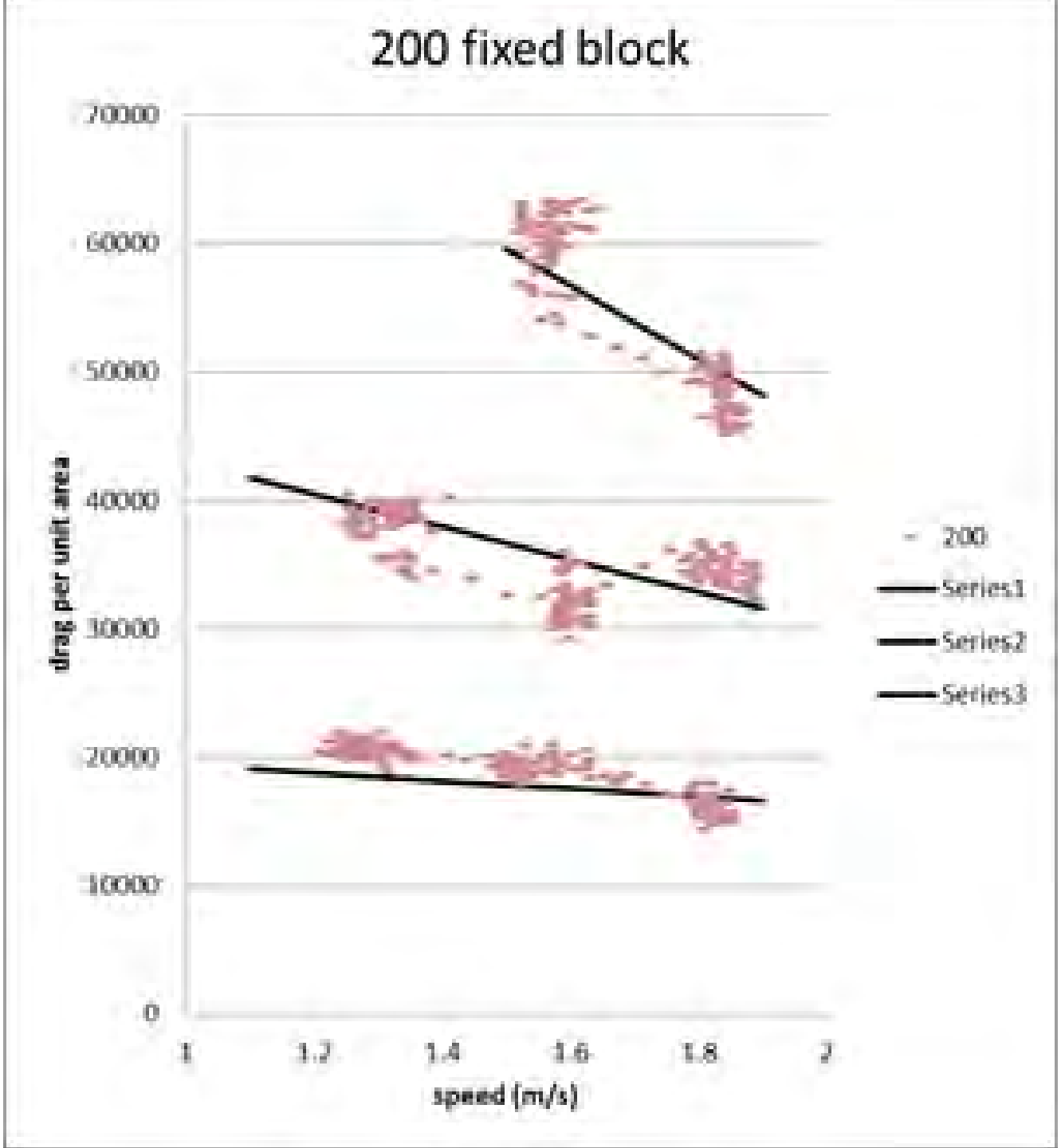
200 fixed block
70000
60000
50000
40000
30000
20000
10000
0
drag per unit area
1
1.2
1.4
1.6
1.8
2
speed (m/s)
200
Series1
Series2
Series3

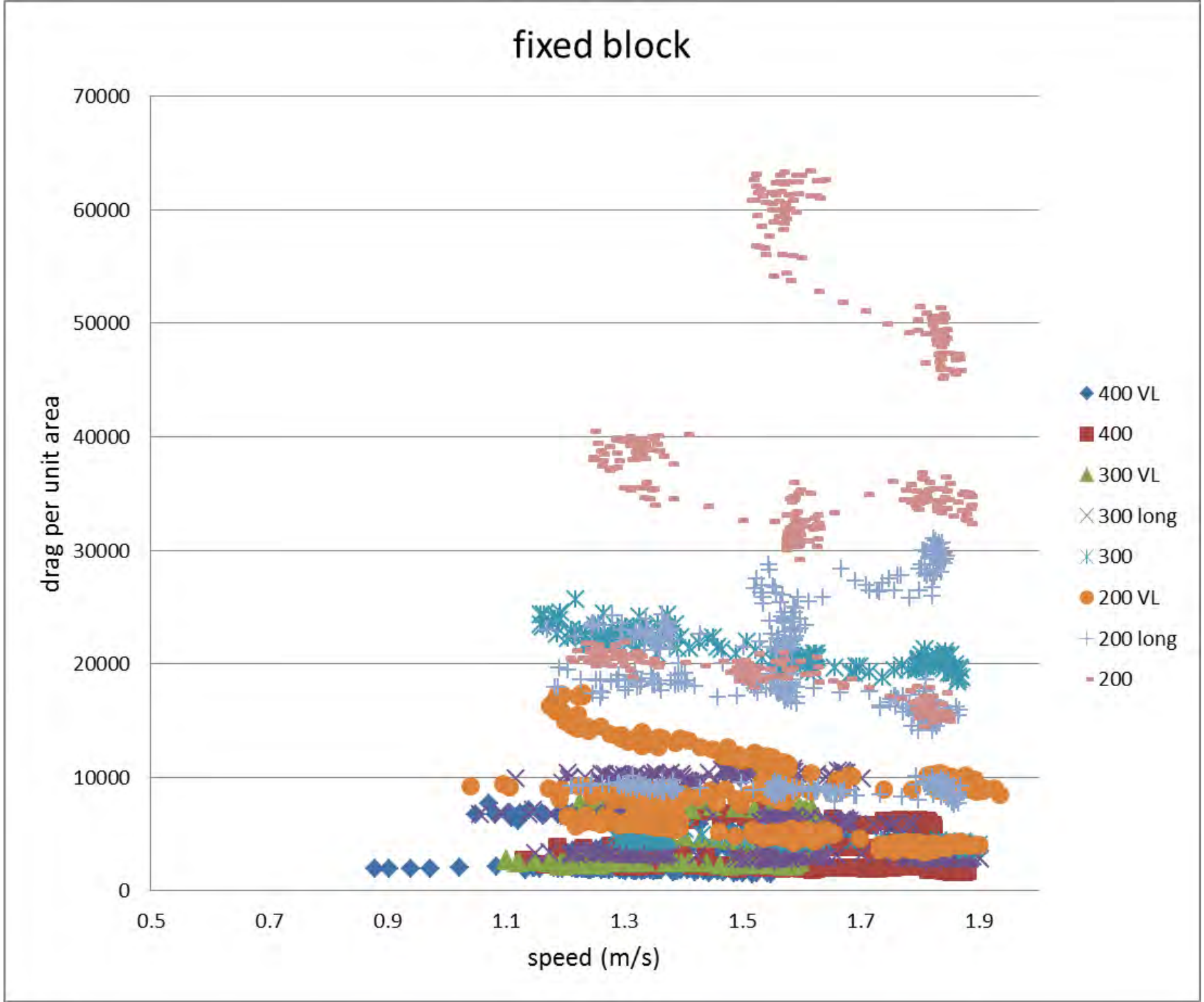
fixed block
70000
60000
50000
40000
30000
20000
10000
0
drag per unit area
0.5
0.7
0.9
1.1
1.3
1.5
1.7
1.9
speed (m/s)
400 VL
400
300 VL
300 long
300
200 VL
200 long
200

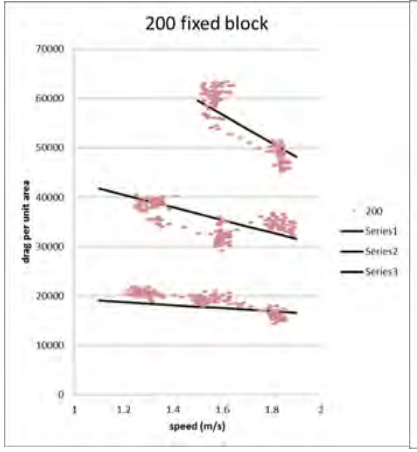
200 fixed block
drag per unit area
speed (m/s)
200
Series1
Series2
Series3

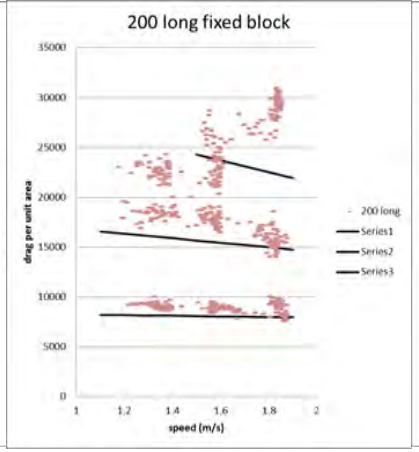
200 long fixed block
drag per unit area
speed (m/s)
200 long
Series1
Series2
Series3

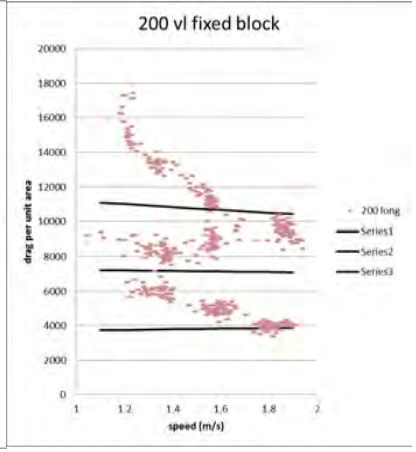
200 vl fixed block
drag per unit area
speed (m/s)
200 long
Series1
Series2
Series3

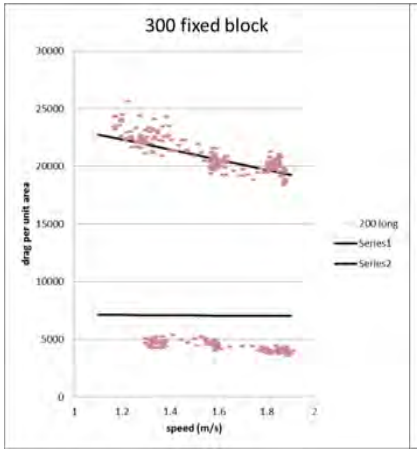
300 fixed block
drag per unit area
speed (m/s)
200 long
Series1
Series2

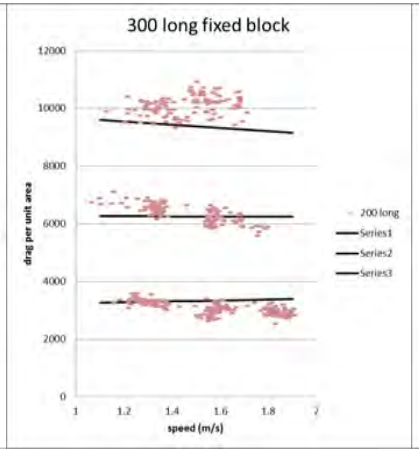
300 long fixed block
drag per unit area
speed (m/s)
200 long
Series1
Series2
Series3

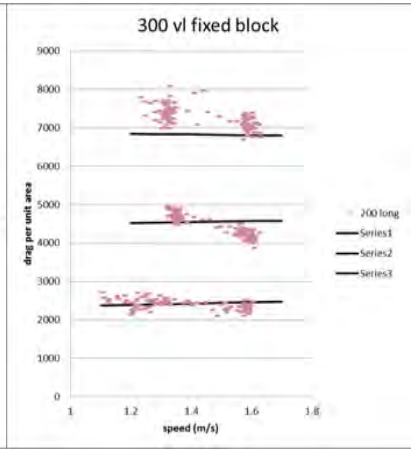
300 vl fixed block
drag per unit area
speed (m/s)
200 long
Series1
Series2
Series3

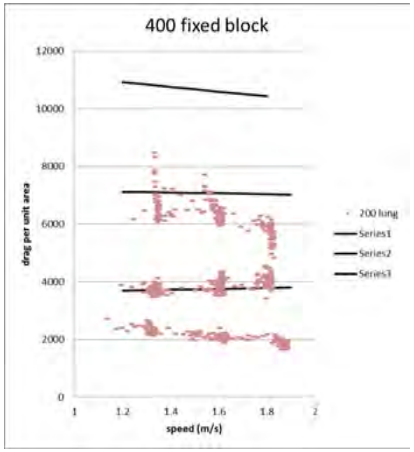
400 fixed block
drag per unit area
speed (m/s)
200 long
Series1
Series2
Series3

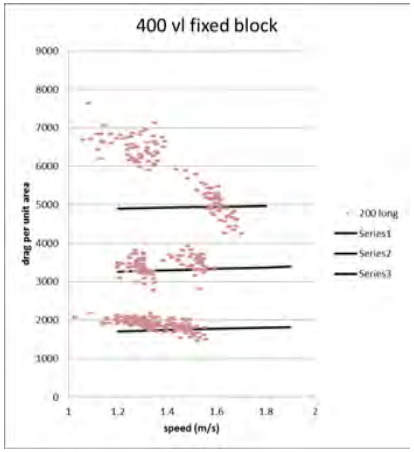
400 vl fixed block
drag per unit area
speed (m/s)
200 long
Series1
Series2
Series3

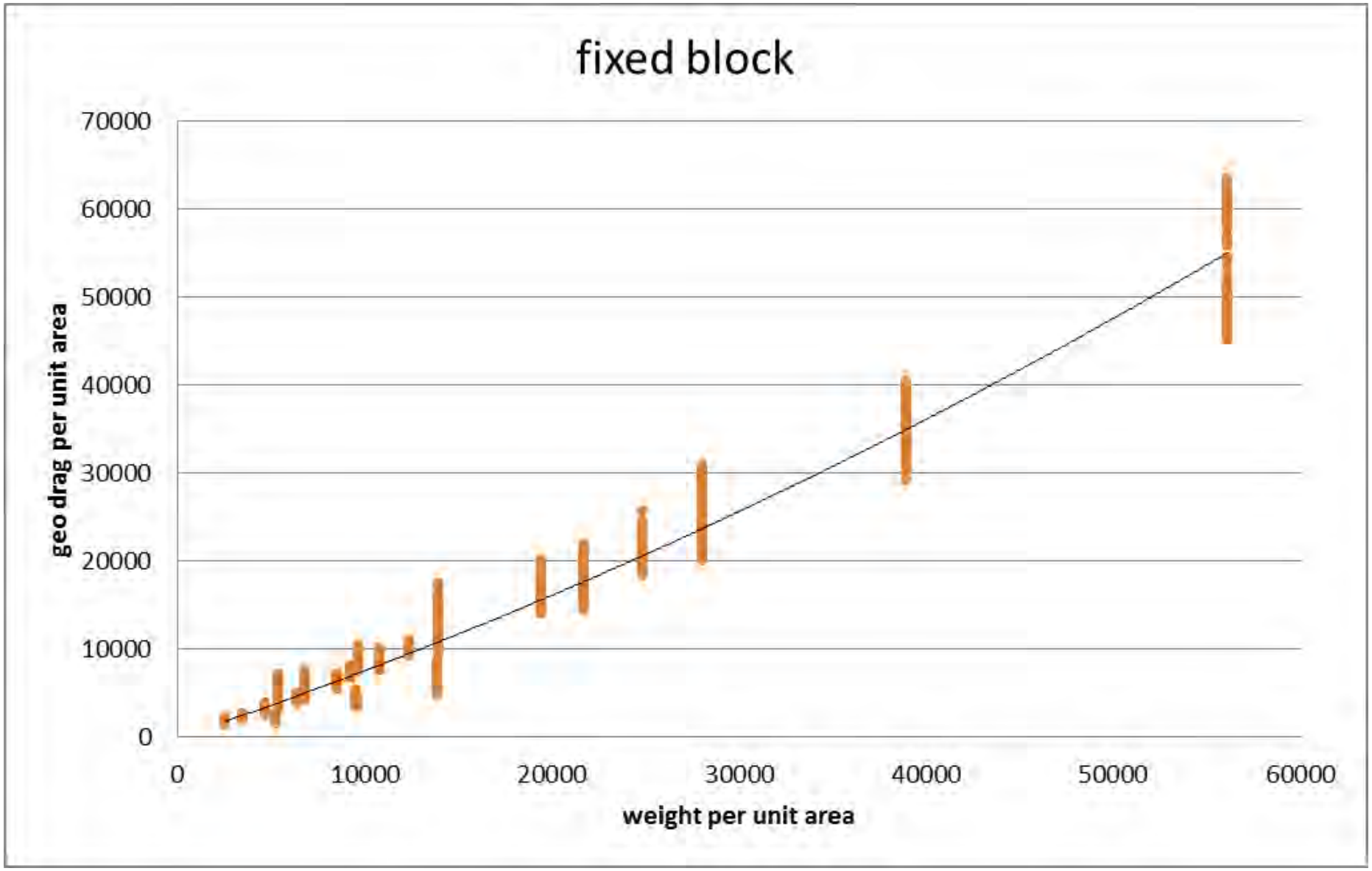
fixed block
70000
60000
50000
40000
30000
20000
10000
0
geo drag per unit area
0
10000
20000
30000
40000
50000
60000
weight per unit area

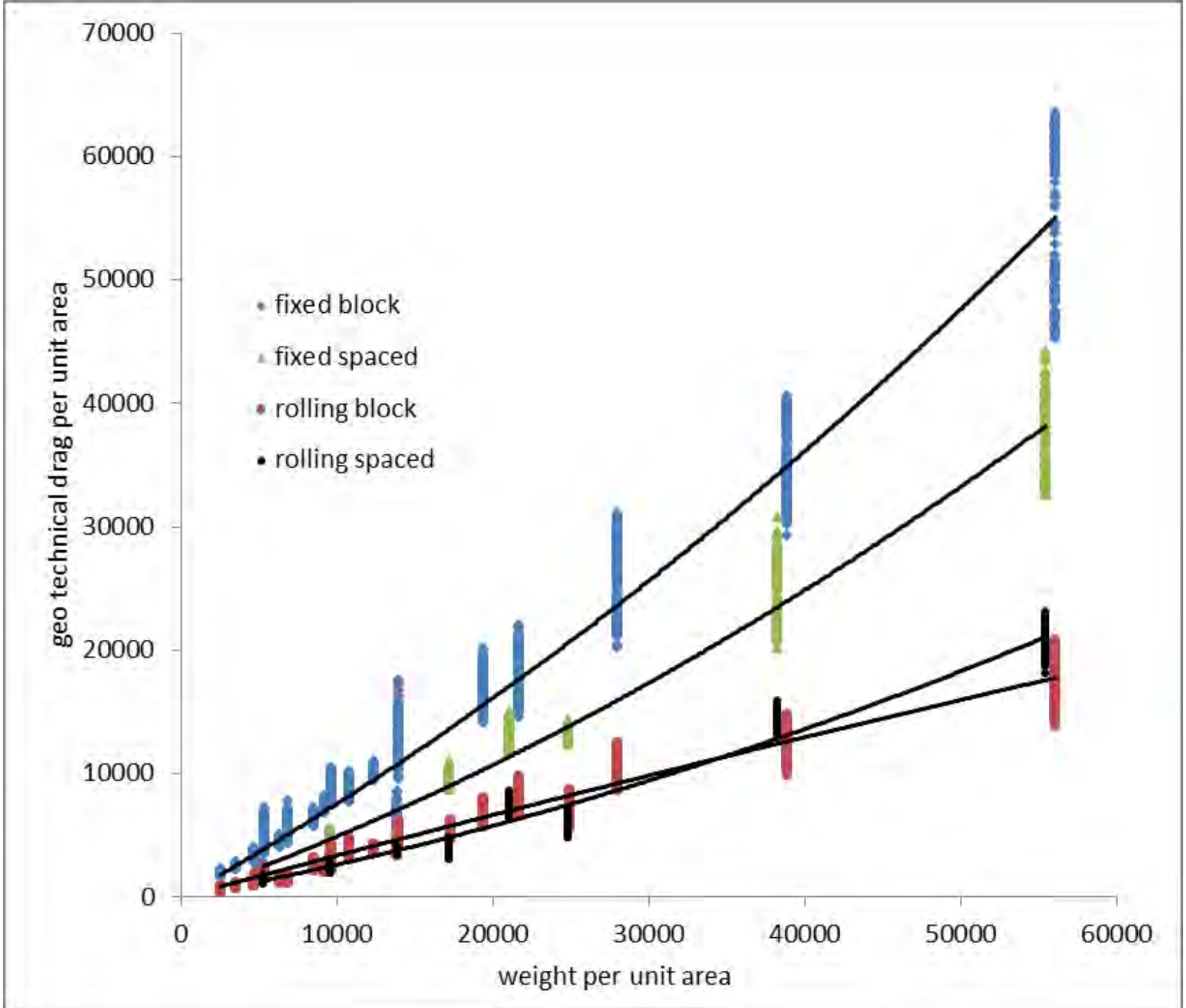
70000
60000
50000
40000
30000
20000
10000
0
geo technical drag per unit area
fixed block
fixed spaced
rolling block
rolling spaced
0
10000
20000
30000
40000
50000
60000
weight per unit area

Geotechnical drag

- geotechnical drag per unit area ~ weight per unit area
  - Secondary effect related to towing speed (but maybe only for fixed heavier components)
- Differences between rolling and fixed components

- For rolling cylinders geotechnical processes are 2 dimensional
- For wider fixed cylinders geotechnical processes are 2 dimensional
- But perhaps not for thinner fixed disks

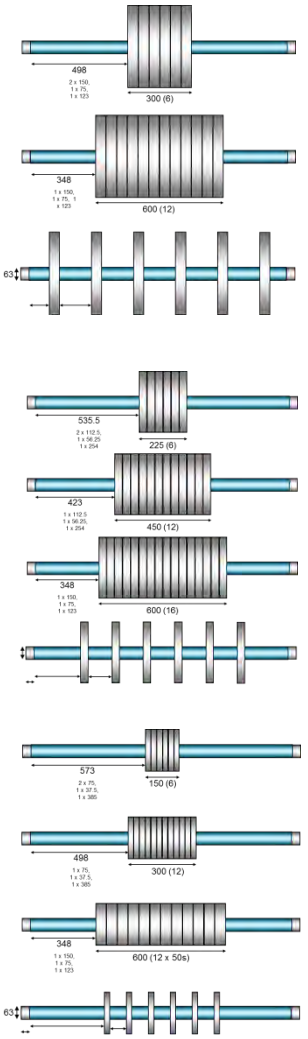

Appendix A16

Simulating the Physical Behaviour of Seine Ropes for Evaluating Fish Herding Properties of Danish Seines

FTFB, New Bedford, 2014

Simulating the Physical Behaviour of Seine Ropes for Evaluating Fish Herding Properties of Danish Seines

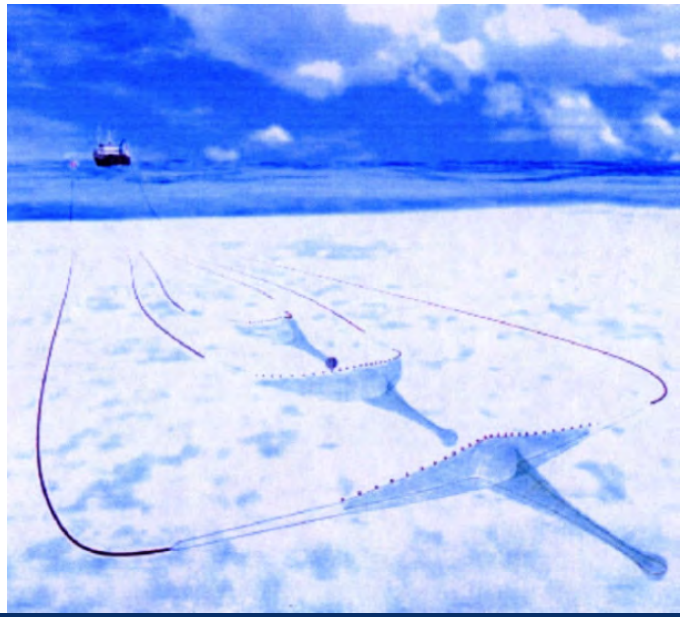

Nina A H Madsen, Karl Gunnar Aarsæther, Bent Herrmann
SINTEF Fisheries and Aquaculture, Fishing Gear Technology

Project

- A national Norwegian three year research project to develop a simulation model for Danish Seine Fishing
  - 2013-2015
  - Physical modelling/simulation of gear behaviour
  - Simulation and prediction of size selection
- Funded by *Research Council of Norway (RCN)* and *Fisheries and Norwegian Seafood Research Fund (FHF)*
- The project Is led by SINTEF and with University of Tromsø as partner (Roger B. Larsen)
- The project uses knowledge from international experts

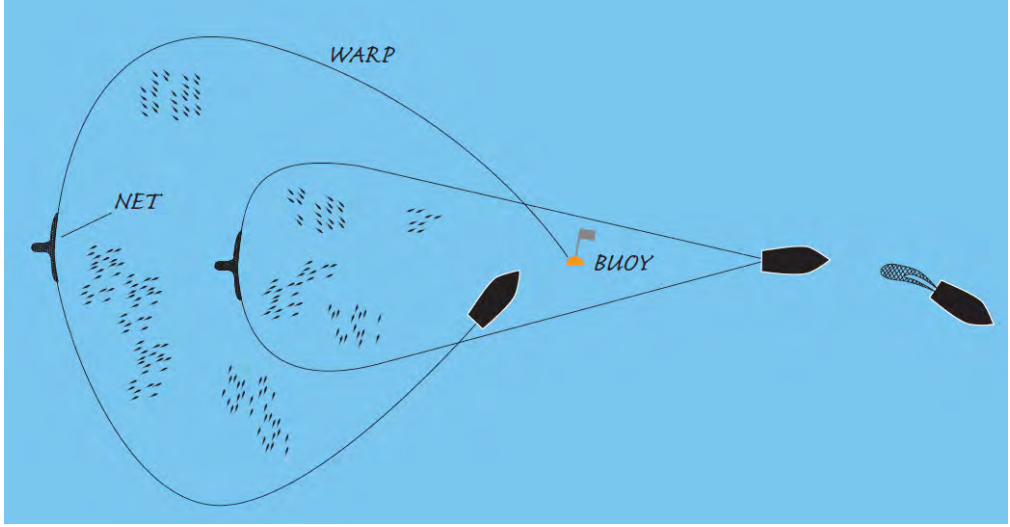

Danish Seine Fishing

- A Danish Seine is an active fishing gear consisting of two long warps (seine ropes) and a fishing net.
  The wings on the net is typically larger than on a bottom trawl net.

- Fishing Procedure
  - The boat will set a buoy, lays out the first warp, the net and then the second warp.
  - The warps are laid out on the seabed to encircle the targeted fish population
  - The boat will then return to the buoy.
  - The boat typically moves forward with a speed of upto 2 knots while simultaneously beginning to winch in the two seine ropes.
- The wings of the seine will gradually change geometry during the fishing process.
- An important function of the seine ropes is to herd the fish into the path of the seine net between the wing tips to ensure they ends up entering the net during the later stages of the fishing process

Seine Ropes and Fish Herding

- The seine ropes(warps) are important since they are sweeping the bottom and mainly responsible for herding the fish in to the path of the seine net
- The fish will react to the approaching warp by swimming perpendicular to the warp
- The movement (shape and speed) of the warps are important for the herding efficiency during the fishing process
  - Too fast and the fish might be overrun by the warp
  - Too slow and the fish might find the warp not to be so scary after all?

- We are going to use experimental data from Norwegian trawl fishing, cod and haddock in establishing a model for herding fish
- Additionally we have sweep herding data from trawl on Plaice and Flounders.
- **More information /data is welcome from anyone !**

Simulation Model

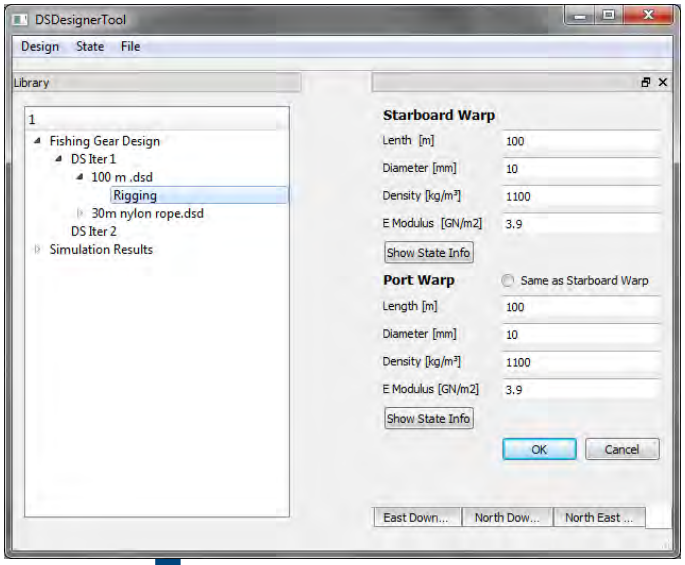

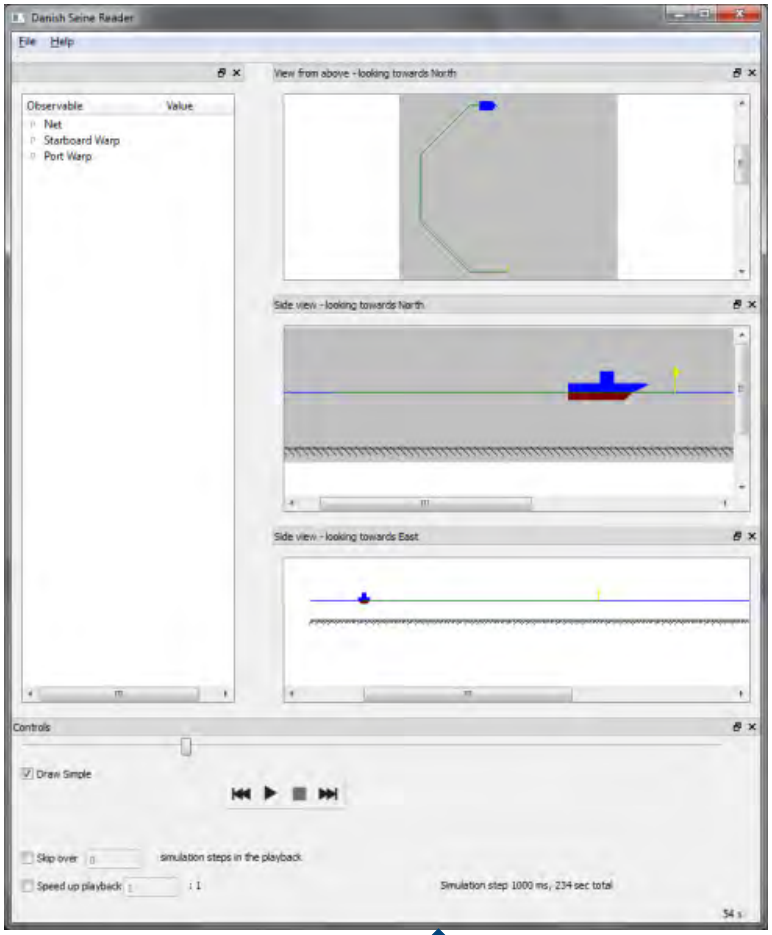

Fishing Operation Description

Environment Description

Fishing Gear Description

Simulation Tool

Simulation Result

Demonstration

Simulation Work Flow

- Vary one description, compare the results
- Effect of gear design

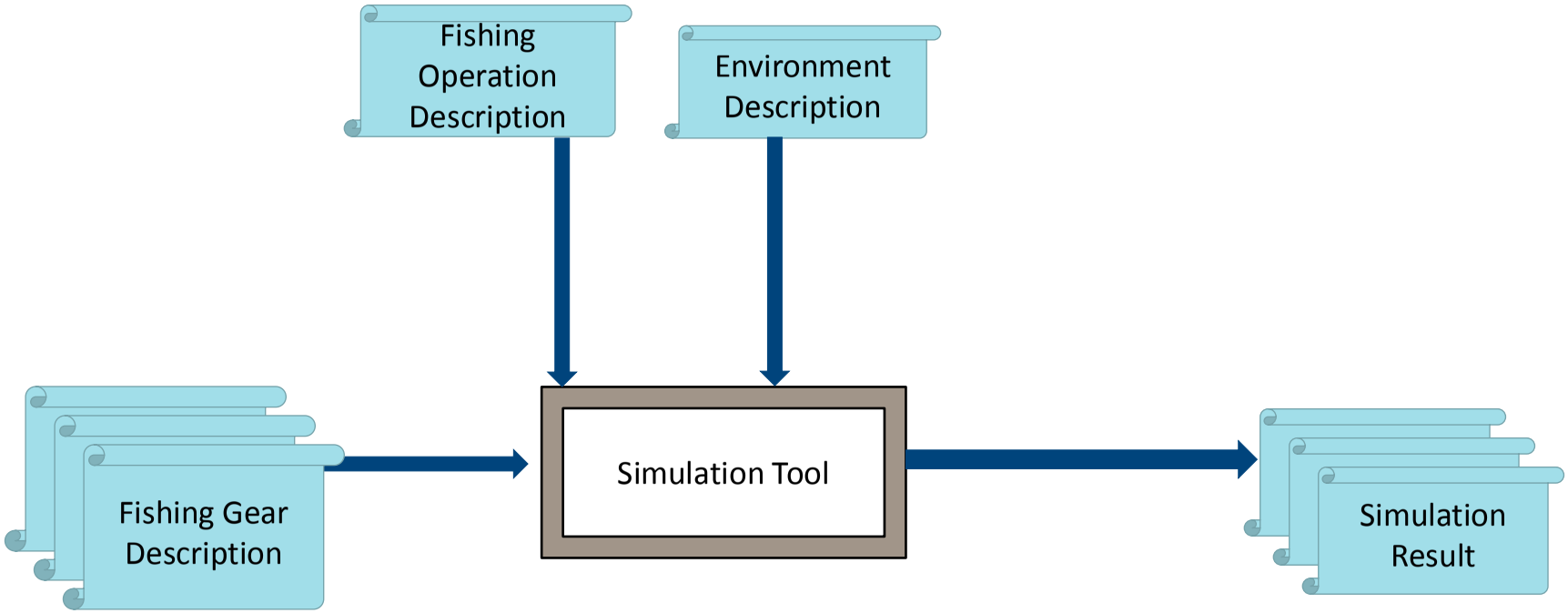

Simulation Work Flow

- Vary one description, compare the results
- Effect of gear design
- Effect of Fishing Operation

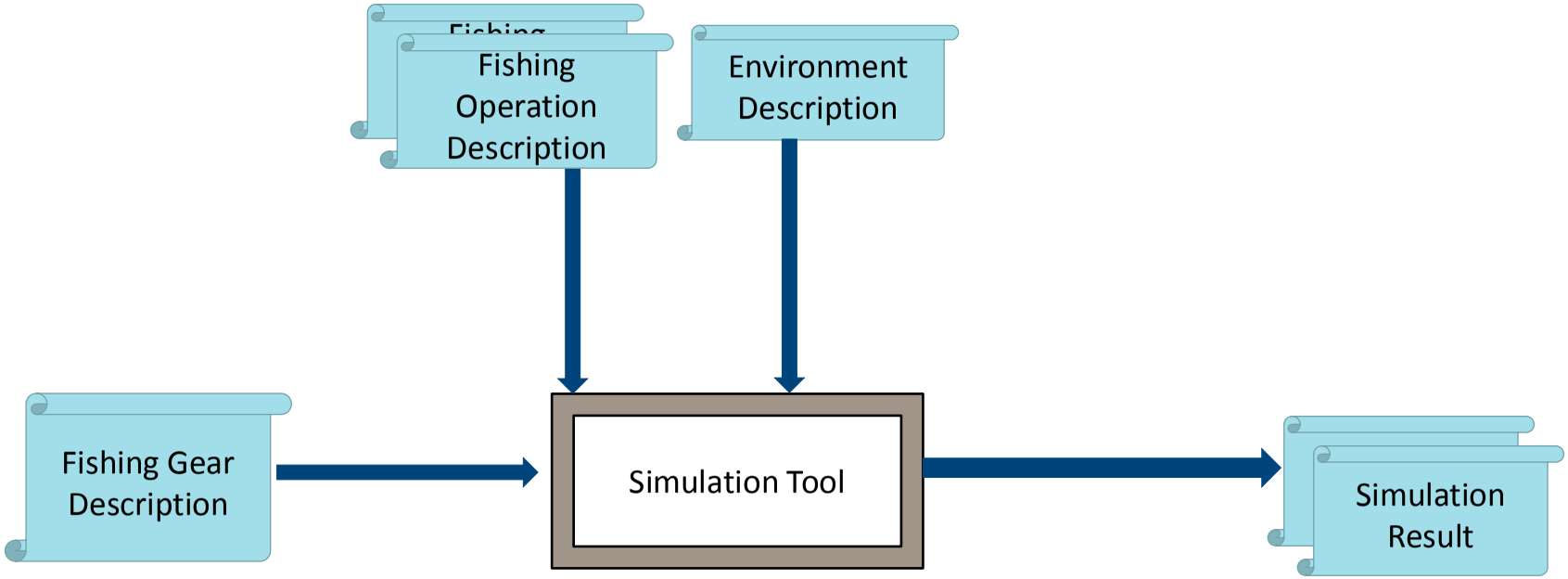

Simulation Work Flow

- Experimentation by simulation

Fishing Gear	Operation	Environment	Result
A	a	e	Aae
B	a	e	Bae
C	a	e	Cae
A	b	e	Abe
A	c	e	Ace

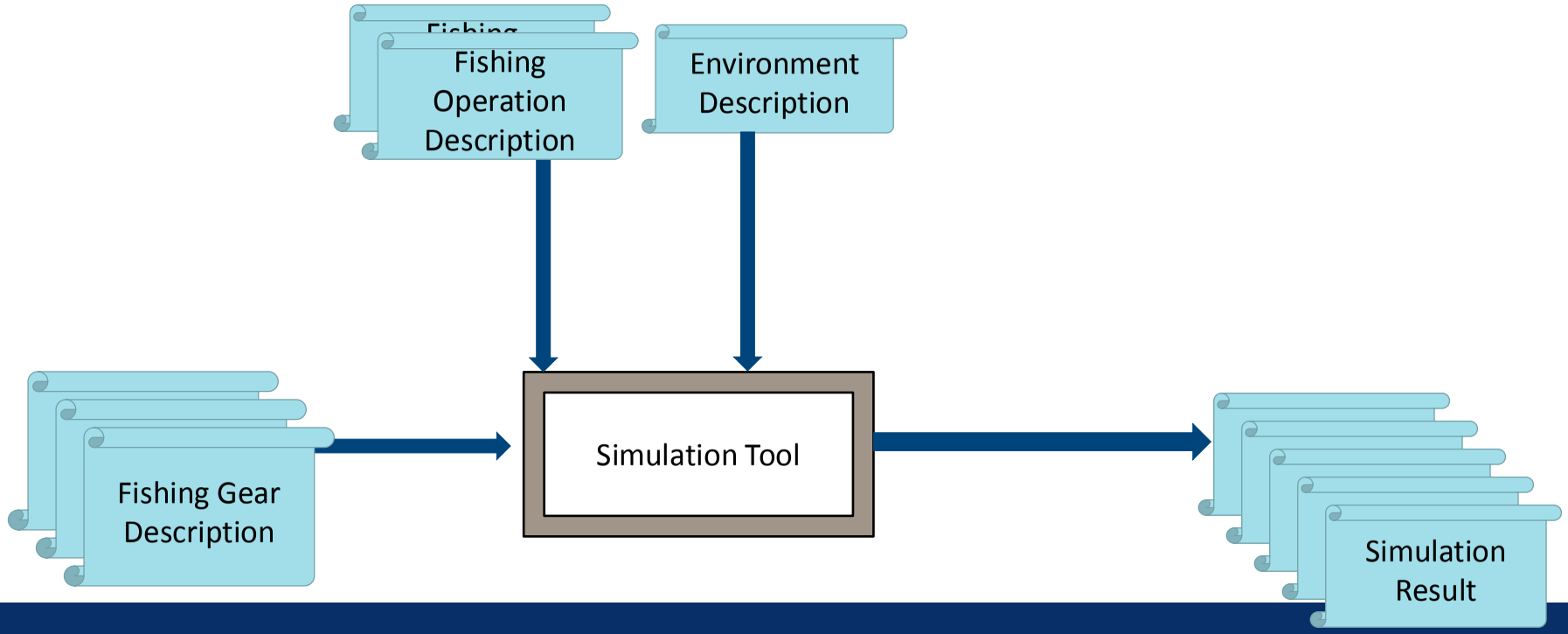

Development Strategy of the Project

- First building a simple model
- Improve it bit by bit – an iterative incremental development approach
- Simulation Model Creation Process
  - Model a setup
  - Compare the setup to experimental data or other simulations
  - Go back and improve the model

Physical Modelling of Danish Seine Rope Behaviour

- The gear geometry is determined by the seine ropes throughout the process
- A physical model is required to demonstrate and predict the effects of
  - Changes to fishing operations – better results with existing gear
  - Changes in gear properties – better results with modified gear
- Seine ropes in use range from 700m combination ropes to 3000m, diameter 36mm to 60mm
- Iterative development of seine rope models – replace models in use with more complex models without changes to model description and usage
  - Complex models provides a more realistic physical modeling

Ongoing Work on Seine Rope Models

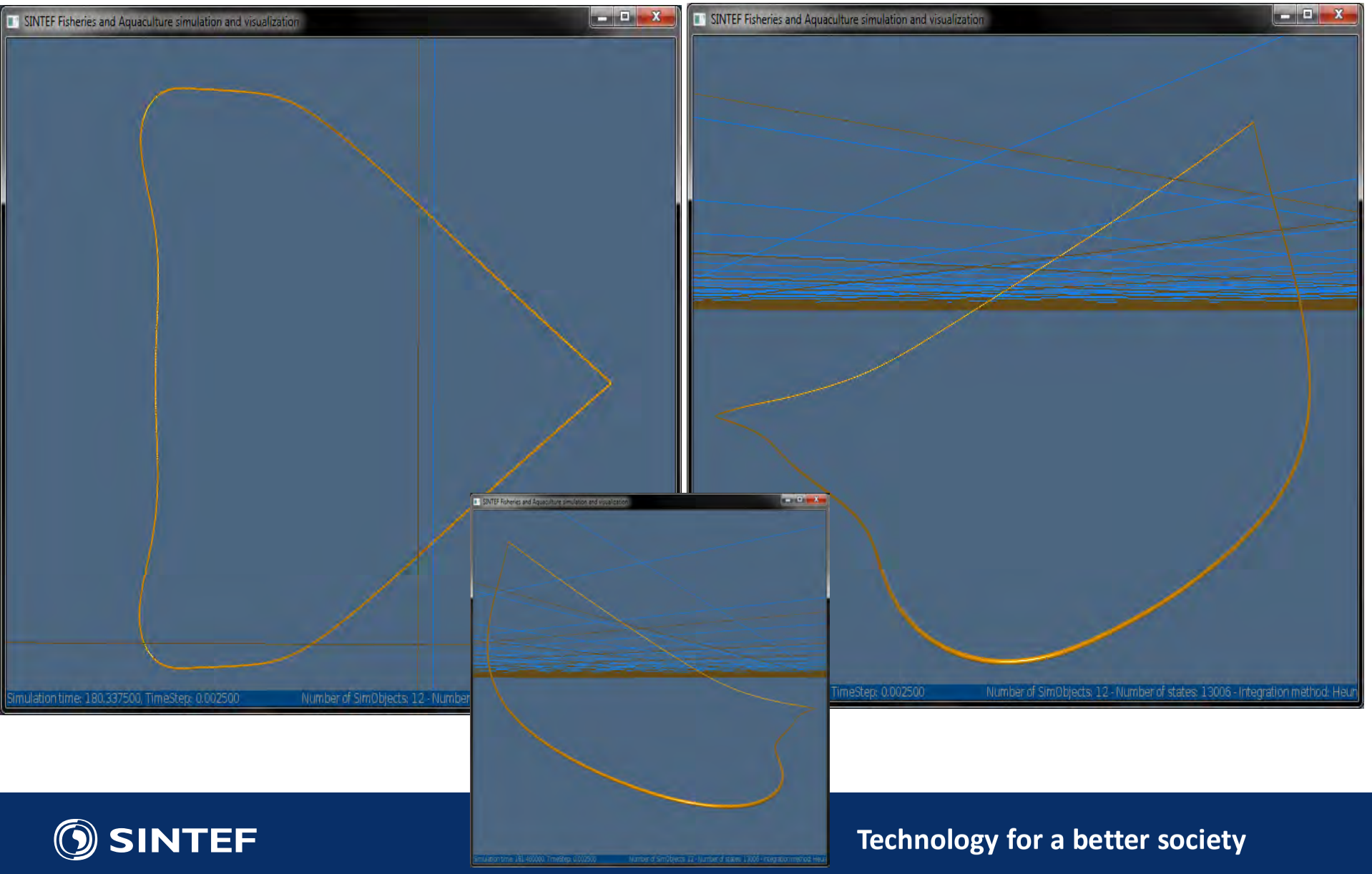

Forces on Danish Seine ropes

- Seine ropes are slender and flexible structures
  - Viscous forces dominate, deformation of structure must be accounted for
- The cables moves through water and in contact with the seabed
  - External forces on ropes
    - Gravity/buoyancy
    - Hydrodynamic lift/drag and added mass
    - Friction/contact forces with seabed
  - Internal forces in ropes – balance external forces
  - Discretization of the rope structure
    - The behavior is determined by the local balance of these forces

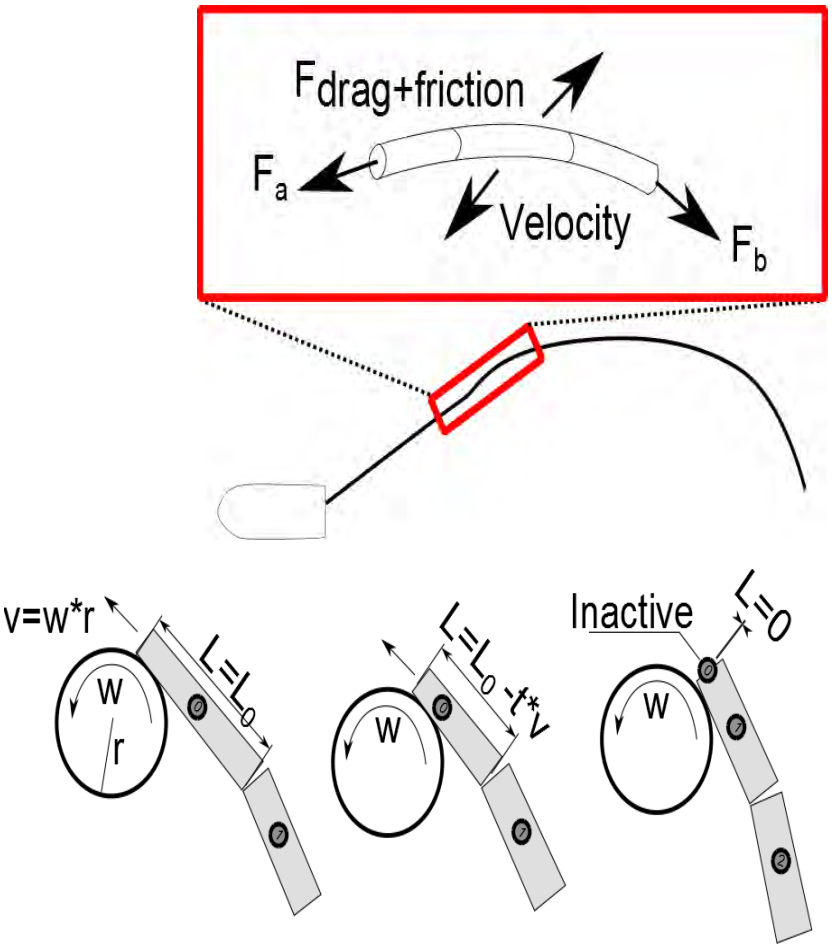

Winching of discrete cable model

Thank you for listening

- We welcome comments, questions and even possible data for use in our studies

Appendix A17

Understanding and predicting size selection of cod (Gadus morhua) in square-mesh codends for Danish Seining: a simulation-based approach

Understanding and predicting size selection of cod (Gadus morhua) in square-mesh codends for Danish Seining: a simulation-based approach

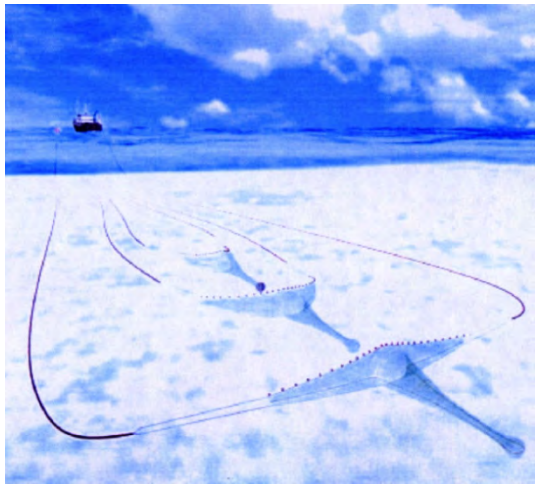

Bent Herrmann, Roger B. Larsen (UIT), Bjørnar Isaksen (IMR), Manu Sistiaga, Nina Madsen, Karl G. Aarsæther

Background

- Danish Seining is an important active fishing method to harvest cod (Gadus morhua) and haddock (Melanogrammus aeglefinus) in Norwegian fisheries. Knowledge about size selectivity in this type of active fishing gear is therefore of importance for managing the exploitation of the cod and haddock resources.

- However very limited scientific published data exists on the size selection of target species in the square mesh codends mostly applied in this fishery.

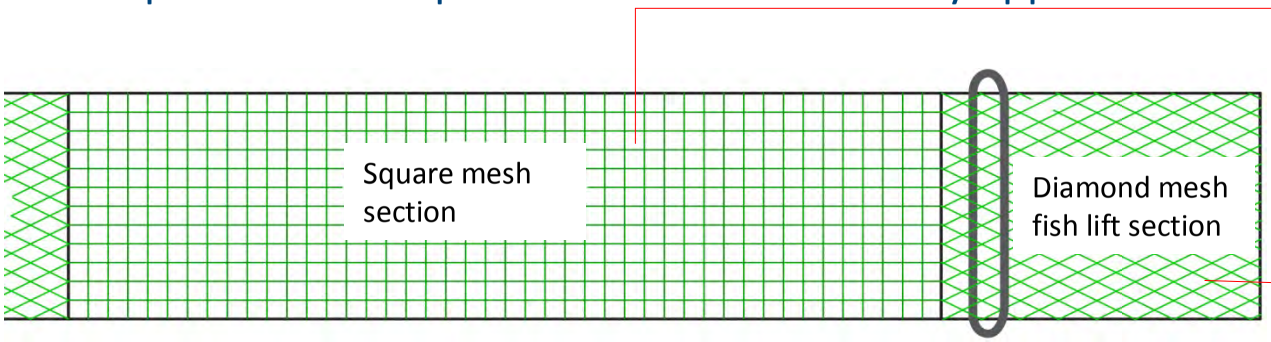

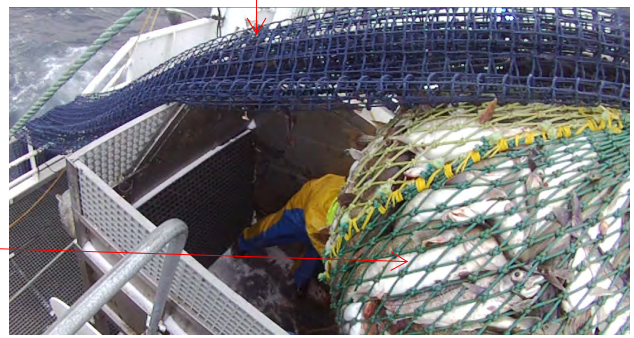

Focus on Cod selectivity in Danish Seine codends

- Cod is the most important species in the Norwegian whitefish fishery when measured in both tonnes landed and in value. Therefore this study focus on cod.
- Around 20% of the Norwegian cod quota is caught using Danish seines.
- The target size for cod in the fishery is sizes from 44 cm. The codends applied should therefore have low retention probability for sizes below 44 cm.

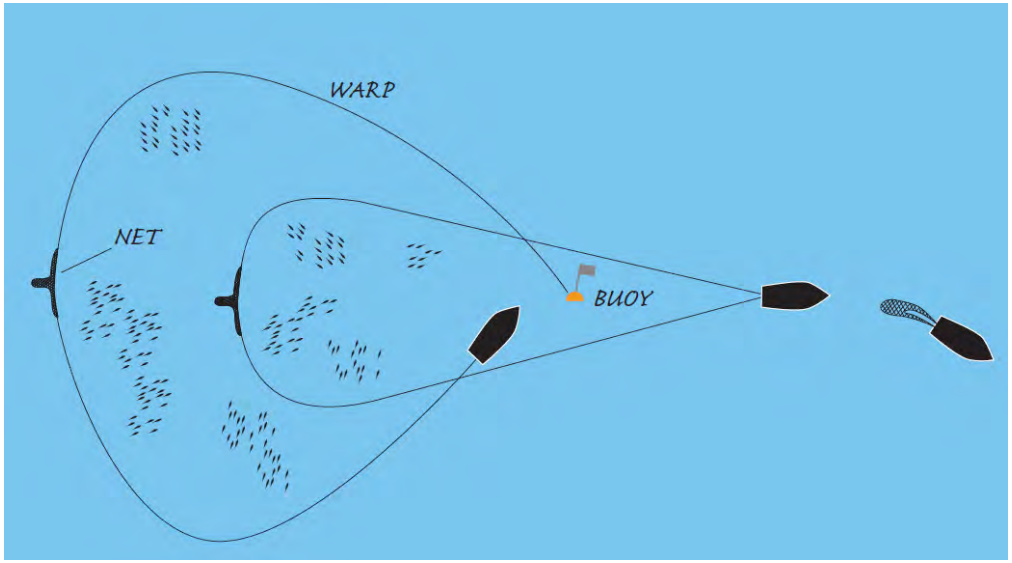

<u>The Danish seine fishing process</u>

Two long seine ropes (warps) which are connect to the wing tips of the seine is laid out on the seabed to encircle the fish population targeted. After the vessel have returned to the buoy marking where the first part of the first seine rope was laid out the vessel typically moves forward with a speed of about 2 knots while simultaneously beginning to winch in the two seine ropes. An important function of the seine ropes is to herd the fish into the path of the seine net between the wing tips to ensure they ends up entering the net during the later stages of the fishing process. The wings of seine will gradually change geometry during the fishing process.

Codend design

- For the Norwegian Danish seine fishing north of 64º it is mandatory to use a square mesh codends in specific areas (mesh size minimum 125 mm).
- The background for requiring a square mesh codend for the Danish seine fishing is to provide better escapement options along the entire length of the codend compared to what would be the situation with a diamond mesh codend under longitudinal tension.
- This is believed to be particular important for the Danish seine fishing with escapement options along the entire codend length compared to with bottom trawling since the fish typically spent far less time in the back part of the codend. Contrary to for the bottom trawl fishery it is not mandatory to use a sorting grid to select out the small fish in the Norwegian Danish seine fishery for cod and the size selection is therefore solely dependent on the size selection in the square mesh codend.

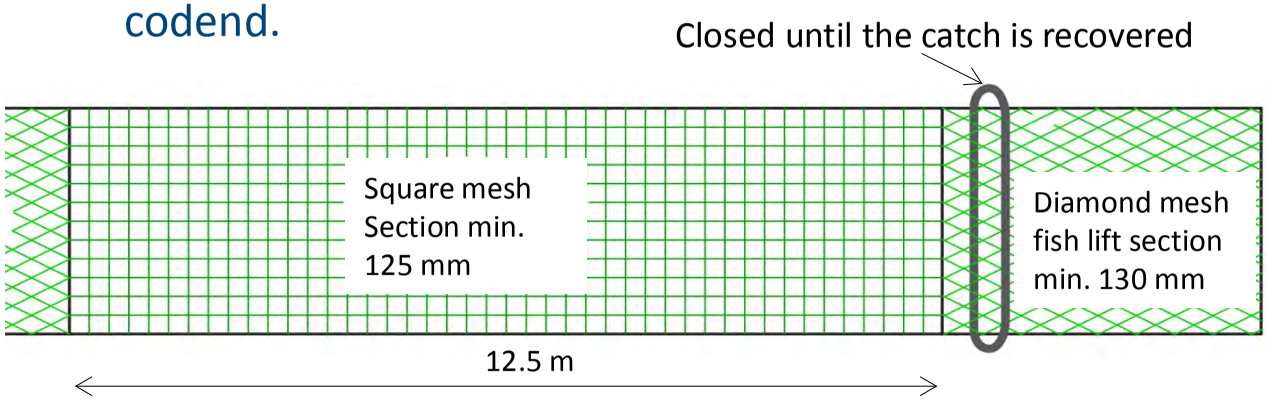

Selectivity at depth

- From underwater recordings it is evident that many fish do escape through the fully or partly open codend square meshes prior to the codend reach the surface.

- Recordings also indicate that at least some fish seem to be able to distort at least tensionless mesh bars during attempts to escape.
- Clear that many meshes are only partly open.

Sacking up and Codend size selection

- The way the catch is recovered to the fishing vessel in Norwegian Danish seine fishing differs considerable from in the trawl fishery.
- A common used method is called "sacking up" and consists of that about 500-1000 kg catch at the time is released to the front part of the codend with diamond meshes which is lifted on board while the rest of the codend remain in surface with slack square meshes.
- Dependent on the amount of catch a fishing process can involve several sacking up operations while the rest of the codend remain at the surface with the remaining fish in the catch surrounded by tensionless square meshes.
- The fish lift of diamond mesh netting may also contribute to the size selection when the fish are released into to this during the catch recovery.

Using FISHSELECT methodology and data

- We applied the fish morphology based simulation method FISHSELECT to investigate the selective potential of the square mesh codends including the diamond mesh fish lift.
- FISHSELECT is a framework of methods, tools, and software developed to determine whether or not a fish is able to penetrate a certain mesh in an active fishing gear. Through computer simulation, FISHSELECT (Herrmann et al. 2009) enables the estimation of the size selectivity for a certain species and selection device by comparing the morphological characteristics of the former and the shape and size of the latter.

Fisheries Research 97 (2009) 59–71

Contents lists available at ScienceDirect

Fisheries Research

journal homepage: www.elsevier.com/locate/fishres

Prediction of selectivity from morphological conditions: Methodology and a case study on cod (*Gadus morhua*)

Bent Herrmann[1], Ludvig A. Krag*,[1], Rikke P. Frandsen, Niels Madsen, Bo Lundgren, Karl-Johan Stæhr

- For this study we used FISHSELECT data collected during experimental trawl fishery in the Barents Sea and morphological models based on analysis of these data. These data and models are described in Sistiaga et al. 2011.

Canadian Journal of Fisheries and Aquatic Sciences, 2011, Vol. 68, No. 5 : pp. 927

Understanding limits to cod and haddock separation using size selectivity in a multispecies trawl fishery: an application of FISHSELECT

Manu Sistiaga, Bent Herrmann, Kåre N. Nielsen, Roger B. Larsen

(doi: 10.1139/f2011-017)

Different mesh states considered in simulations

Due to the observations that the fish will experience codend meshes with different shape and tension states during the Danish Seine fishing process we consider for the simulation different scenario's regarding the distortability of mesh shapes when cod attempt to escape through:

I. Soft/slack mesh model

The fish can fully distort the mesh shape to take shape after the fish cross section

II. Semi soft square mesh model

For partly open square meshes the fish can distort the tensionless mesh bars outwards

(model also applied in Krag et al. (2011) for study of selectivity of haddock in trawl square mesh codends)


Fisheries Research 110 (2011) 225–235

Contents lists available at ScienceDirect

Fisheries Research

journal homepage: www.elsevier.com/locate/fishres

Size selection of haddock (*Melanogrammus aeglefinus*) in square mesh codends: A study based on assessment of decisive morphology for mesh penetration

Ludvig A. Krag[*,1], Bent Herrmann[1], Niels Madsen, Rikke P. Frandsen

III. Stiff mesh model

The fish cannot distort the mesh shape at all neither bars with tension or without tension in

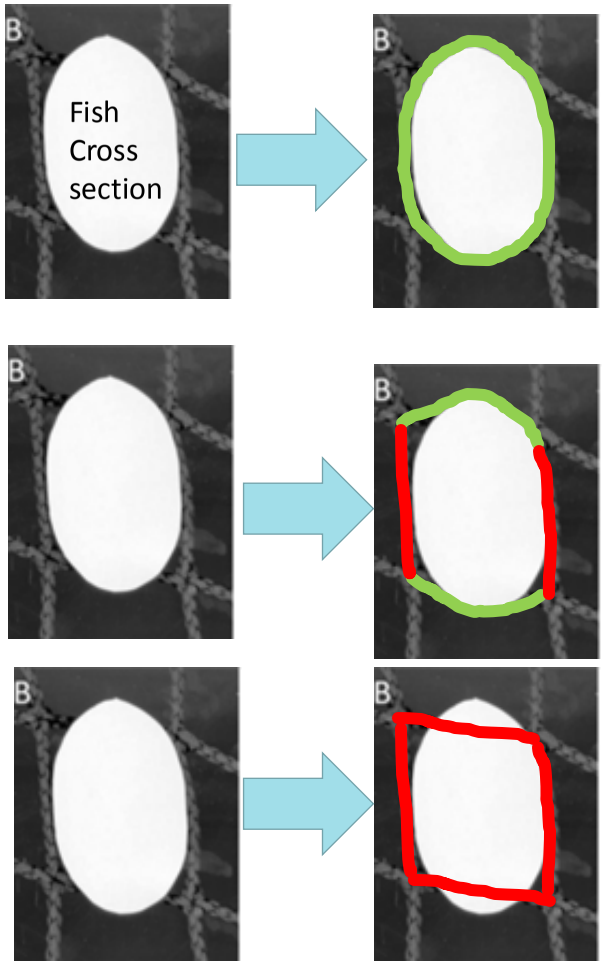

Prediction of Selective potential for the current codend design

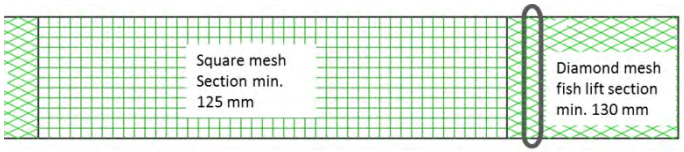

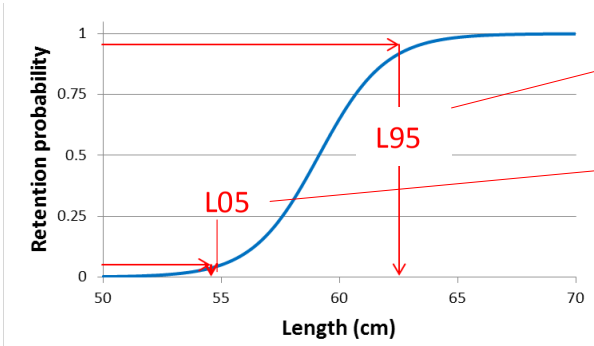

Target size limit at 44 cm

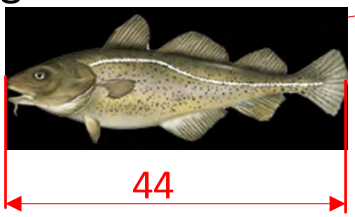

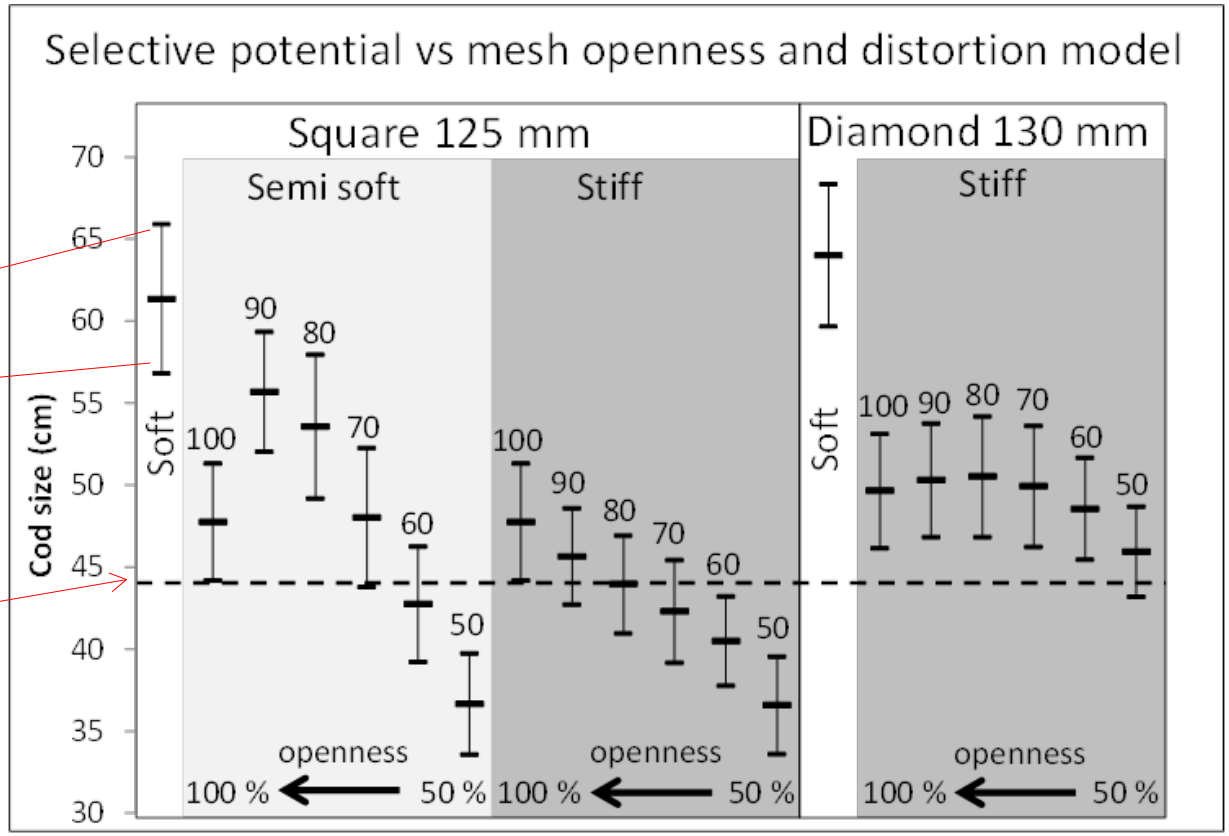

- Soft/slack mesh selectivity if occurring could potentially mean release of cod far above the target limit.
- Semi soft mesh selectivity can if optimal open result in release of cod well above minimum target size. But it need to be at least 70% open to avoid retaining some undersized cod.
- If the cod are not able distort even tensionless mesh bars (stiff mesh) then it is necessary that the square meshes are fully open to avoid risking catching undersized cod.
- The selective potential in the bigger mesh size fish lift can if slack/soft or well open result in potential after selection.

Experimental results from historical codend

- Paired gear data from Isaksen and Larsen (1988)
- Square 120 mm
- Thin and flexible twine construction (thinner and more flexible than applied today)
- Fish lift diamond 110 mm
- Trouser gear data (control 60 mm mesh size)
- Few hauls conducted.
- Re-analysed to obtain confidence limits:

L50	57.33 (54.52 - 85.65)
SR	6.61 (5.37 - 32.43)
1/δ	0.0231 (0.0193 – 100)
SP	0.500 (0.4044 - 0.8603)
P-Value	0.5889
Deviance	3.73
DOF	5

L05	43.48 (39.44 - 53.66)
L10	47.65 (44.14 - 59.44)
L15	50.09 (46.88 - 63.69)
L20	51.82 (48.69 - 66.80)
L25	53.16 (50.09 - 70.31)
L30	54.26 (51.30 - 73.61)
L35	55.18 (52.34 - 76.61)
L40	55.99 (53.18 - 79.57)
L45	56.70 (53.85 - 82.57)
L55	57.90 (55.08 - 88.87)
L60	58.43 (55.61 - 92.29)
L65	58.91 (56.11 - 96.15)
L70	59.35 (56.58 - 100.56)
L75	59.77 (57.10 - 105.58)
L80	60.16 (57.49 - 110.38)
L85	60.52 (57.83 - 116.91)
L90	60.87 (58.36 - 123.78)
L95	61.21 (58.71 - 137.68)

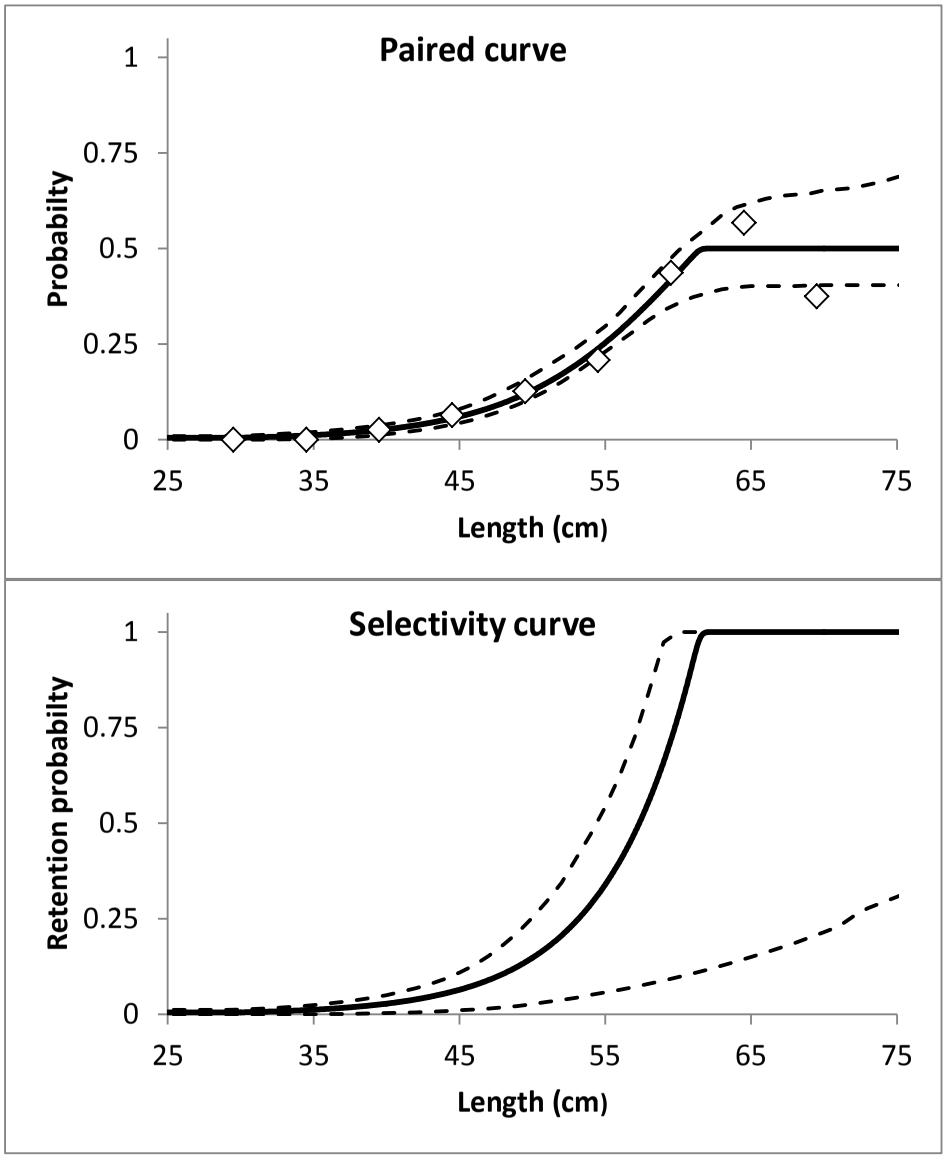

Replicating the historical data by FISHSELECT simulation

- Can we understand the historical data based on the different mesh states models and thereby learn something about size selection of cod in Danish seine codends based on square mesh selection?
- We investigated different scenario's regarding the fish ability to distort the meshes: not (stiff), partly (semi soft), fully (soft) or combinations of these.
- In particular we investigated if the combination of meshes with different openness (%) and different distortion modes would have the potential to replicate the experimentally observed selectivity curve. For doing this we used the technique described in Herrmann et al. (2013) :


Fisheries Research 146 (2013) 59–73

Contents lists available at SciVerse ScienceDirect

Fisheries Research

journal homepage: www.elsevier.com/locate/fishres

Understanding sorting grid and codend size selectivity of Greenland halibut (*Reinhardtius hippoglossoides*)

Bent Herrmann[a,*,1], Manu Sistiaga[b,1], Roger B. Larsen[c], Kåre N. Nielsen[c], Eduardo Grimaldo[b]

Experimental result

$$f(w_1, \ldots, w_n) = \sqrt{\sum_i (L_i - LF(w_1, \ldots, w_n)_i)^2},$$

Simulation result

Contribution factor

$$i \in \{5,10,15,20,25,30,35,40,45,50,55,60,65,70,75,80,85,90,95\}$$

Ability to replicate experimental results for different mesh states scenario's

- Only a combination of semi soft and soft/ slack meshes with a considerable contribution (>60%) can explain the historical data!

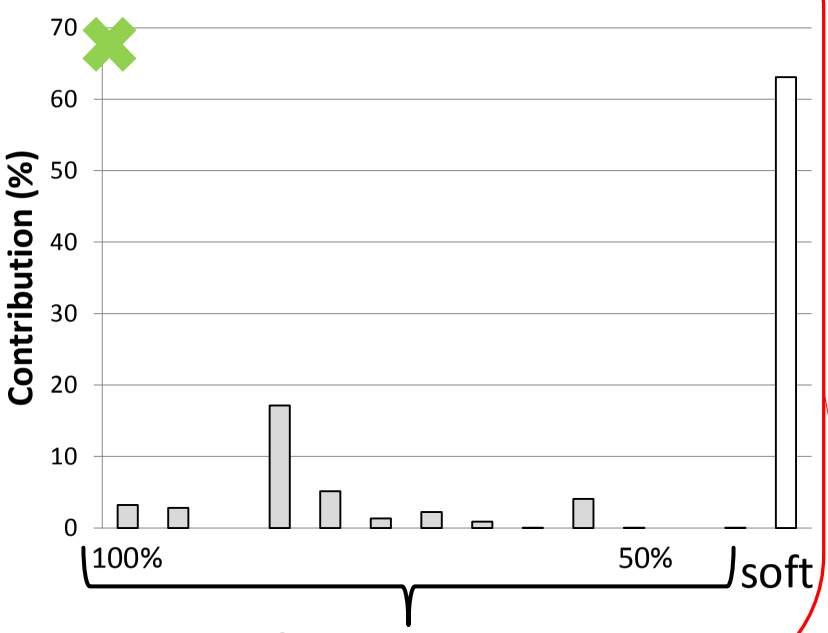

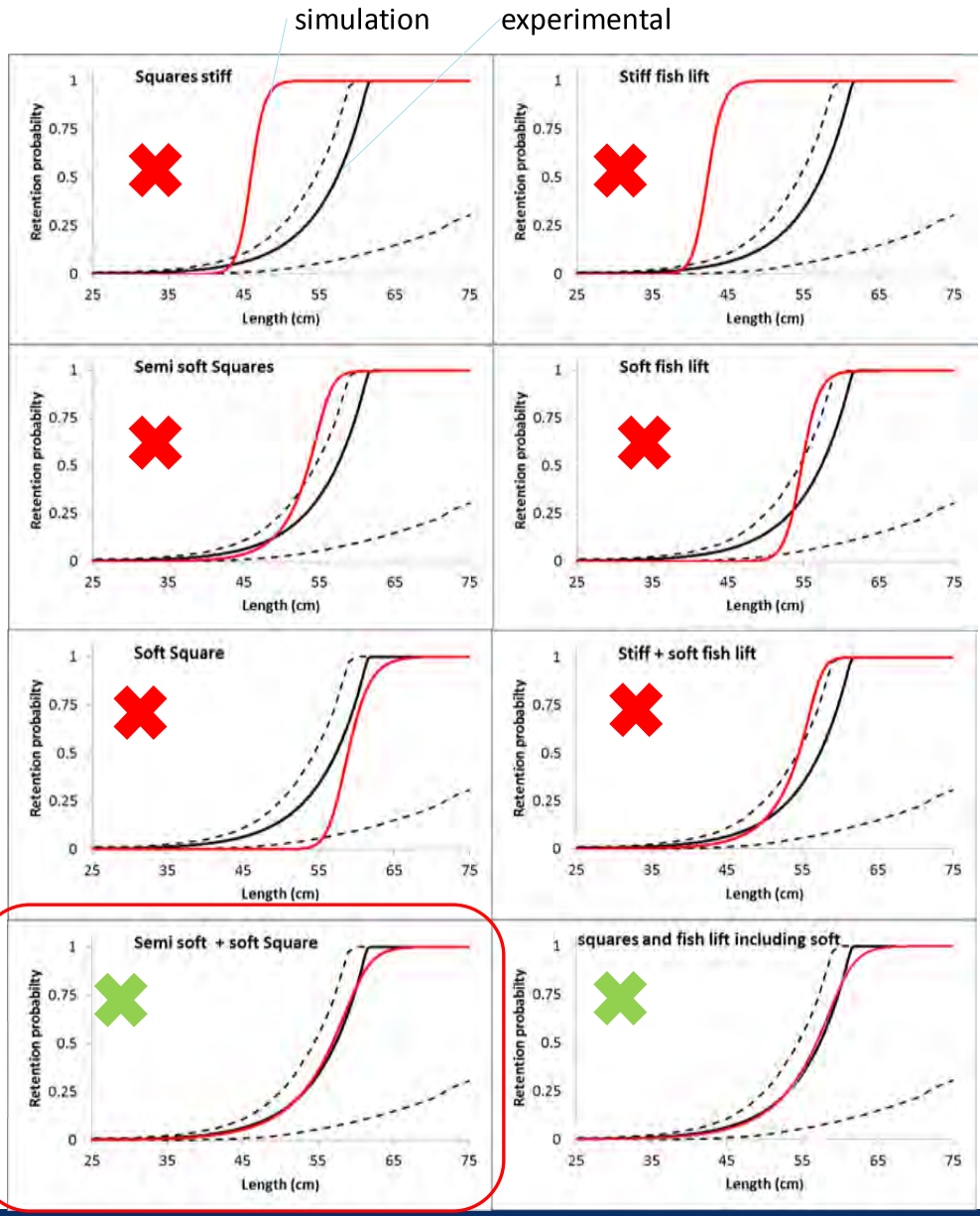

Conclusion/Discussion

- Soft/slack mesh escapement seem to play a big role for the selection process in the historical gear – could speculate when during the fishing process this may occur and what would be the survival rate of those fish.
- The current applied codends are made of stiffer and thicker twine and it can therefore be questioned if soft/slack mesh escapement will play any significant role for the designs applied today.
- Would be beneficial with experimental results for designs made of currently applied codend materials since this would enable predictions for this type of contructions.
- However if cod can as indicated from underwater recordings distort tensionless partly open square meshes (semi soft escapement) then the current applied design support release of all cod below the target sizes (44 cm) if the codend meshes are at least 70 % open.
- If the cod cannot distort the meshes at all (stiff mesh) then the codend meshes needs to be fully open to release all undersized cod through the square meshes of the current design.
- Bigger mesh size in the fish lift than for the square meshes may potentially lead to late escapement of some cod if these meshes are slack or well open.

THANKS!

Work funded by:
Research Council of Norway
and
Norwegian Seafood Research Fund